STRUCTURAL AND TECTONIC EVOLUTION OF THE EASTERN ARUNTA INLIER IN THE HARTS RANGE AREA OF CENTRAL AUSTRALIA



by

Ding Puquan

Department of Geology and geophysics,

The University of Adelaide,

Australia

March, 1988

A thesis submitted to the University of Adelaide
in fulfilment of the requirements for the
degree of Doctor of Philosophy

CONTENTS

Abstract

Acknowledgements

CHAPTER 1 INTRODUCTION ---------- 1

1.1. Introduction ---------- 1

1.2. Regional geological setting ---------- 2

1.3. Previous geological work in the Harts Range area ------- 4

1.4. Original aims of the thesis ---------- 5

1.5. Methods of study ---------- 6

1.6. Logistics ---------- 7

1.7. Stratotectonic subdivision of the Harts Range area ----- 8

1.7.1. Review of previous work ---------- 8

1.7.2. Revised stratotectonic subdivision and thesis layout -- 10

Fig. 1-1 ---------- (13)
(numbers in brackets represent page numbers to be followed)

Fig. 1-2 ---------- (13)

1.8. Summary of the main achievements of this study -------- 14

Fig. 1-3 ---------- (15)

PART ONE -- STRANGWAYS OROGENIC BELT

CHAPTER 2 THE HALE RIVER REGION AND THE ENTIA DOME ---------- 16

2.1. Introduction ---------- 16

Fig. 2-1 ---------- (16)
Fig. 2-2 ---------- (16)
Fig. 2-3 ---------- (16)
Fig. 2-4 ---------- (16)

2.2. Field description and basic petrology of the Hale River Region and the Entia Dome ---------- 17

2.2.1. Introduction ---------- 17

2.2.2. Metasediments ---------- 19

Plate 2.1 ---------- (20)

2.2.3. Mafic and ultramafic rocks ---------- 22

Plate 2.2 ---------- (23)

2.2.4. Acidic to intermediate orthogneiss ---------- 25

Plate 2.3 ---------- (26)

2.2.5. Post tectonic intrusive bodies ---------- 28

2.3. Structure ---------- 28

2.3.1. Introduction ---------- 28

2.3.2. Compositional layering in metasediments and amphibolites ---------- 29

2.3.3. Structures of the first deformation (BD_1) --------- 30

Plate 2.4 ---------- (30)

2.3.4. Structures of the second deformation (BD_2) ---------- 32

2.3.5. Structures of the third deformation (BD_3) --------- 33

Plate 2.5 ---------- (33)

2.3.6. Structures of the fourth deformation (BD_4) ---------- 37

2.3.7. Thrusting within the Entia Dome (BT) ---------- 37

2.4. Metamorphism ---------- 39

2.4.1. Introduction ---------- 39

2.4.2. Regional granulite facies metamorphism ---------- 40

2.4.3. Regional amphibolite facies metamorphism ---------- 41

2.4.4. Retrograde metamorphism ---------- 42

Plate 2.6 ---------- (42)

CHAPTER 3 THE OONAGALABI TONGUE ---------- 44

3.1. Introduction ---------- 44

3.2. Field description and basic petrology of the Oonagalabi Tongue ---------- 44

3.2.1. Metasediments ---------- 45

3.2.2. Mafic rocks ---------- 46

Plate 3.1 ---------- (46)

3.2.2.1. Mafic granulite ---------- 47

3.2.2.2. Amphibolite ---------- 47

3.2.2.3. Deformed and retrograde mafic granulite ---------- 48

3.2.3. Orthogneisses ---------- 49

3.2.4. Migmatitic gneiss ---------- 49

Plate 3.2 ---------- (50)

3.3. Structure ---------- 50

Fig. 3-1 ---------- (50)
Fig. 3-2 ---------- (50)

3.3.1. Introduction ---------- 50

3.3.2. Pre-BD_1 to BD_1 structures ---------- 52

3.3.3. Structures of the second deformation (BD_2) -------- 53

Plate 3.3 ---------- (54)

3.3.4. Structures of the third deformation (BD_3) --------- 55

3.3.5. Structures of the fourth deformation (BD_4) -------- 55

Plate 3.4 ---------- (56)

3.3.6. Shear zones within the Oonagalabi Tongue (BT) --------- 56

3.3.7. Fold interference ---------- 58

3.4. Metamorphism ---------- 60

3.4.1. Granulite facies metamorphism ---------- 60

3.4.2. Amphibolite facies metamorphism ---------- 63

CHAPTER 4 THE FLORENCE / LEAKY SHEAR ZONE ---------- 66

4.1. Introduction ---------- 66

Fig 4-1 ---------- (66)

4.2. Field description ---------- 69

4.2.1. The Florence Shear Zone ---------- 69

Plate 4.1 ---------- (70)

4.2.2. The Leaky Shear Zone ---------- 71

Plate 4.2 ---------- (71)

4.2.3. Coggan Shear Zone ---------- 72

4.2.4. Emma and Cone Klippen ---------- 72

4.3. Petrographic description of the lithologies ---------- 73

Plate 4.3 ---------- (75)

Plate 4.4 ---------- (77)

4.4. Folding within the F/LSZ ---------- 77

4.5. Fabric and microstructure of the mylonitic rocks ------ 78

4.5.1. Fabrics ---------- 78

4.5.2. Deformation of individual mineral phases from within the mylonites in the F/LSZ ---------- 79

Plate 4.5 ---------- (80)

4.6.2. Shear sense assesment ---------- 82

Fig. 4-2 ---------- (84)

4.7. Metamorphism ---------- 85

4.7.1 Metamorphic facies ---------- 85

4.7.2. Temperature and pressure estimates ---------- 86

PART TWO THE HARTS RANGE OROGENIC BELT

CHAPTER 5 LITHOLOGIES AND METAMORPHISM OF THE HARTS RANGE OROGENIC BELT ---------- 89

5.1. Introduction ---------- 89

5.2. Subdivision of lithologic units and stratigraphy in the ISA ---------- 90

5.3. The metasedimentary lithologies ---------- 92

5.3.1. Unit 1: quartz-rich calc-silicate, calc-silicate quartz schist and calc-silicate gneiss ---------- 92

Plate 5.1 ---------- (93)

5.3.2. Unit 2: calc-silicate ---------- 94

5.3.3. Unit 3: marble with minor calc-silicate ---------- 95

5.3.4. Unit 4: pure and impure quartzite ---------- 96

5.3.5. Unit 5: pelitic and semi-pelitic gneiss ---------- 96

Plate 5.2 ---------- (97)

5.4. The Harts Range meta-igneous complex ---------- 98

5.4.1. Unit 6: layered amphibolite ---------- 98

Plate 5.3 ---------- (99)

5.4.2. Metamorphosed ultramafic rocks ---------- 100

5.4.3. Metagabbro ---------- 102

Plate 5.4 ---------- (103)

5.5. Bruna Gneiss ---------- 104

5.5.1. Introduction ---------- 104

5.5.2. Mesoscopic features ---------- 106

Plate 5.5 ---------- (107)

5.5.3. Modal composition and microstructure ---------- 107

CHAPTER 6 THE EARLY STRUCTURES OF THE HARTS RANGE OROGENY --- 109

6.1. Introduction ---------- 109

6.2. Compositional layering and the earliest foliation (CS_0) ---------- 109

6.3. Structures of the CD_1 deformation ---------- 110

Plate 6.1 ---------- (110)
Plate 6.2 ---------- (111)

6.4. Structures of CD_2 deformation ---------- 111

6.4.1. CF_2 folds in the Naringa Well area

6.4.1.1. Major CF_2 folds ---------- 112

6.4.1.2. Minor CF_2 folds ---------- 113

Plate 6.3 ---------- (113)

6.4.1.3. Relationship between CF_2 folds and CF_1 folds -------- 114

Plate 6.4 ---------- (114)

6.4.2. CF_2 folds in the Mt Campbell area ---------- 114

6.4.3. Tectonic significance of CF_2 folds ---------- 115

6.5. Thrust (CT) and nappe structures ---------- 116

6.5.1. Introduction ---------- 116

Fig. 6-1 ---------- (117)

6.5.2. Naringa Thrust ---------- 118

Plate 6.5 ---------- (119)

6.5.3. Riddoch Thrust ---------- 120

6.5.4. Campbell Thrust ---------- 120

6.5.5. Salthole Thrust ---------- 121

Plate 6.6 ---------- (121)
Plate 6.7 ---------- (122)

6.5.6. Ruby Thrust ---------- 122

Plate 6.8 ---------- (123)

6.5.7. Displacement along the CT thrusts ---------- 124

6.6. Metamorphism of the Irindina Spracrustal Assemblage (ISA) ---------- 124

Fig. 6-2 ---------- (129)

CHAPTER 7 THE LATER STRUCTURES OF THE HARTS RANGE OROGENY -- 130

7.1. Introduction ---------- 130

7.2. The Oonagalabi Movement ---------- 132

7.2.1. The Oonagalabi Thrust (HRT_1) ---------- 132

Plate 7.1 ---------- (133)
Plate 7.2 ---------- (134)

7.2.2. Oonagalabi Movement folding (HRF_1/CF_3 folds)--------- 135

7.2.2.1.HRF1 folds ---------- 135

Plate 7.3 ---------- (137)

7.2.2.2.CF3 folds ---------- 137

Plate 7.4 ---------- (140)

7.3. Maud Movement ---------- 140

7.3.1. Maud Thrust (HRT2) ---------- 140

Plate 7.5 ---------- (141)

7.3.2. Maud Movement folding (HRF_2 folds) ---------- 142

Fig. 7-1 ---------- (142)
Fig. 7-2 ---------- (142)

7.3.2.1.The Oonagalabi Fold ---------- 142

7.3.2.2.The Mullocky Fold ---------- 145

7.3.2.3.The Naringa Fold ---------- 146

Plate 7.6 ---------- (147)

7.4. The Bruna Movement ---------- 148

7.4.1. The Bruna Thrust and the Entia Thrust (HRT_3) --------- 148

7.4.1.1. The Bruna Thrust ---------- 148

Fig. 7-3 ---------- (148)
Plate 7.7 ---------- (149)
Plate 7.8 ---------- (150)

7.4.1.2. The Entia Thrust ---------- 151

Plate 7.9 ---------- (151)
Fig. 7-4 ---------- (151)

7.4.1.3. Metamorphism of the Bruna Gneiss ---------- 152

7.4.2. Bruna Movement folding (HRF_3 folds) ---------- 153

7.5. Muller Movement - Muller Thrust (HRT_4) ---------- 155

Plate 7.10 ---------- (155)
Plate 7.11 ---------- (156)

7.6. Post HRO deformation ---------- 157

7.6.1. Open folds ---------- 157

Fig. 7-5 ---------- (157)

7.6.2. Dolerite dyke ---------- 160

Plate 7.12 ---------- (160)

7.6.3. Structures of the Alice Springs Orogeny ---------- 161

7.6.3.1. Shear zones and thrusts ---------- 161

7.6.3.2. Steep faults system ---------- 163

7.6.3.3. Undeformed pegmatite veins ---------- 164

PART THREE -- DISCUSSION AND CONCLUSION

CHAPTER 8 TECTONIC EVOLUTION OF THE HARTS RANGE AREA--------- 166

8.1. Introduction ---------- 166

8.2. Tectonic evolution of the Strangways Orogeny --------- 168

8.2.1. Deposition ---------- 168

8.2.2. Peak metamorphism and its tectonic implications ------ 168

8.2.3. Voluminous syntectonic acidic to intermediate plutonism ---------- 171

8.2.4. The first deformation in the SOB ---------- 173

8.2.5. Implications of the superimposed (BF_2-BF_4)

folding events ---------- 175

Fig. 8-1 ---------- (176)
Fig. 8-2 ---------- (177)
Fig. 8-3 ---------- (178)

8.2.6. Late thrusting of the SOB ---------- 179

8.2.7. Termination of the Strangways Orogeny ---------- 180

Fig. 8-4 ---------- (181)
Fig. 8-5 ---------- (182)
Fig. 8-6 ---------- (182)

8.3. Tectonic evolution of the Harts Range Orogeny -------- 182

8.3.1. The Florence Movement phase ---------- 182

8.3.1.1. Initiation of the Harts Range Detachment Zone -------- 182

8.3.1.2. Deposition of the Harts Range Supracrustal Cover ----- 184

8.3.1.3. Metamorphism within the HRSC ---------- 185

8.3.1.4. CD_1 deformation ---------- 186

8.3.2. The Oonagalabi Movement phase ---------- 187

8.3.2.1. CD_2 deformation ---------- 188

8.3.2.2. Thrusting: the CT thrusts, nappes and the HRT_1 Oonagalabi Thrust ---------- 189

Fig. 8-7 ----------(190)

8.3.2.3. Intrusion of the Bruna Granite ---------- 191

8.3.2.4. Folding (HRF_1) ---------- 191

8.3.3. Maud Movement phase ---------- 192

8.3.3.1. Thrusting: the HRT_2 Maud Thrust ---------- 192

8.3.3.2. Folding (HRF_2) ---------- 193

8.3.4. Bruna Movement phase ---------- 194

8.3.4.1. Thrusting: the HRT_3 Bruna and Entia thrusts ------ 194

8.3.4.2. Folding (HRF_3) ---------- 194

8.3.5. The Muller Movement phase ---------- 195

Fig. 8-8 ---------- (195)

8.3.6. Completion of the HOB ---------- 195

Fig. 8-9 ---------- (198)

8.4. Post HRO evolution ---------- 198

8.5. Conclusion ---------- 200

REFERENCE ---------- 203

APPENDIX I Modal composition of all samples collected from the Harts Range area

APPENDIX II Results from electron microprobe analysis (14 pp.)

LIST OF ENCLOSURES

Map 1, Map 2, Map 3, Map 4, Map 5, Map 6 and Map 7. (These maps are major part of the thesis.)

Four papers are enclosed as separate appendices. They are Appendix III, Appendix IV, Appendix V and Appendix VI. The preprints will be replaced by reprints later.

This thesis contains no material which has been accepted for the award of any other degree or diploma in any University and, to the best of my knowledge and belief, contains no copy or paraphrase of material previously published or written by another person, except where due reference is made in the text of the thesis.

DATED _____ SIGNED _____

UNIVERSITY OF ADELAIDE LIBRARY

STRUCTURAL AND TECTONIC EVOLUTION OF THE EASTERN ARUNTA INLIER IN THE HARTS RANGE AREA OF CENTRAL AUSTRALIA

Abstract

A thick complex detachment zone, the Harts Range Detachment Zone (HRDZ) is recognized between two orogenic belts, an Early-Middle Proterozoic fold belt, the Strangways Orogenic Belt (SOB) and a younger Middle Proterozoic fold belt, the Harts Range Orogenic Belt (HOB), within the high grade metamorphic complex of the eastern Arunta Inlier in the Harts Range area of central Australia. Both orogenic belts contain their own supracrustal sequences and developed sequentially with different orientations.

Rocks of the SOB were deposited and metamorphosed to a maximum grade of granulite facies at about 1800 Ma. They were subsequently intruded by significant proportions of acidic magma at 1767±2 Ma and compressed to form a distinctively NNE-SSW trending orogenic belt. Four generations of large scale ductile folds and one set of thrusts are mapped and described. One of the most impressive geometrical features is the result of the interference between four tight to isoclinal, inclined to recumbent major and minor fold generations.

The HOB is dominated by a thick pile of supracrustals which were metamorphosed to a maximum grade of amphibolite facies without significant pretectonic intrusions of acidic magma. They were compressed to form a distinctively E-W trending orogenic belt. Four generations of large scale ductile folds and one set of thrusts developed within the HOB. These structures are distinctively different in age and orientation to those in the SOB.

Parts of the SOB were intensely reactivated during the Harts Range Orogeny (HRO) and up to seven generations of ductile folds have been recognized in one of the reactivated SOB areas (the

Oonagalabi Tongue). The HRDZ is represented by discrete thrusts and a thick mylonitic complex (the Florence/Leaky Shear Zone), and is recognized as an ancient WNW-ESE trending and shallow north dipping crustal scale detachment zone which formed initially during a period of NNE-SSW crustal extension as a major low-angle normal shear/detachment zone within and crossing at a high angle to the structural trend of the SOB. Extensional movement on this zone initiated the formation of the HROB. This zone has been intermittently active as a zone of crustal weakness since then and controlled the consequential development of the HOB. Granitic magma intruded along the HRDZ into both the SOB and HOB in the middle stage of the HRO at 1747+3/-2 Ma, and forms a major sheet-like body (the Bruna Gneiss), which acted in turn as a lubricant and thus enhanced the movement along the HRDZ. The HRDZ itself was thus actively reworked through the whole period of the HRO, resulting in polyphase alternating operation of thrusting and folding during crustal compression. Four thrusting phases of the HRDZ are distinquished by three intervening folding phases which affected the thrusts sequentially.

Displacement on the HRDZ was a stick-slip process with repeated punctuation of thrust-slip movement by pinning at points located progressively to the south. Each period of cessation of thrust-slip movement was followed by folding of discrete thrusts, of captured basement lobes and of the overlying supracrustal sequence. The individual discrete movement phases and folding episodes are each named and described, as is a model of this unusual type of Proterozoic tectonic activity during which time, the intrusion of a major granitic gneiss along one of the thrust boundaries precisely fixes the time-scale of evolution of the earlier phases of the Harts Range Orogeny.

ACKNOWLEDGEMENTS

I am indebted and grateful to my supervisor, Dr P.R. James, without whose enthusiastic encouragement, this study would not have been started. He not only geologically but also logistically supported my study in the field, and provided constant guidance and inspiration during all stages of the project. He also spent extra effort in correcting my English.

This study was largely financed by an Adelaide University Research Scholarship and also benefitted from an A.R.G.S. Grant number E 82156171, which I gratefully acknowledge.

I extend sincere thanks to the Institute of Geology, Chinese Academy of Geological Sciences, the Ministry of Geology and the State Education Commission of the People's Republic of China, who offerred me an initial grant to visit Australian institutions and permitted my continuing study in Australia towards a Ph.D degree.

Of the many colleagues in the Department of Geology & Geophysics at the University of Adelaide, many thanks are due to Drs. J.A. Cooper, J. Foden and G. Mortimer and Miss M. McBriar for advice and assistance, and to Mr R. Barrett for making the photographic plates for this thesis. Especial thanks are due to Drs. R.L. Oliver and M. Sandiford who read the earlier draft of this thesis, and made constructive comments and provided valuable discussion.

I also extend my thanks to L. Rankin, R.W. Lawrence and G. Scales for their friendly companying in the field and for discussion. Thanks are also due to my friends, Miss J. Flawry, Ms D.

Jacobson and Mrs J. Goraj who proof read some chapters of the thesis.

Finally especial thanks are due to my wife Xu Gu for her encouragement and support throughout my study and the loss of many valuable weekends for the colouring of the maps, and for the preparation of the photographic plates and appendices of the thesis.

CHAPTER 1 INTRODUCTION

1.1 Introduction

The Proterozoic Eon represents an important segment of earth history. There are two most important aspects of Proterozoic history: 1) a declining thermal regime resulting in the growth of stabilized continental crust and a related change from permobile Archaean tectonics to the initiation of modern-style plate tectonics (Dewey & Bird, 1970; Burke & Dewey, 1975); 2) the emergence of an atmosphere and hydrosphere similar in characteristics to those of the present day, with attendant effects on the nature of sedimentation. Although most workers (see Memoir Geological Society of America: 161, 1983) agree that modern-style plate tectonics began by about 1000-800 Ma, the nature and style of early Proterozoic tectonics continues to be a controversial topic. Some workers applied plate tectonic interpretations to early Proterozoic terrains (Windley, 1977, 1983; Dewey & Windley, 1981; Anderson & Burke, 1983), whilst others argued for the development of ensialic orogenic belts during the early Proterozoic, unrelated to the growth and subduction of large ocean basins (Burke, 1980; Baer, 1983; Kroner, 1977a & b, 1981, 1983; Rutland, 1981; Plumb, 1979 and Plumb et al., 1981).

Detailed studies of lithologies, structures and structural evolution, mountain building mechanisms, thermal gradients and metamorphism in early Proterozoic metamorphic terranes are essential to solve these problems. The Arunta Inlier in central Australia is considered to represent one of the best study areas for this task. The conclusion of this study tends to favour ensialic orogenic tectonics.

1.2 Regional geological setting

The area studied in this thesis is situated some 100-150 km NE of Alice Springs in central Australia between 23°00' to 23°30'S and 134°40' to 135°20'E. It runs from Mount Riddoch in the NW via Mount Campbell , Mount Mabel and Mount Mary to Leaky Bore in the SE (see Maps 1 & 2) and covers an area approximately 2500 km^2 in size. This area will be referred to in this thesis as the Harts Range area, but in fact includes the Harts Range plus some adjacent areas.

The Harts Range area lies within the eastern part of the Arunta Inlier (Complex) which is an Early Proterozoic (the definition of capitallized Early, Middle and Late Proterozoic see Plumb & James, 1986) crystalline complex surrounded by Late Proterozoic to Palaeozoic sedimentary cover sequences (see TECTONIC MAP OF AUSTRALIA AND NEW GUINEA, 1971). The subdivisions of Early, Middle and Late Proterozoic in this thesis are in accordance with the Proterozoic I (2500-1600 Ma), Proterozoic II (1600-900 Ma) and Proterozoic III (900-570 Ma) of Plumb & James (1986). The Arunta Inlier was called the Arunta Block prior to Plumb et al. (1981). In this thesis the new name Arunta Inlier will be used even where the previous work is referred to. The Arunta Inlier occupies an area of about 200,000 km^2 along the southern edge of the North Australia Craton (Plumb et al. 1979). Many studies have been carried out within the Arunta Inlier before this study (e.g. Joklik, 1955; Yar Khan, 1972; Marjoribanks & Black, 1974; Marjoribanks, 1975 & 1976; Black, 1975; Shaw & Stewart, 1975 a & b; Shaw, 1979; Shaw, et al., 1979; Allen, 1979; Allen & Black, 1979; Black, et al., 1980; Shaw, et al., 1982. Prior to the initiation of this study systematic papers synthesizing the geology of the Arunta Inlier were published by Plumb (1979a & b), Plumb et al. (1981)

and Rutland (1981). During the course of this study the following synthesis papers have been published: Black et al. (1983), Black and McCulloch (1984), Shaw and Langworthy (1984), Shaw et al. (1984), Shaw & Freeman (1985), Stewart et al. (1984), Teyssier (1985) and Warren (1982, 1983a & 1983b).

According to Plumb et al.(1981), the Arunta Inlier is a typical example of an Early Proterozoic intracontinental polymetamorphic mobile belt. Within the Arunta Inlier, there are three metamorphosed and deformed sequences, which are defined as Division 1, 2 and 3 by Shaw & Stewart (1975a). These sequences are supposedly separated by unconformities and were intruded by granite throughout the Early to Middle Proterozoic. The metamorphic and igneous rocks were then overlain by the Late Proterozoic to Palaeozoic Central Australian Platform Cover (Stewart & Shaw, 1984).

Both Rutland (1981) and Plumb (1978) suggested that the Arunta Inlier lies astride a fundamental deep crust-mantle E-W trending megastructure. Rutland recognized the antiquity of this structure and suggested that it initially separated the essentially platformal Early Proterozoic sequences of the Gawler Province, from the "geosynclinal" sequences of the North Australian Orogenic Province. During its subsequent evolution in Middle to Late Proterozoic times, tectonic activity was largely confined to the Redbank mylonite zone, a north dipping thrust outcropping near the southern margin of the Arunta Inlier (Marjoribanks 1976, Marjoribanks and Black 1974). The Arunta Inlier suffered its last major tectonic movement during the Devono-Carboniferous Alice Springs Orogeny (e.g. Teyssier, 1985). A full list of the previous works in central Australia is presented in Shaw et al. (1979).

1.3 Previous geological work in the Harts Range area

Apart from mineral prospecting, little regional geological work had been carried out before that of Joklik (1955), who was the first to investigate the regional geology and mica fields of the Harts Range area between 1949 to 1953. He compiled the first geological map of the Harts Range which covered an area of 14,000 square miles. Joklik (1955) established a "stratigraphic" sequence for the metamorphic basement in the Harts Range area. In fact, as pointed out in this thesis, Joklik's "stratigraphy" represents a sequence of structural superposition and lacks any real evidence for true stratigraphic order. Joklik's sequence will be further discussed in section 1.7. However the initial systematic geological mapping of the Alice Springs to Harts Range area of the Arunta Inlier was carried out by the Australian Bureau of Mineral Resouces (BMR) between 1970 - 1974 and was reported by Shaw et al. (1979, 1982).

The formal maps of the Australia Geological Series (1:250 000 and 1:100 000) of the Harts Range area and their commentaries were published sequentially during the course of this study (Shaw, et al., 1983, 1984, 1985; Shaw & Langworthy, 1984). Many staff members and students of the University of Adelaide have studied various subjects and subareas within the Harts Range area since 1982, i.e. Bowyer (1982), Ding et al. (1983), Buick (1983, 1985), Martin (1983), Rankin (1983), James et al. (1983, 1984, 1985, 1987), Goscombe (1984), Aoukar (1985), Stewart (1985), Sullivan (1985), Ding and James (1985, Appendix III; in press, Appendix VI), Sivell, et al. (1985), Sivell (1986), McDonald (1986), Nykiel (1986), Parker (1986), Lawrence et al.(1987), Mortimer et al. (1987), James & Ding (in press, Appendix IV), Cooper et al (in press), Oliver et al. (1986; in press, Appendix V), Foden et

al. (in press), Sivell & Foden (in press), Sivell (in press). Their work will be cited or discussed in later relevant chapters.

1.4 Original aims of the thesis

No detailed regional structural geology had been carried out in the area before this study and the previous works were mainly concerned with mineralogy, petrology, geochronology and stratigraphy. Only very brief and primitive descriptions of the structural evolution of the whole Arunta Inlier were presented in earlier tectonic syntheses (Plumb, 1979, Plumb, et al. 1981 and Rutland, 1981). Three fold generations were described as having formed during the Strangways Tectonic Event (Plumb, et al.,1981), but they did not clarify whether the Division 1 and Division 2, both of which occur in the Harts Range area, experienced different deformational and tectonic histories or evolved together, although an unconformity was suggested between the two Divisions.

The aims of this study are to elucidate the structural and tectonic evolution of the Harts Range area, within which the specific tasks are:

1) To produce and prepare detailed geological maps of the Harts Range area.
2) To describe the geological structures in the area.
3) To interpret the deformational history of the area.
4) To study briefly the metamorphism and metamorphic evolution.
5) To discuss the tectonic evolution of the area and compare it with other areas of similar age and tectonic style, in order to erect a possible model for the Proterozoic Tectonic evolution of this region.

1.5 Methods of study

(1) The results presented in this thesis are based, to a large extent, on detailed geological mapping on a regional scale together with precise observation of structures in the field. The general structural concepts and terminology used in this thesis are referred to well known text books, e.g. Billings, 1972; Hills, 1972; Dennis, 1972; Ramsay, 1967; Hobbs et al., 1976). No suitable contoured topographic maps were available before the study. Instead of topographic maps, therefore, colour aerial photographs (airphotos), (about 1:25,000 scale), were used as the base for the field mapping. The major tectonic and lithologic boundaries in the area were observed and mapped during field traverses at many locations. Many boundaries have been observed along their strikes for certain distance. However, most of the boundaries between the observed locations were drawn largely on the basis of stereoscopic airphoto interpretation. A careful preinterpretation of the airphotos greatly benefited the field work, and a reinterpretation of the airphotos after the field trips was even more important in order to complete the detailed geological maps.

All the geological maps in this thesis were compiled using the original airphotos as a basemap without geodetic control or precise topographic correction. The names of localities, the creek systems and the marks of latitude and longitude of these maps were approximately based on the Australia National Topographic Map Series, 1:250,000 (Sheet SF 53-14, Alice Springs and Sheet SF 53-15, Illogwa Creek).

(2) The structural analytical techniques of Turner and Weiss (1963), Ramsay (1967) and Hobbs et al. (1976) were used to determine the sequential evolution of the different fold generations, to interpret the very complex fold interference patterns developed

between these different fold generations, and to demonstrate the relationships between folds, thrusts and shear zones.

(3) The study of lithologies and their microstructures provided important information on the understanding of the metamorphic history, the development of fabrics and the microstructural deformation of the area. The petrological nomenclature used in this thesis are mainly referred to Best (1982), Turner (1981), Miyashiro (1973), Williams, et al. (1982) and Spry (1969).

(4) Electron microprobe techniques have been extensively used in the study of mineralogy and the estimation of the temperatures and pressures which operated during the metamorphism and deformation. The chemical composition of minerals are compared with Deer, et al. (1966).

(5) Because the primary aims of this thesis are to elucidate the structural and tectonic evolution of the Harts Range area, the mineralogy and petrology of this area are only briefly described in the text. Further details of the numerous lithologies are presented in Appendix I for the interested reader. The results of thermobarometric analyses are presented in the text, but the details of the analysed minerals are documented representatively in Appendix II.

1.6 Logistics

Altogether, in five trips, 29 weeks of field work were carried out during three field seasons (1982 - 1984). Sixteen field camps were set down progressively to cover the whole area in addition to the Ruby Mine Base Camp (Map 1). Each camp allowed coverage of an area with a diameter of 5-10 km. Because of the rough nature of the terrain (rugged hill and scrub) vehicles were used mainly for moving camp, thus usually long distance walking

was necessary for access to many of the interesting and important outcrops and for coverage of the whole area.

No residents were living within the mapped area. Water was not readily available and was obtained from nearby dams or bores. Creeks are normally dry in the winter season. Food was purchased from Alice Springs.

1.7 Stratotectonic subdivision of the Harts Range area

It is not considered the major task of this thesis to attempt to establish a complete stratigraphy for the Harts Range area, which may never be possible due to the complex tectono-metamorphic history. Thus the stratigraphic relationships of the Harts Range area are only briefly summarized here. For more detailed work the reader is refered to other workers (Stewart et al, 1984; Shaw et al., 1979, Shaw & Langworthy, 1984). The term "stratotectonic" of Rutland (1976) is used here to emphasise the difference from classical chronological depositional stratigraphy which can be employed in less complex terranes.

1.7.1 Review of previous work

Joklik (1955) first tried to establish a preliminary stratigraphic sequence for the high grade metamorphic rocks of this area, which he named the Harts Range Group and considered Archaean in age. The "Harts Range Group" was overlain unconformably by a sequence of sedimentary rocks which he named the Lower Proterozoic White Range Quartzite and Upper Proterozoic Heavitree Quartzite respectively. The stratigraphic subdivisions of the "Harts Range Group" were defined by Joklik as shown in Table 1-1.

This sequence was based on his conclusion that the Harts

Range area was an anticlinorium. Neither younging criteria nor structural relationships were provided by Joklik to suport his proposition which also was not supported by later workers, e.g. Shaw et al.(1979, 1982, 1984b) and Stewart et al. (1984).

Joklik's subdivisions of the Harts Range area were later modified by the BMR workers (Shaw & Stewart, 1975a; Shaw et al. 1979, 1982; Stewart et al., 1984) as shown in Table 1-2. One of the principal contributions of the BMR workers has been the subdivision of the Arunta Inlier into three broad stratigraphic groups called Division 1, 2 and 3, Division 1 being the oldest and Division 3 being the youngest. Most importantly the Cadney Gneiss was moved from being the top-most unit of Joklik's Harts Range Group into the Division 1 Strangways Metamorphic Complex (Stewart et al.,1984) which includes the Bungitina Metamorphics. In contrast to Joklik's idea of an anticlinorium, the BMR subdivisions were based on the idea of a simple, northerly dipping homocline, with the oldest rocks exposed in the southern most outcrops.

Table 1-1 JOKLIK'S STRATIGRAPHIC SUBDIVISIONS OF THE HARTS RANGE AREA

	SEDIMENTARY	IGNEOUS
Archaeozoic Harts Range Group	Cadney Gneiss	
	Brady Gneiss	
	Irindina Gneiss	
		Riddoch Amphibolite
		Granitized Irindina Gneiss
	Bruna Gneiss	
		Entia Gneiss

The stratotectonic and morphotectonic history of the Arunta

Inlier was summarized by Shaw et al. (1984 a) as: (1) the sequential deposition of Divisions 1, 2 & 3; (2) polyphase deformation including three generations of folds (F_1, F_2 & F_3) affecting all three Divisions; (3) prograde metamorphism with peak temperature attained after the third folding event; and (4) post-tectonic plutonism followed by later mild deformation. F_1 folds of Shaw et al. (1984) were described from within both their Division 1 and Division 2 sequences in the Harts Range area and thus they considered the orogenic evolution of Division 1 and Division 2 to be identical.

Table 1-2 BMR'S STRATIGRAPHIC SUBDIVISIONS OF THE HARTS RANGE AREA

		Brady Gneiss
		Irindina Gneiss
Division 2		Riddoch Amphibolite Member
Harts Range		Naringa Calcareous Member (western area) or Stanovos Member (eastern area)
Group		Bruna Gneiss
		Entia Gneiss
		inferred unconformity
Division 1		Cadney Metamorphics
Strangways		
Metamorphic		Bungitina Metamorphics
Complex		

1.7.2 Revised stratotectonic subdivision and thesis layout

A considerable revision of the previous subdivision and nomenclature has been made since 1983 based on the work of this study (Ding & James, 1985, Appendix III). The metamorphic rocks in the Harts Range area have been subdivided on the basis of their structural and tectonic evolution into three distinct chronologi-

cal groupings: viz. the Basement, the Cover and the Bruna Gneiss. The Basement is considered as an earlier metamorphic complex of predominantly acidic to intermediate gneisses, and includes parts of the Cadney and Bungitina Metamorphics of Stewart et al.(1984). The Cover is a supracrustal sequence of metamorphosed sedimentary and volcanic rocks, and includes most of the Harts Range Group of Stewart et al.(1984). Finally the Bruna Gneiss, which was included in the Harts Range group is now recognised as a discrete, originally intrusive, mylonitized, megacrystic granitic gneiss which forms a major sheet separating Basement from Cover over most of the eastern Harts Range area (Appendix III).

The stratotectonic complexes of the Harts Range area are further proposed as belonging to two separate orogenic belts (James and Ding, in press; Appendix IV): the previous general term "Basement" is now formally named as (part of) the STRANGWAYS OROGENIC BELT (SOB), which was formed during the STRANGWAYS OROGENY (SO). The SOB is described in detail in Chapters 2, 3, and 4. The "Cover", is now referred to as the HARTS RANGE OROGENIC BELT (HOB) formed during the separate and later HARTS RANGE OROGENY (HRO). The HOB is described in detail in Chapters 5, 6, & 7. The relationship between the two orogenic belts is discussed in Chapter 8.

Four individual tectonic domains are recognized as belonging to the SOB in the Harts Range area and are subdivided as such on the legend of Map 2, which can thus be compared with Table 1-1 and 1-2. These domains include the Entia Dome (Shaw, et al., 1982), the Oonagalabi Tongue (Appendix III), the Florence/Leaky Shear Zone (Appendix IV) and the Hale River region (see Chapter 2). The rocks in these separate domains are named the Entia gneiss complex, the Oonagalabi gneiss complex, the Florence/Leaky meta-

morphic complex and the Hale River complex, respectively. These domains are spatially separated by major tectonic boundaries and/or other lithological units, and they are all inferred to belong to the same orogenic cycle. The Entia Dome and the Hale River region are considered to have been comparatively stable or weakly reactivated during the Harts Range Orogeny and will be discussed in Chapter 2. The Oonagalabi Tongue and the Florence/Leaky Shear Zone were intensely reactivated during the Harts Range Orogeny and are interpreted as parts of a crustal detachment zone, which is named the Harts Range Detachment Zone. The Oonagalabi Tongue and the Florence/Leaky Shear Zone will be described separately in Chapters 3 and 4 and will be further discussed in Chapter 8.

The rocks in the HOB as a whole are referred to as the Harts Range Supracrustal Cover (HRSC). The HOB in the Harts Range area is considered a single domain and the rocks within this domain are referred to as the "Irindina Supracrustal Assemblage" (ISA), as defined by Ding & James (1985, Appendex III). The ISA represents a metamorphosed sedimentary sequence plus the Harts Range metaigneous complex which includes a thick sequence of layered amphibolite and some other mafic and ultramafic intrusive bodies. The lithologies of the ISA are described in detail in Chapter 5.

The Brady Gneiss of Joklik (1955) and Stewart et al. (1984) is seen only at the northern margin of the study area. It has not been studied in detail and will thus not be further discussed.

The Bruna gneiss was previously considered to be a stratigraphic unit and was assigned to the Harts Range Group by Joklik (1955) and later to the Division 2 (the Harts Range Group) by Shaw et al. (1982, 1984). It is now redefined as a deformed and metamorphosed intrusive granitic complex. The Bruna Gneiss includes a major sill-like sheet within the Florence/Leaky Shear Zone and a

few individual smaller intrusive bodies in the ISA and is described in Chapter 5.

The quartzite cropping out at the southeastern margin of the Harts Range area was assigned to the Heavitree Quartzite Formation of the Late Proterozoic platform cover sequence by Shaw et al. (1982, 1984b), an assignment which is adopted in this thesis. The lithology and structures of the Late Proterozoic platform cover will not be described in this thesis.

The stratotectonic subdivisions in this thesis are summarized in Table 1-3, and are described in detail in related Chapters.

Table 1-3 MAJOR STRATOTECTONIC SUBDIVISIONS OF THE HARTS RANGE AREA

Late Proterozoic Platform cover	Adelaidean Heavitree Quartzite Formation
	regional unconformity
	Bruna gneiss (metamorphosed granite intruded into both the HOB & SOB)
Early Proterozoic Harts Range Orogeny	Irindina supracrustal assemblage (includes metasedimentary sequence and the Harts Range meta-igneous complex)
	tectonic boundary, sheared unconformity
Early Proterozoic Strangways Orogeny	Oonagalabi gneiss complex
	Entia gneiss complex
	Florence mylonite complex
	Hale River complex

(Distribution of these mapping units are shown on Map 2.)

Fig. 1-1 is a simplified regional geological map of the Harts Range area (Map 2). A refined tectonothermal history of this area is presented as a time-space diagram in Fig. 1-2 which represents a significantly more sophisticated and detailed

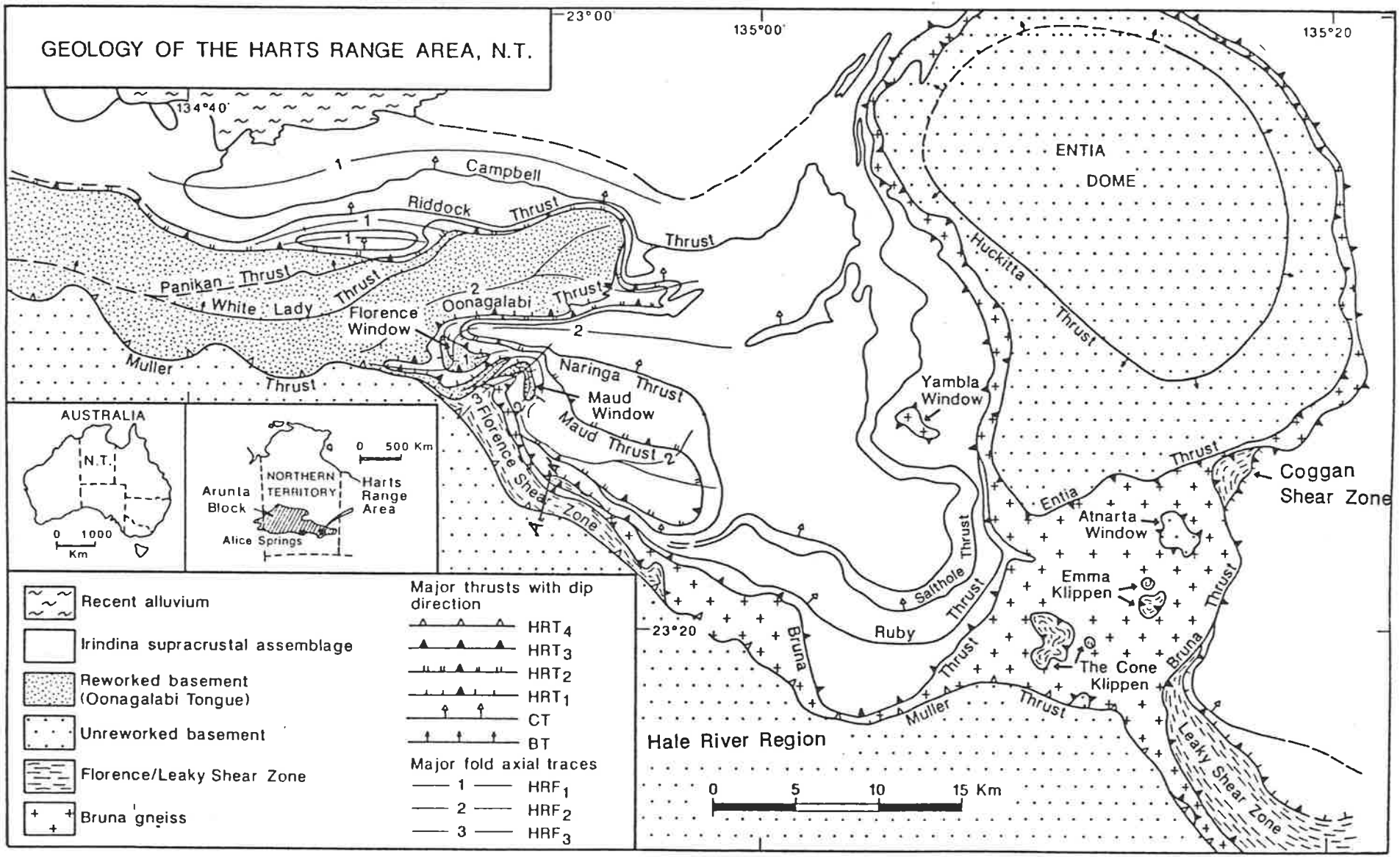

GEOLOGY OF THE HARTS RANGE AREA, N.T.
23°00
135°00
135°20
134°40
23°20
ENTIA
DOME
Campbell
Riddock Thrust
Panikan Thrust
White Lady Thrust
Florence Window
Oonagalabi Thrust
Muller Thrust
Naringa Thrust
Maud Window
Maud Thrust
Florence Shear Zone
Huckitta Thrust
Yambla Window
Entia Thrust
Coggan Shear Zone
Atnarta Window
Emma Klippen
The Cone Klippen
Salthole Thrust
Ruby
Bruna Thrust
Muller Thrust
Leaky Shear Zone
Hale River Region
0 5 10 15 Km
AUSTRALIA
N.T.
0 1000 Km
0 500 Km
NORTHERN TERRITORY
Arunta Block
Harts Range Area
Alice Springs
Recent alluvium
Irindina supracrustal assemblage
Reworked basement (Oonagalabi Tongue)
Unreworked basement
Florence/Leaky Shear Zone
Bruna gneiss
Major thrusts with dip direction
HRT4
HRT3
HRT2
HRT1
CT
BT
Major fold axial traces
1 HRF1
2 HRF2
3 HRF3

Fig. 1–1

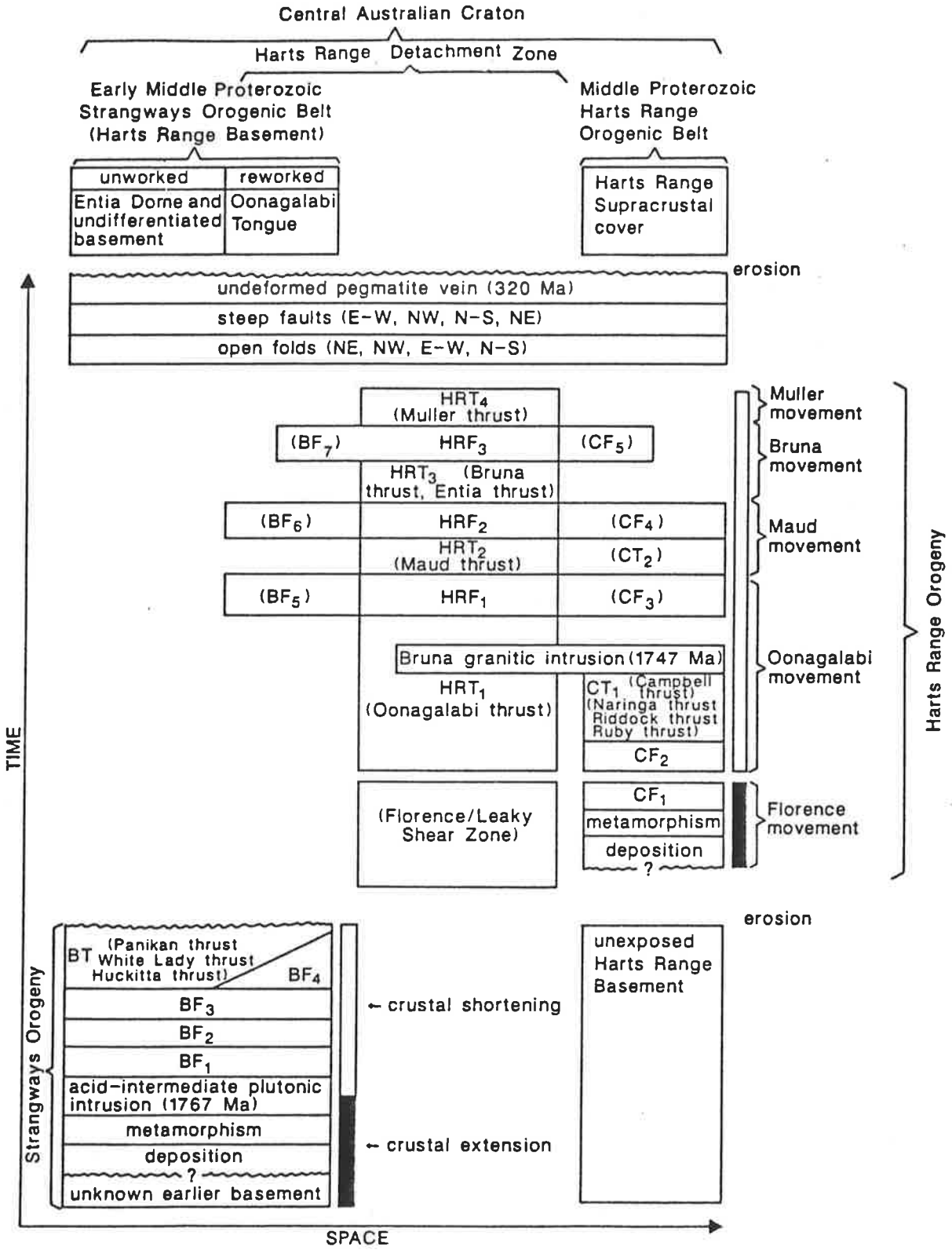

Central Australian Craton
Harts Range Detachment Zone
Early Middle Proterozoic Strangways Orogenic Belt (Harts Range Basement)
Middle Proterozoic Harts Range Orogenic Belt
unworked
reworked
Entia Dome and undifferentiated basement
Oonagalabi Tongue
Harts Range Supracrustal cover
erosion
undeformed pegmatite vein (320 Ma)
steep faults (E-W, NW, N-S, NE)
open folds (NE, NW, E-W, N-S)
HRT4 (Muller thrust)
(BF7)
HRF3
(CF5)
HRT3 (Bruna thrust, Entia thrust)
(BF6)
HRF2
(CF4)
HRT2 (Maud thrust)
(CT2)
(BF5)
HRF1
(CF3)
Bruna granitic intrusion (1747 Ma)
HRT1 (Oonagalabi thrust)
CT1 (Campbell thrust) (Naringa thrust Riddock thrust Ruby thrust)
CF2
(Florence/Leaky Shear Zone)
CF1
metamorphism
deposition
?
Muller movement
Bruna movement
Maud movement
Oonagalabi movement
Florence movement
Harts Range Orogeny
TIME
erosion
BT (Panikan thrust White Lady thrust Huckitta thrust)
BF4
BF3
BF2
BF1
acid-intermediate plutonic intrusion (1767 Ma)
metamorphism
deposition
?
unknown earlier basement
← crustal shortening
← crustal extension
unexposed Harts Range Basement
Strangways Orogeny
SPACE

Fig. 1-2

version of Table II from Ding and James, 1985 (Appendix III) with which it may be compared. The nomanclature for the tectonic events to have affected the Harts Range area introduced in Figs. 1-1 & 1-2 will be described and defined in detail in related chapters and fully discussed in Chapter 8. (The Figs. 1-1 & 1-2 are, however, also the principal scheme describing the structures and tectonic evolutionary sequence for the area and thus need to be referred to frequently throughout the text, especially in the concluding chapter. Thus extra copies of these figures are included as loose leaf separate inserts with Maps, so that the reader may more easily refer to them throughout the thesis).

1.8 Summary of the main achievements of this study

The principal findings presented in this thesis are briefly summarized below:

1) Extraordinarily complex structures within the high grade metamorphic rocks in the Harts Range area have been successfully mapped in detail on the regional scale.

2) The major parts of the Divisions 1 and 2 of Stewart et al. (1984) have been recognized as belonging to two separate sequential orogenic belts, termed the Strangways Orogenic Belt (older) and the Harts Range Orogenic Belt (younger). The two orogenic belts experienced very different structural and tectonic histories during the Early Proterozoic. The Strangways Orogeny was completed before the initiation of the intracontinental Harts Range Orogenic Belt which developed in a direction nearly perpendicular to the trend of the Strangways Orogenic Belt.

3) A spectacularly thick and high grade, mylonite zone, the Florence/Leaky Shear Zone (F/LSZ) has been recognized and mapped

through out the whole Harts Range area. The F/LSZ and the Oonagalabi Tongue are recognized as parts of a deep crustal detachment zone, named the Harts Range Detachment Zone (HRDZ) (see Fig. 1-3) which underwent both large scale extensional and contractional displacements and controlled the development of the younger Harts Range Orogeny.

4) A local stratigraphic sequence for the Harts Range Orogenic Belt has been proposed on the basis of the structural analysis and way-up criteria found in the layered mafic-ultramafic igneous rocks.

5) A major megacrystic gneiss, the Bruna Gneiss, has been recognized as a metamorphosed syntectonic intrusive granitic body.

6) The gneiss complex within the Entia Dome has been reinterpreted as a part of the Strangways Orogenic Belt rather than as the basal unit of the Division 2 Harts Range Group of Stewart et al. (1984). This interpretation has been substantiated by subsequent geochronological data of Cooper et al. (in press).

7) A general tectonic model (Caterpillar Tectonics) has been proposed and developed to explain the evolution and repeated cycles of extension-collision tectonism observed in the Harts Range area (James & Ding, in press, appendix IV). This model has been applied to explain the dramatic change in trend from that of the Strangways Orogenic Belt to that of the Harts Range Orogenic Belt in the Harts Range area. The implications of this model for the evolution of the remainder of the Arunta Inlier, the Northern Australia Craton and other Proterozoic metamorphic terranes are considered.

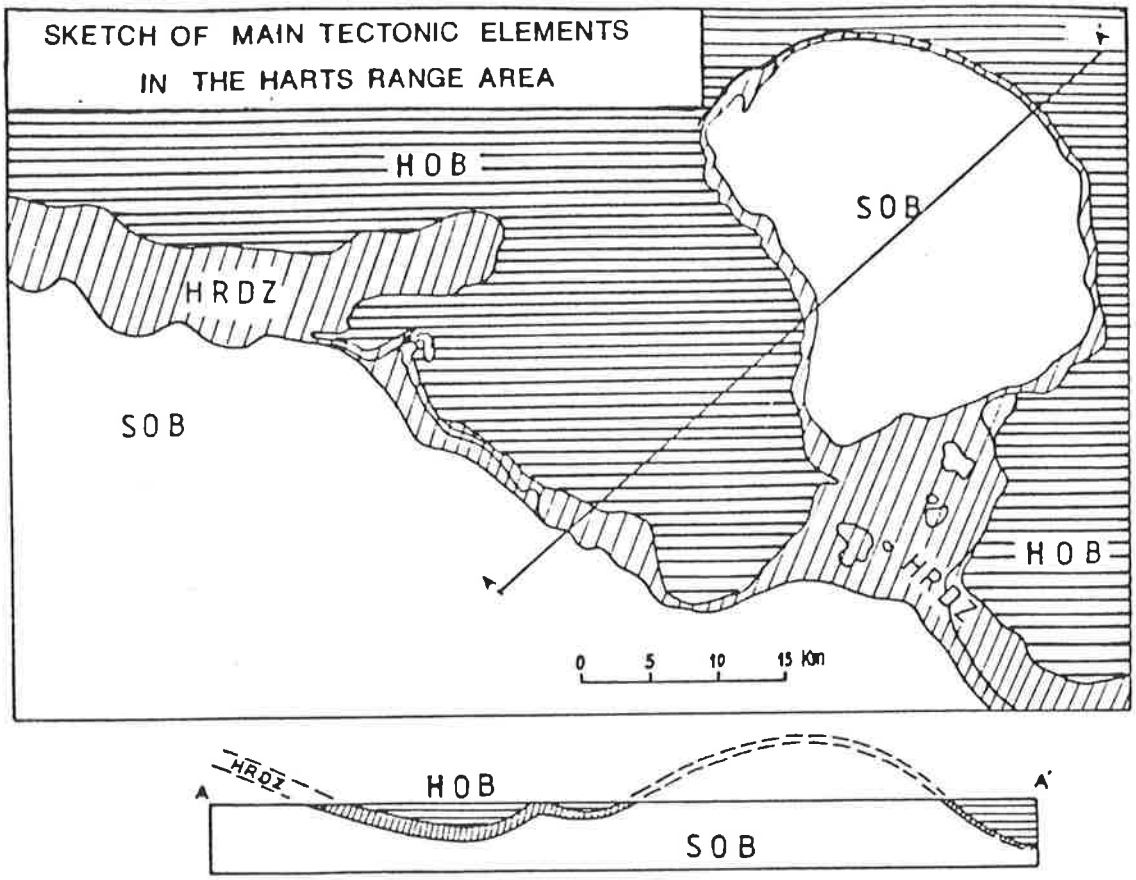

SKETCH OF MAIN TECTONIC ELEMENTS
IN THE HARTS RANGE AREA
HOB
SOB
HRDZ
SOB
HRDZ
HOB
0 5 10 15 Km
HRDZ
HOB
A
A'
SOB

Fig. 1-3

PART ONE

STRANGWAYS OROGENIC BELT

CHAPTER 2 THE HALE RIVER REGION AND THE ENTIA DOME

2.1. Introduction

The Hale River Region is the extensive SOB area south of the Muller Thrust (see Map 2 & Fig. 2-1). Study of the Hale River Region was limited to reconnaissance traverses mainly near the Muller Thrust and the Illogwa Shear Zone. A sketch map of the area (Fig. 2-1) was compiled mainly on the basis of airphoto interpretation together with some modification of the Australia Geological Series (1:250 000, Alice Springs and Illogwa Creek sheets; 1:100 000, Arltunga-Harts Range Region sheet, B.M.R.). In addition, three smaller areas (e.g. Figs. 2-2, 2-3 & 2-4) have been mapped to demonstrate the characteristic outcrop style and detailed structural relationship of this area. The Hale River Region is tectonically divided into three subareas: 1) the Arltunga subarea south of the Illogwa Shear Zone (Fig. 2-1); 2) the Claraville subarea (west of Paradise Well and to the north of the Illogwa Shear Zone; 3) the Illogwa Creek subarea (east of Paradise Well and to the north of the Illogwa Shear Zone). The Arltunga subarea is partially covered by a Late Proterozoic sedimentary sequence, whereas the other two subareas are fully excavated. The inferred boundary between the Claraville and the Illogwa Creek subareas has not been precisely defined. There are three possibilities for this boundary: 1) a single line of a metamorphic isograd; 2) a transitional zone of intercalated granulite and amphibolite facies rocks; 3) a tectonic boundary.

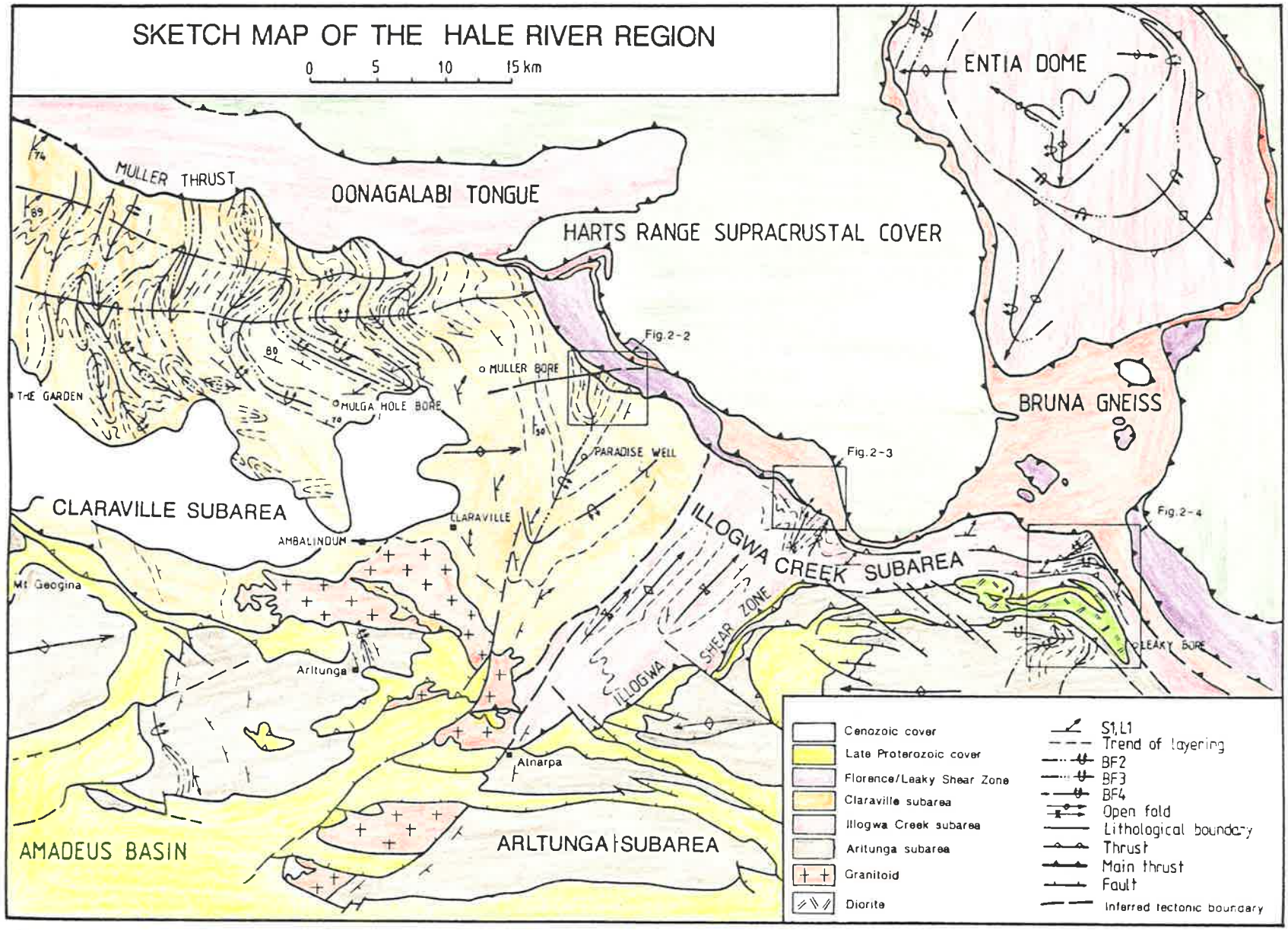

SKETCH MAP OF THE HALE RIVER REGION
0 5 10 15 km
ENTIA DOME
MULLER THRUST
OONAGALABI TONGUE
HARTS RANGE SUPRACRUSTAL COVER
Fig.2-2
MULLER BORE
THE GARDEN
MULGA HOLE BORE
PARADISE WELL
Fig.2-3
BRUNA GNEISS
Fig.2-4
CLARAVILLE SUBAREA
CLARAVILLE
AMBALINDUM
ILLOGWA CREEK SUBAREA
Mt Georgina
Arltunga
ILLOGWA SHEAR ZONE
LEAKY BORE
Alnarpa
AMADEUS BASIN
ARLTUNGA SUBAREA
Cenozoic cover
Late Proterozoic cover
Florence/Leaky Shear Zone
Claraville subarea
Illogwa Creek subarea
Arltunga subarea
Granitoid
Diorite
S1, L1
Trend of layering
BF2
BF3
BF4
Open fold
Lithological boundary
Thrust
Main thrust
Fault
Inferred tectonic boundary

Fig. 2-1

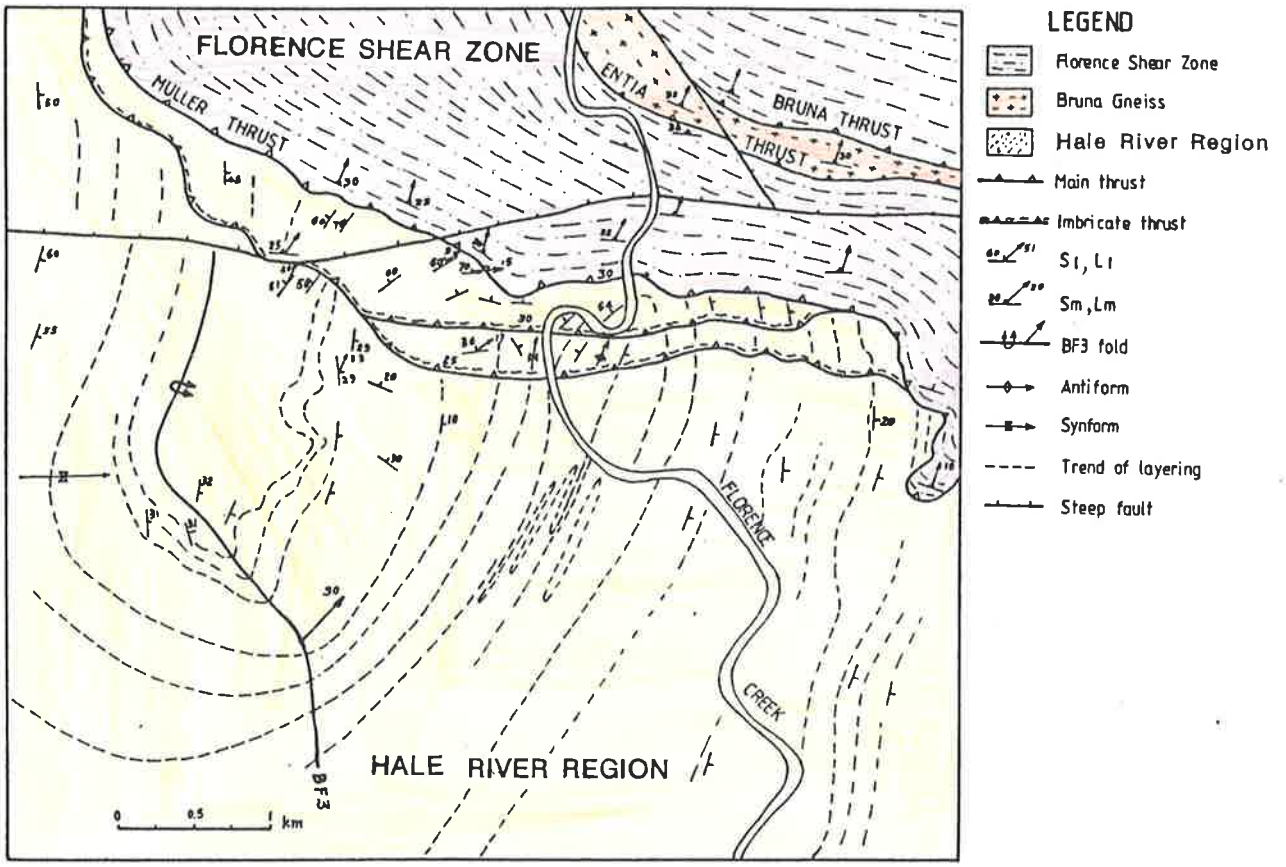

FLORENCE SHEAR ZONE
MULLER THRUST
ENTIA
BRUNA THRUST
THRUST
FLORENCE
CREEK
HALE RIVER REGION
BF3
0 0.5 1 km
LEGEND
Florence Shear Zone
Bruna Gneiss
Hale River Region
Main thrust
Imbricate thrust
S1, L1
Sm, Lm
BF3 fold
Antiform
Synform
Trend of layering
Steep fault

Fig.2-2

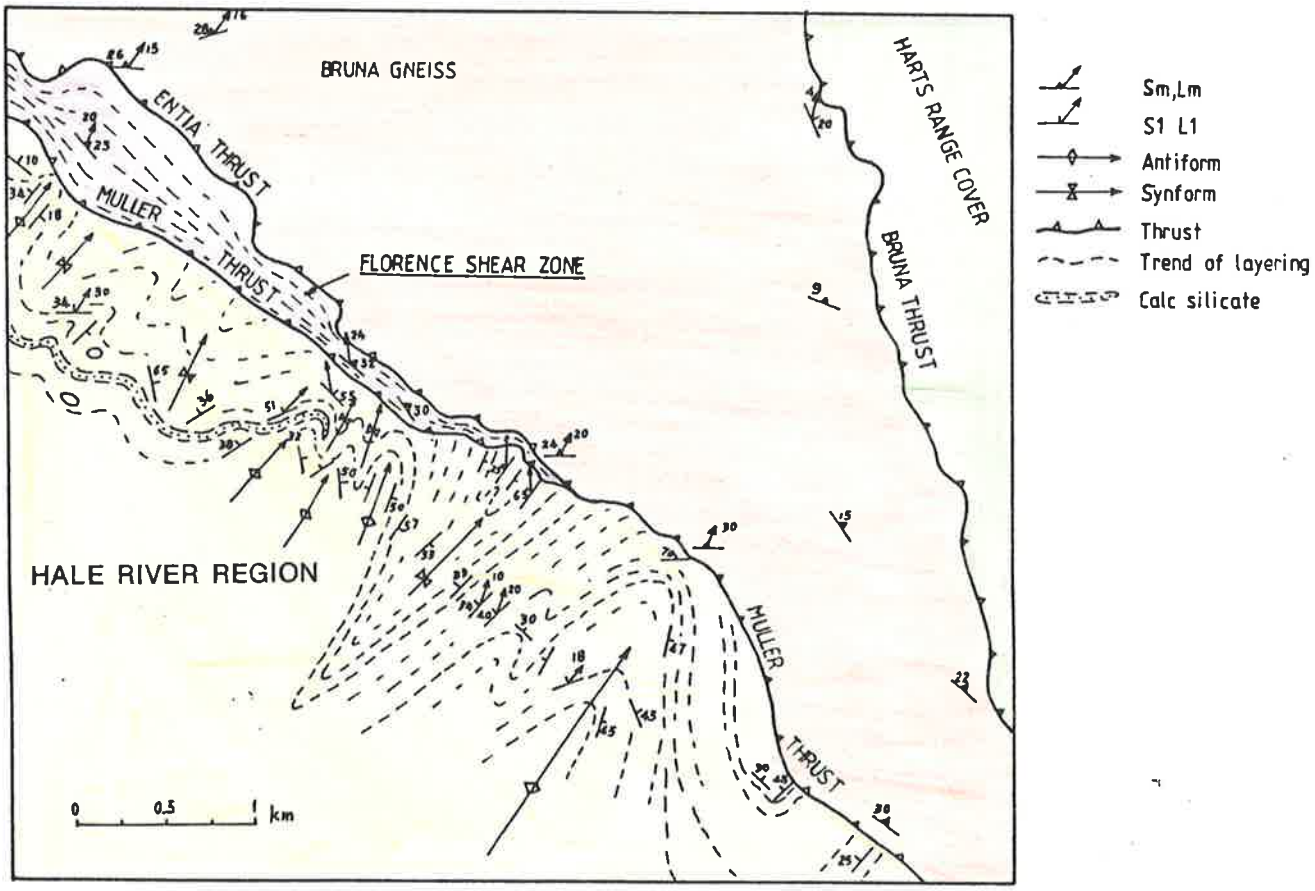

BRUNA GNEISS
ENTIA THRUST
MULLER THRUST
FLORENCE SHEAR ZONE
HALE RIVER REGION
HARTS RANGE COVER
BRUNA THRUST
MULLER THRUST
0 0.5 1 km
Sm,Lm
S1 L1
Antiform
Synform
Thrust
Trend of layering
Calc silicate

Fig. 2-3

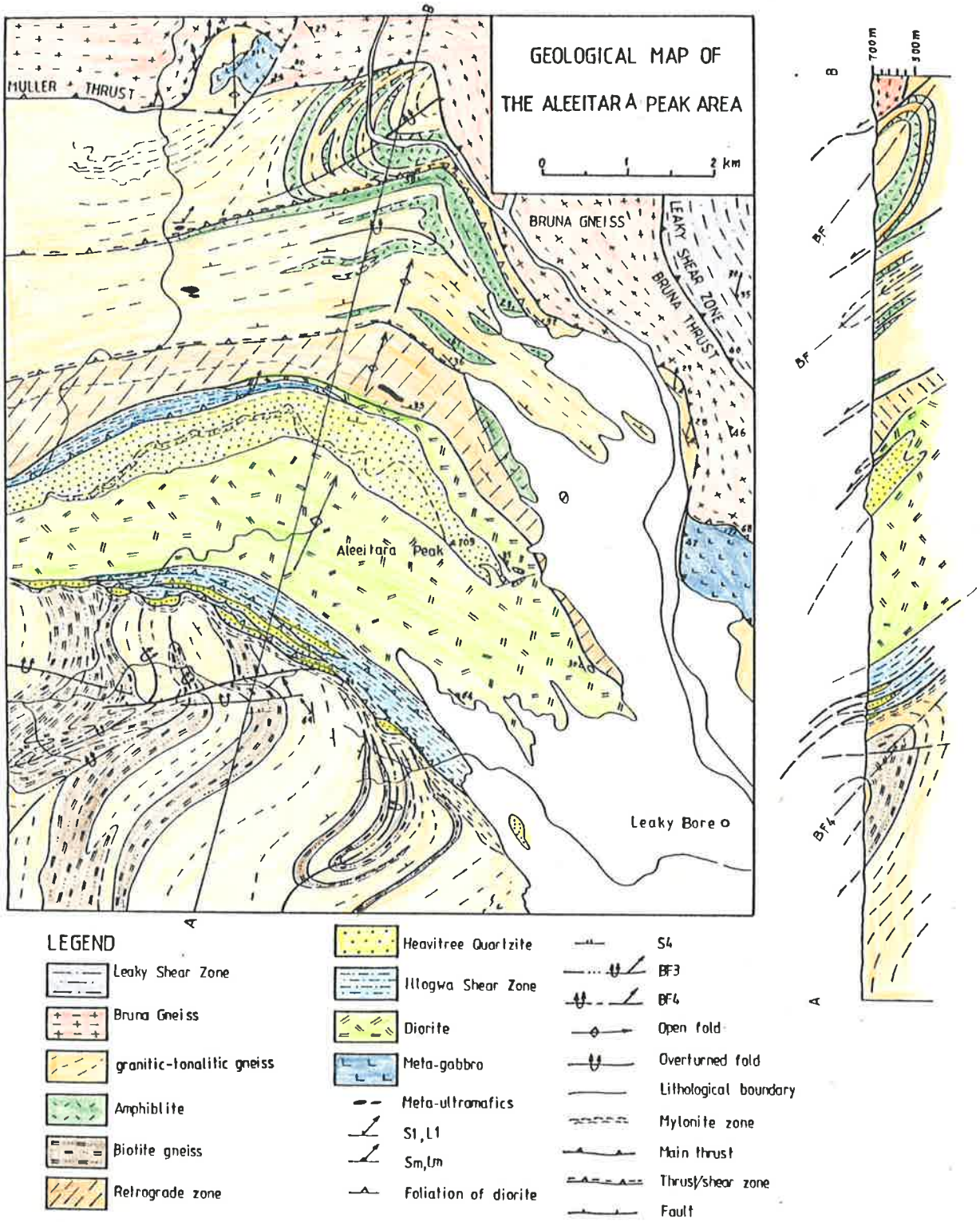

GEOLOGICAL MAP OF
THE ALEEITARA PEAK AREA
0 1 2 km
MULLER THRUST
BRUNA GNEISS
LEAKY SHEAR ZONE
BRUNA THRUST
Aleeitara Peak
Leaky Bore
B
A
700m
500m
BF
BF
BF4
LEGEND
Leaky Shear Zone
Bruna Gneiss
granitic-tonalitic gneiss
Amphiblite
Biotite gneiss
Retrograde zone
Heavitree Quartzite
Illogwa Shear Zone
Diorite
Meta-gabbro
Meta-ultramafics
S1, L1
Sm, Lm
Foliation of diorite
S4
BF3
BF4
Open fold
Overturned fold
Lithological boundary
Mylonite zone
Main thrust
Thrust/shear zone
Fault

Fig.2-4

The Entia Dome, first named by Joklik (1955), is situated in the NE quarter of the Harts Range area (see Maps 2 & 4, and Fig. 1-1) and occupies an area of about 750 km^2. The Entia Dome is completely surrounded by the Bruna gneiss (see chapter 5). Most of the Entia Dome is reasonably well exposed, though its central and northern parts are covered by recent creek deposits.

The stratotectonic position of the metamorphic rocks in the Entia Dome has been reviewed in Chapter 1. The metamorphic complex in the Entia Dome is named the Entia gneiss complex (Appendix III, Ding & James, 1985) which is a non formal term, as the rocks do not constitute a stratigraphic unit but rather they form a complex of acidic to intermediate metamorphosed intrusive rocks (orthogneisses) with minor mafic metamorphics and metasediments. The geology of the Entia gneiss complex has been recently studied in some detail by a number of workers (e.g. Buick, 1983 & 1985; Foden et al., in press; Martin, 1983; Aoukar, 1985; Stewart, 1985; Sullivan, 1985; Macdonald, 1986; Parker, 1986; Nykiel, 1986; Oliver, 1986; Sivell & Foden, in press; Cooper et al, in press).

The Hale River Region and the Entia Dome were relatively stable and only weakly reactivated during the Harts Range Orogeny compared with the Oonagalabi Tongue and the Florence/Leaky Shear Zone. These areas have been affected, but certainly not pervasively deformed, by later thrusting and block movement (e.g. Late Proterozoic to Palaeozoic deformation including the Alice Springs Orogeny).

2.2. Field description and basic petrology of the Hale River Region and the Entia Dome

2.2.1. Introduction

The Entia gneiss complex comprises mainly acidic to interme-

diate orthogneisses and migmatitic gneisses (80-85%), with minor mafic to ultramafic metamorphics (10-12%) and metasediments (<5%) (see map 4). There are a number of different varieties of orthogneisses, but the boundaries between them are gradational and thus are practically not mappable on a regional scale. The mafic metamorphic rocks appear as distinctive dark coloured discrete layers within the light grey or pinkish coloured orthogneiss sequence and form the main mappable geological bodies. The mafic metamorphics are mainly exposed in the marginal, structurally higher, parts of the dome. Most of the meta-ultramafic and metasedimentary bodies are too small to map on a regional scale. The different rock units are intimately interleaved to form a near recumbent gneissic pile.

Within the Hale River Region B.M.R. workers (Shaw et al., 1984) proposed a number of lithostratigraphic subdivisions, including the Cadney metamorphics, the Bungitina metamorphics and some unnamed units, which have been combined into the Hale River complex in this thesis (Map 2 & Fig. 2-1). However lithological variation is apparent within the Hale River complex. In the Claraville subarea the complex consists of mainly charnockitic gneisses (30-35%), mafic granulites (15-20%) and high grade metasediments (up to 50%), whereas in the Illogwa Creek and Arltunga subareas the complex consists mainly of amphibolite facies gneisses (80-85 %), amphibolite (15-18%) with minor metasediments, small isolated bodies of meta-ultramafic rock, metagabbro and mafic granulite. The lithologies in the Illogwa Creek subarea are very similar to those of the Entia gneiss complex. Apart from post tectonic intrusive granites and diorites, individual lithologies within the Hale River complex are not shown on the map (Fig. 2-1).

2.2.2. Metasediments

Metasediments form the oldest recognizable lithologies in the SOB. They include pelitic schists and gneisses, quartzite, marble and calc-silicate which occur as very thin (a few meters to less than one meter) layers or small lenticular bodies within the gneisses. Of all the metasedimentary bodies only one calc-silicate gneiss layer, which is exposed at the middle northern part of the Entia Dome, is sufficiently large to show on the regional map (Map 4).

(1) Pelitic rocks

Aluminous kyanite mica schist forms a minor (<1%) component of the Entia gneiss complex where it occurs as elongate pods enclosed within granitic gneisses. The schist pods are most abundant near the Huckitta Bore (Map 4) where they have been mapped in detail by Buick (1983); but occur sporadically throughout the Entia Dome (Sullivan, 1985; Stewart, 1985; Aoukar, 1985; Shaw, et al., 1982 and Oliver, 1986). The maximum dimension of individual pods varies from a few metres to hundreds of meters. These pods are distributed at distinct levels, probably where an original pelite horizon had been disrupted by plutonism, metamorphism, deformation and possibly partial anatexis (Foden et al, in press).

The pelitic schists are composed mainly of kyanite, muscovite phlogopite and biotite. In places the kyanite makes up 60% of the rocks and forms large porphyroblasts more than 100 mm X 10 mm in dimensions, but more commonly forms a coarse inequigranular granoblastic texture. (Note: the general characteristics of mineral phases, e.g. colour, pleochroism, etc., are omitted in this thesis.)

Metapelite has also been found around Paradise Well in the

Hale Rive Region as small lenticular bodies and thin interlayers within charnockitic gneiss and calc-silicate. It contains almandine-rich garnet, cordierite, plagioclase and quartz (Goscombe, 1984).

(2) Marble

Marbles are mainly found in the Claraville subarea of the Hale River Region and form layers and lenticular bodies within the calc-silicates and gneisses. The marble looks massive and has no fabric, but contains many small slab-like inclusions of distorted calc-silicate rock (Plate 2.1.A). Only very small lenticular bodies (5 X 20 metres) of marble have been found within the Entia Dome. The marble is composed of calcite (80-95%) and minor diopside and epidote.

(3) Calc-silicates

Calc-silicates in the Entia Dome and the Illogwa Creek subarea of the Hale River Region exist as thin (1 to 10 metres) layers or lenticular bodies intercalated with the orthogneisses or amphibolite layers and make up only 1-2 % of the whole rock volume. The calc-silicate rocks invariably have a very well developed millimetre-scale compositional layering, individual layers consisting of different concentrations of various minerals (e.g. Plate 2.4.E)..

The minerals are mainly epidote, diopside, plagioclase and quartz, with occasional calcite, scapolite, hornblende, tourmaline, garnet and biotite. Examples of modal compositions of several calc-silicate samples are listed in Table 2-1. (Mineral abbreviations used in this thesis are listed in Table 2-2.)

Calc-silicates in the Claraville subarea of the Hale River Region are more common and make up about 10% of the whole rock volume around Muller Bore. They form thick or thin greenish layers

FIGURE CAPTIONS OF PLATE 2.1

A: Outcrop of a massive impure marble with inclusion-like calc-silicate slabs. Location No.4124; N of Muller Bore; The Claraville subarea of the Hale River Region.

B: Calc-silicate comprising a mosaic of mainly plagioclase and clinopyroxene (ferrosalite). Small grains of grossular garnet occur along the boundaries between the coarser grains of plagioclase and clinopyroxene. Field of view: 1.7 mm X 2.2 mm; sample 4100; NW of Muller Bore.

C: Close-up of the sample shown in (B:); field of view: 0.43 mm X 0.55 mm. ppl.

D: Same view as in (C:); X polars.

E: Mafic granulite (dark) intruded by acidic charnockitic gneiss (light). A weak foliation within mafic granulite is crosscut by the charnockitic gneiss. Location No.4107; southern Florence Creek.

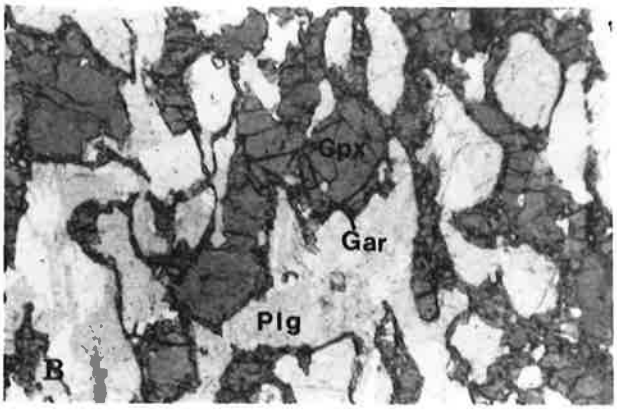
F: Typical granoblastic texture of a hornblende two-pyroxene mafic granulite. The hornblende and pyroxene have similar medium grain size and straight grain boundaries, forming triple point junctions. Sample 4107; field of view: 1.7 mm X 2.2 mm; ppl; from the outcrop in (E:).

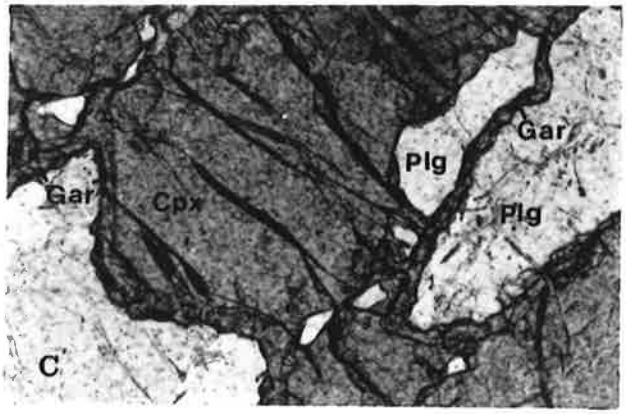
G: Hypersthene in the charnockitic gneiss. Sample 4107A; field of view: 1.7mm X 2.2mm; ppl; from the outcrop in (E:).

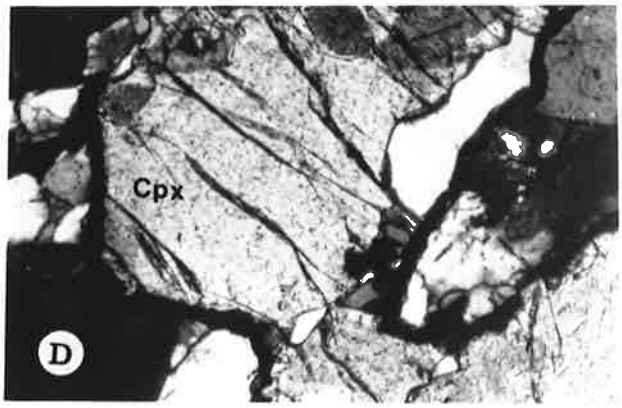
H: Hornblende occurs as reaction rims between plagioclase and mafic minerals, such as hypersthene, clinopyroxene, biotite and opaques. Sample number: 3105a; field of view: 0.43 mm X 0.55 mm; ppl; S of Mt Ruby.

Plate 2.1

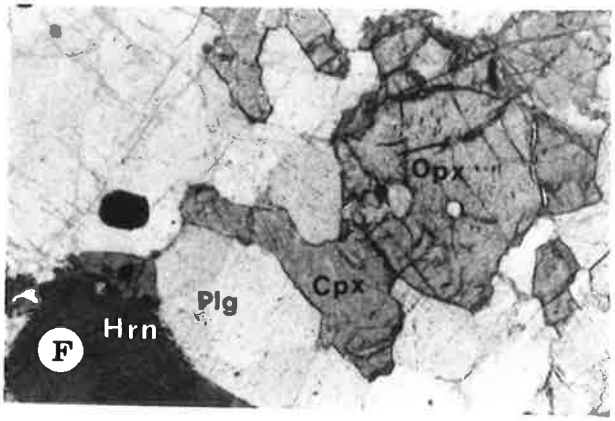

A

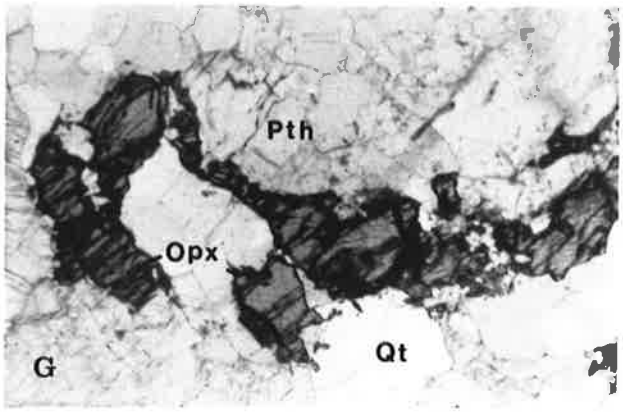

Gpx
Gar
Plg
B

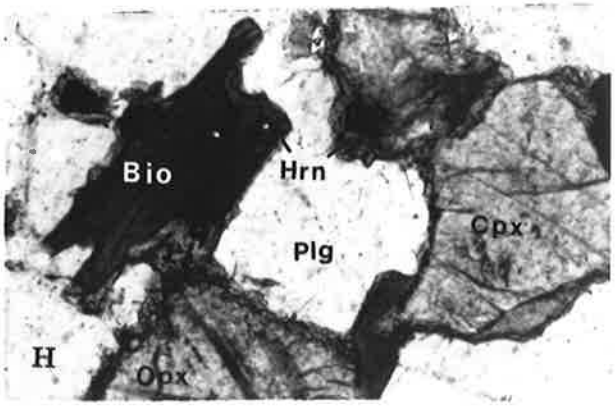

Gar
Cpx
Plg
Gar
Plg
C


Cpx
D


E


Opx
Cpx
Plg
Hrn
F


Pth
Opx
Qt
G


Bio
Hrn
Cpx
Plg
H
Opx

intercalated with minor marble, and consist of mainly diopside (25-30%), garnet (20-30%), scapolite (13-30%), quartz (12-15%), calcite (5-10%) and plagioclase (up to 20%) with or without epidote. Diopside (up to 50%) and garnet (up to 30%) are typically concentrated in darker layers, and plagioclase, quartz, calcite and scapolite in lighter layers (e.g. samples 4100). The garnet is yellow coloured and contains 61% grossular (refer to mineral analysis in appendix II). Commonly, garnet forms narrow coronas about diopside (ferrosalite) and plagioclase grains (Plate 2.1.B, C & D).

Table 2-1 MODAL COMPOSITIONS (%) OF CALC-SILICATE ROCKS

sample number	Dio	Qt	Plg	Scp	Epd	Hrn	Bio	Gar	Clc	Sph	Tum	Opa	Aln
3055	8	30	50		2	10							
3056a	5	34	10		30	20	1			tr		tr	
3056b	5	64	5		25	1							
3056c	20	20			20	40							
3056d	2	28	50		2	15	3						
3056e	10	55			20	13	1			1			
3059	4	58			35								3
3355	9	50			40	1							
4485	5	10	5	25	25	30							
4502	20	20	30	2	20			tr	1	tr	3	3	
4604	5	10	40		15	30				tr			

(Note: Modal compositions (%) given in tables of this thesis are estimated from thin sections; "tr" represents trace amount. Sample number follows the nearest observation location number which is presented in Map 7. For example, sample number 4502 is collected near the observation location labelled 4502. However the term "sample number" will be simplified as "sample" in the text, e.g. sample 4502 means sample number 4502. In this table sample 3056a to 3056e are separate layers within the sample 3056.)

Table 2-2 ABBREVIATION OF MINERAL NAMES

Aln	allanite	Gar	garnet	Pth	perthite
Apt	apatite	Hrn	hornblende	Qt	quartz
Atp	antiperthite	Hyp	hypersthene	Rut	rutile
Amp	colourless amphibole	Ksp	K-feldspar	Sal	salite
Bio	biotite	Kyn	kyanite	Scp	scapolite
Chl	chlorite	Mus	muscovite	Sil	sillimanite
Clc	calcite	Mic	microcline	Sph	sphene
Cpx	clinopyroxene	Olv	olivine	Spn	spinel
Cum	cummingtonite	Opa	opaque	Trm	tremolite
Dio	diopside	Opx	orthopyroxene	Tum	tourmaline
Epd	epidote	Plg	plagioclase	Zir	zircon

2.2.2. Mafic and ultramafic rocks

The mafic and ultramafic rocks, including mafic granulite (in the Hale River Region only), amphibolite, metagabbro and very minor ultramafics, are mappable units in both the Entia Dome and the Hale River Region, but have only been mapped as principal units in the Entia Dome (see Maps 2 & 4). Even within the Entia Dome many very thin layers or small lenticular bodies are too small to show on the regional maps. None of the mafic and ultramafic rocks are shown in the Hale River Region.

(1) Mafic granulite

The mafic granulite occurs as lenticular bodies or layers within the charnockitic gneiss in the Claraville subarea of the Hale River Region (Plate 2.1.E) and to a lesser extent in the Illogwa Creek subarea but does not occur in the Entia Dome. Individual mafic granulite layers and lenses vary from one to one hundred metres in thickness and up to one kilometre in length.

The mafic granulite near Mulga Hole Bore (Fig. 2-1) consists essentially of plagioclase (45%), salite (30%), hypersthene (15%) and iron oxide (5%) (e.g. sample 4100B). The recrystallized fine-grained matrix (20-50%) surrounds porphyroclastic coarser minerals. Fine-grained hornblende (2%) and biotite (3%) occur on the

margins of, and along the cracks within, the pyroxenes. Typical hornblende two-pyroxene mafic granulite is found around Paradise Well (e.g. sample 4107). It has a homogeneous, medium to coarse, equigranular texture comprising labradorite (60%), hypersthene (5%), salite (15%), hornblende (20%) and minor opaques (Plate 2.1.F). Invariably the mafic granulite (e.g. sample 3105A) in the Illogwa Creek subarea contains two generations of hornblende. The first generation hornblende has a similar grain size to the pyroxene, whereas the second generation hornblende is fine grained and rims the pyroxene (Plate 2.1.H).

(2) Amphibolite

Amphibolite occurs as very distinctive dark layers (Plate 2.2.A) or lenticular bodies within the light coloured gneiss sequence in the Entia Dome (Map 4) and the Illogwa Creek subarea of the Hale River Region. The amphibolite is more resistant than the gneisses and thus usually forms low ridges. In the Entia Dome most of the amphibolite layers are found within the marginal zone or structurally highest levels (Map 4). The amphibolite layers vary from hundreds of metres to centimetres in thickness (Plate 2.2.B) with lengths from about 10 km to less than 100 metres. The amphibolite bodies shown on Map 4 are not single lithological units but contain thin layers of gneisses or metasediments (Plate 2.2.A). Some early amphibolites occur as inclusions within granitic gneisses (Plate 2.2.C), but later dyke-like amphibolite intrusions are also found in folded gneisses (Plate 2.2.D).

The amphibolites consist essentially of hornblende (14-90%) and andesine (9-65%) with varying amounts of diopside, (0-35%), garnet (0-20%), epidote (0-20%), scapolite (0-5%), biotite (0-10%), clinozoisite (0-15%), anthophyllite (0-10%) and quartz (0-10%). Accessory minerals are mainly iron oxide and sphene with

FIGURE CAPTIONS OF PLATE 2.2

A: Regular planar leucocratic migmatite layers in a thick sequence of layered amphibolite. North of Harding Springs Well, Entia Dome; location No.3354.

B: Very thin layers of amphibolite within layered tonalitic gneiss. W of Huckitta Bore, the Entia Dome; location No.4529.

C: A block of layered amphibolite occurring as a xenolith within granitic gneiss. Location No.4048; the Illogwa Creek subarea in the Hale River Region.

D: Folded interlayered amphibolite and tonalitic gneiss were intruded by a later massive dyke (amphibolite) along the metamorphic layering and early fractures. Location No. 4420; W of the Entia Dome.

E: The dyke-like amphibolite in (D) showing a weakly foliated granoblastic microstructure. Field of view: 1.7 mm X 2.2 mm; sample 4420-4; southern margin of the Entia Dome.

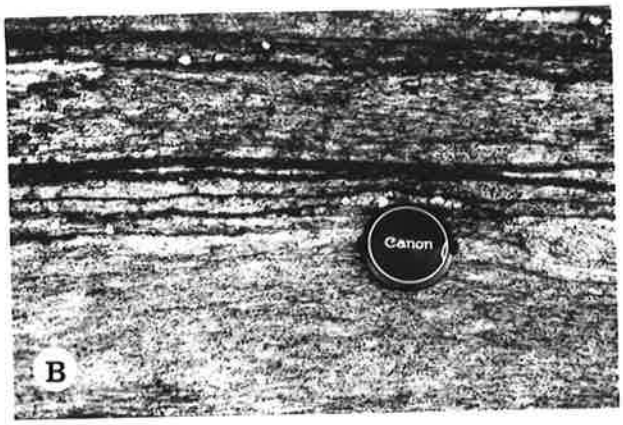
F: Spheroidal outcrop form of the metagabbro at the summit of Black Mountain, a common feature of homogeneous massive rock. Location No.4447; S of the Entia Dome.

G: Typical igneous texture of hypidiomorphic pyroxene and plagioclase from the meta-gabbro described in (F:). Field of view: 1.7 mm X 2.2 mm; sample 4447; X polars.

H: Zoning of a large mafic aggregate which has an olivine core, an orthopyroxene mantle and a myrmekitic rim of intergrown hornblende and quartz. This kind of zoning might be formed during the cooling of gabbro. However metamorphic hornblendes and plagioclase are also present. Field of view: 1.7 mm X 2.2 mm, sample 4447; ppl.

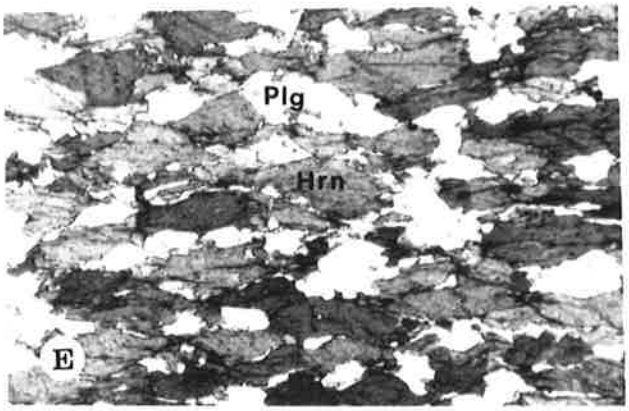
Plate 2.2



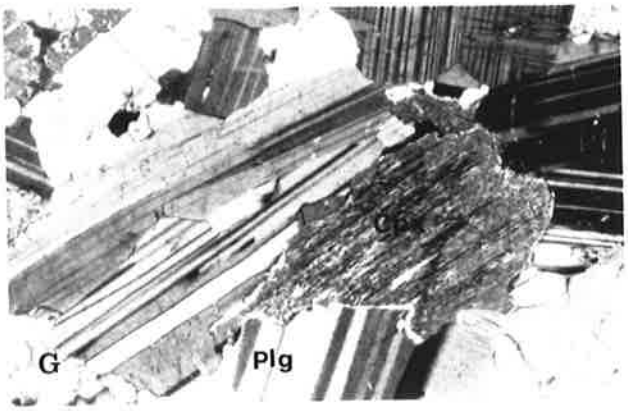


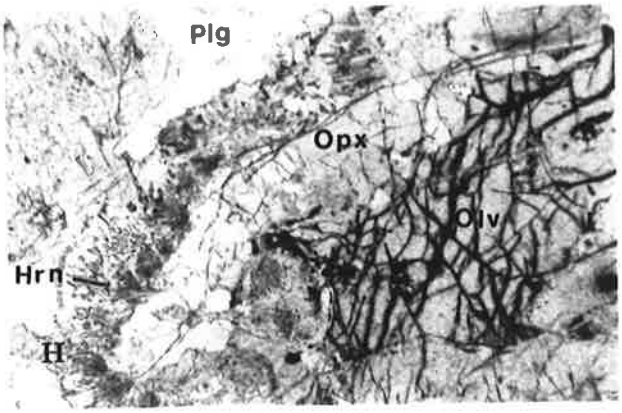












rare apatite, rutile and zircon. Iron oxide (magnetite and/or ilmenite) form as much as 10 % of the whole rock. The amphibolites show weakly foliated equigranular or inequigranular granoblastic microstructures (Plate 2.2.E).

(3) Ultramafics

The ultramafic rocks usually form small lenticular bodies in gneisses as distinctively dark coloured resistant hills and ridges, and usually have a close spatial relationship with the amphibolite layers. No plagioclase is found in the ultramafic rocks. Most of them consist mainly of hornblende and/or cummingtonite (up to 99%) and are thus hornblendite (e.g. sample 4510). Some schistose samples are composed of tremolite and chlorite (e.g. sample 4509).

(4) Metagabbro

Two separate bodies of metagabbro form the bulk and summit of Black Mountain (Plate 2.2.F) in the Entia Dome (Map 4). They are both pod-like lenticular intrusive sheets within the layered granitic gneisses. Each body is about 3 km long and about 150 to 200 metres in maximum thickness. The two metagabbro bodies dip shallowly towards the south and are separated by a thin gneiss layer which is about 20 to 30 metres thick. Gneissic inclusions, about 5 to 10 metres in thickness, have been found within the metagabbro and the gneissic layering is locally cut obliquely by the top-most boundary of the upper metagabbro sill. Similar but smaller intrusive bodies of metagabbro have also been mapped at the northwestern edge of the Entia Dome by Parker (1986).

The metagabbro consists of bytownite (An78) (50%), salite (20%), bronzite (7%), olivine (2%), pale green myrmekitic amphibole and quartz (20%) and minor brownish green hornblende. The coarse grained (1-4 mm) hypidiomorphic plagioclase and pyroxene

show igneous textures (Plate 2.2.G). The bronzite crystals, which usually have olivine cores, are surrounded by pale green myrmekitic amphibole and quartz rims (Plate 2.2.H). The brownish green hornblende is considered to represent part of the original igneous mineral assemblage because it has a similar grain size to the igneous pyroxene. The presence of myrmekitic amphiboles and other fine grained hornblendes, which have formed on the edges and along the cracks of pyroxenes, indicates that the gabbro was slightly metamorphosed under amphibolite facies conditions or altered during a cooling stage (see section 2.4.3).

2.2.3. Acidic to intermediate orthogneiss

Acidic to intermediate orthogneiss includes charnockitic, granitic and tonalitic gneiss. The charnockitic gneiss is only found in the Claraville subarea, whilst the granitic and tonalitic gneisses are found in the Entia Dome and in other subareas of the Hale River Region.

(1) Charnockitic gneiss

Charnockitic gneiss is the principal rock type (50-60%) in the Claraville subarea of the Hale River Region. It forms well layered bodies intercalated with mafic granulite. Charnockitic gneiss is also found as small veinlets intruded into mafic granulite (Plate 2.1.G). Samples from the Illogwa Creek subarea (e.g. sample 3388) have been partially retrogressed, and the hypersthene is pervasively altered to biotite and hornblende. The modal composition of charnockitic gneisses is quite variable (Table 2-3).

Table 2-3 MODAL COMPOSITION OF CHARNOCKITIC GNEISS

sample No.	Qt	Plg	Atp	Pth	Hyp	Cpx	Hrn	Bio	Gar	Opa
3388	20	20	10	20	tr	5	7	18		tr
4100A	40	37			2	2	2	1	16	
4101	20		74		2			tr	1	tr
4107A	20	10	65		5			tr		

Accessory minerals include zircon, apatite and opaques.

(2) granitic and tonalitic gneisses

The predominant rocks of the Entia Dome and the Illogwa Creek subarea of the Hale River Region are granitic gneiss (70%) and tonalitic gneiss (25%). A fine gneissic layering and layer parallel schistosity (Plate 2.3.A) is defined by thin concentrations of mica and/or hornblende and the preferred orientation of the minerals.

The layered granitic gneiss, tonalitic gneiss and some metasedimentary rocks have been locally migmatized (Plate 2.3.B). Leucocratic veinlets comprising mainly quartz and feldspar with very little or no ferromagnisian minerals occur both parallel to, and crosscutting the gneissic foliation. These migmatitic gneisses are not mappable on a regional scale and will not be described further in this thesis.

The boundaries between granitic gneiss layers and tonalitic gneiss layers are usually gradational and are not easily mappable on a regional scale though some workers have attempted this in relatively small areas (e.g. Buick, 1984; Aoukar, 1985; Stewart, 1985; Sullivan, 1985; etc.). For the purpose of this study, the granitic gneiss, tonalitic gneiss, migmatitic gneiss and their intercalated very thin layers of amphibolite and metasediments in the Entia Dome have been treated as a single unit (Map 4).

The granitic and tonalitic gneiss layers are usually concordant with the amphibolite or metasedimentary layers. However,

FIGURE CAPTIONS OF PLATE 2.3

A: Granitic gneiss showing complex folding of fine compositional layering and a layer parallel schistosity. South of Black Mountain, the Entia Dome; location No.4441.

B: Migmatitic gneiss from within layered granitic gneiss. The coarse grained migmatitic veins have formed along both layer parallel schistosity and minor fold axial surfaces. The migmatizaton is a post plutonic but probably a syntectonic feature. Location No.4627, the central Entia Dome.

C: Granitic gneiss intruded into layered amphibolite mainly along the layering (BS_0) but in places injected aross the layering. Location No.4427, S of the Entia Dome.

D: Melanocratic xenoliths within the homogeneous granitic gneiss indicating the early igneous origin of the granitic gneiss. Location No.4356; NW of Huckitta Bore, the Entia Dome.

E: Homogeneous granitic gneiss showing coarser grained augen and a finer grained micaceous schistose matrix. Location No.4631, the central Entia Dome.

F: Typical equigranoblastic texture of tonalitic gneiss. Sample 4510; field of view: 1.7 mm X 2.2 mm; the central Entia Dome.

G: Granitic gneiss sample showing bimodal microstructure including megacrysts of microcline and a foliated granoblastic matrix. Sample 4501; field of view: 1.7 mm X 2.2 mm; the central Entia Dome.

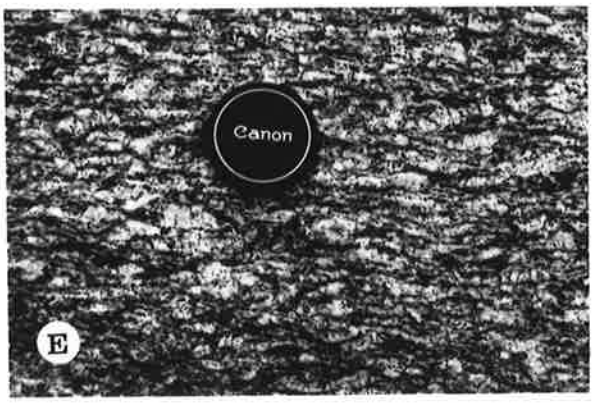
Plate 2.3

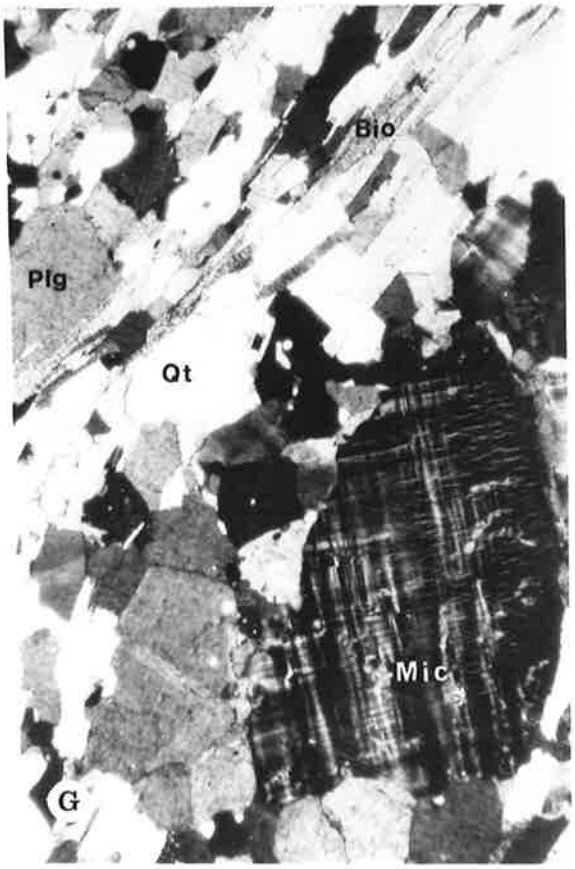


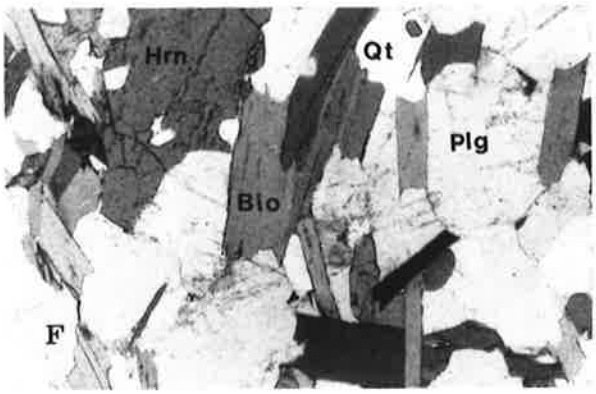












there are indications that the layered amphibolites and metasediments were intruded by the granitic gneiss (Plate 2.3.C). Melanocratic xenoliths (Plate 2.3.D) within some homogeneous thicker granitic gneiss layers in the central part of the Entia Dome (Plate 2.3.E), also support an intrusive origin for the granitic gneisses. Some of the granitic gneisses in the central part of the dome were considered to have diapirically intruded as stock-like granitoids by previous workers (Joklik, 1955; Shaw et al., 1982), and were called the Inkamulla and Huckitta granites. The "Huckitta granite" which is located to the north of Huckitta Bore, was first described as an integral part of the layered gneiss sequence by Buick (1983). Similarly the Inkamulla granite near Inkamulla Bore is now recognized as a separate layered gneiss unit.

The granitic gneiss is composed of K-feldspar (10-72%), plagioclase (5-55%) and quartz (20-30%) with varying amounts of biotite (0-15%), muscovite (0-3%), hornblende (0-6%), epidote (0-1%) and accessory apatite, zircon, sphene and magnetite, with rare tourmaline and rutile. Microcline is dominant but perthitic feldspar is generally absent. Plagioclase is generally oligoclase (An18 to An30). Details of mineral assemblage and modal composition for 39 samples are presented in Appendix I. The typical microstructure of granitic gneiss is equigranular granoblastic with occasional megacrysts of K-feldspar (e.g. Plate 2.3.G).

The tonalitic gneiss is composed of oligoclase (59-70%), quartz (10-30%) and varying amounts of hornblende (0-20%), biotite (5-15%) and epidote (0-5%). K-feldspar is absent. Accessory minerals are similar to those of the granitic gneisses. Details from 14 samples are presented in Appendix I. The tonalitic gneiss shows typical granoblastic microstructure (Plate 2.3.F) similar to that of the granitic gneiss.

2.2.4. Post tectonic intrusive bodies

A diorite intrusive body about 15 km long and 2 km wide is found in the Hale River Region (Fig. 2-1) near Aleeitara Peak (Fig. 2-4). The diorite has a weakly foliated homogeneous character with many inclusions of gneiss, ultramafics, mafic granulite and layered amphibolite. It shows igneous texture and consists of coarse (2-8 mm) plagioclase (70%) and hornblende (30%) with trace amounts of biotite and chlorite. Granite bodies found in the Ambalindum to Atnarpa area have been studied by Sando (1987).

2.3. Structure

2.3.1. Introduction

The major structures of the Hale River Region trend N-S to NNE-SSW (Fig.2-1). Four generations of tight to isoclinal folds have been recognized as belonging to the Strangways Orogeny. The fold structures are truncated to the north by the Muller Thrust which defines the northern margin of the Hale River Region. The Illogwa Shear Zone is a later shear zone in the middle southern part of the area and separates the SOB from Late Proterozoic to Palaeozoic platform cover sequences further south.

The Entia Dome is confined by an originally recumbent marginal thrust (the Entia Thrust) and is separated into two parts by an internal thrust (the Huckitta Thrust), (see Map 4). The lithological layers and structures in the outer (structurally upper) part of the dome are generally parallel to the two thrusts. The lithological layers and structures in the central part of the dome, outcrop as two semi-circles with a straight steep zone between them (see cross section to Map 4). During the Strangways Orogeny three generations of early ductile recumbent folds formed

before the major thrusts were developed. The marginal Entia Thrust itself was later deformed by a further generation of local recumbent folds.

The overall structure of the Entia Dome is similar to other gneiss domes, e.g. the Thor-Odin gneiss dome (Duncan, 1984). The origins of such domal structures often vary and thus usually form topics of controversy (e.g. Duncan, 1984). The Entia Dome is considered to be formed by four sets of late upright open folds, which were finally cut by the latest steep faults. Only the structures of the Strangways Orogeny are described in this chapter, other structures will be described in Chapter 7. The structural events in the Hale River Region and the Entia Dome are compared in Table 2-4.

Table 2-4. COMPARISON OF STRUCTURAL EVENTS IN THE HALE RIVER REGION AND IN THE ENTIA DOME

	Hale River Region	Entia Dome
BD_4	BF_4	BT (Huckitta Thrust)
BD_3	BF_3	BF_3
BD_2	BF_2	BF_2, BS_2, BL_2
BD_1	BF_1?, BS_1, BL_1	BF_1, BS_1, BL_1
pre-BD_1	BS_0	BS_0

Note: In this table and hereafter in this thesis the structural abbreviations are: "B" implies structures belonging to the SOB basement; D = deformation; F = fold; T = thrust or shear zone; S = foliation; L =lineation.

2.3.2. Compositional layering in metasediments and amphibolites

The compositional layering in the calc-silicates is considered to be metamorphosed bedding; the recognition of fine-scale

sequences of up to five compositional layer types (each composed of a different mineral assemblage) is thought unlikely to have been formed by metamorphic or tectonic processes alone, though no convincing sedimentary or volcanic structures have been found. This compositional layering is transected in places by the earliest axial plane schistosity (BS_1, see next section and Plate 2.4.E), and thus must be a pre-BD_1 structure. Other lithological boundaries, such as the boundaries between amphibolites and orthogneisses, similarly show a pre-BD_1 character because these boundaries were also crosscut by an intense BS_1 axial planar fabric (see next section). A weak foliation in the mafic granulite is in places cut obliquely by the charnockitic gneiss (Plate 2.1.E) which suggests that the charnockitic gneiss is younger than the foliation in the mafic granulite and implies a possible earlier deformation phase before the regional plutonism. All the pre-BD_1 fabrics are assigned to BS_0. Thus BD_1 fabrics are the earliest tectonic structures recognized in the area though the possibility of earlier deformations cannot be precluded.

2.3.3. Structures of the first deformation (BD_1)

The earliest mappable folds (BF_1) are found at many localities within the Entia Dome (map 4). The best large-scale example (Plate 2.4.A) occurs at the NE end of the steep zone in the central part of the dome (Fold No.1 on Map 4; note: axial traces of 6 representative folds in the Entia Dome are labelled from No.1 to No.6). This fold is formed by a single amphibolite layer within the granitic gneiss and is isoclinal overall, though the parasitic folds within its hinge zone show an interlimb angle of up to 50^{o}. The fold wavelengths vary from 50 to 100 metres and amplitudes vary from 30 to 150 metres. All limbs of the folds dip shallowly

FIGURE CAPTIONS OF PLATE 2.4

A: A sketch map of BF_1 folds within the Entia Dome (Map4). Location No.4555 to No.4556, NE of Inkumulla Bore.

B: BS_1 fabric, which transects the boundaries between a thin layer of amphibolite and the surrounding granitic gneiss. The amphibolite layer forms the hinge of a BF_1 fold to the left of the picture. Location No.4578; SW of the steep zone, the central Entia Dome.

C: Boundary between dark grey megacrystic tonalitic gneiss on the left and light pinkish granitic gneiss on the right. The predominent schistosity is penetratively discordant to the boundary. Location No.3388; the Illogwa subarea of the Hale River Region.

D: A sketch map showing the relationship between minor BF_1 folds and a larger BF_2 fold. Both the BF_1 and the BF_2 folds are isoclinal. The folds are outlined by amphibolite (dark) and calc-silicate (stipled) layers within granitic gneiss (unshaded). The axial planar fabric is oblique and transects the compositional layering of calc-silicate rock. Location No.3057; N of Harding Spring Well, S of the Entia Dome.

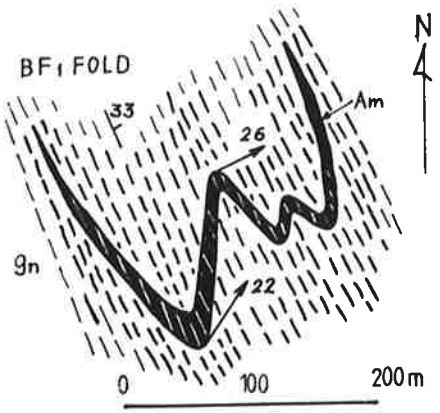
E: The BF_1 fold in D is outlined by the compositional layering of calc-silicate and the axial planar fabric is defined by preferred alignment of elongate epidote. Sample 3057; field of view: 12 mm X 17 mm.

F: Thick amphibolite showing a very complex compositional layering which includes massive amphibolite, fine-scale interlayered mafic and leucocratic amphibolites, layered tonalitic gneiss and a network of migmatitic veins. Location No. 4426, 2 km to the east of Mt. George.

G: A sketch section of a major BF_2 fold with parasitic folds, which show steep fold axial surfaces and subhorizontal fold hinges. A layered amphibolite and its surrounding granitic gneiss form rounded closures and isoclinal limbs with slightly thickened hinges. Weak BS_2 foliation parallel BF_2 axial surfaces and crosscuts the layer parallel BS_1 schistosity. Location No.4603 to No.4605; the central Entia Dome.

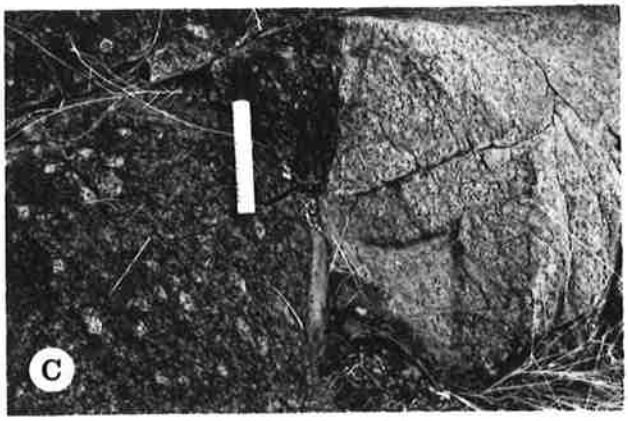
H: BF_2 fold in calc-silicate with a nearly vertical axial surface and a subhorizontal hinge. A weak BS_2 fabric can be seen in the outcrop parallel to the axial surface and transecting the lithological boundary or compositonal layering and layer parallel BS_1 schistosity. Location No.4604; the central Entia Dome.

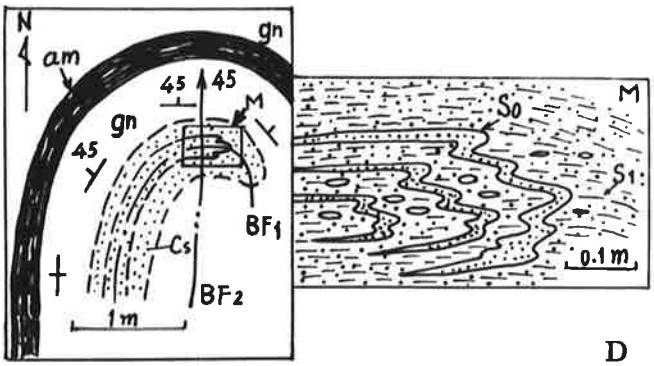
Plate 2.4


BF1 FOLD
N
33
26
22
Am
gn
0
100
200m

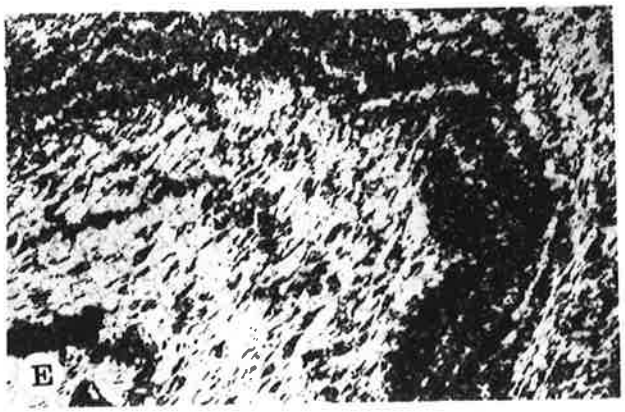
A


B

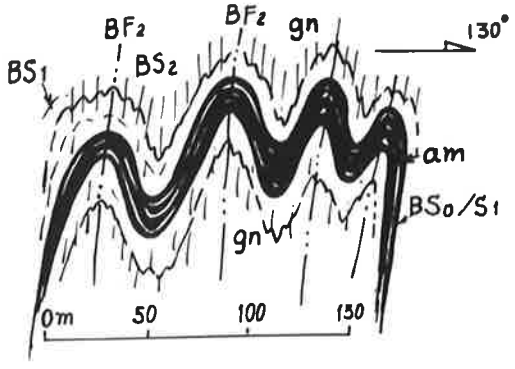

C


N
am
gn
45
45
M
gn
45
BF1
Cs
BF2
1m
So
M
S1
0.1m

D


E


F


BF2
BF2
gn
130°
BS1
BS2
am
BSo/S1
gn
0m
50
100
150

G


H

NE and the major hinge plunges at 22^{o}-035^{o} (22^{o}-035^{o} means plunge angle of 22^{o} towards 35^{o} E of N for all following presentations). A penetrative axial planar schistosity (BS_1), which strikes 345^{o} and dips 33^{o}E, is developed in the amphibolite layer as well as in the surrounding granitic gneiss. The BS_1 foliation is defined by the alignment of mica in the granitic gneiss and the parallel orientation of hornblende and plagioclase in the amphibolite. Similar structures have been observed at the southern end of the same steep zone and a small-scale example is shown in Plate 2.4.B. These BF_1 folds indicate that the orthogneisses developed their main fabric during the BD_1 deformation.

Similar structures are found in the metasediments. Plate 2.4.D is a sketch map of a BF_1 fold outlined by calc-silicate layers. In this fold a preferred orientation of the elongate grains of epidote and diopside within each layer define a schistosity parallel to the fold axial surface but crosscutting the compositional layering (Plate 2.4.E).

No BF_1 folds have been recognized in the Hale River Region, although evidence of crosscutting BS_1 foliations has been observed in the orthogneiss (Plate 2.4.C). However the BS_1 foliation is generally more frequently parallel to the lithological layering reflecting the large limb/hinge ratio in the isoclinal BF_1 folds in this region.

The main compositional layering and schistosity in the granitic gneiss and tonalitic gneisses (e.g. Plate 2.3.A), and in the amphibolite (Plate 2.3.F) have thus been assigned to BS_1 as this is the earliest recognizable and main fabric in these rocks.

A mineral lineation (BL_1) can be invariably seen, on the surface of the BS_1 foliation, paralleling the hinge of BF_1 folds. BL_1 is manifested by the alignment of hornblende in amphibolite

and of mafic minerals such as mica, amphibole and epidote in the granitic and tonalitic gneisses. The BL_1 lineation plunges moderately toward the N to NE or toward the S to SW (see stereogram of BL_1 on Map 4), though locally it may plunge towards the east due to subsequent reorientation caused by the interference of later folds.

2.3.4. Structures of the second deformation (BD_2)

The lithological boundaries, the compositional layering and particularly the main regional schistosity (BS_1) are folded about second generation folds (BF_2).

BF_2 folds are usually very tight to isoclinal, with thickened hinges and attenuated limbs, and only very weakly develop an axial planar schistosity (BS_2). Fold hinges trend NE-SW with variable plunges. The amplitudes and wavelengths of BF_2 folds vary from ten to hundreds of metres.

An excellent example of a major BF_2 fold (fold No.2 on Map 4) occurs to the NW of Huckitta Bore (see Map 1). The fold was interpreted by Buick (1983) from the symmetrical distribution of a series of discrete 10 to 50 metres thick amphibolite layers and lenticular bodies. The major closure of this No.2 BF_2 fold has been mapped during the present study and it shows a rounded hinge which plunges 25^{o} to 34^{o} towards 030^{o} to 037^{o}. The compositional layering and layer parallel schistosity within the amphibolite are clearly folded with the development of only very weak axial planar schistosity (BS_2).

Another major BF_2 fold (see fold No.3 on Map 4; note that it is especially well displayed on the accompanying cross section) occurs in the steep zone in the central part of Entia Dome. The northern closure, which is outlined by a thick layered sequence of

calc-silicate and amphibolite, plunges at 22^{o}-010^{o}, which is oblique to the local BL_1 lineation (plunging at 34^{o}-070^{o}). At the southern closure of this fold the BF_2 fold axes and lineations all plunge S to SW. In the middle part of this BF_2 fold, it shows a steeply NW dipping profile with parasitic folds occurring in its major hinge zone (Plate 2.4.G). The fold axes and lineations plunge subhorizontally NE or SW. Also in this middle part a spaced schistosity is developed at the closure of the BF_2 fold parallel to its axial surface and is superimposed on the layer-parallel BS_1 schistosity (Plate 2.4.G). The BS_2 schistosity is also developed elsewhere within layered mica-rich granitic gneisses (Plate 2.5.A, B & C), where BS_2 is oblique to the compositonal layering (BS_1) of gneisses.

BF_2 folds are well developed in the Claraville subarea of the Hale River Region (Fig. 2-1); they show elliptical outcrop patterns and their hinges all plunge in a similar direction thus implying a three dimensional sheath-like form (Cobbold & Quinquis, 1980; Henderson, 1981). This type of fold has recently been reported by Goscombe (1987) from the eastern part of the Strangways Range in the western extension of the Hale River Region.

2.3.5. Structures of the third deformation (BD_3)

Major BF_3 folds have been mapped throughout the Entia Dome, where they are almost isoclinal and formed originally in a recumbent orientation with subhorizontal fold axes trending NE-SW before the formation of the Entia Dome. The BF_3 folds now show a regional luniform shape on the map with hinge zones plunging both NE and SW, resulting mainly from the superimposition of a later NW trending upright open fold within the Entia Dome (see Map 4). The profiles of the major BF_3 folds are shown by the cross section on

FIGURE CAPTIONS OF PLATE 2.5

A: BS_1 compositional layering in a mica rich granitic gneiss (parallel to the handle of a sledge-hammer) with BS_2 schistosity oblique to the layering. The BS_2 schistosity is steeper than the compositional layering. Location No.4625, the central Entia Dome.

B: A close-up of A. In the picture, the BS_1 is almost horizontal, whereas the BS_2 is inclined towards the right.

C: Banded granitic gneiss with the compositional layering affected by parasitic BF_2 folds. An axial planar BS_2 schistosity lies obviously oblique to the layering (BS_1). Location No.4626; S of the steep zone in the Entia Dome.

D: Small scale interference between BF_3 and BF_2 folds. Location No.3153; SW margin of the Entia Dome.

E: A close-up of the BF_2 fold in (D:) showing the details of its closure area.

F: Intense stretching lineation on the surface of foliation within a mylonitic granite gneiss. South of the Entia Dome.

G: A pair of dextral reclined folds are manifested by the mylonites along the Entia Thrust (the picture facing the SW). Location No. 4530, W of Mt. Long, NE of the Entia Dome.

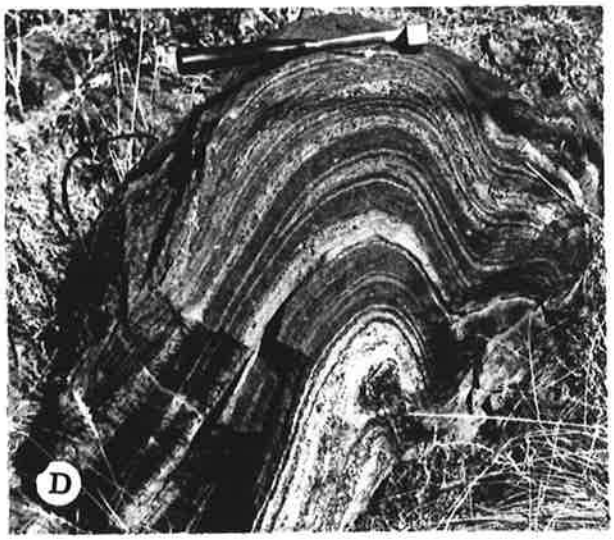
H: A close-up of the fold closures at the upper right corner of (G:).

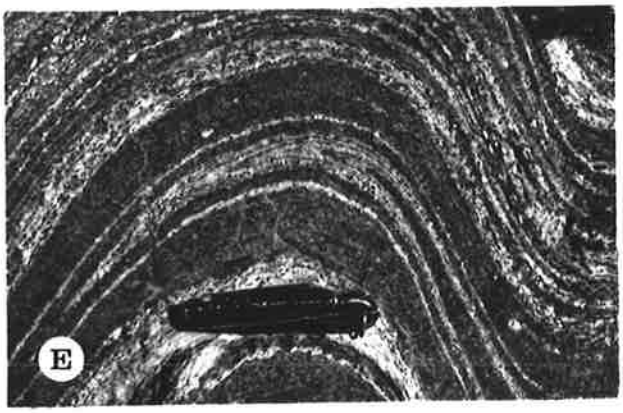
Plate 2.5

















Map 4.

The geological map of the inner Entia Dome shows a very unusual pattern not unlike a human brain in shape. This was interpreted previously as two diapiric semi-domes separated by a steep zone, resulting from the intrusion of "the Inkamulla and Huckitta granodiorites" (Shaw and Freeman, 1985). These two "semi-domes" are interpreted as a pair of major isoclinal BF_3 folds in this study; the right or southeastern half of the "brain" structure was recognized, first by Buick (1983), as a major isoclinal fold closing to the northwest and is here named the Huckitta Fold (fold No.4 on Map 4); the left or northwestern half of the "brain" structure is recognized to be the real structural centre of the Entia Dome and a major isoclinal BF_3 fold, which is named as the Inkamulla Fold (fold No.5 on Map 4). Other major BF_3 folds have been mapped and interpreted in the marginal areas (i.e. at the upper-most structural levels) of the Entia Dome (Map 4), e.g. the Harding Spring Fold (fold No.6 on Map 4).

The axial surface of the Huckitta Fold has been mapped over most of the Dome for 35 km in strike length. Its amplitude, which can be estimated from the cross section, varies from 3 to 10 km depending on which planar elements are concerned. Its half wavelength is about 2.5 km. A granitic gneiss body forms the core of the Huckitta Fold, and an amphibolite sequence, which represents the No.2 major BF_2 fold, forms an ellipse surrounding this core (Map 4). The two limbs of the Huckitta Fold are parallel and dip 23° to 43° SE. Its NE closure plunges at 38°-030° as indicated by the detailed measurements of dips and strikes along the amphibolite layers. BL_1 lineations are slightly oblique to the hinge of the Huckitta Fold with the intersection angle between the two varying from 0° to 27° (see stereogram on Map 4). Its SW closure

plunges at 25°-213° as indicated by the orientation of the BS_1 schistosity around this closure (see stereogram on Map 4), with the intersection angle between the BL_1 lineation and the hinge of BF_3 fold varying from 3° to 27°.

The core or hinge area of the Inkamulla Fold consists of a layered granitic gneiss body, which was called the Inkamulla granodiorite by Shaw and Freeman (1985), but is in fact very similar to the other layered granitic gneisses of the Entia gneiss complex. Its fold axial trace follows a completely closed circuit, for about 15 km of strike length (fold No.5 on Map 4). Its amplitude and wavelength can be estimated from the cross section as about equal to those of the Huckitta Fold. Its southwestern closure is well outlined by a thin, discrete amphibolite layer which can be traced continuously from the lower limb to the upper limb around the granitic gneiss core which plunges at 25°-230°. The northeastern closure of the Inkamulla Fold is not well exposed but its hinge has been measured as plunging at 25°-035°.

The distinctively asymmetric fold profile of the Inkamulla and Huckitta Folds (i.e. the long upper and short lower limbs of the Huckitta fold or the short upper and long lower limbs of the Inkamulla Fold) shows a northwesterly vergence (Bell, 1981) and suggests a major tectonic transport direction from SE to NW during BF_3 folding.

The recognition of the Inkamulla Fold as part of a major overturned fold pair leads to a new interpretation for the overall structure in the Entia Dome. In this interpretation the most important point is the understanding of the steep zone which was previously mapped as an upright synformal fold between two upright antiformal folds of the same generation (and the same as the Entia Dome overall) (Shaw, et al., 1982; Shaw & Freeman, 1985). The

steep zone is now interpreted as the easterly closing hinge of the Inkamulla fold (BF_3). The relationship between the early folds and the BF_3 folds is shown by the cross section on Map 4.

Another excellent example, the Harding Springs Fold (fold No.6 on Map 4), is exposed north of Harding Springs Well and is cored by layered granitic gneiss of about 30 to 50 m in thickness. This fold has two parallel limbs of layered amphibolite, which close to the SE, and which have been traced more than 8 km to the north showing a remarkably large limb/hinge ratio. The thickness of the amphibolite layers has been doubled or tripled at the fold hinge. The axial surface of the fold dips 10^{o} to 35^{o} NW and its hinge plunges at 17^{o}-230^{o}. The axial trace of this fold may extend for more than 20 km to the northwestern part of the Entia Dome (Map 4), but its middle part has been sheared by the Entia Thrust (section 2.3.7) along the west margin of the Entia Dome.

Interference between BF_3 folds and the earlier BF_2 folds has been found also on the outcrop scale (Plate 2.5.D & E). These interference patterns are mainly of Type 3 of Ramsay's (1967) classification. (The types of interference pattern described in this thesis all follow Ramsay's classification, which will not be referred to hereafter.)

BF_3 folds are also developed throughout the Hale River Region (Fig. 2-1) but are best exposed in the Claraville subarea. They have completely isoclinal profiles and rounded closures with amplitudes of approximately 10 km and wavelengths of the order of 1-2 km. The axial surfaces of BF_2 folds are clearly folded by BF_3 folds, and some of the BF_2 folds show luniform or mushroom shapes near to the closure areas of the BF_3 folds (e.g. northeast of The Garden on Fig. 2-1). BF_3 folds have also been mapped around Aleei-tara Peak in the SE (Figs. 2-4 and 2-1) and to the north of

Paradise Well (Figs. 2-1 and 2-2). The latter shows an isoclinal core and a tight but rounded hinge which closes to the south and plunges NE. Its amplitude is approximately 10 km and the wavelenth is of the order of 5 km. A major BF_2 fold (Fig. 2-1) with a calc-silicate gneiss sequence in the core is refolded by this BF_3 fold.

2.3.6. Structures of the fourth deformation (BD_4)

A pair of major E-W trending BF_4 folds is developed in the northern part of the Claraville subarea between The Garden and Muller Bore (Fig. 2-1). BF_3 folds as well as the earlier folds are refolded by these BF_4 folds. These folds are subreclined with moderately north dipping fold axial surfaces, and northerly plunging hinges. The NE trending limbs dip moderately NW, whereas the NW trending limbs dip moderately NE and thus form an easterly closed hinge zone for the northern BF_4 fold and a westerly closed hinge zone for the southern BF_4 fold. The amplitudes and wavelengths vary from 3 to 5 km.

In a small area around Paradise Well (Fig. 2-1), three generations of tight to isoclinal folds (F_2, F_3 & F_4) were mapped and described by Goscombe (1984), and this interpretation is in agreement with the regional system presented in this study. He defined S_1 as the axial fabric of F_1 folds but he also could not provide a convincing example of the F_1 folds. BF_3 folds in the area south of Aleeitara Peak (Fig. 2-4) are also clearly refolded by a set of E-W trending BF_4 folds. No BF_4 folds have been recognized in the Entia Dome.

2.3.7. Thrusting within the Entia Dome (BT)

Small shear zones are common within the Entia Dome, but only one major fault shear zone, named the Huckitta Thrust, has been

mapped within the Entia Dome. (The term "thrust" used in this thesis implies a compressional origin. "Thrusts" in this area do not always show geometrically upwards/reverse shear senses, because most of these thrusts have been subsequently deformed by polyphase ductile folding.) The Huckitta Thrust forms the boundary between the inner and outer parts of the Entia Dome and acted as a slide surface separating two recumbent tectonic sheets (see Map 4). The discordance between the structures on either side of the thrust can be seen clearly on the Map 4. The thrust boundary is characteristically represented by a shear zone. The upper limb of the Huckitta Fold which occurs in the lower tectonic sheet, has been intensely thinned and sheared where it comes close to the thrust. The gneiss sequence and some amphibolite layers are pinched out near the shear zone in the east close to Huckitta Bore (see Map 4 and cross section). The discordance between the Huckitta Thrust and the upper tectonic sheet can be seen most clearly near Black Mountain in the southwestern part of the Entia Dome (Map 4). Amphibolite layers and gneissic layering are cut obliquely by the shear zone, and the structures on both sides of the shear zone are discontinuous.

Schists and blastomylonites (Higgins, 1971) with an intense NE trending stretching lineation (Plate 2.5.F) are found along this shear zone. However the shear zone has not been studied in detail and the shear sense is uncertain. Nykiel (1986) and Macdonald (1986) mapped the NW part of the Entia Dome and described some intensely deformed rocks along what is considered to represent an extension of the Huckitta Thrust. The Huckitta Thrust is temporarily assigned to the SOB structures. However, it is possible, though less likely, that the Huckitta Thrust is part of a later thrust (e.g. the HRT_4 Muller Thrust, see Chapter 7) or was

reworked during the Harts Range Orogeny.

The Entia Dome is completely surrounded by a ductile shear zone. Rocks of the shear zone are intensely mylonitized, and the structures within the Entia Dome are clearly sheared into and truncated by this zone particularly along its western and southern margins (Map 4). A quite sharp contact, which is named the Entia Thrust, can be recognized at many places between the Entia gneiss complex and the mylonite zone. The Entia Thrust is folded by locally developed reclined folds (Plate 2.5.G & H) which may be related to later folds of the Harts Range Orogeny (HRF_3, see Chapter 7). This marginal shear zone, including the Entia Thrust, is a part of the HRDZ and will be described and discussed in detail in Chapters 7 & 8.

A similar type of BT thrust may represent the boundary between the Claraville and Illogwa Creek subareas (Fig. 2-1), however, such a possible tectonic boundary has not yet been recognized.

2.4. Metamorphism

2.4.1. Introduction

The Hale River Region covers a vast area, about 100 km long and up to 40 km wide, and includes regional metamorphic rocks varying from granulite facies to amphibolite facies. The granulite facies lithologies occur mainly in the Claraville subarea, where thin layers or lenticular bodies of mafic granulite are intercalated within dominant charnockitic gneisses. The amphibolite facies lithologies are mainly in other subareas, where thin layers of amphibolite are intercalated mainly with granitic and tonalitic gneisses. The boundary between a predominantly granulite facies terrane and a predominantly amphibolite facies terrane near Para-

dise Well is locally mapped as an isograd by Goscombe (1984) after the B.M.R. who showed a distinctive isograd on the regional geological map (Australia 1: 250000 Geological Series: Alice Springs sheet). A different type of transitional zone is recognized in this work, and is characterized by the intercalation of thin mafic granulite layers and dominant granitic gneisses in the same area but on a broader scale. However, this transitional zone has not been mapped in detail on a regional scale. The whole of the Entia gneiss complex is metamorphosed under typical amphibolite facies conditions. Retrogressive metamorphism has locally occurred and indicates that polyphase metamorphic events have affected the SOB rocks.

2.4.2. Regional granulite facies metamorphism

Granulite facies mineral assemblages include orthopyroxene, clinopyroxene and plagioclase in mafic granulite (e.g. samples 4100B, 4107 and 3105A); hypersthene and perthitic feldspar within charnockitic gneiss (e.g. samples 4100A, 4101 and 4107A); and garnet, biotite, cordierite and perthitic feldspar in metapelite (e.g. Goscombe, 1984). The mafic granulites contain hornblende, which is of a similar grain size to the pyroxenes; the two ferromagnesian minerals are considered to be in equilibrium and the rocks can be called hornblende granulite (Turner, 1981).

The earliest BS_0 foliation in the mafic granulite is defined by the granulite facies minerals thus suggesting that the granulite facies metamorphism was reached before BD_1.

Metamorphic temperatures (ranging from 770 to 830^{o}C) given by mafic granulites were estimated from two-pyroxene geothermometry of Wood & Banno (1973) and of Wells (1977), and are listed in Table 2-5. Because of the disagreement between different methods,

the P-T estimates are provisional.

Table 2-5 TEMPERATURES FROM TWO-PYROXENE GEOTHERMOMETRY

sample No.	Wood & Banno (1973)	Wells (1977)
4100B	785°C	805°C
3105A	780°C	830°C
4107	770°C	785°C

Granulite facies P-T conditions of 700-800°C and 7-8 kb were suggested by Goscombe (1984) for the Paradise Well area (Fig. 2-1). This pressure estimate has been revised to 5-7 kb by Oliver et al. (in press, Appendix V) and represents a burial depth of 18-25 km. Somewhat higher pressures and temperatures, of 850-920°C and 8 ± 1 Kb were estimated by Warren (1983) for metamorphics in the Strangways Range. This represents a burial depth of 25-32 km. The Strangways Range is the western extension of the Hale River Region and may represent a deeper or inner zone to the SOB with a similar thermal gradient.

2.4.3. Regional amphibolite facies metamorphism

The amphibolite facies metamorphism is manifested by the mineral assemblages of kyanite plus biotite plus garnet and plagioclase in pelitic rocks, and of clinopyroxene plus garnet plus hornblende and plagioclase in amphibolite and metagabbro. Using the clinopyroxene - garnet thermobarometry of Ellis & Green (1979), the metamorphic temperature of amphibolite (sample 4428) is estimated as 655°C at 6 kb to 660°C at 8 kb. Peak metamorphic temperatures and pressures of the Entia gneiss complex have been estimated also by many other workers (Buick, 1983; Aoukar, 1985; Stewart, 1985 and Sullivan, 1985), and metamorphic temperatures of 650-825° and pressures of 6-9 kb are indicated.

A P-T estimate of 650-750°C and 7-8 kb is suggested from the present study for the amphibolite facies lithologies in the SOB on

the basis of all the above estimations. The amphibolite facies assemblages show lower temperatures and similar or even higher pressures and consequently lower geothermal gradients than that of the granulite facies assemblage.

2.4.4. Retrograde metamorphism

Most mafic granulites in the Hale River Region remain unretrogressed (Plate 2.1.E & F). However amphibolite facies retrograde metamorphism has been observed locally in the granulite facies rocks of the SOB. For example, secondary garnet (0.01-0.05 mm) rims coarse-grained (0.5-1 mm) plagioclase (Plate 2.1.B, C & D) in some calc-silicates and rims hypersthene in some mafic granulites (e.g. sample 4101). This feature may be interpreted as a result of isobaric cooling (Sandiford, 1985), but its localized distribution favours deformational retrograde metamorphism. Fine-grained hornblende (2%) and biotite (3%) rimming, or occupying cracks within, pyroxene has also been observed in the mafic granulites (sample 4101). Access to water causing this retrograde metamorphism is likely to be provided by nearby basement shear zones (BT) during the last deformational stage of the Strangways Orogeny. Some of the charnocktic gneiss and mafic granulite near the Muller Thrust has been retrogressed to hornblende gneiss and amphibolite.

Evidence of retrograde metamorphism has also been observed in small mafic granulite bodies within granitic gneiss in the Illogwa Creek subarea. In the mafic granulite secondary hornblende rims coarse pyroxene, biotite and iron oxide (Plate 2.1.H).

In some foliated and lineated amphibolite layers, more massive amphibolite cores are found. The massive cores have a mineral assemblage of major plagioclase, clinopyroxene, garnet and minor

FIGURE CAPTIONS OF PLATE 2.6

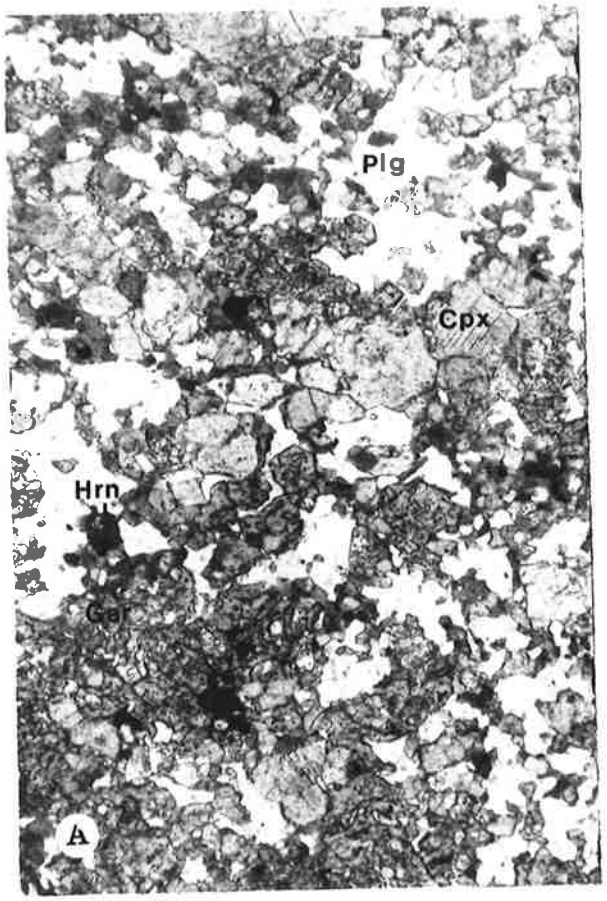
A: Garnet clinopyroxene hornblende plagioclase rock showing an inequigranular granoblastic microstructure. The hornblende grew at the expense of pyroxene and garnet. Field of view: 1.7 mm X 2.2 mm; sample 4428, southern margin of the Entia Dome.

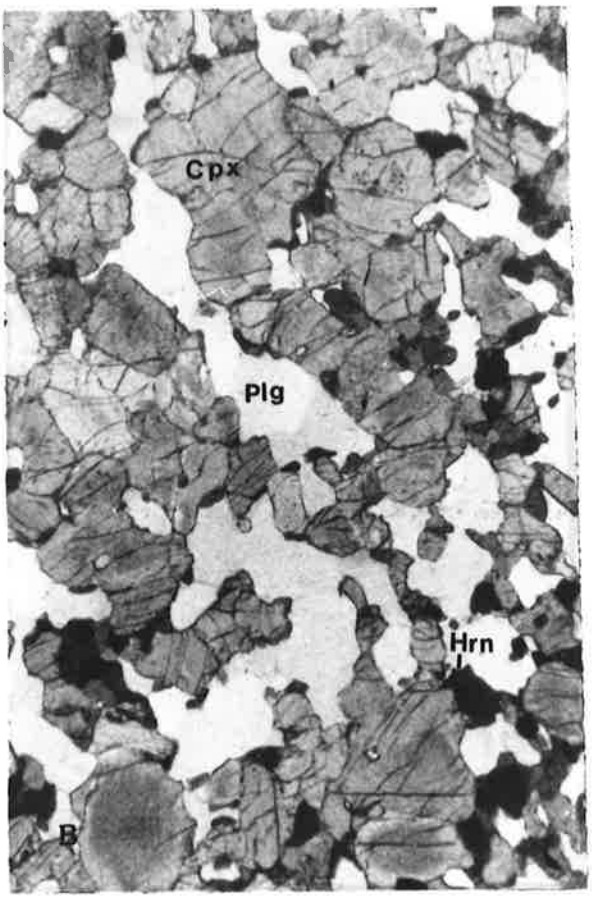
B: Granoblastic textures of clinopyroxene plagioclase rock (which constitutes the massive core of a thick schistose amphibolite layer). Fine grained hornblende occurs along some of the grain boundaries and triple point junctions indicates incipient hydration. Field of view: 1.7 mm X 2.2 mm; sample 4029a; S of the Entia Dome.

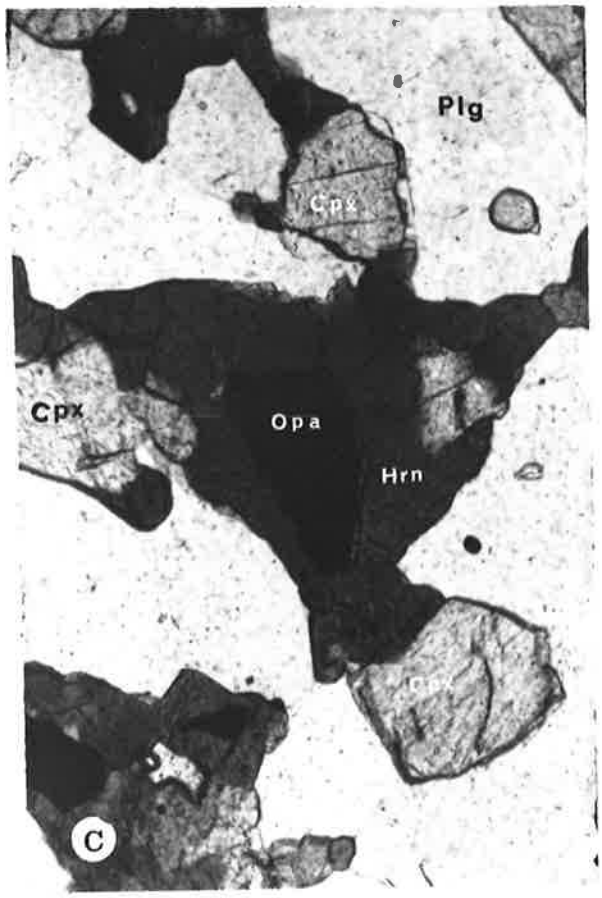
C: A close-up of the texture in (B:). Field of view: 0.43 mm X 0.55 mm.

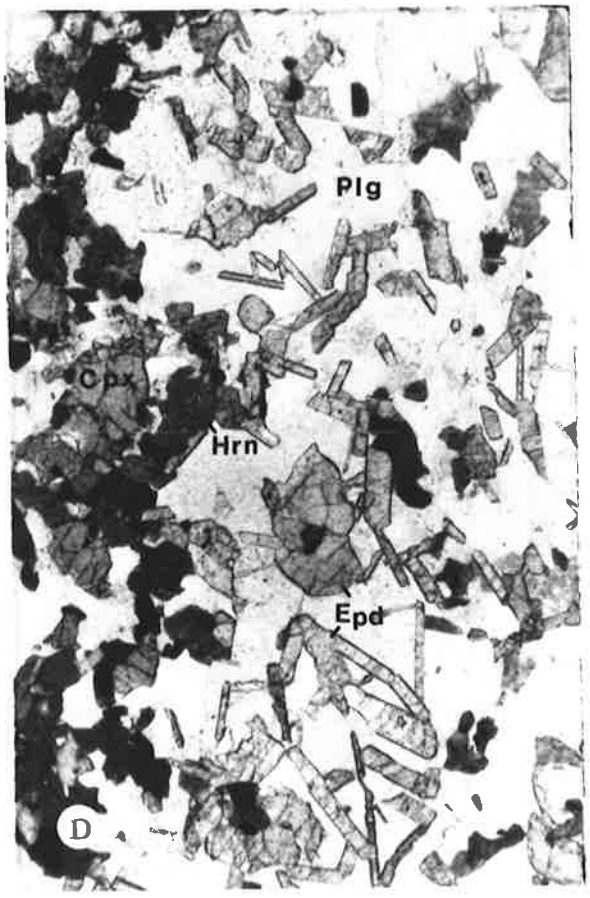
D: Compositional layering of an amphibolite sample (which appears at the margin of the thick amphibolite layer depicted in (B:). Abundance of epidote and hornblende indicate that hydration was extensive within the marginal zone of the mafic layer. Field of view: 1.7 mm X 2.2 mm.

Plate 2.6


Plg
Cpx
Hrn
Gal
A


Cpx
Plg
Hrn
B


Plg
Cpx
Cpx
Opa
Hrn
C


Plg
Cpx
Hrn
Epd
D

hornblende (e.g. Plate 2.6.A, B & C), while their foliated and lineated amphibolite margins comprise plagioclase, hornblende (Plate 2.2.E) and prismatic epidote (Plate 2.6.D). The above examples indicate some degree of retrograde metamorphism during the main ductile deformation (BD_1-BD_4), though both the inner cores and main parts of the rocks are amphibolites. No compositional zoning has developed in the clinopyroxene nor the garnet.

Evidence for greenschist to low amphibolite facies retrograde metamorphism has been observed in the area to the north of Aleeitara Peak (Fig. 2-4). A recrystallized mineral assemblage, including albite, muscovite, oligoclase, epidote, pale brown biotite, pale green amphibole, and minor chlorite, is superimposed on the pre-existing mineral assemblages, which include dark green hornblende, brownish biotite, garnet, plagioclase and potash feldspar, within the SOB complex of amphibolites, granitic and tonalitic gneisses. This retrograde zone was named the Illogwa Schist Zone by Shaw et al. (1984). Fully retrogressed schists along the Illogwa thrust are restricted to only a few metres in thickness. This indicates the limited extent of low amphibolite to greenschist facies metamorphism which has accompanied the shearing (see also Chapter 7).

CHAPTER 3 THE OONAGALABI TONGUE

3.1. Introduction

The Oonagalabi Tongue is situated in the middle west part of the area, and occupies an area of about 200 km^2. Geographically and geologically it is bounded by now tightly folded discrete thrusts and shear zones. The Maud Thrust and the Oonagalabi Thrust define its northern, eastern and southeastern margin, whereas the Muller Thrust defines its southern margin (see map 2 and Fig. 1-1). Only the eastern part of the Oonagalabi Tongue has been mapped in detail (Map 3). The area was previously named as the Oonagalabi Dome by the B.M.R. (Shaw and Wells, 1983; Shaw et al., 1984b) but has since been renamed as the Oonagalabi Tongue by Ding and James (1985, Appendix III), as it does not have the geometry of a domal structure but is rather the tongue-shaped core of a major subreclined fold (Hobbs et al., 1976).

The metamorphic rocks within the Oonagalabi Tongue were previously assigned to the Bungitina metamorphics of Division 1 by Shaw et al. (1979, 1980 and 1984a), but were later named the Oonagalabi gneiss complex by Ding & James (1985) as the original Bungitina metamorphics were named after a subdivision of gneisses in the area to the south of the Muller Thrust, and Ding & James showed that there was no direct continuity between the Bungitina Metamorphics and the Oonagalabi gneiss complex. Like the Entia gneiss complex, the Oonagalabi gneiss complex is not a stratigraphic unit but a non formal subdivision and hence a non capitalized term.

3.2. Field description and basic petrology of the Oonagalabi Tongue

The Oonagalabi gneiss complex comprises predominantly grani-

tic gneiss, tonalitic gneiss and migmatitic gneiss (about 80-85% of the outcrops), minor mafic rocks (10-14%) and very few ultramafics and metasediments. The mafic rocks are mainly distributed in the eastern part of the Oonagalabi Tongue (Map 3), other rocks are evenly distributed through the domain as a strongly interlayered pile of high-grade metamorphic lithologies.

On a regional scale the boundaries between different gneiss types are usually gradational, and thus it is very difficult to produce a meaningful lithological map of the gneisses. Most of the compositional layers within the gneisses are somewhat diffuse and too thin to map. The intercalation between gneissic and mafic layers on a fine scale are characteristic but also not possible to map. The metasediments always occur as small bodies or very thin layers within the Oogagalabi gneiss complex and also cannot be mapped as individual identities. Thus, the predominant granitic gneiss, minor tonalitic gneiss and migmatitic gneiss including small bodies and thin layers of mafic rocks and metasediments are grouped into one mapping unit on Maps 2 and 3.

The mafic rocks include mafic granulite and amphibolite, which have been mapped as two different units. They are mapped either as individual layers where they are very continuous or thick enough, or as groupings of layers where they are intercalated with acidic gneisses on a fine scale. Some mafic layers on Map 3 include thin gneiss layers.

3.2.1. Metasediments

The metasediments include semi-pelitic gneisses, calc-silicates, marble, and rare impure quartzite. They occur as thin layers (a few metres thick) or small lenticular bodies within the granitic gneiss, or as the mesosome of the migmatitic gneiss in

the eastern part of Oonagalabi Tongue, and are usually too small to map as individual geological bodies. They become more abundant in the western part of the Oonagalabi Tongue.

The semi-pelitic gneisses contain biotite (25-30%), garnet (1-5%), plagioclase (28-54%), quartz (20-40%) and minor K-feldspar. They are dark greyish in colour because of the large proportion of biotite. The calc-silicates are identical to those in the Claraville subarea of Hale River Region (chapter 2) and will not be further described here.

3.2.2. Mafic rocks

The mafic metamorphic rocks are mainly found in the middle and eastern part of the Map 3 area, where they form major rather continuous layers and minor lenticular bodies within the gneiss complex and generally parallel the gneissic layering. Their very dark colour makes them easy to map in the field and to recognize from airphotos. The longest layers extend continuously for over 10 km, while many small lenticular bodies, which are sporadically distributed within the gneiss complex, are usually shorter than 20 metres. The thickness of the mafic layers varies from metres to over a hundred metres. The mafic metamorphic rocks are fine to intermediate grained (0.2 to 2 mm) and massive to weakly foliated. It was difficult to identify orthopyroxene during the field work, however subsequent thin sections study allowed the subdivision of three types of mafic rocks. These include: (1) a mafic granulite; (2) an amphibolite; and (3) a rock type representing a deformed and retrogressed equivalent of the mafic granulite.

Some fine grained amphibolite occurs as mafic dykes, which intruded into the granitic gneiss and cross cut its compositional layering (Plate 3.1.A). The amphibolite dykes are usually too

FIGURE CAPTIONS OF PLATE 3.1

A: Mafic dyke (in the centre), now metamorphosed to amphibolite, intruded into complexly folded banded granitic gneiss. Middle south of the Oonagalabi Tongue; location NO.3905.

B: Equigranular texture of an undeformed mafic granulite. The straight boundaries between plagioclase and pyroxene form triple point junctions. Hornblende, plagioclase and two pyroxenes have a similar grain size. Field of view: 1.7 mm X 2.2 mm; sample 3809-1; SE of Oonagalabi Tongue.

C: Amphibolite shows a weakly foliated fine granoblastic texture. The homogeneous texture is in contrast to the bimodal texture of hypersthene-bearing amphibolite (e.g. in D & E). Field of view: 1.7 mm X 2.2 mm, sample 3905, the Oonagalabi Tongue.

D: Fine grained amphibolite containing deformed Opx and Cpx relicts (1 mm long). The elongate pyroxene and fine grained (0.05-0.2 mm) marix of hornblende and plagioclase define a lineation and foliation. Field of view: 1.7 mm X 2.2 mm; sample 3791; north margin of the Oonagalabi Tongue.

E: A large elongate hypersthene within a fine grained amphibolite. Field of view: 1.7 mm X 2.2 mm; sample 3715; north margin of the Oonagalabi Tongue.

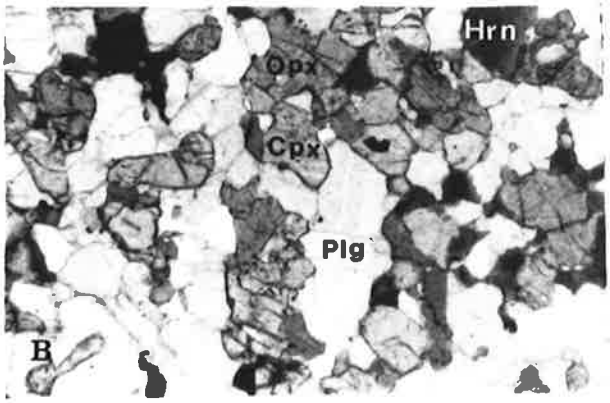
F: Fine grained hypersthene aggregates rim a coarse single hypersthene. Sample 3893; south margin of the Oonagalabi Tongue. Field of view: 0.55 mm X 0.43 mm.

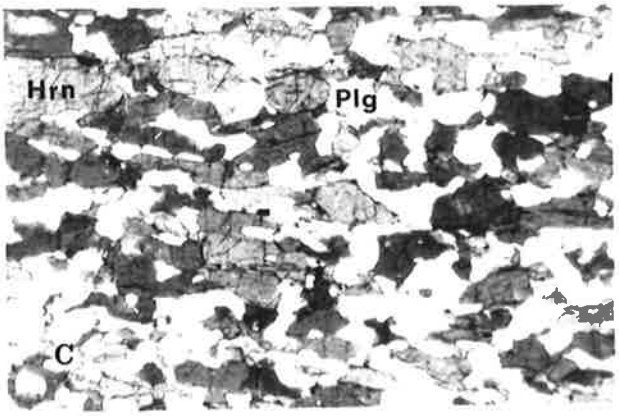
G: A hypersthene showing coronas of hornblende. The intergrowth of garnet and iron oxide may result from the breakdown of some pyroxene. Field of view 1.7 mm X 2.2 mm; sample 3645; Panikan Dame, middle of the Oonagalabi Tongue.

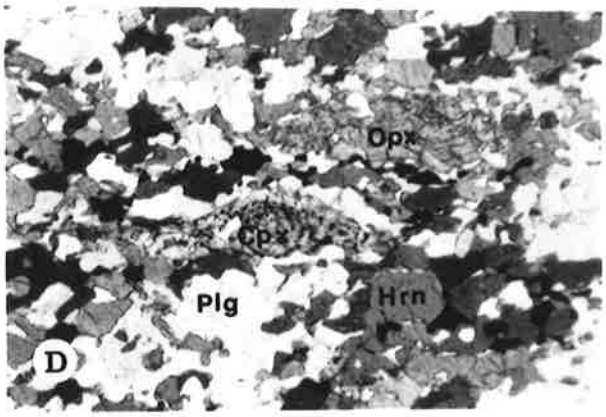
H: Banded granitic gneiss injected by fine leucocratic migmatitic veins, shows the hinge area of a minor open fold. South of Panikan Dam, middle of the Oonagalabi Tongue; location No.3646.

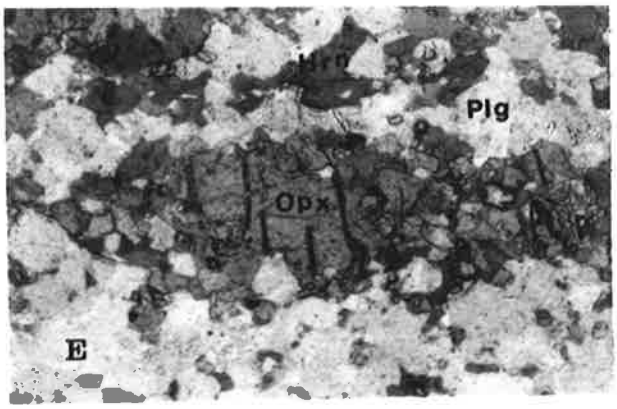
Plate 3.1

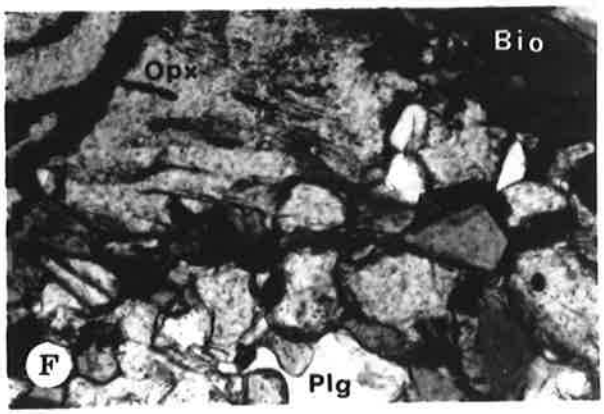

A

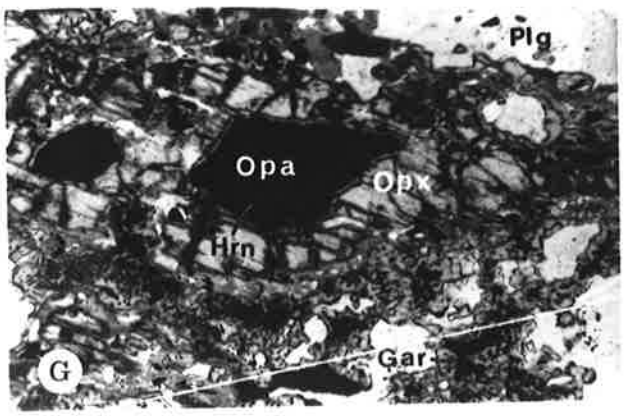

Hrn
Opx
Cpx
Plg
B


Hrn
Plg
C


Opx
Cpx
Plg
Hrn
D


Hrn
Plg
Opx
E


Bio
Opx
F
Plg


Plg
Opa
Opx
Hrn
G
Gar


H

narrow (5-10 cm in width) to show on the regional map.

3.2.2.1. Mafic granulite

Mafic granulite is mainly found in the middle and eastern part of Map 3 and makes up 15-20% of the mafic metamorphic rocks or 2-3% of the whole area. In thin section the typical mafic granulite shows homogeneous fine to intermediate (0.2 to 2 mm) equigranular metamorphic textures with or without a weak foliation (Plate 31.B). It comprises hypersthene (Opx) (10-15%), salite (Cpx) (12-20%), labradorite (50%), hornblende (18-25%) and minor accessory minerals. There are two generations of hornblende within the mafic granulite: the main and older generation is olive brown in colour and shows a similar grain size to the pyroxene, while the second generation of hornblende is green in colour and appears as thin reaction rims between the plagioclase and pyroxene or opaque minerals. Accessory opaque minerals (usually less than 2%) are mainly ilmenite and magnetite with occasional biotite.

3.2.2.2. Amphibolite

Amphibolite is found mainly near to both the western and the eastern margins of Map 3, and represents about 20% of the mafic rock outcrops or about 3% of the area. It usually has a coarser grain size (0.5-2 mm) than the mafic granulite and shows a weak but clearly developed foliation and lineation due to the preferred orientation of prismatic hornblende grains.

Typical amphibolite shows weakly foliated granoblastic texture (similar to Plate 3.1.C) and comprises hornblende (55-66%) and andesine (30-40%) with or without clinopyroxene (0-2%), garnet (0-1%), biotite (0-5%) and quartz (0-3%). Accessory minerals are mainly ilmenite, magnetite and sphene.

3.2.2.3. Deformed and retrograde mafic granulite

Some rocks consisting of mainly hornblende and plagioclase contain mafic granulite relics. This rock type is considered to be derived from the mafic granulite during deformation and retrogression. Outcrops of this rock type make up 60-65% of the overall mafic rocks or 6-9% of the whole area. The rocks show a very intense lineation but also a less well developed foliation. The rock outcrops look very like typical amphibolite but contain individual grains of relict orthopyroxene or elongate aggregates of relict mafic granulite (0.5-1 mm X 2-5 mm) in thin section. The proportion of mafic granulite relics is variable in this rock type, which grade laterally into typical mafic granulite. This lithology and the typical mafic granulite are shown as a single unit on Map 3, because they are in fact two variants of one geological body showing different degrees of deformation and retrogression.

This lithology shows a bimodal microstructure in thin section. It consists of porphyroclasts (1-3 mm) of pyroxene and a matrix (0.05-2 mm) of recrystallized hornblende and plagioclase (Plate 3.1.D & E). The proportions of porphyroclasts vary from 5-50%. The matrix consists of a typical amphibolite mineral assemblage, i.e. plagioclase and hornblende, with or without garnet and biotite. The plagioclase contains 45-54% anorthite, which is less basic than that in the typical mafic granulite described above. Some samples show grain size reduction of the coarse pyroxene, where the aggregates of fine-grained orthopyroxene have replaced the coarse pyroxene porphyroclasts (Plate 3.1.F)

Weakly deformed and retrogressed mafic granulite is found near Panikan Dam. Hypersthene in this rock has coronas of hornblende. The intergrowth of garnet and iron oxide may also result

from the breakdown pyroxene (Plate 3.1.G).

3.2.3. Orthogneisses

The orthogneisses include major granitic gneiss and minor tonalitic gneiss whose relationship to each other is not clear. No charnockitic gneiss has been found in the Oonagalabi Tongue.

The granitic gneiss forms thick layers intercalated with other metamorphic rocks and shows a prominent internal compositional layering and layer parallel schistosity (Plate 3.1.H). It consists essentially of K-feldspar (30-50%), oligoclase (10-30%), quartz (20-30%) and biotite with or without hornblende, garnet, muscovite and epidote. Sillimanite is rare. Accessory minerals are usually zircon, apatite, sphene, allanite and magnetite. The K-feldspars are mainly microcline with minor perthite.

Microscopic study reveals various mineral assemblages. In addition to essential quartz, feldspar and biotite, the assemblages may include: hornblende; garnet; muscovite; sillimanite; hornblende & garnet; hornblende & muscovite; hornblende & epidote; garnet & muscovite; muscovite & epidote.

Tonalitic gneiss was not recognized in the field. However, a few samples show mineral assemblages including plagioclase (60-69 %), quartz (20-25%), hornblende (2-3%), biotite (3-10%), garnet (2-5%) and accessory minerals and thus are recognized as tonalitic gneiss. Some other samples have a mineral assemblage of plagioclase (55%), hornblende (30%), quartz (10%) and biotite (5%), similar to that of quartz diorite (e.g., sample 3669A).

3.2.4. Migmatitic gneiss

Migmatitic gneisses exist sporadically within the Oonagalabi Tongue and grade into granitic gneiss. The leucosome layers in

migmatitic gneiss are usually clearly separated from the mesosomes and parallel the schistosity of the micaceous mesosomes (Plate 3.2.A). However, cross cutting leucosome veinlets also occur (Plate 3.2.B). The mesosomes have similar compositions to the pelitic gneiss, whereas the leucosomes have similar compositions to the granitic gneiss. The origin of the leucosome veinlets is still controversial; some may occur by in situ partial melting, others may occur by injection of molten material from deeper levels.

3.3. Structure

3.3.1. Introduction

The overall structure of the Oonagalabi Tongue is shown on Maps 2 & 3 and Fig. 1-1. Its eastern part is the most complex part of the Harts Range area. No diagnostic stratigraphic markers or younging features are present and none of the major lithological layers can be traced across the whole area. Furthermore there is a great variety of fold scales with fold amplitudes varying from 10 km to a few cm and a very complex structural interference resulting from at least four generations of isoclinal folds (Fig. 3-1 & 3-2). The complex interference patterns and lack of stratigraphic markers have made it very difficult or impossible to identify fold generations in the specific isolated outcrops of this area. However in the central part of the Oonagalabi Tongue a major mafic granulite sequence has been mapped continuously over a strike distance of 10 km, and has allowed a resolution of the macroscopic structure (Map 3 & Fig. 3-2).

Altogether seven overprinted phases of ductile folding deformation plus five phases of thrusting deformation have been recognized and are listed in Table 3-1 with a correlation to other SOB

FIGURE CAPTIONS OF PLATE 3.2

A: Contrasting compositional layering in the migmatitic gneiss. It is formed by alternations of pelitic biotite garnet gneiss with migmatitic leucosomes or pegmatitic veins. Location No.3669; south of the Oonagalabi Tongue.

B: Disharmonic irregular folds within the typical migmatitic gneiss. Most of the leucosome layers are parallel to the schistosity of biotite gneiss. However cross cutting leucosome veinlets are common (at the left margin of the picture). Location No.3869; east of the Oonagalabi Tongue.

C: A profile of a parasitic BF_2 fold in banded granitic gneiss. Its hinge plunges at 17°-033°. North of the Oonagalabi Tongue; location No.3611.

D: A true profile view of a sample collected from the core of the BF_2 fold shown in (C:).

E: A sketch of the photo shown above emphasizing the BS_2 axial planar schistosity. The thickness ratio between the hinge and the limb varies, up to 10:1.

F: Lefy: Isogon diagram of the BF_2 fold shown above shows that it mainly belongs to Class 2 type (similar fold) of Ramsey's (1967) classification but different bands can be assigned to class 1c or class 3 types.

Right: A sketch of the fold shown above showing an apical angle of 30°-37°.

G: Small-scale spiral fold within the SOB marble. Location No.4278, S of the Panikan Dame, The Oonagalabi Tongue.

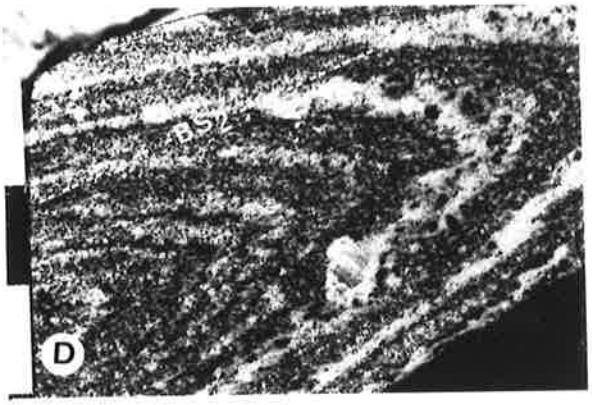
H: Micrograph showing the BS_2 axial planar foliation which transects the BS_1 compositional layering. BS_2 foliation is manifested by the preferred orientation of biotite. Field of view: 11 mm X 15 mm.

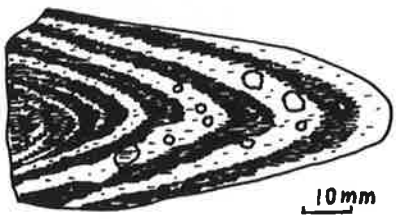
Plate 3.2



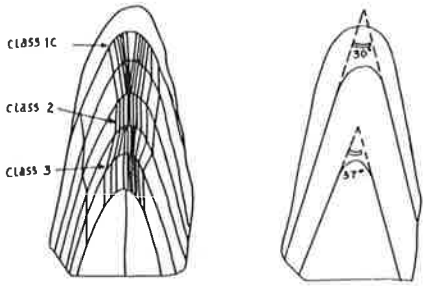




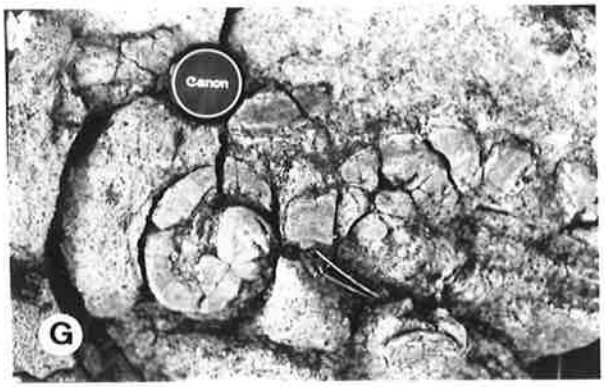


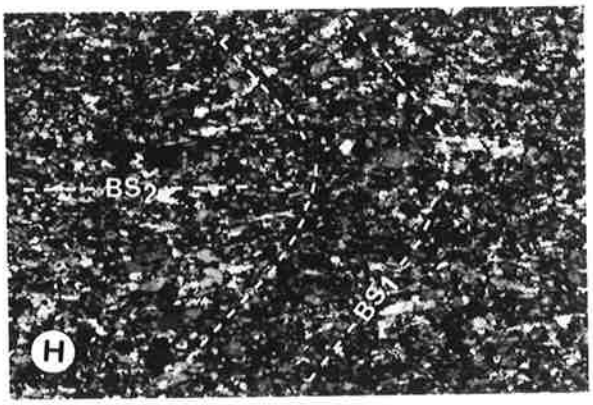


E



F





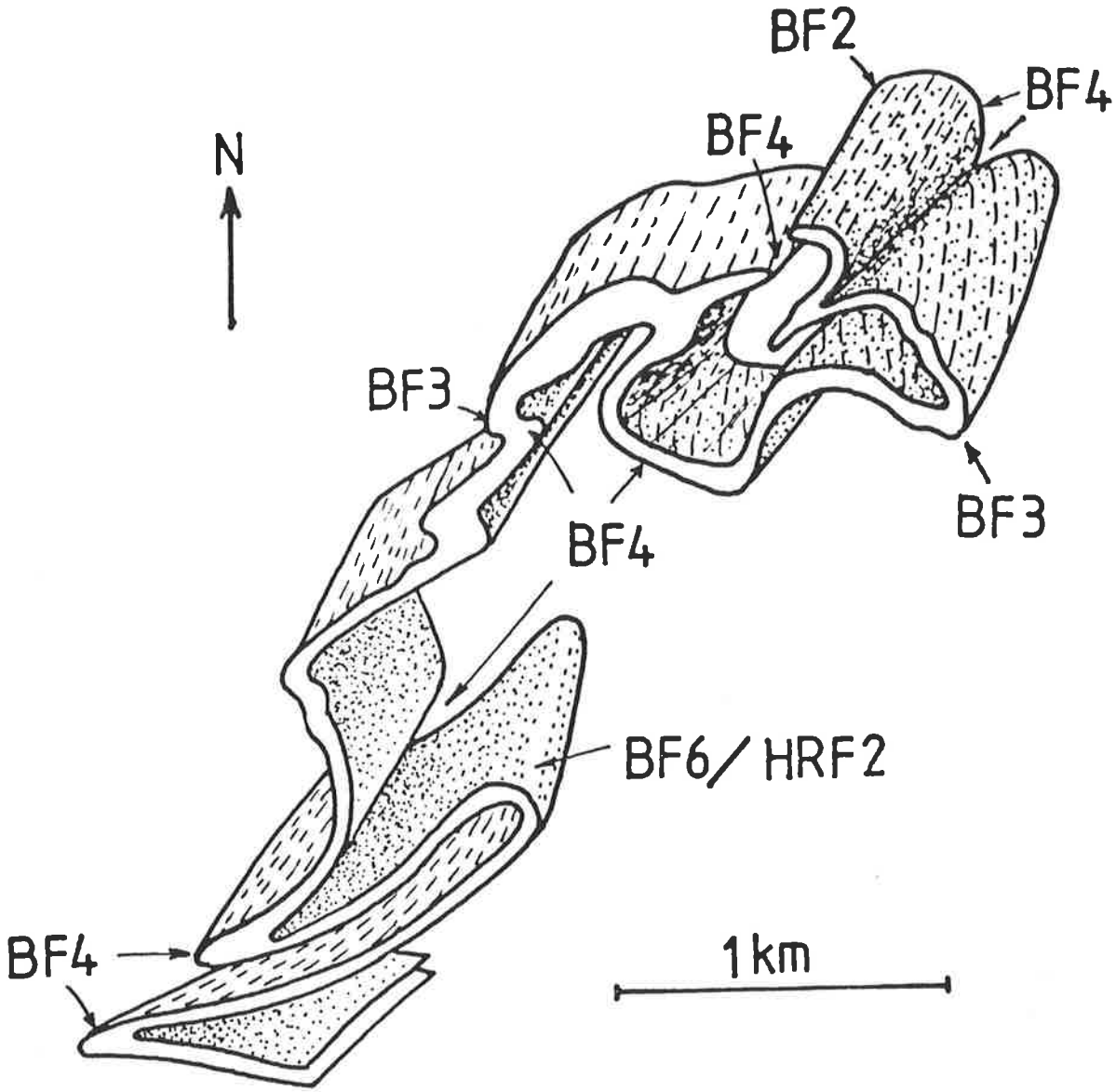


Fig. 3-1 Perspective diagram illustrating the interference between BF_2, BF_3, BF_4 and BF_6 / HRF_2 folds in the central part of Oonagalabi Tongue. The dashed line represents the BL_1 lineation. This diagram is based on the geology depicted in Map 3.

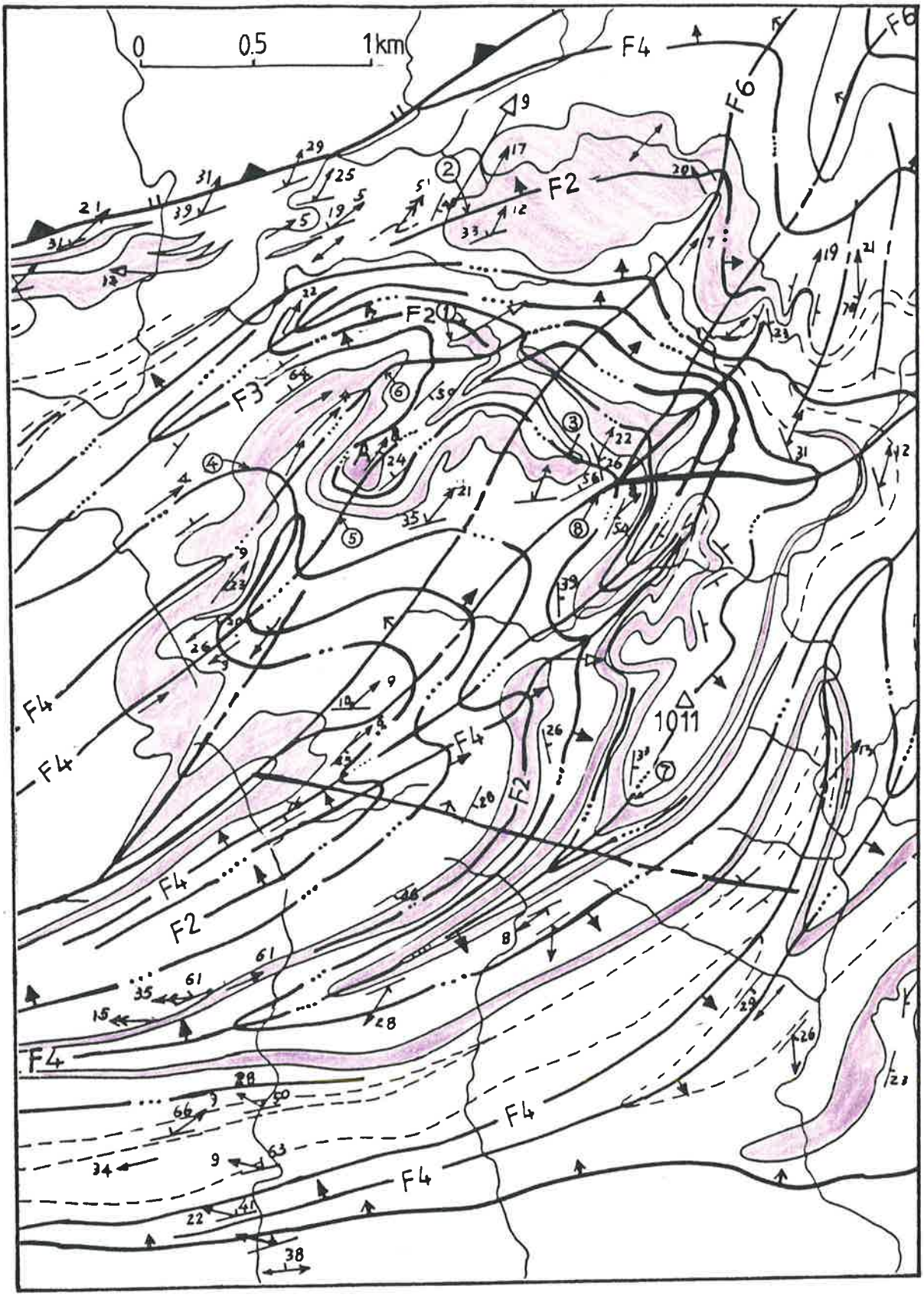


Fig. 3-2

domains.

Table 3-1 CORRELATION OF STRUCTURAL EVENTS WITHIN THE SOB

	Oonagalabi Tongue	Hale River Region and Entia Dome
Post-HRO		Illogwa Shear Zone
deformation	Steep faults	Steep faults
	Open folds	Open folds
Harts Range	HRT_4 (Muller Thrust)	HRT_4 (Muller Thrust)
Orogeny	HRF_3 (BF_7)	Local reclined fold
	HRT_3 (Bruna Thrust)	HRT_3 (Bruna Thrust & Entia Thrust)
	HRF_2 (BF_6)	
	HRT_2 (Maud Thrust)	
	HRF_1 (BF_5)	
	HRT_1 (Oonagalabi Thrust)	
Strangways	BT (White Lady Thrust and Pannikan Thrust)	BT (Huckitta Thrust)
Orogeny	BF_4	BF_4 (in Hale River R.)
	BF_3	BF_3
	BF_2, BS_2, BL_2	BF_2, BS_2, BL_2
	BF_1?, BS_1, BL_1	BF_1, BS_1, BL_1
	BS_0	BS_0

Note: Structural abbreviations "HR" represent structures affecting both the HOB and SOB. Other abbreviations are same as those of Table 2-4, except for the BF_5 to BF_7, which do not imply belonging to the Strangways Orogeny but represent an evolutional sequence within the SOB.

The first four phases of folding (BF_1 to BF_4) and the earliest thrusting (BT) are considered to belong to the Strangways Orogeny and are described here, whereas the other three phases of folding (BF_5 to BF_7) and four phases of thrusting (HRT_1 to HRT_4) are assigned to the Harts Range Orogeny (HRO) and thus are only

introduced in the Table to emphasize the complexity of the structural history of the Oonagalabi Tongue and they will be described in detail in Chapter 7. Post HRO structures are omitted.

3.3.2. Pre-BD_1 to BD_1 structures

The major lithological boundaries between supracrustal layers and orthogneisses, and a layer parallel fabric in the mafic lithologies are recognized as pre-BD_1 planar structural elements (BS_0), similar to those of the Entia Dome and the Hale River Region. Any possible earlier deformation (thrusting) has been obscured by later voluminous plutonic activity.

An ubiquitous compositional layering, layer parallel schistosity and a prominent mineral lineation in the orthogneisses are the main fabrics in the area. As the BS_1 gneissic layering and layer parallel schistosity, and the BL_1 mineral lineation are related to BF_1 folds in the Entia Dome (see chapter 2), it is assumed that the earliest fabrics, BS_1 & BL_1 within the orthogneisses in the Oonagalabi Tongue are also related to BF_1 folds. Unfortunately no large-scale or small-scale BF_1 folds have been found or mapped in the area. The BL_1 lineation is assumed to be parallel to hinges of BF_1 folds in comparison with that found within the Entia Dome.

The BS_1 layer parallel schistosity is manifested by the preferred orientation of mica in gneisses and of prismatic amphiboles in amphibolite while the BL_1 lineation is manifested by the alignment of biotite, amphibole, garnet, etc. (e.g. Plate 3.3.C, D & G), or the streaky shape and preferred orientation of mineral aggregates (e.g. Plate 3.1.D & E).

3.3.3. Structures of the second deformation (BD_2)

BF_2 folds are recognized by the deformation of the BS_1 fabric. One major BF_2 fold (fold No.1 in Fig. 3-2) has been mapped on the regional scale in the northern and central area of the Oonagalabi Tongue (see also Map 3). It is an isoclinal fold with a typically thickened hinge and two intensely attenuated limbs. A layered sequence of mafic granulite, about 20-50 m thick, forms the fold core. The banded granitic gneiss sequence involved can be traced continuously from one limb to the other. The mafic granulite layer is poorly foliated and rather homogeneous, while the surrounding gneiss layers show a very well developed layer parallel schistosity (BS_1) which is folded by the BF_2 fold. This fold closes to the west with a hinge zone plunging at 20^{o}-050^{o}. Its mafic granulite core extends continuously for over 10 km and finally pinches out within the dominant granitic gneisses. No axial plane fabric has been observed at this closure.

Another major BF_2 fold (fold No.2 in Fig. 3-2) shows a greatly thickened hinge zone and short thin limbs with a hinge/limb thickness ratio estimated at about 20:1. An intense elongation lineation parallels the hinge zone and plunges at 18^{o}-042^{o}.

Some small tight inclined angular folds observed on the outcrop scale have been recognized on style, orientation and congruity as parasitic BF_2 folds (Plate 3.2.C). They show thickened hinges and attenuated limbs with a varying hinge/limb thickness ratios of up to 10:1 (Plate 3.2.D & E). The various profiles of different layers (Plate 3.2.F) can be classified as Class 1c, Class 2 and Class 3 types (This and all subsequent fold classifications refer to the isogon classification system of Ramsay, 1967). The apical angles of the two limbs range from 30^{o} to 37^{o} (Plate 3.2.G). An axial planar fabric (BS_2) is visible both on the

outcrop and in specimens (Plate 3.2.D) and is oblique to the compositional layering (BS_1) in the hinge area but parallel to BS_1 in the limbs. A weak intersection lineation (BL_2) also occurs in the hinge.

In thin section, the BS_1 compositional layering and layer parallel biotite flakes have been significantly disturbed by BS_2, which is defined by intensely reorientated biotite flakes and elongate garnet grains within, but oblique to, the compositional layering (Plate 3.2.H).

The BL_1 lineation was obviously folded obliquely by the BF_2 folds. For example, at an outcrop (Plate 3.3.A, C & D) near Panikan Dam, a BF_2 fold shows a very tight profile which involves a layer of quartzofeldspathic gneiss of almost uniform thickness and is classified as Class 1c type (flattened parallel fold) (Plate 3.3.B). A very weak intersection lineation (BL_2), which can be seen on the outcrop and in hand specimens but is not clear on the figure, appears to form only at the fold hinge and parallel the fold axis, whereas an intense BL_1 mineral lineation appears on the surface of the gneissic layering (BS_1), oblique to the fold axis, and can be traced from one limb across the hinge area to the other limb (Plate 3.3.E). BL_1 on the southern limb is almost perpendicular to the BF_2 fold hinge but the angle of intersection is apparently reduced in the hinge area (Plate 3.3.F). This is interpreted as the result of inhomogeneous strain accompanying the BF_2 folding, similar to that occurring in flattened parallel (flexural-slip) folds illustrated by Ramsay (1967, p.466). The rock in the hinge zone has been stretched in the direction of the fold axis.

At many outcrops, the orientation of the BL_1 lineation on the surface of one gneiss layer differs from that of BL_1 on adjacent

FIGURE CAPTIONS OF PLATE 3.3

A: A profile view of a minor BF_2 fold. North of Panikan Dam, middle of the Oonagalabi Tongue; location No.3643.

B: A profile sketch of the minor BF_2 fold in (A:). The more competent leucocratic granitic gneiss layer (stippled), retains almost equal thickness within the less competent biotite-rich granitic gneiss. Isogon diagram of the BF_2 shown above indicates that the fold shown above belongs to Class 1c type of Ramsay's classification.

C: The hinge of the fold in (A:), which plunges towards the camera. The BL_1 lineation is folded around the the BF_2 fold hinge.

D: North or upper limb of the fold in (A:). The fold hinge defines the left margin of the outcrop. An intersection angle between the fold hinge and BL_1 lineation can be seen as about 30°.

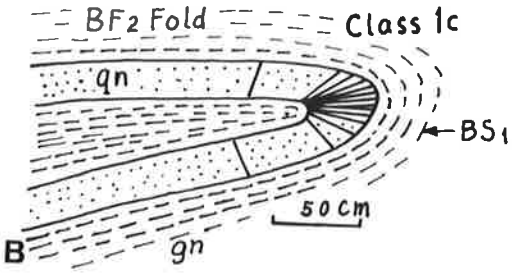
E: Field sketch of the fold in (A:) showing the variation of BL1 lineation on the surface of the leucocratic granitic gneiss. On the south limb of the fold, BL_1 lineations vary from shallowly plunging towards the NW, via horizontally trending E-W to shallowly plunging towards the NE, but on the north limb of the fold all the lineations plunge shallowly towards the NE. The lineation can be traced continuously from one limb to another.

F: Stereogram illustrating the relationship between the BF_2 fold axis, BL_1 and BS_1. The intersection angles between BF_2 fold axis and BL_1 are variable which may imply a stretching along the direction of fold axis.

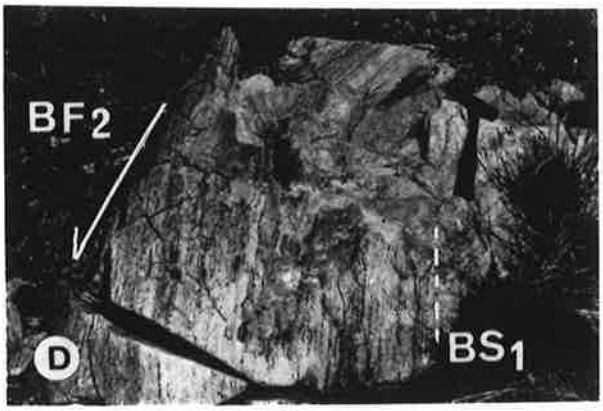
G: BL_1 lineation on adjacent gneissic layers display different orientations. The lineation on the back layer plunges at 10°-279° (parallel to the pocket knife), whereas the lineation on the front layer plunges 10°-057° (parallel to the pencil). Location No.3669; the Oonagalabi Tongue.

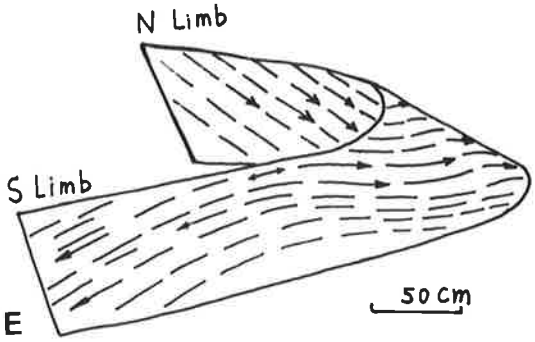
Plate 3.3

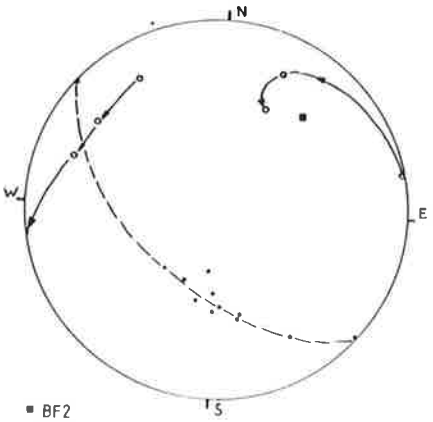

A


BF2 Fold
Class 1c
qn
BS1
50 cm
B
gn


C


BF2
D
BS1


N Limb
S Limb
50 cm
E


N
W
E
S
BF2
BL1
pole of BS1

F


G

layers, thus implying that the two adjacent gneiss layers are probably the same layer which was folded by, and forms the core of, an isoclinal BF_2 fold. Plate 3.3.G is an example which shows that BL_1 on the surface of one gneiss layer plunges at 10^{o}-057^{o}, whereas the BL_1 of the adjacent layer plunges at 10^{o}-279^{o}.

3.3.4. Structures of the third deformation (BD_3)

Four major BF_3 folds have been mapped on the regional scale (Map 3). Two of these (fold Nos. 3 & 4) are indicated by the folded axial surface of the No.1 BF_2 fold (Fig. 3-2). These BF_3 folds are isoclines with amplitudes of about 1.5 km. The upper fold (No. 3) closes to the SE, plunging at 23^{o}-029^{o}, with a gneiss core of about 50 m in thickness and two mafic granulite limbs which are actually the core of the No.1 BF_2 fold. The mafic layers form a rather rounded cylindrical closure but have totally parallel limbs. The lower fold (fold No.4 on Fig. 3-2) closes to the NW with a doubly or triply thickened hinge plunging at 4^{o}-040^{o}. Its gneiss core dips very gently and thus appears very wide on the map. It is very difficult to estimate the real thickness of the hinge, because of the interference of BF_2 folds and other later folds. This BF_3 fold pair does not show a clear vergence (Bell, 1981) but is rather symmetric. The fold axes of BF_3 and BF_2 folds are almost parallel, thus resulting in a type 3 fold interference pattern (Fig. 3-1).

3.3.5. Structures of the fourth deformation (BD_4)

Five major BF_4 folds are shown on Map 3. These folds are mainly inclined tight folds with axial surfaces dipping towards the NW and fold axes plunging towards the NE. The amplitudes of these BF_4 folds range from 0.5 to 1.5 km which is much smaller

than that of the BF_3 and BF_2 folds. One fold pair of an antiform (fold No.6 in Fig. 3-2) and a synform (fold No.5 in Fig. 3-2) shows a SE vergence. The axial surfaces of BF_3 folds are refolded by the BF_4 folds. One isolated outcrop (location A in Fig. 3-2) of mafic granulite in the hinge of the No.5 BF_4 synform is part of the upper limb of the No.3 BF_3 fold, from which it has been separated by erosion due to the very shallow plunge (8^o-034^o) of the No.5 BF_4 synform. Profiles of these BF_4 folds vary from broad in the northern area to narrow or tight in the southern area (see cross section on Map 3). Outcrop scale BF_4 folds have buckled profiles (e.g. Plate 3.4.A & B). Alternating cuspate and lobate folds in these examples were formed due to intercalation of more competent granitic gneiss and less competent mafic (in Plate 3.4.A) or micaceous gneiss (in Plate 3.4.B) lithologies (Ramsay, 1984). The BF_4 and BF_3 folds are also subcoaxial resulting in a type 3 fold interference pattern. The tectonic interpretation of superimposed polyphase folding will be discussed in chapter 8.

3.3.6. Shear zones within the Oonagalabi Tongue (BT)

Shearing deformation occurred after the fourth phase of folding in the Oonagalabi Tongue and produced discrete cross-cutting schist or mylonite zones. A number of shear zones are observed in the field but only two major ones have been mapped as thrusts on a regional scale (Map 2 & Fig. 1-1) and these are regarded as the result of a deformational event of basement thrusting (BT). The thrusts extend for over 30 km and crosscut the lithological layers and fold axial surfaces at various angles. The thrusts are truncated obliquely at both ends by major marginal shear zones of the later Harts Range Orogeny.

The structurally upper thrust is best observed 1 km to the

FIGURE CAPTIONS OF PLATE 3.4

A: Minor BF_4 folds in the hinge of a major BF_4 fold (fold No.7). Fold axes plunge at 15°-252° and axial plane dips 68°-316°. The cuspate and lobate shape of the profile indicates that the granitic gneiss was more competent than the thin layer of mafic granulite during folding. Location No.3680; S of the Oonagalabi Tongue.

B: Profile view of cuspate and lobate folds. The light granitic gneiss was more competent than the thin layer of melanocratic biotite schist during the folding. Location No.3755; S of the Oonagalabi Tongue.

C: Migmatitic gneiss showing a type 3 interference pattern between BF_2 and BF_3 folds. Isoclinal BF_2 folds are folded by very tight to isoclinal BF_3 folds. Location No.3740; N of Panikan Dam, the Oonagalabi Tongue.

D: Fold interference pattern between BF_2 and BF_3 (?) folds. The mafic granulite hinge (stippled) is wrapped around by granitic gneiss (dashed lines). The BF_2 axis parallels the BF_3 axes but is oblique to the BL_1 lineation. Location No.3849; the Oonagalabi Tongue.

E: Interference between BF_2 and BF_3 folds within granitic gneiss. Location No. 3740; the Oonagalabi Tongue.

F: Interference between BF_2 and BF_3 folds within granitic gneiss. Locaton No.3735; the Oonagalabi Tongue.

G: The White Lady Thrust is manifested by a mylonitic shear zone. Location No.4299; SE of Panikan Dam.

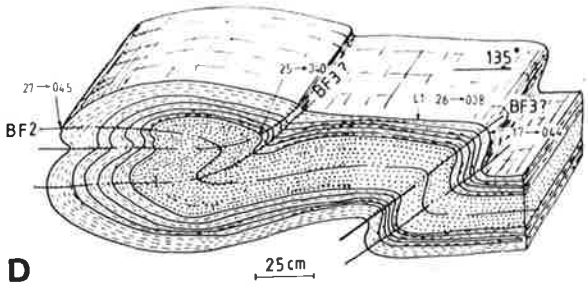
H: An augen-like remnant of granitic gneiss appears in biotite schist from a shear zone along the White Lady Thrust. Location No.4299; SE of Panikan Dam.

Plate 3.4

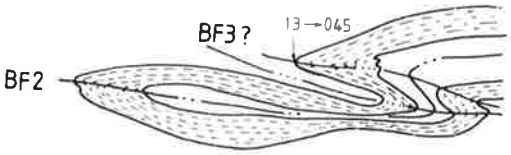

A


B

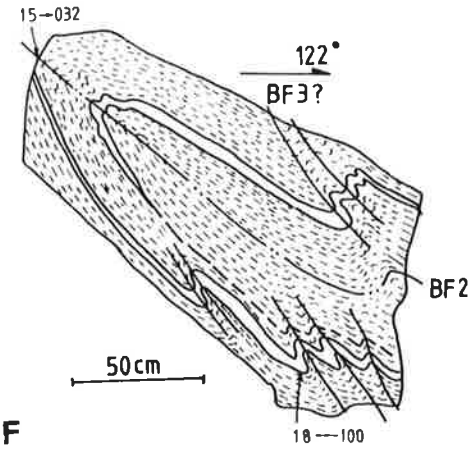

C


135°
BF3?
BF2
25cm

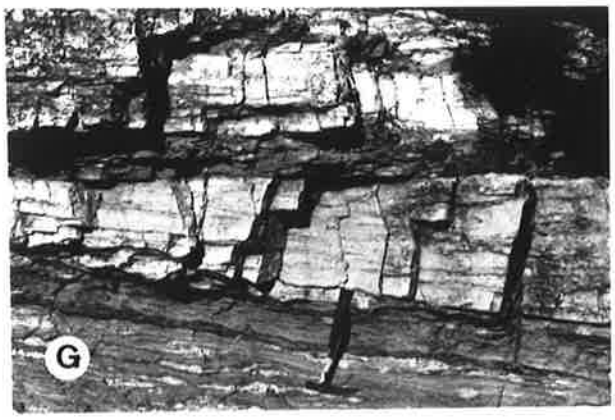
D


BF3?
13→045
BF2

E


15→032
122°
BF3?
BF2
50cm
18→100

F


G


H

south of Panikan Dam and is named the Panikan Thrust (Fig. 1-1). It is defined by a blastomylonite zone, of about 20 meters in thickness, which dips 20-50° N to NE. This thrust is subconcordant to the regional structure of the northern or upper block, but sharply truncates the structure of the southern or lower block which trends northerly and dips nearly vertically (Map 2). However two sets of schistosities, can be detected in the field in the mafic granulite and acidic gneiss layers of the lower block. The later schistosity trends parallel to the blastomylonite zone but crosscuts the early schistosity and gneissic layering (BS_1) at high angles.

The structurally lower zone is named the White Lady Thrust (Fig. 1-1) which lies 2-3 km to the south of the Panikan Thrust, showing similar trends and dips. The structures of the upper block to this zone are truncated at high angles by the White Lady Thrust but are sheared to low angle contacts within 500 metres above the thrust boundary (Map 2). A thrust sheet, about 2-3 km wide or 1-1.5 km in thickness, is thus formed between the two major thrusts. The structures of the foot wall block to the White Lady Thrust are almost parallel to the thrust. An anastomosing shear zone, of about 200 m overall width, is developed along the White Lady Thrust, which includes a few narrow zones of mica schists, blastomylonites and lenses of low strained host rock.

The blastomylonite has a mylonitic microstructure including 80% of coarse grained (0.5-4 mm) porphyroclasts and 20% of fine-grained (0.01-0.25 mm) matrix. The porphyroclasts are perthite, plagioclase and quartz, whereas fine grains of sillimanite (3%) and garnet (very few) are found only within the quartzofeldspathic schistose matrix (e.g. sample No. 4299). The mica schist zone includes 5-10% of porphyroclasts of granitic gneiss (Plate 3.4.G).

These porphyroclasts can be as large as 10 cm and are wrapped around by the schistosity (Plate 3.4.H). This kind of schist is considered to represent a recrystallized mylonitic matrix which was formed during the mylonitization of a coarse-grained granitic gneiss as it is only developed along the thrust boundary. A northerly trending stretching lineation is weakly developed within the blastomylonites.

A short thrust zone (about 3 km long) in the NE corner of the Oonagalabi Tongue, 1 km south of Mt Brassy, and a major thrust zone in the SE of the Oonagalabi Tongue (Map 3) are interpreted as two discrete segments of the White Lady Thrust. This is likely because these segments of thrust zones are structurally at the same level as the White Lady Thrust and are all sheared by the marginal thrusts of the Oonagalabi Tongue.

The Panikan Thrust and the White Lady Thrust are temporally assigned to the SOB. It is also possible that these thrust were developed during the Florence Movement (see chapter 6).

3.3.7. Fold interference

Fold interference patterns formed between two fold generations are quite complicated and their geometry has been systematically examined by Ramsay (1967). Three types of interference patterns have been classified based on the orientation relationships between the interferring folds (Ramsay, 1967), and this classification has been reexamined by Thiessen and Means (1980). The significant influence of early fold shape on the pattern of fold interference has been experimentally tested by Watkinson (1981). However, fold interference patterns between three or even more fold generations are much more complicated and have not been fully examined or classified. Nine possible patterns may potentially be derived from interference between three fold generations

and twenty seven patterns from four fold generations, etc.. Further much more detailed study is necessary for a systematic classification of fold interference patterns. Computer modeling would be a tempting task but it is beyond the aim of this thesis. However, in the Oonagalabi Tongue, an interference between, at least, five fold generations has been recognized and the resulting overprint shapes are described and discussed here.

The interference between the BF_2 and BF_3 folds or between the BF_3 and BF_4 folds is similar to the type 3 interference patterns of Ramsay (1967). The fold axes of these generations are subparallel but the axial surfaces are variably oblique. Outcrop-scale Type 3 fold interference patterns can be seen at many locations. However, it is not always possible to prove whether the interference occurs between BF_2 and BF_3 or between BF_3 and BF_4 or between BF_2 and BF_4. Some examples of fold interference are shown on Plate 3.4.C, D, E & F. The interference between the major BF_2, BF_3 and BF_4 folds is illustrated by the perspective diagram of Fig. 3-1.

The interference between the earlier folds (e.g. BF_2, BF_3 and BF_4) and later folds of the Harts Range Orogeny (e.g. HRF_2 folds, see chapter 7) results in luniform or mushroom shape interference patterns which are similar to the Type 2 fold interference pattern of Ramsay. This is due to the high intersection angles between their hinges (Map 3 and Fig. 3-2). (The interference between HRF_1 and HRF_2 folds also produced excellent luniform and mushroom-shape outcrop patterns, and forms basement windows within the HRSC, see detailed description in Chapter 7).

The high degree of variation of all of the fold axes and BL_1 lineations, though predominantly trending NE, is illustrated by the stereograms shown on Map 3 and is considerd to result from the

complex interference between all fold generations.

3.4. Metamorphism

Lithologies in the Oonagalabi Tongue have been studied in more detail than those of the other SOB domains. Two sequential metamorphic events are recognized; the earlier granulite facies event and the later amphibolite facies event. Evidence of retrogression from granulite to amphibolite facies isobserved. A distinctive feature is the intercalation between granulite facies supracrustal lithologies and amphibolite facies orthogneisses. Various geothermometers have been used to estimate metamorphic temperature, but no reliable pressure has been obtained. A pressure of 7 $\pm$2 kb as estimated from the SOB rocks in the Strangways Range by Warren (1983) and in the Hale River Region by Oliver et al., (in press, Appendix V) has been adopted here.

3.4.1. Granulite facies metamorphism

The mafic granulites in the Oonagalabi Tongue contain orthopyroxene, clinopyroxene, hornblende and feldspar and thus display granulite facies assemblages (Winkler, 1979, pp. 256-271). The chemical composition of these minerals has been analysed by electromicroprobe (see appendex II). The metamorphic temperature of the mafic granulite has been determined by two pyroxene geothermometry and is shown in Table 3-2.

Table 3-2 TEMPERATURES TWO-PYROXENE GEOTHERMOMETRY (MAFIC GRANULITE)

sample number	Wood & Banno (1973)	Wells (1977)
3729	820	865
3645	790	810
3615	780	805
average	795	825

Pelitic-semipelitic gneiss contains biotite and garnet but no orthopyroxene. Its metamorphic temperature has been estimated from different garnet - biotite geothermometers and is shown in Tables 3-3 to 3-6. The centres and rims of garnet have slightly different compositions (Appendix II) and thus yield different temperature ranges, although the biotite does not show compositional zoning.

The temperatures calculated from analyses of garnet-centres and biotite range from 695-875°C using different methods (Table 3-3). The results of Perchuk (1976) and of Thompson (1976) are very close to each other, but a bit lower than the results of the other two methods. The results of Goldman & Albee (1977) are in some cases higher, but in other cases lower than the results of Ferry & Spear (1978). The temperature range (810-875°C) from Ferry & Spear's method (1978) is regarded as the peak temperature of metamorphism of the pelitic-semipelitic gneiss; this is very close to the temperature range (780-865°C) of the mafic granulite. (In this thesis, temperatures estimated from garnet - biotite geothermometer of Ferry & Spear, 1978, are prefered for consideration and discussion. Estimates from other methods are presented without discussion.) The garnet - biotite geothermometry is almost pressure independent as shown by the results in table 3-3. A high water pressure and K content of the metasediments was probably responsible for the predominent occurrence of biotite and lack of orthopyroxene.

Table 3-3 TEMPERATURES FROM GARNET-CENTRE AND BIOTITE IN PELITIC GNEISSES

sample No.	Perchuk (1976)	Thompson (1976)	Goldman & Albee (1977)	Ferry & Spear (1978) 7Kb	7.5Kb	8Kb	8.5Kb
146833	718	750	777	866	868	871	873
3770	695	720	756	814	816	819	821
3734	693	720	755	811	813	816	818
average	703	730	766	830	832	835	837

The temperatures calculated from analyses of garnet-rims and biotite range from 728-842°C (Table 3-4, Ferry & Spear, 1978), which are 30-80°C lower than the peak metamorphic temperature. The composition of garnet-rims may have been affected by Mg-Fe exchange processes during the cooling period but the zoned structure of garnet suggests that the cooling system was not equilibrated.

Table 3-4 TEMPERATURES FROM GARNET-RIMS AND BIOTITE (PELITIC GNEISS)

sample No.	Perchuk (1976)	Thompson (1976)	Goldman & Albee (1977)	Ferry & Spear (1978) 7Kb	7.5Kb	8Kb	8.5Kb
146833	704	735	765	835	837	840	842
3770	661	675	728	744	746	749	751
3734	652	660	721	728	730	733	735
average	673	690	738	769	771	774	776

A few biotite flakes occur as inclusions within garnet crystals and show slightly different compositions from other biotite. Metamorphic temperatures of the pelitic-semipelitic gneiss have thus also been calculated from analyses of these garnet-centres and adjacent biotite inclusions and are shown in Table 3-5.

Table 3-5 TEMPERATURES FROM GARNET-CENTRES AND BIOTITE INCLUSIONS (PELITIC GNEISS)

sample No.	Perchuk (1976)	Thompson (1976)	Goldman & Albee (1977)	Ferry & Spear (1978) 7Kb	7.5Kb	8Kb	8.5Kb
146833	630	630	702	683	685	688	690
3770	631	640	704	686	688	691	693
average	631	635	703	685	687	690	692

The temperature range from 685-695°C (Ferry & Spear) is 135-180°C lower than the peak metamorphic temperature of the pelitic-semipelitic gneiss. It is possible that the temperature from garnet-centres and biotite inclusions represents an earlier amphibolite facies metamorphism and the peak temperature represents a

later granulite facies metamorphism during the Strangways Orogeny. However it is more likely that the lower temperature represents a result of local Mg-Fe exchange during later cooling, as the Mg-Fe exchange between biotite inclusions and the host garnet might be more effective.

3.4.2. Amphibolite facies metamorphism

The granitic gneiss in this area contains biotite and garnet but no orthopyroxene, which contrasts with the charnockitic gneiss within the Claraville subarea of the Hale River Region (see chapter 2). The granitic gneiss would thus seem to indicate the effects of the amphibolite facies metamorphism; either due to lower temperature or to higher water pressure, or theoretically to both.

The metamorphic temperature of the granitic gneiss has been derived from the application of biotite - garnet geothermometers. Temperatures derived from analyses of garnet centres and biotite are considered to represent the peak temperature of the granitic gneiss and are shown in Table 3-6. A wide range of 553-790°C (Ferry & Spear) is obtained from various localities. The temperature range is about 85-255°C lower than the peak metamorphic temperature of the pelitic gneiss or 75-225°C lower than that of mafic granulite.

Table 3-6 PEAK TEMPERATURES FROM GARNET-CENTRES AND BIOTITE (GRANITIC GNEISS)

sample No.	Perchuk (1976)	Thompson (1976)	Goldman & Albee (1977)	Ferry & Spear (1978) 7Kb	7.5Kb	8Kb	8.5Kb
146835	680	700	744	783	785	788	790
3780	567	555	655	571	573	576	578
3780A	633	650	706	689	691	694	696
3781	673	695	738	770	772	775	777
3783	556	550	647	553	555	558	560
average	622	632	698	673	675	678	680

Temperatures calculated from analyses of garnet-rims and

biotite are shown in Table 3-7, which are 20-135°C lower than the temperatures from garnet-centres of each sample, but the average temperature ranges are only 25°C lower than those in Table 3-6.

Temperatures calculated from analyses of garnet-centres and associated biotite inclusions are shown in Table 3-8, which are 0-154°C lower, but the average temperature range (555-560°C) is only about 20°C lower than the peak temperature of the granitic gneiss. This temperature variation is also interpreted as the effect of cooling.

Table 3-7 TEMPERATURES FROM GARNET-RIMS AND BIOTITE (GRANITIC GNEISS)

sample No.	Perchuk (1976)	Thompson (1976)	Goldman & Albee (1977)	Ferry & Spear (1978) 7Kb	7.5Kb	8Kb	8.5Kb
146835	610	608	688	647	649	652	654
3780	558	550	649	556	558	561	563
3780A	608	610	686	643	645	648	650
3781	654	678	722	731	733	735	737
3783	619	630	694	663	665	668	670
average	610	615	688	648	650	653	655

Table 3-8 TEMPERATURES FROM GARNET-CENTRES AND BIOTITE INCLUSION (GRANITIC GNEISS)

sample No.	Perchuk (1976)	Thompson (1976)	Goldman & Albee (1977)	Ferry & Spear (1978) 7Kb	7.5Kb	8Kb	8.5Kb
146835	600	595	680	629	631	634	636
3780	507	480	612	473	475	478	480
3780A	596	590	677	622	624	627	629
3783	556	550	647	553	555	558	561
average	565	554	654	555	557	560	562

The intercalation between the granitic gneiss and mafic granulite layers, as well as small inclusions of mafic granulite within the granitic gneiss suggests that the granite intruded into a granulite sequence in a later (post granulite metamorphism)

stage and was subsequently meta-morphosed under amphibolite facies conditions.

The amphibolite in the Oonagalabi Tongue also displays evidence of typical amphibolite facies metamorphic conditions. The garnet - hornblende thermobarometry of Graham & Powell (1984) has been applied to the garnetiferous amphibolite (e.g. sample 3641), and yields a temperature of 655-660^{o}C at 6-7Kb.

Most of the mafic granulite in the Oonagalabi Tongue, has been partially retrogressed to amphibolite. Some of the hypersthene relics have coronas of hornblende or have been partially altered to garnet, magnetite and ilmenite (Plate 3.1.G). The temperature of this amphibolite facies metamorphism has been estimated from the clinopyroxene - garnet thermobarometry of Ellis & Green (1979) as 680^{o}C at 6-7 Kb, which is within the temperature range shown by the granitic gneiss described above.

In the NE part of the Oonagalabi Tongue, rocks are intensly deformed. Some of the mafic granulite has been intensly retrogressed to amphibolite with minor relics of hypersthene (Plate 3.1.D & E) thus implying a locallized retrogressive amphibolite facies metamorphism accompanying the shearing along thrusts. The temperature of the retrogressive metamorphism is indicated by the composition of coexisting recrystallised garnet and hornblende (Graham & Powell, 1984) as 660^{o}C (6-7Kb).

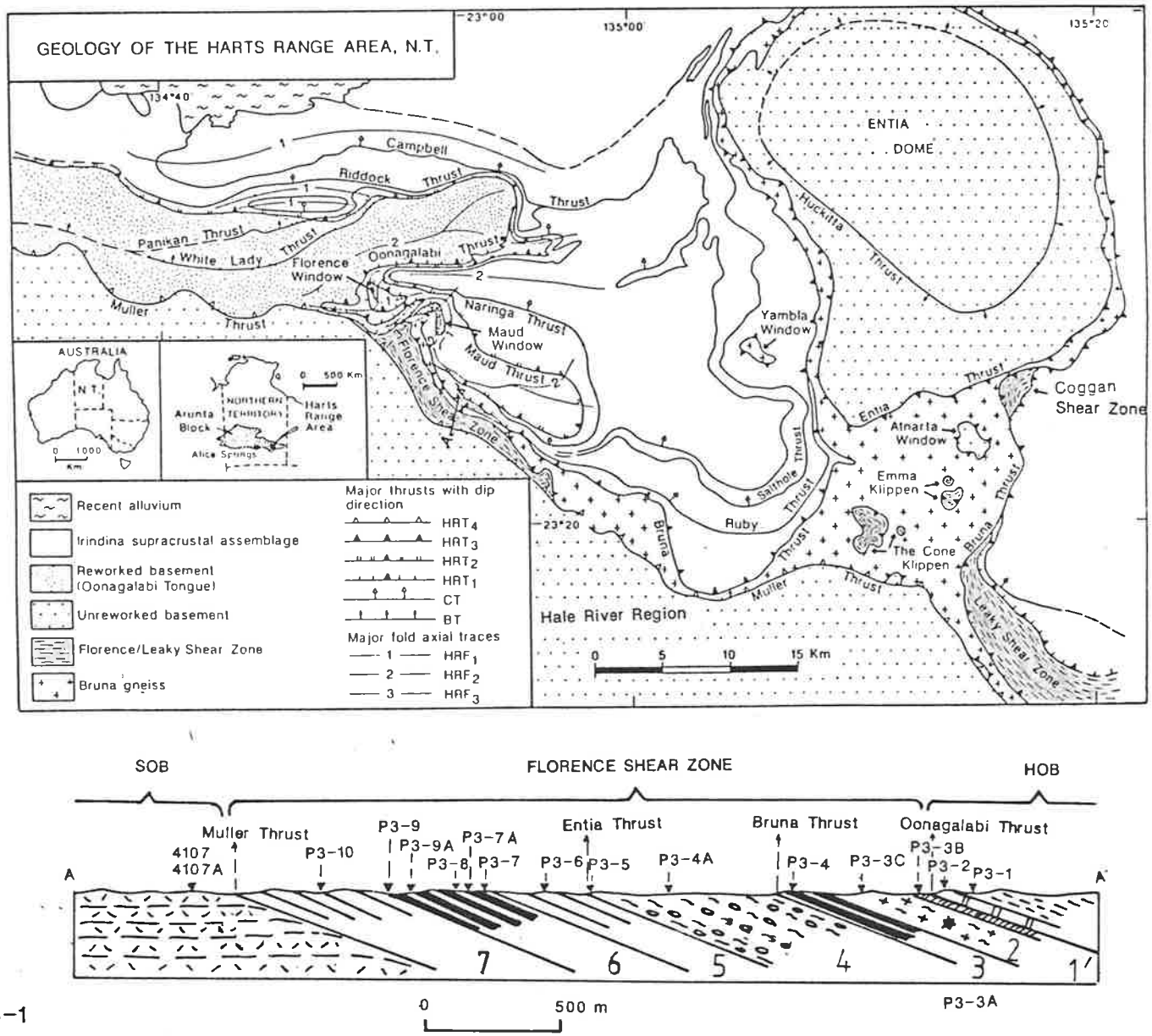
The migmatization probably occurred after peak metamorphism, because the leucosome veinlets were emplaced both along and across the schistosity within the metasediments (Plate 3.2.B).

CHAPTER 4 THE FLORENCE / LEAKY SHEAR ZONE

4.1. Introduction

A large regional shear zone between the Hale River Region of SOB and the Harts Range Supracrustal Cover (HRSC) has been recognized and mapped for the first time in this study (Map 2 & Fig 1-1). This shear zone is a thick sheet-like unit of SOB which has been intensly redeformed by ductile shearing. The zone trends WNW-ESE at right angles to the main structural trend of the Hale River Region of the SOB. The western and structurally lower part of the zone is named the Florence (Creek) Shear Zone (FSZ), whereas the east and structurally upper part is named the Leaky (Bore) Shear Zone (LSZ). Also included as part of the Florence/Leaky Shear Zone (F/LSZ) are a few klippen and smaller isolated shear zone relics, i.e. the Emma Klippen, the Cone Klippen and the Coggan Shear Zone (Fig. 4-1).

The F/LSZ is recognized to have initiated as a part of a major regional extensional detachment zone (see Chapter 7) which was later intruded subconcordantly by metagabbro sills and a major sheet-like body of megacrystic gneissic granite, the Bruna Gneiss, during the earlier stage of the Harts Range Orogeny (Chapter 5), and was reworked by reverse thrusting during the later stage of the HRO (Chapter 7). Four major thrusts are related to the F/LSZ; the Oonagalabi Thrust lies at the top and the Muller Thrust at the base of the F/LSZ, while the Bruna Thrust and the Entia Thrust bound the top and base of the Bruna Gneiss sheet within the F/LSZ. These thrusts will be described in detail in Chapter 7. The Bruna Gneiss sheet, which was also intensly deformed by later polyphase shearing, now lies structurally above the FSZ, but below the LSZ, the Coggan Shear Zone and the Emma & Cone Klippen which were


GEOLOGY OF THE HARTS RANGE AREA, N.T.
23°00
135°00
135°20
134°40
ENTIA
DOME
Campbell
Riddock
Thrust
Panikan Thrust
White Lady
Florence Window
Oonagalabi Thrust
Muller Thrust
Naringa Thrust
Maud Window
Maud Thrust
Florence Shear Zone
Huckitta Thrust
Yambla Window
Coggan Shear Zone
Entia
Atnarta Window
Emma Klippen
The Cone Klippen
Saithole Thrust
Ruby
Bruna
Leaky Shear Zone
Hale River Region
23°20
0 5 10 15 Km
AUSTRALIA
N.T.
0 1000 Km
NORTHERN TERRITORY
Arunta Block
Harts Range Area
Alice Springs
0 500 Km
Recent alluvium
Irindina supracrustal assemblage
Reworked basement (Oonagalabi Tongue)
Unreworked basement
Florence/Leaky Shear Zone
Bruna gneiss
Major thrusts with dip direction
HRT4
HRT3
HRT2
HRT1
CT
BT
Major fold axial traces
1 HRF1
2 HRF2
3 HRF3

SOB
FLORENCE SHEAR ZONE
HOB
Muller Thrust
Entia Thrust
Bruna Thrust
Oonagalabi Thrust
4107
4107A
P3-10
P3-9
P3-9A
P3-8
P3-7A
P3-7
P3-6
P3-5
P3-4A
P3-4
P3-3C
P3-3B
P3-2
P3-1
P3-3A
A
A'
7
6
5
4
3
2
1'
0
500 m

Fig. 4-1

originally parts of the major shear zone but became isolated due to open folding and recent erosion. The metagabbro and Bruna Gneiss will be fully described in Chapter 5.

The F/LSZ is a complex of protomylonites, mylonites and mylonitic gneisses and shows a very complicated deformational and metamorphic history. Some mylonites exhibit granulite facies metamorphic assemblages while others show amphibolite facies assemlages.

Shear zones have been studied by generations of geologists, and have been demonstrated to have formed at many different levels of the crust (Ramsay, 1980; Coward, 1983, 1984; Davies & Coward, 1982; Behr, 1980). Major shear zones usually control the structural framework of an area, for example the Moine Thrust Zone in the NW Scotland (Butler, 1982; White et al., 1982), the Limpopo Mobile Belt in southern Africa (Coward et al., 1976), the Redbank Shear Zone and Harry Creek Shear Zone in central Australia (Allen & Black, 1979), the thrust series in the Himalayas (Coward, 1983), and the Sanbagawa Belt in Japan (Faure, 1983, 1985 a & b). These examples typically show retrograde metamorphic characters. Mylonitization under granulite facies conditions, such as the early phase of mylonitization in the F/LSZ, has rarely been documented.

The significance and petrogenesis of mylonitic rock has been summarized by Tullis et al.(1982). The term "mylonitic rock" was suggested by Tullis et al. to includes three implied features: "(1) grain size reduction, although this is difficult to document if the protolith is not visible, (2) occurrence in a relatively narrow planar zone, although the zone could be tens of kilometres wide, and (3) enhanced foliation ("fluxion structure") and/or lineation, in most cases due to strain concentration."

The term "mylonite" has been recently redefined by Mawer

(1986), who added two points to the definition of Tullis et al. (1982), to include 1) the predominance of the ductile deformation process and 2) a suite of diagnostic asymmetric structures. This is the definition which is adopted in this thesis.

Many studies have concentrated on the microstructure, fabric development and deformational processes of mylonites with special emphasis on the deformation of quartz and feldspars (Stauffer, 1970; Higgins, 1971; Hobbs et al., 1972; Bell & Etheridge, 1973, 1976; Ross, 1973; Vernon, 1974; Wilson, 1975; Boullier & Gueguen, 1975; Wakefield, 1977; Price, 1978; Etheridge & Wilkie, 1979; Grunsky et al., 1980; Vauchez, 1980; Lister & Price, 1978; Lister & Paterson, 1979; Lister & Williams, 1979; Lister, 1981; Lister & Snoke, 1984; Passchier, 1983; White et al., 1980, White, 1982, White & White, 1983;). The deformation process of other minerals such as, garnet, sillimanite, hornblende and pyroxene has not been well documented. However the deformation features of such minerals are described here and may attract interest for further studies. In this thesis particular attention is paid to the tectonic significance of shear zones rather than detailed work on mylonites themselves.

The interpretation of shear sense within shear zones is usually based on the sense of the major asymmetric structures, the metamorphic grade of adjacent blocks, as well as both the mesoscopic and microscopic structures of the mylonites. The asymmetric structures of mylonite as indicators of shear sense in shear zones have been well studied in many other examples (e.g. Faure, 1983, 1985 a & b; Lister & Snoke, 1984).

Shear zones have long been considered to result from compressional tectonism. There has been considerable recent interest in large scale detachment shear zones which are believed to develop

during extensional tectonic regimes (Davis & Coney, 1979; Wernicke, 1981, 1985, Wernick & Burchfiel, 1982; Lister et al, 1986, 1987). One frequently cited regional example is the Basin and Range Province of the Rocky Mountain Cordillera of western North America where sediments are thought to have been deposited directly above low angle detachment shear zones and have been subsequently juxtaposed gradually over the top of old basement, the Cordilleran metamorphic core complexes. However Early Proterozoic detachment shear zones have not been precisely described and neither has the conversion of a detachment zone from extensional shearing to compressional shearing. The F/LSZ represents the relict part of an original excellent example of a long-lived complex detachment zone, the Harts Range Detachment Zone (HRDZ), which will be defined and fully discussed in chapter 8.

4.2 Field description

4.2.1. The Florence Shear Zone

The Florence Shear Zone is exposed continuously from Muller Flat Dam to the west of Mt Ruby (Map 2) and extends for about 30 km along strike. This shear zone was not recognized by previous workers (Shaw et al. 1984) and was simply included into their Division 1. Its thickest part is about 2.5-3 km in outcrop width or 1-1.5 km in true thickness around the Florence Creek. This shear zone is separated from the SOB of the Hale River Region at its base by the Muller Thrust, and from the HRSC at its top by the Bruna Thrust and a part of the Oonagalabi Thrust. A sheet-like body of the Bruna Gneiss lies along the top boundary of the FSZ except for a short section of the Bruna Gneiss sheet which occurs within the shear zone (Map 2, Fig. 1-1). An ubiquitous mylonitic schistosity (Plate 4.1.A) dips towards the N to NE with a charac-

teristic intense stretching lineation (Plate 4.1.B), plunging shallowly to moderately towards the NNE. Its planar aspect and very fine grained texture are in distinct contrast to the schistose and coarse-grained garnet sillimanite biotite gneisses of the overlying ISA.

The intercalation of mafic and acidic mylonite layers is the most characteristic feature of the FSZ. Porphyroclasts within the granitic mylonites are visible in the field whereas prophyroclasts within the mafic mylonites can only be seen in thin section. The various mylonites are so complexly interlayered that it is not possible to describe each one individually, neither to map all the mylonite layers. However, the mylonites are described in seven grouped units (from top to bottom) from a 2.5 km cross section (2.5 km) along the Florence Creek (see Fig. 4-1; no legend is drawn for the cross section and the lithologies of each unit are described below).

It is obvious that these units have no sequential and regional significance but are described to give an indication of the style and magnitude of mylonite variation within the zone. The thickness of each grouped unit changes along strike. These grouped units are:

(1) Light grey ultramylonite of granitic gneiss (5-10 m).

(2) Pinkish mylonitized granitic gneiss (about 100 m thick, Plate 4.1.C).

(3) Mylonitized major mafic granulite and minor granitic gneiss (about 100 m thick).

(4) Mylonitized Bruna Gneiss (about 300 m thick).

(5) Interlayered mylonitized granitic gneiss, light grey ultramylonite of tonalitic gneiss and dark mylonitized mafic granulite which exists occasionally as deformed xenolith

FIGURE CAPTIONS OF PLATE 4.1

A: XZ view of an intense mylonitic schistosity and compositional layering within a light grey ultramylonite of tonalitic gneiss composition. Florence Creek. It comprises 5% porphyroclasts and 95% matrix. (Z is defined as the pole of foliation; X: represent the direction of lineation; Y: perpendicular to XZ; refer to fabric axes of Flinn, 1969.)

B: Stretching lineation on the layer parallel fabric surface of an intensly mylonitized granitic gneiss. Location No.4106, 3 km east of the Florence Creek.

C: XZ view of a mylonitized granitic gneiss, 3 km east of Florence Creek; location No.3581.

D: A view, normal to the mylonitic lineation of interlayered mylonitized granitic gneiss and mylonitized mafic granulite in the Florence creek. The mylonitic schistosity transects the lithological boundaries. Small bodies of the mylonitized mafic granulite appear as inclusions within the mylonitized granitic gneiss and some granitic gneiss appears as veinlets within the mafic granulite. Location No.3538.

E: Isoclinal folds in mylonite, from west of Florence Creek. The mylonitic schistosity occurs as an axial planar fabric and the fold hinges are normal to the picture (and parallel to the intense mylonitic lineation). Location No.4270.

F: An XZ view of the intercalated mylonitized granitic gneiss (light) and very fine grained mafic mylonite (dark). Location No.3556, Florence Creek.

G: A YZ view of intercalated mylonitized granitic gneiss and very fine grained mafic mylonite showing disharmonic folds, with fold hinges parallel to the stretching lineation. Location No.3556, Florence Creek.

H: Interfingering relationship between mylonitized mafic granulite and intermediate gneiss. The mylonitic schistosity is obviously discordant and oblique to the lithological boundary (similar to that seen in Fig. 4-4). The mafic layer pinches out at the upper left corner. Location No.3378, NE of Leaky Bore.

Plate 4.1





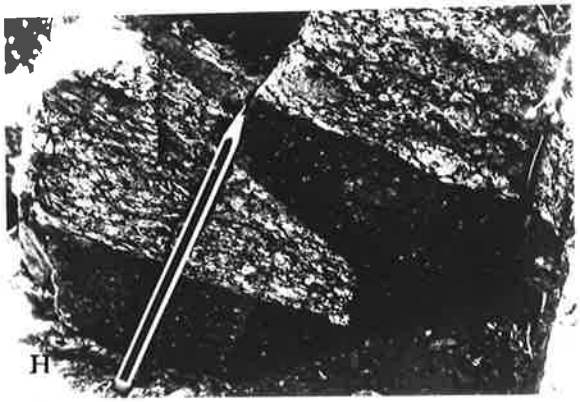












within the mylonitized granitic gneiss (Plate 4.1.D) or which has been intruded by thin veinlets of mylonitized granitic gneiss (Plate 4.1.E), (150 m ±).

(6) Ultramylonite of mafic granulite intercalated with many thin ultramylonite layers of tonalitic gneiss (Plate 4.1.A), (about 150 m thick).

(7) Intercalated mylonitized granitic gneiss and very fine grained mafic ultramylonite (about 200 m thick). The thickness of single layers varies from 0.05-2 metres (Plate 4.1.F & G).

4.2.2. The Leaky Shear Zone

The Leaky Shear Zone is exposed NE of Leaky Bore, in the SE corner of the Harts Range area and is about 20 km long, 4 km in outcrop width and 2 km in true thickness at the thickest part. An ubiquitous mylonitic foliation dips moderately towards the NE with an intense stretching lineation plunging towards the NNE. It overlies the Bruna Gneiss along the Bruna Thrust but underlies an amphibolite sequence of the ISA along the Oonagalabi Thrust. This shear zone was assigned to the Irindina Gneiss of Division 2 by Shaw et al. (1984b) and has been first recognized and reinterpreted as an allochthonous tectonic sheet of mylonitized SOB complex in this study (Ding & James, 1985, Appendix III).

This shear zone includes two parts: the lower part comprises intercalated mylonitized mafic granulite and mylonitized charnockitic gneiss or intermediate gneiss (Plate 4.1.H); while the upper part is made up of intercalated mylonitized metasediments and mylonitized granitic gneiss. Observed field relations suggest that the mafic granulite was originally intruded by the intermediate gneiss which mainly forms concordant layers with occasional discordant apophyses (Plate 4.2.A). The intermediate gneiss and

FIGURE CAPTION OF PLATE 4.2

A: Minor folds in the Leaky Shear Zone outlined by the boundary between mafic mylonite and mylonitized intermediate gneiss. The folded thin layer of mylonitized intermediate gneiss is connected to the thick layered intermediate gneiss (at the upper part of the figue) and is considered to be an apophysy from the layered intrusive body. Location No.4067, NE of Leaky Bore.

B: The Cone, where well layered mylonitized SOB basement (forming the major part of The Cone) sits horizontally on top of Bruna Gneiss (forming the foot og the hill and the plain area in the background.

C: Lenticular porphyroclast (0.7 mm X 1.25 mm) of hypersthene showing undulatory extinction oriented symmetrically within the intensely schistose matrix of a mylonitized intermediate charnockitic gneiss. Field of view: 1.7 mm X 2.2 mm; ppl; sample 4008.

D: Compositional layering within a banded fine grained mafic granulite which is a recrystallized ultramylonite of coarse grained mafic granulite as revealed by the lenticular hypersthene aggregate. Field of view: 1.7 mm X 2.2 mm; ppl; sample P3-7.

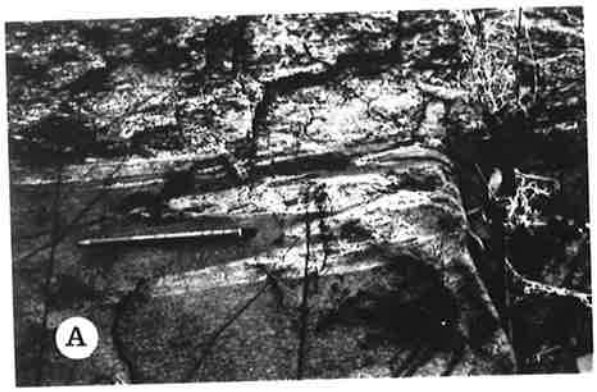
E: Mylonitized charnockitic gneiss showing intense fluxion microstructure: porphyroclasts of lenticular hypersthene and garnet are suspended in the very fine grained matrix of quartz ribbons and granular feldspar. Field of view: 1.7 mm X 2.2 mm; ppl; sample 3368.

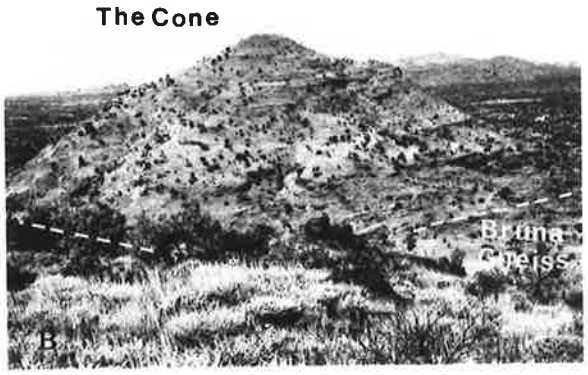
F: Microstructure of a mylonitized charnockitic gneiss showing porphyroclasts of deformed plagioclase and very fine grained matrix which contains some small grains of garnet. Field of view: 1.7 mm X 2.2 mm; ppl; sample 3368.

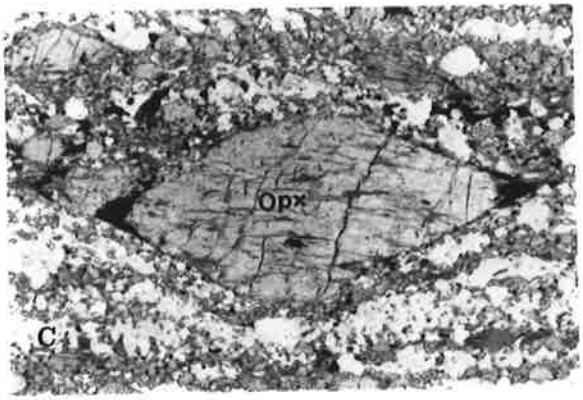
G: XZ view of a polished surface of the mylonitized nonpyroxene-bearing intermediate gneiss shows very large lenticular porphyroclasts of feldspar with short tails. Field of view: 28 mm X 40 mm; sample 3379, NE of Leaky Bore.

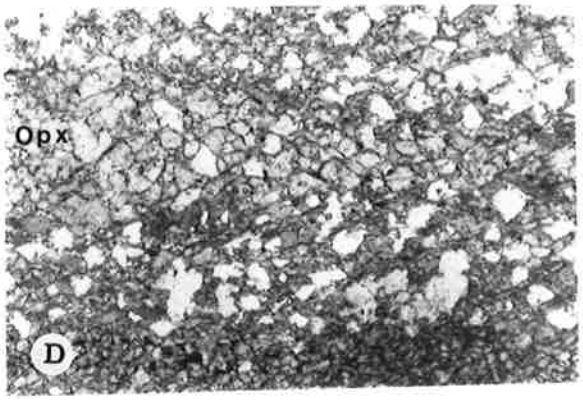
H: XZ view of a polished surface of mylonitized garnetiferous intermediate gneiss showing fairly rounded porphyroclasts with short tails which indicate a sinistral (northwards) simple shear of the upper block, similar to sample 3379. Field of view: 28 mm X 40 mm; sample 4068, Leaky Shear Zone.

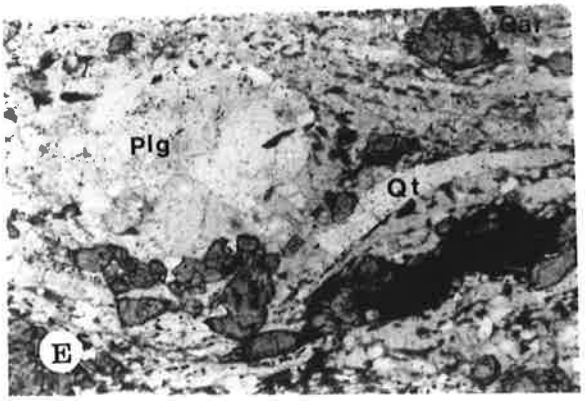
Plate 4.2

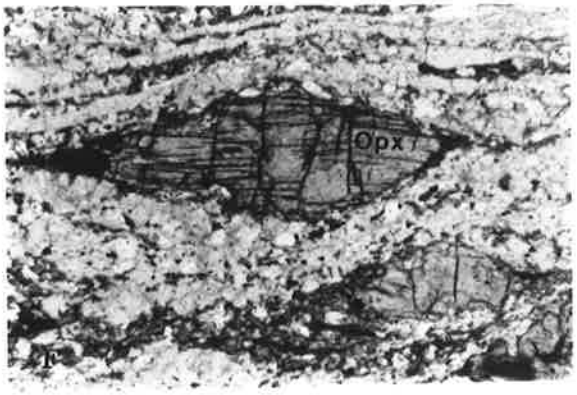


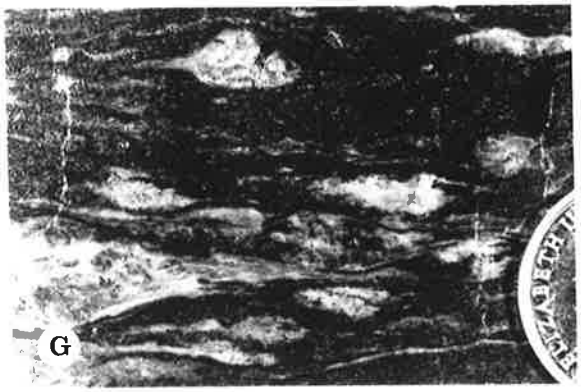














mafic granulite were then folded and mylonitized as the mylonitic schistosity is distinctly oblique to the lithological contact between the two (Plate 4.1.H). The LSZ shows identical characteristics to the FSZ, though as it lies above the Bruna Gneiss it occupies a higher structural lever than, and has an original lithological assemblage slightly different from, that of Florence Shear Zone.

The mylonitic metasediments look similar to the pelitic gneiss of the ISA but have less biotite and more garnet in their mineral assemblages, and most importantly have a distinct linear and planar mylonitic fabric.

4.2.3. Coggan Shear Zone

The Coggan Shear Zone outcrops in the hills between the Atnarta Dam and the Coggan Bore, an area of about 4 km^2. Its structural position is the same as, and should thus be the extension of, the Leaky Shear Zone. Its base sits on top of the upper ultramylonite zone of the Bruna Gneiss sheet, whereas its top is defined by a thrust boundary which is the base of the HOB and has been correlated with the Oonagalabi Thrust (see Chapter 7). The lithology (e.g. samples 4058 & 4061) and structural characteristics of this shear zone are identical to those of the Leaky Shear Zone. However there is a significant change in the orientation of the lineations and minor fold axes which plunge 10-25^o towards 107-118^o. This is most likely caused by bulk rotation of the allochthonous sheet by about 80^o during later deformation.

4.2.4. Emma and Cone Klippen

The Emma Klippen, including two isolated outcrops, representing about 3 km^2 in total area, were mapped as intrusive gabbro

bodies within the Bruna gneiss by B.M.R. workers (Shaw et al., 1984b). In fact they are mainly interlayered mylonites of mafic granulite, charnockitic gneiss (e.g. sample 4516c) and acidic gneisses (e.g. samples 4516 a & b), with intense NNE trending stretching lineations and subhorizontal mylonitic foliations. However, thin sills of metagabbro have also been found. The klippen sit subhorizontally on top of the upper mylonite zone of the Bruna Gneiss at the same level as the Leaky Shear Zone and the Coggan Shear Zone. Their subhorizontal attitude has been caused by later open folding, and erosion has made them two isolated klippen forming the cap to Mount Emma.

The Cone Klippen, also including two isolated outcrops, crop out about 8 km south of Harding Springs Well and occupy an area of 6 km^2. The Cone Klippen were also mapped as Irindina Gneiss of the Division 2, Harts Range Group, by B.M.R. workers. These geological bodies form an intercalated sequence of mylonitized charnockitic gneiss, mafic granulite and some felsic gneiss with intense, NNE trending, stretching lineation and subhorizontal mylonitic foliation. The klippen sit horizontally on the top mylonite zone of the Bruna Gneiss (Plate 4.2.B). Their lithology is very similar to that of the LSZ, but differs from the "Irindina Gneiss" (see Chapter 5).

4.3. Petrographic description of the lithologies

The protoliths of the mylonites within the F/LSZ are similar to those originally formed in the Claraville subarea of the Hale River Region. A brief petrographic description is given in this section, whereas the fabrics and microstructures of the mylonites will be described later (in section 4.5.).

(1) Mylonitized mafic granulite

Mylonitized mafic granulite is found all through the F/LSZ, and is mainly preserved in the lower levels of the LSZ and in the upper levels of the FSZ. It makes up 10-20% of the whole shear zone.

It consists of a very fine-grained (0.01-0.1 mm) matrix (50-85%) and coarser (0.25-5 mm) porphyroclasts (15-50%) (Plate 4.2.C), and mineralogically comprises plagioclase (40%), garnet (5-30%), hypersthene (10-15%), salite (10-15%), hornblende (5-10%), opaques (1-4%) and biotite (1-5%).

(2) Ultramylonite of mafic granulite composition

This rock type shows a marked streaky character of fine-grained (0.1-0.3 mm) light and dark mineral aggregates which are derived from plagioclase and pyroxene, respectively. No single large crystals have survived, though lenticular aggregates of pyroxene have been found (Plate 4.2.D). This rock type comprises plagioclase (40%), hornblende (29%), hypersthene (15%) and clinopyroxene (15%) and biotite (1%).

(3) Ultramylonite of amphibolite composition

Some of the mafic ultramylonites are very fine-grained (0.1-0.3 mm) amphibolite without any newly formed or relict of orthopyroxene. Sample P3-10, for example, comprises plagioclase (45%), hornblende (35%), clinopyroxene (10%), garnet (7%), biotite (2%) and minor calcite. Large garnets (0.5-2 mm) occur as post-mylonitization porphyroblasts.

(4) Mylonitized charnockitic gneiss

Mylonitized charnockitic gneiss is found within the Leaky Shear Zone (e.g. sample 3379A) and the Cone Klippen (e.g. sample 4001 and 3368) as thin dark grey layers. It comprises coarse (0.5-3mm) porphyroclasts (19-32%) and a very fine-grained (0.01-0.1 mm) matrix (68-81%). The porphyroclasts include garnet (15-20%), hy-

persthene (2-5%), salite (2%) and perthitic feldspar (5%), whereas the matrix comprises feldspar (38-55%), biotite (5%), hornblende (3%), pyroxene (3%) and quartz (10-20%) (e.g. Plate 4.2.E & F).

(5) Ultramylonite of charnockitic gneiss composition

This type of ultramylonite is very fine-grained (0.01-0.2 mm) and totally recrystallized and could be called a fine granulite. It comprises feldspar (63%), hypersthene (10%), salite (5%), hornblende (10%), opaque minerals (2%) and quartz ribbons (10%) (e.g. sample 4516c). It shows very fine compositional layers which contain three different mineral assemblages: i.e. hypersthene + hornblende + feldspar; salite + feldspar; hornblende + feldspar.

(6) Mylonitized intermediate gneiss (without pyroxene)

Mylonitized intermediate gneiss has been found all along the F/LSZ. It contains large porphyroclasts (up to 20 X 30 mm, see Plate 4.2.G & H) of perthitic feldspar (15-20%) and porphyroblasts (about 2 mm, see Plate 4.3.A & B) of garnet (15%) within a very dark and fine-grained (0.05-1 mm) matrix. The matrix consists of biotite (20%), hornblende (15%), garnet (10%), quartz ribbons (5%) and a very fine-grained mixture of quartz and feldspar (35%) (Plate 4.3.A & B). Some of the mylonitized intermediate gneiss has an appearance similar to the mylonitized charnockitic gneiss and could not be distinquished from it in the field.

(7) Ultramylonite of intermediate gneiss composition

This type of ultramylonite is found as very thin layers in the FSZ. It contains no relics of the original rock but 5% of porphyroblastic garnet (0.5-2 mm) and 95% of very fine-grained (0.02-0.2 mm) matrix which comprises andesine (An.48) plagioclase (60-65%), quartz (5-10%), hornblende (5-15%), biotite (10-20%) and trace amounts of epidote and apatite (e.g. samples P3-6A & P3-7A).

(8) Mylonitized granitic gneiss

FIGURE CAPTIONS OF PLATE 4.3

A: Porphyroclasts of garnet with small biotite inclusions and larger biotite flakes in the pressure shadow. Field of view: 3.4 mm X 2.2 mm; ppl; sample 3379, Leaky Shear Zone.

B: Garnet porphyroclasts with long tails of small recrystallized garnets. field of view: 3.4 mm X 2.2 mm; ppl; sample 3379, N of the Leaky Bore.

C: A polished sample surface of mylonitized garnetiferous quartzofeldspathic gneiss shows intense mylonitic structure. Field of view: 45 mm X 70 mm; sample 3380A.

D: Large thin section from the sample (3380A) above. Garnets are much more competent than quartz and feldspar, and remain undeformed. Field of view: 21 mm X 14 mm; ppl.

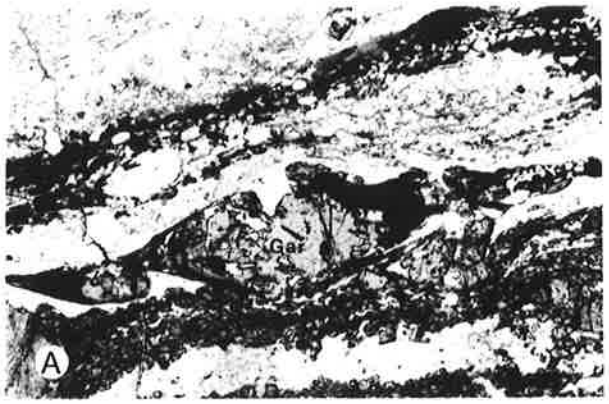
E: Large sillimanite porphyroclast wrapped around by mylonitic matrix. The sillimanite has been slightly broken by cracks and shows greater competence than quartz and feldspar. It also has been altered by biotite. Field of view: 3.4 mm X 2.2 mm; ppl; sample 3380A.

F: Mylonitized granitic gneiss showing a large porphyroclast of plagioclase (0.5 X 1.5 mm) and the ribbon-like matrix of fine grained potash feldspar and quartz. The porphyroclast has developed a symmetric long tail at its right end (north) and an asymmetric short tail at its left end, which is interpreted to result from dominant superplastic flow of minor dextral (downwards or northwards) shear. Field of view: 3.4 mm X 2.2 mm; X polars; sample P3-3b, Florence Creek.

G: Large thin section of sample 3581 (Fig. 4-3) showing strained porphyroclasts and mylonitic schistosity. The low angle oblique,leftinclined schistosity and the long axes of porphyroclasts is interpreted to define an S fabric whereas the subhorizontal schistosity may define a C fabric of S-C mylonite. This relationship may indicate a dextral (northward) shear sense. Field of view: 60 mm X 40 mm; ppl.

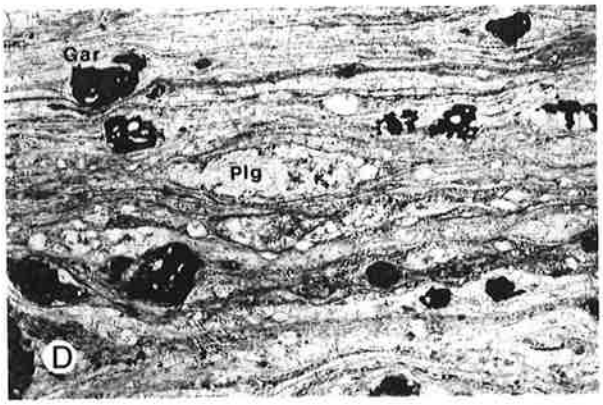
H: Same view as above (G); X polars.

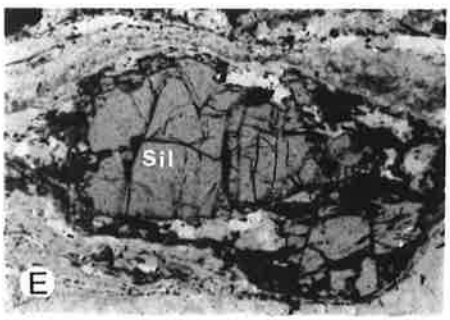
Plate 4.3

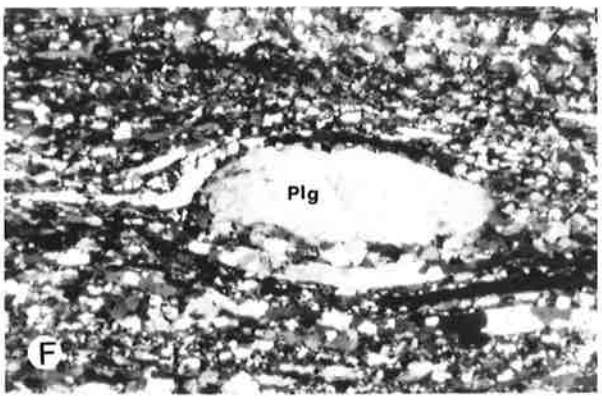


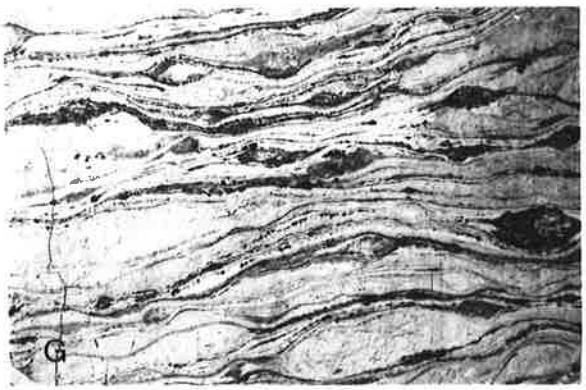














Mylonitized granitic gneiss has been found within the whole F/LSZ, and makes up 50% of the FSZ and 20% of the LSZ. It comprises coarse (0.5-1.5 mm) porphyroclasts (10-50%) of major feldspar and minor hornblende and a very fine-grained (0.01-0.1 mm) matrix (50-90%) which consists of microcline perthite (30-35%) and plagioclase (20-25%), ribbon-like (0.1-0.5 mm wide and more than 5mm long) quartz (22-40%), garnet (0-5%), hornblende (0-1%), biotite (2-3%) and minor opaques (e.g. Plate 4.3.F, G & H).

Sample 3380A represents the uppermost level of LSZ. It comprises 15% porphyroclasts and 85% matrix (Plate 4.3.C & D). The porphyroclasts include garnet (0.2-6 mm, up to 10% in Plate 4.3.C), sillimanite (up to 2 X 5 mm, about 2%, e.g. in Plate 4.3.E), plagioclase and perthite (1-4 mm, 3%). The matrix comprises quartz ribbons (40%), very fine-grained (0.01-0.1 mm) feldspar aggregates (43%) and biotite (2%). The widths of quartz ribbons range from 0.2-2 mm with individual grains ranging from 0.2 X 0.5 mm to 1 X 5 mm. It is difficult to classify the protolith of this rock which could be either metasedimentary or metaigneous in origin.

(9) Ultramylonite of granitic composition

This type of ultramylonite is found at the top of the FSZ. It comprises 5% porphyroclasts (0.5 X 1.5 mm) or aggregates of fragmentary plagioclase and 95% recrystallized very fine-grained (0.01-0.2 mm) matrix which consists of potash feldspar (40%), plagioclase (30%), quartz (20%), clinopyroxene (3%), hornblende (3%), opaques (3%), biotite (1%) and trace amounts of apatite, zircon and sphene (e.g. sample P3-3).

Recrystallized ultramylonite of granitic composition is found in the middle level of the Florence Shear Zone. It comprises 5-10% of porphyroclasts (5-10 mm) of plagioclase and 90-95% of matrix

(0.1-0.4 mm), which includes potash feldspar (30%), plagioclase (44%), quartz (20%), biotite (5%) and trace amounts of garnet, sphene, epidote and apatite (e.g. sample P3-6). Its porphyroclasts and matrix are coarser than in other ultramylonites but the porphyroclasts make up less than 10% of the whole rock which is thus refered to as recrystallized ultramylonite.

(10) Protomylonite of granitic gneiss

Weakly foliated protomylonite of granitic gneiss is found within a lenticular body of mylonitized granitic gneiss in the Florence Shear Zone (e.g. sample P3-3A). It is mainly a coarse-grained (2-5 mm) granitic gneiss with about 40% deformed and finely recrystallized (0.01-0.2 mm) matrix, and mineralogically comprises perthite (50%), plagioclase (20%), quartz (20%), clinopyroxene (3%), biotite (3%), magnetite/ilmenite (3%), and trace amounts of apatite and allanite.

Mylonitized white-coloured garnet-bearing felsic gneisses outcrop as thin layers within the Cone Klippen. Its character is similar to other mylonitized granitic gneiss but it contains mainly plagioclase (40%), potash feldspar (30%), quartz (20%) with only 2% of garnet (e.g. Plate 4.4.A).

4.4. Folding within the F/LSZ

As the whole sequence of the F/LSZ has been intensely flattened and stretched, the earlier folds (BF_1 to BF_4) in the zone have been intensely flattened and deformed by mylonitization, and thus no major folds have been mapped on a regional scale, though small isoclinal folds have been seen at a few places.

These folds are outlined by the boundaries between mafic mylonites and felsic mylonites (e.g. Plates 4.4.B, 4.1.E & 4.2.A). The folds are isoclinal with narrow, rounded or angular

FIGURW CAPTIONS OF PLATE 4.4

A: Mylonitized garnet-bearing felsic gneiss showing a similar microstructure to that of the charnockitic gneiss (Plate 4.2.F). Field of view: 1.7 mm X 2.2 mm; X polars; sample 3367, W of The Cone.

B: YZ view of an isoclinal fold hinge in the mylonite sequence. The mylonitic schistosity is developed as its axial planar fabric and the fold hinge parallels the mylonitic lineation. Location No.4106, E of the Florence Creek.

C: XZ view of intensely mylonitized granitic gneiss. Location No.4106; E of Florence Creek.

D: Weakly mylonitized charnockitic gneiss showing a protomylonitic microstructure. The deformed porpyroclasts of Cpx, Opx, quartz and feldspar and laminated matrix define a mylonitic foliation. Field of view: 1.7 mm X 2.2 mm; ppl; sample 4001; W of The Cone.

E: Same view as above (D); X polars.

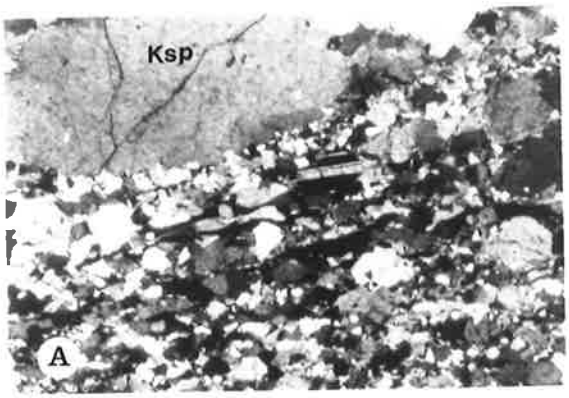
F-H: Polished surfaces of one intensely mylonitized granitic gneiss sample. The bulk strain ratio is difficult to estimate because the deformation is largely inhomogeneous. location No: 4106, east of the Florence Creek.

F: XZ view; 48 mm X 70 mm;

G: YZ view; 36 mm X 52 mm;

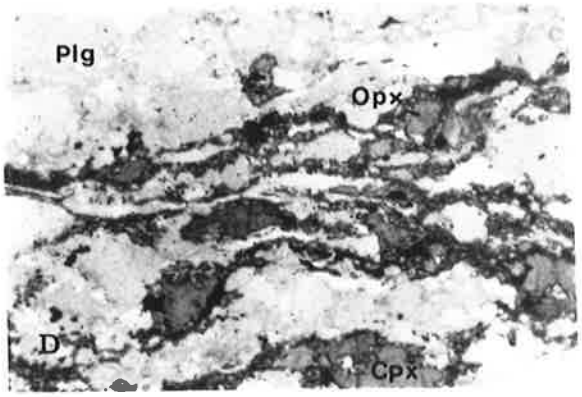
H: XY view; 48 mm X 70 mm.

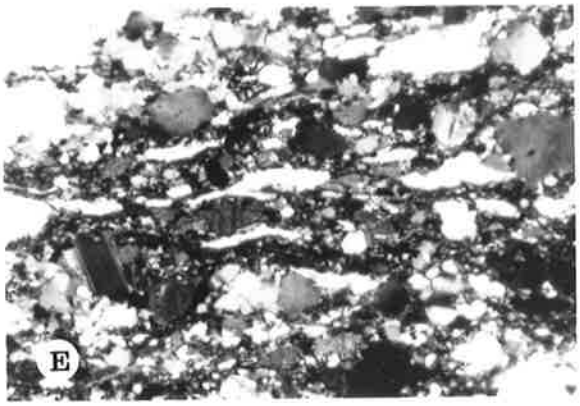
Plate 4.4

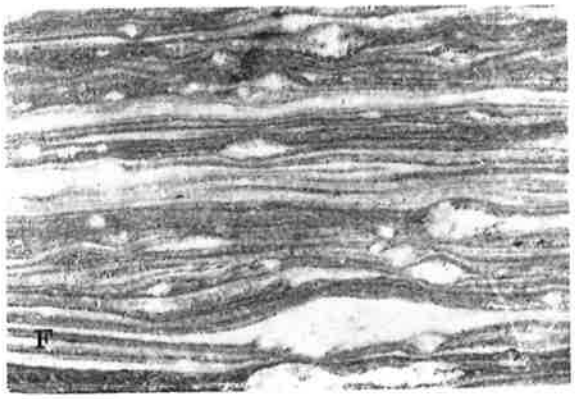


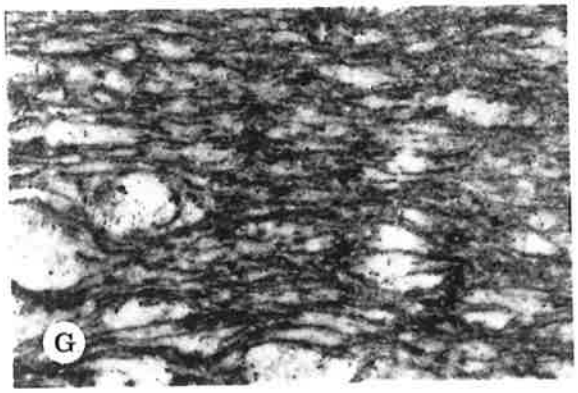














closures. The mylonitic foliation is parallel to the fold limbs but penetrates the lithological boundaries in the hinge. An intense stretching lineation parallels the fold hinges.

In Plate 4.2.A, a small folded veinlet is lithologicaly identical to a thick layered intermediate gneiss and is thus interpreted as an apophysis of the major intermediate gneiss body intruded into the mafic granulite. The major boundary between the mylonitized mafic granulite and the intermediate gneiss remains straight. It is not possible to tell whether these small isoclinal folds are flattened early folds or generated during the mylonitization.

Only some small-scale disharmonic folds within the mylonite sequence are certain to have been formed during the mylonitization and have fold hinges parallel to the direction of the mylonitic lineation (e.g. Plate 4.1.D & G).

4.5. Fabric and microstructure of the mylonitic rocks

4.5.1. Fabrics

The original fabric (i.e. BS_1 and BL_1) of the SOB complex within the F/LSZ has been completely replaced by a very intense and ubiquitous mylonitic fabric, though lithological boundaries are still visible (e.g. Plates 4.1.E & H, and 4.4.B). Indurated mylonites with very intense linear and planar mylonitic fabrics are the most characteristic feature of this shear zone and differ markedly from the weak fissile schists or phyllites commonly developed in other anastomosing mylonitic zones, e.g. the widespread retrograde schist zones of the Broken Hill Block (Hobbs et al., 1984) and the slaty mylonite (phyllite) along the Woodroffe Thrust in the Musgrave Range (Bell and Etheridge, 1976).

The mylonitic foliation is manifested by a compositional

layering (e.g. Plates 4.1.B, F & G and 4.3.C) and/or the parallel prefered orientation of flaky minerals (e.g. biotite) in the matrix and of flattened porphyroclasts (e.g. Plate 4.4.F, G & H).

The mylonitic lineation can be clearly seen on all outcrops (e.g. Plate 4.1.B). It is manifested by a streaking of mineral aggregates, i.e. ribbon-like aggregates of pyroxene (Plate 4.5.G), garnet (Plate 4.3.B), hornblende (Plate 4.3.H), feldspar and quartz (Plate 4.3.F) and/or by the parallel preferred orientation of prismatic minerals (e.g. hornblende). It is also defined by long tails of deformed porphyroclasts, which show large X/Z aspect ratios (e.g. Plates 4.2.G and 4.4.F) and large X/Y aspect ratios (Plate 4.4.H), but small Y/Z aspect ratios (e.g. Plate 4.4.G).

The field aspect and the microstructures of the mylonitic fabrics within the Florence Shear Zone contrast sharply with those of the unmylonitized SOB, the latter retaining their coarse equigranular texture (e.g. Plate 2.1.F in Chapter 2).

4.5.2. Deformation of individual mineral phases from within the mylonites in the F/LSZ

Many deformational features are observed within the mylonites, but no detailed study has been made as it is beyond the scope of this thesis. However, some significant features are described here and may attract interest for further studies. An order of mineral competence during mylonitization of, from low to high: quartz, feldspar, pyroxene & hornblende, garnet, sillimanite, zircon, is established on the basis of observation without however, the confirmation of experimental evidence.

(1)Quartz

Quartz is the least competent mineral during ductile deforma-

tion. Quartz ribbons are the most common feature within the mylonitized gneissic rocks (e.g. Plate 4.3.F), whereas quartz porphyroclasts are rare. The individual grains within the quartz ribbons are coarser than the grains of feldspar in the matrix. This may imply that ductile flow or recovery of strain is much easier in quartz than in feldspar (Tullis, 1977). The quartz ribbons have an optical preferred orientation which can be seen by the subparallel extinction of individual quartz grains. However no crystallographic work was carried out in this study.

(2)Feldspar

Feldspar is usually more competent than quartz during ductile deformation and thus forms porphyroclasts in the mylonitized quartzofeldspethic gneisses. The feldspar porphroclasts usually show undulatory extinction (e.g. Plate 4.5.F). However, most of the original feldspar has been deformed to elongate aggregates or ribbon-like laminae of very fine grained feldspar intercalated with quartz ribbons (e.g. Plates 4.3.F & 4.5.A),

(3) Pyroxene

In mylonitized mafic granulite, pyroxene shows slightly higher competence than plagioclase. For example, in sample P3-4, much of the pyroxene remains as porphyroclasts which show evidence of brittle deformation (Plate 4.5.D) with micro-faults and cracks, though some parts of the original pyroxene have also been deformed and recrystallized to very fine-grained (0.01-0.1 mm) aggregates of hypersthene, salite, hornblende and plagioclase (Plate 4.5.C & G). In contrast, most of the original plagioclase has been deformed and recrystallized to elongate aggregates of very fine grained plagioclase (0.05-0.1 mm) (Plate 4.5.B & G) and only a few fragments of relict plagioclase are preserved with fractures, kinks and dragilike structures (e.g.Plate 4.5.E & F). The process of the

FIGURE CAPTIONS OF PLATE 4.5

A: A large zircon crystal in the centre retains its euhedral shape during the intense mylonizaton to show the most resistant character. Field of view: 0.55 mm X 0.85 mm; ppl; sample 3380, Leaky Shear Zone.

B: Mylonitized mafic granulite showing porphyroclasts of orthopyroxene (mainly hypersthene with thin laminae of augite). About 10-20% Of the pyroxenes have been deformed and recrystallized. New generations of fine-grained hypersthene, salite and hornblende occur around the large pyroxene porphyroclasts and form the matrix of mylonite. The plagioclase has been totally deformed and recrystallized. Field of view: 3.4 mm X 2.2 mm; ppl; sample P3-4, Florence Creek.

C: About 70% of a large pyroxene has been recrystallized to fine-grained hypersthene, salite, hornblende and minor plagioclase. Field of view: 3.4 mm X 2.2 mm; ppl, sample P3-4.

D: A large porphyroclast of pyroxene shows opposite senses of displacement along both the augite laminae and the microfaults. The hornblende altered after pyroxene along its microfaults and laminae. Field of view: 3.4 mm X 2.2 mm; ppl; sample P3-4.

E: A large porphyroclast of plagioclase is surrounded by fine-grained mafic granulite which was recrystallized after deformed large grains of pyroxene. Fine hornblende grains mainly occur along the boundary between the plagioclase porphyroclast and the mafic granulite. The plagioclase porphyroclast shows bending and undulatory extincton. Sample P3-4; ppl; field of view: 3.4 mm X 2.2 mm.

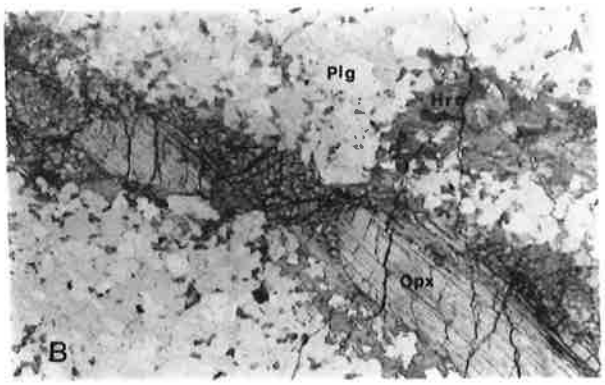
F: Same sample as above (E); X polars.

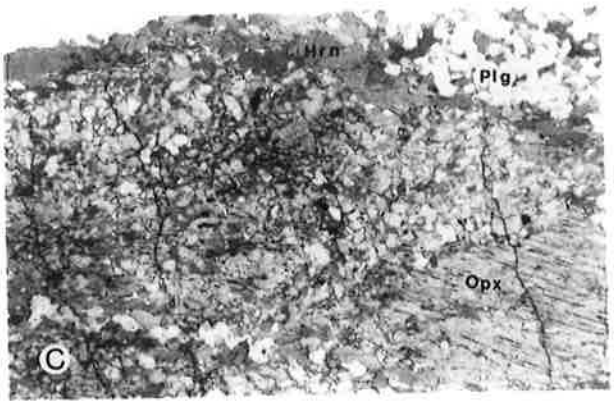
G: Hornblende forms as thin layers between fine-grained pyroxene and plagioclase layers, which are deformed and recrystallized former megacrysts of pyroxene and plagioclase. Field of view: 3.4 mm X 2.2 mm; ppl; sample P3-4.

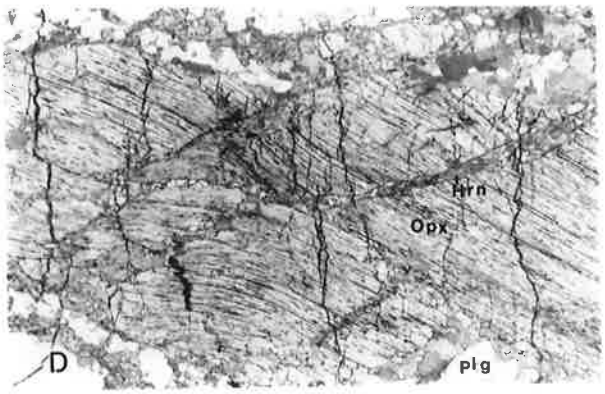
H: Fine-grained pyroxene has been totally replaced by hornblende thus forming a fine-grained banded amphibolite. Field of view: 3.4 mm X 2.2 mm; ppl; sample P3-4.

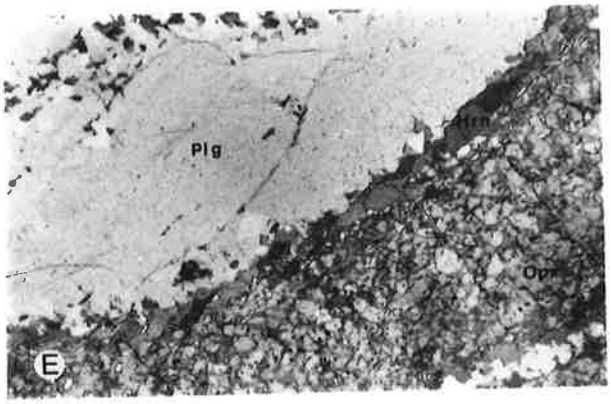
Plate 4.5

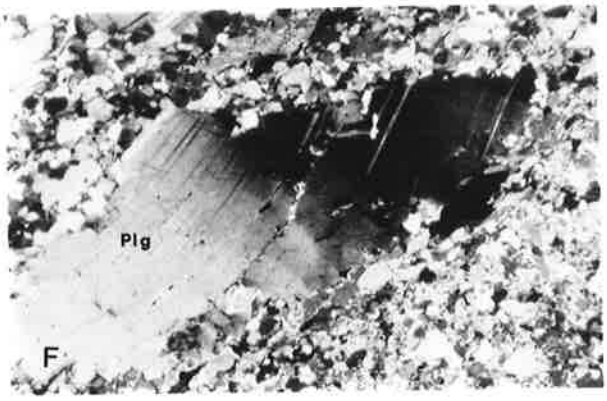

Zir
A

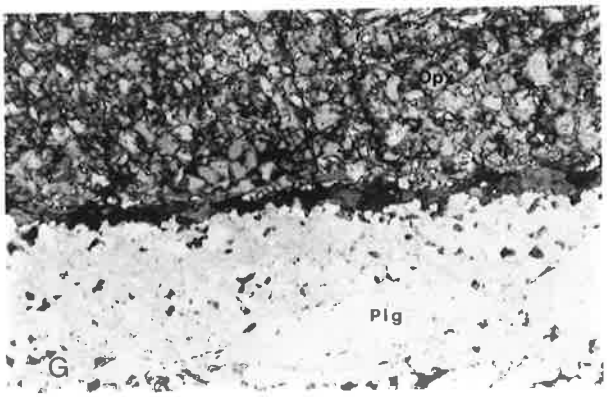

Plg
Hrn
Opx
B

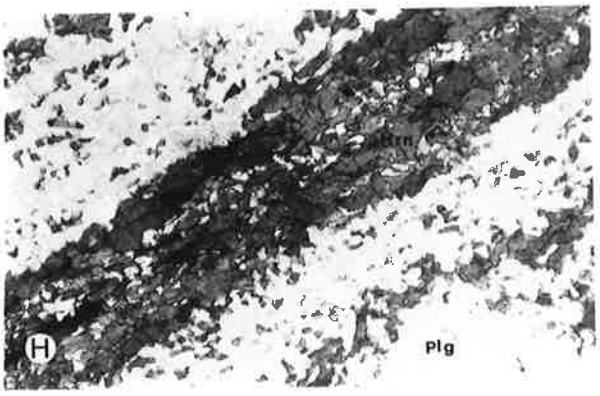

Hrn
Plg
Opx
C


Hrn
Opx
D
Plg


Plg
Hrn
Opx
E


Plg
F


Opx
Plg
G


Hrn
Plg
H

formation of compositional layering within the mylonitized mafic granulite is illustrated from Plate 4.5.B to H. The tension fractures (Plate 4.5.B) were probably related to a later brittle deformation, because some of them extend into the mylonitic matrix.

Within the ultramylonitized mafic granulite, no porphyroclasts of single minerals have survived and the original pyroxene and plagioclase has been deformed to streaky elongate aggregates and thin laminae. Further petrofabric work is necessary to gain a fuller understanding of the deformational mechanisms of pyroxene.

(4) Hornblende

Hornblende porphyroclasts (0.3-1mm) and long stretched tails of very fine grained hornblende (0.01-0.1mm) have also been found in the mylonitized mafic granulite. The petrofabrics of hornblende aggregates in some of the mafic mylonites within the Florence Shear Zone has been studied by Liu and James (1987) who suggested that the crystallographic prefered orientation of hornblende implies a predominant ductile deformation.

(5) Garnet

Garnet is usually very competent during mylonitization. Undeformed large poikiloblastic garnets, containing undeformed inclusions of biotite, quartz and feldspar, are usually wrapped around by a very fine-grained mylonitic matrix of quartz, biotite and feldspar (Plate 4.3.C & D). However flattened garnets have been studied by Ross (1973) from the mylonitic rocks in the southern Okanagan of British Columbia, who has used their deformed outlines and internal zoning for strain analysis.

Intensely deformed garnet has also been observed within the F/LSZ in many rock types including mylonitized charnockitic gneiss, intermediate gneiss, granitic gneiss, and mafic granulite.

The garnets form porphyroclasts (0.3-1 mm) with long stretched tails and/or elongate aggregates of fine grained garnet (0.05-0.1 mm) (Plate 4.3.A & B). It is most difficult to study the deformation mechanisms of such isotropic minerals. However the feature that very small polygonal garnets form tails of porphyroclastic large garnets or form elongate aggregates strongly implies that a ductile deformation is most likely to have occurred during the mylonitization within such a high grade (granulite facies) terrain.

(6) Sillimanite

Sillimanite has been found as porphyroclasts within the mylonitized garnetiferous rocks in the LSZ (Plate 4.3.E). Large (1-2 mm) sillimanites show weak undulatory extinction or deformation bands and are wrapped around by a very fine-grained mylonitic matrix. However brittle deformation is dominant as the sillimanites are deformed by cracks and sometimes broken to small angular fragments. No subgrains developed in large sillimanites to form elongate aggregates.

(7) Zircon

Zircon is observed as being very competent, always retaining its undeformed euhedral shape within mylonitess with long axes parallel to the mylonitic foliation (e.g. Plate 4.5.A). This is likely to be caused by rigid rotation during non-coaxial shear.

4.6.2. Shear sense assesment

Most of the mylonites in the F/LSZ show a dominant symmetry of structure and only one set of mylonitic foliations is generally observed (Plates 4.1.A & 4.3.C). Lenticular porphyroclasts or elongate aggregates in many thin sections are symmetrically orientated in relation to the mylonitic foliation of the matrix (e.g.

Plates 4.2.C & D, 4.3.B and 4.5.A). This feature suggests a co-axial strain ellipsoid for the mylonitic deformation (Plate 4.4.F, G & H). Symmetrically stretched tails of porphyroclasts may indicate superplastic flow (Boullier & Gueguen, 1975). The displacements on fractures within some large pyroxene porphyroclasts show symmetrical conjugate orientation and shear sense: i.e. a dextral shear along the growth laminae and a sinistral shear along micro-faults (Plate 4.5.D). Transverse tension cracks also develop within porphyroclasts at right angles to the main mylonitic foliation (Plate 4.2.E). All these features indicate a prolonged co-axial strain ellipsoid during mylonitization and may imply a major amount of pure shear. Thus these features cannot be used as indicators of shear sense.

However, there are some asymmetric stretched tails and pressure shadows around porphyroclasts which may indicate shear sense. Asymmetric structural features in mylonites have been used as indicators of shear sense in shear zones by many authors (e.g. Berthe et al. 1979; Lister & Snoke, 1984; Simpson & Schmidt, 1983; Faure, 1983, 1985 a & b). The shear criteria in rocks have been recently reviewed by Cobbold & Gapais, 1987 and Choukroune et al. 1987. Typical asymmetric structural features are described in so called S-C mylonites (Berthe et al., 1979; Lister & Snoke, 1984). There are two surfaces of foliation in S-C mylonites: (1) S-surfaces related to the accumulation of finite strain; (2) C-surfaces related to localized high shear strains (where "C" stands for "cisaillement" or shear). Some S-C mylonites has been observed in the F/LSZ but appear to have been largely destroyed by the intensity of flattening and stretching. A similar analysis can be applied to other mylonites which are not typical S-C mylonites but show asymmetric structures. For example the long axes of

porphyroclasts may be considered to represent the S-surfaces whereas the tails are considered to represent the C-surfaces (Fig. 4-2).

In some of the mylonitized intermediate gneisses (Plate 4.2.G & H) the lenticular or ellipsoidal feldspar porphyroclasts have weakly asymmetric tails which indicate a northward (sinistral in the picture) shear sense. (The northward or southward shear means movement direction of the hanging wall or upper plate). In some other examples (Plates 4.2.F and 4.3.F) large feldspar porphyroclasts within mylonitized granitic or charnockitic gneisses have long symmetric tails at the right ends (north) but asymmetric short tails at the lower left ends; this feature is also interpreted as an indicator of northward shear sense (dextral in the pictures). The petrofabrics of hornblende in some of the mafic mylonites within the Florence Shear Zone has been studied by Liu and James (1987) and the crystallographic prefered orientation of hornblende has been interpreted to indicate a northward shear sense.

From the evidence described above, an extensional northward shear sense is considered dominant within the F/LSZ. Because the use of these weak asymmetric tails may be arguable, the shear sense of the F/LSZ will be substantiated mainly on the basis of regional structures and tectonic considerations which confirm the northward shear sense (see Chapter 8).

However, reverse southward shear sense has also been found from some mylonites within the F/LSZ. The reverse shear sense is related to the thrusting of later HRO deformation (HRT_1 to HRT_4) and will be described in Chapter 7. Polyphase shear zones have been found in some other granulite belts, e.g. along the margins of Bohemian Massif (Behr, 1980).

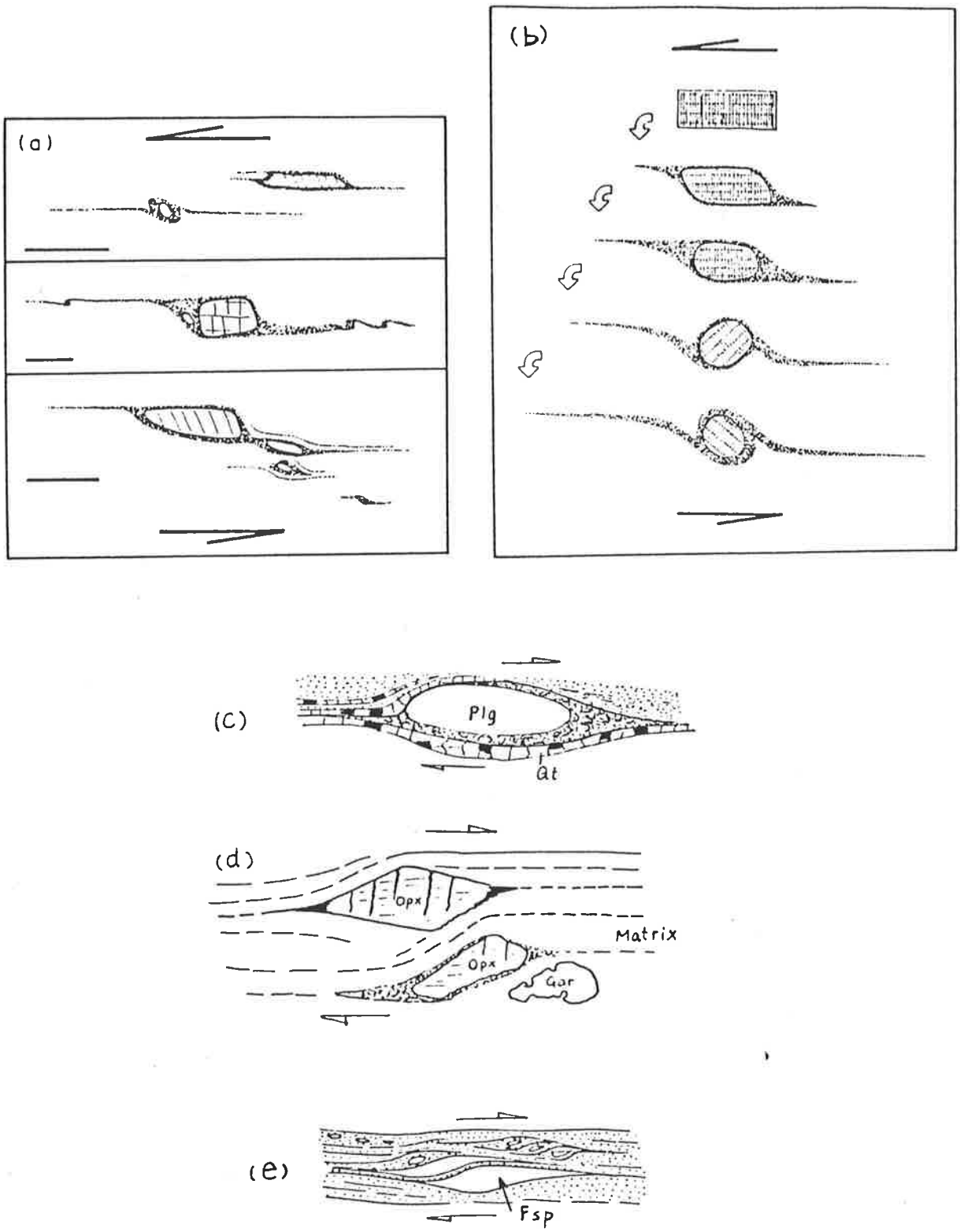


Fig. 4-2. Sketch of shear sense from porphyroclasts and asymmetric tails within mylonite.

a & b: Diagrams adopted from Mawer (1987) for comparison.

c: Sketch from Plate 4.3.F;

d: Sketch from Plate 4.2.F;

e: Sketch from Plate 4.4.F.

4.7. Metamorphism

4.7.1 Metamorphic facies

The porphyroclasts within the mylonitized mafic granulite, charnockitic gneiss and metasediments in the F/LSZ show an original granulite facies metamorphism defined by the mineral assemblage of hypersthene, salite, perthite, garnet and sillimanite. The porphyroclasts within the mylonitized granitic gneiss show an original amphibolite facies metamorphism defined by the mineral assemblage of garnet, biotite, hornblende and feldspar. Field evidence (section 4.2.; Plate 4.1.D & E) shows that the mylonitized granulite sequence was intruded by granitic gneiss in a similar relationship to that found in the Oonagalabi Tongue, and then both the granite and the granulite sequence were mylonitized together.

The early mylonitization occurred under dry conditions as is shown by the recrystallized mineral assemblage of hypersthene, salite, garnet and plagioclase with very little hornblende in the matrix of the mylonitized mafic granulite (e.g. samples 4008, 3379A) and the charnockitic gneiss (e.g. samples 4001, 3368). However, inhomogenous retrogressive or hydrous metamorphism has occurred during prolonged mylonitization. In some mylonitized mafic granulite, recrystallized hornblende occurs along the boundaries between plagioclase and hypersthene (Plate 4.5.F, G & H), and also along microfaults, mineral cleavages and exsolution lamellae within pyroxene (Plate 4.5.D), whereas in some other mafic ultramylonites, most of the matrix has been recrystallized to very fine grained amphibolite (e.g. sample P3-10). In some mylonitized intermediate gneiss, most of the matrix has been recrystallized to very fine grained biotite, hornblende and garnet (e.g. sample 3379).

The amphibolite facies metamorphism must have lasted for a fairly long perid during and after the prolonged mylonitization as is indicated by some large post-tectonic porphyroblasts of garnet. This is also indicated by the fact that the unstrained and coarser grained light brown biotite and light green hornblende formed in transverse tension cracks, which cut the mylonitic foliation. Also the alteration is seen to form along the mylonitic foliation near to the cracks with a decreasing intensity away from them.

4.7.2. Temperature and pressure estimates

No specific pressure estimate has been made for the F/LSZ, so the pressure (7-9 kb) estimated from the other SOB areas is adopted for the F/LSZ on the basis of their structural relationship.

The metamorphic temperatures of mylonitized mafic granulites have been estimated from two-pyroxene geothermometry. The mylonitic matrix contains granulite facies mineral assemblages and reveals a similar temperature (Table 4-1) to the porphyroclasts, ranging from 800° to 815°C, average 805°C (Wood & Banno, 1973) or from 800° to 840°C, average 815°C (Wells, 1977).

Table 4-1 TEMPERATURE FROM TWO-PYROXENE GEOTHERMOMETRY (MYLONITIZED MAFIC GRANULITES)

sample No.	Wood & Banno (1973)	Wells (1977)
P3-4A	805	810
P3-7	800	800
3379A	815	840
average	805	816

The metamorphic temperature has also been estimated from biotite - garnet geothermometers. The results are consistent for the matrix and for the porphyroclasts, but are more complicated than the results from two-pyroxene geothermometry. Mylonitized

charnockitic gneiss (samples 3368, 3379A) and intermediate gneiss (sample P3-7a), for example, show a higher equilibrated peak temperature, which is represented by the garnet-centre and biotite, but the mylonitized granitic gneiss (sample 3380) shows a 100-140°C lower peak temperature (Table 4-2). All the samples show a cooling temperature calculated from the garnet-rims and biotite in contact with garnet.

Table 4-2 TEMPERATURES FROM BIOTITE - GARNET GEOTHERMOMETRY (MYLONITIZED VARIOUS GNEISSES)

sample No.	Perchuk (1976)	Thompson (1976)	Goldman & Albee (1977)	Ferry & Spear (1978) 7kb	7.5kb	8kb	8.5kb
3368							
peak	719	760	777	867	869	872	874
cooling	672	692	737	767	769	771	773
P3-7A							
peak	717	735	776	863	865	868	870
cooling	671	690	736	764	766	769	771
3379A							
peak	699	730	760	824	826	829	831
coolng	589	580	671	608	610	613	615
3380							
peak	649	670	718	721	723	726	728
cooling	619	630	695	664	666	669	671

Note: peak T from garnet-centres; cooling T from garnet-rims.

The garnet - hornblende geothermometer of Graham & Powell (1984) gives 690°C for the mylonitized intermediate gneiss (sample P3-7A) and 740°C for the mylonitized charnockitic gneiss (sample 3379A).

The clinopyroxene - garnet thermobarometer of Ellis & Green (1979) gives 700°C (7-9 kb) for sample 3379A.

From these data, the peak temperature of the granulite facies metamorphism which operated during the mylonitization can be suggested as 800-865°C. The peak temperature of the late amphibolite facies metamorphism which operated during continuous mylonitiza-

tion can be suggested as 690-740°C, which is about 110-125°C lower than that of granulite metamorphism but agrees with the cooling temperature (610-765°C) of the mylonitized charnockitic gneiss.

The temperature (720°C) of the mylonitized granitic gneiss (sample 3380) is within the temperatures range (650-740°C) of Bruna gneiss (see chapter 5) and very similar to the temperature (690-740°C) of the amphibolite facies mylonitization.

PART TWO THE HARTS RANGE OROGENIC BELT

CHAPTER 5 LITHOLOGIES AND METAMORPHISM OF THE HARTS RANGE OROGENIC BELT

5.1. Introduction

The lithologies comprising the Harts Range Orogenic Belt (HOB) include a metamorphosed supracrustal sequence, named the Harts Range Supracrustal Cover (HRSC), and an intrusive gneissic meta-granitoid complex, named the Bruna Gneiss. The HRSC extends into adjacent areas to the west, north and east of the study area. The specific part of HRSC in the study area sits structurally above the metamorphic complexes of the Strangways Orogenic Belt (SOB) and has been generally described and named as the Irindina supracrustal assemblage (ISA) (Appendix III, Ding & James, 1985). This assemblage includes a metasedimentary sequence plus a layered mostly mafic complex, the Harts Range metaigneous complex. The ISA covers an area of 1200 km^2 from Mt Riddoch to Leaky Bore (Map 2), The Harts Range metaigneous Complex includes a major sequence of layered amphibolite and small isolated bodies, or thin layers, of ultramafic anorthosite and metagabbro. The subdivision of strato-tectonic units has been introduced and reviewed in chapter 1. A brief description of lithologies is presented in this chapter based on the present study. Various lithologies within the ISA have also been described in some detail by Stewart et al.(1984), Lawrence et al.(1987) and Lawrence (1987). The HOB area forms mainly hills and mountain ranges which have a relative relief of a few hundred metres and are intersected by many bushy creeks.

5.2. Subdivision of lithologic units and stratigraphy in the ISA

Since no primary depositional features, such as cross bedding and graded bedding or volcanic structures, have been identified within the ISA throughout the whole field investigation, no depositional younging or way-up criteria have been recognized. In addition, the whole supracrustal sequence has been complexly folded and sheared, so the recognition of a formal stratigraphy in the supracrustal sequence is very difficult. However, the following lines of evidence have been used to deduce a stratigraphic order.

Some igneous features within the Fiskenaesset Anorthosite Complex have been used as a stratigraphic key to the tectonic evolution of the West Greenland gneiss complex (3000-2800 Ma) by Myers (1981). The sequence of the Harts Range meta-igneous complex has similarly been used in this thesis to determine local younging directions (e.g. see section 5.4.2). Assuming that the mafic and ultramafic bodies intruded into the metasediments and crystallized at an early stage before the occurrence of major recumbent folding, then the younging directions proposed for the layered mafic and ultramafic bodies may be used to represent the younging direction of the metasedimentary sequence as a whole. Based on these younging directions from the meta-igneous bodies and a detailed regional structural analysis (see Maps 2, 5 & 6), possible local stratigraphic sequences are suggested and correlated in Table 5.1. The layered amphibolite constantly appears to be located in the highest stratigraphic position and thus has been treated as a stratigraphic unit. Finally, throughout the area it has been possible to use a pure or impure quartzite layer as a marker horizon. The stratigraphic sequence proposed for the Irindina Supracrustal Assemblage is provided in Table 5.2.

Table 5.1 STRATIGRAPHIC CORRELATION BETWEEN THREE HOB NAPPE SHEETS

Naringa Nappe	Irindina Nappe	Riddoch & Campbell Nappes
(not found)	layered amphibolite	layered amphibolite
pelitic & semi-pelitic gneiss	pelitic & semi-pelitic gneiss with small lenses of amphibolite	pelitic & semi-pelitic gneiss with small lenses of amphibolite
pure and impure quartzite	pure and impure quartzite	
marble with minor calc-silicate	marble & calc-silicate	
calc-silicate		
calc-silicate gneiss and calc-silicate quartz schist		
---------- thrust ----------		
Strangways Orogenic Belt		

Note: details of the nappes are referred to in Chapter 6.

Table 5.2 STRATIGRAPHIC SEQUENCE FOR THE WHOLE ISA

(6)	layered amphibolite (meta-basaltic lava) with thin layers of meta-sediments ------	up to 2,000 m
(5)	pelitic & semi-pelitic gneiss with amphibolite lenses at the uppermost position of this unit ----------	up to 500 m
(4)	pure and impure quartzite ----------	up to 20 m
(3)	marble with minor calc-silicate ----------	up to 400 m
(2)	calc-silicate ----------	up to 200 m
(1)	quartz-rich calc-silicate, calc-silicate quartz schist and calc-silicate gneiss ----------	up to 800 m
---------- thrust (possible original unconformity) ----------		
Strangways Orogenic Belt basement		

Although the stratigraphic sequence is tentative and cannot be fully substantiated, the relative order of this sequence has proved to be very consistant and has been useful for detailed

mapping on all scales. Most of the lithological units (1-6 of Table 5.2) are continuous and traceable even though they have been intensely deformed and metamorphosed. This is in marked contrast to the supracrustal layers in the SOB, for which no stratigraphic relations have been proposed.

The sequence represents two depositional cycles, i.e. an early cycle from calcareous sandstone to limestone, and a later cycle from sandstone to siltstone or greywacke with ultimately basaltic lava flow.

The present maximum total thickness of the ISA is estimated to be about 4,000 metres. This includes the combination of repetition by folding and thinning by flattening deformation, but excludes any thickening caused by repetition of nappe sheets. Its original thickness is difficult to estimate, but it may very likely have been many times thicker than it is now, especially as the real top and base of the sequence are no longer evident. The present thickness of each lithological unit varies from a maximum (shown in Table 5.1) down to a few metres.

The Bruna Gneiss and the intrusive mafic and ultramafic metamorphics have been mapped as non-stratigraphic individual bodies, in contrast to the metasediments and layered amphibolite sequence, because they intruded into various levels of the stratigraphic sequence.

5.3. The metasedimentary lithologies

5.3.1. Unit 1: quartz-rich calc-silicate, calc-silicate quartz schist and calc-silicate gneiss

This unit is best exposed in the Naringa Well area (see Map 5) and represents the lowest stratigraphic level of the whole supracrustal sequence. This unit shows a greyish to greenish

colour because of the presence of clinopyroxene and/or epidote. The rocks are hard and resistant to weathering and usually form ridges or hills, with a set of closely spaced joints developed in some places at a high angle to the layering (Plate 5.1.A). These rocks always show a well developed, flaggy, compositional layering which most likely represents metamorphosed and attenuated or transposed original bedding (Plate 5.1.B). This unit is exposed almost continuously for over 60 km from the northern margin of the Oonagalabi Tongue to the west of Brumby Bore and finally pinches out at both ends due to ductile shearing (see Maps 2, 5 and 6). Its topographic features and light colour provide excellent criteria for airphoto interpretation.

Twelve thin sections from this unit give a wide mineralogical variation as shown in Table 5.3. Eight mineral assemblages have been identified and assigned into four rock types, which are named as: A. biotite calc-silicate gneiss; B. quartz rich calc-silicate; C. calc-silicate quartzite; and D. scapolite hornblende biotite quartz schist.

Table 5.3 MODAL COMPOSITIONS OF ROCKS IN UNIT 1 OF THE ISA

rock type	sample number	Dio	Qt	Plg	Scp	Epd	Hrn	Bio	Clc	Sph	Tum	Trm	Opa
A (1)	3406a	30	10	45	2			10		1			2
	3406b	45	10	40				tr	2	2			1
	3789	25	30	20	20			5		tr	tr		tr
(2)	3625a	20	30	5	20		5	20		tr	tr	tr	
(3)	3625b	30	40	7	15	5	1	1		1			
(4)	3534	40	30	1	15	1	1	1	5	1		5	
B (5)	3531	40	40		16		1	1	1	1			
	4120	50	20		18			10	1	tr		1	
	3400	40	50		5		tr	3	tr	tr	2		
C (6)	P4-9	8	69	tr	10	3	3	1	5				
(7)	4195		79		5	5	4					7	
D (8)	3403		50		10		10	30					

FIGURE CAPTIONS OF PLATE 5.1

A: A set of closely spaced cleavage is developed at right angles to a quartzite layer surface (which a hammer lies on). Transverse and oblique joints are also developed. Location No.3511, N of Brumby Bore.

B: Fine-scale compositional layering within the unit 1 calc-silicate gneiss. Location No.3402, NW of Naringa Well.

C: A typical equigranular granoblastic texture within calc-silicate which consists mainly of scapolite, calcite, diopside and plagioclase. The planar and curved grain boundaries form triple points junctions. Field of view: 0.43 mm X 0.55 mm; ppl; sample P4-8.

D: A large lense of boudinaged amphibolite showing a folded tail. Location No.4071, Spriggs Creek, SW of Ruby Mine.

E: Boudinaged thin layers of amphibolite within the massive marble. Location No.4071.

F: Folded calc-silicate marble. The regular and very continuous compositional layering (CS_0) is considered as having been inherited from sedimentary bedding. Location No.4120, E of the Oonagalabi Tongue.

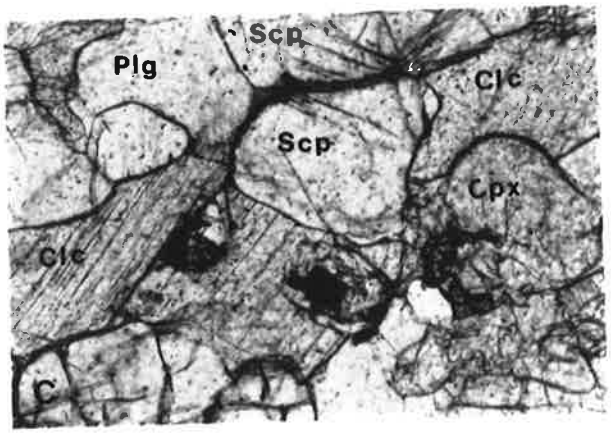
G: Dark needle like crystals of amphibole on the surface of an impure quartzite defining a mineral lineation (CL_1). Field of view: 15 cm X 10 cm; location No.3461, middle east of the Naringa Well area.

H: Slightly migmatized pelitic gneiss showing intense but irregular schistosity and disharmonic small folds. Location No.3916, W of Mt Campbell.

Plate 5.1

















The rocks have predominant polygonal granoblastic textures, and the major minerals, such as diopside, scapolite, quartz and plagioclase, have a similar grain size with straight grain boundaries and triple point junctions. Deformed (mylonitic) microstructures have also been found in the rocks exposed near to major shear zones (e.g. Naringa and Maud Thrusts in chapter 6). The rock compositions suggest that this unit was originally a calcareous sandstone or sandy limestone.

5.3.2. Unit 2: calc-silicate

Unit 2 is best exposed and mapped in the middle of the Naringa Well area. Its thickness varies from 50 to 200 metres. This unit shows a light grey colour for the fresh rock and a brownish colour for the weathered rock. It is less hard and less resistant to weathering because of the greater calcite component and lesser quartz. The field aspect of its fine scale compositional layering is very similar to unit 1.

The boundaries between this unit and the neighbouring units above and below are gradational and arbitrary. However,it proved useful to map out this unit separately from the marble and calc-silicate gneiss to show details of the major structures. This unit is only shown on the map of the Naringa Well area (Map 5) and has been combined with marble or calc-silicate gneiss in other areas (Maps 2 and 6).

The calc-silicate rock includes two rock types; A: typical calc-silicate, and B: quartz bearing calc-silicate. The various mineral assemblages of the calc-silicates are shown in Table 5.4. The calc-silicate has a typical polygonal granoblastic microstructure (Plate 5.1.C) similar to that of unit 1.

Table 5.4 MODAL COMPOSITIONS OF ROCKS IN UNIT 2 OF THE ISA

rock type		sample number	Dio	Qt	Plg	Scp	Epd	Hrn	Bio	Clc	Sph	Tum	Trm	Opa
A	(1)	P4-1	20	5	40	10	20	2		2	1	tr		
	(2)	P4-8	30		35	15		tr	3	15	2			tr
	(3)	3410	46		10	40	tr	tr	2	tr	2			
B	(4)	3520	70	15		13					1	tr	tr	

5.3.3. Unit 3: marble with minor calc-silicate

The fresh outcrops of this unit are white or light grey coloured, whereas when weathered they show yellow or brown colour. The marble is usually massive or thick (10-50 cm) layered (Plate 5.1.D), whereas the calc-silicate marble usually shows a well developed fine scale (1-5 cm) compositional layering (Plate 5.1.F) The main marble and calc-silicate marble extend continuously for about 50 km from the eastern margin of the Oonagalabi Tongue to the NW of Brumby Bore, but the discrete layers, or lenticular bodies, of marble are also found within the pelitic gneiss. Marble and calc-silicate marble are softer and weaker than the previous units and usually form the hill slopes and valleys, though occasionally they form hills and cliffs. Thin layers of amphibolite are boudinaged in some places within the marble (Plate 5.1.D & E). Eight thin sections have been studied (Table 5.5). The textures of these rocks are similar to those of units 1 and 2.

Table 5.5 MODAL COMPOSITIONS OF ROCKS IN UNIT 3 OF THE ISA

rock type	sample number	Clc	Qt	Bio	Trm	Dio	Scp	Plg	Epd	Mus	Sph	Zir
(1)	3399	99	1									
	4125	99	1									
(2)	3417	90	tr	2	7	1						
	3418	90	7	2	tr			1		tr	tr	tr
(3)	3557-3	71	20		1			8			tr	tr
	3333	79		15	1		5					
	3334	60				20	15	5			tr	
	3399A	50		5		40	3		2			

This unit includes three rock types: (1) pure marble (more than 98% calcite), (2) impure marble (calcite between 90% to 98%) and (3) calc-silicate marble (calcite between 50% to 90%).

5.3.4. Unit 4: pure and impure quartzite

Quartzite occurs frequently between the marble of unit 3 and the pelitic gneiss of unit 5, and is very well layered with fine (mm scale) compositional layering. Fresh surfaces of the quartzite are white, whereas its weathered surface is yellow to pale brown. The quartzite displays sharp upper and lower boundaries and is best exposed in the Naringa Well area (Map 5) and less well exposed in the Spriggs Creek area (Map 2, 134°58'E and 23°08'S) It is usually about 1-2 metres or less in thickness, and is thus too thin to present on the map. Sometimes it appears as a thick layer, up to 20 metres in thickness, due to repetition by folding and has been shown on the regional maps. This can be seen in the Spriggs Creek area (Map2) and in the area to the NW of Brumby Bore (Map 5). To show the continuity of this marker horizon, the width of quartzite on the maps has been exaggerated in some places.

This unit includes two rock types: (1) Pure quartzite containing 97% to 99% quartz and minor muscovite, e.g. sample 4165, which usually shows undulatory extinction of individual quartz grains and mosaic grain boundaries; (2) Impure quartzite containing 50% to 90 % quartz and different amounts of diopside, tremolite, epidote and mica, e.g. samples 3416 & 3514, which thus can be conveniently called calc-silicate quartzite. The prismatic tremolites (Plate 5.1.G) define a clear mineral lineation (CL_1, see Chapter 6).

5.3.5. Unit 5: pelitic and semi-pelitic gneiss

This unit is poorly layered but strongly foliated (Plate

5.1.H). It occupies about 50% of the outcrops of the whole Irindina Supracrustal Assemblage (ISA), and extends through the whole ISA area. The rocks are usually deeply weathered, showing a dark brown weathering surface, and easy to erode and form depressional topography. The pelitic gneiss is intercalated with very thin layers of amphibolite in some places (Plate 5.2.A).

Altogether fifteen thin sections have been studied. Their modal compositions are listed in Table 5.6. The pelitic gneisses (rock types 1 to 4 in Table 5.6) contain high amounts (25-56 %) of mica, garnet and sillimanite, compared with the semipelitic gneisses (rock types 5 to 7). K-feldspar is usually absent.

Table 5.6 MODAL COMPOSITIONS OF ROCKS IN UNIT 5 OF THE ISA

rock type	sample number	Qt	Plg	Bio	Gar	Sil	Mus	Scp	Epd	Hrn	Opa	Tum
(1)	P2-7	25	30	40	5						tr	
	3405	29	30	40	1						tr	tr
	4306	30	33	30	5					1		1
(2)	3264	37	20	30	5		2		2	3		
(3)	P3-1	25	20	45	4	2						
	3209	20	21	45	1	10	3					
(4)	P4-4	25	35	29				8	2			1
	3404	30	30	30				10				
(5)	4261	40	40	10			10					
(6)	3053D	50	40	5	5							
	3149	49	20	20	1							
	3287	58	20	12	10							
	3305	57	20	20	3						tr	tr
	P2-6	30	50	15	5	tr						
(7)	4254	50	38	5		3	1				3	

Minerals in most of the pelitic and semipelitic gneisses are mainly evenly distributed (Plate 5.2.B) forming granoblastic microstructure with an intense foliation which is defined by the pre-

FIGURE CAPTIONS OF PLATE 5.2

A: Very fine-scale intercalation of amphibolite and garnetiferous biotite gneiss. The latter shows gradational variation within each layer but sharp contacts between adjacent layers. It was probably a sequence of interlayered tuffacious and fine-grained clastic material. The possible younging direction (gradation from quartzofeldspathic to micaceous) is downwards. Location No.3287, N of Mt Ruby.

B: Biotite plagioclase gneiss showing typical granoblastic texture with evenly distributed biotite. Field of view: 3.4 mm X 2.2 mm; ppl; sample 3149, N of Mt Ruby.

C: Biotite within a pelitic gneiss showing intense foliation which is truncated by the euhedral porphyroblastic garnet. Field of view: 3.4 mm X 2.2 mm; ppl; sample P2-7.

D: Biotite within pelitic gneiss defines an intense foliation and is bent around a syntectonic garnet megacryst. Field of view: 3.4 mm X 2.2 mm; ppl; sample 3204.

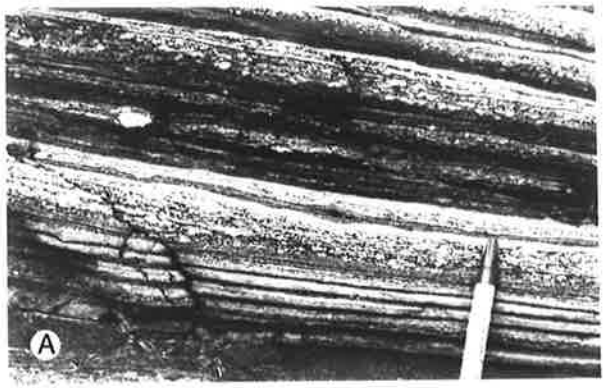
E: Two sets joints developed at right angles to each other and perpendicular to the layering of a thick amphibolite sequence. The northerly trending joints parallel the mineral lineation. Location No.3224, NW of Mt Ruby.

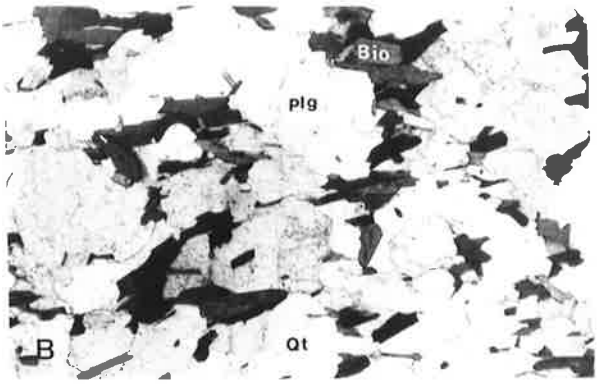
F: Spheroidal weathered surfaces of the thick amphibolite sequence at the summit of Mt Ruby. Location No.3009.

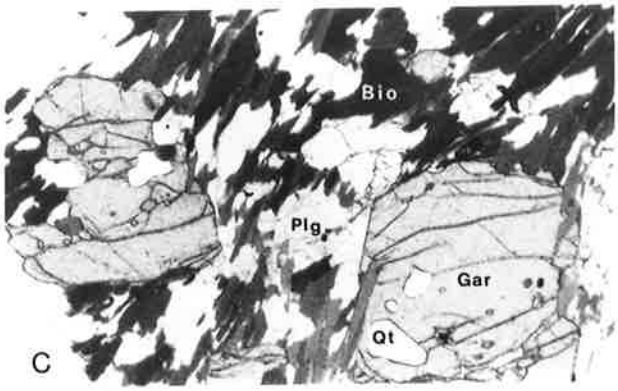
G: Compositional layering within a thick amphibolite sequence. Some layers show a internal gradational variation between the leucocratic part and the melanocratic part. N of Ruby Mine.

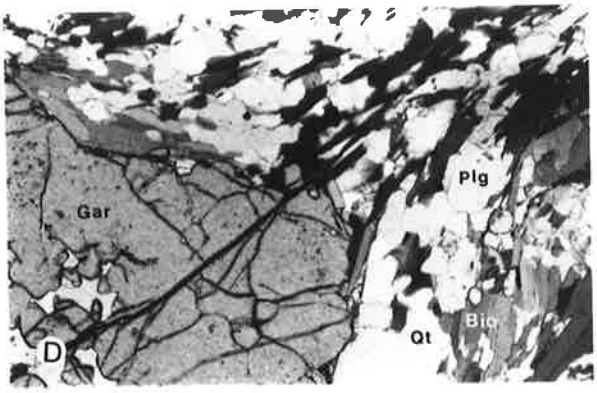
H: Weakly migmatized layered amphibolite. The quartz plagioclase veinlets were emplaced into the amphibolite mainly along a small shear zone, but also entered the layering and cleavage. The relationship of cleavage and layering indicates a dextral shearing which is coincident with the regional shear sense of the Bruna Thrust at the bottom of the thick amphibolite sequence of Ruby Nappe sheet (see chapter 7). Location No. 3041, W of Mt Ruby.

Plate 5.2

















ferred orientation of micas (Plate 5.2.C). Lineations are usually lacking or very weak, but become obvious in the sillimanite-rich pelitic gneiss where a mineral lineation is defined by the long axes of sillimanite. Mylonitic textures are rarely found even within shear zones. Sometimes the pelitic and semipelitic gneisses show porphyroblastic textures with garnet and plagioclase mega-crysts developed within an equigranular gneissic matrix (Plate 5.2.C & D).

5.4. The Harts Range meta-igneous complex

5.4.1. Unit 6: layered amphibolite

A continuous layered sequence of amphibolite has been mapped within the Irindina Supracrustal Assemblage and includes three major regional lithological sheet-like bodies. The upper and northernmost one is confined within the Campbell Nappe (see Fig. 6-1 & Chapter 6)and extends for over 100 km in strike length with its thickest part (about 1,000 m in thickness) in the Mt Campbell area. The lower one is confined within the Riddoch Nappe (Chapter 6) and extends for over 35 km in strike length with its thickest part (about 1,500 m in thickness) in the Mt Riddoch area. The southernmost one is confined within the Ruby Nappe (Chapter 6) and extends for over 50 km in strike length with its thickest part (about 2,000 m in thickness) in the Mt Ruby area. However this latter sheet thins rapidly towards both ends.

Thin layers of amphibolite, as well as small amphibolite boudins, can also be found within the pelitic gneiss. Plate 5.2.A shows an example of very fine scale intercalation of amphibolite and garnetiferous biotite gneiss.

The amphibolite is black coloured both on fresh and weathered surfaces, and is easy to identify in the field and to interpret

from the airphotos. Some massive amphibolite develops three joint sets (Plate 5.2.E), which are approximately perpendicular to each other, and which thus form spheroidally weathered outcrops at hill crests (Plate 5.2.F). The amphibolite is erosion resistant and usually forms the ranges or peaks of this area.

There is a great variety of rock types in this amphibolite unit. Some amphibolites are thick layered whereas others develop a fine scaled compositional layering, about a few to tens of mm in thickness. Slightly migmatized amphibolites are found locally (e.g. Plate 5.2.H). Some amphibolites consist of intercalated leucocratic thin layers and melanocratic thin layers. Each layer has a gradational boundary at one side and a sharp boundary at the other side (Plate 5.2.G), which may thus indicate the direction of younging if it were interpreted as a relict cryptic feature (Best, 1982). However, the true origin of this feature is not really understood.

Some thin, but very continuous, layers of garnet bearing quartzite and biotite schist have been found within the amphibolite sequence. The extremely continuous distribution of the amphibolite sequence and the intercalated thin layers of quartzite suggest that the layered amphibolite represents mainly metamorphosed basaltic lava, though no intrusive or extrusive textures have been found. This interpretation has been strongly supported by the geochemical interpretation of Sivell & Foden (1984). However some lenticular discrete bodies of amphibolite show some similarity to metagabbro or meta-ultramafic bodies and thus have been interpreted as intrusive bodies (e.g. the swarm of small amphibolite bodies SE of Boots Dam on Map 2).

The amphibolites mainly show unstrained coarse equigranular granoblastic (Plate 5.3.A) and elongate granoblastic textures

FIGURE CAPTIONS OF PLATE 5.3

A: Amphibolite showing typical unstrained coarse equigranular granoblastic texture with straight grain boundaries and triple points junctions. Field of view: 3.4 mm X 2.2 mm; ppl; sample P2-7A.

B: An example of slightly elongate granoblastic texture of amphibolite. Field of view: 3.4 mm X 2.2 mm; ppl; sample P1-2c.

C: Deformed migmatized amphibolite showing porphyroclasts of hornblende and a mylonitic matrix which comprises fine-grained recrystallized quartz, plagioclase and hornblende. The quartz ribbon might be a syntectonic veinlet as it is less deformed than plagioclase and also quartz is usually not contained in normal amphibolite. Field of view: 3.4 mm X 2.2 mm; ppl; sample 3008, Mt Ruby.

D: Same view as above; X-polars.

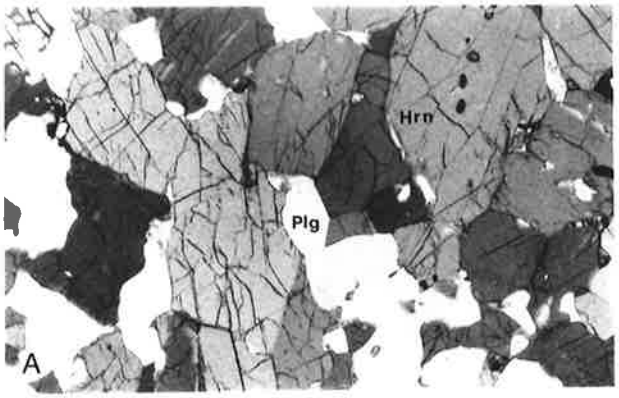
E: Weakly deformed amphibolite showing compositonal layering of alternating dominant hornblende and dominant plagioclase. Much of the plagioclase has been recrystallized to form a fine-grained matrix. A few plagioclase porphyroclasts show undulatory extinction. Grain size has been greatly reduced along the margins of large hornblendes and plagioclases. Field of view: 3.4 mm X 2.2 mm; ppl; sample 3205, near the Ruby Thrust.

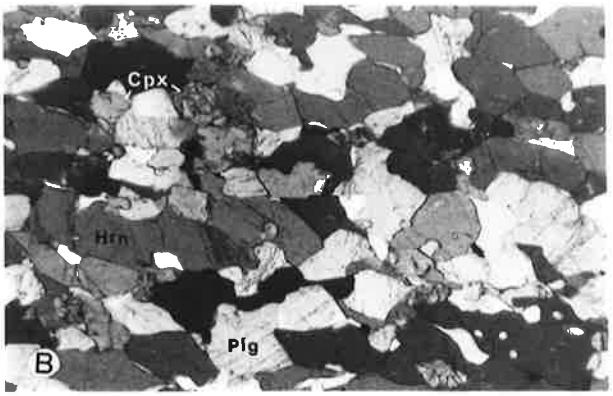
F: Same view as above; X-polars.

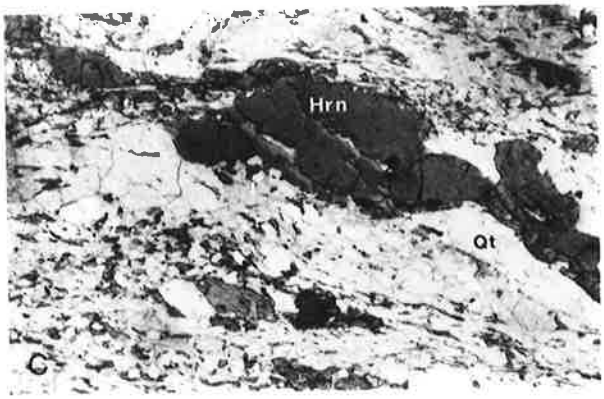
G: Meta-ultramafic rock comprising cummintonite, two pyroxenes and spinel and showing typical granoblastic texture. Field of view: 3.4 mm X 2.2 mm; ppl; sample 4317, N of Pannikan Dam.

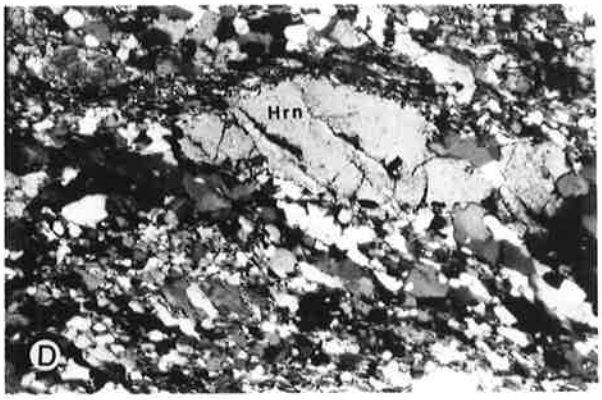
H: A hard and very dark coloured ultramafic rock body stands out from the soft pelitic gneiss. Location 3082.

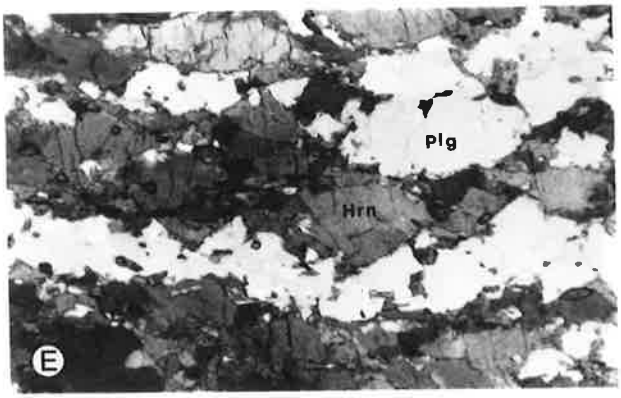
Plate 5.3

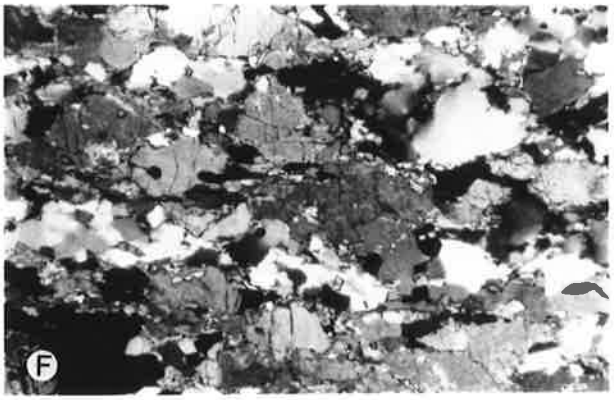


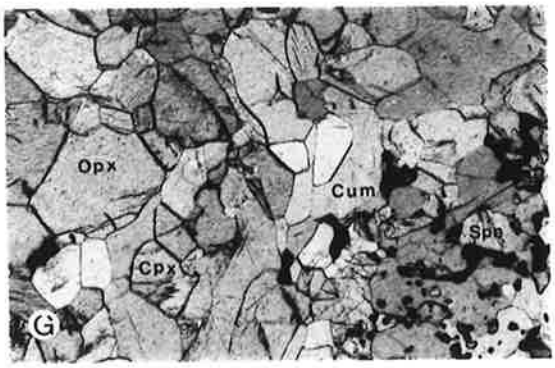














(Plate 5.3.B). Deformed microstructures (e.g. Plate 5.3.C, D, E & F) are found near thrust boundaries (see Chapter 6). The mineral assemblages of amphibolites are essentially hornblende and andesine plagioclase with different amounts of garnet, clinopyroxene, biotite, epidote, scapolite and quartz. Accessory minerals are mainly iron oxide, sphene, and occasionally apatite, rutile and zircon. No orthopyroxene has been found within twenty six thin sections of amphibolite studied. Their average modal compositions are listed in Table 5.7.

Table 5.7 AVERAGE MODAL COMPOSITIONS OF AMPHIBOLITES IN THE ISA

rock type	number of samples averaged	Plg	Hrn	Cpx	Gar	Qt	Scp	Cum?	Opa	Sph
1	7	36	54	9					tr	
2	1	30	58	2			8			2
3	1	25	65	5	3					1
4	2	30	64	5					1	
5	13	36	64						tr	tr
6	1	48	50	tr		2				tr
7	1	28						70	2	

There are 7 varieties of mineral assemblages within the amphibolites. The modal composition of each sample are listed in Appendix I.

5.4.2. Metamorphosed ultramafic rocks

Most of the ultramafic rocks found in the area are too small to show on the regional maps except for two major bodies. One is a layered body within the amphibolite sequence, about 2 km NE of Pannikan Dam (see Maps 2 and 6). Its outcrop is about 2 km long and 30-50 m wide, trending E-W parallel to the surrounding amphibolite layering. Within the ultramafic body a weak layer parallel schistosity is manifested by the preferred orientation of amphiboles. A representative sample (4317) comprises cummingtonite

UNIVERSITY OF ADELAIDE LIBRARY

(77%), orthopyroxene (10%), clinopyroxene(7%), garnet (3%), dark green spinel(3%) and minor opaque minerals and shows a typical coarse metamorphic microstructure of equigranular polygonal mineral grains forming triple point junctions (Plate 5.3.G).

The second body has a rounded outcrop and lies within the pelitic gneiss sequence 3 km SE of Mt Riddoch (see map 2 & 6). It has a dimension of about 300 X 500 m. This ultramafic body is only weakly deformed and is enwrapped by schistose pelitic gneiss, thus resembling a rigid body in a viscous matrix (Ghosh & Ramberg, 1975). A number of rock types are found in this ultramafic body, including pyroxenite and pyroxene garnet rock. An anorthosite vein, only 5 cm wide, has straight and undeformed vein walls and contains perfect hexagonal prismatic crystals of white corundum, which are 0.5 to 1.5 cm in size. The corundum crystals have not been studied in detail but their appearence looks different from the pink-coloured ruby crystals in the Ruby Mine area (Lawrence et al., 1987).

Smaller ultramafic bodies within the pelitic gneiss usually form small black hills or mounds probably due to the competence contrast between the ultramafic rocks and the surrounding pelitic gneisses (Plate 5.3.H). The ultramafic rocks commonly show equigranular textures, however some ultramafic rocks have been partly altered by chlorite which forms a weak schistosity. The modal compositions of some samples are listed in Table 5.8.

Table 5.8 MODAL COMPOSITIONS OF ULTRAMAFICS

	3086	3083	3094A
olivine	10	10	
orthopyroxene	50		
colorless amphibole	37	85	89
chlorite	tr	4	10
spinel	2		
opaque	1	1	1

An overturned mafic to ultramafic sequence occurs about 2-3 km NE of Boots Dam, within the pelitic gneisses. This mafic to ultramafic metamorphic body comprises three gradational layers of different rock types: an ultramafic layer (sample 3086) at the top; a plagioclase-rich amphibolite layer at the base; and a plagioclase-poor (more mafic) melanocratic amphibolite layer in the middle. This kind of layering is considered to result from igneous differentiation and is similar to the cumulate-type structure found in the gabbro layer of oceanic crust (Best, 1982). Typically in such an igneous sequence the ultramafic layer occurs at the base, the normal gabbro in the middle and the leucocratic gabbro or anorthosite at the top (Best, 1982). Thus the mafic to ultramafic body described above shows an inverted sequence and implies an overturned position for this mafic to ultramafic body and its surrounding metasedimentary rocks. This feature has been used as one line of evidence to establish a local stratigraphic sequence (see section 5.2.).

In the northern central part of the Harts Range (the Ruby Mine area), a well layered ultramafic-anorthosite complex (Katz, 1981) possesses a local stratigraphic relationship (Lawrence et al. 1986), but it has not been found elsewhere in the area and will not be further discussed in this thesis.

5.4.3. Metagabbro

Metagabbro bodies have been found within the HRSC, the major sheet of Bruna Gneiss, the Florence/Leaky Shear Zone and in the other SOB areas (e.g. the metagabbro bodies at Black Mountain in the Entia Dome, see chapter 2).

Some of the metagabbros in the HRSC retain a typical relict

gabbroic microstructure which can be observed in thin section (Plate 5.4.A & B). This relict igneous microstructure is the main criterion differentiating the metagabbros from other small amphibolite bodies, whose origin is still uncertain, i.e. these latter may represent completely metamorphosed gabbroic bodies or boudinaged thin layers of metamorphosed mafic volcanic rocks.

A large lenticular body of gabbro occurs within the Bruna gneiss, 3 km east of Salthole Dam and 4 km south of Harding Springs Well. It is about 2.5 km long and 2 km wide, over 500 metres thick in the middle and pinches out rapidly at both ends. It forms a prominent black hill within a flat area of Bruna Gneiss. Most parts of this body retain relics of the original gabbroic microstructure (Plate 5.4.A & B), though some pyroxenes have been recrystallized and altered to amphibole and biotite (e.g. sample 3096A). However, at the margins of this metagabbro body, a mylonitic fabric (e.g. sample 3364) has been found.

Five thin sections of this gabbro body have been studied, and their modal compositions are shown in Table 5.9.

Table 5.9 MODAL COMPOSITIONS OF METAGABBROS IN THE HRSC

sample number	Plg	Hyp	Sal	Amp	Hrn	Bio	Gar	Opa	Chl	Epd	Sca
3364	50	15	15		15		5				
3096	40	10	5		38	5		1			1
3069	50	10	8		30			1			1
3098	50				30				10	5	
3096A	49			40	5	5		1			

Smaller metagabbro bodies are mainly found just to the north of Mt. Ruby. The size of each body varies from 50 to 500 metres. Their modal compositions are summarized as: labradorite (An50-An60) (50%), hypersthene (13-20%), salite or augite (10-20%), hornblende (10-20%) with occasional garnet (5%)and olivine (1%).

FIGURE CAPTIONS OF PLATE 5.4

A: A relict hypidiomorphic igneous texture of metagabbro. Small-grained hornblende occurs along the margin of coarse-grained orthopyroxenes. Bending and undulatory extinction can be seen within coarse grains of plagioclase. Field of view: 3.4 mm X 2.2 mm; ppl; sample 3096; S of Harding Spring Well.

B: Same view as above; X-polars.

C: Thin layers of mafic ultramylonite, which are identical to the lithology of the Florence Shear Zone, appear in the thick Bruna Gneiss body as xenolithic layers. Location No.3576.

D: A close-up of the mafic ultramylonite in (C:) showing that the mafic layer was slightly boudinaged.

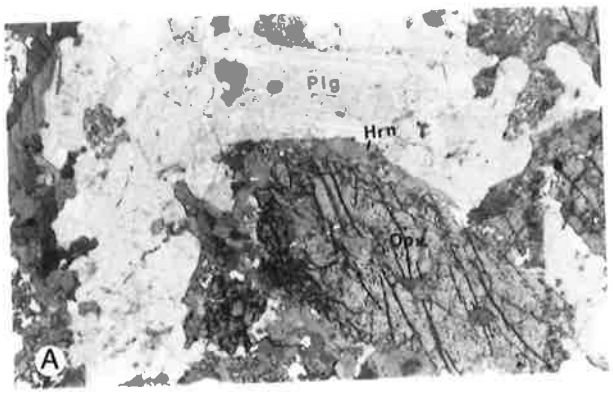
E: Unmylonitized Bruna Gneiss showing typical megacrystic texture. A micaceous xenolith at the top margin of the outcrop (above the hammer) provides one of the lines of evidence for its intrusive origin. Location No.4242.

F: A close up view of the biotite rich mylonitized megacrystic Bruna Gneiss is a YZ section showing variable shear sense within different levels; the upper part shows a dextral shear sense whereas the lower part shows a sinistral shear sense. Different megacrysts of potash feldspar also show different intensities of deformation. One megacryst remains undeformed with its long axis perpendicular to the mylonitic foliation (up left). Location No.3097.

G: A sharp contact between two rock types within the Bruna Gneiss complex. The lower part is the typical and major one, the biotite rich megacrystic Bruna Gneiss (augen gneiss); the upper part is nonmegacrystic granitic gneiss, SW of Harding Springs Well.

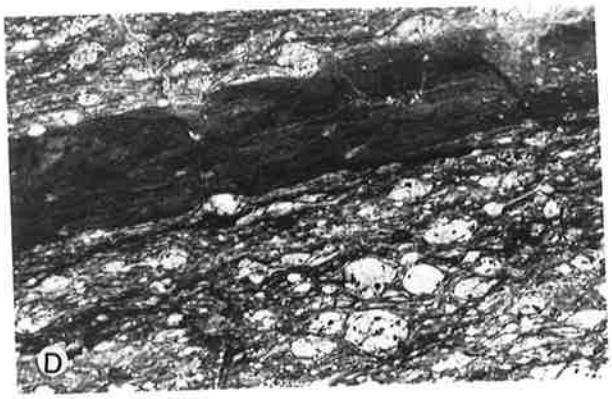
H: Mylonitic schistosity is oblique to and transect the lithological boundary between two rock types of the Bruna Gneiss. The nonmegacrystic granitic gneiss behaves more competently than the biotite rich megacrystic gneiss which has been deformed to blastomylonite. Location No,4007.

Plate 5.4

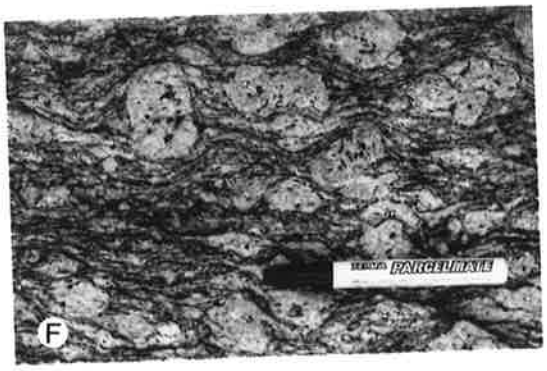


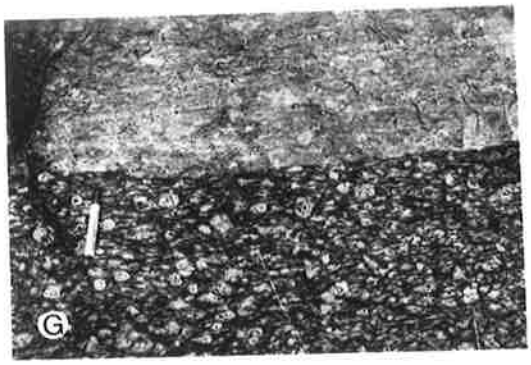














The metagabbro bodies within the HOB (including those within the Bruna Gneiss) and the SOB, though now spatially isolated, are all very similar and thus are probably formed from a magma source similar to that of the layered amphibolite (originally basaltic lava) of the ISA. The coexistence of layered amphibolite and metagabbro suggests that the gabbro must have formed later than the extrusion of the basaltic lava sequence, because mafic magma crystallizes to form gabbros only at deeper crustal levels. It means, that when the gabbros intruded into the supracrustal, the originally basaltic lava had been subsided to the same deep crustal level from the earth's surface and metamorphosed to form amphibolite. The large metagabbro body near Salthole Dam occurs as an inclusion within the major sheet of the Bruna Gneiss, thus confirming that the main intrusive event of the mafic magma predated the intrusion of the Bruna Gneiss granitoid during the Harts range Orogeny.

5.5. Bruna Gneiss

5.5.1. Introduction

The Bruna Gneiss was described as a stratigraphic unit of metamorphosed arkosic sedimentary rock by Joklik (1955), or of metamorphosed acid vocanic lava and ignimbrite by Shaw et al., (1979). It was also described as underlying and older than the Irindina Gneiss (Joklik; Shaw, et al., op cit). Recent studies have revealed that the Bruna Gneiss is a metamorphosed syntectonic intrusive granitoid complex (Ding et al., 1983; James et al, 1983, Ding & James, 1985). This has been partly accepted by Shaw et al. (1984b).

The Bruna Gneiss was mainly intruded along the Florence/Leaky Shear Zone (see chapter 4), and was also emplaced into both the

SOB and HOB (Maps 2 & 5). The major sheet-like body of Bruna Gneiss extends from the west of Florence Creek, around the margin of the Entia Dome, to the east of Leaky Bore, and covers an area of outcrop of about 240 km^2. It appears at the bottom of the Leaky Shear Zone to the east and transgresses upwards gradually to the top of the Florence Shear Zone in the west (Map 2). The major sheet of Bruna Gneiss is quite thick (possibly over 1,000 m) in the Harding Springs Well to Leaky Bore area, but it thins gradually towards both the north and west. It is only 20-30 m thick at the north and NE margin of the Entia Dome and finally pinches out altogether at the western end of the Florence Shear Zone. Metagabbro bodies and thin layers of mylonitized mafic granulite are found as inclusions within the major sheet of Bruna Gneiss (Plate 5.4.C & D). Typical micaceous xenoliths are also found within the Bruna Gneiss (e.g. Plate 5.4.E).

At the western edge of Map 5, a small sill-like body of Bruna Gneiss has intruded along the Oonagalabi Thrust (HRT_1, see Chapter 7) and has been further sheared by a later intermittent movement of this Thrust. Small laccolithic or sill-like bodies of megacrystic granitic gneiss are also found within the (ISA) calc-silicate layers at the northern margin of the Oonagalabi Tongue (Map 6), and within the marble and pelitic gneiss of the ISA in the western part of the Naringa Well area (Map 5), and also within the amphibolite layers north of the Ruby Mine area. These small intrusive bodies are petrographically identical to the major sheet of Bruna Gneiss. Some granitic gneiss bodies in the Entia Gneiss are petrographically similar to the Bruna Gneiss and show clearly intrusive origins (see chapter 2) but have not been separated out from other granitic gneisses during mapping. All evidence suggests an intrusive precursor of the Bruna Gneiss.

5.5.2. Mesoscopic features

The outcrops of Bruna Gneiss are pink coloured and usually form prominent hills. Three sets of major joints are developed within the Bruna Gneiss and are oriented perpendicular to each other with one set parallel to the gneissic foliation. These have formed due to its rather homogeneous structure, and are like those commonly observed in unmetamorphosed granitoid rocks. The cube-like joints system results in a characteristic topography, and provides a good criteria for airphoto interpretation.

The Bruna Gneiss comprises two main phases. The first and major one is a biotite-rich granitic gneiss with significant megacrysts of potash feldspar (Plate 5.4.F), which are very similar to those in some unmetamorphosed megacrystic granites, e.g. the Cambrian Victor Harbor Granite in South Australia (Milnes, 1977). The megacrysts in the Bruna Gneiss are considered the remainder of igneous phanocrysts not porpyroblasts similar to that discussed by Vernon (1986), though a metamorphic origin for the megacrysts cannot be excluded (Shaw et al., 1984). This rock type has been intensly deformed and shows the typical structure of an augen gneiss (Plate 5.4.F), i.e. large megacrysts form porphyroclasts which are wrapped around by a fined grained schistose matrix. In appearance it is thus very similar to a blastomylonite defined by Higgins (1971).

The second and minor type is an equigranular leucocratic granitic gneiss without megacrysts (Plate 5.4.G), which is exposed mainly along the west, north and east margins of the Entia Dome (Lawrence et al, 1987; Macdonald, 1986; Parker, 1986).

The schistosity within the Bruna Gneiss is found in some places oblique to, and transecting, the boundary between the megacrystic and equigranular phases (Plate 5.4.H). The equigranu-

lar granitic gneiss behaves in a more competent way than the biotite rich megacrystic granite gneiss, and has been boudinaged during deformation (Plate 5.5.A & B). A weak compositional layering in the equigranular granitic gneiss is somewhat truncated by the megacrystic Bruna Gneiss along an irregular boundary, indicating that the former one intruded slightly earlier than the latter.

Some very large megacrysts of potash feldspar, about 20 cm long, may represent the fragments of early pegmatite veins after intense mylonitization (Plate 5.5.C). Typical mylonite or ultramylonite occurs within the major Bruna gneiss sheet, particularly at its topmost and basal margins (the Bruna Thrust and the Entia Thrust) and will be discussed later in Chapter 7.

5.5.3. Modal composition and microstructure

The modal compositions of Bruna Gneiss samples have been estimated from 20 thin sections and are listed in Table 5.10.

Mylonitic microstructures (Plate 5.5.D) are dominant in these thin sections studied. Hornblende and garnet are competent during the mylonitization and remain as weakly deformed or undeformed megacrysts (Plate 5.5.E & F). This contrasts markedly with the intense deformation of hornblende and garnet in the mylonites of the Florence Shear Zone. Some of the coarse-grained plagioclase and microcline feldspars also remain as porphyroclasts whereas others have been intensely deformed and recrystallized to form the fine-grained matrix and quartz ribbons (Plate 5.5.G). However the the matrix of the mylonitized Bruna Gneiss is coarser than typical very fine grained mylonite.

FIGURE CAPTIONS OF PLATE 5.5

A: Weak compositional layering within a thin layer of nonmegacrystic granitic gneiss is truncated by the biotite-rich megacrystic Bruna Gneiss. The foliation within the Bruna Gneiss is oblique to the lithological boundary. Location No. 4005, NW of Leaky Bore.

B: Boudinaged nonmegacrystic granitic gneiss layer within the biotite rich megacrystic Bruna Gneiss. Location No.4005.

C: Close-up of the upper left corner of (B:). Mylonitic schistosity within the biotite-rich megacrystic bruna Gneiss is oblique to, and transects, the lithological boundary. The shape of this lenticular body of nonmegacrystic granitic gneiss and its long tail looks very similar to the typical microstructure of porphyroclasts in mylonite.

D: A very large megacryst of potash feldspar within the typical mylonitized Bruna Gneiss. It might be a remnant of pegmatite which was much more competent than the Bruna Gneiss during the mylonitization. Location No.3026.

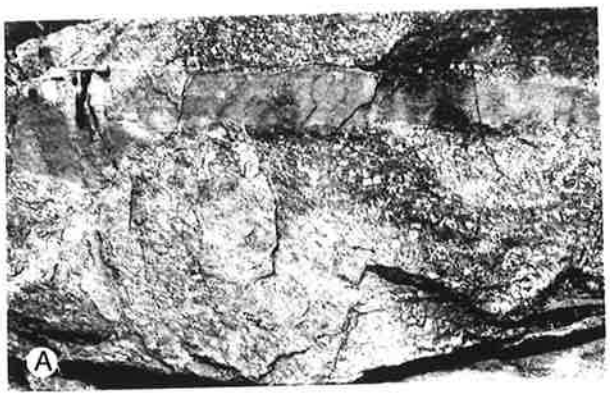
E: Typical mylonitized biotite rich megacrystic Bruna Gneiss showing weakly strained porphyroclasts of potash feldspar and intensely foliated fine-grained matrix. Field of view: 55 mm X 38 mm; sample No.P3-4; X polars.

F: A large porphyroclast of hornblende within the fine- grained matrix of mylonitized Bruna Gneiss. A large biotite inclusion within the hornblende porphyroclast is oriented at right angles to the mylonitic foliation. It suggests that the biotite inclusion occurred before the mylonitization. Field of view: 3.4 mm X 2.2 mm; ppl; sample No.P1-4.

G: A megacryst of garnet within a fined grained matrix of mylonitized Bruna Gneiss. The zoned interior structure of the garnet is discordant to the mylonitic foliation and thus suggests an earlier history before mylonitization. Field of view: 3.4 mm X 2.2 mm; ppl; sample No.P1-4.

H: Porphyroclast of plagioclase and an attached quartz ribbon fringe within fine-grained matrix of mylonitized Bruna gneiss. Field of view: 3.4 mm X 2.2 mm; X polars; sample No.P1-3.

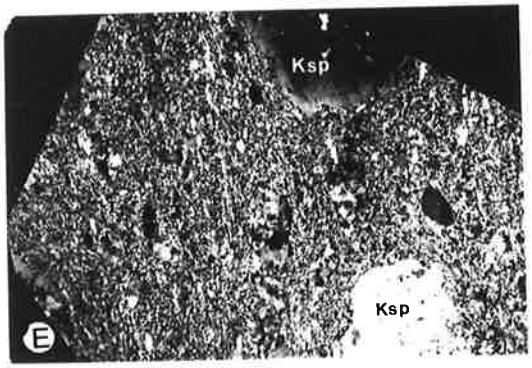
Plate 5.5

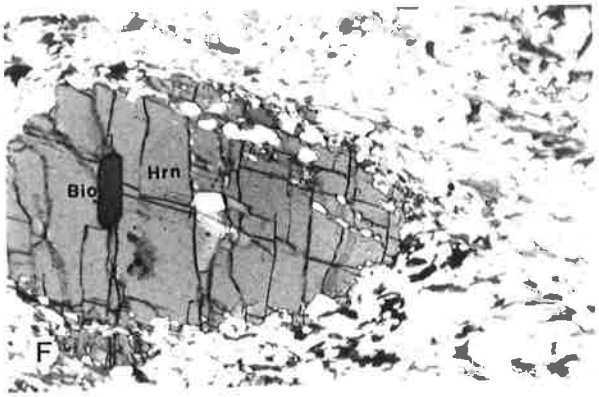


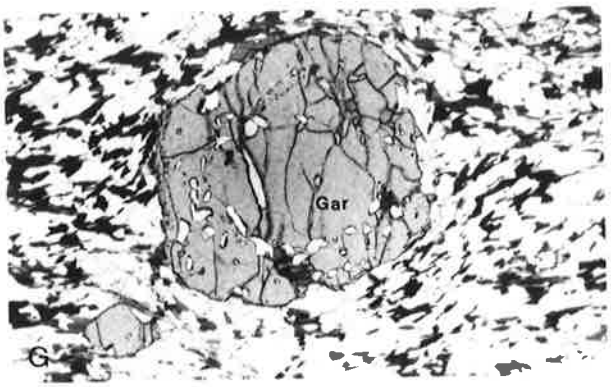












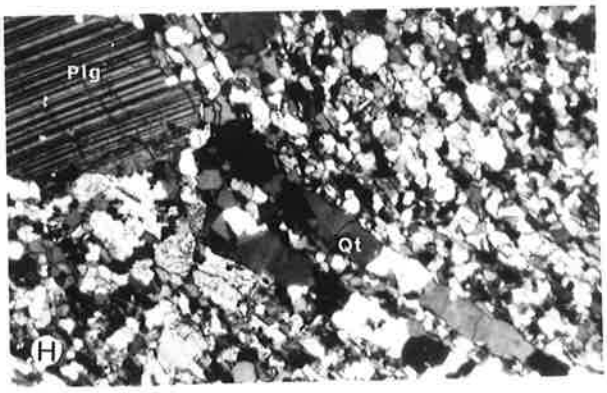


Table 5.10 MODAL COMPOSITIONS OF SAMPLES FROM THE BRUNA GNEISS

rock type	sample number	Qt	Plg	Atp	Pth	Mcl/Ksp	Bio	Hrn	Gar	Mus	Opa	Epd
1.	4190	30	30		5	19	1	15				
	4641	20	55			15	8	1		tr		1
2.	3006	40	30			20	5		5			
3.	P1-3	30	30			35	5			tr		
	4004	30	8			50	10					2
4.	3210	26	30		1	29	8	3	2			
	3013	20	30			30	15	2	3			
	3557-1	13	30			40	10	3	2		2	
	P3-3B	11	20			60	3	3	2		1	
	P1-2A	30	30	3			30	2	5			tr
	P1-2B	30	33	2			15	15	5			tr
	P1-2D	20	25	10			30	5	10			tr
	P1-6	30	40			7	17	1	2			3
	P1-7	25	30			5	25	5	5			5
	P1-4	28	30			15	22	3	1			1
	3538	30	32	1		19	10	5	3			tr
	3004	34	10			30	16	5	5			
	3382	11	30			38	15	2	1			3
	P1-5	17	19			49	8	2	4			1
	3151	10	10			64	10	2	3			tr

CHAPTER 6 THE EARLY STRUCTURES OF THE HARTS RANGE OROGENY

6.1. Introduction

The structures of the Harts Range Orogeny were formed during two sequential tectonic stages. The deformational regime involved a simple compression from north to south during the earlier stage but became a very complicated process of intermittent thrusting and folding during the later stage. The structures formed during the earlier stage, which mainly affected the Harts Range Orogenic Belt (HOB) itself, are presented in this chapter, whereas the structures formed during the later stage, which affected both the HOB and the SOB, will be presented in the next chapter.

6.2. Compositional layering and the earliest foliation (CS_0)

The boundaries of the lithological units and the fine-scale compositional layering within each unit are the essential planar elements used in this study to mark the overall structural geometry. The compositional layering in some of the metasediments is very likely to represent metamorphosed and deformed sedimentary bedding, and is thus labelled as CS_0. There are two important features supporting this interpretation: (1) this type complex compositional variation (up to 5 compositionally different thin layers in one single calc-silicate specimen) is unlikely to have formed merely by metamorphic differentiation; (2) the extreme continuity of the compositional layering is unlikely to be due only to deformation. In contrast, the compositional layering within the amphibolite sequence is considered to have formed mainly by metamorphic differentiation and partial melting (Lawrence et al., 1987), or intrusion of tonalitic magma (Sivell & Foden, 1985). Some amphibolites have fine-scale graded compositional layering

(Plate 5.2.G), which may represent the original bedding of tuffs, but this cannot be substantiated with certainty. However, metamorphism and deformation must have greatly assisted the development of the fine-scale compositional layering by the flattening and/or elongation of CS_0.

6.3. Structures of the CD_1 deformation

The first structures recognized to have deformed the CS_o compositional layering are CF_1 folds, a CS_1 axial plane foliation and a CL_1 mineral lineation.

The CF_1 folds are found mainly on a small-scale. However, a pair of mappable CF_1 folds have been recognized about 5 km SE of Mt Riddoch (Map 6). The folds have E-W trending axial surfaces and NW plunging hinges. The southern fold is outlined by amphibolite layers (unit 6) with pelitic gneiss (unit 5) in the core. It is isoclinal with an axial plane dipping 50^o N and a hinge plunging at 23^o-298^o. Along the fold axial trace, further to the west, small-scale CF_1 folds have caused intimate interfingering of pelitic gneiss and amphibolite. Within the pelitic gneiss an axial planar fabric (CS_1) is dominant with no recognizable CS_0, whereas in the amphibolite layers the CS_1 is subordinate in comparison with the CS_0. The compositional layering (CS_0) within the boudinaged amphibolite is clearly truncated by the schistosity (CS_1) within the pelitic gneiss (Plate 6.1.A, B & C).

The northern CF_1 fold of the pair (Map 6) is manifested by folded pelitic gneiss, marble and calc-silicate with amphibolite in the core. It shows a similar profile to the southern one and plunges at 17^o-303^o. A mineral lineation lies parallel to the fold hinge and is considered to have formed during the CF_1 folding and is thus recognized as CL_1. Arcuate CL_1 lineations also occur at

FIGURE CAPTIONS OF PLATE 6.1

A: Boudinaged amphibolite body in migmatized pelitic gneiss. Location No.3916, west of Mt Campbell.

B: A close-up of (A) showing the schistosity within the migmatized pelitic gneiss wrapping around the edge of the amphibolite body, whereas the layering (CS_0) within the amphibolite is truncated by the schistosity (CS_1).

C: Details of the S_0 foliation in the amphibolite (the darkest upper part), the S_1 schistosity in the pelitic gneiss (left-lower part) and the garnetiferous migmatitic veinlet (coarse, massive and light coloured in the middle) in (B).

D: Curved CL_1 lineation on the S_1 surface of a pelitic gneiss layer. The lineation on the left plunges at 16°-010°, whereas the lineation on the right plunges at 40°-032°. Location No. 3915, W of Mt Campbell.

E: Small CF_1 folds. Thin layers of quartzite within the calc-silicate gneiss are folded and transposed to form intrafolial rootless folds, which have thinned parallel limbs and thickened rounded closures (Class 2 type) This outcrop is situated near to the hinge of a regional scale CF_2 fold, which plunges at 20°-300° whereas the small CF_1 folds plunge at 36°-100°. The intersection angle between the hinge of CF_1 and that of CF_2 is about 56°. Location No.3588, W of Naringa Well.

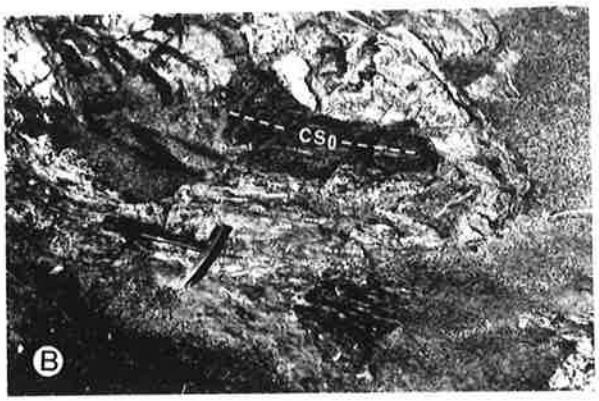
F: CF_1 folds are clearly seen within the calc-silicate layer with limbs transposed along the main contacts between calc-silicate and marble. Location No.3520; N of Brumby Bore.

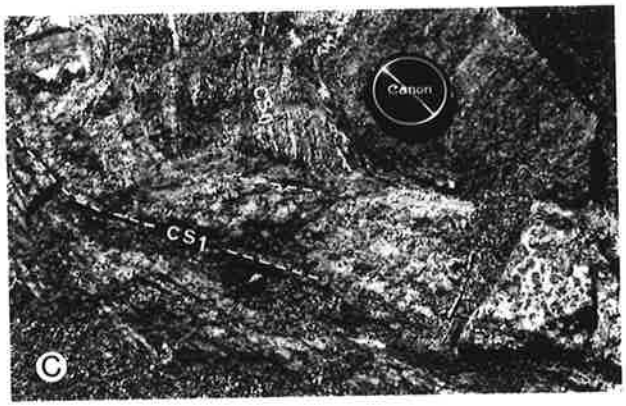
G: Details of the CF_1 folds in (F) showing the profile of Class 2 type fold, with parallel dip isogon (Ramsey,1967); a weak axial planar cleavage can be seen in the field transecting the layering around the fold closure; its hinge plunges at 10°-360°.

H: Micrograph of a calc-silicate collected from the core of the CF_1 fold in (G), showing folded compositional layering (CS_0) and the weak axial planar schistosity. Field of view: 55 mm X 37mm; ppl; sample 3520.

Plate 6.1



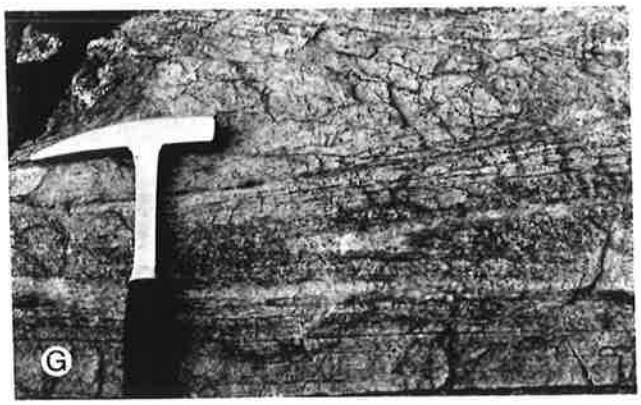














the outcrop scale (Plate 6.1.D). These are interpreted as having been deformed by inhomogenous elongation in a northerly direction parallel to the transport direction of later major folds (CF_2) and/or shear direction of the later CT thrusts (see section 6.5). This is similar to those described for the development of arcuate lineations and sheath folds within large shear zones (Henderson, 1981).

Minor CF_1 folds have been found in the Naringa Well area (e.g. Plate 6.1.E). Here Class 1c to 2 type isoclinal CF_1 folds are manifested by thin quartzite layers within calc-silicate gneiss. They have steeply dipping axial surfaces and steeply plunging hinges without any visible axial planar fabric. The fold limbs have been virtually transposed, thus only the intrafolial rootless closures are preserved.

Small isoclinal CF_1 folds are also found within marble (Plate 6.1.F & G), calc-silicate (Plate 6.2.C) and impure quartzite (Plate 6.2.A & B). The CF_1 fold limbs usually appear to be transposed along straight CS_1 surfaces, whereas in the closure area a weak axial planar fabric (CS_1) can be seen clearly oblique to the layering (CS_0) on the outcrop (Plate 6.1.G) as well as in thin section (Plate 6.1.H). Some of the intercalated pelitic gneiss layers within the major amphibolite sequence may have resulted from the CF_1 folding but fold closures or stratigraphic evidence is lacking.

6.4. Structures of CD_2 deformation

CF_2 folds have been mapped throughout the whole area, whilst the best examples are found in the Naringa Well area (Map 5) and the Mt Campbell area (Map 6). The CF_2 folds in the Spriggs Creek

FIGURE CAPTIONS OF PLATE 6.2

A: A CF_1 fold within impure quartzite showing a nearly Class 2 type profile on a larger scale. It is an intrafolial fold with its upper limb transposed along the main lithological boundary; location No.3565.

B: A profile view of a CF_1 fold. Its lower limb is transposed along the top boundary of an adjacent impure quartzite layer. A weak axial planar schistosity can be seen cutting through the hinge zone; location No.3508.

C: A larger CF_1 fold within a thick calc-silicate sequence appears on a cliff. Its fold hinge plunges at 5°-090°. Length of the view: 20 metres. Location No.3553, western part of the Naringa Well area.

D: A major CF_2 fold (No.5 on Map 5) within the calc-silicate gneiss. The outcrop on the hill slope provides a perspective profile of the fold closure with a steep north dipping axial plane and a shallow WNW plunging fold hinge. Location No. 3588, W of Naringa Well.

E: Profile view of the core of a major CF_2 fold (No.2 on Map 5) within calc-silicate. The rock layers have uniform thickness in the limb area, but have been slightly thickened in the hinge area. Location No.4194, N of the Florence Window.

F: A view along the subhorizontal hinges of the folds in (E) showing the total parallelism of rock layers.

G: An outcrop scale CF_2 fold in the hinge area of a major CF_2 fold (No.1 on Map 5) within the calc-silicate. Location No. 4206.

H: Dip isogon diagram of the fold in (G).

Plate 6.2





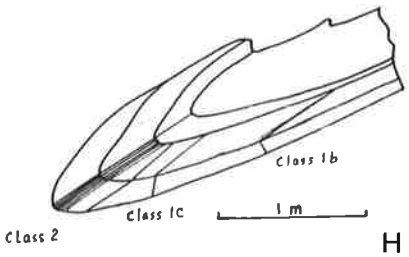












H

area (Map 2), to the east of Oonagalabi Tongue, have not been mapped in detail, thus will not be further described. No CF_2 folds have been mapped in the lower structural level of the HOB, where CF_2 folds implied by the repetition of lithological units may have been obscured by intense shearing and attenuation near the HRDZ (see Chapter 7).

6.4.1. CF_2 folds in the Naringa Well area

6.4.1.1. Major CF_2 folds

Major CF_2 folds can be seen in three dimensional perspective in the field (Plate 6.2.D). Four major synformal CF_2 folds and three major antiformal CF_2 folds have been mapped on the regional scale and marked with reference numbers from 1 to 7 (Map 5). Here the lowest stratigraphic unit (No. 1, see Chapter 5) outcrops in the cores of synformal folds whereas the upper units (Nos. 2 & 3 outcrop in the cores of antiformal folds. The downward-facing style of these CF_2 folds implies that they are on the overturned lower limb of a major isoclinal CF_1 fold, of which the normal upward-facing limb has been sheared off by later thrusting (CT). The closure of this inferred major CF_1 fold cannot be found, and the situation is similar to that described in the Broken Hill Block by Hobbs et al. (1984), where only minor F_1 folds have been observed in outcrop, but major F_1 folds have similarly been inferred by recognition of downward-facing F_2.

The orientations of CF_2 fold axial surfaces are quite variable due to later refolding (especially the HRF_1 and HRF_2 folds (see Chapter 7). It is very likely that the CF_2 folds were all originally nearly recumbent with E-W trending fold axes. However, the major portion of CF_2 folds now show northerly dipping axial surfaces with hinges plunging shallowly towards east or west in

different subareas (see stereograms on Map 5).

Major CF_2 folds are recognized by the symmetrical repetation of lithological units and by their rounded closures. The limbs of each CF_2 fold are always subparallel, but clearly close in the hinge zone where smaller parasitic folds and intersection lineations (CL_2) are well developed. The amplitudes of major CF_2 folds vary from about one hundred metres to over one km, and the ratio of wavelength/amplitude varies from 1:3 to 1:5. The axial traces and closures of these major folds, and the interference relationship between CF_2 folds and other folds are shown on Map 5 and its cross sections.

The profiles of major CF_2 folds are of Class 1c type flattened parallel folds (Plate 6.2.E). Because the fold hinges are subhorizontal, the rock layers are mainly parallel on horizontal surfaces without showing any of their closures (Plate 6.2.F).

Many smaller but mappable CF_2 folds in the western part of the Naringa area are shown by their closed lithological boundaries (Map 5).

6.4.1.2. Minor CF_2 folds

Many outcrop-scale CF_2 folds (e.g. Plates 6.2.G & 6.3.A) occur near the hinge zones of major CF_2 folds. The profiles of these minor folds show the characteristic styles of Class 2 to 1c type in their hinge area, but of Class 1b type in their limb areas, where the rock layers retain constant thicknesses (Plates 6.2.H & 6.3.D). The interlayering of different rock types and the different thicknesses of layers usually produce a disharmonic CF_2 fold profile which indicates that the amphibolite is more competent than the tonalitic migmatite (Plate 6.3.B), whereas the quartzite is more competent than the biotite gneiss (Plate 6.3.C).

fIGURE CAPTIONS OF PLATE 6.3

A: A large outcrop scale CF_2 fold within calc-silicate. Location No.4206. Note the significant continuity of the fold along its axial surface, thus indicating a near "similar" style.

B: An example of parasitic CF_2 folds within the migmatitic pelitic gneiss showing disharmonic relationships between different layers. Location No.3125.

C: CF_2 folds within impure quartzite showing a disharmonic relation between different layers. Location No.3416.

D: A polished surface of sample 3412 showing the profile of a CF_2 fold. Its thickened hinge has characters of Class 1c to 2 type, but its limbs retain uniform equal thickness and thus belong to style 1b. This sample was collected from the core of a major CF_2 fold (No.4 on Map 5).

E: A profile view of CF_2 fold within impure quartzite. Its axial plane dips 58° towards the north and the fold hinge plunges at 45°-030°. Location No.4266, NE of the Florence Window. A weak axial plane schistosity (CS_2) is developed in the closure, cutting through the compositional layering (CS_0/CS_1). This impure quartzite core is wrapped around by pelitic gneiss and belongs to the characteristic Class 1b to 1c type fold.

F: Micrograph shows well developed axial planar schistosity defined by elongate quartz grains. Field of view: 55mm X 37mm; X polars; sample 4266, collected from the core of the fold in (E).

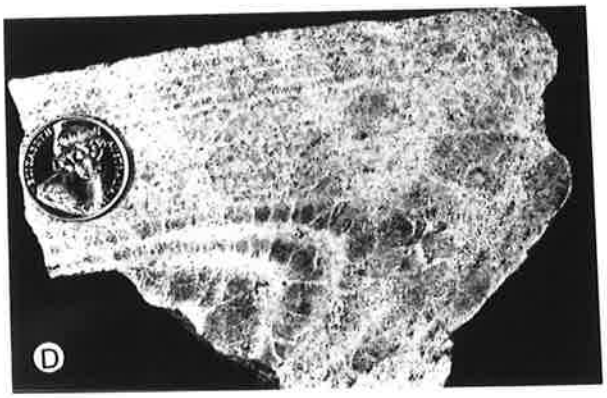
G: Enlarged micrograph showing the CS_2 schistosity from the same sample (4266). Field of view: 27.5mm X 18.5mm; X polars.

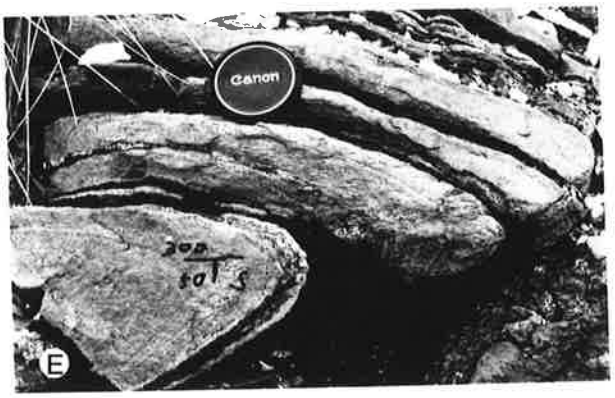
Plate 6.3

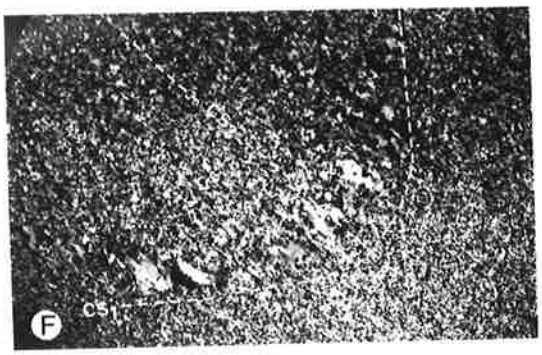














Disharmonic folding and its cause due to the influence of rock compeence and layer thickness on fold geometry has been well reviewed by Ramsay (1984).

An axial plane schistosity (CS_2) is clearly developed within impure quartzite but is less intense than CS_1. Plate 6.3.E shows an axial plane schistosity (CS_2) cutting through the compositional layering (S_0/S_1) of impure quartzite which forms the core of a CF_2 fold surrounded by pelitic gneiss. In thin section the CS_2 is defined by elongated quartz grains (Plate 6.3.F & G). Hinges of parasitic CF_2 folds and the intersection lineaton of CS_2 and CS_0/CS_1 define the CL_2 lineation. Mullion structures have been found occasionally in the hinge area of CF_2 folds (Plate 6.4.A).

6.4.1.3. Relationship between CF_2 folds and CF_1 folds

The CL_1 mineral lineation is often found oblique to the hinge of CF_2 folds and sometimes can be seen wrapping around these hinges (Plate 6.4.B, C & G), where the CL_1 mineral lineation on the layer surface can be traced from one limb to the other. The intersection angles between the CL_1 lineations and the CF_2 fold hinge are variable (Plate 6.4.D & E) due to the curved orientation of CL_1 lineations themselves, which may be caused by ductile stretching along the direction parallel to the CF_2 fold hinge. Interference between CF_2 and CF_1 folds is found occasionally at outcrop scale (Plate 6.4.H). Steeply plunging CF_1 folds (e.g. Plate 6.1.C) occur in the shallow plunging hinge area of a major CF_2 fold, 6 km NW of Naringa Well (see Map 5), which provides the evidence of relative age relationship between CF_1 and CF_2.

6.4.2. CF_2 folds in the Mt Campbell area

FIGURE CAPTIONS OF PLATE 6.4

A: A mullion structure formed in the hinge zone of a CF_2 fold which involved a quartzite layer in the core and pelitic gneiss in the limbs. The hinge lines of parasitic CF_2 folds and the cleavage/layering intersection lineation define CL_2. Location No.3505.

B: An outcrop scale recumbent isoclinal CF_2 fold in quartzite with only its hinge and upper limb exposed. An oblique mineral lineation on the layer surface can be traced from upper limb to lower limb (not naturally exposed), passing through the hinge zone. Location No. 3579, N of Brumby Bore.

C: The hinge of the fold in (B) showing an intersection angle of 18° between the CL_1 lineation and the CF_2 fold hinge (parallel the pencil).

D: A sketch of the curved CL_1 lineation on the upper limb of the CF_2 fold in (B).

E: Stereogram for the CL_1 lineations in (D).

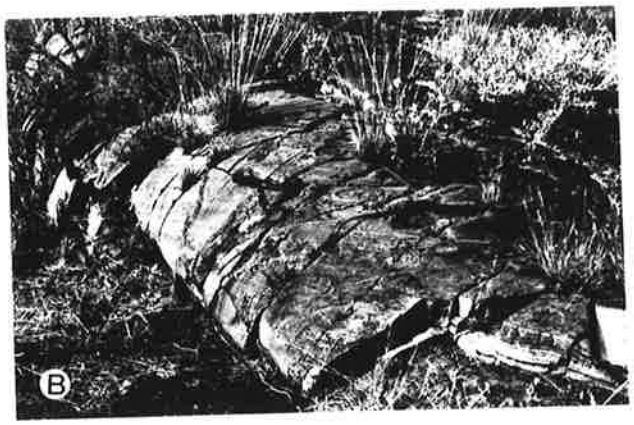
F: The profile view of parasitic CF_2 folds in calc-silicate showing very little change in the layer thicknesses. These folds belong to Class 1b to 1c type. Location No.3677.

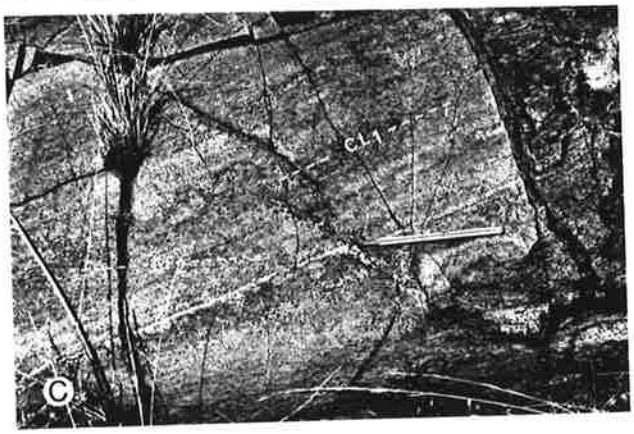
G: The hinge of a CF_2 fold in (F) showing that the CL_1 lineation is folded around the CF_2 fold hinge, which plunges at 14°-087° wheras the CL_1 lineation plunges at 20°-067° on the upper limb and plunges at 30°-247° on the lower limb.

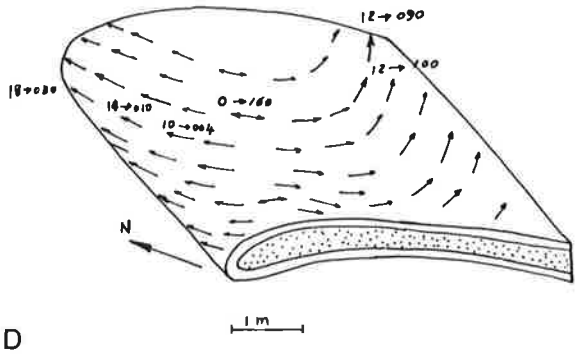
H: Interference between CF_1 and CF_2 folds within the impure quartzite. Isoclinal CF_1 folds showing Class 2 type closures; CF_2 fold showing characteristics of Class 1b to 1c type. Location No.3561.

Plate 6.4

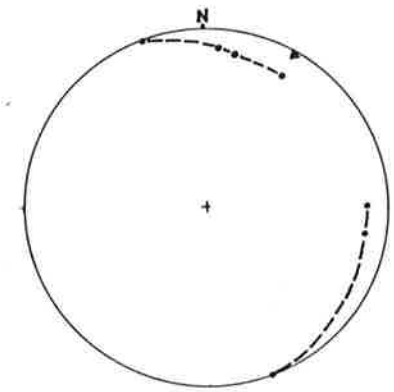








D



• CL1
▲ CF2

E







One major CF_2 fold and two smaller CF_2 folds have been mapped in the Mt Campbell area and are shown on Map 6. The major fold consists of a pelitic gneiss core and thick amphibolite limbs; and it closes to the south. Its northern limb has been affected by a later thrust (Campbell Thrust, see later section). The pelitic gneiss in the fold core extends for about 30 km along strike, thus implying an E-W trending subhorizontal hinge line. Two smaller CF_2 folds within the amphibolite sequence are easier to recognize, because they show quite rounded closures with hinges plunging shallowly towards the west. Some of the CL_1 lineations trend at high angles to the axes of CF_2 folds whereas these two CF_2 folds have been clearly folded coaxially by, and show opposite vergence to, the major CF_3 folds as can be seen on Map 6 and cross section A-A'. The interference feature between CF_2 and CF_3 folds can be seen also on outcrop scale (see Chapter 7).

6.4.3. Tectonic significance of CF_2 folds

Since the CF_2 folds have been complexly refolded by later large scale folds (HRF_1/CF_3 and HRF_2/CF_4, in Chapter 7), it is impossible to describe their original orientation and vergence of the fold system or its transport direction. However, from their present distribution, it is considered that they may have formed in an E-W orientation (i.e. almost at rights to the regional trends of the SOB) with northerly dipping fold axial surfaces and shallow hinges plunging towards the east or west. The major CF_2 folds in the Naringa Well area show a southward vergence (see section A-B on Map 5) and may imply a southward transportation. No strain analysis can be made as no strain markers are available and the original thickness of any of the metamorphic layers is not

known. Geometrically the CF_2 folding may have shortened this rock sequence to 1/6 - 1/10 of its original width, as the wavelength / amplitude ratios of the CF_2 folds vary between 1/3 - 1/5.

6.5. Thrust (CT) and nappe structures

6.5.1. Introduction

Thrusts are commonly defined as low angle reverse faults, which developed mainly in Late Proterozoic to Phanerozoic compressional orogenic belts where the displacement can be determined by comparing stratigraphic units. Examples of this kind of structure are found in the Canadian Rocky Mountains, the Alpine-Himalayan Mountain chain, and the westernmost part of the Appalachian Mountains (Hobbs et al., 1976). Fold nappes have been well studied in the European Alps which involved large-scale recumbent folds and long distance tectonic transport (Heim, 1878, 1919; see de Sitter, 1956). Now the term "nappe" has been applied to any large, more-or-less horizontal sheet of rocks that has been displaced for a considerable distance from its original place of origin (Hobbs et al., 1976, p. 411), e.g. the Himalayas (Coward, 1983).

In high grade metamorphic terranes the original transport directions or the transport distances are very difficult to prove. However, some similarity between the Early Proterozoic orogenic belts and the European Alps has been recognized and the terms "thrust" and "Nappe" have also been applied to Early-Middle Proterozoic tectonics, e.g. the structures in the eastern Svecokarelides of Finland (Bowes, et al., 1984) and in the Mt Isa Inlier of Australia (Bell, 1983; Bettess, 1987; Loosveld, 1987).

Thus the major shear zone boundaries in the HOB are called thrusts in spite of their present geometries, and the geological

bodies between the major thrusts are called nappes where evidence of long distance displacement between these geological bodies can be found (see later sections).

Major discrete shearing occurred following the CF_2 folding and formed a set of large scale CT thrusts (CT is an abbreviation of Cover Thrust), which are similar to the fold nappe structures defined in the European Alps. These major CT thrusts have been named the Naringa Thrust, the Riddoch Thrust, the Campbell Thrust, the Salthole Thrust, and the Ruby Thrust, whereas the geological bodies between these major thrusts are named the Naringa, the Irindina, the Campbell, the Riddoch, the Ruby and the Salthole Nappes, respectively (Figs. 1-1, 6-1 & Map 2. The nappes in fig. 6-1 are informally coloured: the Campbell Nappe, green; the Riddoch Nappe, blue; the Irindina Nappe, brown; the Naringa Nappe, orange; the Salthole Nappe, light brown; and the Ruby Nappe, apple green). Shear zones within the major nappes have been omitted on the maps although small scale shear zones are found frequently cutting lithological boundaries and CF_2 folds.

The CT thrusts occur mainly along boundaries between major lithological units of great competence contrast, e.g. the boundaries between pelitic gneiss and amphibolite or between pelitic gneiss and calc-silicate rock. Intensely schistose amphibolite or calc-silicate rock, recrystallized fine-grained schists or blastomylonites formed along these thrusts, with northerly plunging stretching lineations. These tectonites are not very fine-grained typical mylonites but contrast markedly to those rocks within the intervening nappes further away from the thrusts.

These major thrusts were considered as normal boundaries between major stratigraphic or lithological units by previous workers (Shaw et al., 1982; Lawrence et al., 1987). The main

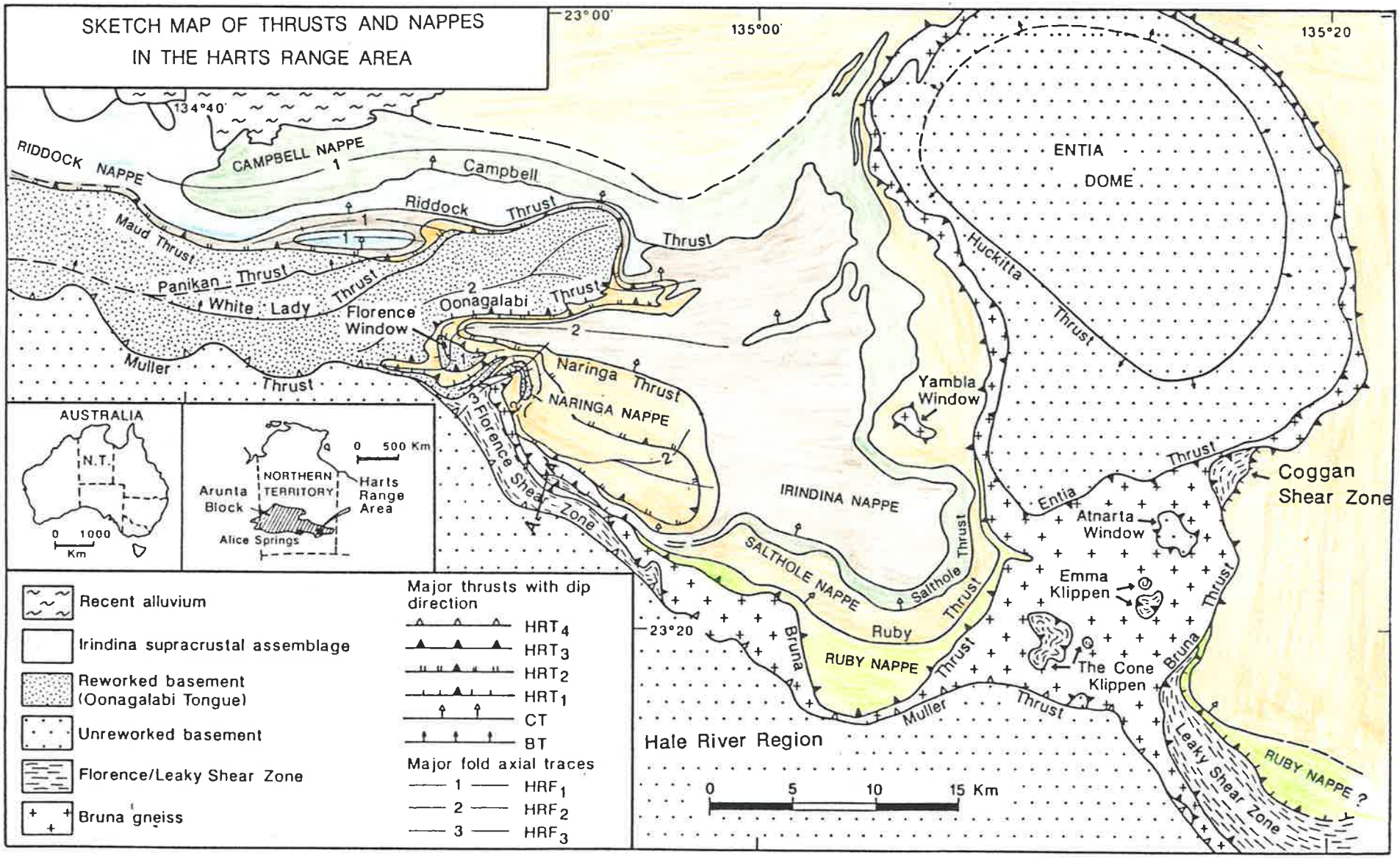

SKETCH MAP OF THRUSTS AND NAPPES
IN THE HARTS RANGE AREA
23°00'
135°00'
135°20'
134°40'
23°20'
RIDDOCK NAPPE
CAMPBELL NAPPE
Campbell
Riddock Thrust
Maud Thrust
Panikan Thrust
White Lady Thrust
Florence Window
Oonagalabi Thrust
Thrust
Muller Thrust
Naringa Thrust
NARINGA NAPPE
Florence Shear Zone
IRINDINA NAPPE
SALTHOLE NAPPE
Salthole Thrust
Ruby
RUBY NAPPE
Bruna Thrust
Muller Thrust
Hale River Region
ENTIA DOME
Huckitta Thrust
Yambla Window
Entia Thrust
Atnarta Window
Emma Klippen
The Cone Klippen
Coggan Shear Zone
Leaky Shear Zone
RUBY NAPPE ?
0 5 10 15 Km
AUSTRALIA
N.T.
0 1000 Km
NORTHERN TERRITORY
Arunta Block
Harts Range Area
Alice Springs
0 500 Km
Recent alluvium
Irindina supracrustal assemblage
Reworked basement (Oonagalabi Tongue)
Unreworked basement
Florence/Leaky Shear Zone
Bruna gneiss
Major thrusts with dip direction
HRT4
HRT3
HRT2
HRT1
CT
BT
Major fold axial traces
1 HRF1
2 HRF2
3 HRF3

Fig. 6-1

criterion to identify these thrusts is that the stratigraphic or major lithological boundaries within the Iridina Supracrustal Assemblage (Chapter 5) and the axial traces of CF_1 and CF_2 folds are truncated, though at very low angles, by these major boundaries on the regional scale. Subconcordant relationships are commonly at the outcrop scale and over limited distances. According to the definition of Ramsay (1967) and Hobbs et al. (1976), obvious dislocation along a planar surface or zone is the diagnostic criterion for a fault or thrust, and thus these mapped major boundaries certainly represent fault-boundaries. However, the regional discordance along these boundaries may have been initiated and been further enhanced by contraction during and after CF_2 folding.

Thrusts usually formed following the main regional folding events and indicate a change of deformational conditions from ductile to semiductile. Possible factors influencing this are isobaric cooling, uplift and fabric/texture homogenization due to complex refolding of the foliated rock sequence, which may have facilitated the change of deformational conditions.

6.5.2. Naringa Thrust

The trace of the Naringa Thrust extends for about 55 km along strike from east of the Oonagalabi Tongue to west of Brumby Bore. This thrust has been folded by later regional folds (HRF_2, Chapter 7) and shows a very variable attitude. However, it defines the original basal boundary of the Irindina Nappe and the upper boundary of the Naringa Nappe which now lies directly above the SOB basement. The thickness and also possibly the originally depositional facies of the stratigraphic units, change rapidly cross the Naringa Thrust, i.e. rocks in the Irindina nappe are mainly thick

pelitic to semipelitic gneisses with minor marble and calc-silicate, while rocks in the Naringa Nappe are dominantly marble and calc-silicate with minor pelitic to semipelitic gneisses. This provides evidence for a long distance displacement between the two nappes.

The CF_2 folds and a gradational lithological boundary between calc-silicate marble and calc-silicate gneiss within the Naringa Nappe are truncated by the Naringa Thrust (Map 5). In some places, for example, east of the Oonagalabi Tongue, CF_2 folds in the calc-silicate marble (Plate 6.5.A & B) are truncated at high angles by this thrust, which is represented by a planar tectonite of calc-silicate schist composition, which shows mylonitic structures on outcrop scale but a totally recrystallized granoblastic microstructure (Plate 6.5.C).

Some layers of pelitic gneiss and marble in the Irindina Nappe are also truncated by and sheared into the Naringa Thrust. Blastomylonites of pelitic composition also occur along this thrust (Plate.6.5.D) in contrast to the typical pelitic gneiss found within the Irindina Nappe further away from the thrust/shear zone (refer to Chapter 5, Plate 5.2.C).

A typical mylonitic calc-silicate gneiss is found to the NW of Brumby Bore (Plate 6.5.E, F, G & H). It is a very fine-grained dark layer, about one metre thick. No porphyroclasts can be seen in handspecimen or outcrop, but it shows a typical type 1 S-C mylonite microstructure (Lister and Snoke, 1984). The porphyroclasts of original minerals, including plagioclase, K-feldspar, quartz, muscovite, calcite, tourmaline, epidote, clinozoisite and zircon, are only 0.1 to 0.2 mm in size whereas the matrix is very fine (0.005 to 0.01 mm) and is mainly composed of quartz. Its XZ section shows an obviously asymmetric microstructure, interpreted

FIGURE CAPTIONS OF PLATE 6.5

A: A field view of the Naringa Thrust. A planar shear zone is exposed at the top of the outcrop but is obscured by the vegetation. The folded calc-silicate marble below is truncated at a high angle by, and sheared into the shear zone. Location No. 4120, to the east of Oonagalabi Tongue.

B: A sketch from the location in (A) showing the relationship between the folded calc-silicate marble and the shear zone of Naringa Thrust.

C: Schistose calc-silicate showing an intense fabric. The microstructure is not typically mylonitic, but the ribbon-like quartz layers and the fabric defined by biotites and elongated diopsides contrasts with the equigranular granoblastic texture of unsheared calc-silicate rock (see chapter 5). Sample 4120; Field of view: 3.4mm X 2.2mm; X polars.

D: Blastomylonite of pelitic gneiss composition collected from within the Naringa Thrust. Porphyroclasts of plagioclase (1 to 3mm) are wrapped around by small but inequigranular matrix and quartz ribbons (1mm wide). It is not a typical mylonite but obviously different from unsheared pelitic gneiss. Field of view: 3.4mm X 2.2mm; X polars; sample 3404.

E-H: A typical mylonite of calc-silicate composition collected from the Naringa Thrust showing microstructure of type 1 S-C mylonite (Lister, 1986). It shows a constant sinistral (southwards) simple shear sense. Field of view: 3.4mm X 2.2mm; sample 3333, N of Brumby Bore.

E: XZ section, ppl;

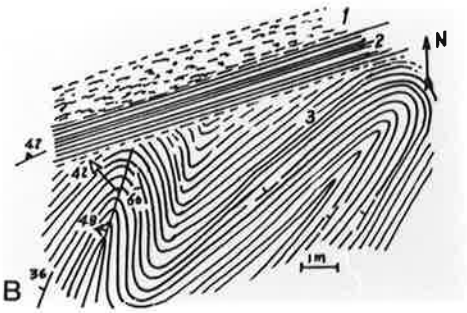
F: YZ section, ppl;

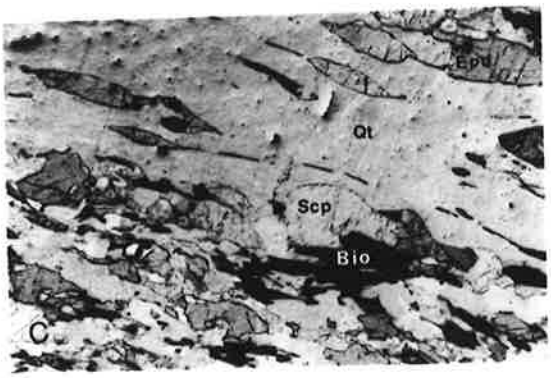
G: XZ section, X-polars;

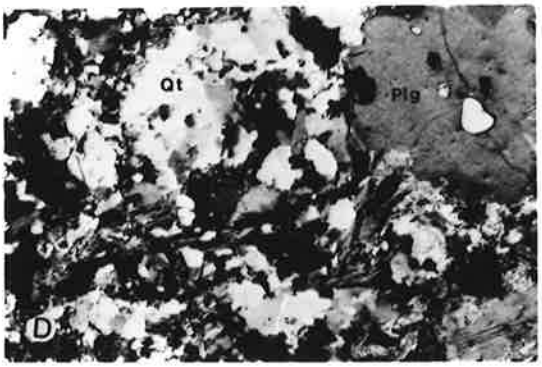
H: YZ section, X polars.

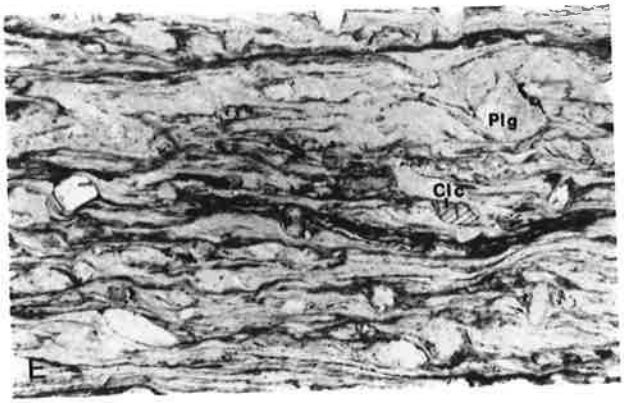
Plate 6.5

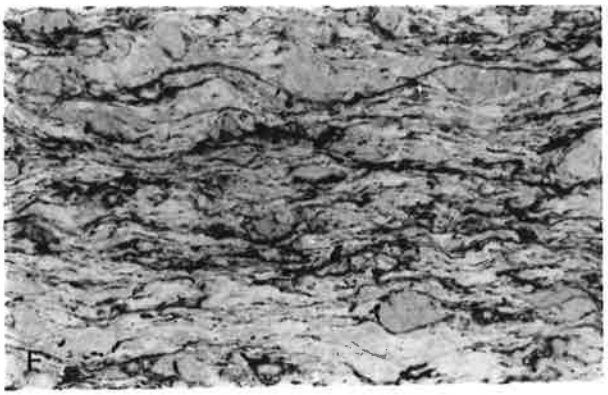


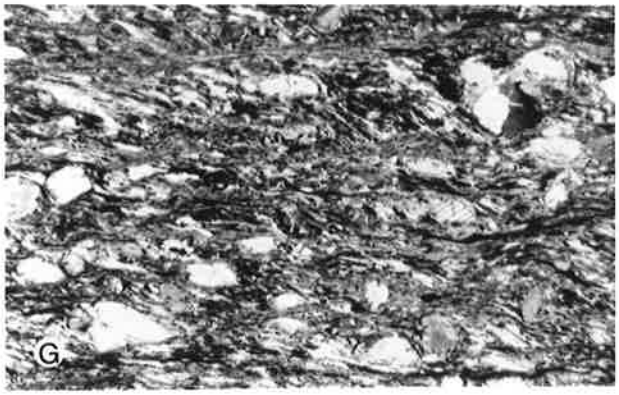














to present a southwards, i.e. overthrust, shear sense (Plate 6.5 E & G), whereas its YZ section shows a symmetric microstructure (Plate 6.5.F & H). This kind of mylonite is not common in the HOB and might have formed by later reworking (see Chapter 7).

6.5.3. Riddoch Thrust

The trace of Riddoch Thrust extends for about 45 km E-W from south of Mt Riddoch to east of the Oonagalabi Tongue, finally merging into the Campbell Thrust at a very small angle (less than 10^{o}). This thrust dips shallowly towards the north and forms the basal boundary of the Riddoch Nappe and the western upper boundary of the Irindina Nappe. The pelitic gneiss and marble within the Irindina Nappe are sheared at a low angle by this thrust. Layered amphibolites appear as a continuous sequence at the lowest levels of the Riddoch Nappe and extend almost parallel to the trace of the Riddoch Thrust. This is in contrast with the lenticular amphibolite bodies within the dominant pelitic gneiss of the Irindina Nappe below.

An isolated amphibolite sequence occurs in the centre of a CF_3 synform (see Chapter 7) situated to the north of Panikan Dam, and forms a klippe which was formerly a part of the Riddoch Nappe. This klippe has been separated by later folding (see Chapter 7) and recent erosion. The tectonite along this thrust is similar to those of other CT thrusts.

6.5.4. Campbell Thrust

The Campbell Thrust defines the boundary between the Campbell Nappe and the Riddoch Nappe, and the boundary between the eastern

parts of the Campbell Nappe and the Irindina Nappe (Fig.6-1 & Map 6). This thrust has been tightly folded by later folding events (CF_3 and HRF_2) and its trace extends as a sinuous line for over 100 km along strike from west of Mt Campbell, across the middle part of the area to the east of Florence Creek (Map 2). The Campbell Nappe consist of a dominant thick-layered amphibolite sequence and thin interlayers of metasediments. Compared with the lithologies in the Riddoch and Irindina Nappes. The displacement between the Campbell and the Riddoch Nappe may be smaller than that between the Riddoch and the Irindina Nappes. The displacement between the Campbell and the Irindina Nappes is the combination of the two displacements discussed above, and an abrupt facies vatiation is obvious between the Campbell and the Irindina Nappes. Many layers on both sides of the thrust are sheared into the thrust boundary on the map scale (Map 2). Ductile fluxion structures are found within the amphibolite layers along the thrust boundary (Plate 6.6.A) where lenticular bodies of low strained massive amphibolite are wrapped around by schistose amphibolites which are not typical mylonites but S-tectonites. On the outcrop scale both pelitic gneiss and amphibolite layers are truncated by, and sheared into, the thrust (Plate 6.6.B). Boudinaged lenticular bodies of amphibolite are common within the pelitic gneiss blastomylonite (Plate 6.6.C). During the shearing, the amphibolite behaved in a semi-brittle manner to form asymmetric shear boudins, i.e. deformed by offset along minor faults, but the pelitic gneiss behaved in a purely ductile manner, i.e. forming continuous layers of blastomylonite (Plate 6.6.D & E).

6.5.5. Salthole Thrust

The Salthole Thrust defines the boundary between the Campbell

fIGURE CAPTIONS OF PLATE 6.6

A: The Campbell Thrust is exposed in the middle of the photo, between the pelitic gneiss above (Irindina Nappe Sheet) and the amphibolite below (Campbell Nappe Sheet), and pass through the bottom of the small cave. The lenticular bodies of low strained massive amphibolite are wrapped around by schistose amphibolite. This macroscopic flow structure looks like a expanded microstructure of typical mylonite. Location No. 3329.

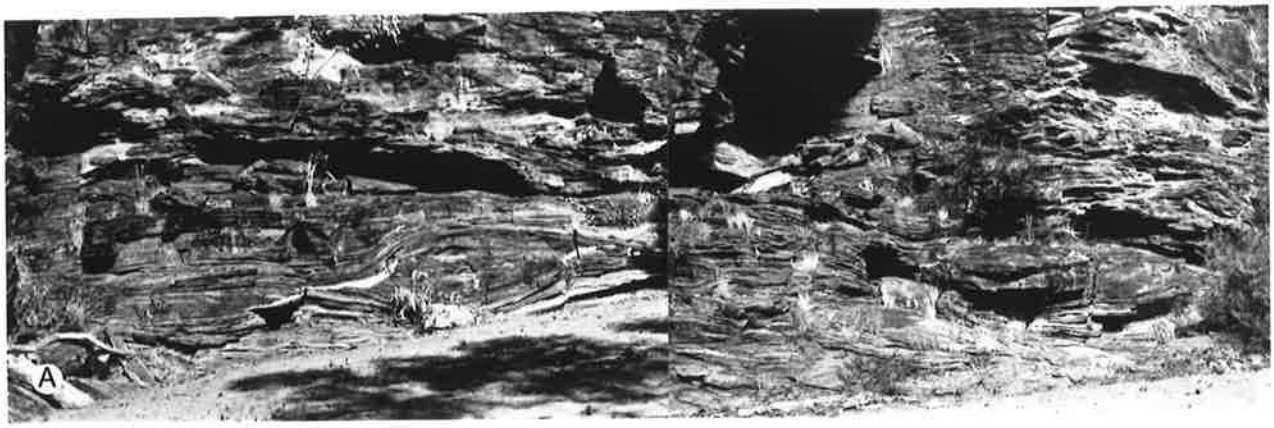
B: An outcrop of the Campbell Thrust. The lithological layering within both the pelitic gneiss above and the amphibolite below are truncated by and sheared into the thrust (in the middle of the picture, passing through the position of the hammer). Location No.3299.

C: A boudinaged amphibolite body within blastomylonite of pelitic gneiss composition indicating that an important ductile flow must have occurred within the pelitic gneiss and must have accommodated a great amount of displacement along the shear zone. Location No.3299.

D: An outcrop of the Campbell Thrust showing the discordant relationship between two sides of the thrust. The competent amphibolite below deformed by small extensional faults whereas the pelitic gneiss above deformed by ductile flow forming continuous layers of blastomylonite. Both the blastomylonite and amphibolite remained cohesive during the shearing. Location No.3288.

E: A closer-up of the view in (D) showing the relationship between the blastomylonite and truncated amphibolite.

Plate 6.6











Nappe and the Salthole Nappe. The thrust trace extends from the west of Brumby Bore to the NW of the Entia Dome. The amphibolite sequence with intercalated metasediments within the Campbell Nappe is truncated by, and sheared into Salthole Thrust. This is particularly clear along its southern section near the Salthole Dam, where the lower part of the amphibolite sequence, of about 1000 metres in width but only about 250 metres in true thickness (including two thin intercalated pelitic gneiss layers) are clearly pinched out by shearing along the thrust boundary. The Salthole Nappe consists mainly of pelitic to semi-pelitic gneiss and is lithologically identical to the Irindina Nappe. Blastomylonites are developed within the Salthole Nappe all along the thrust boundary (Plate 6.7.A).

Because the Campbell Nappe forms the cores of major CF_3 folds (see Chapter 7) in the Mt Campbell area, whilst the Irindina and Riddoch Nappe form the southern limb of the major CF_3 fold and the Salthole Nappe forms its northern limb (see Fig.6-1, Maps 2 & 6), the Salthole Thrust and the Campbell Thrust are considered to represent two now separated outcrops of one folded thrust and the Salthole Nappe is interpreted as a former part of the Irindina Nappe.

6.5.6. Ruby Thrust

The Ruby Thrust defines the northern and western boundary of Ruby Nappe and its trace extends for 30 km from west of Brumby Bore to east of Yambla Dam where it merges into the Bruna Thrust (Map 2).

Blastomylonites are developed all along the boundary (Plate 6.7.B). A typical augen gneiss consists of large porphyroclasts of feldspar and fine-grained schistose matrix (Plate 6.7.C) with a

fIGURE CAPTIONS OF PLATE 6.7

A: Large garnet containing biotite inclusions remains as a porphtroclast within blastomylonite, whereas the other minerals deformed to form the fine-grained matrix (0.05 to 0.5mm) and quartz ribbon. Field of view: 3.4mm X2.2mm; ppl; sample 3264, from the Salthole Thrust.

B: Intense stretching lineation on the surface of a mylonite layer above the Ruby Thrust. Location No. 3337.

C: Large porphyroclasts of garnet and plagioclase within the fine grained matrix of a blastomylonite. Field of view: 55mm X 37mm; ppl; sample 3172, from the Ruby Thrust.

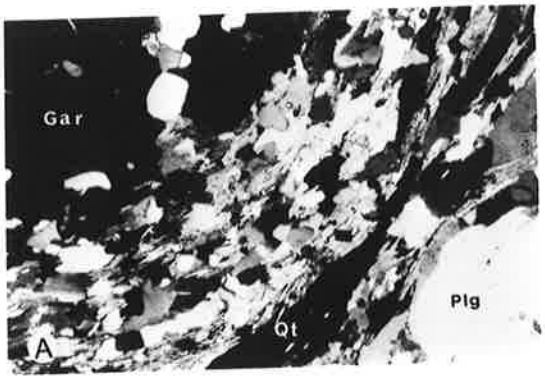
D: An outcrop showing both XZ section view (left) and YZ section view (right) of the blastomylonite found along the Ruby Thrust. The porphyroclasts are mainly deformed feldspar megacrysts. Location No.3338.

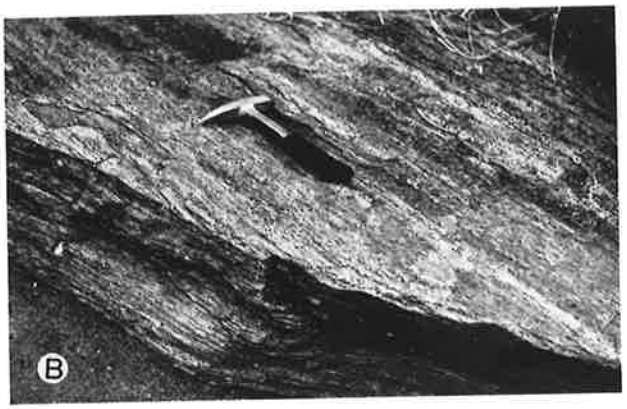
E: A protomylonite of amphibolite composition showing partly deformed and recrystallized hornblende and totally deformed and recrystallized plagioclase. Field of view: 3.4mm X 2.2mm; sample 3339; ppl.

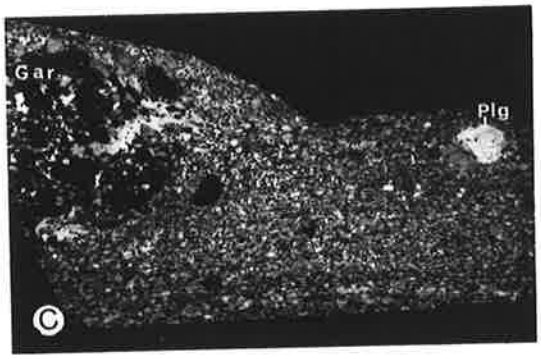
F: Same view as in (E), X polars.

G: Angular fragments of plagioclase, quartz, garnet and biotite are "cemented" by fine calcite matrix within a fault breccia rock collected along the Ruby Thrust. Sample 3186; field of view: 3.4 mm X 1.7 mm; X polars.

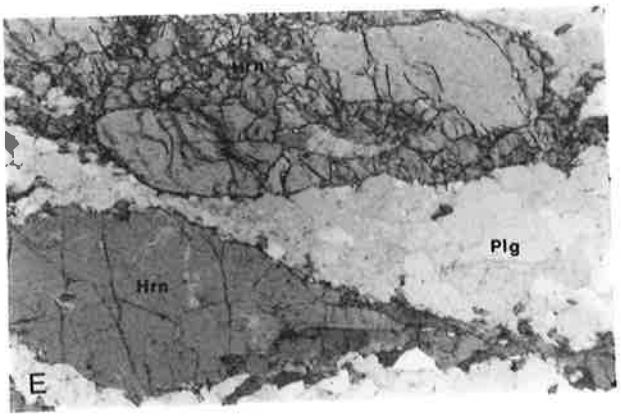
Plate 6.7

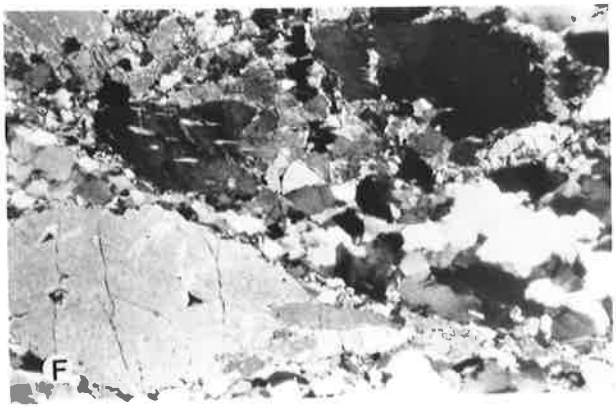


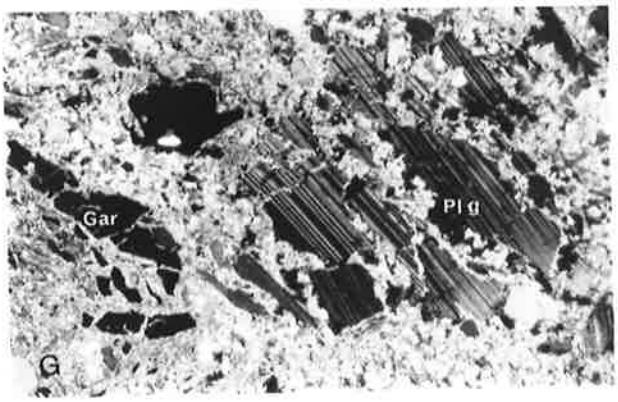












northerly plunging intense stretching lineation within the mylonitic foliation (Plate 6.7.D). Protomylonites are developed within the amphibolites which crop out closely below the thrust boundary (Plate 6.7.E & F). Fault breccia is found locally along the boundary (e.g. Plate 6.7.G) and implies a change of deformational conditions from ductile to brittle. It is likely that the breccia is a product of reworking along this thrust during or after major uplift, because fault breccias are usually formed at shallow crustal levels.

The Ruby Thrust and the Ruby Nappe can be traced discontinuously close to the upper boundary of the Bruna Gneiss sheet, around the western, northern and eastern margin of the Entia Dome (Martin, 1983) to the east of Harts Range area. Intense macroscopic shearing structures are found within the amphibolite sequence. The structures on the outcrop scale looking very like "megamylonite". Plate 6.8.A, for example, shows large lenticular bodies of less deformed amphibolite within curved thin layers of amphibolite and migmatitic veins. The competent amphibolites are boudinaged, rotated and sheared with internal compositional layering truncated along their sheared surfaces, like prophyroclasts in a mylonite matrix (Plate 6.8.B & E). The schistosity in the tonalitic gneiss wraps around the boudinaged amphibolites and behaves in a manner similar to that of a mylonitic matrix. The microstructures indicate a dextral (southward) shear sense (Plate 6.8.B, C & D). However, the tonalitic gneiss is not a mylonite but a typical gneiss, which is considered evidence of syn-metamorphic ductile shearing under high P-T conditions (see later sections).

Based on their structural analysis, the Ruby Thrust is very likely a relict part of the Salthole Thrust, which was correlated with the Campbell Thrust in the previous section. Thus the Ruby

FIGURE CAPTIONS OF PLATE 6.8

A-E: Flow-like structures within an amphibolite sequence; NE of Coggan Bore.

A: A boudinaged thick amphibolite layer looking like a mylonitic porphyroclast, whereas the schistose thin layers look like mylonitic matrix.

B: Compositional layering within the lenticular body of the boudinaged amphibolite layer is truncated and dragged into the schistose biotite hornblende gneiss. This suggests a dextral shear sense, which coincides with the shear sense shown by the folds within the gneiss.

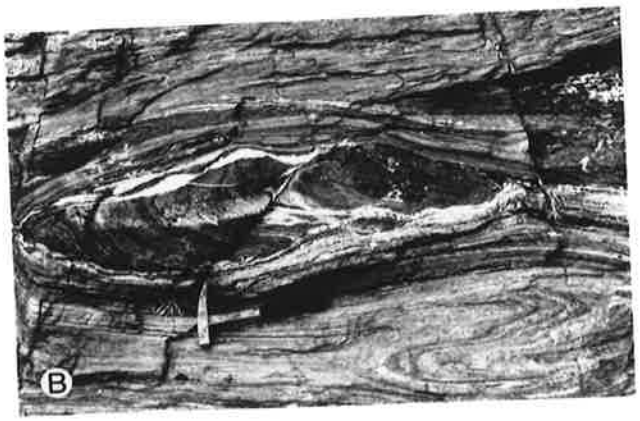
C: A sketch from the photo in (B) showing shear sense.

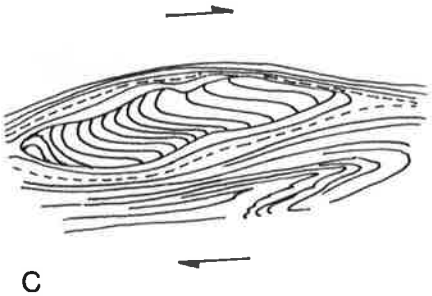
D: A lenticular amphibolite body within biotite hornblende gneiss showing the competence contrast between these two rock types. The amphibolite behaved like a competent porphyroclast whereas the gneiss behaved like an incompetent matrix. The S shaped folds have thinned limbs on both sides of the lenticular amphibolite body and were probably formed by dextral shearing.

E: Disharmonic relationship between the gneissic schistosity and the compositional layering within a folded amphiblite layer.

Plate 6.8






C





Nappe is interpreted as originally a part of the Campbell Nappe, which has been later folded by a regional HRF_2 fold and is now separated by intense shearing along the Bruna Thrust (Chapter 7). Unfortunately this relationship could not be definitly substantiated, because the area of their original connection, near the Florence Creek, has been destroyed by the shearing (see Maps 2 & 5).

6.5.7. Displacement along the CT thrusts

From the description above, the thickness of each lithological unit can be seen to vary dramatically from one nappe to another. These differences must imply a large (tens of kilometres) displacement along each major CT thrust and a total (more than one hundred km)shortening between the series of nappes. Balanced cross sections (Elliott, 1983) have been constructed in some Phanerozoic fold belts (Price, 1981; Boyer & Elliott, 1982, Butler, 1983; McClay & Way, 1986). No examples of balanced cross sections for high grade gneiss terranes have been found in the literature. It is also impossible to constract a balanced regional cross section for the HOB, because neither detailed drill nor geophysical exploration data are available to produce a detailed cross section and a true stratigraphy of these high grade metamorphic lithological units has not been established yet.

6.6. Metamorphism of the Irindina Supracrustal Assemblage (ISA)

The ISA has been completely metamorphosed to the amphibolite facies. This is shown by the metamorphic mineral assemblages of different rock types described in Chapter 5 (e.g. plagioclase + hornblende + clinopyroxene + garnet in amphibolite and metagabbro;

predominant magnesio-hornblende and cummingtonite in meta-ultramafics; garnet + sillimanite + biotite + plagioclase in pelitic to semi-pelitic gneisses.

The ISA reached its peak metamorphism probably during the earliest deformation when the CS_o and CS_1 fabrics formed because these earlier fabrics are defined by amphibolite facies mineral assemblages. However the amphibolite facies conditions must have persisted for a long period because later fabrics accompanying the HOB structures also show amphibolite facies metamorphic mineral assemblages. The regional amphibolite facies metamorphism was homogeneous and complete in the metasediments and layered amphibolites but was inhomogeneous and unequilibrated in the metagabbros and meta-ultramafics, within which the olivene and orthopyroxene are partially preserved, although grain size reduction of pyroxene is common. The pyroxenes were clearly partially altered to ferromagnesian amphibole or hornblende, which forms reaction rims between pyroxenes and plagioclases (Plate 5.4.A & B). A thorough alteration from pyroxene to hornblende is also occasionaly found in the metagabbro.

The metamorphic temperature and pressure of the ISA was estimated by Bowyer (1982) as 755-783^{o}C and 8kb, and recently concluded as 680-780^{o}C and 6-8 kb by Oliver et al. (in press, Appendix V).

Various methods of thermobarometry have been used for testing the P-T of the ISA during this study. Some results have been included in the conclusions of Oliver et al. (Appendix V), but the details of P-T estimates from this study are presented here. Biotite - garnet geothermometers and a garnet - plagioclase thermobarometer have been used for pelitic and semipelitic gneiss, whereas the garnet - clinopyroxene thermobarometer has been used

for amphibolite.

The garnet in the pelitic gneiss has a narrow rim which shows a slightly different composition from the main part of the garnet. The biotite does not show compositional zoning, but the biotite inclusions within the garnet have a slightly different composition from other biotite. The peak temperature (Table 6.1) of regional metamorphism in the ISA was calculated from the garnet-centres and biotite not incontact with garnet. The temperature range obtained of 690-750°C at 6-8 kb (Ferry & Spear, 1978) is within the range suggested by Oliver et al. (Appendix V). The cooling evidence is shown by the lower temperature calculated from garnet-rims and biotite in contacted with garnet (640-650°C in Table 6.2) and from the garnet-centres and the biotite inclusions (560-570°C in Table 6.3). The cooling temperatures are 50-130°C lower than the peak temperature of regional metamorphism.

Table 6.1 TEMPERATURES FROM GARNET-CENTRES & BIOTITE NOT IN CONTACT WITH THEM (IN PELITIC GNEISSES)

sample No.	Perchuk (1976)	Thompson (1976)	Goldman & Albee (1977)	Ferry & Spear (1978) 7Kb	7.5Kb	8Kb	8.5Kb
3405	637	650	709	698	700	703	705
3732	637	650	709	697	699	702	704
average	637	650	709	698	700	703	705

Table 6.2 TEMPERATURES FROM GARNET-RIM & BIOTITE IN CONTACT WITH IT (IN PELITIC GNEISSES)

sample No.	Perchuk (1976)	Thompson (1976)	Goldman & Albee (1977)	Ferry & Spear (1978) 7Kb	7.5Kb	8Kb	8.5Kb
3405	609	620	687	645	647	650	652

Table 6.3 TEMPERATURES FROM GARNET & BIOTITE INCLUSIONS IN PELITIC GNEISSES

sample No.	Perchuk (1976)	Thompson (1976)	Goldman & Albee (1977)	Ferry & Spear (1978) 7Kb	7.5Kb	8Kb	8.5Kb
3405	564	558	653	564	566	569	571

From the mylonitized pelitic gneiss or blastomylonitic pelitic gneiss which formed along CT shear zones, higher peak metamorphic temperatures and different cooling temperatures are obtained (Table 6.4). The average peak metamorphic temperature is 120°C higher than that of the unmylonitized rocks in the ISA. Similarly the cooling temperature calculated from garnet-rims and biotite (Table 6.5) is 110°C lower than the peak temperature of mylonitized pelitic gneisses, but is equal to the peak metamorphic temperature of the unmylonitized rocks in the ISA. Thus it is interpreted that the metamorphic temperatures nearby the CT shear zones were higher than the temperatures of the country rocks. Mylonitization may produce frictional heating (Sibson, 1986) and thus may increase the local metamorphic temperature. This process can be proved from the mylonitization which has occurred within unmetamorphosed sedimentary rock sequences where the matrixes within mylonites are usually greenschist facies phyllonites or phyllites conditions. Mylonites found in high grade metamorphic terrains usually represent retrogressive metamorphism and show lower metamorphic temperatures than those of their country rocks, e.g. the anastomosing shear zones in the Broken Hill Block (Hobbs et al., 1984) and the Illogwa Shear Zone in this area (Shaw et al, 1984; and Chapter 7 of this thesis). This type of mylonitization is interpreted as occurring after cooling and uplift of the country rocks, where the local frictional heating is still lower than the previous high temperature of regional metamorphism.

Table 6.4 TEMPERATURES FROM GARNET-CENTRES & BIOTITE IN MYLONITIC PELITIC GNEISSES

sample No.	Perchuk (1976)	Thompson (1976)	Goldman & Albee (1977)	Ferry & Spear (1978) 7Kb	7.5Kb	8Kb	8.5Kb
3305	703	730	763	831	833	836	838
3172	699	730	760	823	825	828	830
3209	695	720	757	815	817	820	822
P2-7	696	720	758	818	820	823	825
average	698	725	760	822	824	827	829

Note: Sample 3305 is from the Naringa Thrust, sample 3172 is from the Ruby Thrust, samples 3209 and P2-7 are from the basal thrust of the HRSC (see Chapter 7).

Table 6.5 TEMPERATURES FROM GARNET-RIMS & BIOTITE IN MYLONITIC PELITIC GNEISSES

sample No.	Perchuk (1976)	Thompson (1976)	Goldman & Albee (1977)	Ferry & Spear (1978) 7Kb	7.5Kb	8Kb	8.5Kb
3209	608	605	685	642	644	647	649
3305	684	705	747	772	774	777	779
P2-7	644	663	714	711	713	716	718
average	645	648	715	708	710	713	715

Sample 3209 has been tested by garnet - plagioclase thermobarometer of Harris & Jayaram (1982). The pressure range for assumed temperature range (from peak to cooling temperature) is 7 to 10.4 kb (Table 6.6). The pressures estimated from the garnet-centres and garnet-rims do not show obvious differences.

Table 6.6 P-T FROM MYLONITIZED PELITIC GNEISS (Harris & Jayaram)

sample number	T (^{o}C)	P (kb)	
		garnet-centre	garnet-rim
3209	650	7	
	700	8.1	8.1
	750	9.2	
	800	10.4	10.2

Garnet - clinopyroxene thermobarometry of Ellis & Green (1979) has been applied to amphibolite. It can be regarded as a

pressure-independent geothermometer (Table 6.7).

Table 6.7 P-T FROM GARNET & CLINOPYROXENE IN AMPHIBOLITE (Ellis & Green, 1979)

sample No.	P (Kb)	average T (^{o}C.)
3205	6	710
	7	713
	8	716
	9	719
	10	722

This method is actually pressure-independent as it is apparent that there are only 3 degrees difference per Kb from this method. However, the reliability of this method needs further examination, because the temperatures calculated from different garnet - clinopyroxene pairs give a variation greater than the influence of pressure changes. Four garnet - clinopyroxene pairs in sample 3205 gave four temperatures: 682, 709, 727 and 735^{o}C at 7 kb (average: 713^{o}C.). The temperature estimates from Perchuk (1976), Thompson (1976) and Graham & Powell (1984) are usually 50-100^{o}C lower than the values from other methods. The P-T values from Ferry & Spear (1978), Harris & Jayaram (1982) and Ellis & Green (1979) are very close to each other and are thus preferably considered in this thesis.

Based on the above data, the metamorphic temperature and pressure of the ISA are suggested as 650-720^{o}C and 7-8 kb (Fig. 6-2). The minimum burial depth of the ISA is thus estimated as 24-28 km on the basis of a depth/pressure dependence of 3.5 km / 1 kb (Winkler, 1979).

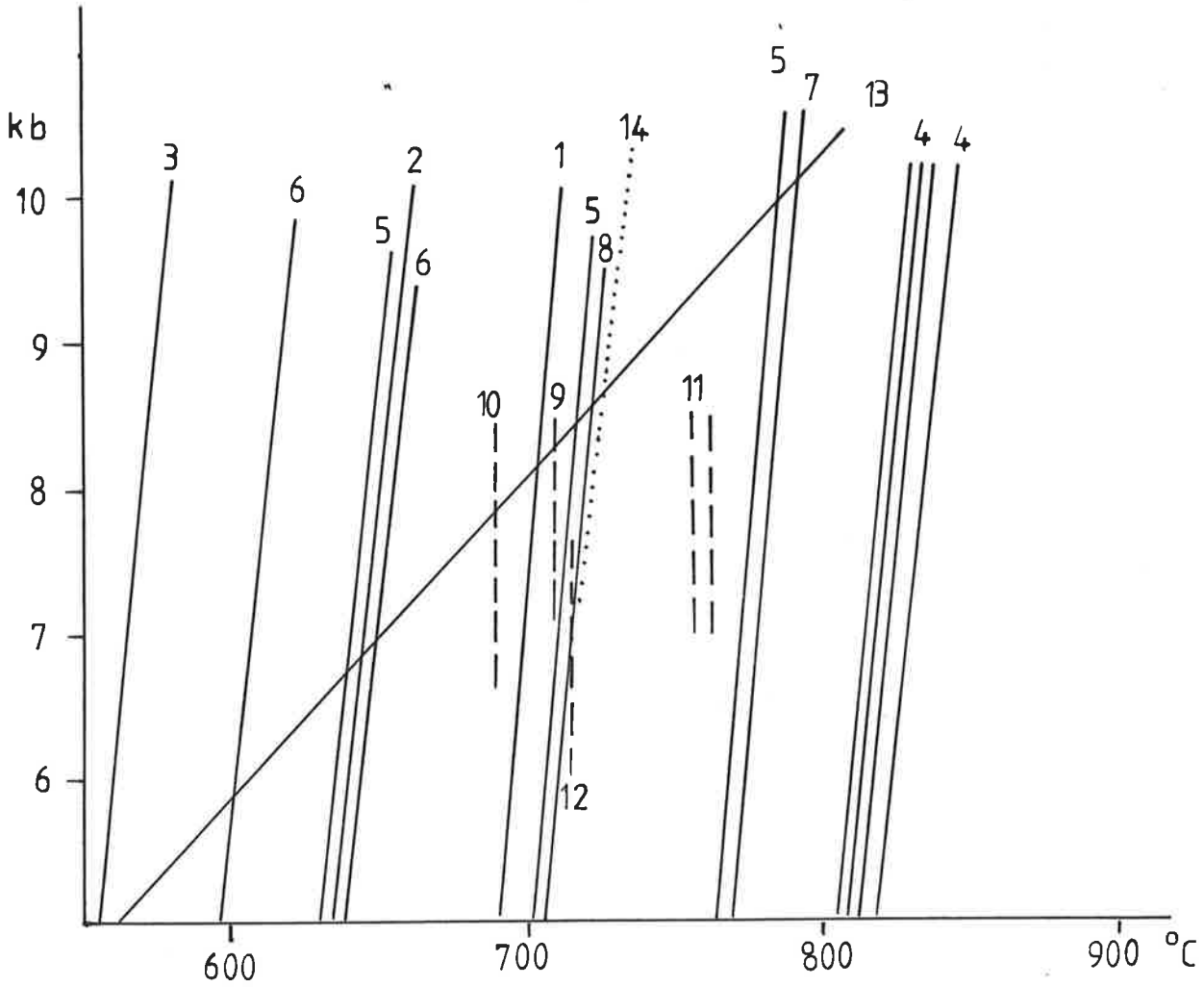


Fig.6-2 Diagram of P-T estimates for the ISA and the Bruna Gneiss.

A: Ferry & Spear (1978): (1) pelitic gneiss; garnet centre + biotite; (2) pelitic gneiss; garnet rim + biotite; (3) pelitic gneiss; garnet + biotite inclusion; (4) mylonitic pelitic gneiss; garnet centre + biotite; (5) mylonitic pelitic gneiss; garnet rim + biotite; (6) Bruna Gneiss; garnet + biotite; (7) ultramylonite (from Bruna Gneiss); garnet centre + biotite; (8) ultramylonite (from Bruna Gneiss); garnet rim + biotite.

B: Goldman & Albee (1977): (9) pelitic gneiss; garnet centre + biotite; (10) pelitic gneiss; garnet rim + biotite; (11) mylonitic pelitic gneiss; garnet centre + biotite; (12) mylonitic pelitic gneiss; garnet rim + biotite.

C: Harris & Jayaram (1982): (13) mylonitic pelitic gneiss; garnet + plagioclase (with sillimanite in the mineral assemblage).

D: Ellis & Green (1979): (14) amphibolite; garnet + clinopyroxene.

CHAPTER 7 LATER STRUCTURES OF THE HARTS RANGE OROGENY

7.1. Introduction

The structural evolution during the later stages of the Harts Range Orogeny involved both the HRSC and the directly underlying SOB. During this time thrusting and folding operated alternately in a different style of unusually cyclical tectonic activity.

The sequential development of monophase folds and thrust-faults in fold belts has been contradictorily interpreted. Folding was considered by Heim (1921) to initiate the process and then to be terminated by thrusting, or it was considered a consequence of earlier thrusting movement by Buxtorf (1916), while a third possibility was proposed by de Sitter (1956, p. 242), that thrust-fault developed in a much earlier stage of folding than Heim's conclusion and in a much later phase than Buxtorf's. However, in the study area, the polyphase thrusting and folding are much more complex than that reviewed above. It appears that earlier thrusting was terminated by folding, and the resultant folds were then cut by another phase of thrusting. The thrusting and folding appear as a sequential but intermittent process.

For convenience, each deformation cycle presented here begins with a period of thrusting and is completed by folding, as discrete shear/thrusting appears to be the first event during this tectonic stage. The thrusts and shear zones must have been developed under semi-ductile conditions, and were then apparently folded under a fully ductile environment. The folded thrusts and nappes were then sheared by renewed thrust boundaries, and a new cycle began. Each cycle is here named a "Movement" phase, and four Movement phases have been recognized on the basis of the thrust/fold alternation. They are the Oonagalabi, the Maud, the

Bruna, and the Muller Movement phases respectively (Fig. 1-2).

During the Oonagalabi Movement the first major thrust (the Oonagalabi Thrust) developed along the bottom of the HRSC and the top of HRDZ. This is the first thrusting phase to affect the HRDZ and is abbreviated as HRT_1 (i.e. HRDZ Thrusting Event 1; Fig. 1-1). The HRT_1 Thrust was then involved in a phase of large scale folding, which is the first folding phase to affect the HRDZ and is abbreviated as HRF_1 (HRDZ Folding Event 1).

During the Maud Movement, the Maud Thrust (HRT_2), developed along or near the top margin of the HRDZ, truncating both the HRT_1 thrust and the HRF_1 fold. The Maud Thrust was consequently folded by a set of large scale sub-neutral folds (HRF_2).

During the Bruna Movement, two HRT_3 thrusts, the Bruna and Entia Thrusts, cut through the HRF_2 folds close to the basal boundary of the HRDZ. The HRT_3 thrusts were then folded by locally developed sub-neutral folds (HRF_3). As a concluding phase, the Muller Thrust (HRT_4) developed during the Muller Movement and carried the HOB and the HRDZ up to lie above the Hale River Region of the SOB.

To complete this tectonic period, widespread upright open folds and high angle faults developed at shallower crustal levels and affected both the HOB and SOB in the Harts Range area, as well as other areas within the Arunta Inlier (Shaw et al., 1984a). Undeformed dolerite dykes, which are correlated with the Stuart Dykes (Black et al, 1980), have been found within the Bruna Gneiss. Undeformed pegmatite veins were injected along some of the faults and have been interpreted as occurring during the Late Palaeozoic Alice Springs Orogeny (Shaw et al, 1984). As all of these events significantly postdated the main Proterozoic Orogenies and do not really belong to the HRO, they are not of critical

concern to this thesis and are thus described only briefly at the end of this chapter.

7.2. The Oonagalabi Movement

7.2.1. The Oonagalabi Thrust (HRT_1)

The boundary between the HOB and SOB is recognized as a major tectonic boundary (labeled as HRT-1 by Ding and James, 1985, Appendix III), and has since been reinterpreted as a complex boundary comprising the Oonagalabi (HRT_1), the Maud (HRT_2) and the Bruna (HRT_3) Thrusts.

It is assumed that the Oonagalabi Thrust (James and Ding, in press, Appendix IV) originally extended throughout the whole area. However, it is now preserved only within the area defined by the Maud Thrust and Bruna Thrust (Fig. 1-1). The Oonagalabi Thrust everywhere separates the amphibolite facies ISA from the underlying granulite facies SOB. There are four separate and discrete thrust sections belonging to the HRT_1.

The first and major section of the HRT_1 fault trace extends continuously for more than 25 km along strike from the eastern margin of the Oonagalabi Tongue to the west of Maud Creek (Map 4). The margins of the Florence and Maud Windows are considered to represent the folded and isolated exposures of this section. The second section of the HRT_1, about 5 km long, forms the upper boundary of the Florence Shear Zone (see Fig. 1-1 & Map 5). The third one, about 5 km long, defines the upper boundary of the Coggan Shear Zone and the fourth one defines the topmost boundary of the Leaky Shear Zone (Fig. 1-1) and is exposed for more than 15 km extending out of the eastern margin of the area.

Along the Oonagalabi Thrust to the south of the Oonagalabi Tongue, different lithological units of the ISA, including marble,

pelitic gneiss and quartzite, are progressively in contact with the SOB gneiss complex, showing a low angle discordant relationship. The axial plane of one CF_2 fold closely adjacent to the thrust is also truncated at a low angle (Map 5). The pelitic gneiss core and calc-silicate or marble limbs of CF_2 fold are gradually sheared into the boundary (Map 5). Occasionally, on a local scale, the lithological layers of the HRSC are truncated at higher angles by the HRT_1 thrust (Plate 7.1.A). The gneissic layering and major and minor folds within the SOB are also truncated by the thrust boundary (Map 3 and Plate 7.1.B).

Rocks closely adjacent to the HRT_1 thrust are obviously deformed. A mylonitic microstructure is typical in quartzite (e.g. sample 4165) but not in pelitic gneiss, whilst marble is deformed to calcite schist along the thrust. Some white, massive and very fine grained ultramylonite derived from marble, is a cryptocrystalline rock, within which a schistosity is visible in thin section but the individual grains of calcite are too small to observe even at this microscopic scale. Thin layers of Bruna Gneiss intruded along HRT_1 (Map 5) and have been mylonitized (Plate 7.1.C). Mylonites have also been found within the basement gneiss (Plates 7.1.D and 7.2.A) adjacent to HRT_1 in both the Florence and Maud windows (see Fig. 1-1). However, compared with the F/LSZ, the mylonite zone along HRT1 is very narrow (1-2 metres).

Around Camp site 12 (see Map 1), the boundary between the marble and basement gneiss looks like an unsheared unconformity. The marble layers extend parallel to the boundary while the layering within the underlying SOB gneiss is truncated by the boundary at high angle (Plate 7.2.B). However, this relationship is unlikely to represent a stratigraphic unconformity as the marble is not the basal unit of the HRSC (see Chapter 5). One explanation is

FIGURE CAPTIONS OF PLATE 7.1

A: A field sketch of the HRT_1 Oonagalabi Thrust showing a discordant relationship between the SOB and the HRSC. The marble layers of the HRSC were truncated by and sheared into the thrust. Location No.4125.

B: A close-up of the HRT1 thrust boundary at the bottom of the cliff showing the obvious discordance between the compositional layering of mylonitized granitic gneiss of the SOB and the HRT_1 thrust boundary.

C: Thin layers of mylonitized Bruna Gneiss intruded along the Oonagalabi Thrust are folded by parasitic HRF_1 folds which show steep axial planes but subhorizontal fold hinges. Location No.3691, south of Oonagalabi Tongue.

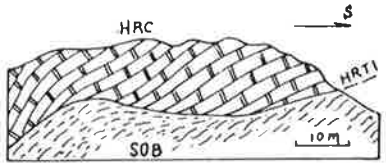
D-F: An excellent example of a sheath fold found at the junction point of the HRT_1 Oonagalabi Thrust and the HRT_3 Bruna Thrust. The sample was about 15cm long, and the structure looks like a tube or a piece of sausage, before being cut. Photos show the similarity between the sequential profiles of four segments cut at different positions of the sheath fold sample. Location No.4258; Maud Window.

D: A profile of the sheath fold. field of view: 50 mm X 80 mm.

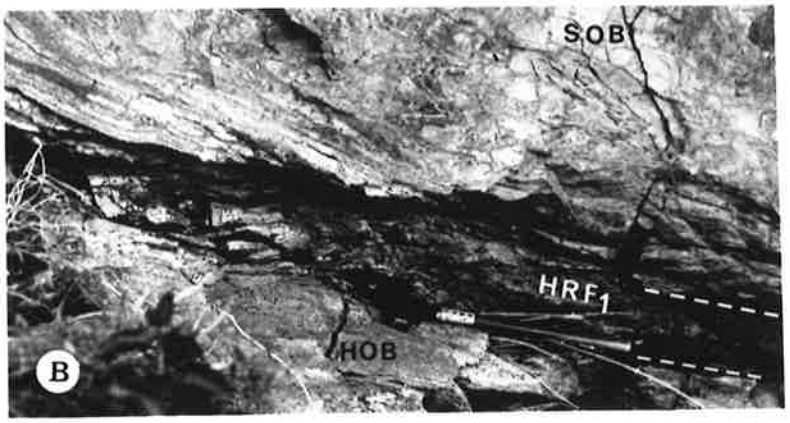
E: Microstructure of the sheath fold showing circular mylonitic foliation. Field of view: 55mm X 37mm; X polars; sample 4258.

F: Four samples showing the gradual variation from one end to the other;

Plate 7.1

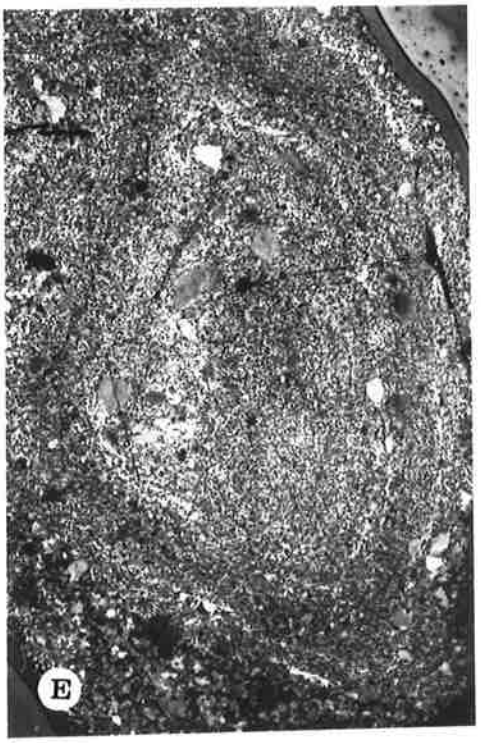


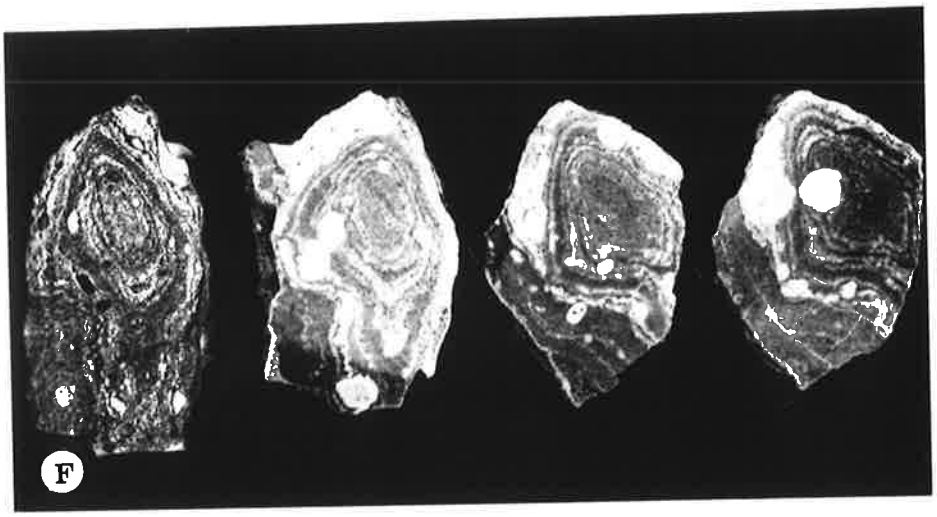
A











that the present marble layer is probably recrystallized mylonite, which accommodated most of the shearing strain, as calcite recrystallizes easily.

Marble and pelitic gneiss are in contact with the Florence Shear Zone along the second section of the HRT_1 boundary. An ultramylonite layer (up to 20 m in thickness) at the top of the Florence Shear Zone has been described in Chapter 4. It is difficult to differentiate the influence of HRT_1 in relation to that of the original F/LSZ (Chapter 4). Compared with the underlying mylonitized mafic granulite, this ultramylonite layer must have been intensely reworked during the HRT_1 shearing. This ultramylonite layer separates the amphibolite facies ISA from the mylonitized granulite facies rocks within the Florence Shear Zone. The mineralogies of the mylonites indicate amphibolite facies metamorphic conditions during thrusting.

Amphibolite layers of the ISA are in contact with the Coggan and Leaky Shear Zone along the easternmost sections of HRT_1 (Map 2). A thick amphibolite sequence of the ISA is abruptly sheared into the HRT_1 above the Leaky Shear Zone. The mylonites below the HRT_1 have been described in detail in Chapter 4, but the mylonites derived from the ISA have not been studied in detail.

It has not been possible to deduce the shear sense for HRT_1 from mylonitic structures. However, the curved drag of layers in the HOB suggests that the HOB has been thrust up to overlie the SOB. It is thus interpreted that while the HRSC was significantly shortened by compressional deformation during the CF_2 folding, the Oonagalabi Thrust may have behaved as a sliding surface along the basal margin of the HOB by reverse sense shearing, as there is no evidence to indicate that HRT_1 has ever been affected by the CF_2 folds.

FIGURE CAPTIONS OF PLATE 7.2

A: Microstructure of a folded (HRF_3) mylonite collected from the marginal HRT_1 Oonagalabi Thrust of the Maud Window. An intense mylonitic scistosity developed within the mylonite and forms the axial planar fabric of the HRF_3 fold. The new fabric is best shown within a folded quartz layer (probably previous quartz ribbon). Sample 3765; X polars; field of view: 55mm X 37mm;

B: A field sketch of the HRT_1 Oonagalabi Thrust showing the discordant relationship between the SOB granitic gneiss and the ISA marble. The marble layer looks completely parallel to the HRT_1 boundary whereas the gneissic layering is truncated at a high angle by the HRT_1 boundary. Location No.4263 to NO.4264.

C: An enlarged view of the microstructure in (A). Field of view: 2.1mm X 1.4mm.

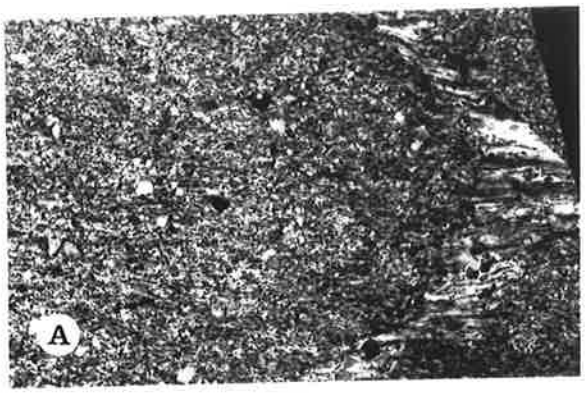
D: The HRF_1 folds exposed on a cliff. The HRT_1 Oonagalabi Thrust between the ISA mable (left) and the mylonitized SOB granitic gneiss (right) is also folded. The marble is squeezed into the core of a cuspate HRF_1 parasitic fold (in the centre) which thus indicates that the marble is less competent than granitic gneiss. Location No.4204; Width of view: 10 metres.

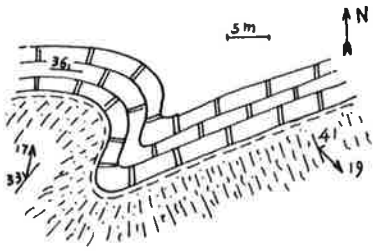
E: A close-up view of the folded HRT1 boundary in (D).

F: A profile view of a pair of HRF_1 (CF_3) folds in calc-silicate layers. The recumbent attitude results from the interference of a major HRF_2 fold. Location No.3525, in the central Naringa Well area.

G: Outcrop scale parasitic HRF_1 (CF_3) folds in impure quartzite showing discrete axial plane cleavage. Location No.3565.

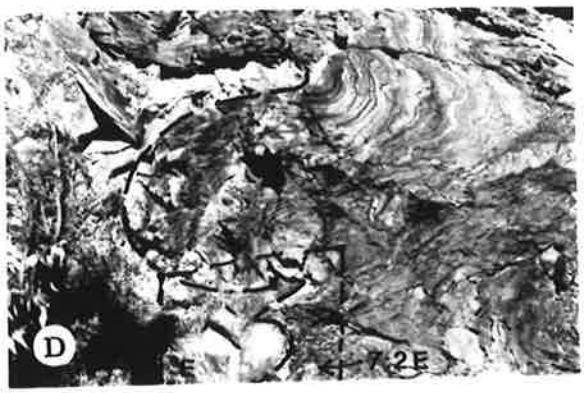
Plate 7.2





B











7.2.2. Oonagalabi Movement folds (HRF_1/CF_3)

Movement along HRT_1 must have stopped by the time that part of the SOB (e.g. the present Oonagalabi Tongue) and the whole of the HRSC became involved in the next major folding event. This fold generation is labelled HRF_1 for those folds which display SOB basement cores, but is labelled CF_3 for other folds which do not expose SOB basement cores, as these folds represent the third generation of folds within the HRSC.

7.2.2.1. HRF1 folds

Basement rocks in fold belts are commonly found to form cores of anticlines. In the Swiss Alps which formed under compressional tectonism, some of the folded nappe structures of the Lower Pennic Alpine involve Hercynian basement within their cores (Kruhl, 1987). Other examples are exposed in the Basin and Range Province of the central Rocky Mountains of western North America, where metamorphic core complexes formed by extensional tectonism and erosion (Davis & Coney, 1979). However, in the Harts Range area the orthogneissic SOB forms tightly infolded cores within the HOB lithologies which have themselves been metamorphosed to amphibolite facies condition.

HRF_1 folds were originally E-W trending and steeply north dipping with subhorizontal hinge lines. They have since become doubly plunging or luniform folds due to the interference of HRF_2 and later open folds. Three pairs (antiforms and synforms) of HRF_1 folds have been mapped along the eastern and southern margin of the Oonagalabi Tongue and throughout the Naringa Well area (Map 4).

The structurally northern-most pair of these is a major one and will be described in detail. This is a luniform shaped antiform (the result of interference between HRF_1 and HRF_2 folds)

which has a core of SOB gneiss. It is named the Florence Window (Fig. 1-1) and is surrounded by marble layers of the ISA (Map 5). Its fold axial surface is curved and dips shallowly towards the north in its SE half and dips steeply towards the east in its NW half. Its two eastern limbs dip in a similar direction and are subparallel to the fold axial surface, whereas its two western limbs dip in opposite directions at the surface. The eastern closure plunges at 22^{o}-052^{o} but the northern closure plunges at 32^{o} N.

The profile of the folded marble in the closure area is of Class 1b to 1c type, i.e. the thickness of each layer does not change markedly. Minor parasitic folds are found around the major closure area as well as along the southern limb. Some parasitic HRF_1 folds are found on a cliff in the area where they are outlined by the folded HRT_1 boundary (Plate 7.2.D & E). The layering within the SOB gneiss has been obviously affected by these folds but is cut obliquely by HRT_1 (Plate 7.1.B). The marble has been sheared near the thrust but is also squeezed into the cores of parasitic synforms.

This antiform can be traced to the east and into the upper levels of the ISA, where it is exposed now in the central part of the Naringa Well area. There, major CF_2 folds are refolded by this antiformal HRF_1 fold. Smaller scale parasitic folds are found around the major hinge zone of the HRF_1 antiform. All the HRF_1 folds were clearly refolded (by the HRF_2 fold, see section 7.3.2.) and change their orientation in different positions. Plate 7.2.F, for example, shows a pair of recumbent HRF_1 folds located within a major HRF_2 fold. Discrete axial planar foliations are only found occasionally (Plate 7.2.G).

There is a major HRF_1 synform, lying just to the south of the

Florence Window, consisting mainly of marble with subordinate pelitic gneiss. The latter is exposed in the hinge areas of a few doubly plunging CF_2 folds which are distributed symmetrically about the axial plane of the HRF_1 fold. Their mappable closures and variably oriented hinges are shown on Map 5. This synform can be further traced to the east and appears as a doubly plunging isoclinal fold (Map 5), where the CF_2 folds were obviously folded by the HRF_1 fold (which has also been refolded by a major HRF_2 fold). Intersection lineations and mullion hinges of parasitic folds were developed parallel to the fold axis of the major HRF_1 synform (Plate 7.3.A).

Two other pairs of HRF_1 folds are exposed at the southern and eastern margins of the Oonagalabi Tongue. Their closures are well exposed with fold hinges plunging towards the NE (Maps 2 and 5). Thin layers of mylonitic Bruna Gneiss are involved with these parasitic HRF_1 folds (Plate 7.1.C).

7.2.2.2. CF_3 folds

CF_3 folds are best preserved in the Mt Riddoch to Mt Campbell area, to the north of the Oonagalabi Tongue (Map 6). They have very tight to isoclinal profiles but vertical or steeply north dipping axial surfaces. Six pairs of CF_3 synformal and antiformal folds have been mapped in this area. The lithological layers of the ISA, the axial planes of CF_2 folds, the CT thrusts (e.g. the Campbell Thrust and Riddoch Thrust) and the associated nappes have been folded by these folds. The folded thrusts and nappes are very similar to those formed in Phanerozoic orogenic belts, e.g. the European Alps (Platt & Lister, 1985a & b), and the Himalayas (Coward, 1983), as well as in Precambrian ones (Bowes et al., 1984; Myers, 1984).

FIGURE CAPTIONS OF PLATE 7.3

A: Very small parasitic HRF_1 (CF_3) folds form mullion structures on the surface of a calc-silicate layer near the closure area of a major HRF_1 fold in the southern Naringa Well area. The hinges of small HRF_1 (CF_3) folds define a marked lineation which plunges 30° towards 340°, and parallels the hinge of the major HRF_1 fold. Location No.3566, NW of Brumby Bore.

B: Two sets of lineations appear on the surface of a calc-silicate layer. The pencil in the picture is parallel to the CL_1 mineral lineation plunging 66° towards 203°, which is folded by a major CF_3 fold (see Map 6). The CL_3 cleavage/layering intersection lineation is weakly developed plunging 34° towards 288° (parallel to the arrow mark) and parallels the fold hinge of a major CF_3 fold. Location No.3626, SW of Mt Mabel.

C: A sketch profile of a pair of CF_3 folds showing the relative position of pictures in (D, E, F & G). 7-12 b, c , d & e.

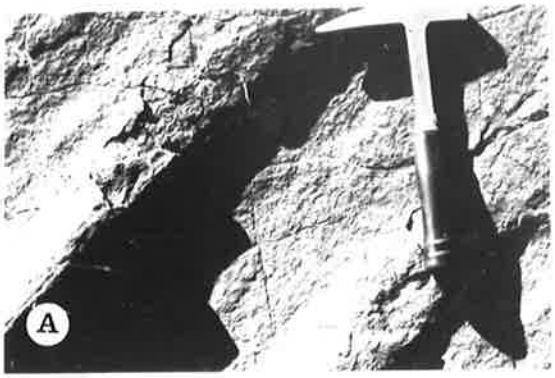
D: A field perspective view of a major synformal CF_3 fold (the northern one on Map 5) which is adjacent to the north or top of a major antiformal CF_3 fold. Its two limbs close laterally to the north (left) through a vertically dipping hinge zone. location No.3548.

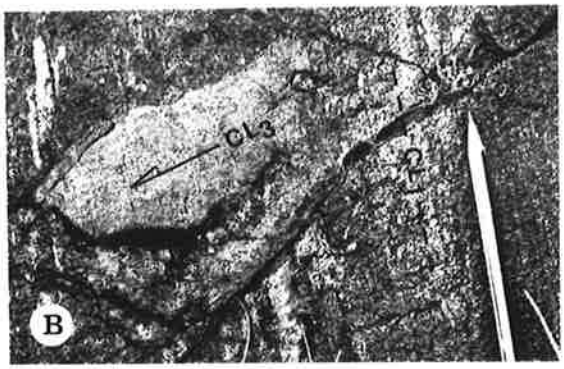
E: This vertically dipping hinge zone of the antiformal CF_3 fold (see Plate 7.3.C) connects the southerly dipping upper limb and the northerly dipping lower limb. The hinge zone plunges 0-13° towards 090°. Location No.3549.

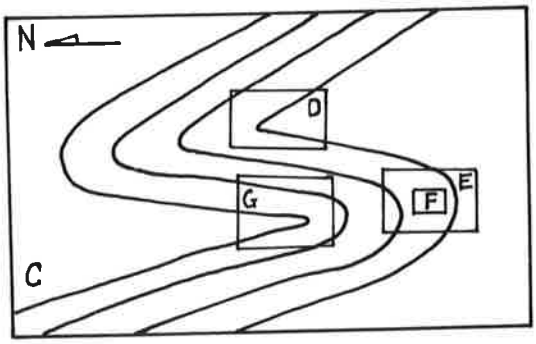
F: A close-up of the vertically dipping hinge zone in (E) which forms a cliff. Location No.3548.

G: A field perspective view of a major antiformal CF_3 fold showing a recumbent axial surface. The two shallow dipping limbs close laterally towards the south (right) via a vertically dipping hinge zone which plunges subhorizontally towards the E-W. location No: 4205, the northern ridge of the Naringa Well area.

Plate 7.3















A weak and discrete CS_3 axial planar schistosity and CL_3 intersection lineation can be found within the calc-silicate gneiss, coexisting with the CS_0-CS_1 compositional layering and CL_1 mineral/elongation lineation (Plate 7.3.B). The CL_3 lineation has also been found within the amphibolite in the hinge areas of CF_3 folds and is parallel to the CF_3 fold axes, which plunge subhorizontally towards the east or west, due to the interference of N-S trending later open folds (Map 6).

The CF_2 folds are refolded by CF_3 folds in a subcoaxial manner and form type 2 interference patterns. The profiles of CF_3 folds are strongly disharmonic between the amphibolite and pelitic gneiss layers. The map-scale cuspate and lobate fold profile in the Mt Campbell area shows that the curvature of the boundary between amphibolite and pelitic gneiss is greatest where the pelitic gneiss lies on the inside of a fold arc and indicates that the amphibolite is more competent than the pelitic gneiss. The amphibolite layers show a more or less constant orthogonal thickness (convergent dip isogon folds, Class 1b to 1c type), whereas the pelitic gneiss sandwiched between thick amphibolite layers shows remarkable thickness increase in the hinge zone, and remarkable thickness decrease in the two limbs (divergent dip isogon folds, Class 3 type). These features can be seen on Map 6 and its cross sections.

The steeply north dipping axial surfaces of the northern five pairs of CF_3 folds become gradually more gently north dipping, as they extend to the east. They eventually become nearly horizontal as they come close to the Bruna Shear Zone, where they pass the hinge zone of a major HRF_2 (CF_4) fold (the Oonagalabi Fold; see later section) and form its overturned limb, extending to the west and southwest. These CF_3 folds become totally isoclinal and very

attenuated in the area from Ruby Mine to Mt Ruby, so that no closure can be mapped out, though the repetition of lithological units is obvious (Lawrence et al., 1987).

The southernmost pair of CF_3 folds in the Mt Campbell area show asymmetric profiles (Map 6 and cross section B-B') which differ from the other CF_3 folds. It is considered that the more competent SOB basement gneiss which was directly underlying the HRSC may have protected this fold pair from further shortening. A thin layer of Bruna Gneiss within the calc-silicate layers is folded by this pair of CF_3 folds (in the centre of Map 6) and this thus defines the upper age limit for the Bruna Gneiss.

A pair of major CF_3 folds has been mapped in the Naringa Well area (Map 5) with fold amplitudes varying from 200 to 500 metres (Plate 7.3.C). They originally had steeply dipping axial surfaces and subhorizontal hinge lines before these were significantly affected by HRF_2 and later open folding. However, they now show shallow dipping axial surfaces in the northern Naringa Well area. Here, the shallowly north dipping limb connects with the shallowly south-dipping limb by passing through a vertically dipping hinge zone around a subhorizontal fold axial surface of a synform at a higher structural level (Plate 7.3.D) This then passes through another vertically dipping hinge zone (Plate 7.3.E & F) to form an adjacent antiform at a lower structural level (Plate 7.3.G). The Naringa Thrust and five individual CF_2 folds are affected by these CF_3 folds. In the central part of the CF_3 synform, the pelitic gneiss forms an isolated core produced by two closures plunging towards each other. This pair of CF_3 folds is probably the associated part of the southernmost pair of CF_3 folds in the Mt Campbell area (Map 6), but this correlation is not certain.

CF_3 folds are refolded by HRF_2 folds (see section 7.3.2.) and change orientation at different locations. In the hinge area of a major HRF_2 fold, north of Naringa Well, a CF_3 fold (No.2 on Map 5) shows that its axial plane dips shallowly towards the NE whereas its fold hinge plunges shallowly towards 340° (Plate 7.4.A, B & C). At this outcrop discrete axial planar foliation can be seen in the hinge zone (Plate 7.4.D & E) and the CL_3 intersection lineation can be clearly seen on the layer surface (Plate 7.4.F).

7.3. Maud Movement

7.3.1. Maud Thrust (HRT2)

The sinuous trace of the Maud Thrust extends for over 80 km from south of Mt Riddoch to the central part of the Naringa Well area. It separates HRSC from SOB at the northern margin of the Oonagalabi Tongue but crosses gradually up into the HRSC as it extends to the south (see Fig. 1-1). The HRF_1/CF_3 folds, the CT Naringa Thrust and HRT1 Oonagalabi Thrust are clearly sheared and very shallowly truncated by the Maud Thrust. At the northern margin of the Oonagalabi Tongue, the CT thrusts and a thin sheet of Bruna Gneiss within calc-silicate are obviously involved in the southernmost pair of CF_3 folds, whereas the Maud Thrust between the ISA and the Oonagalabi gneiss complex is not affected by CF_3 folds but truncates their fold axial traces (see Map 6). This contrasts with the Oonagalabi Thrust, which defines the eastern and southern margin of the Oonagalabi Tongue and has been very obviously involved with the HRF_1 folds. Further to the south and east, the HRF_1 folds are clearly truncated by the Maud Thrust (see Map 5).

A mylonitic zone, about 5-20 metres wide, is found along the

FIGURE CAPTIONS OF PLATE 7.4

A: A sketch profile of the major antiformal CF_3 fold within the calc-silicate at the eastern margin of Naringa Well area (see Map 5) showing the relative position of pictures in (B, C, D, E & F). Location No.3563.

B: The overall view of the fold. Its two limbs close towards the west (left) and its hinge plunges at 8°-340°.

C: The fold core of the fold above which shows Class 1b to 1c type dip isogon patterns. The lithological layering retains equal thickness in the limb areas but is slightly thickened in the hinge area.

D: A discrete spaced foliation (CS_3) occurs in the hinge area of the CF_3 fold.

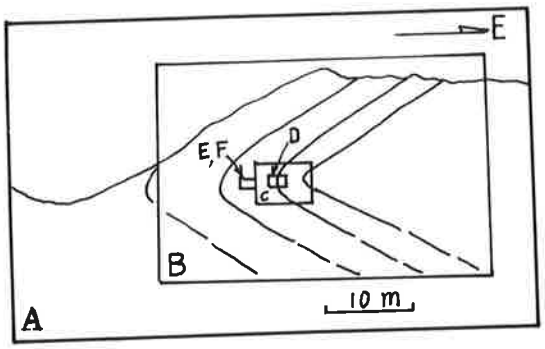
E: A CS_3 spaced axial planar foliation is well developed in calc-silicate gneiss and transects the compositional layering.

F: The CL_3 cleavage/layering intersection lineation on the layer surface (CS_0 or CS_1).

G: Blastomylonitic microstructure. A porphyroclast (full size 2 mm X 2.5 mm) of perthite (lower right corner) within a recrystallized fine (0.01-0.001 mm) matrix of quartz and feldspar and quartz ribbons. The perthite porphyroclast has a deformed and recrystallized margin. Northeastern margin of the Oonagalabi Tongue, along the Maud Thrust; Sample 3650; field of view: 3.4mm X 2.2mm; X polars.

H: Coarse, equigranular granoblastic texture of granitic gneiss, which is the parent rock of the blastomylonite in (G), and was collected from an outcrop 30-40 metres away from the HRT_2 Maud Thrust. Sample 3651; field of view: 3.4mm X 2.2mm; X polars.

Plate 7.4





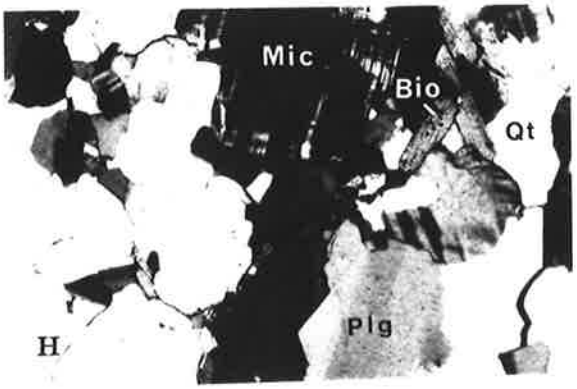












northern margin of Oonagalabi Tongue. This is typically composed of blastomylonites, which show an intense foliation and stretching lineation. Relics of large perthitic feldspar form porphyroclasts, while fine grains of deformed feldspar and quartz ribbons form the matrix (e.g. Plate 7.4.G). This mylonite was derived from the underlying granitic gneiss within the Oonagalabi Tongue. The thin Bruna Gneiss sill within the calc-silicate of the ISA is locally sheared by the Maud Thrust (Rankin, 1983). In contrast, the granitic gneiss within the Oonagalabi Tongue, 20 metres away from the mylonitic zone, shows typical random granoblastic textures in thin section (Plate 7.4.H). The petrofabrics of this mylonitic gneiss show a low angle cross girdle quartz <C> axis petrofabric pattern (Rankin, 1983) , which indicates a high temperature (>700^{o}C) competition between basal and prismatic slip or a low strain rate (Tullis et al., 1973).

Mylonitization is also found along other parts of the Maud Thrust. In Plate 7.5.A, a deformed calc-silicate shows an intense lineation and foliation, which is defined by elongate mineral aggregates of diopside, scapolite, plagioclase and quartz. It is not a typical mylonite but contrasts markedly with the equigranular granoblastic microstructure of the calc-silicate (e.g. Plate 5.1.C) collected further away from the shear zone.

Typical ultramylonite is locally found at the southern end of the Maud Thrust. In outcrop it forms a dark massive layer which looks like limestone containing small fragments. However, in thin section it shows a typical mylonitic microstructure, comprising 10% very small (0.1-2 mm) porphyroclasts and 90% matrix (0.001-0.01 mm). The porphyroclasts include quartz, plagioclase and phlogopite, and are deformed and strained. Small sheath folds are manifested by thin fragments of quartz and can be seen on the

FIGURE CAPTIONS OF PLATE 7.5

A: A deformed calc-silicate showing an intense fabric (compared with the undeformed calc-silicate in chapter 5). This sample was collected a few tens of metres away from the HRT_2 Maud Thrust in the Naringa Well area. Sample P4-9; field of view: 3.4mm X 2.2mm; ppl.

B: Microstructure of a marble ultramylonite showing deformed and recrystallized folded porphyroclasts of quartz, plagioclase and mica in a very fine grained calcite schistose matrix. This sample was collected at the location where the CT Naringa Thrust was sheared into the HRT2 Maud Thrust. Sample No: 3418; field of view: 3.4mm X 2.2mm; ppl;

C: Same view as in (B); X polars.

D: Outcrop scale HRF_2 folds in layered amphibolite. The thin interlayers of tonalitic gneiss (grey) show less competence than the amphibolite layers (dark). The migmatitic veinlet (white) reveals a weak fold axial plane schistosity. About 2 km N of the Ruby Mine.

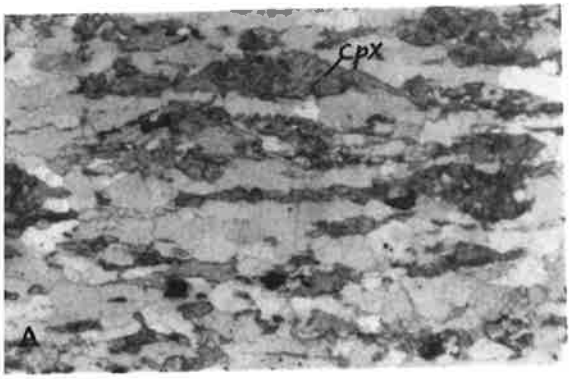
E: A close-up of the lower left part of the folds in (D).

F: Dip isogon diagram of the HRF_2 fold described above. The amphibolite layers (am) show Class 1c type profiles, whereas the tonalitic gneiss layers (to) show Class 3 type profiles.

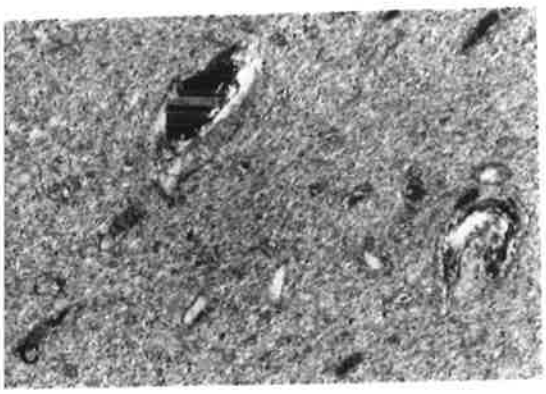
G: A mullion structure with intense lineation within the layered amphibolite. About 1 km S of the Ruby Mine.

H: Discrete foliation developed within the calc-silicate marble parallel to the axial surface of the HRF_2 Mullocky Fold. N of the Muller Flat Dam; location No.4273.

Plate 7.5

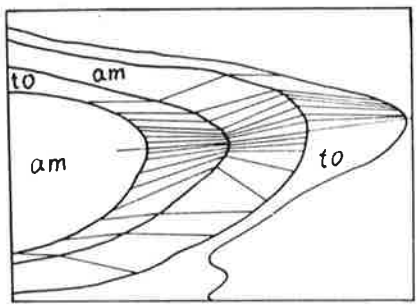












F





sample scale as well as in thin section (Plate 7.5.B & C). The matrix comprises very fine grained calcite showing a clear schistosity. This ultramylonite is probably a product of superimposed shear strain of a later thrusting phase (HRT_3).

7.3.2. Maud Movement folds (HRF_2)

Two pairs of large scale dextral sub-neutral HRF_2 folds occur in the major part of the HOB and in the western part of the HRDZ, but only the northern three have been fully mapped, of which two close towards the east and one closes towards the west (Map 2 and Fig. 1-1). These are named, from north to south, the Oonagalabi, the Mullocky and the Naringa Folds. The southernmost one is only inferred from the lithological symmetry and structural interpretation. Three dimensional geometries of these HRF_2 folds are better illustrated by structural contours on the bounding thrusts of the Oonagalabi Tongue (Fig. 7-1) and on the fault planes of the Maud, the Naringa and the Campbell Thrusts (Fig. 7-2).

7.3.2.1. The Oonagalabi Fold

The northernmost Oonagalabi Fold closes towards the east and its axial surface extends E-W for over 20 km, from the western margin of the Harts Range area to the north of Mt Bruna (Fig. 1-1 & Map 2). It is a very large and very complex fold showing a variable but roughly north-dipping axial surface and north-plunging fold hinges. The fold geometry varies, depending upon which of the different planar elements are considered (e.g. the lithological boundaries; the thrust boundaries; and the axial planes of different folds). This is because these elements were not parallel before the HRF_2 folding. The axial surface of HRF_1 is the best and

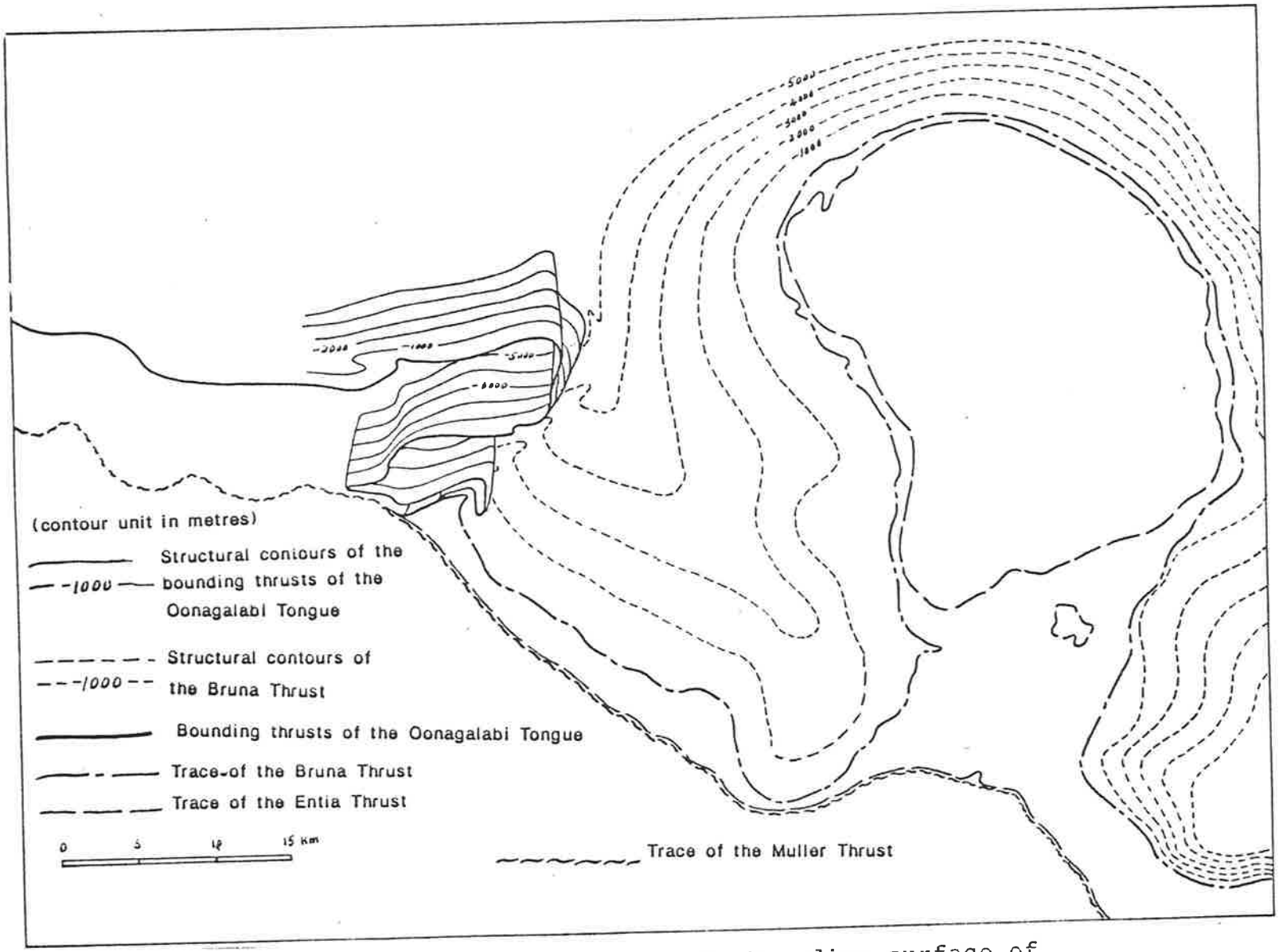


Fig. 7-1 A structural contour diagram for the bounding surface of the Oonagalabi Tongue and the Bruna Thrust.

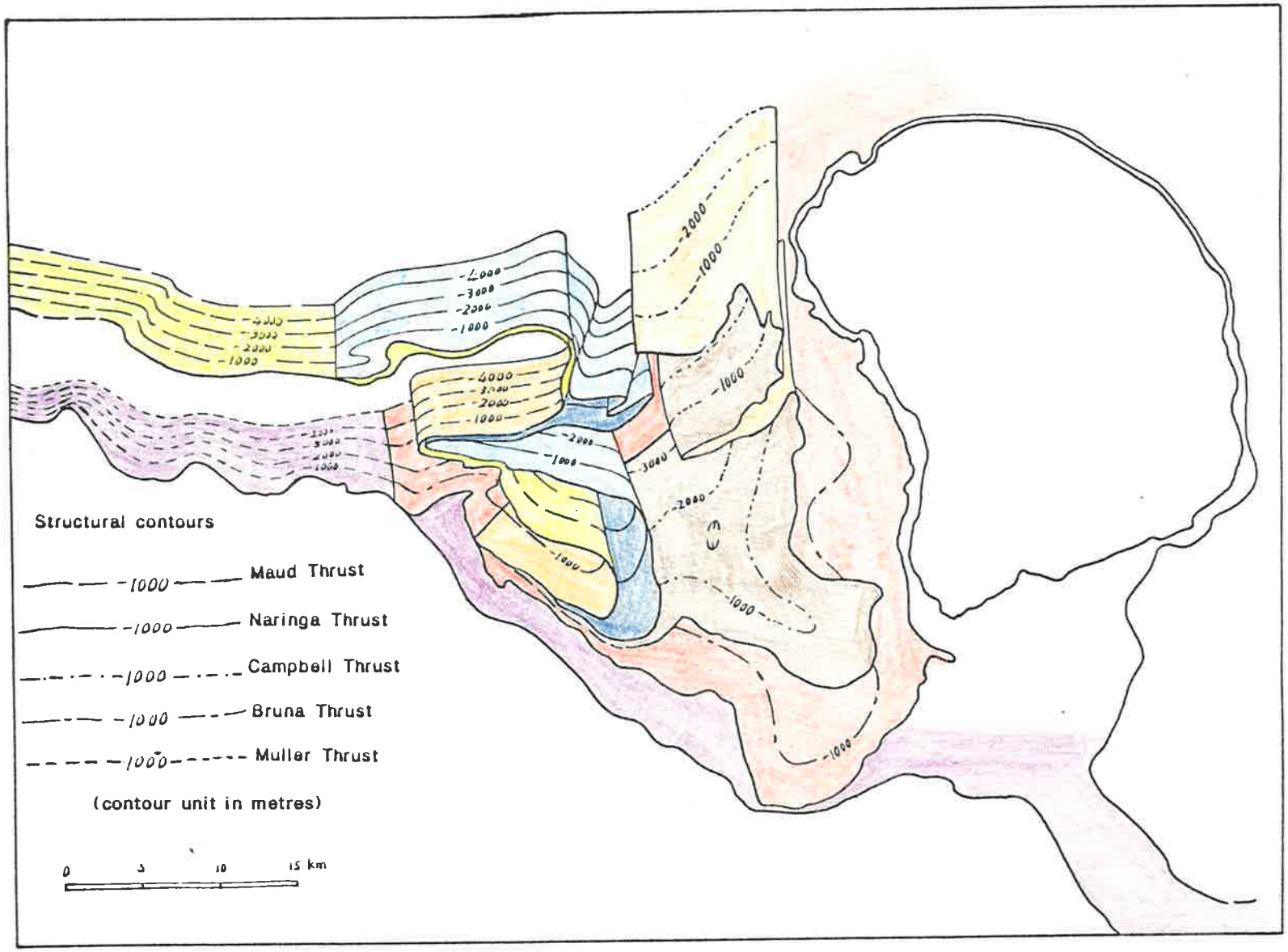


Fig. 7-2 A structural contour diagram for part of the Maud, Naringa, Campbell, Bruna and Muller Thrusts showing the HRF_2 folds.

most representative planar element to describe the geometry of the HRF_2 folds. The overall geometry of the HRF_2 folds is neutral and isoclinal with regard to either the axial surface of HRF_1 or the major thrust boundaries.

The Oonagalabi gneiss complex forms the inner core of the Oonagalabi Fold. The neutral character of HRF_2 makes the surface outcrop of the core a tongue shape, which thus explains its name as the Oonagalabi Tongue (see Chapter 4 and Appendix III). Most of the axial traces of the BF_4 folds appear to extend from the northern limb of the HRF_2 fold across its closure to its southern limb (Map 3). The BL_1 lineation, and BF_2, BF_3 and HRF_1 folds are also affected by the HRF_2 fold as is shown by their fold axial traces on Map 3 and its attached stereograms.

The outline of the Oonagalabi Tongue is manifested by the bounding HRT_1 and HRT_2 thrusts, and shows a pear shaped profile with rectangular closure and parallel limbs, (see Maps 2 and 3). Its wide rounded closure indicates that the gneiss complex within the Oonagalabi Tongue was more competent than the surrounding sequence of the ISA. The northern limb is apparently planar and unfolded, and extends for over 40km out of the mapping area, whereas its southern limb is about 17 km long thus defining the amplitude of the Oonagalabi Fold. However the amplitude of the Oonagalabi Fold decreases eastward (structurally upward) from 17 km for the Oonagalabi Thrust, to 13 km for the Maud Thrust and the Naringa Thrust and to only 7 km for the Campbell Thrust. A single easterly trending fold axial surface diverges into two of different directions in the closure area. One trends northeasterly and dips towards the northwest, the other trends easterly and dips towards the north. Some folds in the closure area of the HRF_2 fold are interpreted as parasitic folds (Map 3).

The trend and plunge of the hinge of the Oonagalabi Fold is extremely variable. In its very tight inner core, two limbs are virtually in contact with each other where the hinge line plunges 10-15° towards the NNE, whereas in its rounded outer closure area, the hinge lines plunge about 40° towards the north or slightly NNE. This change of hinge orientation is interpreted as the result of non-parallelism between the lithological layers and the thrust boundaries, as well as of the effect of rotation.

The ISA forms the outer part of the Oonagalabi Fold enveloping the Oonagalabi Tongue and the geometry of the Oonagalabi Fold becomes more complex within the ISA. There are many smaller or parasitic HRF_2 folds which indicate that the metasedimentary rocks of the ISA are less competent and/or more highly layered than the basement gneisses. Disharmonic folds develop locally around the hinge area of the Oonagalabi Tongue.

The disharmonic profile of HRF_2 within the ISA indicates an order of rock competence (Ramsay, 1984), from highest to lowest, of amphibolite, calc-silicate gneiss, marble and biotite gneiss (Ramsay, 1984). Within the amphibolite sequence, the thin interlayers of tonalitic gneiss show less competence than the amphibolite layers. The outcrop scale HRF_2 folds (Plate 7.5.D & E) show a remarkable similarity to the regional HRF_2 fold. The more competent amphibolite layers form Class 1c type folds, whereas the less competent tonalitic gneiss layers form Class 3 type folds (Plate 7.5.F).

A weak axial plane schistosity develops locally in the hinge areas of HRF_2 folds (Plate 7.5.D & E). Intense stretching is seen in the easternmost part of the Oonagalabi Fold, near the Bruna Thrust (the western margin of Entia Dome), and results in mullion structures in the HRF2 hinges (Plate 7.5.G) where the CL_1 linea-

tion has been rotated to nearly parallel to the HRF_2 hinge, though other trends of CL_1 lineations are seen occasionally. However, the CL_1 lineations and fold axes of CF_2 and HRF_1/CF_3 are clearly folded by the Oonagalabi Fold in the area close to the Oonagalabi Tongue (Map 5 and attached stereograms).

The HRF_2 fold axes are almost perpendicular to the HRF_1/CF_3 and CF_2 fold axes (see Map 3 & 5), which thus produce mushroom shaped or luniform folds, similar to type 3 superimposed fold interference patterns. The interference patterns between three or more non-coaxial fold phases are extremely complex and have not been studied in detail.

The HRF_2 (CF_4) folds described here were described as F_2 in the Ruby Mine area by Lawrence et al. (1987). Their F_2 is a local terminology for that specific area because the earlier CF_1, CF_2 and CF_3 folds mapped on the regional scale in this study could not be identified in the Ruby Mine area due to the intense attenuation and stretching by the closely adjacent HRT_3 Bruna Thrust. The F_1 structures of Lawrence et al. (1987) thus include all folds which are earlier than HRF_2 folds defined by this study.

7.3.2.2. The Mullocky Fold

The Mullocky Fold lies just 3-4 km to the south of the Oonagalabi Fold, closing to the west, and has an axial trace extending for over 30 km. Like the Oonagalabi Fold it has a northerly dipping axial plane, parallel limbs and northerly plunging major fold hinges (Map 2, Map 5 and Fig. 1-1). With reference to the Naringa Thrust, its amplitude is about 13 km but is reduced to only 7 km with reference to the Campbell Thrust to the east. Its very tight core is occupied by amphibolite of the Campbell Nappe (Map 2 and Fig. 1-1). The disharmonic profile can be seen on Map 5 and indi-

cates an identical order of competence to that described in the previous section. A rounded and rectangular closure formed along the outer boundary of the calc-silicate and calc-silicate gneiss, whereas a sharp cuspate closure formed along the outer boundary of the marble, where the marble lies in contact with the granitic gneiss in the basement. This indicates that marble is less competent than the granitic gneiss or the calc-silicate.

The CL_1 lineation and fold axes of CF_2 and HRF_1/CF_3 folds are all folded around the closure area of the Mullocky Fold, as is shown on Map 5 and its attached stereogram. A major HRF_1 fold is exposed as a luniform tectonic window (the Florence Window) (see Chapter 6), formed by the interference between HRF_1 and HRF_2 major folds. The distorted axial surface of the Mullocky Fold is attributed to the interference of a competent basement gneiss core of the HRF_1 fold. Discrete cleavage found within the marble in the western closure of the HRF_2 fold might be its axial planar fabric (Plate 7.5.H).

7.3.2.3. The Naringa Fold

The Naringa fold is situated 2-7 km south of the Mullocky Fold, and closes to the east. Its northerly dipping axial surface extends for over 25 km along strike and has been itself refolded by HRF_3 and later open folds. Its northerly plunging fold hinge varies in trend from NE to NW. The Naringa Fold shows a pear shaped surface outline, very similar to the Oonagalabi Tongue, with a rounded closure and two parallel limbs in the centre but a rectangular closure and two convergent limbs in its outer part.

Its amplitude is about 15 km with reference to the Maud Thrust and the Naringa Thrust. In the western part of the Naringa Fold, the basement gneiss forms its inner core, which has been

truncated and intensely sheared by the HRT_3 Bruna Thrust, and is thus exposed as a tectonic window, named as the Maud Window. The amplitude of the basement core is only about 4 km. The folded HRT_1 Oonagalabi Thrust shows a NNE plunging closure and forms totally parallel limbs.

In the middle region of the Naringa Fold, marble forms its core and shows a cylindrical closure plunging towards the NNW with totally parallel limbs (see Map 5). The axes of HRF_1/CF_3 folds are folded around the closure of the HRF_2 fold. Plate 7.6.A is an oblique aerial view of the marble core (Appendix III, Ding & James, 1985). A closure of a refolded HRF1 fold (see Map 5) appears in the lower part of the photo. The thickness of the folded rock pile remains almost unchanged and thus forms a Class 1b type fold. The significant variation in thickness at the southern limb of the Naringa Fold is considered to result from the combination of, shearing caused mainly by CT and HRT_2 thrusts before HRF_2 folding, and by HRT_3 thrusting after HRF_2 folding. The chronological relationship between different overprinting fold phases is best shown by the fold axial traces on Map 5. The relationship between the HRF_2 and earlier fold axes is illustrated by the attached stereograms of Map 5.

The Naringa Thrust forms the outer part of the Naringa Fold and has a pear shaped profile with a wide rounded rectangular closure and convergent limbs. This indicates once again that the calc-silicate gneiss is much more competent than the pelitic gneiss. A single axial surface within the fold core diverges to form two axial surfaces to the east. One trends NE-SW and dips towards the NW, another trends E-W and dips towards the north (Map 5 and Fig. 1-1). There appears to be a distinct geometric similarity between the outline of the Oonagalabi Tongue and the outline

FIGURE CAPTIONS OF PLATE 7.6

A: Oblique aerial view (facing towards east) showing the core of the HRF_2 Naringa Fold (compare with Map 5). Marble layers (white) form the lower ridges whereas the calc-silicate and calc-silicate gneiss layers (darker) form the higher ridges. A major HRF_1 fold can be seen refolded by the HRF_2 fold. The closure of the HRF_1 fold is manifested by the calc-silicate gneiss layers (at the lowest part of the picture). The HRT_2 Maud Thrust separates the hilly area of mainly marble calc-silicate lithologies to the north from the area of subdued relief to the south where the dominant lithology is the ISA pelitic gneiss. S of the Naringa Well area.

B: K-feldspar porphyroclasts (0.5-2 mm) within the very fine grained (0.001-0.02 mm) matrix of an ultramylonite of Bruna Gneiss, collected from the Bruna Thrust. The mylonitic foliation is defined by recrystallized biotite in the matrix. The foliation seems not to be affected by the syntectonic and post-tectonic garnet. Sample 3210; NW of Mt Ruby; field of view: 3.4mm X 2.2mm; ppl.

C: Same view as in (B); X polars.

D: Mylonitized Bruna Gneiss along the Bruna Thrust showing heterogenous fabric development. S of Mt Ruby; location No.3026.

E: A large porphyroclast of K-feldspar within mylonitized Bruna Gneiss along the Bruna Thrust at the western margin of the Entia Dome; location No.3151.

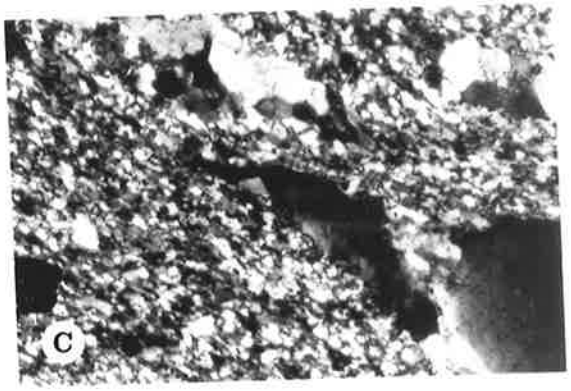
F: A Polished XZ surface of a mylonitized Bruna Gneiss sample (3151) shown in (E).

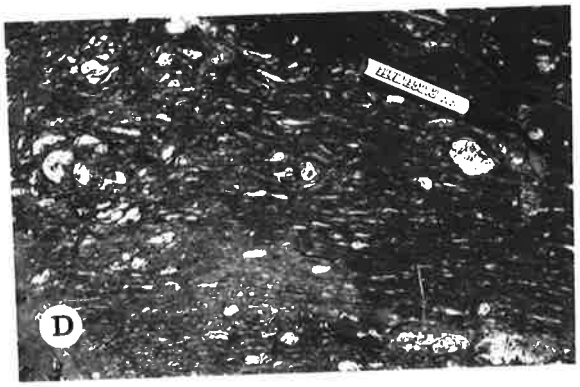
G: An ultramylonite layer defines the Bruna Thrust at the top of the major Bruna Gneiss sheet. Location No.4008; N of Leaky Bore.

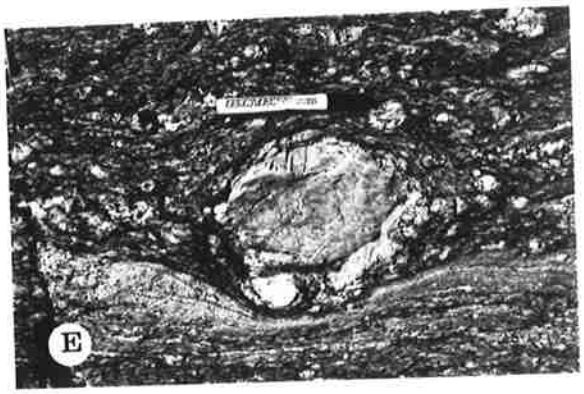
Plate 7.6

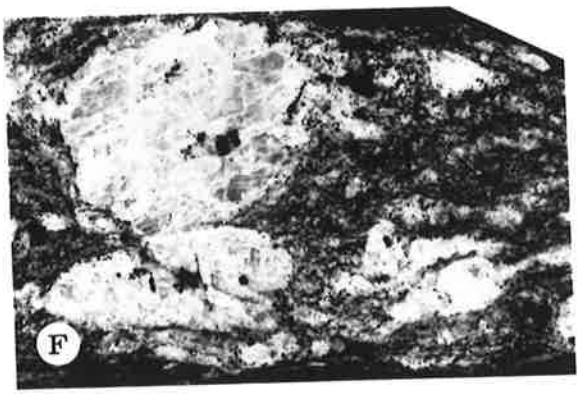














of the Naringa Thrust within the Naringa Fold.

7.4. The Bruna Movement

7.4.1. The Bruna Thrust and the Entia Thrust (HRT_3)

Intense shearing occurred along the margin of, and within, the major sheet of Bruna Gneiss (see chapter 5) during the Bruna Movement and a heterogeneous mylonitic fabric formed ubiquitously within the whole Bruna Gneiss body (also see James et al., in press). In contrast, the typical mylonites and ultramylonites developed within relatively narrow zones along both the top and basal margins of the major Bruna Gneiss sheet. These two narrow mylonite and ultramylonite zones are recognized as major thrust fault boundaries since they truncate the Oonagalabi and the Maud Thrusts, and lithological boundaries within both the ISA and the F/LSZ. The top boundary is named the Bruna Thrust and the basal zone is named the Entia Thrust (Fig. 1-1 & Map 2). The three dimensional geometry of the present Bruna Gneiss sheet is illustrated by structural contours on both the Bruna and the Entia Thrusts (Fig. 7-3).

7.4.1.1. The Bruna Thrust

The irregular fault trace of the Bruna Thrust extends for over 140 km, trending SE from west of Florence Creek to the south of Mt Ruby before it turns north, passing around the Entia Dome, and finally trends south, passing through the Leaky Bore and out of the study area. Its complex exposure is due to the influence of later open folds. The exposed fault trace of the Bruna Thrust reveals an original thrust surface of 75 km in original length (in WNW-ESE direction) and 50 km in width (in NE-SW direction). Its

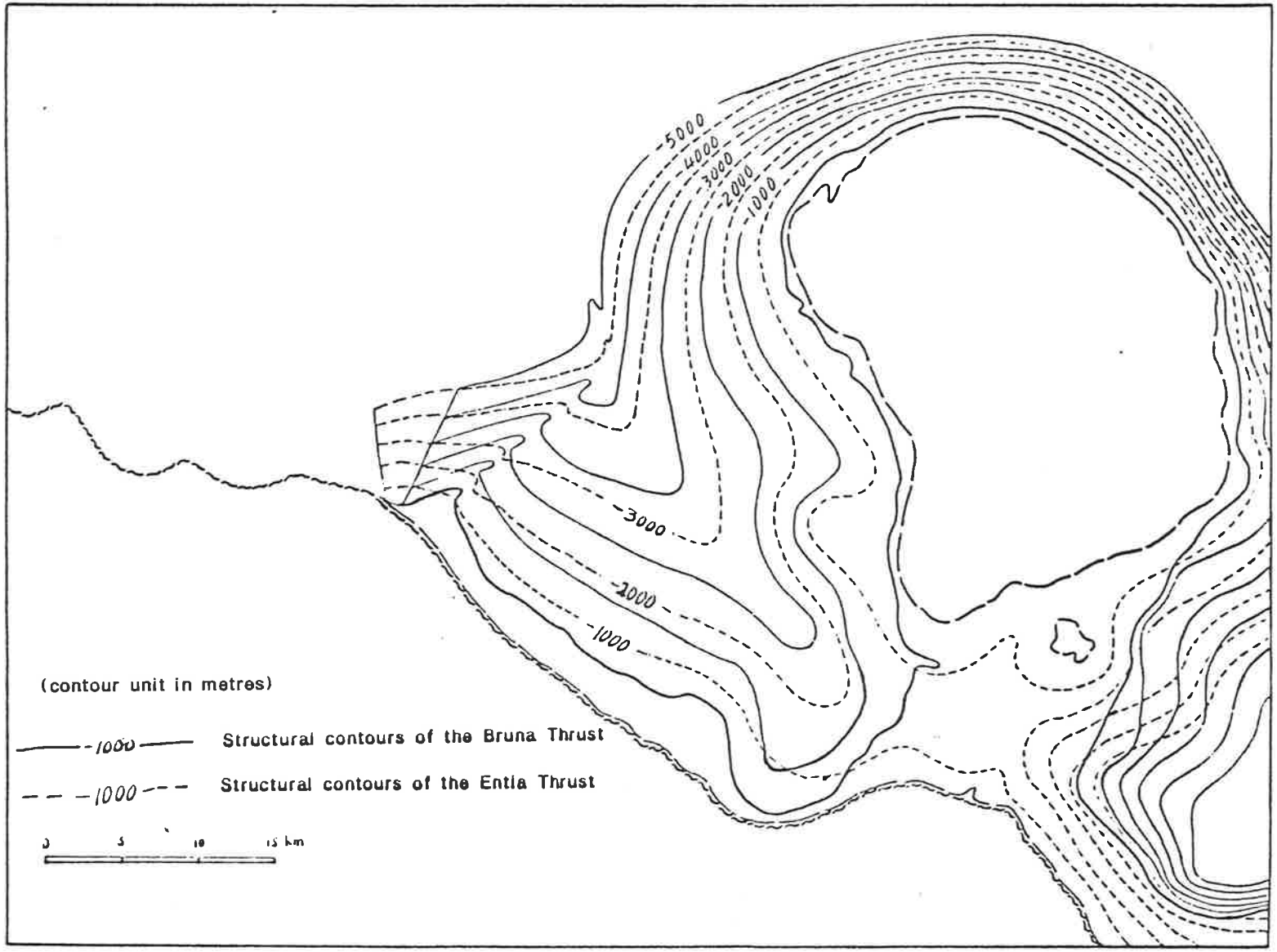


Fig. 7-3 A structural contour diagram for the HRT_3 Bruna and Entia Thrusts.

present three dimensional geometry is better shown by the diagram of structural contours on the thrust surface (Fig. 7-3).

Mylonite and ultramylonite occur all along the thrust trace with intense planar foliation and northerly trending transverse lineation (Mattauer, 1981). Representative samples were collected from many places, e.g. the west of Mt Ruby (e.g. Plate 7.6.B & C), the south of Mt Ruby (Plate 7.6.D), the western margin of Entia Dome (Plate 7.6.E & F) and the north of Leaky Bore (Plate 7.6.G). A thin layer of recrystallized pelitic ultramylonite usually occurs above the Bruna Thrust, particularly between the thick Ruby amphibolite pile and the major Bruna Gneiss sheet (Plate 7.7.A, B, C & D). It is not always possible to tell the original precursor of the ultramylonite.

The fabrics developed within the mylonite are extremely heterogeneous. Some weakly deformed feldspar megacrysts retain their original rounded shapes, whilst some other intensely deformed megacrysts form streaky (Plate 7.7.E) or folded ribbons (Plate 7.7.F & G). The process of the formation of folded feldspar ribbons is probably similar to that of curved lineations (Bell, 1978) and of sheath folds (Cobbold & Quinquis, 1980; Henderson, 1981). At the junction of the HRT_1 and the Bruna Thrust at the southern margin of the Maud Window the HRT_1 mylonites have been significantly stretched during the development of HRT_3 and form typical sheath folds (Plate 7.1.D, E & F). Individual sheath folds look like pipes or tubes which imply a very large strain ratio of X/YZ (Sanderson, 1973; Cobbold & Quinquis, 1980; Henderson, 1981; Faure, 1985). The mylonites along the Bruna Thrust were formed under amphibolite facies conditions which have been discussed in Chapter 5.

Mesoscopic and microscopic structures within mylonites have

FIGURE CAPTIONS OF PLATE 7.7

A: Microstructure of (ISA) mylonitized pelitic gneiss from directly above the Bruna Thrust, south of Mt George at the western margin of the Entia Dome, showing porphyroclasts of plagioclase (1-2 mm), garnet (0.5 mm) and biotite in a recrystallized matrix of fine-grained (0.01-0.1 mm) biotite, plagioclase and quartz ribbons. Sample P2-6; field of view: 3.4mm X 2.2mm; ppl.

B: Same view as in (A), X polars.

C: Microstructure of a recrystallized ultramylonite derived from the (ISA) pelitic gneiss directly above the Bruna Thrust, west of Mt Ruby, showing a porphyroclast of garnet surounded by fine grained sillimanite biotite gneiss. The garnet remains undeformed. Grain size of the recrystallized matrix is still much smaller than the unmylonitized pelitic gneiss (described in chapter 5). Sample 3209; ppl; field of view: 3.4mm X 2.2mm.

D: An enlarged view from (C) showing the recrystallized sillimanite in the matrix; ppl; field of view: o.85mm X 0.55mm.

E: An outcrop of ultramylonite along the Bruna Thrust, from the south of Mt Ruby, showing the evidence of heterogeneous strain. Some megacrysts have been intensly stretched whereas others remain elliptical. Location No.3004.

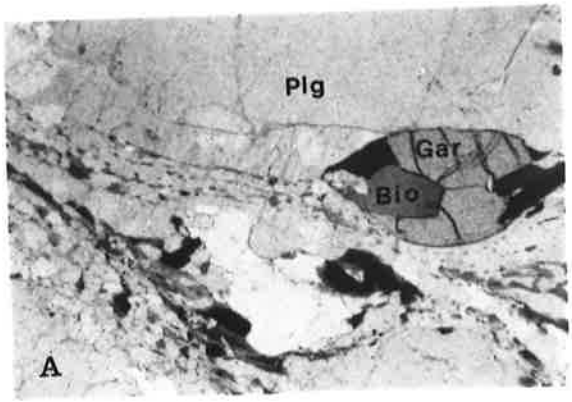
F-G: Heterogenous fabric within mylonitized Bruna Gneiss layer. SW of the Coggan Bore; location No.4506.

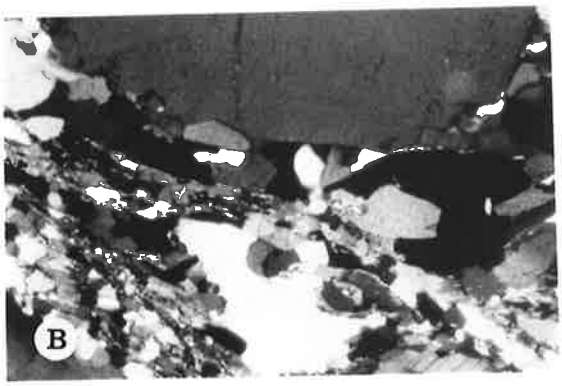
F: A view of a joint surface perpendicular to the foliation but slightly oblique to the elongation lineation.

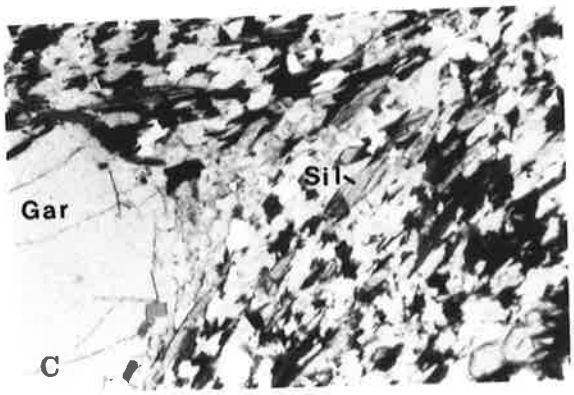
G: A view of the layer surface. Some of the megacrysts remain weakly deformed whereas others have been intensly deformed to be ribbon-like and sheath-like aggregates of very fine grained feldspar.

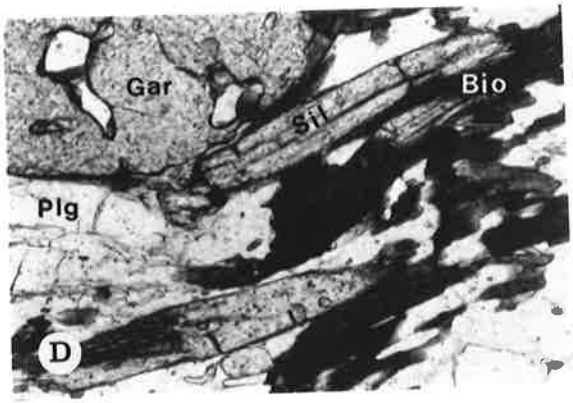
H: Asymmetric structure within blastomylonite along the northerly dipping Bruna Thrust showing a sinistral shear sense (southwards upthrusting). Location No.P1-2, S of Mt Ruby.

Plate 7.7

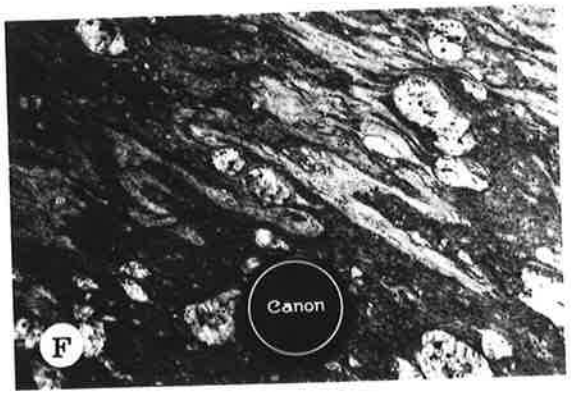
















been used to indicate the shear sense in shear zones by many authors (e.g. Boullier and Gueguen, 1975; Faure, 1983, 1985 a & b; Berthe et al., 1979; Lister & Snoke, 1984). The shear criteria in rocks have been recently reviewed by Cobbold and Gappais (1987). Excellent examples are presented by Choukroune et al. (1987), and by Mawer (1987). The application of these shear criteria has also been previously discussed in Chapter 4. However, the shear sense within the Bruna Gneiss indicated by these shear creteria is variable. Some mylonitic gneisses show northerly shear sense, while others show opposite southerly sense (see also MacDonald, 1986; James et al., 1987). This probably reflects a heterogeneous ductile flow during mylonitization as can be seen from Plate 7.7.G. The kinematic principle here appears similar to that of the formation of folds, where the opposite limbs show opposite shear senses. This interpretation may also be applied to many of the thick shear zones in this area, e.g. the F/LSZ (see Chapter 4). Limited samples and/or outcrop observations cannot be used as conclusive evidence to interpret the shear sense of the whole shear zone. However the predominant shear sense represented by the Bruna Thrust and the Bruna Gneiss seems to be southward overthrusting (Plates 7.7.H & 7.8.A, B & C).

No quartz c-axis fabric work has been carried out along the HRT_3 thrusts. As the typical mylonites of the Bruna Gneiss give a temperature (see Chapter 6) ranging from 710-740°C (Goldman & Albee, 1977) to 710-780°C (at 7kb after Ferry & Spear, 1978), this discouraged any attempt at quartz c-axis fabric measurement, because high temperature (>700°C) mylonites usually show a symmetric cross girdle pattern of quartz c-axis fabric and can not be used as indicators of shear sense (see HRT_2 in section 7.3.1.).

The predominant southward shear sense is also confirmed by

FIGURE CAPTIONS OF PLATE 7.8

A: A polished XZ surface of an ultramylonite sample collected from the outcrop described in Plate 7.7.E, showing the structral details and a southward (dextral) shear sense from asymmatric tails around feldspar augens. Sample 3004; field of view: 28 mm X 63 mm.

B: A large thin section of the sample above showing the recrystallization within porphyroclasts presumably due to deformation. Field of view: 26 mm X 39 mm; X polars.

C: Polished XZ surface of a mylonitized Bruna Gneiss sample (No. P1-4) collected from the Bruna Thrust showing a dextral shear sense. Field of view: 28 mm X 40 mm; S of Mt Ruby.

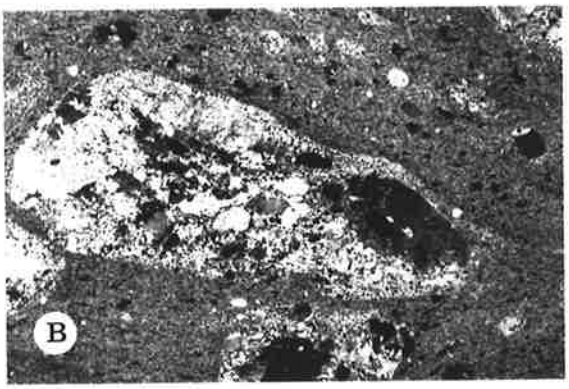
D: A cross section from Mt Ruby to the Yambla Window (B-B' section on Fig. 7-5) showing the large scale southwards shearing of the Ruby nappe sheet above the Bruna Thrust. Dragging and stretching are obvious along and near the thrust surface.

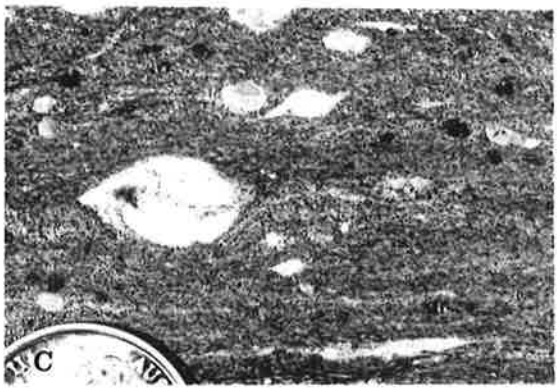
E: A sketch section of the Entia Thrust showing a very planar layer of ultramylonite (3), developed between the mylonitized Bruna Gneiss and the unmylonitized amphibolite and tonalitic gneiss of the Entia gneiss complex. The axial surfaces of the folds within the Entia gneiss complex are clearly truncated by the thrust boundary, whereas the axial surfaces of folds within the ultramylonite are parallel to the thrust boundary. The typical Bruna Gneiss (5) sits at the top of the hill. Location No.P2-3; S of Mt Geoge, Entia Dome.

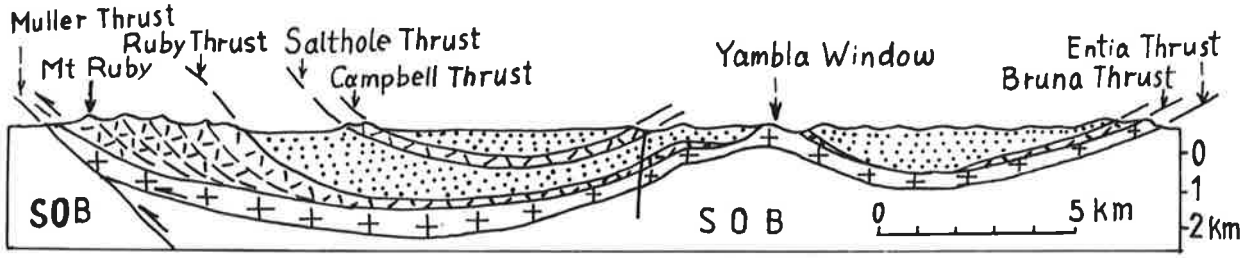
F: A field view of the Entia Thrust at the southern margin of the Entia Dome. The subhorizontal oriented Bruna Gneiss forms a cliff above the thrust. The Entia gneiss beneath the thrust dips moberately towards the south and becomes very shallow dipping where it approaches the thrust boundary. Location No.3358.

Plate 7.8

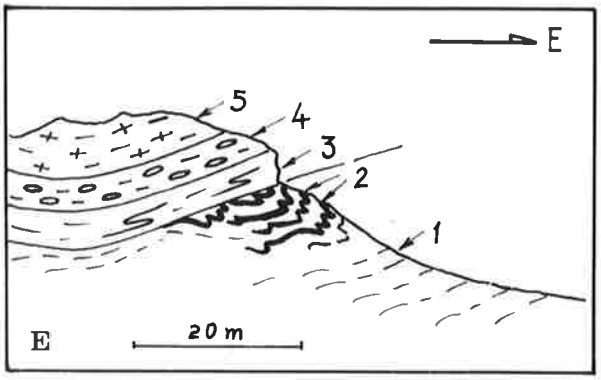


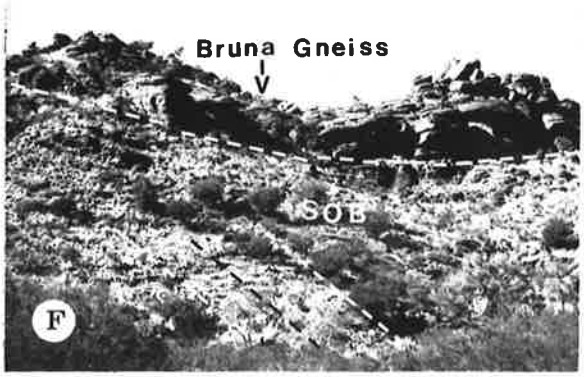






D Pelitic gneiss Amphibolite Bruna Gneiss





the regional displacement of the whole structure above the Bruna Thrust. A cross section through Mt Ruby (Plate 7.8.D) shows a thick pile of amphibolite, which dips moderately towards the north, has been truncated and dragged to shallower dips by southward shearing and is also thinned where it approaches the Bruna Thrust. The HRT_1 Oonagalabi Thrust, the HRF_2 folds and the HRT_2 Maud Thrust are also obviously truncated by and sheared into the western part of the Bruna Thrust with a similar sense (Map 5).

7.4.1.2. The Entia Thrust

The trace of the Entia Thrust has similar dimensions to that of the Bruna Thrust (Fig. 1-1). Its full exposure around the Entia Dome is about 100 km and it has been mentioned in Chapter 2 as the marginal shear zone of the Dome. Its three dimensional geometry is shown by a structural contour diagram (Figs. 7-3 and 7-4).

Along the southern margin of the Entia Dome, the Bruna Gneiss dips gently towards the south and sits above the Entia gneiss complex (Plate 7.8.F) which is truncated by the Entia Thrust at an angle of about 30^{o}. However, the Entia gneiss layers become subparallel to the thrust boundary where these gneiss layers approach the thrust boundary. At the SW margin of the Entia Dome, a thin layer of ultramylonite, about 5-10 metres thick, lies at the top of the folded Entia gneiss complex with an impressively sharp contact (Plate 7.8.E). Intrafolial isoclinal folds (Plate 7.9.A & B) are found within the ultramylonite layers, with fold hinges parallel to the mylonitic lineation. These are interpreted as a result of rotation by intense stretching (Sanderson, 1973; Bell, 1978; Berthe and Brun, 1980). The strain must have been very large to produce an $80\text{-}90^{o}$ rotation of mylonitic fold hinges by stretching along the shear direction, in comparison with the example deve-

FIGURE CAPTIONS OF PLATE 7.9

A: A YZ (perpendicular to the mylonitic lineation) polished sample surface of the ultramylonite described in Plate 7.8.E showing an isoclinal fold within the ultramylonite. Size of view: 50 mm X 125 mm; sample P2-3.

B: A small-scale micrograph of the same sample in (A); X polars; field of view: 28 mm X 37 mm.

C: An XZ view of the microstructure of the same sample showing a intense foliation which is manifested by quartz ribbon and feldspar aggregates, and the alignment of recrystalized epidote. X polars; field of view: 1.7 mm X 2.2 mm.

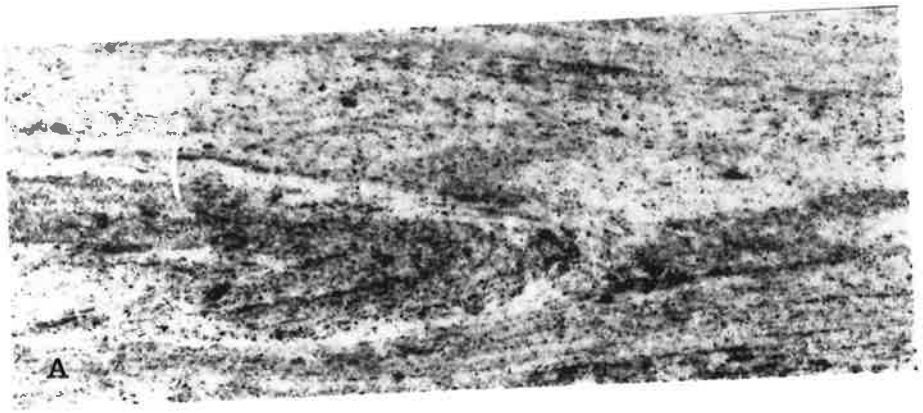
D: Microstructure of a blastomylonite collected from near the base of the Bruna Gneiss sheet at the SW of Mt Ruby showing a weak S-C relationship. The horizontal elongation fabric (S) was intersected by a set of displacement foliation (C) which is gently inclined towards the right and suggests a dextral (southwards) shear sense; field of view 28 mm X 39 mm; ppl.

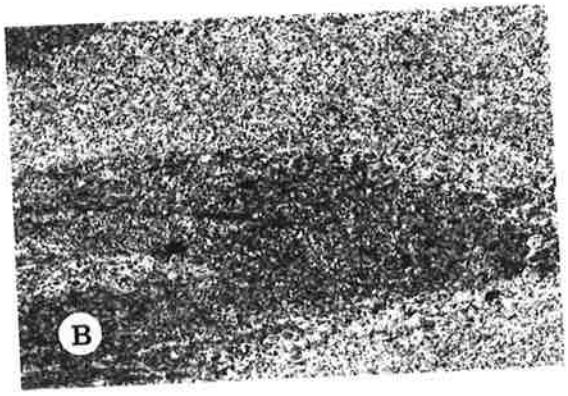
E: Asymmetric HRF_3 fold within the HRSC near the Bruna Thrust. Florence Creek.

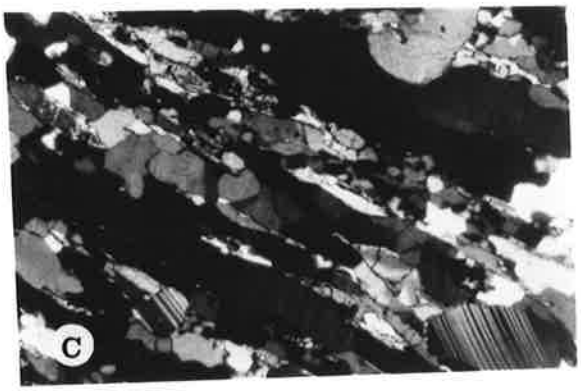
F: An example of a reclined HRF_3 fold at the southern margin of the Entia Dome (the picture faces NNE). The mylonitized Bruna gneiss and the amphibolite (in the core of the fold) of the Entia gneiss complex were folded together. Location No.3359.

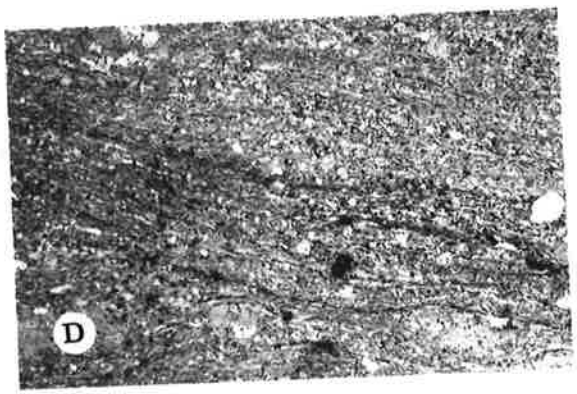
G: A sketch of the fold in (F) showing its disharmonic profile and a near Class 2 dip isogon pattern.

Plate 7.9


A

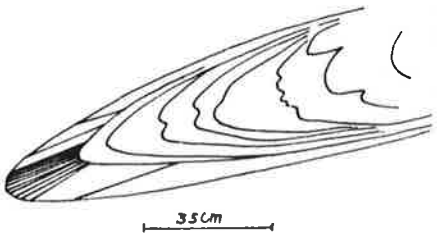

B


C


D


E


F



G

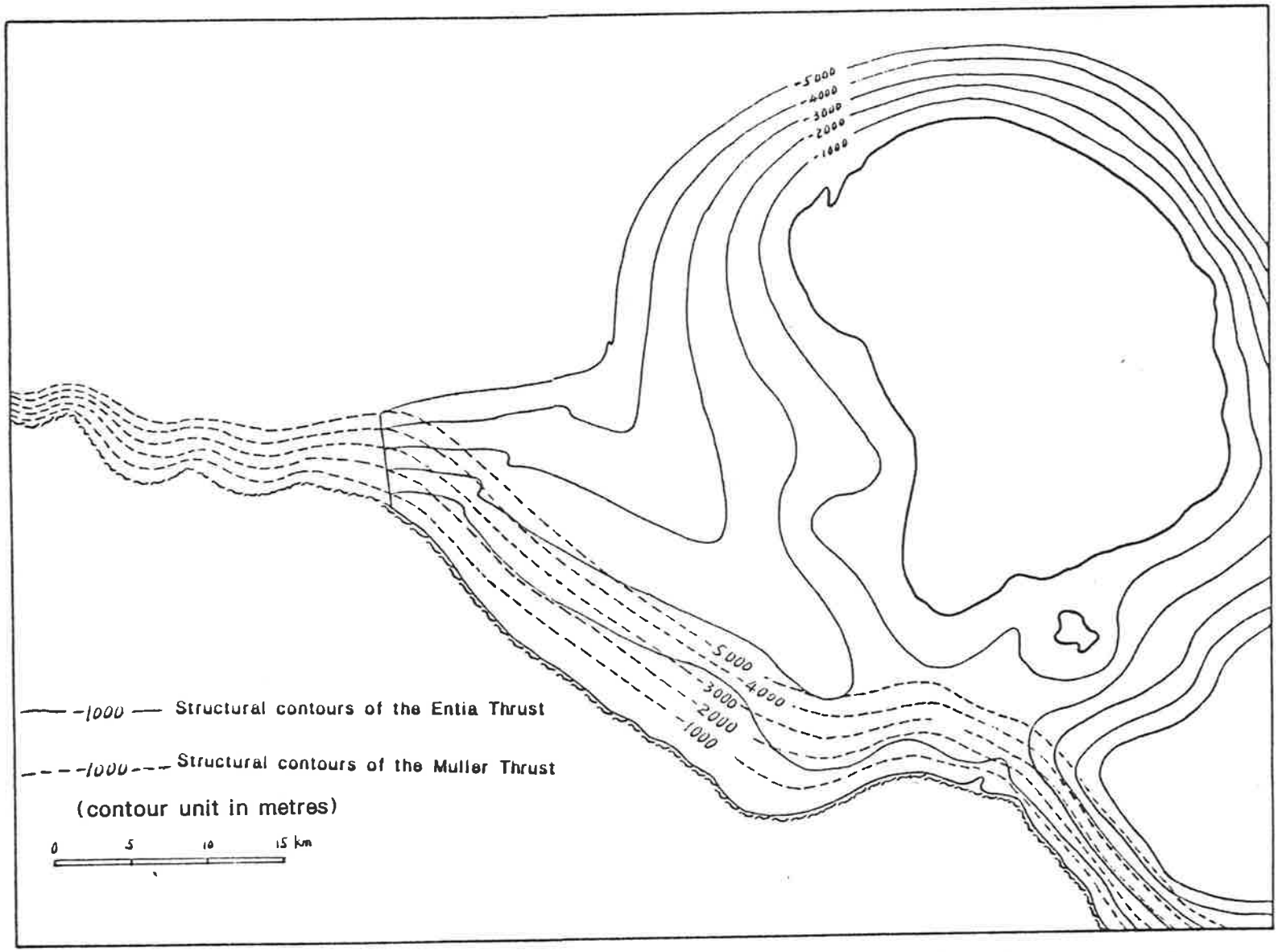


Fig. 7-4 A structural contour diagram for the HRT_3 Entia Thrust and the HRT_4 Muller Thrust.

oped by Sanderson (1973). The ultramylonite has been totally ecrystallized and shows intense ribbon structure without any symmetric kinematic indicators (Plate 7.9.C). Further detailed ork has been carried out in the NW section (MacDonald, 1986; arker, 1986 and James et al., 1987) and in the NE section Martin, 1984). These studies all suport the observations of this tudy, i.e. that the boundary between the Entia gneiss and the runa Gneiss is a large scale shear zone.

Similar ultramylonite has been found along the southern mar-in of the Bruna Gneiss sheet, from the Florence Creek (see FSZ in hapter 4) to the south of Mt. Ruby. The microstructure of the ltramylonite indicates a southward shear sense (Plate 7.9.D), but t might have been reworked by the later HRT_4 Muller Thrust. It is very likely that the granulite facies mylonites within the lorence/Leaky Shear Zone were reworked under amphibolite facies conditions during the Bruna Movement.

7.4.1.3. Metamorphism of the Bruna Gneiss

The Bruna Gneiss has been metamorphosed under amphibolite facies conditions as is shown by the mineral assemblage of biotite, hornblende, garnet, epidote, plagioclase and microcline with minor muscovite. Garnet within the Bruna Gneiss does not show compositional zoning.

A metamorphic temperature has been calculated from coexisting biotite and garnet (Table 7.1).

Table 7.1 TEMPERATURES FRON GARNET & BIOTITE IN THE BRUNA GNEISS

sample No.	Perchuk (1976)	Thompson (1976)	Goldman & Albee (1977)	Ferry & Spear (1978) 7Kb	7.5Kb	8Kb	8.5Kb
P3-4	610	605	688	649	651	654	656
3382	588	580	671	607	609	612	614
average	599	603	680	628	630	633	635

The temperatures range from 600°C to 660°C (Ferry & Spear, 1978), or 670-690°C (Goldman & Albee, 1977). In comparison with the results from other samples, the metamorphic temperature of the Bruna Gneiss is about 70°C lower than the peak temperature of the ISA, but very similar to the cooling temperature of the ISA. It is thus suggested that the Bruna Gneiss was metamorphosed under a decreased geothermal gradient.

The peak temperature derived from the ultramylonite of the Bruna Gneiss (Table 7.2) is 150°C higher than the average temperature of typical Bruna Gneiss. The temperature derived from garnet-rims is lower than that from garnet-centres but still about 90°C higher than the typical Bruna Gneiss. A local heating from deformation is suggested as a possible reason for the higher temperature recorded within the ultramylonite. This is similar to the results from the CT shear zones. Fig. 6-2, a P-T diagram in Chapter 6, may be referred to in order to compare the metamorphic conditions between the ISA and the Bruna Gneiss.

Table 7.2 TEMPERATURES FROM GARNET & BIOTITE IN AN ULTRAMYLONITE OF THE BRUNA GNEISS

sample No. 3004	Perchuk (1976)	Thompson (1976)	Goldman & Albee (1977)	Ferry & Spear (1978) 7Kb	7.5Kb	8Kb	8.5Kb
centre	677	685	742	778	780	783	785
rim	647	650	717	716	718	721	723
difference	20	35	25	62	62	62	62

7.4.2. Bruna Movement folding (HRF_3 folds)

The HRT_3 thrusts and their adjacent lithologies, including the Bruna Gneiss sheet, the Florence metamorphic complex, the Entia gneiss complex and the ISA, were all locally affected by

HRF_3 folds on a mappable scale. However the HRF_3 folds cannot be traced very far away from HRT_3 thrusts.

The HRF_3 folds are plunging inclined and show an asymmetric dextral (easterly) vergence, similar to that of the HRF_2 folds (Fig. 1-1). The HRF_3 folds show profiles varying from open to tight, and locally isoclinal, with fold hinge trends varying from NNW to NNE. One major HRF_3 fold has been mapped in the Florence Creek area (see the major HRF_3 axial trace on the SW corner of Map 5). This major fold is quite open in its core near to the base of the Florence Shear Zone, but it becomes tight and locally isoclinal NE towards its outer arc, where the Maud Window (HRF_2), the Bruna Gneiss sheet and HRT_3 thrusts are folded around it. Further to the NE its intensity decreases again. There are also many parasitic HRF_3 folds around this major one but most of these are too small to show on the maps (Plate 7.9.E).

Plate 7.2.A & C shows an example of mylonite along the HRT_1, which was refolded by HRF_3, with an axial planar schistosity developed within the mylonite, and particularly within one single quartz ribbon. Some other HRF_3 folds have been found along the southern and eastern margins of the Entia Dome (Plate 7.9.F & G; see also Plate 2.5.G & H in Chapter 2), where the mylonitized Bruna Gneiss and the gneisses within the Entia Dome, as well as the Entia Thrust between them, have been locally folded at a mappable scale. The profiles of the local folds vary from tight asymmetric to isoclinal neutral, with fold hinge trends varying from NNW to NNE. A pair of major dextral asymmetric folds around the Ruby Mine area have been mapped and assigned to a local F_3 by Lawrence et al. (1987). They are correlated with the HRF_3 folds in this thesis.

7.5. Muller Movement - Muller Thrust (HRT_4)

The Harts Range Orogeny was terminated by upthrusting along the HRT_4 Muller Thrust. This is the northern marginal bounding thrust of the Hale River Region of the SOB, within which the structural trends are distinctly truncated.

The Muller Thrust has been mapped for over 80 km of strike length across the whole area. Its westerly extension most likely passes through the northern margin of the Strangways Range (see Australia 1:100 000 Geological Series: Arltunga - Harts Range Region N.T., B.M.R., 1984), whereas its easterly extension is covered by Cenozoic sediments. The Muller Thrust truncates the HRF_3 folds, the HRT_3 thrusts and other earlier structures (Fig. 1-1). The Oonagalabi Tongue, the Florence/Leaky Shear Zone and the whole HRSC sequence were carried up over the essentially stabilized SOB in the Hale River Region. There is no evidence that the Muller Thrust has been affected by any of the HRF_3 folds or earlier HRF_2 and HRF_1 folds.

A wide (one hundred meters thick) biotite muscovite schist zone is developed in the western part of the Muller Thrust and separates the Oonagalabi Tongue from the Hale River Region. Typical mylonite (Plate 7.10 A & B) also is found within discrete small shear zones, which are parallel to, and within the upper block of, the main thrust boundary. This part of the thrust dips 40-50° N.

The central part of the Muller Thrust is represented by a rather narrow schist zone which dips 15° to 30° towards the N to NE and separates the thick mylonite sequence of the Florence Shear Zone from the almost undisturbed metamorphic rocks of the Hale River Region SOB. Typical sheath folds (Faure, 1985), which show tongue shaped hinge lines, have been found within this schist

FIGURE CAPTIONS OF PLATE 7.10

A: A polished YZ surface of a typical mylonite sample (No.4285) showing folded mylonitic layering in a direction perpendicular to the mylonitic lineation. The fold hinges are parallel to the stretching lineation. Field of view: 77 mm X 53 mm. About 6 km S of Panikan Dam, close to the Muller Thrust.

B: A large thin section from sample 4285; X polars; Field of view: 55 X 37 mm.

C: A sharp contact (the Muller Thrust) between the mylonitized Bruna gneiss (dark) above and the layered quartzofelspathic gneiss (light) below, which is recrystallized ultramylonite. Location No.3395; NW of Leaky Bore.

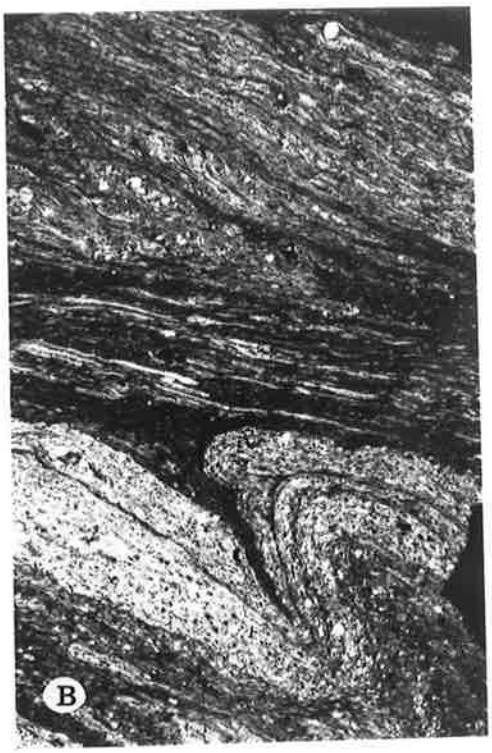
D: Sketch section across the Muller Thrust showing the sharp contact between the Bruna Gneiss above and the unreactivated SOB below. The foliation of the mylonitized Bruna Gneiss and the layering of the felsic ultramylonite within the SOB are both truncated by the thrust surface. The folded ultramylonite reveals a southward shear sense. Location No.3020, S of Mt Ruby.

E: A polished surface of a folded felsic ultramylonite sample from the core of the fold in (D). Scale bar: in cms.

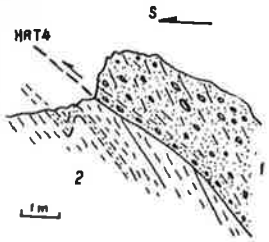
F: A stereogram showing the relationship between the fold hinge of the mylonite fold and the mylonitic lineation which has been refolded during the continuous mylonitization. (LN: lineation on the north limb; LS: lineation on the south limb; B: fold axis)

Plate 7.10

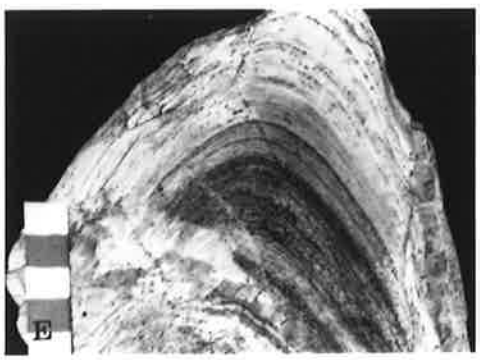


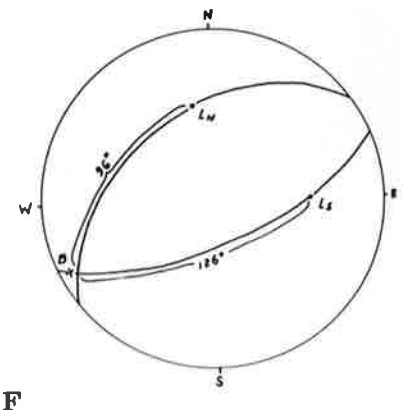






D





F

zone. Small imbricate thrusts are also found within the footwall block (see Chapter 2 and Fig. 2-2).

The eastern part of the Muller Thrust, which dips at 20-50° towards the N and NE, is represented by a narrow (a few meters thick) ultramylonite zone which separates the Bruna Gneiss from the Hale River Region (Plate 7.10.C). Only one mylonitic foliation can be seen within the ultramylonite. The extremely intense shearing may have destroyed any initial noncoaxial structure resembling S-C type mylonites (Lister & Snoke, 1984). However, the mylonitic lineation and foliation have been further folded by small parasitic folds during the later stages of thrusting and indicate a southward overthrust shear sense. One example of this type of structure is shown in Plate 7.10.D & E. The intersection angle between the mylonitic lineation and the fold hinge within the ultramylonite varies from 90° in its upper (northern) limb, to 45° in its lower limb (Plate 7.10.F). The trends of the mylonitic lineation generally vary from 350° to 020°. Typical mylonitised granitic gneiss (Plate 7.11.A & B) in the footwall block has been found along small imbricate shear zones within a few hundred metres of the main thrust boundary.

The kinematic indicators within rocks of the Muller Thrust, e.g. asymmetric tails of porphyroclasts (Plate 7.11.A), the relationship of shear bands and mylonitic foliation (Plate 7.11.C) and the asymmetric folds of the mylonitic foliation (Plate 7.11.D). all indicate a rather constant southward overthrust shear sense.

The northern extension of the Muller Thrust is not clear, and two interpretations have been given. One is shown by inferred structural contours on the thrust surface (Fig. 7-4), based on the knowledge that the Muller Thrust is not exposed in the Entia Dome, thus a thick wedge of rocks must separate the Entia Thrust from

FIGURE CAPTIONS OF PLATE 7.11

A: A polished surface of a felsic ultramylonite sample (No. 3014) showing a southward (sinistral) shear sense. Field of view: 26 mm X 63 mm; S of Mt Ruby.

B: Microstructure of the sample above showing an intense mylonitic foliation which is manifested by a ribbon structure of feldspar and quartz, and the very long stretched tail from a porphyroclast of K-feldspar which has been totally recrystallized to form an aggregate of small grains which show the same size to those within the tails. Field of view: 1.7 mm X 2.2 mm.

C: A blastomylonite of deformed granitic gneiss showing a southward (dextral) shear sense by a type of S-C mylonitic fabric and asymmetric tails. Width of view: 40 cm; Location No. 3384; about 4 km N of Leaky Bore.

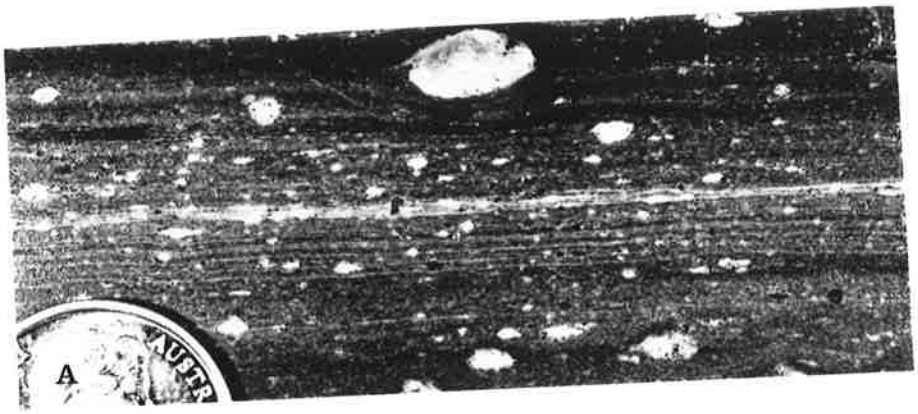
D: Intrafolial folds of the mylonitic foliation showing a southward (dextral) shear sense. Location No.3384.

E: An example of open folds within the calc-silicate unit. Location No.3869.

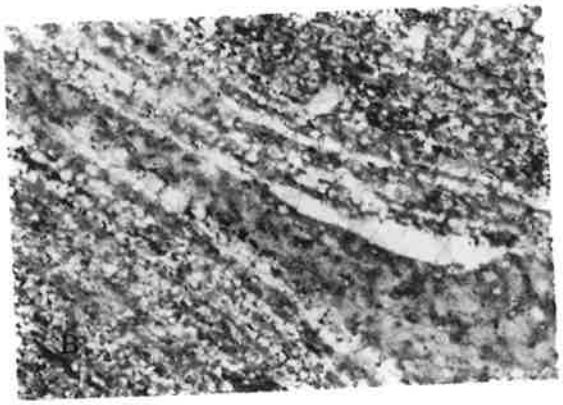
F: Open folds manifested by joint surfaces. Location No.4118, within the Florence Creek.

G: A sketch of the folded joints in (F). The joints (represented by long and rather continuous lines) are perpendicular to the mylonitic foliation (represented by short lines), which becomes fanning where the joints are curved.

Plate 7.11



A



B



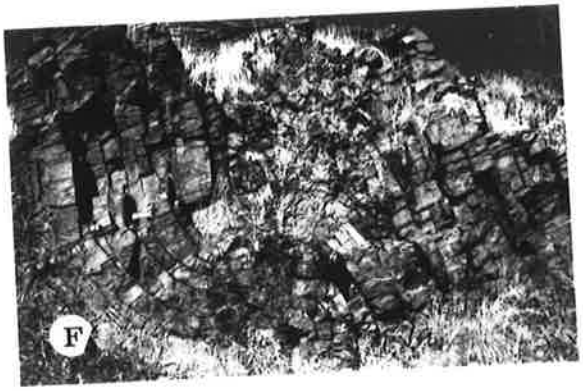
C



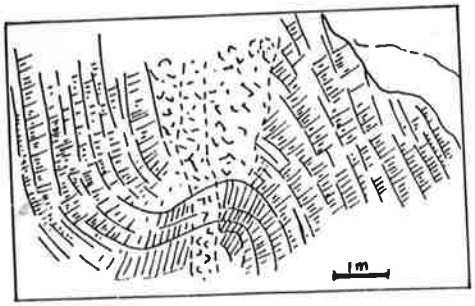
D



E



F



G

the Muller Thrust. Another is that the Muller Thrust and the Entia Thrust become a single thrust surface to the north, i.e. the Entia Thrust around the Entia Dome is also a part of the Muller Thrust.

7.6. Post HRO deformation

Many structures in the study area have apparently been formed later than the HRT_4 Muller Thrust and are simply assigned to post HRO deformations. Some structures were probably formed during the Late Proterozoic, others were certainly formed during or after the Late Palaeozoic Alice Springs Orogeny. All these post HRO structures are relatively less ductile and less significant than those structures formed during the Strangways and the Harts Range Orogenies.

7.6.1. Open folds

Upright to asymmetrically inclined open folds occurred after the Muller Movement, as the HRT_4 Muller Thrust and the earlier structures have been affected by these open folds. Their axial surfaces trend in four directions: NE, NW, E-W and N-S. The mappable open folds of the Harts Range area are shown on the tectonic sketch map of Fig. 7-5.

Open folds are easy to recognize where the lithological units have parallel and sub-horizontal attitudes, e.g. within the Entia Dome (see Map 4) and the central part of HOB, and where the geometry of open folds can be defined by the lithological layers and layer parallel foliation. However, it is very difficult to work out the evolutionary order of these folds by geometric analysis.

The overall geometry of the Entia Dome, which dips moderately away from the centre in all directions (Map 4), was formed by the interference of major antiformal open folds. The NE-SW trending

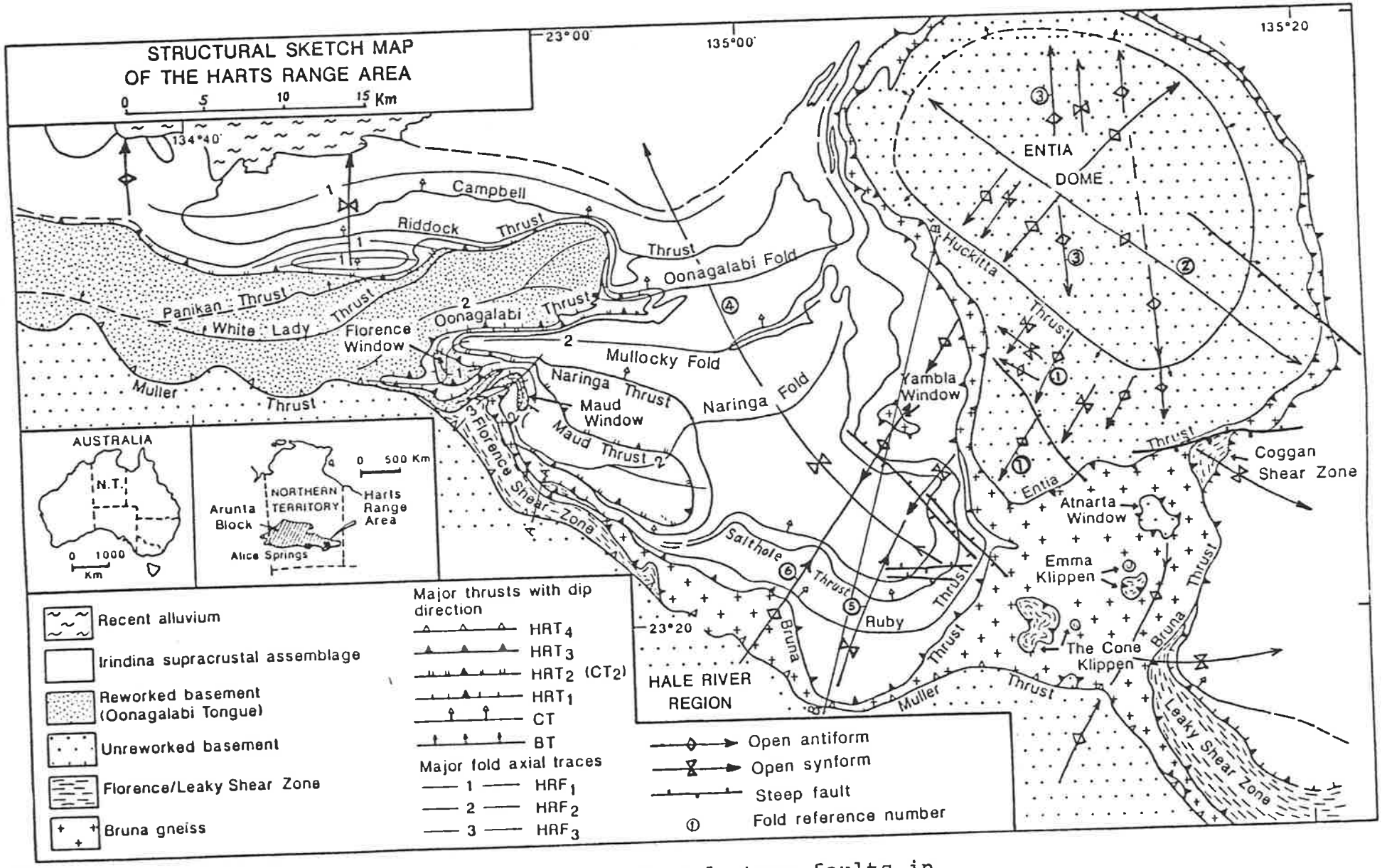


Fig. 7-5 A tectonic sketch map of open folds and steep faults in the Harts Range area.

major open fold (No.1 in Fig. 7-5) has been mapped in detail in the southwestern part of the dome to the north of Harding Springs Well. The isoclinal Harding Springs Fold (BF_3) was clearly folded around the closure of this open fold which plunges gently towards the SW. Parasitic open folds of this orientation are also found at Black Mountain (Map 4). The SE limbs of antiforms usually dip slightly steeper than the NW limbs, and thus define steeply NW dipping (80-85^o) axial surfaces. The Huckitta Thrust might have acted as a detachment boundary during the later deformation phase of upright open folding. The disharmony between the upright open folds above and below this shear zone can be seen clearly on Map 4 and its cross section.

The NW-SE trending major open folds (No.2 in Fig. 7-5) can be traced from the NW to the SE corner of the Entia Dome (Map 4). The BL_1 lineation and the early fold axes are folded by this open fold, and plunge towards the NE and SW in the NE and SW limbs of the open fold. Smaller open folds of this orientation have been mapped in the SW corner of the dome, where small domal and basin-like structures were formed by the interference of the NE and NW trending open folds (Map 4). The NE limbs of antiforms usually dip slightly steeper than the SW limbs, and thus define steeply SW dipping (80^o to 85^o) axial surfaces.

Many E-W folds of small to moderate scale have been mapped in the inner part of the Entia Dome, where the general attitude of the gneiss complex is nearly horizontal (Buick, 1983; Sullivan, 1985; and Aoukar, 1985), as well as at the NW margin of the Dome (Macdonald, 1986). The northern limbs of antiforms are usually steeper (to nearly vertical in some places) than the southern limbs, thus defining south dipping (60^o-85^o) axial surfaces.

The N-S trending open folds are better seen in the central

part of the dome (see Map 4), with steeply west dipping axial surfaces, but also extend into the southern area adjacent to the Entia Dome.

Upright open folds are also developed in the Hale River Region but have not been studied in detail. Examples of NNE trending open folds have been mapped in the area SW of Mount Ruby (Figs. 2-1 and 2-3), where many parasitic folds occur on the limbs of a major synform. The western limbs of the parasitic antiforms trend 340° to 020° and dip 25° to 60° easterly, whereas the eastern limbs trend 040° to 055° and dip 30° to 80° westerly. The fold hinges plunge 10° to 20° toward the NE with almost vertical axial surfaces.

A large NW trending synformal open fold (No.4 in Fig. 7-5) appears in the central part of the HOB with an amplitude similar to that of the No.2 antiform. The interference between this NW trending synform and the No.3 antiform produces a large saddle-like structure which results in the major exposure of the Bruna Gneiss.

Interference between the NW trending synform (No.4) and the NE trending synform (No.5 in Fig. 7-5) produces a basin-like structure. Smaller structural domes formed by the interference between antiforms are the Yambla and Atnarta Windows (Fig.1-5).

Outcrop scale open folds are common (Plate 7.11.E.) The layers involved retain almost equal thickness and thus form Class 1b type folds. Within the Florence Shear Zone, a very interesting and unusual structure is found in which a set of joints originally formed at right angles to the mylonitic foliation has since been folded (Plate 7.11.F & G). The folded joints show a similar profile to the open fold outlined by the lithological layering and the joint sheets show the characteristics of Class 1b type dip

isogons. The axial plane of the folded joint sheets and the axial plane of the folded mylonitic foliation intersect each other at a high angle. This confusing structure may be attributed to the influence of a local fault which could have dragged the structure.

A more difficult task is the analysis of the influence of open folds on an originally non-parallel set of geological layers. The geometry of an open fold depends on the orientation of the planar element considered and this geometry, of a folded lithological layer, may not represent the real characteristics of open folding. This concept is similar to the modification of two inclined surfaces by flexural-slip folds illustrated by Ramsay (1967, pp. 499). Early linear structures may be more important in structural analysis in many cases, if they are originally fairly constant (Turner & Weiss, 1972). Some variations in lineation trends provide evidence for open folds, e.g. the plunge reversal of CL_1 and other later lineations in the Mt Campbell area (see Map 6), though the lithological layering does not show the lateral bending, because the bending has been produced in a direction parallel to the lithological layering. The influence of such open folds can be observed over the whole area, e.g. similar plunge variations of early lineation and fold axes, but the general geometry of the open fold interference structures has not been studied in detail.

7.6.2. Dolerite dykes

Undeformed or weakly deformed dolerite dykes have been found within the intensly mylonitized Bruna Gneiss. The dykes trend mainly in a NE-SW direction and show a close relationship to the NE trending antiforms. The dykes are about 1-2 metres wide and tens to hundreds of metres in length with steep dyke walls which

FIGURE CAPTIONS OF PLATE 7.12

A: Microstructure of a dolerite dyke within the Bruna Gneiss. Sample 3024; S of Mt Ruby; field of view: 1.7mm X 2.4mm; X polars.

B: Mica schist developed between the SOB and the Heavitree Quartzite, along the basal thrust of the Illogwa Shear Zone showing two sets of schistosities. The earlier schistosity within a fragment of the parental rock (in the centre of the picture) is truncated by the later predominent schistosity. Sample 3370A; W of Leaky Bore and N of the Aleeitara Peak; field of view: 1.7mm X 2.2mm; X polars.

C: Tight reclined folds within a quartzite sliver along the Aleeitara Thrust. Its fold hinges plunge steeply towards the north and are parallel the stretching lineation. Location No. 4027; about 3 km SW of the Apleeitara Peak.

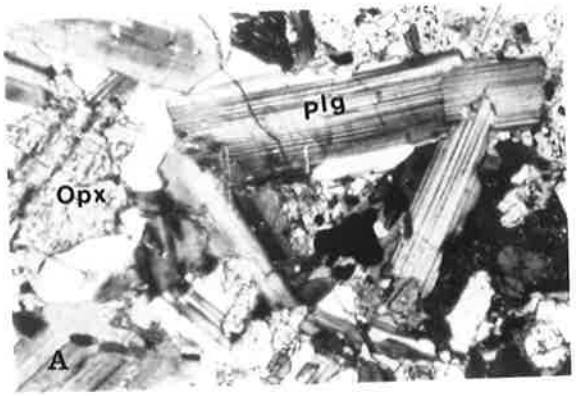
D: Fault breccia along a NW trending steep fault zone. Location No.3291.

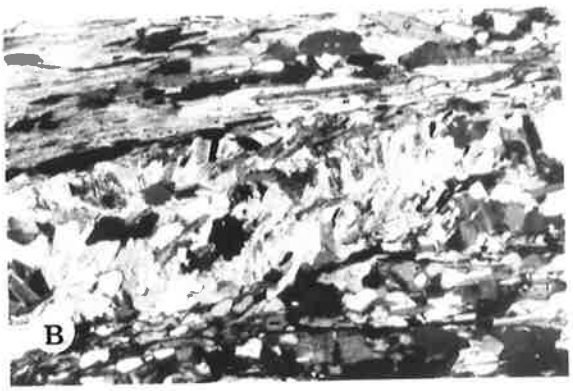
E: Microstructure of the fault breccia showing typical brittle deformation. Sample 3127.

F: Zigzag-shaped pegmatite vein within an intensly foliated ISA sequence does not have an apparent fabric, E of Coggan Bore.

G: A pegmatite vein (0.5 m wide) intruded into a vertical fault within the Cone Klippen. Location No.4002.

Plate 7.12

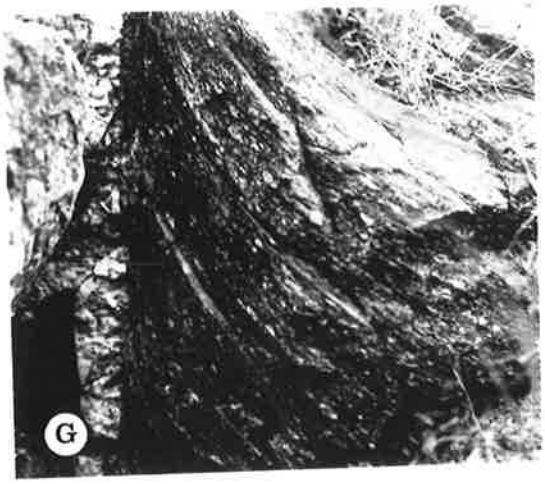














truncate the mylonitic fabric within the Bruna Gneiss at high angles.

The dolerite shows a typical igneous texture (e.g. sample 3024; Plate 7.12.A) comprising labradorite plagioclase (35%), hypersthene (10%), augite (40%), hornblende (3%), biotite (10%) and minor opaques. These dolerite dykes have not been studied in detail but may be correlated with the Stuart Dykes which have been dated at 897±9 Ma (Black et al, 1980). Swarms of the Stuart Dykes are mainly exposed in the Alice Springs area unconformably underlying and thus predating the later Proterozoic Heavitree Quartzite.

7.6.3 Structures of the Alice Springs Orogeny

The Alice Springs Orogeny refers to the deformation which mainly affected the Amadeus Basin during the Devonian to Carboniferous Periods (Stewart, 1967). Thrusting and nappe formation have been proposed by many workers (e.g. Stewart (1967), Forman (1971), Yar Khan (1972) and Stewart & Oaks (1987)), as forming a major component of the ASO deformation at the southern margin of the Arunta Inlier. Teyssier (1985) and Collins & Teyssier (1987) have reinterpreted most of the HOB thrusts as the products of the ASO. However, from the geological evolution described in previous chapters, the effects of the ASO on the Harts Range area are considered to be minimal (James & Ding, in press, Appendix VI). As the ASO is not a part of the aims of this thesis, it will not be discussed in detail except for the Illogwa Shear Zone and some of the steep faults and undeformed pegmatite veins.

7.6.3.1 Shear zones and thrusts

One major shear zone has been observed at the northern margin

of the Amadeus Basin. The SOB gneiss complexes in the Illogwa Creek and Claraville subareas are thrust over the Heavitree Quartzite (the basal formation of Late Proterozoic platform cover within the Amadeus Basin, see Chapter 1). This shear zone is a part of the Illogwa Schist Zone which is defined by Shaw et al (1984a). However, the major part of the rocks within the Illogwa Schist Zone are not typical schists but deformed and partially retrogressed SOB gneisses. Typical schists are found only within narrow zones (less than 10 metres in true thickness) along a set of descrete thrust boundaries (Fig. 2-4). Furthermore a structural term "Illogwa Shear Zone" is preferable and is suggested here to replace the lithological term "Illogwa Schist Zone" as the name of the major tectonic boundary between the Arunta Inlier and the Amadeus Basin.

On a regional scale the Illogwa Shear Zone extends E-W for over 100 km, and dips 18^{o} to 40^{o} towards the N, NW and NE (Fig. 2-1). Rocks within the shear zone vary gradually from greenschist or phyllonite in the west (e.g. NE of Mt Geogina and N of the Atnarpa Homestead) to biotite muscovite schist in the east (N of Aleeitara Peak).

Two sets of schistosity can be seen within the mica schist in thin section (Plate 7.12.B). The earlier one was folded and truncated by the later one which is the predominant schistosity subparallel to the thrust plane.

The Heavitree Quartzite layers in the footwall block of the shear zone become lenticular bodies (tens to one hundred metres in thickness and a few kilometres long) towards the east in the Aleeitara area (Map 2 & Fig. 2-1). The thrust boundary becomes uncertain further to the southeast where a weakly foliated diorite intrudes into both sides of the quartzite, and the schist zone

disappears. A small lenticular body of the quartzite (about 10 X 50m) appears to form a xenolithic inclusion within the diorite (Fig. 2-4). Similarly the thrust boundary about 10 km to the west is intruded by another meta-diorite body as is mapped by Shaw et al. (1986). This may therefore imply that the meta-diorite was intruded into the thrust during or after the ASO, partially preventing a further movement along the Illogwa Shear Zone. There is another possibility that the meta-diorite is Proterozoic in age and the small lenticular body of quartzite described above is a tectonic sliver within the meta-diorite, therefore it implies that the displacement along the Illogwa Shear Zone was not significant during the ASO. The age of this meta-diorite might be one of the critical features in the understanding of ASO.

Imbricate thrusts have been observed to the SW of Aleeitara Peak (Fig. 2-4). They include a set of fault planes which are manifested by many small discrete quartzite slivers within a mica schist zone dipping steeply towards the NE (Map 2). Small ductile sheath folds have been found within these quartzite slivers (Plate 7.12.C) with hinges plunging at 73^{o}-300^{o}. The low angle between the fold hinges and the mylonitic lineation indicates a high degree of stretching of the quartzite sliver within the shear zone (Sanderson, 1973). The repetition of the quartzite also suggests that the uplift along the imbricate thrusts is limited, otherwise the quartzite slivers would not be exposed at the same level.

7.6.3.2 Steep faults system

Steep faults can be interpreted easily from airphotos by their linear alignment and the offset of geological boundaries across them. Some of the steep faults have been omitted during the compilation of Map 2 in order to avoiding disturbing the more

important geological features, but they are shown on the tectonic sketch map (Fig. 7-5). The steep faults may have formed at different stages.

Typical fault breccia developed along the NW trending steep fault lines (Plate 7.12.D & E), thus implying brittle deformation conditions. Small veins of calcite and barite cement the fault breccia. The NE and N-S trending faults are short and less important.

The offsets along the steep faults have been recognized as the result of mainly normal fault displacements. The true displacements of steep faults are usually very small in the Harts Range area (from a few metres to several tens of metres). The importance of these late steep faults, particularly the NW trending faults, has been overemphasized and used to define different blocks (Shaw et al., 1984), though the displacement between any two adjacent blocks may be very small or not visible on the regional maps (e.g. the Australia 1:100 000 Geological Special, Geology of the Strangways Range Region, N.T., B.M.R., 1984).

In the Arltunga subarea steep faults become more important with greater displacements and wider breccia zones (1 to 100 metres) within the quartzite. The structures along the northern margin of the Amadeus Basin are currently being studied by Ding & James (in press, Appendix VI) and will not be further discussed in this thesis.

7.6.3.3 Undeformed pegmatite veins

Swarms of post-tectonic undeformed pegmatite veins have been emplaced along cracks and steep faults in the western part of Entia Dome and the adjacent ISA, as well as within the F/LSZ (Plate 7.12.G). The pegmatite has been dated as 320 ma (Cooper

et.al. 1986) and was thus probably emplaced during the Alice Springs Orogeny. Some pegmatite veins seem folded (Plate 7.12.F), but this is unlikely to represent a fold phase, because the metamorphic country rocks were not folded, and the fabric within the metamorphic rocks does not penetrate the pegmatite. The zigzag outline of the pegmatite veins probably formed by following two sets of joints.

PART THREE DISCUSSION AND CONCLUSION

CHAPTER 8 TECTONIC EVOLUTION OF THE HARTS RANGE AREA

8.1. Introduction

In this chapter the geology of the Harts Range area is summarized with a view to establishing a tectonic model. Modern-style plate tectonics, characterised by the growth and subsequent closure of ocean basins, has been applied to early Proterozoic terranes (Windley, 1983; Anderson & Burke, 1983). A model of underthrusting of one extremely attenuated basin margin under another (A-subduction) has been used to interpret the deformation of Precambrian intracontinental geosynclinal basins (Kroner, 1983); a model which has been applied to the Arunta Inlier by Shaw et al. (1984) who proposed polyphase extension - compression (from limited rifting to A-subduction) to explain the complex stratigraphic and structural relations in the Inlier. On the other hand Foden et al. (in press) proposed that the granitic gneisses in the Entia Dome are like the granites of the modern Cordilleran Belts on both geochemical and petrographic criteria, suggesting that at least this part of the Arunta Inlier may represent a fold belt developed along a collisional B-subduction zone (Bally, 1981), though no relics of oceanic lithosphere have yet been identified within the Arunta Inlier.

There has been considerable recent interest in the proposal that large scale extensional detachment may be an important mechanism for the formation of intraplate basins and regional metamorphism incorporating high geothermal gradients (Wernicke and Burchfiel, 1982; Oxburgh, 1984; Wernicke, 1985; Sandiford and Powell, 1986). A model incorporating these ideas has been invoked to

explain the metamorphism and structural evolution of the Harts Range area and is presented (James & Ding, Appendix IV) and reviewed here.

As a conclusion to this thesis, a new model is developed to explain primarily the evolution of the HOB, and is also tentatively discussed as a possible cause of the SOB tectonic evolution. This new model outlines how the HRSC sequence was possibly deposited accompanying extensional displacement along a major crustal detachment zone, and was concomitantly metamorphosed under a consequently increased geothermal gradient, and was then deformed subsequently by folding and overthrusting under a compressional tectonic regime, with a concluding decrease in the geothermal gradient. This model may also be applied to the SOB, although, as the basement to the SOB and/or a bounding detachment zone have not yet been recognized, the model for the evolution of the SOB is poorly constrained.

A major part of the model outlined here is the recognition of the spatial juxtoposition of two separate orogenic belts along a regional detachment zone. The different structural character of the various domains has been described in considerable detail in the preceding chapters, and indicates that both the intensely reworked Florence/Leaky Shear Zone (including the major Bruna gneiss sheet) and the Oonagalabi Tongue represent part of a large-scale and long-lived crustal detachment zone, which is here named the Harts Range Detachment Zone (HRDZ) (see Fig. 1-3), whilst the Entia Dome and the Hale River Region represent separated relics of the cratonized SOB basement.

In terms of a chronological sequence of events in the early Precambrian, the tectonic evolution of the Harts Range area has been temporally divided into three stages (see Fig. 1-2): the

Strangways Orogeny, the Harts Range Orogeny and post Harts Range Orogeny events (which includes the effects of the Palaeozoic Alice Springs Orogeny).

8.2. Tectonic evolution of the Strangways Orogeny

8.2.1 Deposition

The small relict layers and lenses of supracrustal rocks within the SOB represent an originally sedimentary and volcanic sequence, possibly deposited in a subsiding basin in central Australia during the Early Proterozoic and subsequently metamorphosed to granulite and amphibolite facies rocks. The 1980±190 Ma (Sm-Nd) age determined from these granulite facies metamorphic rocks has been suggested as their depositional age by Black & McCulloch (1984). (Fig.1-2). A comparable example is the Namaqua Mobile Belt in Eastern Namaqua Land, South Africa, of which the entire sedimentary cycle is dated between 1800-2100 Ma (Botha and Grobler, 1979).

No basement to these supracrustals has yet been discovered. Thus neither the existence nor style of any possible earlier basement to the (SOB) basin, nor the original thickness of the (SOB) supracrustals are known. The (SOB) rocks in the Harts Range area are very similar to the bimodal lithological sequence described from the Strangways Ranges (Warren, 1979 and 1983; Shaw and Langworthy, 1984). It seems probable that the sequences from the two adjacent areas have a common origin.

8.2.2. Peak metamorphism and its tectonic implications

The supracrustals of the SOB preserved in the Harts Range area have been metamorphosed to granulite facies lithologies in

the Oonagalabi Tongue and the Claraville subarea of the Hale River Region, and to amphibolite facies lithologies in the Entia Dome and other subareas, with local migmatization indicating partial melting. Lower grade metamorphism must have occurred in the upper levels of the supracrustal sequence , but now only the high grade metamorphic rocks from the lower levels are preserved and exposed within the SOB, as a consequence of deep level erosion. The 1790±35 Ma Rb-Sr age of these granulite facies rocks in the Arunta Inlier has been suggested as their metamorphic age by Black et al. (1983).

The peak metamorphic P-T conditions are suggested from this study as 750-870°C at 7-8 kb using mineral assemblages in the pelitic gneiss, and as 770-870°C from the mafic granulite. Higher P-T conditions (850-920°C and 8±1 kb) are proposed from the granulite facies rocks in the Strangways Range by Warren (1983), whereas lower P-T conditions are estimated as 700-800°C and 5-7 kb from granulite facies rocks in the Claraville subarea within the Hale River Region by Oliver et al. (in press, Appendix V). In the Entia Dome, a significantly lower peak metamorphic temperature range (650-750°C) and a similar pressure (7-8 kb) (Chapter 2) are estimated from the upper amphibolite facies rocks. Thus the earliest high-grade metamorphism of the SOB appears to decrease in grade from WNW to ESE across the Harts Range area. This is further supported by the work of Warren (1979 and 1983) who recognized a granulite facies thermal peak in the Strangways Range to the NW, which she also described as decreasing in temperature locally from west to east. Further lower grade equivalents of the SOB supracrustals have not been found in the Harts Range area.

The peak metamorphism reached in the earliest stage of the tectonothermal evolution (Fig. 1-2) as the maximum P-T conditions

are obtained from the mineral assemblages which define the BS_0 fabric within the SOB supracrustal layers. The mineral assemblages which define the BS_1 fabric in granitic gneiss, indicate lower P-T conditions for the second metamorphic event (see later). This conclusion is different from that suggested by Shaw et al. (1984) who described a late thermal culmination following the main folding deformation in their Strangways Event, but agrees with that of Warren (1983) who emphasised that the peak metamorphism must have occured soon after original deposition of the sequence. From the current data of depositional age and metamorphic age of the SOB supracrustals, the depositional process lasted for a period of about 200 Ma.

This early peak metamorphism recognized in the SOB therefore, suggests that the lower parts of the supracrustal sequence were at depths of at least 25-32 km (7-8 kb). Such a depth (25-32 km) is significantly greater than the depth to the base of present sedimentary basins (Davis & Coney, 1979). One possibility is that the supracrustals were stacked up and greatly thickened by early imbricate thrusts or nappes during an earlier stage of compressional tectonism. This could also account for the production of the BS_0 layering and layer-parallel foliations formed during this event. Examples of pre-F_1 nappes are described from cover rocks of the Svecokarelides of eastern Central Finland (Bowes et al., 1984). However, pre-BF_1 thrusts cannot be proved from the field geology preserved today in the study area, as most of the early structures have been obscured during the long and extremely complex history of later deformations. An alternative crustal extension model is favoured as a mechanism for the pre-BF_1 subsidence of the supracrustal sequence (James & Ding, in press, Appendix IV). This model envisages continuous extension associated with,

and subsidence above, a possible throughgoing asymmetric extensional detachment zone (Wernicke, 1985). The great thickness (up to 25-30 km) of supracrustal deposits required to form in the basin produced by this extensional model has not been documented from studies of moden basin developments, which typically record a maximum subsidence of only 10 km (Wernicke, 1985; Davis & Coney, 1979). However, the possibility of a greater subsidence under extensional tectonism cannot be precluded, particularly when the Archaean or Early Proterozoic orogenic belts are considered. For example, the platform sedimentary sequence near to the basement-cover unconformity in the Grenville Province has reached a depth of more than 15 km (Wynne-Edwards, 1976). Furthermore a possible complex polyphase extensional history may result in an extremely thick sedimentary succession over a long time scale, i.e. a period of 100-200 Ma (Mckenzie, 1978). During a single extensional period, a sedimentary sequence of 10-15 km in thickness could be formed. However, the thinned lithospheric plate could be then subsequently isostatically recovered during a tectonic pause, and the recovered lithospheric plate will allow further extension and subsidence. A similar example of such a polyphase extensional and depositional history can be found in the Adelaide Geosyncline whose aggregate thickness of known strata significantly exceeds 20 km (Preiss, 1987, p.258), and which has been interpreted as the result of two phases of active crustal extension, each followed by prolonged periods of thermal subsidence (Jenkins, in press).

8.2.3. Voluminous syntectonic acidic to intermediate plutonism

The granitic gneisses in the SOB are interpreted as orthogneisses (see section 8.2.4.) because there are xenolithic inclusions of metasediments and mafic rocks within them and cross-

cutting gneiss veinlets within the supracrustal rocks. Syntectonic acidic to intermediate magma was emplaced subconcordantly into the deeper levels of the metamorphosed supracrustals, similar to that in the deep levels of a model hypothesized by Gastil (1979). The supracrustals were consequently disrupted and became discrete thin layers and lenticular bodies within dominant granitoids and thus any possible primary features and early structures (e.g. early imbricates) would have been largely obscured by this plutonism. It is interesting to note that in contrast to the metamorphic gradation of decreasing temperature from west to east, the most voluminous granitoids are found in the Illogwa Creek subarea of the Hale River Region and in the Entia Dome, where they comprise often more than (80-85%) of the total rocks. The granitoids make up 75-80% of the total rocks in the Oonagalabi Tongue and become more subordinate to the SOB supracrustals in the Claraville subarea of the Hale River Region. This also supports the interpretation of an intrusive origin for the granitic gneiss rather than an origin of in situ melting. This is because the higher metamorphic temperature in the Claraville subarea should have produced more melting than that of the Entia Dome and the Illogwa Creek subarea. According to Foden et al.(in press), the orthogneisses in the Entia Dome represent typical I-type granodiorite (Chappell & White, 1974).

A zircon age of 1767±1 Ma for the granitic gneiss in the Entia Dome is believed to be the intrusive age of the orthogneiss protolith (Cooper et al., in press.), suggesting that the plutonism just postdated (by 0-60 Ma) the metamorphic age (1790±35 Ma) of granulite facies supracrustals. This is also likely to have been a time of considerable underplating of the continental crust by mafic melts (Foden et al. in press) and further reflects the

tectonic / metamorphic instability associated with early stages of the SOB.

8.2.4. The first deformation in the SOB

During the first recognized deformation of the Strangways Orogeny, fine compositional layering and intense layer parallel foliation (BS_1) developed in the granitoids to form the axial planar foliation of isoclinal BF_1 folds, which indicates a fundamental change in stress conditions from the subhorizontal tension, inferred by the extension during the early prograde metamorphism, to a phase of major compressional stress. The BF_1 folds are manifested by the folded supracrustal layers (Chapter 2). BS_0 and BS_1 are distinguishable in fold hinges but cannot be distinguished in fold limbs. The granitoids were thus converted to orthogneisses by a major phase of syntectonic metamorphism; charnockitic gneiss formed in granulite facies environments (e.g. in the Claraville subarea) and granitic - tonalitic gneiss in amphibolite facies environments. However, a marked change in metamorphic conditions (also associated with the change from a tensional to a compressional stress regime) is indicated by the intimate intercalation of amphibolite facies granitic gneisses with partially retrogressed mafic granulites in the Oonagalabi Tongue. The supracrustal amphibolite layers in the Entia Dome are also slightly retrogressed though they are still within the range of amphibolite facies metamorphism (see Chapter 2). All these features indicate a transitional amphibolite to granulite facies metamorphic environment for the BD_1 deformation. The lower temperatures and similar pressures of the granitic gneisses suggest a decrease of the geothermal gradient accompanying the compressional stress and contractional deformation. However, the charnockitic gneisses in

the Claraville subarea contain granulite facies assemblages suggesting that this cooling during the BD_1 deformation was relatively small.

Orthogneisses with minor intercalated or included mafic and metasedimentary rocks, which as has been demonstrated obviously comprise a significant portion of the SOB terrain in the Harts Range area, are very common in Archaean gneiss terrains, such as: the Ancient Gneiss Complex in the Kaapvaal Province of Swaziland, South Africa (Jackson, 1984), the Amitsoq Gneiss (Nutman, 1984) and the Fiskenaesset Complex (Myers, 1981, 1984) of West Greenland, the gneiss domes in the Wabigoon Subprovince of the Canadian Shield (Schwerdtner, 1984), the basement to the Early-Middle Proterozoic Svecokarelides in central Finland (Bowes, et al., 1984), and the Napier complex of East Antarctica (James and Tingey, 1983) and are often referred to as "grey gneiss" in such terrains. However, this kind of orthogneiss complex is much less common in Proterozoic mobile belts. Comparable examples may be the Rayner complex of East Antarctica (Ding & James, in press; James & Ding, in press) and the gneiss complex of the Musgrave Range in central Australia (Collerson, et al., 1972).

Some workers (Stewart et al., 1984) considered that the gneiss complexes within the Arunta Inlier were metamorphosed immature sediments and felsic volcanic rocks which reached their peak metamorphism during a single event, the Strangways Event. The evidence presented previously (Chapters 2 & 3) for a plutonic precursor for the orthogneisses, including the presence of xenolithic inclusions of metasediments and mafic rocks in the gneisses and cross-cutting gneiss veinlets within the mafic rocks may be argued to result from ductile deformation (e.g. boudinage as an alternative origin for the xenoliths and transposition for the

veinlets). However, the intercalation of amphibolite facies granitic gneiss and the granulite facies mafic layers in the Oonagalabi Tongue conclusively support an intrusive origin for the precursor to the granitic gneiss. The mafic granulites must represent the products of an earlier stage anhydrous metamorphism, whereas the amphibolite facies granitic gneisses must represent the results of later hydrous metamorphism of intrusive granitoids. Later crosscutting mafic dykes in the Oonagalabi Tongue (Chapter 3) and in the Entia Dome (Chapter 2) have also been metamorphosed to amphibolites. The coexistence of mafic granulite layers and crosscutting amphibolite dykes also strongly supports the interpretation of two separate metamorphic events: an earlier granulite facies event and a later amphibolite facies event.

In terms of mappable BD_1 features, only minor BF_1 isoclines were recognized from the Entia Dome, along with the dominant BS_1 foliation. An early, typically layer-parallel tectonic foliation, usually described as S_1, is the most predominant foliation in many Precambrian gneiss terrains (e.g. Coward, 1973). However, associated F_1 folds are the most difficult structures to map because of intense transposition along the S_1 foliation, which has usually destroyed the fold structures and separated the fold hinges from their limbs. The latter in consequence have become discrete thin layers or lenticular bodies (e.g. Bowes, et al., 1984; Myers, 1978). This condition has also been described for the Fold Island and the Bunger Hills areas of East Antarctica (Ding & James, in press; James & Ding, in press).

8.2.5. Implications of the superimposed (BF_2-BF_4) folding events

The post BD_1 foliated gneiss sequence provided a ubiquitous planar element to facilitate further fold deformations during the

continuing SOB compression. Thus the SOB displays repeatedly superimposed primarily subrecumbent isoclinal folds (BF_2 to BF_4) developed under amphibolite to granulite facies conditions.

Two major superimposed fold generations have been recognised in the Entia Dome (BF_2 & BF_3 in Chapter 2; Foden et al. in press) and three in the other basement areas (Chapters 2 & 3). Superimposed fold hinges are commonly subcoaxial with mineral and/or stretching lineations subparallel to the fold hinges which attests to the overall intensity of the strains involved. The predominant NNE-SSW orientation of these basement linear fabrics are interpreted as resulting from the main compressional phases of the Strangways Orogeny which operated in an ESE-WNW direction.

Such repeated refolding and repetition of lithologies about primarily subrecumbent axial surfaces can be explained by various processes.

1) Where an originally subhorizontal rock sequence (S_0) is folded under a variably oriented stress field, with alternating subhorizontal and vertical compression.

During subhorizontal compression the crust is shortened laterally in the direction of maximum compressive stress, and thickened vertically (Fig. 8-1). From this model an original rock sequence of subhorizontal layers of different competence should form upright to inclined folds by buckling (Fig. 8-1a & b). When this subhorizontal maximum compressive stress is released, the overthickened crust will act under a gravitational influence to produce a vertical maximum compressional stress and a subhorizontal tensile stress. Deformation under such a deviatoric stress regime will cause the upright folds in the lower levels of the crust to be refolded and flattened to form recumbent refolds (Fig. 8-1c), as the crust extends laterally (Wynne-Edwards, 1963).

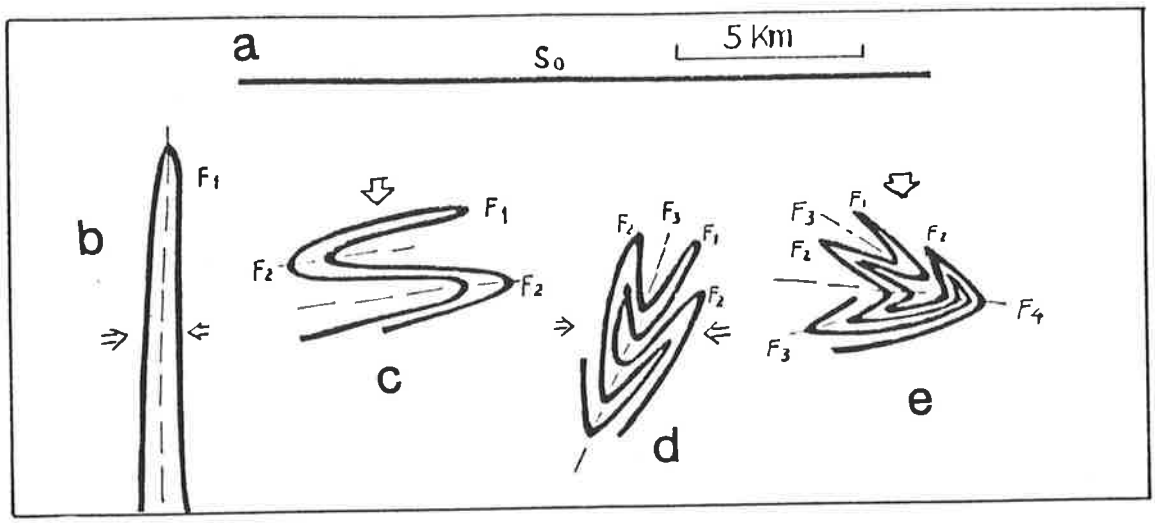


Fig. 8-1 Two dimensional schematic diagrams showing progressive evolution of large-scale superimposed folds by sequential horizontal and vertical compression. The process is initiated from a subhorizontal rock sequence.

During any subsequent (or even a continuously varying) subhorizontal compression, the recumbent earlier folds may be further refolded to form upright folds of a third generation (Fig. 8-1d), and finally the necessarily reimposed vertical stress (gravitational "body" force), generated as a consequence of crustal thickening, will flatten all the earlier folds and produce an overall recumbent attitude for all folds (Fig. 8-1e).

2) Where originally subhorizontal F_1 folds and an S_1 foliation in the orthogneisses are folded under a variably oriented stress field, with alternating subhorizontal and vertical compression.

It is difficult for the first model to explain some of the more important characteristics of the folds in the SOB. These include the pervasive and intense BS_1 foliation in the orthogneisses; the very large amplitudes (more than 10 km) of the BF_2 folds and the obviously asymmetric vergence of the BF_3 fold profiles, which do not support the initial development of upright folds. In order to interpret the fold structures in the SOB, one important modification is that the F_1 folds and S_1 foliation in the orthogneisses are assumed to have been formed originally in a subhorizontal attitude (Fig. 8-2a & e) by different process, which may be similar to the model discussed in the next paragraph. These subhorizontal D_1 structures were subsequently deformed under alternating subhorizontal and vertical compression and thus formed upright to inclined F_2 folds (Fig. 8-2 b & f), recumbent F_3 folds (Fig. 8-2 c & g) and upright to inclined F_4 folds (Fig. 8-2 d & h). This modified model matches the geometry of the SOB folds, particularly the folds in the Oonagalabi Tongue.

3) Another completely different model for the evolution of the refolded sequence involves an originally subhorizontal rock

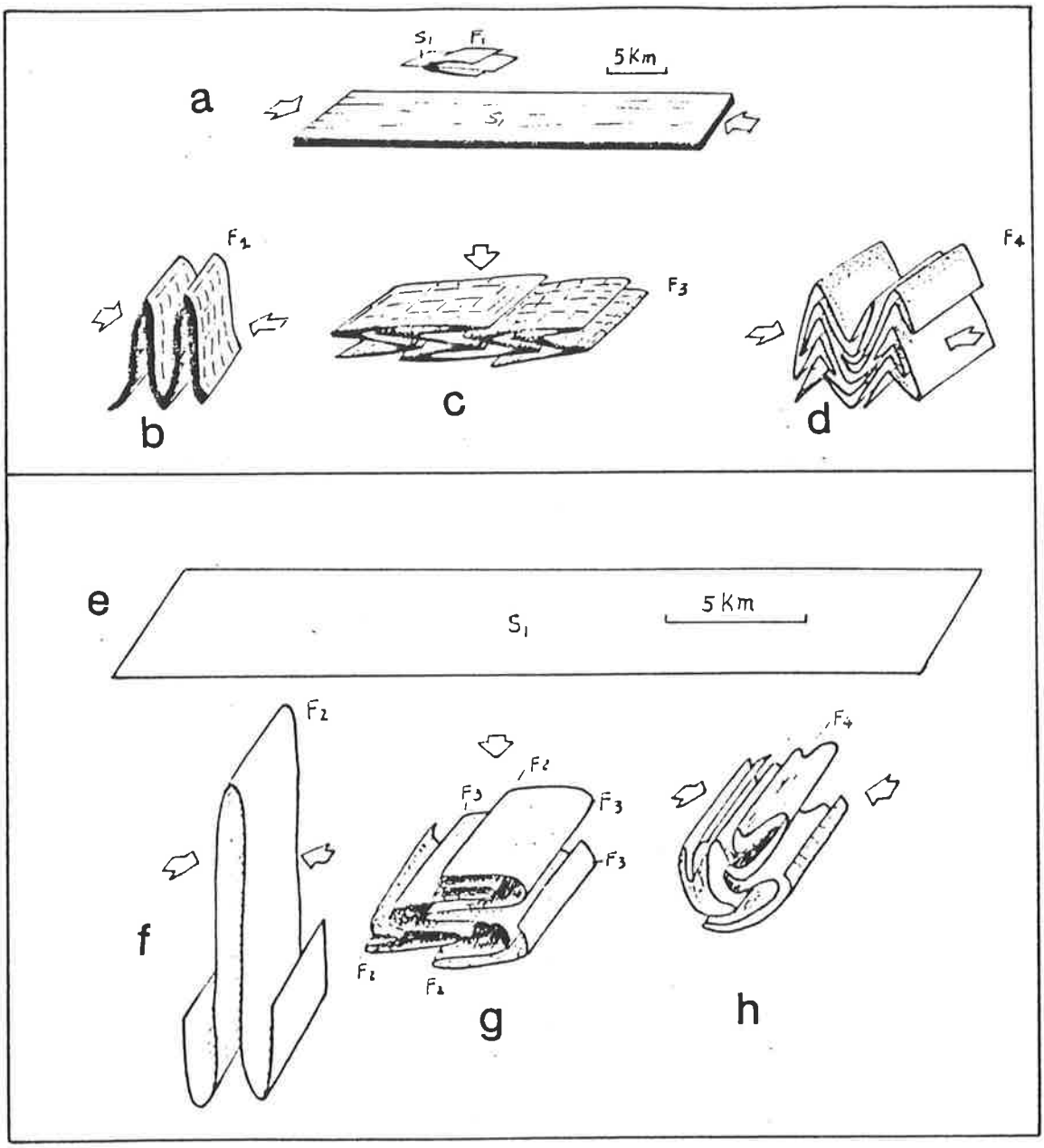


Fig. 8-2 Three dimensional sketches for the tectonic and geometrical evolution of four generations of SOB folds, particularly for that observed in the Oonagalabi Tongue. This model is slightly different from that in Fig. 8-1, as this process is initiated from an already developed subhorizontal BS_1 foliation and BF_1 axial surface.

a to d: Show the evolution of a single rock layer with the involvment of intralayer strain. The single thick layer becames very thin after the polyphase folding and flattening.

e to h Show equivalent geometry for a single planar element without the involvment of internal strain.

sequence (S_0) which is folded during the application of a variable stress field with the alternation of subhorizontal unidirectional shearing and gravitational collapse.

Continuous but heterogeneous subhorizontal unidirectional shearing may develop from a regional horizontal compression and be located along a low-angle deep crustal detachment zone. During the shearing, subhorizontal rock layers at lower crustal levels may form inclined asymmetric F_1 folds (Fig. 8-3 a & b). The crust is thus locally shortened and thickened. When the compression is released the thickened crust collapses and laterally extends under the increased gravitational force to form recumbent F_1 folds and S_1 axial surface foliations and gneissic layering (Fig. 8-3 c). As the first principal schistosity develops in the rock, particularly in the orthogneisses, the newly formed S_1 foliation and gneissic layering will facilitate a further development of F_2 folds (Fig. 8-3 d & e). A repetition of such a process may produce recumbent F_3 folds (Fig. 8-3 f & g) and F_4 folds etc..

This process explains well the geometry and evolution of the SOB fold sequence. However, several phases of folding will finally produce an almost homogeneous rather than a layered and well foliated structure within the crust (e.g. three fold generations in the Entia Dome and four fold generations in the other SOB domains).

The total strain within the SOB, however, cannot be estimated with any confidence. Some individual mafic layers show a significant ductile thinning from hundreds of metres down to less than one metre. In contrast these isoclinally folded rock layers seem to indicate a very high degree of shortening and consequently an equivalently high thickening (by the frequent repetition of each layer) of the rock sequence. However, such a thickening (which may

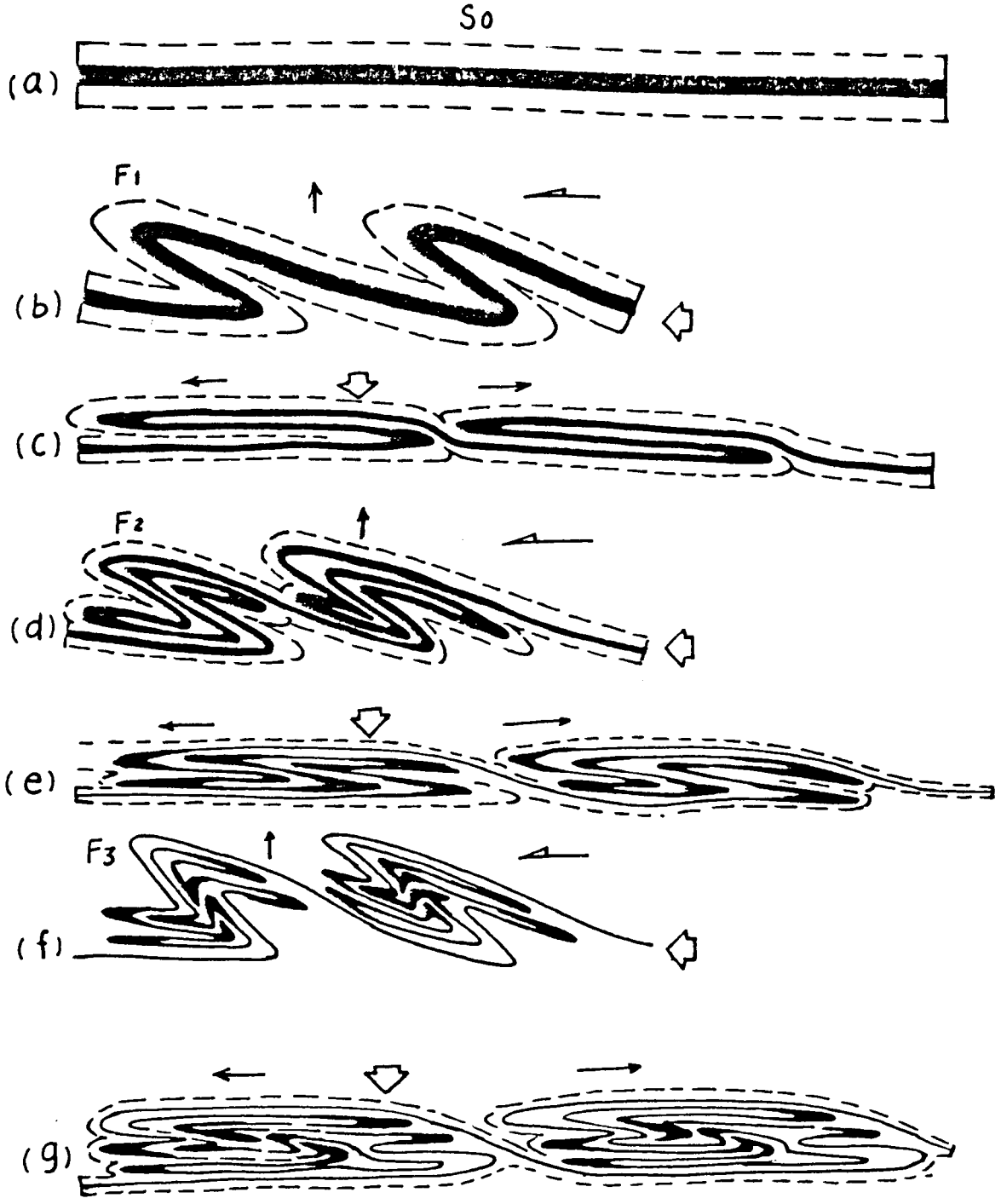


Fig. 8-3 Two dimensional schematic diagrams showing a model of sequential unidirectional compression (and/or shear) and gravitational collapse. The folding shortened and thickened the crust whilst the collapse thinned and extended the crust. The rock volume remains the same while the individual layers have been extremely strained. The present length of a single rock layer may be 10 times its original length, and the present thickness of the same rock layer may be less than 1 tenth of its original thickness except in some of the fold hinges.

be up to ten times, according to the lithological repetition; see Fig. 8-3 g) of the crust (e.g. to 300-400 km thick) is impossible to envisage. Thus the overall strain within the SOB must be much less than simple fold length estimates as the overall thickening can not be greater than 100%. This total strain could even be almost zero in fact, if the crust was finally returned to normal crustal thickness, though the strain within single rock layers is apparently very large (Fig. 8-3). This process is similar to that of the making of a marble cake; i.e. the continuous folding and refolding of a ball of dough.

The third model is preferred as it can best explain the devolopment of polyphase folding within the SOB. It appears that the SOB was deformed under a strain field controlled by a prolonged subhorizontal ESE-WNW shearing deformation with a predominant NNE-SSW principal elongation, which is illustrated by the consistent trends of fold axes (see Map 5 and Fig.2-1). The actual sense of shear is not clear, though the regional BF_3 folds in the Entia Dome show a relative shear sense of its upper plate to lower plate from the ESE towards the WNW.

8.2.6. Late thrusting of the SOB

The folded SOB was finally deformed by thrusting (BT of Fig. 1-2). This indicates a significant change in the rheological condition during deformation from a bulk pervasive ductile to a discrete semi-ductile environment, a common feature at the end of orogenic cycles. The BT thrusts are typically developed at low angles of intersection with the fold axial surfaces, and the thrust traces are usually subparallel to the lithological layers. As with those of the ductile events, the original transport direc-

tions of this terminal thrusting are also not clear. The change of rheology and strain field may be a result of the crustal uplift which is a function of the thickening of the SOB after the last folding (BF_4).

8.2.7. Termination of the Strangways Orogeny

The Arunta Inlier was proposed as comprising part of a major ensialic E-W trending polycyclic Proterozoic mobile belt (Shaw et al., 1984). The proposed E-W trend is mainly based on the distribution of their three Divisions and only represents the primary structural trend of Divisions 2 & 3. However, this interpretation does not explain the generally northerly trending structures within their Division 1 (SOB of this study). From the similarity in the NNE-SSW structural trends throughout all SOB domains in the Harts Range area and also the similarly NNE-SSW alignment of metamorphic and plutonic zonation, it is suggested here that the SOB itself was probably a significant and unified N-S or NNE-SSW trending orogenic belt, but was later reworked during the Harts Range Orogeny and possibly the Alice Springs Orogeny), to form an apparent E-W trending megastructure. It is further inferred that while the SOB formed in a NNE-SSW direction, the main extension - collision orogenic activity occurred in a WNW-ESE direction. This is supported by the vergence of both the metamorphic and plutonic asymmetry.

As was introduced in Section 8.1., many models may be applied to interpret the tectonic environment of the SOB, but none is overwhelmingly convincing. For the detachment model, the inferred master detachment zone may have originally dipped towards the ESE, and its surface trace may have defined the western margin of the SOB. However, it has not been recognized from the surface geology

or, as is more likely, it is now under the cover of young sediments. No fossilized subduction zones or sutures have been recognized within the Arunta Inlier to support a possible B-subduction model.

Based on the model of extension - collision along a detachment zone, the perturbed geothermal gradient illustrated by the spatial variation in metamorphic maxima reaches a culmination in the Strangways Range which may therefore represent an internal tectonic zone to the Strangways Orogeny and therefore may have at that time overlain the location of maximum lithospheric thinning on the extensional detachment zone (Sandiford and Powell, 1986).

The age of the oldest metamorphosed sequence in the Arunta Inlier has been tentatively correlated with the Halls Creek Group in the Halls Creek Mobile Zone by Plumb (1979) (Fig.8-4). The N-S or NNE-SSW trend of the SOB is here structurally correlated with the N-S trending North Australian Orogenic Province (NAOP) (Plumb, 1979), though most exposures of the NAOP show only greenschist to amphibolite facies metamorphic grade. The amphibolite to granulite facies exposures of the SOB in the Arunta Inlier are interpreted as the result of further uplift during the Harts Range Orogeny (belonging to the Central Australian Orogenic Province (CAOP) of Plumb, 1979; see later) and Alice Springs Orogeny, and may thus represent the lower or internal zone of the NAOP. N-S trending structures are predominant in the Halls Creek Inlier, the Pine Creek Inlier, the Arnhem Inlier, the Murphy Inlier, the Tennant Creek Inlier of the NAOP, and in the the Argylla Formation (1780 Ma basement) of the Mount Isa Inlier of the CAOP (Fig. 8-4). However, further study, especially detailed mapping and regional synthesis in those areas is necessary before the architecture of the SOB and its relation to the Early Proterozoic basement geology

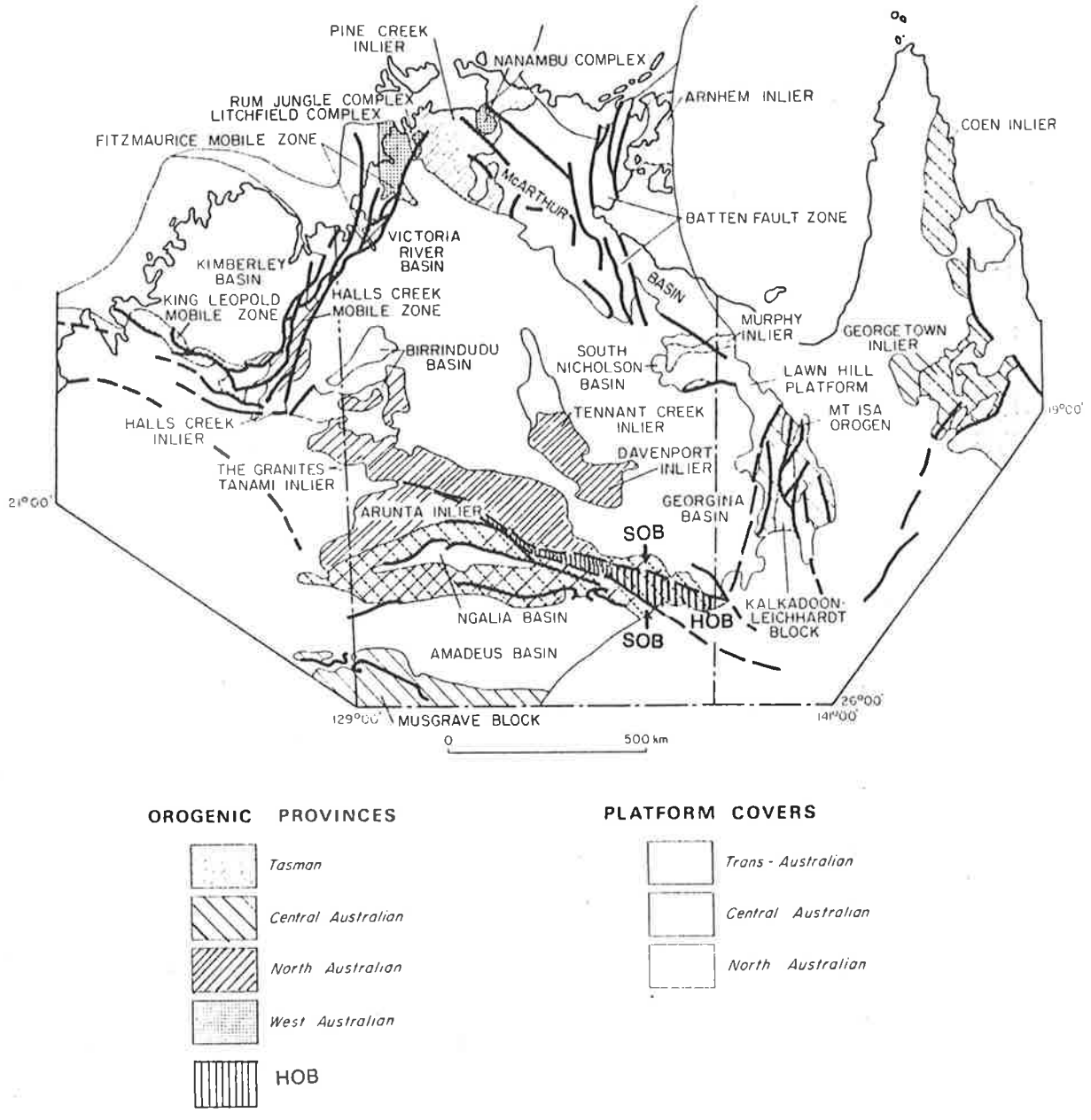


Fig. 8-4 Tectonic sketch of northern Australia showing the present setting of Proterozoic orogenic provinces and platform cover (modified from Plumb, 1979). Note the present spatial relationship between the HOB and the Mt Isa Orogen, and also between the SOB and the other part of the Arunta Inlier.

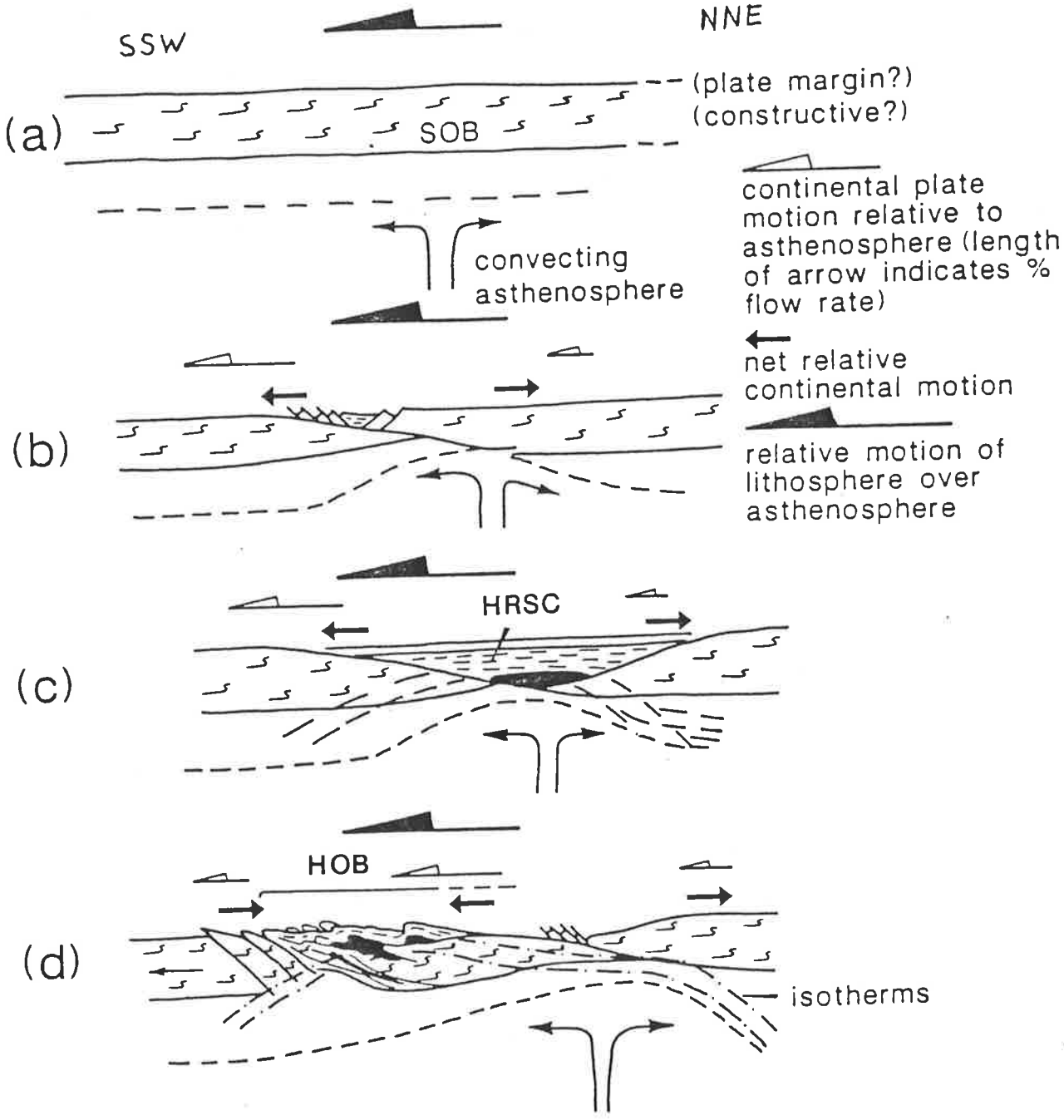


Fig. 8-5 Sketch sections showing a "Caterpillar Tectonic" model (modified from the Detachment model of Wernicke, 1985 and the Millipede model of Wynne-Edwards, 1976) for the evolution of the HOB. SOB - Strangways Orogenic Belt, HRSC - Harts Range Supracrustal Cover, HOB - Harts Range Orogenic Belt.

of Northern Australia can be fully demonstrated.

8.3. Tectonic evolution of the Harts Range Orogeny

There are two main models considered as possible causes of the original relationship between the HOB and the SOB. Firstly it is possible that the HOB represent a totally allocthonous unit with respect to the structurally lower SOB and was deposited thousands of kilometres away from the present location of the SOB in a totally different tectonic environment. Comparable examples are well known from many collisional orogenic belts, e.g. the northern Scandinavian Caledonides (Hodges et al., 1982) and the intracontinental collision and subduction in the Himalayas (Bird, 1975). Alternatively the HOB may represent a para-autocthonous sequence deposited in an intra-continental orogen. In this thesis the latter scheme is favoured and a scenario is outline for the deposition and subsequent tectonothermal evolution of the HOB, where it displays an intimate relationship with extension - collision movement along a master crustal detachment zone. However, this interpretation is certainly not exclusive.

The tectonic evolution of the HOB is considered to have occurred in five discrete periods which have in the preceeding chapters been named and described as separate Movement Phases (Fig.1-2).

8.3.1. The Florence Movement phase

8.3.1.1 Initiation of the Harts Range Detachment Zone

The Florence movement (Fig. 1-2) defines the beginning of a cycle of large-scale crustal extension-collision (Figs. 8-5 and 8-6), with a NNE-SSW principal horizontal extension, initiating an

Fig. 8-6 Block diagrams showing the development of the Harts Range Orogenic Belt.

(a) Initiation of the Harts Range Detachment Zone. Rifting, block subsidence and formation of the HRSC occurred during the early stage of the extensional Florence Movement phase.

(b) Full extension and juxtaposition of the HRSC over mylonitized high-grade rocks of the HRDZ.

(c) HRF_1 folds developed during shortening of the Oonagalabi Movement phase.

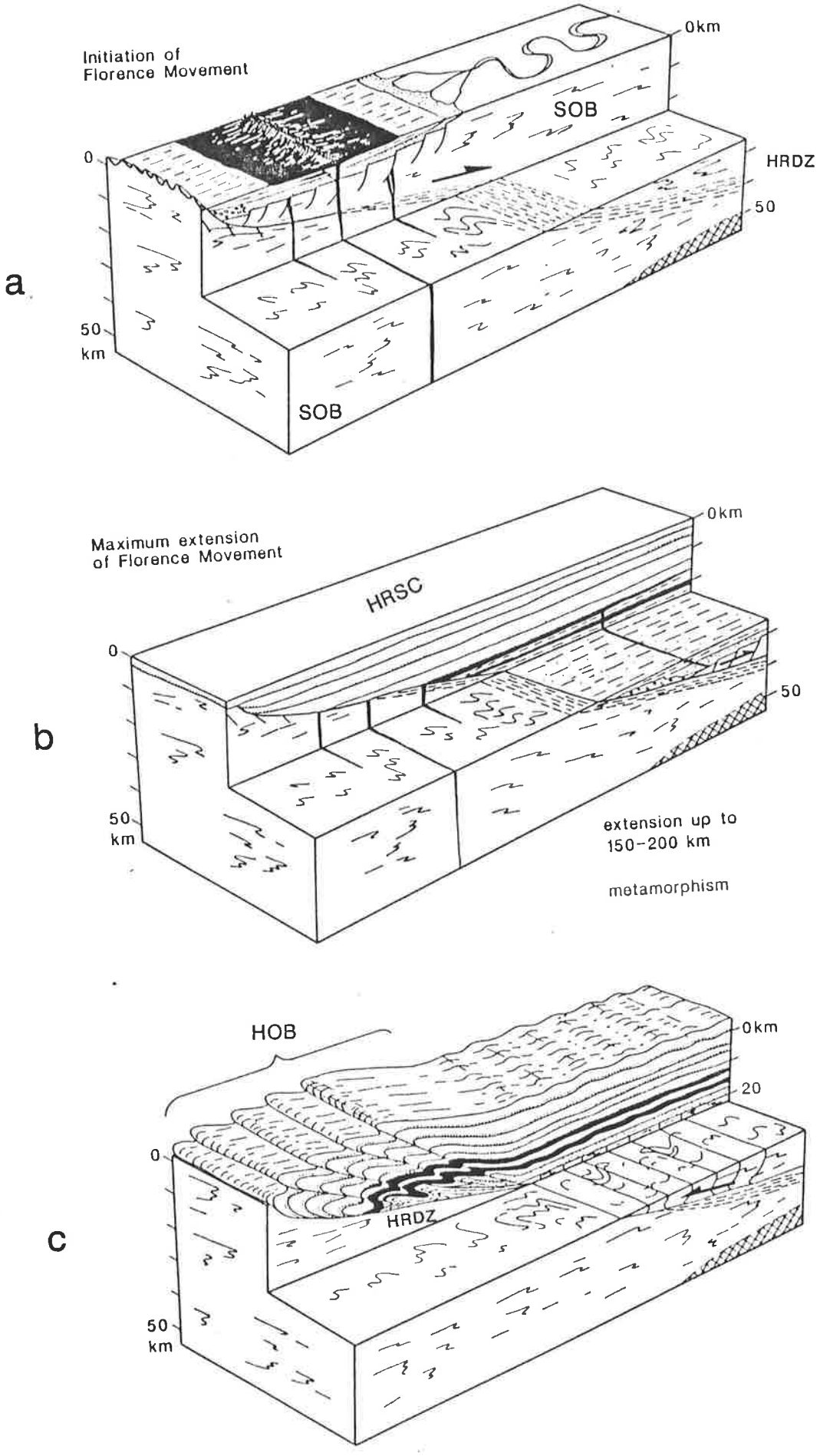

a
Initiation of
Florence Movement
0km
SOB
HRDZ
0
50
50
km
SOB
b
Maximum extension
of Florence Movement
0km
HRSC
0
50
50
km
extension up to
150–200 km
metamorphism
c
HOB
0km
20
0
HRDZ
50
km

Fig. 8-6

SE-WNW orogen at high angles to the trend of the SOB. The difference in structural trend further confirms the fundamental relative temporal difference between the HOB and the SOB. It also emphasises the fundamental change in crustal stress conditions from horizontal WNW-ESE compression to horizontal NNE-SSW tension.

Extensional strain was concentrated along a master detachment zone (Fig. 8-5b), named the Harts Range Detachment Zone (HRDZ) (James & Ding, in press, Appendix IV). The form of the HRDZ matches closely that of the type of gently dipping low angle normal shear or detachment zone, described as a model for explaining the anomalous thickness of the sediments in the Basin-Range Province and metamorphic core complexes of central west U.S.A. (Wernicke, 1981 and 1985, Davis and Coney, 1979). The model also fits the concept of deep crustal metamorphism of Sandiford and Powell (1986).

During the initial development of the HRDZ, the zone at lower crustal levels may have consisted of a discrete detachment fault bounded on either side by high-grade, granulite facies mylonite zones (Fig. 8-6a). They are now only recognized to a very limited extent largely because of the significant later disruption by the tectonic activity during the Harts Range Orogeny. The preserved parts of the HRDZ are now recognised as including the separate relics of the Florence and Leaky Shear Zones, each up to 2 km thick (Figs. 1-1, 1-2 & 8-5), together with the minor intervening tectonic klippen and the less intensely mylonitized Oonagalabi Tongue, which is a relict section of the HRDZ, folded during later reactivation in the compressional phase of the Harts Range Orogeny. The F/LSZ shear zone exhibits strongly layered protomylonites and mylonites, with intense layer-parallel fluxion foliation and consistently north or northeasterly trending stretching linea-

tions. Microstructures provide evidence of finely comminuted granulite facies mineralogies (two-pyroxene, plagioclase and hornblende), though retrograde metamorphism is common due to later shearing. The character of these zones indicates deeply located shearing at high temperatures estimated as 800-870°C (chapter 4), similar to those of the SOB. Most of the mylonites show symmetric microstructures. However, some asymmetric structures within the mylonites indicate a downward or northward (i.e. extensional) shear sense of the upper block.

The detachment zone must have originally continued updip to form a Basin-Range type brittle extending orogen (Angelier & Colletta, 1983)(see Figs. 8-5b & 8-6), which has been eroded during the later uplift events.

8.3.1.2 Deposition of the Harts Range Supracrustal Cover

The extensional movement along the HRDZ produced a subsiding basin with an uplifted northern margin (Fig. 8-5c). The original sediments of the HRSC sequence were deposited into the subsiding basin (Fig. 8-6 A) under initially shallow water conditions and now occur in the most southerly (and likely earliest) sequences within the Naringa Nappe. Deeper water conditions producing arkoses and greywackes formed later in the deepening basin further to the north and are now mainly found within the Irindina Nappe sheet. Further extension led to fracturing of the continental crust and the eruption of extensive basaltic lava, which now forms the thick amphibolite pile (the highest unit) within the present HRSC sequence. The eruption was accompanied by mafic and ultramafic intrusions which formed the Harts Range metaigneous complex. These igneous rocks are now mainly found within the Riddoch and Campbell Nappe sheets, and may be more closely associated with the

northern exposures of the deeper water sediments as would be expected in an extending orogen over a thinning lower crust. The upper part (i.e. unmetamorphosed) of the HRSC is not exposed in this area and must have been eroded. Importantly, no relics of oceanic crust (Hsu, 1984) have been recognized within the HRSC.

8.3.1.3 Metamorphism within the HRSC

Continued extension during the Florence Movement drew the HRSC down to deeper crustal levels until it eventually came into direct contact with the granulite facies SOB complex of the lower (footwall) plate (Figs. 8-5 c & 8-6 b). During this time it is possible that sedimentary deposits attained sufficient depths that they underwent progressive metamorphism at conditions of upper amphibolite facies. Such metamorphism would have been accompanied by minor dehydration and partial melting during the development of metamorphic layering and weak layer-parallel foliation (CS_0). The peak metamorphic temperature of the Iridina Supracrustal Assemblage (ISA), at the lower level of the HRSC, has been estimated as 650-720^{o}C (7-8 kb). This is about 100-150^{o}C lower than the peak metamorphic temperature of granulite facies rocks of the SOB.

A problem, similar to that of the SOB discussed previously (see section 8.2.2), concerns how the HOB supracrustals were able to subside to depths of 25-32 km as indicated by the high metamorphic pressure (7-8 kb). It is possible that prograde equilibration occurred after the HRSC was thickened by thrust/nappe stacking during an early contractional event. However, no such early thrusting deformation has been recognized during the field study and it is suggested that the very thick depositional basin was developed by a polyphase extensional process with intervening periods of thermal subsidence (Jenkins, in press).

The total extensional movement can be estimated geometrically from the maximum thickness (32 km) of the HRSC, and as a function of the dip of the HRDZ. The estimates of possible extension are listed in Table 8-1. The possible dip range of 3-7° and extension range of 250-600 km are preferred (see section 8.3.2.2).

Table 8-1 ESTMATES OF POSSIBLE EXTENSION ALONG THE HRDZ

assumed dips of the HRDZ	possible extension	
1°	1882 km	
2°	914 km	
3°	615 km	most likely options
4°	457 km	
5°	368 km	
7°	260 km	
10°	182 km	
15°	119 km	
20°	88 km	
25°	69 km	
30°	55 km	

8.3.1.4 CD_1 deformation

The HRSC underwent early intense deformation and formed CF_1 isoclinal folds, which have an intense axial planar schistosity (CS_1) in pelitic gneiss and a weak lineation (CL_1) which parallels the CF_1 hinges. The CF_1 folds have been largely transposed in the limb areas, where the CS_0 and CS_1 fabrics are parallel. As the main fabric (CS_1) is actually a layer-parallel schistosity and formed in a subhorizontal attitude, it closely resembles the types of fabrics formed early in the structural history in many other gneiss belts (Coward, 1973; Park, 1980). As all folds have been transposed, no vergence has been recognized, and no microstructural movement indicators could be found. The relatively variable trend of CL_1 lineations and CF_1 fold hinges in the HOB is somewhat difficult to explain.

Whether the CF_1 folds were formed under contractional or

extensional deformation conditions is not clear. This event is described as the last part of the Florence Movement phase. That phase has been mentioned as primarily extensional and is succeeded by the contractional Oonagalabi Movement phase. Thus the inability to recognize the tectonic style of CD_1 has meant that it is only included within the former for convenience (James & Ding, in press, Appendix IV), but may have actually formed either as the initiation of the Oonagalabi Movement phase or during a transitional event between the two Movement phases.

If the CF_1 folds were formed by extensional shearing, then they may have formed under such a specific strain field with lateral shortening perpendicular to the maximum elogation direction controlling the trends of fold hinges. In this case the fold hinges should mainly parallel the extension direction. However, as curvature of the CL_1 lineations occurs on the layer surfaces (CS_o) or within the CS_1 foliation, the CF_1 folds are, perhaps better interpreted to have formed by contractional shearing process like that forming typical sheath folds (Cobbold & Quinquis, 1979). They were probably initiated with fold hinges and CL_1 lineations in an E-W direction at high angles to the contractional shearing direction and parallel to the intermediate principal strain axis, and were consequently rotated by ductile stretching (elongation) parallel to the direction of continuous shearing deformation (Sanderson,1973; Henderson, 1981).

8.3.2 The Oonagalabi Movement phase

The end of the extensional Florence Movement phase saw a major change in tectonic style (as also occured after the major plutonism in the SOB). The HRSC began to deform under a continuou-

sly NNE-SSW contractional regime which performed an unusually complex tectonic style of stick-slip thrusting and folding. This movement led to the southward shallow overthrusting and gradual thickening of the HRSC in the upper plate of the HRDZ, with most displacement concentrated along bounding thrusts of the detachment zone. It is noteworthy that a similar but less extensive intrusion of acidic magma occured, as the protolith of the Bruna granitic gneiss (see later) was intruded as a major sheet soon after the change from a horizontal tensile to a horizontal compressive stress regime in this Harts Range Orogenic cycle, thus repeating a similar cycle of events first recognised in the SOB.

Contractional orogenies typically involve thin-skinned foreland folding and thrusting (Coward, 1983) with large overthrust nappes containing small-scale asymmetric inclined to recumbent folds. The HOB exhibits many features typically of such terrains, though the structures within the present HOB were formed at deeper levels than that recognized for typical thin-skinned tectonics.

8.3.2.1 CD_2 deformation

The Irindina Supracrustal Assemblage in the HOB was intensly deformed by compressional tectonism and formed a series of E-W trending tight to isoclinal CF_2 folds on a regional scale with E-W trending and shallowly plunging hinges at a high angle to the regional shortening direction (Fig. 8-6 C). Similar types of folds are common structures found in orogenic fold belts of all ages. Examples can be found from the Archaean terrain in SW Greenland (Chadwick & Nutman, 1979); the Proterozoic complex of the eastern Svecokarelides of Finland (Bowes et al.,1984); the basement of the West Africa Craton (Villenevve & Dallmeyer , 1987) and in the Mt Isa Region of Australia (Loosveld, 1987; Bettess, 1987); as well

as in Phanerozoic geosynclines (Townsend et al., 1986). The attitudes of major folds may vary at different crustal levels, i.e. forming upright to inclined folds at higher levels and recumbent folds at lower levels.

The CF_1 and CF_2 folds are generally not coaxial with hinge-intersection angles varying from zero to almost 90^{o}. However, the subhorizontal CF_2 fold hinges remain dominantly E-W trending in contrast to those of the CF_1 folds, and may indicate little involvment of stretching and rotation.

8.3.2.2 Thrusting: the CT thrusts, nappes and the HRT_1 Oonagalabi Thrust

The CF_2 folding deformation was followed by southwards overthrusting (CT) within the HOB, and occurred with successive formation and overriding of the major Naringa, Irindina/Salthole, Riddoch and Campbell/Ruby Nappes. The precise displacement along each CT thrust cannot be determined from the present data but a very large bulk displacement of 150 to 200 km is proposed here, partly because the thicknesses of individual lithologic units change abruptly from one nappe sheet to another, and also because each nappe may have been transported for over 50 km (the present width of the HOB in the study area). A subhorizontal shearing from north to south, which is represented by the northerly trending lineations found along the CT boundaries, may explain the development of the CT thrusts and nappe structures (Fig. 8-6 C). It is not clear whether these nappes were formed simultaneously or sequentially like those described as piggy-back by Butler (1987).

With the development of the nappe structures, the HOB may have been upthrust to overlie the granulite facies SOB along the top principal bounding fault (the Oonagalabi Thrust) of the HRDZ

(Fig. 8-7a). To explain this particular relationship between the amphibolite facies HOB and the granulite facies SOB, the HRSC must have been moved down to a level lower than that of the granulite facies rocks in the SOB within the footwall plate of the HRDZ during the extensional Florence Movement phase, when the HRSC within the hanging wall plate was being metamorphosed under amphibolite facies conditions (Figs. 8-6b & 8-7a). In that situation the amphibolite facies HRSC could thus be upthrust to lie over the granulite facies rocks within the SOB (Fig 8-6c). In addition to the extensional shear sense indicated by some of the kinematic indicators in the mylonites within the F/LSZ, this is one of the main lines of evidence to support the interpretation of an extensional initiation for the HRDZ. However the displacement along the Oonagalabi Thrust is not possible to estimate, because the HOB and the SOB are totally different terrains, and no related marker lithologies have been found from both sides of the Oonagalabi Thrust.

It was also during this movement phase that a large component of displacement was accommodated along the basal bounding fault of the HRDZ (Fig. 8-7a), similar to the movement within a duplex (Cooper et al., 1983). This basal fault has been largely replaced by the later HRT_3 Entia Thrust (Fig. 8-7f) and HRT_4 Muller Thrust (Fig. 8-7g). This brought parts of the granulite facies HRDZ up to lie on top of the amphibolite facies Entia gneiss complex as can be seen in the Leaky shear zone and the Coggan Shear Zone (Map 2 & Fig. 1-1). The very low angle dip of the HRDZ requires a very large displacement along the base of the HRDZ to bring the thick pile of granulite facies mylonites to overlie an amphibolite facies domain. The displacement must be greater than the width plus thickness of the Entia gneiss complex, i.e. 75 km, as no

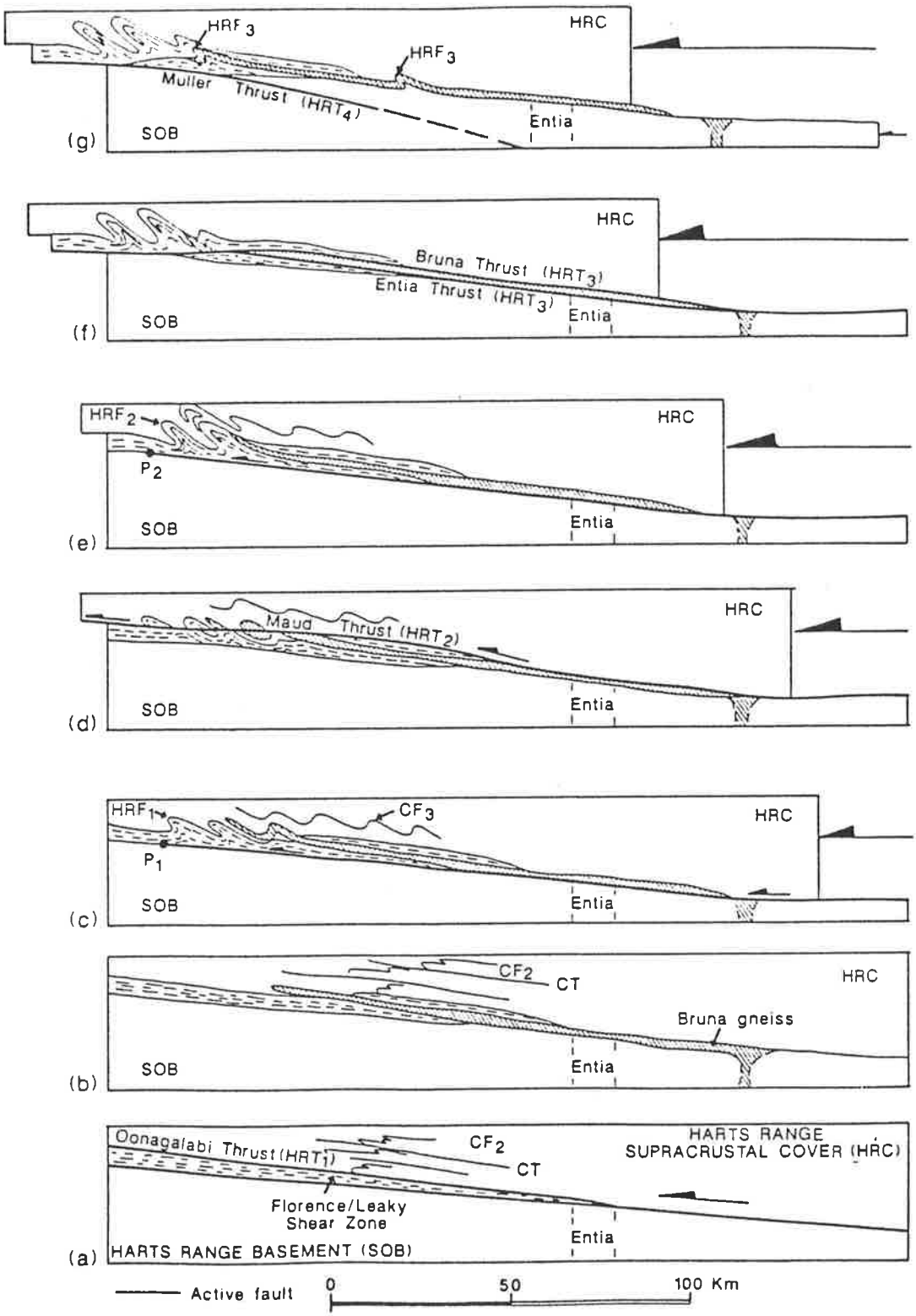


Fig. 8-7 Cartoon showing the evolution of the Harts Range orogeny. (a)-(c) Oonagalabi Movement phase (compare with Fig. 8-6 (c); (d) and (e) Maud movement phase; (f) and (g) Bruna and Muller Movement phases.

rocks witin the Entia Dome are similar to those within the overlying Leaky Shear Zone. The total displacement during this thrusting event is thus probably more than 250 - 300 km. This estimate suggests that the dip of the HRDZ must have been shallower than 7^{o} during the extensional phase (see section 8.3.1.2; Table 8-1).

8.3.2.3 Intrusion of the Bruna Granite

The protolith to the Bruna Gneiss is interpreted to have preferentially intruded along the active F/LSZ of the HRDZ during the Oonagalabi Movement phase. The whole premise is based on the correlation between the small intrusive granitic gneiss bodies within the HRSC and the major Bruna Gneiss sheet. The magma probably intruded near the base of the HRDZ in the east, and transgressed up to near its top in the west, where the small stocks and sills previously mentioned crosscut the HRSC sequence. This sill-like plutonic body was subsequently deformed and metamorphosed to form the Bruna Gneiss (see Figs. 1-2 and 8-7b). The F/LSZ mylonites and other shear zone products remain as large xenolithic fragments within the Bruna gneiss. Further shearing (as also happened in the later Bruna Movements) deformed and mylonitised the Bruna Gneiss with the strain preferentially partitioned into shear zones at the margins and occasionally within the Bruna gneiss.

The zircon date of 1747+3-2 Ma records the intrusive age of the Bruna Gneiss (Cooper et al., in press). This provides a usefull time marker for the tectonic evolution of the Harts Range Orogeny, and will be further discussed in Section 8.3.6.

8.3.2.4 Folding (HRF_1)

During the continued contraction of the Oonagalabi Movement phase the displacement along the bottom bounding fault of the HRDZ is assumed to have become pinned (see Butler, 1987) along a line near to the southern margin of the active orogenic belt. This is shown as the pin-point P1 of Fig. 8-7c. Continued movement of the upper plate led to the development of buckles and subsequently major HRF_1 (CF_3) folds in the HOB and in that part of the SOB, which had been previously incorporated within the HRDZ (e.g. the Florence Window), as well as also in the Bruna Gneiss. All major HRF_1 (CF_3) folds are very tight to isoclinal, inclined and asymmetric, with a constant southerly vergence indicating continued overriding from the north caused by the consistent subhorizontal compression. This is the first fold generation recognised to have affected the thrust boundary of the HRDZ. The fold axes of HRF_1 (CF_3) folds trend E-W similar to those of CF_2 folds, but the CF_2 and other earlier folds as well as thrusts (BT and CT) were all obviously refolded by this fold generation (Maps 2, 3 & 5).

8.3.3. Maud Movement phase

8.3.3.1 Thrusting: the HRT_2 Maud Thrust

Folding of the detachment zone at the end of the Oonagalabi Movement phase was succeeded by renewed thrusting on a new thrust plane, the Maud Thrust (HRT_2) (Figs. 1-1, 1-2 & 8-7d). The Maud Thrust has now a complexly folded geometry, but can be seen on the maps to ramp up from its lower position as the basement-cover boundary at the northern edge of the Oonagalabi Tongue to a central layer-parallel position in the Naringa Well area until it is finally truncated in the south by the Bruna Thrust. This clearly illustrates a major example of out-of-sequence, break back thrusting as defined by Boyer and Elliot (1982) and Butler (1987).

8.3.3.2 Folding (HRF_2)

Then followed probably the most dramatic event in the development of the HRDZ, with the change to a major E-W transpressional movement. For the second time, thrust movement at the base of the HRDZ was pinned, this time at an assumed point P2 shown on Fig. 8-9e, and a major slab of reworked SOB basement, the Oonagalabi gneiss complex, which had earlier been intensly affected by and incorporated into the HRDZ, and its overlying HRSC, together with all the preexisting thrusts and folds, were thrown into a regional HRF_2 fold pair. The HRF_2 folds are subreclined or subneutral isoclinal folds, which have E-W trending fold axial surfaces and shallow to intermediate northerly plunging fold axes with amplitudes varying from 7 to 17 km.

The geometry, scale, kinematic pattern and tectonic position of the HRF_2 folds all show a marked similarity to that described for the development of the Hazara and Nanga Parbat syntaxes of the western Himalayas in northern Pakistan (Coward, 1983), which he described as forming due to a process of pinning on bounding thrust surfaces.

The easterly vergence of these structures, plus their style, suggests E-W subhorizontal shearing of the hanging wall upper plate as the most likely cause, with dextral transcurrent shear concentrated on the major northerly inclined HRDZ. The change from southerly overthrusting, to eastwards overfolding in a low angle transpressional regime could well have been imposed on the zone as a local rotation or scissor movement of the moving upper plate, caused by the initial pinning of its thrust movement at a single point, rather than along a line, as appeared to occur during the earlier Oonagalabi phase.

8.3.4. Bruna Movement phase

8.3.4.1 Thrusting: the HRT_3 Bruna and Entia thrusts

Compression from the north continued with a return to intense thrusting and ductile shearing which occurred over a large part of the HRDZ. This movement, which was not involved in, but rather transected the HRF_2 folds, was partitioned mainly along both the top and basal margins of the sill-like Bruna gneiss body, where it formed the Bruna and Entia Thrusts, respectively (Fig. 1-2 and 8-7f). Movement also took place within the main Bruna Gneiss body forming stacked heterogeneous protomylonite, mylonite and ultramylonite zones. The trends of all stretching lineations indicate a N-S or NNE-SSW principal shear direction, while rotational criteria such as asymmetric augen and asymmetric shear bands indicate primarily overthrusting of the HRSC towards the south over the SOB. The mylonitic layering is frequently folded on a small scale within the Bruna gneiss forming asymmetrical folds. These also indicate a southwards vergence and thus overthrusting movement.

As thrusting continued it seems to have become more localised in the HRDZ, probably indicating either a lessening of the subhorizontal compression and/or noncoaxial flow rate and most likely a gradual decrease of rock ductility, as would be expected for progressive continental obduction of an upward moving upper plate (Sibson, 1986).

8.3.4.2 Folding (HRF_3)

The HRT_3 thrusts as well as the adjacent basement and supracrustals were then locally folded by HRF_3 folds, at a mappable scale. These are asymmetric, tight to isoclinal, subneutral folds with fold axes trending NNE similar to those of the HRF_2 folds. Although they are local in effect, one HRF_3 fold is as large as a

few km in amplitude and this phase marks the last intense ductile deformation which affected the HRDZ and HOB (Fig. 8-7g).

8.3.5. The Muller Movement phase

The Harts Range Orogenic Cycle was terminated by up thrusting movement along the Muller Thrust (HRT_4), which crosscuts HRF_3 folds and other earlier structures, and spatially bounds the southern margin of the HOB. The Muller Thrust is marked by a mylonite/schist zone with muscovite and biotite developed internally in typical retrograde assemblages associated with epidotisation. Relict high grade mylonites within the F/LSZ suggest that this relatively narrow zone became the locus of displacement as the whole area moved up through the ductile/brittle transition. This movement thus carried the HRDZ up to its current position relative to the SOB of the Hale River Region, along with the remainder of the overlying HOB (Fig. 8-8). The northern extension of the Muller Thrust is considered to extend under the Entia Dome and thus has not been exposed yet. However, the possibility cannot be excluded that the Huckitta Thrust (in this thesis tentatively assigned to the BT phase) within the Entia Dome is the northern extension of the Muller Thrust, because the Huckitta Thrust has a similar NE trending stretching lineation and also was not affected by HRF_3. However, direct evidence supporting or contradicting these possibilities are lacking.

8.3.6. Completion of the HOB

The pervasive CF_2 and CF_3 folds and the low angle thrusts within the HOB define an ESE-WNW trending typical collisional orogenic belt, with inferred NNE-SSW contraction, which truncates the structural trend of the SOB at a high angle. However, the

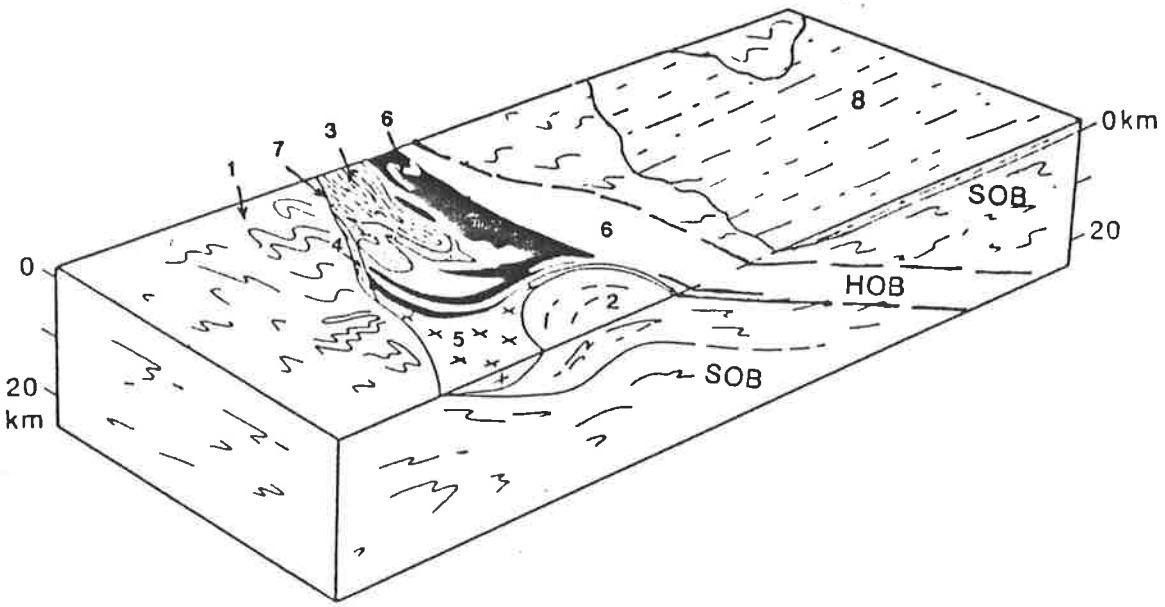


Fig. 8-8

Block diagram showing the final structure of the Harts Range area at the present erosion level. 1. The Hale River Region; 2. the Entia Dome; 3. The Oonagalabi Tongue; 4. the Florence Shear Zone; 5. the Bruna Gneiss; 6. the Harts Range Supracrustal Cover; 7. The Muller Thrust; 8. the SOB in the north of the Harts Range area with Late Proterozoic to Palaeozoic platform cover.

northerly plunging HRF_2 and HRF_3 folds may reflect a more complex reworking of both the SOB and the HOB by the later stages of the HOB collision.

The Harts Range area belongs to the Central Australian Orogenic Province of Plumb (1979) but the HOB is first recognized in this thesis as a geosynclinal orogenic belt in its own right. This orogenic belt is different from the mobile belts defined as mainly reworked older basements (Witschard,1984; Hunter et al., 1981). Using the zircon age of 1747+3/-2 Ma for the Bruna gneiss as a time marker for the end of the extensional movement along the HRDZ and the end of HRSC deposition, and the zircon age (1767 $\pm$1 Ma) of the granitic gneiss in the Entia Dome as the end of the SOB evolution, only a very short span (20 Ma) is allowed for the HRSC to be deposited as was suggested by James & Ding (Appendix IV). This is sedimentologically viable during such a short period, as it is possible to accumulate 20 km of sediments with only a rate of 1 mm of deposits per year, or 30 km of sediments with a rate of 1.5 mm of deposits per year over the apparently short time span as 20 Ma.

The deformational time-scale for the Harts Range Orogeny is still not precisely known. In fact, no age data have been derived directly either from the HRSC itself or from the small granitic gneiss bodies which intruded into the HRSC. The small intrusive bodies are only tentatively correlated with the major Bruna Gneiss sheet on the basis of their petrographic similarity without geochemical or geochronological evidence. Thus the reliability of the suggested timing of the Harts Range Orogeny lacks complete substantiation. Other interpretations should therefore not be excluded and two other possibilities are discussed here.

Firstly it is possible that the HRSC and the small intrusive

granitic gneiss bodies within the HRSC are younger than the Bruna Gneiss, In this case, the relationship between the Bruna Gneiss and the HRSC is not definitely known. Thus if, for example, the Bruna Gneiss intruded into the Florence Shear Zone during the extensional Florence Movement phase, its age can be regarded as the time marker only for the begining of the Harts Range orogeny which would have been at 1747+3/-2 Ma. This would leave a more flexible and possibly longer time span for the Harts Range Orogeny subsequent to that time.

The second one is that those small intrusive granitic gneiss bodies within the HRSC are of the same age as the Bruna Gneiss, but the HRSC has a similar age to that of the SOB. In this case the HOB and SOB may have formed during a similar time period but in different areas and were juxtoposed later by large scale thrusting as suggested by Oliver et al. (in press, Appendix V). The juxtoposition may have occurred before the intrusion of the Bruna Gneiss or more likely during the intrusive event which could even have been enhanced by the presence of the sheet-like magma body (Hollister and Crawford, 1986).

The HOB may be correlated with the Mount Isa Orogen (Plumb, 1979) whose basement (Argylla Formation) has a similar age (1780 Ma) to that of the SOB in the Harts Range area. The first sedimentary deposit above the Argylla Formation in the Mt Isa orogen was deformed between 1670-1620 Ma (Page, 1976c). The trend of the HOB and that of the Mount Isa Orogen are nearly perpendicular. This relationship is very similar to that of the WNW trending King Leopold Mobile Zone and the NNE trending Halls Creek Mobile Zone, which bound the southern and eastern margins of the Kimberley Basin (Plumb, 1979 & Fig. 8-4; Hancock and Rutland, 1984). This relationship is also similar to the geometry of transfer and

extensional faults in continental extension terrains (Lister et al., 1987; Etheridge, 1987). It is possible that at the end of the Strangways Orogeny, the SOB was bordered by a subduction zone at its eastern margin and was crosscut by large scale transfer faults (Fig. 8-9 a) similar to the "Collision-induced rifting " model of Gorden and Hempton (1986). A rectangular basin may have formed following these megastructures during a subsequent extensional movement (Fig. 8-9 b) as the granulite facies SOB basement became exposed on both sides of the HOB. When the HOB was deformed by N-S contraction (e.g. CF_2 and HRF_1 folds), the western margin of the Mount Isa Orogen may have acted as a major sinistral strike-slip shear zone (Fig. 8-9 c), and subsequently whilst the Mount Isa Orogen was deformed by E-W contraction (Loosveld, 1987; Bettes, 1987), the HOB may have been affected by dextral transcurrent shearing (e.g. HRF2 & HRF3; see Fig. 8-9 d). This may compromise the contradictory interpretations about the complex movement directions during the formation of D_1 duplex thrusts in the Mt Isa Orogen (e.g. a southerly movement proposed by Bell,1983 and a westerly movement proposed by Bettes, 1987). Unfortunately the connection between the two orogenic belts is hidden by younger platform cover.

8.4. Post HRO evolution

The end of the Harts Range Orogeny may be the begining of another orogeny as illustrated by the model of "Caterpillar Tectonics" proposed by James & Ding (Appendix IV, see Fig. 8-5 d). The Division 3 sequence of the B.M.R in the Chewings Range area (Amri et al, 1987) may represent part of that following orogenic belt.

The open folds and steep faults in the Harts Range area are

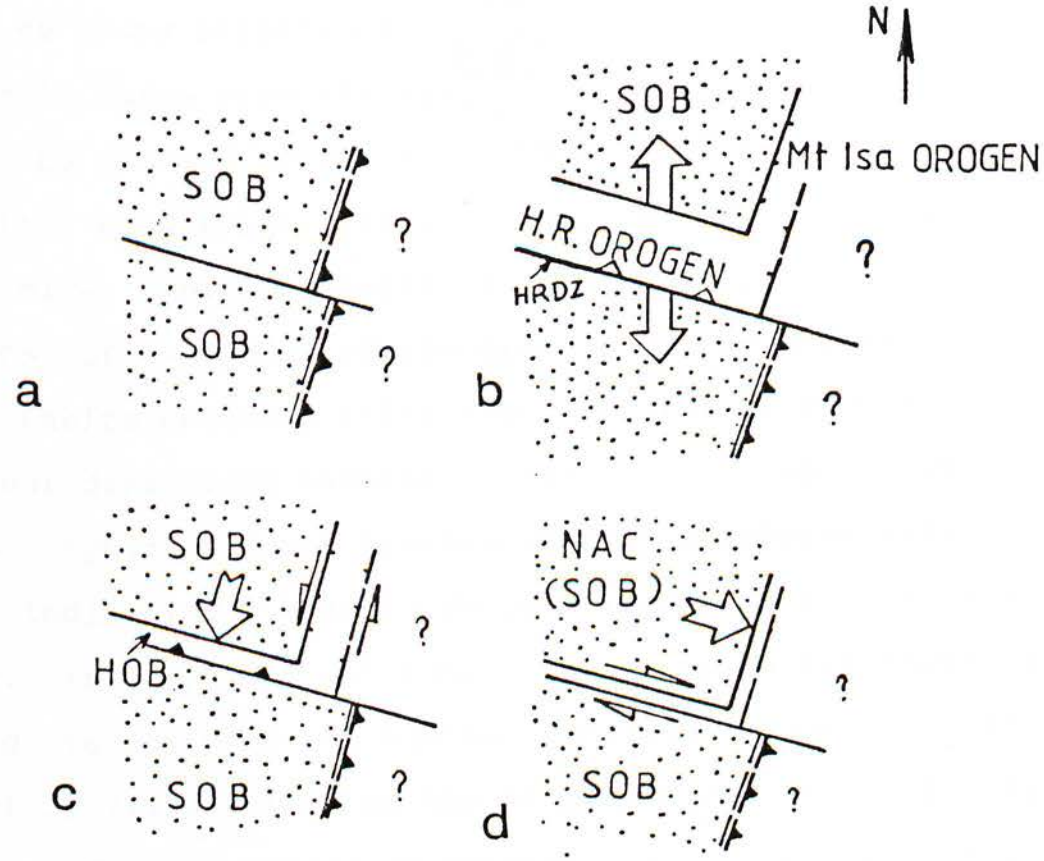


Fig. 8-9 Cartoon showing possible tectonic evolution of central Australia during the Harts Range Orogeny. No scale implied.

(a) End of the SOB: the SOB may have been formed by collision with an older continental (?) or oceanic (?) plate. An early transfer fault may have formed in a direction perpendicular to the trend of the SOB.

(b) Opening of the Harts Range Orogen along a northerly dipping detachment zone, and possibly initiation of the Mt Isa Orogen simultaneousely.

(c) Formation of the HOB by compressional movement along the Harts Range Detachment Zone with inferred sinistral shearing (?) in the Mt Isa Orogen.

(d) Contractional movement in the Mt Isa Orogen may have caused the dextral shearing in the HOB and may explain the dextral vergence of the regional scale HRF_2 and local HRF_3 folds.

considered to represent post HRO deformation, as the change of fold styles from recumbent tight/isoclinal to upright/inclined usually implies a change of deformational conditions from higher strain to lower strain, or from deeper levels to shallower levels. The Harts Range area may have been uplifted to shallower levels after the HRO and before the formation of the upright to inclined asymmetric open folds. The four (NE, NW, E-W, S-N) trends of these open folds imply a complex change in strain field, though the sequence of evolution of the open folds has not been recognized. Steep faults occurred later than the open folds but developed in the four directions similar to them, and also cut the open fold system. Typical fault breccia usually developed along the fault planes indicating a brittle deformational environment and further uplift. It is still not known whether these deformations may be related to which of the various subsequent events as proposed by Shaw et al (1984), such as the Aileron Event (1700-1600 Ma; including the Chewings phase of deformation) or to the Anmatjira Event (1500-1400 Ma).

Post-tectonic dolerite dykes, which may be equivalent to the Stuart Dykes (897±9 Ma) in the Alice Springs area (Black et al, 1980), have been found in the Harts Range area particularly within the mylonitized Bruna Gneiss. Their emplacement may be chronologically related to the Ormiston Event (1050-900 Ma) of Shaw et al., 1984. Swarms of post-tectonic pegmatite veins were emplaced along fractures and steep faults at 315 Ma (Mortimer et al., 1987) and are considered to represent the main products of the Alice Springs Orogeny (ASO) (400-300 Ma; Shaw et al., 1984) in the Harts Range area.

Other definite ASO structures, including folds, faults and the Illogwa Shear Zone, are found at the southern margin of the

Harts Range area particularly within the Arltunga subarea where they affected the Late Proterozoic Heavitree Quartzite (Forman, 1971; Forman & Shaw, 1973).

8.5 Conclusion

Based largely on the detailed large-scale geological maps presented in this thesis, together with the petrographic and structural analysis, a number of significant conclusions are presented concerning the tectono-metamorphic evolution of the Harts Range area within the Arunta Inlier.

(1) The Early Proterozoic high grade metamorphic rocks in the Harts Range area of the eastern Arunta Inlier are now recognized as belonging to three tectonic terranes:

a) the NNE-SSW trending Strangways Orogenic Belt (SOB) in the southern or lower structural position;

b) the ESE-WNW trending Harts Range Orogenic Belt (HOB) in the northern or upper structural position;

c) the Harts Range Detachment Zone (HRDZ) which defines the base or southern margin of the HOB and separates the two orogenic belts.

(2) The deformational history of the gneiss complex within the Entia Dome is considered to be different from that of the HOB but very similar to that of the SOB in the Illogwa Creek subarea of the Hale River Region. Therefore in contrast to earlier propositions (Shaw et al, 1984), the Entia gneiss complex is assigned to the SOB.

(3) The major part of the acidic to intermediate gneiss within the SOB has been recognized as syntectonic deep crustal intrusive orthogneisses.

(4) Two separate granulite to amphibolite facies metamorphic

events are recognized to have occurred during the Strangways Orogeny; an earlier and higher metamophic event preserved in the supracrustals and a later and lower grade metamorphic event shown only in the orthogneisses.

(5) Four large scale ductile folding phases and one thrusting event are recognized to have occurred during the Strangways Orogeny.

(6) The SOB is interpreted to have a NNE-SSW regional trend before being affected by the Harts Range Orogeny. The granulite facies complex in the west and the amphibolite facies complex in the east may represent two tectonic zones, an internal (root) zone in the west, and an external zone (externides) in the east.

(7) A stratigraphic sequence for the Irindina Supracrustal Assemblage within the HOB is proposed on the basis of structural analysis and way-up criteria found in the layered mafic-ultramafic igneous rocks, has been recognized throughout the HOB in the Harts Range area.

(8) Two early folding phases and one thrusting event during the Harts Range Orogeny are recognized to form a major sequence of stacked nappe-like structures within the HOB before the overthrusting along the Oonagalabi Thrust.

(9) The HRDZ is a major deep crustal detachment zone and includes intensely reworked SOB (the Oonagalabi Tongue), an intensely mylonitized thick granulite facies SOB rock sequence (the Florence/Leaky Shear Zone), and the sill-like body of mylonitized Bruna Gneiss (metamorphosed syntectonic intrusive granitic body within the HRDZ).

(10) The HOB and the HRDZ were deformed together during the later stage of the Harts Range Orogeny resulting in polyphase alternating operation of thrusting and folding during crustal

compression. Four sequential thrusting phases of the HRDZ are distinquished by three intervening folding phases which affected the thrusts sequentially. This complex history has led to the recognition of up to seven generations of ductile folds in the Oonagalabi Tongue. Displacement on the HRDZ was a stick-slip process with repeated punctuation of thrust-slip movement by pinning at points located progressively to the south. Each period of cessation of thrust-slip movement was followed by folding of discrete thrusts, of captured basement lobes and of the overlying supracrustal sequence.

REFERENCES

Allen, A.R., 1979. Metamorphism of a depleted granulite facies terrain in the Arunta Block, central Australia. Part I: Geochemical evidence. Contrib. Mineral. Petrol., 71: 85-98.

Allen, A.R. and Black, L.P.,1979. The Harry Creek Deformation Zone, a retrograde schist zone of the Arunta Block, central Australia. Geol. Soc. Aust., J. 26: 17-28.

Allen, R., 1986. Relationship of thermal evolution to tectonic processes in a Proterozoic fold belt: Halls Creek Mobile Zone, East Kimberley, West Australia. Ph.D. thesis, University of Adelaide.

Amri, C., Hobbs, B.E. & Ralser, S., 1987. The Iwupataka Complex: A key area of the Proterozoic and Paleozoic thrust system in the south Arunta Block and its kinematic significance. International Conference on Deformation of Crustal Rocks. Geol. Soc. Aust. Abstracts No. 19, p. 56.

Anderson, S.L. and Burke, K.,1983. A Wilson Cycle approach to some Proterozoic problems in eastern North America. In: Proterozoic Geology, Geol. Soc. Amer. Mem. 161: pp. 75-94.

Angelier, J. & Colletta, B., 1983. Tension fractures and extensional tectonics. Nature, 301: 49-51.

Aoukar, N., 1985. A geological review of the southwest Entia Dome, with emphasis on the Inkamulla Granite gneiss, Harts Range, eastern Arunta Block, Northern Territory. Honours thesis, University of Adelaide, (Unpublished).

Australia 1:250 000 Geological Series: Alice Springs N.T., sheet SF 53-14, B.M.R., 1983.

Australia 1:250 000 Geological Series: Illogwa Creek N.T., sheet SF 53-15, B.M.R., 1985.

Australia 1:100 000 Geological Series: Arltunga-Harts Range Region N.T., B.M.R., 1984.

Australia 1:250 000 Geological Series: Huckitta N.T., sheet SF 53-11, B.M.R., 1985.

Baer, A.J., 1983. Proterozoic orogenies and crustal evolution. In: Proterozoic Geology, Geol. Soc. Amer. Mem. 161: pp. 47-58.

Behr, H.J., 1980. Polyphase shear zones in the granulite belt along the margins of the Bohemian Massif. Journal of Structural Geology, Vol. 2, No. 1/2, pp. 249-254.

Bell, A.M., 1981. Vergence: an evaluation. Journal of Structural Geology, Vol. 3, No. 3, pp. 197-202.

Bell, T.H., 1983. Thrusting and duplex formation at Mt. Isa, Qld. Aust. Nature, V. 304, pp. 493-497.

Bell, T.H. & Etheridge, M.A., 1973: Microstructure of mylonites and their descriptive terminology. Lithos 6, 337-348.

Bell, T.H. and Etheridge, M.A., 1976. The deformation and recrystallization of quartz in a mylonite zone, Central Australia. Tectonophysics, 32, 235-267

Bell, T.H., 1978. Progressive deformation and reorientation of fold axes in a ductile mylonite zone: the Woodroffe Thrust. Tectonophysics, 44: 285-320.

Berthe, D., Choukroune, P. & Jegouzo, P., 1979. Orthogneiss, mylonite and non coaxial deformation of granites: the example of the South Armorican Shear Zone. Journal of Structural Geology, Vol.1, No.1, pp. 31-42.

Berthe, D. and Brun, J.P., 1980. Evolution of folds during progressive shear in the South Armorican Shear Zone, France. Journal of Structural Geology, Vol.2, No.1/2, pp. 127-133.

Best, M.G., 1982. Igneous and metamorphic petrology. Freeman, San Francisco, 630 pp..

Bettess, D.E., 1987. The structural evolution of the Deighton Thrust Nappe Complex, Mount Isa, Queensland. Geol. Soc. Aust. Abstracts No. 19, p. 41.

Billings, M.P., 1972, 3rd. ed.. Structural Geology, Prentice-Hall Inc. Englewood Cliffs, N.J., 606 pp.

Bird, P., 1978. Initiation of intracontinental subduction in the Himalayas. J. Geophys. Res., 83: 4975-87.

Black, L.P., 1975. Present status of geochronological research in the Arunta Block, N.T.. Geol. Soc. Aust., 1st Aust. Geol. Conv., Abstracts, p. 37.

Black, L.P., Shaw, R.D. and Offe, L.A., 1980. The age of the Stuart Dyke Swarm and its bearing on the onset of Late Precambrian sedimentation in central Australia. Geol. Soc. Aust. J. 27: 151-155.

Black, L.P., Shaw, R.D. and Stewart, A.J., 1983. Rb-Sr geochronology of Proterozoic events in the Arunta Inlier, central Australia. BMR Journal of Australia Geology and Geophysics, 8: 129-137.

Black, L.P. and McCulloch, M.T., 1984. Sm-Nd ages of the Arunta, Tennant Creek, andGeogetown Inliers of northern Australia. Aust. J. Earth Sci., 31: 39-60.

Botha, B.J.V. and Grobler, N.J.,1979. Models for the geotectonic evolution of the Middle to Late Precambrian Namaqua Mobile Belt in eastern Namaqualand, South Africa. Precambrian Research, 10: 21-41.

Boullier, A.M., and Gueguen, Y., 1975. SP-Mylonite: Origin of some mylonites by superplastic flow. Contrib. Mineral. Petrol. 50, 93-104.

Bowes, D.R., Halden, N.M. and Park, A.F., 1984. Structural features of basement snd cover rocks in the eastern Svecokarelides, Finland. In Kroner, A. and Greiling, R., eds. Precambrian Tectonics Illustrated, pp. 147-171.

Bowyer, D.G., 1982. Geology of part of the Harts Range, Northern Territory, Australia: Petrology, geochemistry and structure. Honours thesis, University of Adelaide. (unpublished)

Boyer, S.E. & Elliot, D., 1982. Thrust systems. AAPG Bul. 66, 1196-1230.

Buick, I.S., 1983. The geology, petrology and geochemistry of the Huckitta granodioritic gneiss and associated granitoids, Harts Range, central Australia. Honours thesis, University of Adelaide. (Unpublished)

Buick, I.S., 1985. The petrology of granitic rocks from the Entia Domal structure, Eastern Arunta Block. Msc. thesis (unpubl.), University of Adelaide.

Burke, K. and Dewey, J.F., 1973. An outline of Precambrian plate development. In Tarling, D.H. and Runcorn, S.K. eds, Implications of Continental Drift to the Earth Sciences, pp. 1035-1045. Academic Press, London.

Burke, K.,1980. Intracontinental rifts and aulacogens. In: Continental Tectonics, pp. 42-49. National Research Council, Geophysics Study Committe, Washington.

Butler, R.W.H., 1982. A structural analysis of the Moine Thrust Zone between Loch Eriboll and Foinaven, NW Scotland. Journal of Structural Geology, Vol.4, No.1, pp.19-29.

Butler, R.W.H., 1983. Balanced cross-sections and their implications for the deep structure of the northwest Alps. Journal of Structural Geology, Vol.5, No.2, pp.125-137.

Butler, R.W.H., 1987. Thrust sequences. J. Geol. Soc. Lond., 144, 619-634.

Chadwick, B. and Nutman, A.P.,1979. Archean structural evoluton in the northwest of the Buksefjorden, southern West Greenland. Precambrian Research, 9: 199-226.

Chappell, B.W. and White, A.J.R., 1974. Two contrasting granite types. Pacific Geology, 8: 173-174.

Choukroune, P.,Gapais, D. & Merie, O., 1987. Shear criteria and structural symmetry. Journal of Structural Geology, Vol. 9, No. 5/6, pp.525-530.

Cobbold, P.R. and Quinquis, H., 1978. Development of sheath folds in shear regimes. Journal of Structural Geology. Vol.2, No.1/2, pp. 119-126.

Cobbold, P.R. & Gapais, D., 1987. Shear criteria in rocks: an introductory review. Journal of Structural Geology, Vol. 9, No. 5/6, pp. 521-523.

Collerson, K., Oliver, R.L. & Rutland, R.W.R. An example of structural and metamorphic relationships in the Musgrave Orogenic Belt, central Australia. J. Geol. Soc. Aust. Vol. 18, Pt 4, pp. 379-393, plats 22-24.

Collins, W.J. & Teyssier, C., 1987. Crustal-scale ductile fault systems in the Arunta Inlier, central Australia. International Conference on Deformation of Crustal Rocks. Geol. Soc. Aust. Abstracts No. 19.

Cooper, J.A., Mortimer, G.E. and James, P.R. (in press.) Rate of Arunta Inlier evolution as indicated at the eastern margin of the Entia Dome, central Australia.

Cooper, M.A., Garton, M.R. and Hossack, J.R.,1983. The origin of the Basse Normandie duplex, Boulonnais, France. Journal of Structural Geology. Vol.5, No.2, 139-152.

Coward, M.P., 1983. Thrust tectonics, thin skinned or thick skinned, and the continuation of thrusts to deep in the crust. Journal of Structural Geology. Vol.5, No.2, 113-123.

Coward, M.P., 1984. Major shear zones in the Precambrian crust; examples from NW Scotland and southern Africa and their significance, in Kroner A. and Greiling, R., eds., Precambrian Tectonics Illustrated, pp.207-236.

Coward, M.P., James, P.R., Wright, L., 1976. Northern margin of the Limpopo mobile belt, southern Africa. Geol. Soc. America Bull., v.87, p.601-611.

Coward, M.P., 1973. Flat-lying structures within the Lewisian basement gneiss complex of NW Scotland. Proc. Geol. Assoc., 85: 459-472.

Davis, G.H. & Coney, P.J., 1979. Geological development of cordilleran metamorphic core complexes. Geology, 7: 120-124.

Davies, C.J. and Coward, M.P., 1982. The structural evolution of the Gariep Arc in Southern Namibia (South-west Africa). Precambrian Research, 17: 173-198.

Deer, W.A., Howie, R.A. and Zussman, J., 1966. An introductin to the rock-forming minerals. Longman Group Limited, London.

Dennis, J.G., 1972. Structural Geology, Ronald Press Co., New York, 532 pp.

de Sitter, L.U., 1964. Structural Geology, 2nd. ed., McGraw-Hill, New York, 551 pp.

Dewey, J.F. and Windley, B.F., 1981. Growth and differentiation of the continent crust. R. Soc. Lond., Phil. Trans., Ser. A 301: 189-206.

Dewey, J.F. and Bird, J.M. 1970. Moutain belts and the new global tectonics. Geophys. Resear., J. 75, 2625-2647.

Ding, P., James, P.R. and Lawrence, R.W., 1983. Structural evolution of the Harts Range Group, central Australia. Geol. Soc. Aust., Abstract Series 9: 67-68.

Ding, P. and James, P.R., 1985. Structural evolution of the Harts Range area and its implication for the developemnt of the Arunta Block, central Australia. Precambrian Research, 27: 251-176.

Ding, P. & James, P.R., 1987. The Harts Range Mobile Belt: A short-lived Proterozoic intraplate orogen from the eastern Arunta Inlier of central Australia. International Conference on Deformation of Crustal Rocks. Geol. Soc. Aust. Abstracts No. 19, p. 53.

Ding, P. & James, P.R.. Structural evolution of the Bunger Hills area of East Antarctica (in press).

Ding, P. & James, P.R.. Discussion on the paper by W.J. Collins & Teyssier, entitled: Crustal scale ductile fault system in the Arunta Inlier, central Australia (in press).

Duncan, I.J.,1984. Structural evolution of the Thor-Odin gneiss dome. Tectonophysics, 101: 87-130.

Elliott, D., 1983. The construction of balanced cross-sections. Journal of Structural Geology, Vol.5, No.2, p. 101.

Ellis, D.J. & Green, D.H., 1979. An experimental study of the effect of Ca exchange upon Garnet-clinopyroxene Fe-Mg exchange equilibria. Contrib. Mineral. Petrol. 71: 13-22.

Etheridge, M.A. and Wilkie, J.C., 1979. Grain size reduction, grain boundary sliding and the flow strength of mylonite. In: T.H. Bell and R.H. Vernon (editors), Microstructural Process during Deformation and Metamorphism. Tectonophysics, 58: 159-178.

Etheridge, M.A., 1987. The geometry and tectonic significance of transfer faults in continental extension terranes, Queensland. Geol. Soc. Aust. Abstracts No. 19, p. 78.

Faure, M.,1983. Eastward ductile shear during the early tectonic phase in the Sanbagawa Belt. Journal of the Geological Society of Japan, Vol.89, No.6, 319-329.

Faure, M., 1985. Microtectonic evidence for eastward ductile shear in the Jurassic orogen of SW Japan. Journal of Structural Geology, Vol.7, No.2, pp. 175 to 186.

Faure, M., 1985. The Pre-Cretaceous structure of the outer belt of southwest Japan. Tectonophysics, 113: 139-165.

Foden, J.D., Buick, I.S. and Mortimer, G.E. (in press). The petrology of granitic gneisses from the east Arunta Inlier, central Australia: implications for Proterozoic crustal development.

Ferry, J.M. and Spear, F.S., 1978. Experimental calibration of the partitioning of Fe and Mg between biotite and garnet. Contrib. Mineral. Petrol., 66: 113-117.

Flinn, D., 1965. On symmetry and the deformation ellipsoid. Geol. Mag. Vol. 102, No.1, p.34-45.

Forman, D.J., 1971. The Arltunga Nappe Complex, MacDonnell Range, Northern Territory, Australia. J. Geol. Soc. Aust. 18: 173-182.

Forman, D.J. and Shaw, R.D.,1973. Deformation of crust and mantle in central australia. Bur. Miner. Resour., Geol. Geophys. Aust., Bulletin 144.

Gastil, R.G., 1979. A conceptual hypothesis for the relation of differing tectonic terranes to plutonic emplacement. Geology, Vol.7, p. 542-544.

Ghosh, S.K. & Ramberg, H., 1975. Reversal of the spiral direction of inclusion trails in paratectonic porphyroblasts. Tectonophysics, 51: 83-97.

Goldman, D.S. and Albee, A.L., 1977. Correlation of Mg/Fe partitioning between garnet and biotite with O^{18}/O^{16} partitioning between quartz and magnetite. Am. J. Sci., 277: 750-767.

Gordon, M.B. & Hempton, M.R., 1986. Collision-induced rifting: the Grenville Orogeny and the Keweenawan rift of north America. Tectonophys., 127: 1-25.

Goscombe, B.D., 1984. The structure, metamorphism, petrology and geochemistry of the Paradise Well in the Harts Range, eastern Arunta Block. Honours thesis, University of Adelaide, (unpubl.)

Goscombe, B.D., 1987. Regional rotational shear accompanying high grade metamorphism in the east Strangeways Range, Arunta Block. International Conference on Deformation of Crustal Rocks. Geol. Soc. Aust. Abstracts No. 19, p. 58.

Graham, C.M., and Powell, R., 1984. A garnet-hornblende geothermometer: calibration, testing and application to the Pelona Schist, Southern California. J. Metamorphic Geol., 2: 13-31.

Grunsky,E.C., Robin, P.Y.F.and Schwerdtner, W.M., 1980.Orientation of feldspar porphyroclasts in mylonite samples from the southern Churchill Province, Canadian Shield. In: W.M. Schwerdtner, P.J. Huddleston and J.M. Dixon (Editors), Analytical Studies in Structural Geology. Tectonophysics, 66: 213-224.

Hancock, S.L. & Rutland, R.W.R., 1984. Tectonics of an Early Proterozoic geosuture: the Halls Creek Orogenic sub-province, Northern Australia. Journal of Geodynamics, 1: 387-432.

Harris, N.B.W. and Jataram, S., 1982. Metamorphism of cordierite gneisses from the Bangalore region of the Indian Archean. Lithos., 15: 89-98.

Heinrich, E.W., 1965. Microscopic identification of minerals. McGraw-Hill, 414 pp.

Henderson, J.R., 1981. Structural analysis of sheath folds with horizontal X-axes, northeast Canada. Journal of Structural Geology, Vol.3, No.3, pp. 203 to 210.

Higgins, M.W., 1971. Cataclastic Rocks. The United States Geological Survey Professional Paper 687, 97p.

Hills, E.S., 1972, 2nd. ed., Elements of Structural Geology, Wiley, New York, 502 pp.

Hobbs, B.E., Mclaren, A.C. & Paterson, M.S., 1972. Plastisity of single crystals of synthetic quartz. Geophys. Monogr. Ser., 16: 29-53.

Hobbs, B.E., Means, W.D. and Williams, P.F., 1976. An outline of structural geology. Wiley. 571 pp.

Hobbs, B.E., Archibald, N.J., Etheridge, M.A. and Wall, V.J., 1984. Tectonic history of the Broken Hill Block, Aystralia. In Kroner, A. and Greiling, R. eds, Precambrian Tectonics Illustrated. pp. 353-368.

Hodges, K.V., Bartley, J.M., and Burchfiel, B.C., 1982. Structural evolution of an A-type subduction zone, Lofoton-Rombak area, Northern Scandinavian Caledonides. Tectonics, Vol. 1, No. 5, pp.441-462.

Hollister, L.S. & Crawford, M.L., 1986. Melt-enhanced deformation: a major tectonic process. Geology 14: 558-561.

Hsu, K.J., 1984. Geosynclines in plate-tectonic settings: Sediments in mountains. In: Mountain building processes, edited by K.J. Hsu.

Hunter, D.R. and Pretorius, D.A., 1981. Southern Africa Structural Framework, in Hunter, D.R. ed., Precambrian of the Southern Hemisphere, Development in Precambrian Geology, Vol. 2, pp. 397-422. Elsevier, Amsterdam.

James, P.R., Ding, P., Lawrence, R.W., 1983. Precambrian stratigraphy and tectonics of the Harts Range Group, Arunta Complex, central Australia. Abstracts, International Symposium on Precambrian crustal Evolution, Beijing, China.

James, P.R., Ding, P., Lawrence, R.W., Martin, A.R., Rankin, L. and Scales, G.P.,1984. Tectonic evolution and fabric development of the Arunta Complex in the Harts Range area, central Australia. Abstracts, International Conference On Multiple Deformation and Foliation Development, Bermagui, Australia.

James, P.R., Ding, P. Rankin, L. and Scales, G., 1985. Displacement and strain within the nappe sequences of the Harts Range area, central Australia. Abstracts, International Conference On Tectonics and Geochemistry of Early to Middle Proterozoic Fold Belts, Darwin, Australia.

James, P.R. & Ding, P.,1987. An Early Middle Proterozoic short-lived extension-collision intraplate orogeny: the Strangways Orogeny of the eastern Arunta Inlier, central australia. International Conference on Deformation of Crustal Rocks. Geol. Sci. Aust. Abstracts No. 19.

James, P.R. & Ding, P., 1988. "Caterpillar Tectonics" in the Harts Range area: a kinship between two sequential Proterozoic orogenic belts within the eastern Arunta Inlier of central Australia. Precambrian Research, in press.

James, P.R., Ding, P. & Rankin, L.R., in press. Structural Geology of the early Precambrian gneisses of northern Fold Island, Mawson coast, Kemp Land, East Antarctica.

James, P.R., Macdonald, P. and Parker, M.D.,1987. Strain and displacement in the Bruna Gneiss at the western margin of the Entia Dome, Harts Range, central Australia. International Conference on Deformation of Crustal Rocks. Geol. Soc. Aust. Abstracts No. 19, p. 60.

James, P.R. & Tingey, 1983. The Precambrian geological evolution of the East Antarctic metamorphic shield - A review. In Oliver et al (eds): Antarctic Earth Science, Australian Academy of Science, Canberra, pp.5-10.

Jackson, M.P.A., 1984. Archaean structural atyles in the Ancient Gneiss Complex of Swaziland, South Africa, In Kroner, A. and Greiling, R. eds., Precambrian Tectonics Illustrated. pp. 1-18.

Jenkins, R.J.F., 1988. The Adelaide fold belt: tectonic reappraisal (in press).

Joklik, G.F., 1955. The geology and mica fields of the Harts Range, central Australia. Bureau of Mineral Resources, Australia, Bulletin 26.

Katz, M.B., 1981. Note on the layered anorthosite complex of the Harts Range ruby deposit in the Arunta Block, central Australia. Geol. Soc. Aust. J., 28: 247-248.

Kroner, A., 1977a. The Precambrian geotectonic evolution of Africa: Plate accretion versus plate destruction. Precambrian Research, 4: 163-213.

Kroner, A., 1977b. Precambrian mobile belts of southern and eastern Africa - ancient sutures or sites of ensialic mobility? A case for crustal evolution towards plate tectonics. Tectonophysics, Vol.40, p. 101-135.

Kroner, A., 1981b. Precambrian plate tectonics, in Kroner, A., ed., Precambrian plate tectonics. Elsevier, Amsterdam, p.57-90.

Kroner, A., 1983. Proterozoic mobile belts compatible with the plate tectonic concept. In: Proterozoic Geology, Geol. Soc. Amer. Mem. 161: pp. 59-74.

Lawrence, R.W., James, P.R. and Oliver, R.L., 1987. Relative timing of folding and metamorphism in the ruby mine area of Harts Range, central Australia. Aust. J. Earth Sci. 34: 293-309.

Lister, G.S. and Price G.P., 1978. Fabric development in a quartz-feldspar mylonite. Tectonophysics, 49: 37-78.

Lister,G.S., and Paterson, M.S.,1979. The simulation of fabric development during plastic deformation and its application to quartzite: fabric transitions. Journal of Structural Geology, Vol.1, No.2, 99-115.

Lister, G.S., and Williams, P.F., 1979. Fabric development in shear zones: theoretical contrals and observed phenomena. Journal of Structural Geology, Vol.1, No.4, 283-297.

Lister, G.S., 1981. The effect of basal-prism mechanism switch on fabric development during plastic deformation of quartzite. Journal of Structural Geology, Vol.3, No.1, pp. 67-75.

Lister, G.S. and Snoke, A.W., 1984. S-C mylonites. Journal of Structural Geology, Vol.6, No.6, pp. 617-638.

Lister, G.S., Etheridge, M.A. & Symonds, P.A., 1986. Detachment faulting and the evolution of passive continental margins. Geology, Vol. 14, p. 246-250.

Lister, G.S., Etheridge, M.A. & Symonds, P.A., 1987. Detachment Model for the formation of passive continental margins. Tectonics, in press. (also Geol. Soc. Aust. Abstracts, No. 19, p. 80.)

Liu, Y. & James, P.R., 1987. Ductile deformation of amphibole in the Florence Shear Zone, southern Harts Range, central Australia. Geol. Soc. Aust. Abstracts No. 19, p. 93.

Loosveld, Ramon J.H., 1987. A complex fold nappe within the Soldier Cap Group, Mount Isa Inlier, Queensland, Australia. Geol. Soc. Aust. Abstracts No 19, pp. 45-46.

Macdonald, P., 1986. The structural geology of the western margin of the Entia Dome, Harts Range, eastern Arunta Inlier. Honours thesis (unpubl.), University of Adelaide.

Mackenzie, D.P., 1978. Some remarks on the development of sedimentary basins. Earth Planet. Sci. Lett., 40: 25-32.

Marjoribanks, R.W. and Black, L.P., 1974. Geology and geochronology of the Arunta Complex, north of Ormiston, central Australia. Geol. Soc. Aust., J. 21: 291-299.

Marjoribanks, R.W., 1975. The structural and metamorphic geology of the Ormiston area, central australia. Aust. Bur. Miner. Resour., Geol. Geophys., Rec. 1975/13.

Marjoribanks, R.W., 1976. The relation between macrofabric and strain in a progressively deformed quartzite sequence from central Australia. Tectonophysics, 32: 269-293.

Martin, A., 1983. The geology and structural geology of the Harts Range Group on the east flank of the Entia Dome, eastern Arunta Block, Northern Territory. Honours thesis, University of Adelaide. (unpublished)

Mattauer, M., 1981. Transverse lineation and large-scale structures related to Alpine obductin in Corsica. Journal of Structural Geology, Vol.3, No.4, pp. 401-409.

McClay, K.R. & Way, N., 1986. Balanced geological cross-sections. Short course notes, pp.113.

Mawer, C.K., 1986. What is mylonite? Geoscience Canada, Vol.13, No.1.

Mawer, C.K., 1987. Shear criteria in the Grenville Province, Ontario, Canada. Journal of Structural Geology, Vol. 9, No. 5/6, pp. 531-539.

Milnes, A.R., Compston, W. & Daily, B. 1977. Pre- to syn-tectonic emplacement of early Palaeozoic granites in southern South Australia. J. Geol. Soc. Aust. Vol. 24, Pt 1, pp.87-107.

Miyashiro, A., 1973. Metamorphism and metamorphic belts. George Allen & Unwin.

Mortimer, G.E., Copper, J.A. & James, P.R., 1986. Geochronological studies in the eastern Entia Dome, Arunta Inlier. Geol. Soc. Aust. 8th A.G.C. Abstracts, 15: 48-49.

Mortimer, G.E., Cooper, J.A. & James, P.R., 1987. U-Pb and Rb-Sr geochronology and geological evolution of the Harts Range ruby mine area of the Arunta Inlier, central Australia. Lithos, 20 (1987) 445-467.

Myers, J.S., 1978. Formation of banded gneisses by deformation of igneous rocks. Precambrian Research, 6: 43-64.

Myers, J.S., 1981. The Fiskenaesset Anorthosite Complex - a stratigraphic key to tectonic evolution of the west Greenland gneiss complex 3000-2800 M.Y. ago. Spec. Publs geol. Soc. Aust., 7: 351-360.

Myers, J.S., 1984a. Archaean tectonics in the Fiskenaesset region of southwest Greenland. In Kroner, A. and Greiling, R. eds., Precambrian Tectonics Illustrated. pp. 95-112.

Myers, J.S., 1984b. The Nagssugtoqidian mobile belt of Greenland. In Kroner, A. and Greiling, R. eds., Precambrian Tectonics Illustrated. pp. 237-250.

Nutman, A.P., 1984. Early Archaean crustal evolution of the Isukasia area, southern West Greenland. In Kroner, A. and Greiling, R. eds., Precambrian Tectonics Illustrated. pp. 79-94.

Nykiel, A.J., 1986. The geology, petrology and geochemistry of the area north of Spriggs Creek Bore, Western margin of the Entia Dome, Harts Range, eastern Arunta Block, Northern Territory. Honours thesis, University of Adelaide, unpublished.

Oliver, R.L., Foden, J.D. and Sullivan, S.J., 1986. Metamorphism and melting in the eastern Harts Range, Northern Territory. Abstrtacts, number 15, p.216, Geol. Soc. Aust, Eighth Australian Geological convention.

Oliver, R.L., Lawrence, R.W., Goscombe, B.D., Ding, P., Sivell, W.J., and Bowyer, D.G., 1988. Metamorphism and crustal considerations in the Harts Range and neighbouring regions, Arunta Inlier, Central Australia. Precambrian, in press.

Oxburgh, E.R., 1984. Heterogenous lithospheric stretching in early history of orogenic belts. In Hsu, K.J. (ed.): Mountain building process.

Page, R.W., 1976. Reinterpretation of isotopic ages from the Halls Creek Mobile Zone, northwest Australia. BMR J. Aust. Geol. Geophys., 1: 79-81.

Park, R.G., 1980. Origin of horizontal structure in high-grade Archaean Terrains. In Glover, J.E. and Groves, D.I. (eds.): Archaean Geology, 2nd international Symposium, Perth.

Park, R.G., 1981. Shear-zone deformation and bulk strain in granite-greenstone terrain of the western Superior Province, Canada. Precambrian Research, 14: 31-47.

Parker, M.D., 1986. A structural and lithological investigation of the southern Mt Bruna area, with special reference to the Bruna Gneiss, western Entia Dome, Harts Range, central Australia. Honours thesis (unpubl.), University of Adelaide.

Passchier, C.W., 1983. The reliability of asymmetric c-axis fabric of quartz to determine sense of vorticity. Tectonophysics, 99: T9-T18.

Perchuk, L.L., 1967. Biotite-garnet geothermometer. Dokl. Akad. Nauh. SSSR., 177: 199-213.

Platt, J.P. and Lister, G.S., 1985. Structural history of high-pressure metamorphic rock in the southern Vanoise massif, French Alps, and their relation to Alpine tectonic events. Journal of Structural Geology, Vol.7, No.1, pp. 19-35.

Platt, J.P. and Lister, G.S., 1985. Structural evolution of a nappe complex, southern Vanoise massif, French Penninic Alps. Journal of Structural Geology, Vol.7, No.2, pp. 145-160.

Plumb, K.A.,1979a. Structure and tectonic style of the Precambrian shields and platforms of northern Australia. Tectonophysics, 58: 291-325.

Plumb, K.A., 1979b. The tectonic evolution of Australia. Earth Sci. Rev., 14: 205-249.

Plumb, K.A., Derrick, G.M., Needham, R.S. and Shaw, R.D.,1981. The Proterozoic of northern Australia. In: Precambrian of the Southern Hemisphere, edited by Hunter, D.R., 205-307. Elsevier Scientific Publishing Company, Amsterdam.

Plumb, K.A. & James, H.L., 1986. Subdivision of Precambrian time: recommendations and suggestions by the subcommission on Precambrian stratigraphy. Precambrian Research, 32: 65-92.

Preiss, W.V. (compiler), 1987. The Adelaide Geosyncline, Bulletin 53, Geological Survey of South Australia. pp.438.

Price, R.A., 1981. The Cordilleran foreland fold and thrust belt in the southern Canadian Rocky Mountains. In McClay, K.R. & Price, N.J. (eds.): Thrust and Nappe tectonics. Geol. Soc. Lond. sp. pub., No.9, 427-448.

Ramsay, J.G., 1967. Folding and Fracturing of rocks, 568 pp.. McGraw Hill Book Company.

Ramsay, J.G., 1980. Shear zone geometry: a review. Journal of Structural Geology, Vol.2, No.1/2, pp.83-99.

Ramsay, J.G., 1983. The techniques of modern structural geology, 307 pp.. Academic Press.

Ramsay, J.G., 1984. Rock ductility and its influenc on the development of tectonic structures in mountain belts. In: Mountain Building Process, edited by K.J. Hsu.

Rankin, L., 1983. The structural geology and fabric development in the Mt. Mabel area of the Harts Range, eastern Arunta Block. Honours thesis, University of Adelaide. (unpublished)

Ross, J.V., 1973. Mylonitic rocks and flattened garnets in the southern Okanagan of British Columbia. Canadian Jouenal of Earth Sciences, Vol.10, No.1, pp. 1-17.

Rutland, R.W.R., 1973a. The tectonic Map of Australia and New Guinea in the context of tectonic history. Geol. Soc. Aust., Tect. Struct. Newsl. 2: 47-52.

Rutland, R.W.R., 1973b. Tectonic evolution of the continental crust of Australia. In Tarling, D.H. and Runcorn, S.K. eds., Implications of continental drift to the Earth sciences. Vol.2, pp. 1011-1033. Academic Press, London.

Rutland, R.W.R., 1976. Orogenic evolution of Australia. Earth. Sci. Rev., 12: 161-169.

Rutland, R.W.R., 1981. Structural framework of the Australian Precambrian. In D.R. Hunter (ed.): Precambrian of the Southern Hemisphere, Elsevier, Amsterdam, pp. 1-32.

Sanderson, D.J., 1973. The development of fold axes oblique to the regional trend. Tectonophysics, 15: 55-70.

Sandford, M. & Powell, R., 1986. Deep crustal metamorphism during continental extension: modern and ancient examples. Earth and Planet Sci. Lett., 79: 151-158.

Sandford, M., 1985. The metamorphic evolution of granulites at Fyfe Hills; implications for Archaean crustal thickness in Enderby Land, Antarctica. J. Metamorphic Geol. 1985, 3, 155-178.

Sando, B.G., 1987. The geology, petrology & geochemistry of the Tommys Gap area in the Giles Creek Synform, Macdonnel Range, southeastern Arunta Block, Northern Territory. Honours thesis, University of Adelaide, unpublished.

Schwerdtner, W.M., 1984. Archaean gneiss domes in the Wabigoon subprovince of the Canadian Shield, northwestern Ontario. In Kroner, A. and Greiling, R. eds., Precambrian Tectonics Illustrated. pp. 129-134.

Shaw, R.D. and Stewart, A.J., 1975a. Towards a stratigraphy of the Arunta Block. Geol. Soc. Aust., 1st Aust. Geol. Conv., Abstr., p. 35.

Shaw, R.D. and Stewart, A.J., 1975b. Arunta Block - regional geology. In Knight, C.L. ed., Economic Geology of Australia and Papua New Guinea. Australas. Inst. Min. Metall., Monogr., No.5, pp. 437-445.

Shaw, R.D., 1979. Basement evolution and mineral potential of Alice Springs region. 8th BMR Symp., Abstr., P. 19 (also as Aust., Bur. Miner. Resour., Geol. Geophys., Rec. 1979/13)

Shaw, R.D., Langworthy, A.P., Offe, L.A., Stewart, A.J., Allen, A.R., Senior, B.R. and Clarke, D.B., 1979. Geological report on 1:250 000 scale mapping of southeastern Arunta Block, Northern Territory. Aust., Mur. Miner. Resour., Geol. Geophys. Rec. 1979/47: BMR Microform MF 133.

Shaw, R.D., Freeman, M.J., Offe, L.A. and Senior, B.R., 1982. Geology of the Illogwa Creek 1:250 000 Sheet area, central Australia - preliminary data, 1979-80 survey. Aust., Bur. Miner. Resour., Geol. Geophys. Rec. 1982/23.

Shaw, R.D. and Wells, A., 1983. Alice Springs, Northern Territory (second edition). 1:250 000 Geological Series - Explanatory Notes. Bur. miner. Resour., Geol. Geophys.

Shaw, R.D. and Freeman, M.J., 1985. Illogwa Creek, Northern Territory (second edition). 1:250 000 Geological Series - Explanatory Notes. Bur. miner. Resour., Geol. Geophys.

Shaw, R.D. and Langworthy, A.P., 1984. Strangways Range region, Northern Territory. Aust., Bur. Miner. Resour., Geol. Geophys., 1:100 000 Map Commentary.

Shaw, R.D., Stewart, A.J. and Black, L.P., 1984. The Arunta Inlier: a complex ensialic mobile belt in central Australia. Part 2: tectonic history. Aust. J. Earth Sci., 31: 457-484.

Shaw, R.D., Stewart, A.J. and Rickard, M.J., 1984. 1:100 000 geological map commentary: Arltunga-Harts Range region, Northern Territory. Bureau of Mineral Resources, Geology and Geophysics, Australia.

Sibson, R.H., 1986. Earthquakes and rock deformation in crustal fault zones. Ann. Rev. Earth Planet, Sci. 1986, 14: 149-175.

Simpson, C. & Schmidt, S.M., 1983. An evaluation of criteria to deduce the sense of movement in sheared rocks. Bull. Geol. Soc. Am. 94: 1281-1288.

Sivell, W.J. and Foden, J.D., 1985. Banded amphibolites of the Harts Range metaigneous complex, central Australia: a bimodal basalt tonalite suite. Precambrian Research 28: 223-252.

Sivell, W.J., Foden, J.D., Lawrence, R.W., 1985. The Entire Anorthositic gneiss, eastern Arunta Inlier, central Australia: geochemistry and petrogenesis. Australia Journal of Earth Sciences. Aust. J. Earth Sci. 32: (in press).

Sivell, W.J., 1986. A basaltic-ferrobasaltic granulite association, Oonagalabi gneiss complex, central Australia: magmatic variation in an Early Proterozoic rift. Contrib. Mineral. Petrol.,

93: 381-394.

Sivell, W.J., (in press). Geochemistry of mafic - ultramafic associations from the Harts Range, Central Australia: Implications for mantle source heterogenity in a Proterozoic mobile belt.

Sivell, W.J. & Foden, J. (in press). Amphibolites from the Entia gneiss complex, Eastern Arunta Inlier: Geochemical evidence for a Proterozoic transition from extensional to compressional tectonics.

Spry, A., 1969. Metamorphic textures. Pergamon Press, Oxford. 350 pp.

Stauffer, M.R.,1970. Deformation textures in tectonites. Candian Journal of Earth Sciences, Vol.7, pp.498-511.

Stewart, A.J., 1967. An interpretation of the structure of the Blatherskite Nappe, Alice Springs, Northern Territory. J. Geol. Soc. Aust. 14: 179-185.

Stewart, A.J., Shaw, R.D. and Black, L.P.,1984. The Arunta Inlier: a complex ensialic mobile belt in central Australia. Part 1: stratigraphy, correlations and origin. Aust. J. Earth Sci., 31: 445-455.

Stewart, A.J. & Oaks, R.Q., 1987. Nappes in the northeastern Amadeus Basin, Northern Territory. International Conference on Deformation of Crustal Rocks. Geol. Sci. Aust. Abstract No. 19, p.51.

Stewart, K.P., 1985. The petrological significance of calc-silicate and associated gneisses, Inkamulla Bore area, Entia Dome, Harts Range, eastern Arunta Block. Honours thesis, University of Adelaide. (unpublished)

Sullivan, S.J., 1985. A detailed geological investigation of the Entia Gneiss and leucocratic gneiss intrusive, northern Entia Dome, Harts Range, eastern Arunta Block. Honours thesis, University of Adelaide. (unpublished)

Tectonic Map of Australia and New Guinea, Aust. Geol. Soc.,1971.

Teyssier, C., 1985. A crustal thrust system in an intracratonic enviroment. Journal of Structural Geology, Vol.7, No.6, pp. 689-700.

Thiessen, R.L. and Means, W.D.,1980. Classification of fold interference patterns: a reexamination. Journal of Structural Geology, Vol.2, No.3, pp.311-316.

Thompson, A.B., 1976. Mineral reactions in pelitic rocks: II calculation of some P-T-X (Fe-Mg) phase relations. Am. J. Sci., 276: 425-454.

Townsend, C., Roberts, D., Rice, A.H.N. and Gayer, R.A., 1986. The Gaissa Nappe, Finnmark, North Norway: an example of deeply eroded external imbricate zone within the Scandinavian Caledonides. Journal of Structural geology, Vol.8, Nos. 3/4, pp.431 to 440.

Tullis, J., Christie, J.M. and Gripps, D.T., 1973. Microstructures

and preferred orientations of experimentally deformed quartzites. Geol. Soc. Am. Bull. 84: 297-314.

Tullis, J., 1977. Preferred orientation of quartz produced by slip during plane strain. Tectonophysics, Vol. 39, pp. 87-102.

Tullis, J., Snoke, A.W., Todd, V.R.,1982. Significance and petrogenesis of mylonitic rocks. Penrose Conference Report.

Turner, F.J. and Weiss, L.E., 1963. Structural analysis of metamorphic tectonites, McGraw-Hill Book Company, Inc..

Turner, F.J., 1981. Metamorphic petrology; mineralogical and field aspects. 2nd. ed. McGraw-Hill Book Company, New York.

Vauchez, A., 1980. Ribbon texture and deformation mechanisms of quartz in a mylonitized granite of Great Kabylia (Algeria). Tectonophysics, 67: 1-12.

Vernon R.H., 1974. Controls of mylonitic compositional layering during non-cataclastic deformation. Geol. Mag. 111 (2), pp.121-123.

Vernon, R.H., 1975. Metamorphic Process, Murby, London, 247 pp.

Vernon, R.H., 1986. K-feldspar megacrysts in granites - phanocrysts, not porphyroblasts. Earth Sci. Rev. 23, 1-63.

Villeneuve, M. & Dallmeyer, R.D., 1987. Geodynamic evolution of the Mauritanide Bassaride, and Pokelide Orogens (West Africa). Precambrian Research Vol.37: No.1 pp. 19-28.

Wakefield, J.,1977. Mylonitizatin in the Lethakane shear zone, eastern Botswana. Journal of Geology, Soc. Lond. Vol.133, pp263-275.

Warren, R.G., 1979. Volcanogenic and sedimentary origins to sapphirine-bearing rocks in the Arunta Block, central Australia. Nature 278: 159-161.

Warren, R.G., 1982. Tectonic setting of the easternmost Arunta Block. Aust., Bur. Miner. Resour., Geol. Geophys. Rep. 221.

Warren, R.G., 1983. Granulite and the tectonic evolution of the Arunta Block. Geol. Soc. Aust., 6th. Aust. Geol. Conv., Abstr. Ser. 9, pp 69-70.

Warren, R.G., 1983. Metamorphic and tectonic evolution of granulites, Arunta Block, central Australia. Nature., 305, no. 5932: 300-303.

Watkinson, A.J., 1981. Patterns of fold interference: influence of early fold shapes. Journal of Geology, Vol.3, No.1, pp.19-23.

Wells, P.R.A., 1977. Pyroxene thermetry in simple and complex systems. Contrib. Mineral. Petrol., 62: 129-139.

Wernicke, B., 1981. Low-angle normal faults in the Basin and Range Province - nappe tectonics in an extending orogen. Nature 291:

645-648.

Wernicke, B. and Burchfiel, B.C., 1982. Modes of extensional tectonics. J. Struct. Geol., Vol.4, No.2, 105-115.

Wernicke, B., 1985. Uniform-sense normal simple shear of the continental lithosphere. Can. Earth Sci., 22: 108-125.

White, S.H., Burrows, S.E., Carreras, J., Shaw, N.D. and Humphreys, F.J., 1980. On mylonites in ductile shear zones. Journal of Structural Geology, Vol.2, No.1/2, pp.175-187.

White, S., 1982. Fault rocks of the Moine Thrust Zone: a guide of their nomenclature. Textures and Microstructures, Vol.4, pp.211-221.

White, S.H., Evans, D.J. and Zhong, D.L., 1982. Fault rocks of the Moine Thrust Zone: microstructures and textures of selected mylonites. Textures and microstructures, Vol.5, pp.33-61.

White, J.C. and White, S.H., 1983. Semi-ductile deformation within the Alpine fault zone, New Zealand. Journal of Geology, Vol.5, No.6, pp.579-589.

Williams, H., Turner, F.J. & Gilbert, C.M., 1982. Petrography, 2nd ed., Freeman, San Francisco.

Wilson, C.J.L., 1975. Preferred orientation in quartz ribbon mylonites. Geol. Soc. Amer. Bull., Vol. 86, pp. 968-974.

Windley, B.F., 1977. The evolving Continents. Wiley, London, 385 pp.

Windley, B.F., 1983. A tectonic review of the Proterozoic. In: Proterozoic Geology: Selected Papers From An International Proterozoic Symposium. pp. 1-10. Published by The Geological Society of America. Inc.

Winkler, H.J.F., 1979. Petrogenesis of Metamorphic Rocks (fifth edition), Springer Verlag.

Witschard, F., 1984. The geological and tectonic evolution of the Precambrian of northern Sweden - A case for basement reactivation? Precambrian Research, 23: 273-315.

Wood, B.J. and Banno, S., 1973. Garnet-orthopyroxene and orthopyroxene-clinopyroxene relationships in simple and complex systems. Contrib. Mineral. Petrol., 42: 109-124.

Wynne-Edwards, H.R., 1963. Flow folding. Am. Jour. Sci., V. 261, pp. 793-814.

Wynne-Edwards, H.R., 1976. Proterozoic ensialic orogenesis: the millipede model of ductile plate tectonics. Amer. J. Sci., 276: 927-953.

Yar Khan, M. 1972. The structure and microfabric of a part of the Arltunga Nappe Complex, central Australia. PhD thesis, Australia National University, Camberra (unpublished).

APPENDIX I

MODAL COMPOSITIONS OF ALL SAMPLES COLLECTED FROM THE HARTS RANGE AREA

1. Introduction

Modal compositions of all samples collected from the Harts Range area are documented in this appendix on the basis of the whole area irrespective of age or subarea. The aim of this appendix is to present some of the information which has not been described in detail within the text of the thesis, but may be useful for further study and any interested reader. It is not exhaustive in terms of petrology, for example the deformational structures are not considered with the classification. On the basis of composition, rocks in this area are grouped into two major parts: (1) meta-igneous rocks and migmatitic gneisses, which have similar modal compositions to igneous rocks; (2) metasediments, which have similar mineralogical compositions to sedimentary rocks.

The meta-igneous rocks and migmatitic gneisses will be presented in three groups, i.e. ultramafic rocks, mafic rocks and acidic to intermediate gneisses. The metasediments will be presented in four groups, i.e. psammitic, pelitic to semi-pelitic, calcareous and calc-silicate rocks.

About 400 thin sections have been studied under the optical microscope and 75 polished thin sections have been studied using the electron microprobe.

The abbreviations of minerals used in this appendix are listed in Table I-1. Modal compositions are presented by percentages (%) which are omitted in the Tables hereafter.

Table I-1 ABBREVIATIONS OF MINERAL NAMES

Aln	allenite	Gar	garnet	Qt	quartz
Apt	apatite	Hrn	hornblende	Rut	rutile
Atp	antiperthite	Hyp	hyperthene	Sal	salite
Amp	colourless amphybole	Ksp	K-feldspar	Scp	scapolite
Bio	biotite	Kyn	kyanite	Sil	sillimanite
Chl	chlorite	Mus	muscovite	Sph	sphene
Clc	calcite	Mic	microcline	Spn	spinel
Cpx	clinopyroxene	Olv	olivine	Trm	tremolite
Cum	cummingtonite	Opa	opaque	Tum	tourmaline
Czt	clinozoisite	Opx	orthopyroxene	Zir	zircon
Dio	diopside	Plg	plagioclase		
Epd	epidote	Pth	perthite		

2. Ultramafic rocks

Ultramafic rocks consist of mafic minerals only, thus quartz and feldspar are usually absent. Twelve thin sections of ultramafic rocks have been studied and their modal compositions are listed in Table I-2.

Table I-2 MODAL COMPOSITIONS (%) OF ULTRAMAFIC ROCKS

sample No.	Olv	Opx	Cpx	Cum	Chl	Gar	Spn	Opa	Hrn	Epd	Qt	Plg	Trm	Mus
3083	10			85	4			1						
3086	10	50		37	tr		2	1						
3904			90						8		2			
3094A				89	10			1						
3245				30	68		tr	2						
3369				90						10				
4016b		tr			4				95	tr				
4051				40	10				50					
4052				19					80		1			
4067			1						98			1		
4317		7	10	70	tr	10	3							
4509		tr			50								50	
4510					tr				97	1	1			<1

Note: "tr" represents trace amount.

3. Mafic rocks

Mafic rocks are assigned into three subgroups, i.e. metagabbros (including dolerite), mafic granulites and amphibolites.

3.1 Metagabbros

Twenty thin sections of metagabbros have been studied and their modal compositions are listed in TABLE I-3. The modal compositions of one dolerite sample is listed in Table I-3A.

Table I-3 MODAL COMPOSITIONS OF METAGABBROS

sample No.	Plg	Olv	Opx	Cpx	Amp	Hrn	Bio	Gar	Opa	Chl	Epd	Scp	Sph	Rut
3032B	50		13	13		22			2					
3069	50		10	9		30			1			1		
3096	40		10	5		38	5		1			1		
3096A	49				40	5	5		1					
3098	52					30			1	10	5		1	1
3165	50		20	20		10			tr					
3257	50	1	16	10		13		5	5					
3364	50		15	15		15		5						
3366	50		15	20		1	3	10	tr					tr
3385A	50		5	40		3	2		tr					
3385B	50		5	30		15								
3385c	25					74	tr			1				
3388E	50		20	20		5	5		tr					
3388	50			2		30	5	5	8					
3747	50		18	19		10	2		1					
3888	50		15	18		15			2					
4015	40		10	20		25	tr	4						
4447	50	2	7	20		20								
4516D	50		16	20		10	1	2	1					
P2-5	50		tr	30		15			5					

Note: in this Table the Plg is mainly labradorite (An52 to An70, containing 52-70% anorthite component), except in sample 3165 where the Plg is bytownite (An80). The Opx varies from brownzite to hypersthene, and the Cpx varies from salite to augite.

Table I-3A MODAL COMPOSITIONS OF DOLERITE

sample No.	Plg	Opx	Cpx	Hrn	Bio	Opa
3024	35	10	40	3	10	2

3.2 Mafic granulites

Mafic granulites were found only within the SOB. The general term mafic granulite used here includes typical mafic granulites and some amphibolites which were derived by deformation and retrogression from original mafic granulites but still contain certain amount of granulite relicts. Typical mafic granulite shows equigranular texture, whereas most of the mafic granulites within the Florence/Leaky Shear Zone have been mylonitized. The porphyro-

clasts are about 1-3 mm in size, while the matrix are only 0.05-0.2 mm. The proportions of porphyroclastic minerals vary from 1% to 80%, as listed in Table I-4.

Table I-4 PROPORTIONS (%) OF PORPHYROCLASTS IN MYLONITIZED MAFIC GRANULITES

sample No.	proportion (%) of porphyroclast	sample No.	proportion (%) of porphyroclast
P3-7	5	P3-8	0
P3-9	1	3379A	10
3645	20	3715	0
3729	50	3791	5
4008	15	4061	50
4067	50	4100B	50
4116A	1	4116B	20
4117	80	4162	10
4162A	5	4293	85

Twenty four thin sections of mafic granulites have been studied and their modal compositions are listed in Table I-5.

Table I-5 MODAL COMPOSITIONS OF MAFIC GRANULITES

sample No.	Plg	Opx	Cpx	Hrn	Bio	Gar	Opa	Scp	Qt
3105A	55	20	10	10	4		1		
3379A	50	15	15	10	3	5	2		
3615	50	10	20	18			2		
3645	40	5	8	20		12			10
3715	45	10	10	29			1	5	
3729	50	20	20	9			1		
3791	50	1	3	40		5	1		
3793	50	10	14	25			1		
3890-1	50	10	12	25	3		tr		
3894	50	15	14	20			1		
4008	40	10	10	5	1	30	4		
4061	50	10	20	10		10	tr		
4067	50	15	3	10		20	2		
4100B	45	15	30	2	3		5		
4107	60	5	15	20					
4116A	50	20	25	4			1		
4116B	50	15	13	20			2		
4117	50	10	8	30			2		
4162A	50	15	13	15	5		2		
4293	50	10	9	30			1		1
P3-7	40	15	15	29	1		tr		
P3-8	20	10	5	58	5		2		
P3-9	40	tr	16	40	2		tr		1

Note: in this Table the Plg is labradorite (An45 to An71); the Opx is hypersthene; the Cpx is salite, and the opaques are ilmenite and magnetite.

3.3 Amphibolites

Amphibolites consist of essential hornblende and andesine plagioclase with different amount of garnet, clinopyroxene, biotite, epidote, scapolite and quartz. Accessory minerals are mainly iron oxide, sphene, with occasional apatite, rutile and zircon. Sixty six thin sections of amphibolites have been studied. There are eighteen rock types of amphibolites which have different mineral assemblages, of which the average modal compositions are listed in Table I-6.

Table I-6 AVERAGE MODAL COMPOSITIONS OF EACH AMPHIBOLITE ROCK TYPE

rock type	number of samples	Plg	Hrn	Cpx	Gar	Bio	Qt	Epd	Czt	Scp	Ath	Cum?	Opa	Sph
1	16	36	54	9									1	
2	1	35	49	1			5						10	
3	1	50	20	10				20						
4	1	40	30	5			10		15					
5	1	30	58	2						8				2
6	2	33	42	13	12								tr	tr
7	2	35	51	7	5	2							tr	
8	2	54	20	2	10		5						9	
9	3	30	64	5									1	
10	17	36	64										tr	tr
11	3	44	49				6							1
12	2	30	48			8	4						tr	
13	7	39	54			5							1	1
14	1	65	30							5			tr	
15	2	26	44					30						tr
16	2	35	55				3		7				tr	
17	1	58	20				10				10		2	
18	1	28										70	2	

Modal compositions of all amphibolite samples are listed in Table I-7.

Table I-7 MODAL COMPOSITIONS OF AMPHIBOLITES

rock type	sample number	Plg	Hrn	Cpx	Gar	Bio	Qt	Epd	Czt	Scp	Ath	Cum?	Opa	Sph
(1)	3339	25	70	5										tr
	3700	50	40	10									tr	
	3785a	50	20	30										
	3785/1	30	50	20										
(1)	3785/b	38	59	2										1
	3839	38	60	2										
	3905	40	60	tr		tr								
	4029A	50	14	35										
	4029B	55	20	25										
	4030	18	80	2										
	4038	9	90	1										
	4436-5	32	65	tr									tr	tr
	4482	30	65	5				tr						tr
	4539	30	65	5										tr
	P1-2C	40	55	5		tr							tr	tr
	P2-7A	46	50	3			tr	tr					1	tr
	4493	49	45	5									1	
(2)	3792	35	49	1			5						10	
(3)	4029C	50	20	10				20						
(4)	4604	40	30	5			10		15					
(5)	3202	30	58	2						8				2
(6)	3205	25	65	5	3									1
	4428	40	18	20	20	tr							1	
(7)	P3-10	45	35	10	7	2							tr	
	3538	25	66	4	3	2								
(8)	4436-3	55	20	2	10		5						8	
	3641	54	20	1	10		5						10	
(9)	3380	30	57		10	3							tr	
	3217	30	63		4								1	
	3604	28	70		tr								2	
(10)	3085	20	78										2	tr
	3086	23	75											
	3105B	18	80											
	3119	18	80										2	
	3123	19	80										1	tr
	3132	49	50											1
	3193	49	50											1
	3219	30	70										tr	
	3287	23	75			tr							2	tr
	3780B	20	80											tr
	3786	40	59										tr	
	3787	44	55										1	
	3788	40	58									2	tr	
	4016	70	30			tr								
	4016A	60	40										tr	

TABLE I-7 continued

		Plg	Hrn	Cpx	Gar	Bio	Qt	Epd	Czt	Scp	Ath	Cum?	Opa	Sph
	4106	45	50										5	tr
	4428-1	35	65										tr	tr
(11)	4525	50	38			tr	10							1
	4557	34	50				5							1
	P1-1	48	50	tr			2							tr
(12)	P2-1A	25	60			10	5					tr	tr	
	3735	35	35		tr	5	3						tr	
(13)	3388G	30	65			5							tr	tr
	4048	60	25			10							5	
	4420-4	30	69			1							tr	
	4420-1a	41	50			4							tr	tr
	4420-1b	31	60			4							5	tr
	4529	40	50			10								
	4623	39	60			1							tr	
(14)	4436-1	65	30			tr			tr	5			tr	
(15)	3230A	33	28					39						
	4065	19	60					20						tr
(16)	P1-10A	39	50			tr	5	tr	5				tr	
	3038a	30	60				tr		10					
(17)	P2-1B	58	20			tr	10				10		2	
(18)	3084	28				tr						70	2	

The eighteen amphibolite rock types are not evenly distributed over the whole area, as can be seen in Table I-8.

TABLE I-8 SPACE DISTRIBUTION OF THE AMPHIBOLITE SAMPLES

	HOB	SOB			
Rock type	ISA	Entia Dome	Oonagalabi Tongue	Florence shear zone	Hale River Region
(1)	P1-2C	4029a	3893		
	P2-7A	4029b	3905		
	3339	4030			
	3700	4038			
	3785a	4436-5			
	3785/1	4482			
	3785b	4539			
(2)			3792		
(3)		4029C			
(4)		4604			

TABLE I-8 continued

	HOB		SOB			
rock type	ISA		Entia Dome	Oonagalabi Tongue	Florence shear zone	Hale River Region
(5)	3202					
(6)	3205		4428			
(7)					3538 P3-1	
(8)			4436-3			
(9)	3217 3604				3380	
(10)	3085 3086 3119 3123 3132 3193 3219 3287	3219 3287 3780B 3786 3787 3788 4106	4428-1			3105B 4106 4106A
(11)	P1-1		4525 4557			
(12)			P2-1	3735		
(13)			4420-1a 4420-1b 4420-4 4529 4623			4048
(14)			4436-1			
(15)						3230A 4065
(16)						P1-10A 3038A
(17)			P2-1B			
(18)	3084					

Most of the amphibolite varieties are found in the ISA of the HOB and the Entia Dome of the SOB. None of the 18 types of amphibolite is ubiquitously distributed throughout the whole area.

4. Acidic to intermediate gneiss

Gneisses of similar mineralogical composition to the acidic to intermediate igneous rocks will be assigned into this group, which includes three subgroups: acid to intermediate hypersthene bearing charnockitic gneiss; tonalitic to dioritic gneiss; and granitic gneiss.

4.1 Acid to intermediate hypersthene bearing charnockitic gneiss

Hypersthene bearing charnockitic gneiss exists in the SOB basement only. Most samples were collected within the Florence/Leaky Shear Zone, the others were found within the Hale River Region and the Pannikan Dam area of the Oonagalabi Tongue. It consists of mainly quartz, perthitic feldspar, hypersthene, salite, hornblende, biotite and garnet. Accessory minerals are zircon, apatite and opaque minerals. Twelve samples have been studied under the microscope and most of these samples have also been studied using the electron microprobe. Their modal compositions are listed in TABLE I-9.

TABLE I-9 MODAL COMPOSITION OF CHARNOCKITIC GNEISS

domain	sample number	mineral proportion (%) Qt	Plg	Atp	Pth	Ksp	Hyp	Cpx	Hrn	Bio	Gar	Opa
Floren ɔ / Leaky Shear Zone	3368	20	43				6	3	3	5	20	
	3379	13	10	12	20		tr	tr	10	12	20	tr
	3379A	10	10	40			5	5	3	3	20	3
	4001	10	40	20			5	3	8	5	5	4
	4001A	10	tr	60			2	2	5	5	15	1
	4001B	10	tr	60			2	2	5	5	15	1
	4516C	10	63				10	5	10			2
Hale River Region	3388	20	20	10	20		tr	5	7	18		tr
	4100A	40	37				2	2	2	1	16	
	4101	20		74			2			tr	1	tr
	4107A	20	10	65			5			tr		
Oonagalabi Tongue	4288	20	40			10	7	10	2	10		tr

4.2 Tonalitic to dioritic gneisses

The tonalitic to dioritic gneisses consist of mainly andesine plagioclase, quartz and some of the ferromagnesian/mafic minerals, such as, hornblende, biotite, garnet and epidote etc.. Accessory minerals are zircon, apatite, sphene and opaques. Tourmaline and rutile are rare. K-feldspar is usually absent.

Twenty three thin sections have been studied and their modal compositions are listed in Table I-10.

Table I-10 MODAL COMPOSITION OF TONALITIC TO DIORITIC GNEISS

type of mineral assemblage	sample number	mineral proportion (%) Qt	Plg	Hrn	Bio	Gar	Epd	Scp	Dio	Chl	Opa
(1)	P3-6A	5	63	15	10	5	1				
	P3-7A	10	60	5	20	5					
	3780A	20	69	3	3	5					
	3903	25	60	2	10	2			tr		
(2)	3669A	10	55	30	5						
	4116C	20	48	10	20		tr	1			
	4510a	10	70	10	5			5			
	4510b	20	50	10	15						
	4623	30	59	3	8		tr				
	4529	20	65	5	10		tr				
(3)	3008	35	40	25							
(4)	3371	10	57	5	10		13			5	
	3372	10	40	5	10		30			4	
	4585	10	65	10	13		2				
	4611	10	62	20	5		5				
(5)	3104A	30	43	18			7		tr		
(6)	3099	33	40	10	1	15					tr
	3029	50	35	10		5					tr
(7)	P2-1	20	70		7		tr			tr	3
	4420-2	25	63		10						

The distribution of these samples is listed in Table I-11.

Table I-12 DISTRIBUTION OF THE TONALITIC TO DIORITIC GNEISS

	type of mineral assemblage					
	(1)	(2)	(3)	(4)	(5)	(6)	(7)
HRSC			3008			3099 3029	
Florence shear zone	P3-6A P3-7A	4116C					
Oonagalabi Tongue	3780A 3903	3669A					
Entia Dome		4529 4623 4510a 4510b		4611 4585			P2-1 4420-2
Hale River Region				3371 3372	3104A		

4.3 Granitic gneiss

Granitic gneiss comprises mainly quartz, alkali-feldspar and plagioclase with small and variable amounts of mafic minerals. Accessory minerals are usually zircon, apatite, sphene, allanite and opaques.

One hundred and twenty seven thin sections have been studied. According to the percentages of quartz, granitic gneiss can be divided into quartz rich granitic gneiss (quartz more than 20%) and quartz poor granitic gneiss (quartz less than 20%). Based on the ratio of alkali-feldspar to total feldspars, the quartz rich and quartz poor granitic gneisses are further divided into five groups (see Table I-12).

TABLE I-12 CLASIFICATION ON THE BASIS OF RATIO OF ALKALI-FELDSPAR TO PLAGIOCLASE

	ratio of alkali-feldspar to total feldspars
A. plagioclase granitic gneiss	less 1/9
B. plagioclase rich granitic gneiss	between 1/9 and 2/5
C. two feldspars granitic gneiss	between 2/5 and 2.5
D. alkali-feldspar rich granitic gneiss	between 2.5 and 9
E. alkali-feldspar granitic gneiss	more than 9

On the basis of the amount of all mafic minerals, the granitic gneisses are assigned into three kinds, as in Table I-13.

Table I-13 CLASSIFICATION ON THE BASIS OF MAFIC MINERAL

	amount of mafic minerals
L. leucocratic acidic gneiss	less than 5%
N. normal acidic gneiss	between 5% and 15%
M. melanocratic acidic gneiss	more than 15%

Modal compositions of the granitic gneiss in the whole area are listed in Table I-16. Twenty five kinds of combinations of mafic mineral assemblages and 79 rock types can be found from Table I-16.

It is possible to use 79 names for the 79 types of granitic gneisses. For example ,type 43 can be called "melanocratic biotite garnet hornblende bearing quartz-rich plagioclase gneiss". But this kind of full name for each type of acidic gneiss is not very usefull for the purpose of this study, so the general name "granitic gneiss" is still preferred.

Table I-16 (1) MODAL COMPOSITIONS OF GRANITIC GNEISS

rock type	sample number	Qt	Plg	Atp	Pth	Mcl	Ksp	Bio	Hrn	Gar	Mus	Cpx	Opa
(1)	3647a	25	35			5	30						
(2)	4114A	30	10			60							
(3)	4598	20	5		5	67							3
(4)	3740A	40	55	1		1		3					
(5)	3161	30	50			15		5					
(6)	P1-8	30	30			39		1					
	4116	30	30				35	3					2
	P3-5	30	30			39		1					
	3643-2	30	30			38		tr					
	3740Ba	20	7	30	30	10		3					
(7)	3647b	25	20			45		9					
	4615-2	20	35			40		5					
	3388Ha	20	30		5		38	7					
(8)	P3-9A	40	9			10	40	1					
	4114	30	10				56	3					1
(9)	3650	30	10		20	30		10					
	4629	25	15			52		8					
(10)	3279	20	55				10		10				5
(11)	3689	25	20		50				5				
(12)	3367	20	48				30			2			
(13)	3252	30	30				20				20		
(14)	146831	35	15		5	25	10				15		
(15)	4047	65				30					5		
(16)	3782	40	46			10		2	1				1
(17)	146832	30	50			15		5	tr				
	3765	30	54			10		1	5				
	4048	25	50	15				5	5				
(18)	4258	30	40	5			15	4	5				
	146837	20	30		38			3	8				
	3790	30	24		10	30		5	1				
(19)	4190	30	30		5	19		1	15				
(20)	3732	20	20			50		10	tr				
	4270	30	20				44	5	1				
	4628	24	20			45		5	1				
(21)	4106	30	5				58	5	1				
(22)	3388D	5	45		5			25	19				

TABLE I-18 (1) (continued)

		Qt	Plg	Atp	Pth	Mcl	Ksp	Bio	Hrn	Gar	Mus	Cpx	Opa
(23)	A-1	34	23		32			8		3			
	3006	40	30			20		5		5			
	3032C	20	30				40	5		5			
	3162A	20	39			30		10		1			
	3710	20	45		5	20		7		1			
	3784	30	30		34			3		3			
	4516A	40	25				30	tr		3			2
	3162	40	30				15	10		5			
	3740Bb	20		63				10		5			
(24)	3163	30	20		34			15		1			
	3172	20	30			30		19		1			
(25)	4181	40	15				40	tr		5			
(26)	4265	45	7		45			1				1	
(27)	P3-3A	20	20		50			3				3	3
(28)	4625	25	55			10		7			3		
(29)	3251	25	40				18	15			2		
	3385	40	10			41		3			5		
(30)	3890	30	30			36		1			2		
	4031	30	3[illegible]			30		1			1		
	4615-1	20	3[illegible]			40		3			tr		

Table I-16 (2)

		Qt	Plg	Mcl	ksp	Bio	Mus
(31)	P1-3	30	30	35		5	tr
	3376	40	21		30	3	5
	3651	30	30	34		5	1
	4033	20	40	30		10	tr
	4616	25	30	40		5	tr
(32)	4420-3	30	34	20		15	tr
(33)	4639	30	10	60		tr	tr
(34)	4436-2	25	5	70		tr	tr
	4486	20	5	72		1	1

Table I-16 (3)

		Qt	Plg	Atp	Pth	Mcl	Ksp	Bio	Epd
(35)	3017	30	30			38		1	tr
(36)	3048	20	30			40		8	tr
	3105	20	14	20	40			5	1
	P3-6	20	44			15	15	5	tr
(37)	4004	30	8			50		10	2
(38)	3376A	10	30			40		15	5

Table I-16 (4)

		Qt	Plg	Atp	Pth	Mcl	Ksp	Bio	Hrn	Gar	Mus	Cpx	Sil
(39)	4299	30	46		20			1					3
(40)	3689A	20	15		50				5			10	
(41)	3055	30					45		10			15	
(42)	4192	45	10	4		40					tr	tr	
(43)	3210	26	30		1	5	24	8	3	2			
	146834	30	24			40		5	1				
(44)	P3-4	20	26			15	15	20	1	3			
	3013	20	30				30	15	2	3			
	3014	20	30				30	9	11	5			
	4056	20	26				26	15	2	5			
	146835	20	19			30		15	15	1			
(45)	3781	25	20			54		1	tr	tr			
(46)	4269-1	30	10		49	5		1	2	3			
	4269-2	30	10		30		20	2	3	5			

Table I-16 (5)

		Qt	Plg	Atp	Pth	Mcl	Ksp	Bio	Hrn	Gar	Mus	Cpx	Opa
(47)	3557-1	13	30			40		10	3	2			2
(48)	P3-3B	11	20			20	40	3	3	2			1
(49)	3388	10	20	35	5			20	5	2			2
(50)	P3-3	20	30				40	1	3			3	3
(51)	3388Hb	18	20	10	22			18	7			5	
(52)	3733	20	19			50		10	1		tr		
(53)	4190A	30	30			24		1	15		tr		

Table I-16 (6)

		Qt	Plg	Pth	Mcl	Ksp	Bio	Hrn	Gar	Mus	Epd	Scp
(54)	3225	20	20	9	40		5	5			1	
	4501	20	10		58		4	6			1	
(55)	4116D	20	45			5	20	10				tr
(56)	4283	20	38		40		1		1	tr		
(57)	3780	20	50			20	5		5	tr		
	3783	30	40		24		5		1	tr		
(58)	3204	29	30		25		20		5	1		
	3160	30	27			15	15		3	10		

Table I-16 (7)

		Qt	Plg	Pth	Mcl	Ksp	Bio	Gar	Sil
(59)	3380-A	34	30	20			4	10	2

Table I-16 (8)

		Qt	Plg	Pth	Mcl	Ksp	Bio	Hrn	Gar	Mus	Cpx	Epd	Opa
(60)	P1-10	30	30		37		2			tr		tr	1
	3017B	30	30		38		1			1		tr	
(61)	3038	20	30		38		2			8		2	
	4105	20	30		39		6			4		tr	1
(62)	3016A	35	25		15		8			6		10	
(63)	3003	35	10		49		1			5		tr	
	3226	30	20		45		3			1		1	
	3230	20	10		58		tr			10		tr	
(64)	3016C	20	8		30		5			25		10	
(65)	3395	45	5		45		2			3		tr	
(66)	P4-6	10	35			47	2			3		tr	
(67)	3890-2	30	48	10			5	tr	5		tr		
(68)	3380	22	25	20		23	3	1	5		tr		1
	3581	25	24	40			2	3	5		tr		1

Table I-16 (9)

		Qt	Plg	Atp	Mcl	Ksp	Bio	Hrn	Gar	Epd
(69)	P1-2A	30	30	3			30	2	5	1
	P1-2B	30	33	2			15	15	5	tr
	P1-2D	20	25	10			30	5	10	tr
(70)	P1-6	30	40		7		17	1	2	3
	P1-7	25	30		5		25	5	5	5
(71)	P1-4	28	30		5	10	22	3	1	1
	3538	30	32	1		19	10	5	3	tr
(72)	3004	34	10		30		16	5	5	tr
(73)	3382	11	30		38		15	2	1	3
(74)	P1-5	17	19		49		8	2	4	1
(75)	3151	10	10		64		10	2	3	tr

Table I-16 (10)

		Qt	Plg	Mcl	Bio	Hrn	Gar	Mus	Epd
(76)	4641	20	55	15	8	1		tr	1
(77)	4631	20	20	50	7	2		tr	tr
(78)	3200	30	15	45	2		1	6	tr
(79)	3039D	30	18	40	10	tr	1	tr	tr

The spatial distribution of each sample of the granitic gneiss is summarized in Table I-17.

Table I-17 DISTRIBUTION OF GRANITIC GNEISS SAMPLES

	sample number (rock type)				
HRSC	P1-2A(69)	P1-2B(69)	P1-2D(69)	P4-6(66)	3160(58)
	3161(5)	3162(23)	3162A(23)	3163(24)	3172(24)
	3200(78)	3204(58)	3251(29)	3252(13)	4192(42)
	146831(14)				
Bruna Gneiss	P1-3(31)	P1-4(71)	P1-5(74)	P1-6(70)	P1-7(70)
	P1-8(6)	P3-4(44)	3004(72)	3006(23)	3013(44)
	3151(75)	3210(43)	3382(73)	3557-1(47)	4004(37)
	4056(44)	4190(19)	4269-1(46)	4269-2(46)	
Entia Dome	4031(30)	4033(31)	4420-3(32)	4436-2(34)	4486(34)
	4501(54)	4598(3)	4615-1(30)	4615-2(7)	4616(31)
	4625(28)	4628(20)	4629(9)	4631(77)	4639(33)
	4641(76)				
Oonagalabi Tongue	A-1(23)	3643-2(6)	3647a(1)	3647b(7)	3650(9)
	3651(31)	3710(23)	3732(20)	3733(52)	3740A(4)
	3740Ba(6)	3740Bb(23)	3780(57)	3781(45)	3782(16)
	3783(57)	3784(23)	3790(18)	3890(30)	3890-2(67)
	4105(61)	4583(56)	4299(39)	6832(17)	6834(43)
	6835(44)	6837(18)			

Table I-17 (continued)

Florence / Leaky Shear Zone	P3-3(50)	P3-3A(27)	P3-3B(48)	P3-5(6)	P3-6(36)
	P3-9(8)	3055(41)	3225(54)	3279(10)	3367(12)
	3380(68)	3380A(59)	3538(71)	3581(68)	3689(11)
	3689A(40)	3765(17)	4106(21)	4114(8)	4114A(2)
	4116(6)	4116D(55)	4181(25)	4190(53)	4258(18)
	4265(26)	4270(20)	4516A(23)		
Hale River Region	P1-10(60)	3003(63)	3014(44)	3016A(62)	3016C(64)
	3017(35)	3017B(60)	3032C(23)	3038(61)	3039D(79)
	3048(36)	3105(36)	3226(63)	3230(63)	3376(31)
	3376A(38)	3385(29)	3388(49)	3388Ha(7)	3388Hb(51)
	3388D(22)	3395(65)	4047(15)	4048(17)	

5. Metasediments

5.1. Psammitic metamorphic rocks

Modal compositions of psammitic rocks are listed in Table I-18.

Table I-18 MODAL COMPOSITION OF PSAMITIC ROCKS

	sample number	Qt	Mus	Trm	Dio	Bio	Hrn	Epd	Gar	Sil	Scp	Plg	Ksp	Aln
(1)	3370	98	2											
	4053	99				tr						tr		
	4027	98	1			3								
	4165	97	3											
(2)	3416	85		6	3	tr		tr					7	
	P4-9	69			8	1	3	3			10		tr	
	4195	79		7			4	5			5			
(3)	3188	80							20					
(4)	4291	60				3			20	10			5	
(5)	6836	80			20	tr								
(6)	4053A	75	15			3						5	5	
	3370A	59	30			10							1	
(7)	3230B	88		1			1	10						
	3246a	70					4	25						
	(3246b	10					8	80	)					
	3246	50					6	43						
(8)	3403	50				30	10				10			

Note: 3246b is an epidote-rich band in the epidote quartzite and should named as quartz epidote rock.

5.2. Pelitic and semi-pelitic gneiss

Modal compositions of 25 thin sections are listed in Table I-19 (of the ISA) and Table I-20 (of the SOB). They contains 22% to 57% mafic minerals and variable amount of quartz and plagioclase. K-feldspar is usually absent.

Table I-19 MODAL COMPOSITION OF PELITIC SEMI-PELITIC GNEISS IN THE ISA

rock type	sample number	Qt	Plg	Bio	Gar	Sil	Mus	Scp	Epd	Hrn	Opa	Tum
(1)	P2-7	25	30	40	5						tr	
	3053D	50	40	5	5							
	3149	49	20	20	1							
	3287	58	20	12	10							
	3305	57	20	20	3						tr	tr
	3405	29	30	40	1						tr	tr
	4306	30	33	30	5					1		1
(2)	3264	37	20	30	5		2		2	3		
(3)	P2-6	30	50	15	5	tr						
	P3-1	25	20	45	4	2						
	3209	20	21	45	1	10	3					
(4)	4254	50	38	5		3	1				3	
(5)	P4-4	25	35	29				8	2			1
	3404	30	30	30				10				
(6)	4261	40	40	10			10					

Table I-20 MODAL COMPOSITION OF PELITIC SEMI-PELITIC GNEISS IN THE SOB

rock type	sample number	Qt	Plg	Bio	Gar	Sil	Mus	Scp	Epd	Hrn	Opa	Ksp	Tum	Chl
(7)	4024a	50	20				20		10					
	4024b	50	30				10		10					
(8)	3403	50		30				10		10				
(9)	3170	25		tr			53							20
(10)	4025a	20	43	20							7		10	
	4025b	24	10	40	1				3		10		13	
(11)	3669B	25	53	20	2				tr		tr			
	3770	20	54	25	1				tr		tr			
	6833	40	28	30	1				tr			1		
	3740B	20	63	10	5				tr		tr	2		

5.3. Calcareous metamorphic rocks

Only nine thin sections have been studied (TAable I-24). They were all collected from the ISA except sample 3794 which is from the Oonagalabi Tongue.

Table I-21 MODAL COMPOSITIONS OF MARBLE

rock type	sample number	Clc	Qt	Bio	Trm	Dio	Scp	Plg	Epd	Mus	Sph	Zir
(1)	3399	99	1									
	4125	99	1									
(2)	3417	90	tr	2	7	1						
	3418	90	7	2	tr			1		tr	tr	tr
(3)	3557-3	71	20		1			8			tr	tr
	3333	79		15	1		5					
	3334	60				20	15	5			tr	
	3399A	50		5		40	3		2			
(4)	3794	80				20						

5.4. Calc-silicate rocks

The mineralogical compositions of calc-silicate rocks are very variable and range from the calc-silicate marble to calc-silicate quartzite. Many rocks have complicated compositional layering, which is defined by either different mineral assemblages or different proportions of the same mineral. For example, in sample 3056, there are five compositional layering, which are labeled as 3056a, 3056b, 3056c, 3056d and 3056e. The mineralogical compositions of each sample and its different compositonal layers is listed in Table I-22. Rock types A to C are found within the ISA, whereas rock types D to I are found within the SOB.

Within the mineral asaemblages of calc-silicate rocks, the epidote occurs both in the ISA and the SOB, whereas the garnet occurs only in the SOB and the biotite is mainly found in the ISA.

Table I-22A MODAL COMPOSITIONS OF CALC-SILICATE

Rock types		Sample number	Dio	Qt	Plg	Scp	Epd	Hrn	Bio	Clc	Sph	Tum	Trm	Opa
A	(1)	3046	30	10	45	2			10		1			2
		3789	25	30	20	20			5		tr	tr		tr
	(2)	3625a	20	30	5	20		5	20		tr	tr	tr	
	(3)	3625b	30	40	5	15	5	1	1		1			
	(4)	3406	45	10	40				tr	2	2			1
	(5)	3534	40	30	1	15	1	1	1	5	1		5	
	(6)	3559	40	40	10		2						8	
B	(7)	3531	40	40		16		1	1	1	1			
		4120	50	20		18			10	1	tr		1	
		4180	12	42		30		13	2		tr			
		3400	40	50		5		tr	3	tr	tr	2		
	(8)	3520	70	15		13					1	tr	tr	
C	(9)	P4-1	20	5	40	10	20	2		2	1	tr		
	(10)	P4-8	30		35	15		tr	3	15	2			tr
	(11)	3410	46		10	40	tr	tr	2	tr	2			

Table I-22B MODAL COMPOSITIONS OF CALC-SILICATE

Rock types		Sample number	Dio	Qt	Plg	Scp	Epd	Hrn	Gar	Clc	Sph	Tum	Opa	Ksp
D	(12)	4502	20	20	30	2	20		tr	1	tr	3	3	
	(13)	4485	5	10	5	25	25	30						
	(14)	P2-3	5	50	15		18		5		2			
	(15)	4604	5	10	40		20	30			tr			
		3055	8	30	50		2	10						
	(16)	4100a	50	4	10	6			30		tr			
		4100b	12	20	30	20			8	10	tr			tr
	(17)	4279a	20	10	40	2	16	1	5	1	tr		tr	5
	(18)	4279b	10	30	55								5	
E	(19)	4058	16	1		5		10	65		3			
	(20)	4102	30	15	tr	30			20	5	tr			
	(21)	4279c	40	8			20		30	2				
F	(22)	4279d	12		60	20	5						3	
	(23)	3643-1	30		55			5	5		5		tr	
G	(24)	3355	9	50			40	1						
	(25)	3059	4	58			38							
H	(26)	3104		44	30		20	5						
		3016B		30	19		30	20						
		3388F		30	30		30	10						

Table I-22A MODAL COMPOSITIONS OF CALC-SILICATE

Rock types	Sample number	Dio	Qt	Plg	Scp	Epd	Hrn	Gar	Clc	Sph	Tum	Opa	Bio
I (27)	3056a	5	34	10		30	20			tr		tr	1
	3056b	5	64	5		25	1						
	3056c	20	20	20		40							
	3056d	2	28	50		2	15						3
	3056e	10	55			20	13			1			1

APPENDIX II

RESULTS FROM ELECTRON MICROPROBE ANALYSIS

1. Introduction

Seventy five samples have been studied using the electron microprobe. Mineral types analysed within each sample can be found from Table II-1, whereas sample index numbers which contain each type of mineral analysed can be found from Table II-2. The mineral abbreviations used in this appendix are the same as those in the thesis (see Chapter 1).

Table II-1 INDEX INFORMATION OF MINERALS ANALYSED IN EACH SAMPLE

stratotectonic units	rock type	sample number	minerals analysed					
Entia Dome	amphibolite	4428	Cpx	Gar	Bio	Hrn	Plg	
		4428-1	Hrn	Plg				
	calc-silicate	3055	Cpx	Hrn	Epd	Plg	Ksp	Alb
Hale river Region	mafic granulite	3105A	Opx	Cpx	Bio	Plg		
		4100B	Opx	Cpx	Hrn	Plg		
		4107	Opx	Cpx	Hrn	Plg		
	charnockitic gneiss	4100A	Gar	Bio	Plg	Ksp		
		4101	Opx	Cpx	Gar	Plg	Ksp	
	calc-silicate	4100	Cpx	Gar				
Oonagalabi Tongue	mafic granulite	3615	Opx	Cpx	Hrn	Plg		
		3645	Opx	Cpx	Gar	Hrn	Plg	
		3729	Opx	Cpx	Hrn	Plg		
		3791	Opx	Cpx	Gar	Hrn		
	amphibolite	3643-1	Cpx	Hrn	Plg			
		3792	Cpx	Hrn	Plg			
		3641	Cpx	Gar	Hrn	Plg		
		3735	Hrn	Bio	Plg			
	granitic-tonalitic gneiss	3643-2	Bio	Plg	Ksp			
		3732	Gar	Bio	Plg	Ksp		
		3733	Hrn	Bio	Plg	Ksp		
		3780	Gar	Bio	Plg	Ksp		
		3780A	Gar	Bio	Plg	Ksp		
		3780B	Hrn	Plg				
		3781	Gar	Bio	Plg	Ksp		
		3782	Hrn	Plg	Ksp			
		3783	Gar	Bio	Plg	Ksp		
		3784	Gar	Bio	Plg	Ksp		
		3790	Hrn	Bio	Plg	Ksp		
		4283	Gar	Bio				

Table II-1 (continued)

	granitic-tonalitic gneiss	146832	Hrn	Bio	Plg	Ksp		
		146834	Bio	Plg	Ksp			
		146835	Gar	Bio	Hrn	Plg	Ksp	
		146836	Hrn	Bio				
		166831	Hrn	Bio	Plg	Ksp		
	pelitic gneiss	146833	Gar	Bio	Plg			
		3770	Gar	Bio	Plg			
		3734	Gar	Bio	Plg			
	calc-silicate	3789	Cpx	Bio	Plg	Ksp		
Florence-Leaky Shear Zone	mylonitized mafic rock	P3-4A	Opx	Cpx	Hrn	Plg		
		P3-7	Opx	Cpx	Hrn	Bio	Plg	
		P3-7A	Opx	Cpx	Gar	Bio	Plg	
		P3-9	Cpx	Hrn	Plg	Bio		
		3379A	Opx	Cpx	Hrn	Gar	Bio	P
		3538-1	Cpx	Gar	Bio	Hrn	Plg	K
	charnockitic gneiss	3368	Opx	Cpx	Gar	Bio	Ksp	
		3379	Opx	Cpx	Gar	Hrn	Bio	P
			Ksp	Mag	Ilm	Epd		
	granitic gneiss	3538-2	Gar	Bio	Plg	Ksp		
	pelitic gneiss	3380A	Gar	Bio	Sil	Plg	Ksp	
		4068	Gar	Bio	Plg	Ksp		
Harts Range Supracrustal Cover	pelitic gneiss	3172	Gar	Bio	Plg			
		3209	Gar	Bio	Sil	Plg		
		3305	Gar	Bio				
		3405	Gar	Bio				
		P2-7	Gar	Bio				
	amphibolite	3008	Hrn	Plg				
		3205	Cpx	Gar	Plg			
		3217	Gar	Hrn	Plg			
		3086A	Gar	Hrn	Plg			
		3785	Cpx	Hrn	Plg			
		3785/1	Cpx	Hrn	Plg			
		3786	Hrn	Plg				
		3787	Hrn	Plg				
		3788	Hrn	Plg				
	calc-silicate	4502	Cpx	plg				
Bruna Gneiss		3004	Gar	Bio	Hrn	Plg		
		3382	Gar	Bio	Epd	Plg	Ksp	
		P3-4	Gar	Bio	Ksp			
Metagabbro		3024	Opx	Cpx	Bio	Plg		
		3032B	Opx	Cpx	Hrn	Plg		
		3165	Opx	Cpx	Hrn	Plg		
		3366	Opx	Cpx	Hrn	Plg		
		3385A	Opx	Cpx	Hrn	Plg		
		4447	Opx	Cpx	Hrn	Plg		

Table II-2. INDEX OF SAMPLES FOR EACH MINERAL ANALYSED

mineral	samples analysed						
orhtopyroxene	3024	3032B	3105A	3165	3366	3368	3379
	3379A	3385A	3615	3645	3729	3791	4100B
	4101	4107	4447	P3-4A	P3-7	P3-7A	
clinopyroxene	3024	3032B	3055	3105A	3165	3205	3366
	3368	3379	3379A	3385A	3538-1	3615	3645
	3785	3785/1	3789	3791	4100	4100B	4101
	4107	4428	4447	P3-4A	P3-7	P3-7A	P3-9
hornblende	3004	3008	3032B	3055	3086A	3165	3217
	3366	3379	3379A	3385A	3538-1	3615	3641
	3643-1	3645	3729	3733	3735	3780B	3782
	3785	3785/1	3786	3788	3790	3791	3792
	4100B	4107	4428	4428-1	4447	146831	146832
	146835	166831	P3-4A	P3-7	P3-7A	P3-9	
Garnet	3004	3086A	3172	3205	3209	3217	3305
	3368	3379	3379A	3380A	3382	3405	3538
	3641	3645	3732	3734	3770	3780	3780A
	3781	3783	3784	3791	4068	4100	4100A
	4101	4283	4428	146833	146835	P2-7	P3-4
	P4-7A						
biotite	3004	3024	3105A	3172	3209	3305	3368
	3379	3379A	3380A	3382	3405	3538-1	3643-2
	3732	3733	3734	3735	3770	3780	3780A
	3781	3783	3784	3789	3790	4068	4100A
	4283	4299	4428	146831	146832	146833	146834
	146835	146836	166831	P2-7	P3-4	P3-7	P3-7A
	P3-9						
Plagioclase	3004	3008	3024	3032B	3055	3086A	3105A
	3165	3172	3205	3209	3217	3366	3379
	3379A	3380A	3382,	3385A	3538-1	3538-2	3615
	3641	3643,	3643-1	3643-2	3645	3729	3732
	3733	3734	3735	3770	3780	3780A	3781
	3783	3784	3785	3786	3786/1	3787	3788
	3789	3790	3792	4068	4100A	4100B	4101
	4107	4299	4428	4428-1	4447	4502	146831
	146832	146833	146834	146835	166831	P3-4A	P3-7
	P3-7A	P3-9					
K-feldspar	3055	3369	3379	3380A	3382	3538-1	3538-2
	3643-2	3732	3733	3780	3780A	3781	3782
	3783	3784	3789	3790	4068	4100A	4101
	4299	146831	146832	146834	146835	166831	P3-4
magnitite	3379						
ilmanite	3379						
epidote	3055	3379	3382				
sillimanite	3209	3380a	4299				

2. Representative data

More than one thousand points have been analysed, but on small number of representative data are documented in Tables to II-9.

Table II-3 MICROPROBE DATA FROM ORTHOPYROXENE

sample No.	3105A	4100B	3615	3645	3729 clast	3729 matrix
		(weight percentage %)				
SiO2	51.37	50.98	50.21	51.51	51.22	52.64
Al2O3	1.15	1.08	1.44	1.00	1.26	1.25
FeO	28.51	29.09	28.52	27.88	30.20	29.60
MnO	0.58	0.64	0.75	0.73	0.91	0.94
MgO	17.84	17.74	17.04	18.33	16.48	17.17
CaO	0.39	0.47	0.49	0.99	0.48	0.39
K2O			0.09			
Na2O	0.21					
summe	100.05	100.00	98.61	100.45	100.48	101.99
	(structural formula based on 6 oxygen per formula unit)					
Si	1.9717	1.9648	1.9634	1.9672	1.9748	1.9859
Al	0.0520	0.0489	0.0663	0.0451	0.0572	0.0555
Fe	0.9152	0.9375	0.9327	0.8906	0.9733	0.9339
Mn	0.0189	0.0210	0.0247	0.0235	0.0298	0.0299
Mg	1.0205	1.0192	0.9934	1.0432	0.9467	0.9655
Ca	0.0160	0.0193	0.0206	0.0407	0.0164	0.0156
K			0.0045			
Na	0.0157					
summe	4.0101	4.0107	4.0100	4.0102	3.9974	3.9863
Mg/(Mg+Fe)	52.7	52.1	51.6	53.9	49.3	50.8
Ca:Mg:Fe	1:52:47	1:52:47	1:51:48	2:53:45	1:49:50	1:50:49

sample No.	3791	4107	3379A clast	3379A matrix	P3-7	P3-7A
		(weight percentage %)				
SiO2	52.01	51.18	50.99	51.12	52.26	51.79
TiO2		0.17				
Al2O3	1.51	1.22	1.57	1.57	1.42	1.41
Cr2O3		0.14				
FeO	25.54	28.83	27.25	26.75	24.30	24.48
MnO	0.71	0.74	0.81	0.89	0.72	0.51
MgO	20.42	16.93	18.82	18.21	21.00	20.94
CaO	0.21	0.62	0.49	0.35	0.23	0.19
Na2O		0.18				
summe	100.42	100.00	99.93	98.89	99.94	99.32
	(structural formula based on 6 oxygen per formula unit)					
Si	1.9837	1.9717	1.9510	1.9704	1.9657	1.9618
Ti		0.0050				
Al	0.0671	0.0554	0.0707	0.0714	0.0631	0.0629
Cr		0.0042				
Fe	0.8044	0.9288	0.8721	0.8623	0.7644	0.7756
Mn	0.0227	0.0240	0.0263	0.0289	0.0229	0.0164
Mg	1.1464	0.9719	1.0733	1.0464	1.1774	1.1822
Ca	0.0086	0.0258	0.0201	0.0146	0.0092	0.0079
Na		0.0134				
summe	4.0077	4.0002	4.0136	3.9939	4.0028	4.0067
Mg/(Mg+Fe)	58.8	51.1	55.2	54.8	60.6	60.4
Ca:Mg:Fe	1:58:41	1:51:48	1:55:44	1:54:45	1:60:39	1:60:39

Table II-3 (continued) MICROPROBE DATA FROM ORTHOPYROXENE

sample No.	3379	3368	4101	P3-4A matrix	P3-4A clast
		(weight percentage %)			
SiO2	50.94	49.78	49.64	51.90	51.79
TiO2	0.12				
Al2O3	1.40	1.88	1.85	0.82	0.77
FeO	26.86	24.30	32.83	24.59	23.70
MnO	0.80	1.10	0.75	0.54	0.51
MgO	18.22	19.54	14.14	21.22	21.23
CaO	0.69	0.44	0.46	0.40	0.31
Na2O			0.32		
summe	99.03	97.46	100.00	99.47	98.30
	(structural formula based on 6 oxygen per formula unit)				
Si	1.9647	1.9378	1.9527	1.9669	1.9770
Ti	0.0035				
Al	0.0636	0.0861	0.0857	0.0367	0.0629
Fe	0.8664	0.7910	1.0799	0.7794	0.7756
Mn	0.0260	0.0364	0.0251	0.0172	0.0164
Mg	1.0472	1.1336	0.8293	1.1985	1.2080
Ca	0.0285	0.0185	0.0196	0.0161	0.0126
Na			0.0244		
summe	4.0000	4.0351	4.0166	4.0147	4.0055
Mg/(Mg+Fe)	54.7	58.9	43.4	60.6	61.5
Ca:Mg:Fe	2:54:45	1:58:40	1:43:56	1:60:39	1:61:38

sample No.	3024	3032B	3165	3366	3385A	4447
		(weight percentage %)				
SiO2	50.95	51.86	52.76	51.48	52.64	54.15
Al2O3	1.17	2.81	2.15	1.38	1.04	2.61
FeO	24.15	19.93	22.10	27.94	23.46	15.51
MnO	0.57	0.47	0.48	0.63	0.55	0.22
MgO	20.05	23.11	22.05	18.11	21.93	27.52
CaO	0.33	0.24	0.45	0.46	0.39	
summe	97.23	98.42	100.00	100.00	100.00	100.00
	(structural formula based on 6 oxygen per formula unit)					
Si	1.9735	1.9648	1.9634	1.9701	1.9703	1.9859
Al	0.0536	0.0489	0.0663	0.0623	0.0459	0.0555
Fe	0.7823	0.9375	0.9327	0.8941	0.7343	0.9339
Mn	0.0186	0.0210	0.02470	0.0204	0.0173	0.0299
Mg	1.1579	1.0.92	0.9934	1.0331	1.2233	0.9655
Ca	0.0139	0.0193	0.0206	0.0188	0.0158	0.0156
summe	3.9997	4.0107	4.0100	3.9988	4.0068	3.9863
Mg/(Mg+Fe)	59.7	67.4	64.0	53.6	62.5	76
Ca:Mg:Fe	1:59:40	1:67:32	1:63:36	1:53:46	1:62:37	0:76:24

Table II-4 MICROPROBE DATA FROM CLINOPYROXENE

sample No.	3105A	4447	3205	4502	4107	4100
		(weight percentage %)				
SiO2	51.92	49.88	51.03	48.09	52.26	48.57
TiO2		0.23				
Al2O3	2.14	3.01	1.67	3.14	1.77	2.77
Cr2O3		0.29	0.18			
FeO	10.46	5.94	9.85	12.99	10.74	19.02
MnO	0.18			0.27	0.24	0.17
MgO	12.22	14.97	11.62	9.22	12.10	6.10
CaO	22.04	20.77	22.17	22.44	22.43	23.00
Na2O	0.34	0.27	0.34	0.31	0.45	0.37
summe	99.30	75.36	96.86	96.46	100.00	100.00
	(structural	formula based on 6 oxygen		per formula	unit)	
Si	1.9630	1.9239	1.9771	1.9121	1.9679	1.9149
Ti		0.0066				
Al	0.0954	0.1367	0.0762	0.1469	0.0785	0.1289
Cr		0.0089	0.0056			
Fe	0.3309	0.1915	0.3192	0.4320	0.3382	0.6271
Mn	0.0057			0.0092	0.0078	0.0055
Mg	0.6889	0.8605	0.6709	0.5465	0.6793	0.3583
Ca	0.8930	0.8584	0.9203	0.9559	0.9048	0.9717
Na	0.0247	0.0203	0.0254	0.0239	0.0330	0.0284
summe	4.0016	4.0069	3.9947	4.0264	4.0094	4.0348
Mg/(Mg+Fe)	67.6	81.8	67.8	55.9	66.8	36.4
Ca:Mg:Fe	47:36:17	45:45:10	48:35:17	50:28:22	47:35:18	50:18:32

sample No.	4428	3055	4100B	3615	3165	3785
		(weight percentage %)				
SiO2	52.83	52.28	51.85	52.22	53.39	52.52
TiO2		0.23			0.14	
Al2O3	1.17	2.15	2.32	2.14	2.04	1.87
Cr2O3		0.29	0.17			
FeO	11.64	9.08	11.02	10.74	6.60	8.44
MnO	0.19	0.73	0.21	0.17	0.24	0.20
MgO	11.61	11.85	11.87	11.85	14.30	12.59
CaO	22.27	22.73	22.04	22.50	23.13	23.31
Na2O	0.30	0.94	0.51	0.38	0.39	0.37
summe	100.00	99.76	100.00	100.00	100.00	98.92
	(structural	formula based on 6 oxygen		per formula	unit)	
Si	1.9926	1.9666	1.9542	1.9645	1.9701	1.9780
Ti		0.0066			0.0040	
Al	0.0518	0.0953	0.1028	0.0948	0.0887	0.0830
Cr		0.0089	0.0052			
Fe	0.3673	0.2856	0.3473	0.3379	0.2038	0.2658
Mn	0.0059	0.0234	0.0068	0.0055	0.0078	0.0063
Mg	0.6527	0.6644	0.6670	0.6645	0.7867	0.7068
Ca	0.9002	0.9161	0.8897	0.9071	0.9143	0.9460
Na	0.0218	0.0686	0.0376	0.0276	0.0282	
summe	3.9923	4.0200	4.0106	4.0019	3.9957	3.9805
Mg/(Mg+Fe)	64.0	69.9	65.8	66.3	79.4	72.7
Ca:Mg:Fe	47:34:19	49:36:15	47:35:18	47:35:18	48:41:11	49:37:14

Table II-4 (continued) MICROPROBE DATA FROM CLINOPYROXENE

sample No.	3789	P3-4A	3641	3792
		(weight percentage %)		
SiO2	53.77	53.77	50.38	51.97
TiO2			0.24	
Al2O3	0.95	1.37	2.88	2.05
Cr2O3	0.12		0.17	
FeO	6.26	7.83	8.96	9.59
MnO	0.14	0.17	0.52	0.58
MgO	14.27	14.31	12.68	12.79
CaO	24.06	23.06	22.64	21.95
Na2O	0.23		0.18	0.39
summe	99.79	100.50	98.49	99.32
	(structural formula based on 6 oxygen per formula unit			
Si	1.9878	1.9832	1.9191	1.9606
Ti			0.0069	
Al	0.0415	0.0594	0.1295	0.0912
Cr	0.0036		0.0052	
Fe	0.1937	0.2414	0.2855	0.3027
Mn	0.0042	0.0052	0.0168	0.0185
Mg	0.7862	0.7867	0.7202	0.7190
Ca	0.9528	0.9111	0.9243	0.8875
Na	0.0162		0.0135	0.0288
summe	3.9860	3.9871	4.0158	4.0082
Mg/(Mg+Fe)	80.2	76.5	71.6	70.4
Ca:Mg:Fe	49:41:10	47:41:12	48:37:15	46:38:16

Table II-5 MICROPROBE DATA FROM HORNBLENDE

sample No.	3217	4447	4107	3055	4428	4100B
		(weight percentage %)				
SiO2	45.98	43.50	42.07	42.40	40.32	40.90
TiO2	0.92	1.04	1.64	0.42	1.32	2.11
Al2O3	10.39	14.89	11.93	11.57	11.97	12.90
FeO	12.81	9.29	17.24	15.71	16.70	15.93
MnO			0.21	0.71		
MgO	12.43	13.97	9.69	11.30	8.75	9.98
CaO	10.92	11.73	11.36	11.78	10.59	11.57
K2O		0.52	1.24	1.60	0.75	2.46
Na2O	1.46	2.05	1.62	1.55	2.07	1.47
summe	94.91	97.00	97.0	97.05	92.48	97.33
	(structural formula based on 23 oxygen per formula unit)					
Si	6.8643	6.3172	6.3963	6.4322	6.4112	6.1950
Ti	0.1035	0.1138	0.1876	0.0484	0.1583	0.2403
Al	1.8285	2.5492	2.1374	2.0681	2.2435	2.3030
Fe	1.5989	1.1283	2.1922	1.9931	2.2212	2.0178
Mn			0.0272	0.0918		
Mg	2.7658	3.0243	2.1968	2.5539	2.0746	2.2541
Ca	1.7460	1.8248	1.8502	1.9141	1.8045	1.8783
K		0.0971	0.2411	0.3102	0.1515	0.4752
Na	0.4219	0.5763	0.4780	0.4568	0.6392	0.4315
summe	15.3288	15.6310	15.7068	15.8686	15.7040	15.7954
Mg/(Mg+Fe)	63.4	72.8	50.1	56.2	48.3	52.8
Ca:Mg:Fe	29:45:26	30:51:19	30:35:35	30:39:31	30:34:36	30:37:33

sample No.	3785	P3-4A	3641	3735
		(weight percentage %)		
SiO2	45.63	43.61	41.65	41.50
TiO2	1.19	1.45	0.90	2.05
Al2O3	11.18	11.82	12.20	12.28
FeO	14.49	14.47	15.73	17.42
MnO	0.27		0.16	0.24
MgO	11.73	11.57	10.91	8.95
CaO	11.44	12.06	11.77	11.65
K2O	0.07	0.93	1.77	1.75
Na2O	1.93	1.55	0.89	1.46
summe	97.93	97.45	95.97	97.30
	(structural formula based on 23 oxygen per formula unit)			
Si	6.6920	6.4859	6.3706	6.3244
Ti	0.1316	0.1618	0.1034	0.2348
Al	1.9324	2.0717	2.1989	2.2062
Fe	1.7775	1.7995	2.0117	2.2196
Mn	0.0338		0.0213	0.0309
Mg	2.5645	2.5652	2.4869	2.0334
Ca	1.7974	1.9213	1.9297	1.9023
K	0.0130	0.1764	0.3454	0.3411
Na	0.5487	0.4456	0.2626	0.4311
summe	15.4909	15.6273	15.7304	15.6337
Mg/(Mg+Fe)	59.1	58.8	55.3	47.8
Ca:Mg:Fe	29:42:29	30:41:29	30:39:31	31:33:36

Table II-6 MICROPROBE DATA FROM GARNET

sample No.	3217	3205	4101	3405 rim	3405 centre	4100
		(weight percentage %)				
SiO2	39.02	37.80	38.50	38.39	38.40	37.90
TiO2						0.14
Al2O3	22.09	21.13	19.50	21.93	21.84	13.25
FeO	27.39	24.66	30.28	25.41	24.75	19.40
MnO	2.94	2.37	2.03	1.88	2.97	1.25
MgO	5.28	3.38	3.23	5.28	5.21	0.39
CaO	5.54	9.69	6.46	7.10	6.83	27.66
Na2O						
summe	102.27	99.04	100.00	100.00	100.00	100.00
	(structural formula based on 24 oxygen per formula unit)					
Si	5.9918	6.0074	6.1502	5.9878	5.9955	6.1896
Ti						0.0175
Al	3.9982	3.9572	3.6705	4.0309	4.0192	2.5505
Fe	3.5164	3.2777	4.0446	3.3145	3.2321	2.6502
Mn	0.3822	0.3195	0.2747	0.2480	0.3932	0.1735
Mg	1.2092	0.8011	0.7692	1.2285	1.2118	0.0959
Ca	0.9111	1.6508	1.1050	1.1866	1.1428	4.8401
Na						
summe	16.0089	16.0137	16.0142	15.9964	15.9947	16.5147
Mg/(Mg+Fe)	25.6	19.6	16.0	27.0	27.3	3.5
Ca:Mg:Fe	16:22:62	29:14:57	19:13:68	21:21:58	20:22:58	64:1:35

sample No.	4428	146835 rim	146835 centre	3770 rim	3770 centre	3004 rim
		(weight percentage %)				
SiO2	37.67	37.20	36.46	37.21	37.55	37.24
TiO2						
Al2O3	20.90	20.58	20.04	20.79	21.28	20.68
FeO	28.61	25.14	27.00	26.36	26.60	24.64
MnO	1.20	8.37	4.80	4.77	4.24	2.30
MgO	2.68	1.42	2.01	3.01	3.59	2.73
CaO	8.93	6.68	6.44	6.05	5.92	10.08
Na2O			0.17		0.24	0.31
summe	100.00	99.39	96.92	98.63	99.42	97.98
	(structural formula based on 24 oxygen per formula unit)					
Si	5.9954	6.0138	6.0201	5.9866	5.9646	5.9957
Ti						
Al	3.9201	3.9206	3.8992	3.9420	3.9846	3.9241
Fe	3.8081	3.3985	3.7290	3.5471	3.5336	3.3175
Mn	0.1622	1.1468	0.6713	0.6502	0.5701	0.3141
Mg	0.6360	0.3419	0.4941	0.7215	0.8512	0.6545
Ca	1.5224	1.1573	1.1401	1.1204	1.0077	1.7388
Na			0.0555		0.0734	0.0953
summe	16.0442	15.9289	16.0093	15.9679	15.9252	16.0400
Mg/(Mg+Fe)	14.3	9.1	11.7	16.9	19.4	16.5
Ca:Mg:Fe	25:11:64	24:7:69	11:9:70	21:13:66	19:16:65	30:12:58

Table II-6 (continued) MICROPROBE DATA FROM GARNET

sample No.	3004 centre	3172 rim	3172 centre	3209 rim	3209 centre	P3-7A rim
	(weight percentage %)					
SiO2	36.70	36.85	36.47	36.38	37.43	37.54
Al2O3	20.33	21.03	20.53	20.80	21.78	21.44
FeO	23.24	23.60	27.07	29.40	29.54	24.42
MnO	4.79	3.22	4.10	1.86	1.85	1.69
MgO	2.69	2.40	2.69	4.93	5.47	6.21
CaO	9.23	9.81	6.66	2.72	2.62	6.27
K2O	0.06				0.13	
Na2O	0.31	0.21	0.27	0.35	0.52	0.19
summe	97.36	97.11	96.80	96.45	99.34	97.75
	(structural formula based on 24 oxygen per formula unit)					
Si	5.9888	5.9777	6.0201	5.9672	5.9310	5.9594
Al	3.9092	4.0200	3.8992	4.0220	4.0669	4.0104
Fe	3.1716	3.2007	3.7290	4.0338	3.9141	3.2415
Mn	0.6626	0.4423	0.6713	0.2583	0.2488	0.2274
Mg	0.6553	0.5800	0.4941	1.2058	1.2911	1.4685
Ca	1.6139	1.7047	1.1401	0.4781	0.4451	1.0661
K	0.0133				0.0273	
Na	0.0966	0.0656	0.0555	0.1129	0.1585	0.0571
summe	16.1113	15.9911	16.0093	16.0779	16.0828	16.0305
Mg/(Mg+Fe)	17.1	15.3	15.0	23.0	24.8	31.2
Ca:Mg:Fe	30:12:58	31:11:58	19:12:69	8:21:71	8:23:69	19:25:56

sample No.	P3-7A centre	146833 rim	146833 centre	3641
	(weight percentage %)			
SiO2	37.56	37.07	36.94	38.31
Al2O3	21.41	21.14	21.33	21.00
FeO	23.54	31.22	32.09	22.66
MnO	1.88	2.89	2.91	6.14
MgO	6.76	3.58	3.82	3.41
CaO	6.04	3.08	1.92	8.99
K2O				
Na2O	0.35	0.23	0.23	
summe	97.53	99.21	99.24	100.52
	(structural formula based on 24 oxygen per formula unit)			
Si	5.9643	5.9739	5.9454	6.0247
Al	4.0068	4.0156	4.0452	3.8923
Fe	3.1265	4.2074	4.3195	2.9797
Mn	0.2527	0.3942	0.3969	0.8178
Mg	1.6002	0.8592	0.9170	0.8001
Ca	1.0282	0.5322	0.3309	1.5144
K				
Na	0.1065	0.0720	0.0710	
summe	16.0853	16.0542	16.0259	16.0290
Mg/(Mg+Fe)	33.9	17.0	17.5	21.2
Ca:Mg:Fe	18:28:54	10:15:75	6:16:78	29:15:56

Table II-7 MICROPROBE DATA FROM BIOTITE

sample No.	3405 iso.	3405 inc.	146835 inc.	146835 iso.	3770 iso.	3770 inc.
		(weight percentage %)				
SiO2	36.65	36.99	34.28	33.74	34.87	34.96
TiO2	2.35	2.95	4.65	3.84	3.97	4.10
Al2O3	15.92	15.12	13.34	13.41	15.28	15.06
FeO	13.87	11.84	22.23	24.79	20.39	18.22
MgO	13.91	16.25	8.24	6.49	9.16	10.87
K2O	9.02	8.18	8.51	8.65	9.30	9.04
Na2O		0.19				
	(structural formula based on 24 oxygen per formula unit)					
Si	6.1482	6.1362	6.0738	6.0943	6.0048	5.9969
Ti	0.2961	0.3684	0.6201	0.5210	0.5145	0.5285
Al	3.1468	2.9562	2.7855	2.8543	3.1018	3.0440
Fe	1.9462	1.6422	3.2942	3.7438	2.9369	2.6141
Mg	3.4794	4.0175	2.1777	1.7470	2.3501	2.7796
K	1.9306	1.7313	1.9239	1.9939	2.0431	1.9785
Na		0.0620				
summe	16.9474	16.9138	16.8751	16.9543	16.9511	16.9416
summe	91.72	91.53	91.25	90.91	92.97	92.25
Mg/(Mg+Fe)	64.1	71.0	39.8	31.8	44.5	51.5

sample No.	3004 iso.	3004 inc.	3172 iso.	3172 inc.	3209 iso.	3209 inc.
		(weight percentage %)				
SiO2	34.59	34.23	33.17	34.15	33.55	33.84
TiO2	3.22	4.81	3.05	3.20	2.18	2.37
Al2O3	15.20	14.45	15.08	15.62	17.51	18.09
FeO	19.80	20.15	21.70	21.86	16.72	17.76
MnO			0.19			
MgO	8.87	7.97	7.07	7.24	9.31	9.74
K2O	8.85	8.80	8.31	8.66	8.65	8.99
Na2O	0.17	0.23				0.20
summe	90.70	90.64	88.50	90.74	87.92	91.00
Mg/(Mg+Fe)	44.4	41.4	36.7	37.1	49.8	49.4
	(structural formula based on 24 oxygen per formula unit)					
Si	6.0822	6.0497	6.0440	6.0568	5.9768	5.8626
Ti	0.4261	0.6389	0.4177	0.4274	0.2916	0.3088
Al	3.1509	3.0093	3.2379	3.2636	3.6763	3.6938
Fe	2.9123	2.9982	3.3062	3.2424	2.4920	2.5733
Mn			0.0294			
Mg	2.3240	2.0999	1.9190	1.9145	2.4931	2.5161
K	1.9845	1.9832	1.9302	1.9582	1.9668	1.9863
Na	0.0567	0.0777				0.0674
summe	16.9366	16.8370	16.8843	16.8629	16.8766	17.0084

Note: iso.= isolated; inc.= inclusion.

Table II-7 (continued) MICROPROBE DATA FROM BIOTITE

sample No.	P3-7A iso.	P3-7A inc.	146833 iso.	146833 inc.
		(weight percentage %)		
SiO2	34.91	35.29	34.26	34.66
TiO2	6.38	3.71	3.95	4.53
Al2O3	14.32	15.38	15.28	15.82
FeO	15.40	13.72	21.62	18.65
MgO	11.95	13.64	7.81	9.69
K2O	8.95	8.61	9.04	8.87
Na2O				0.34
summe	91.92	90.35	91.96	92.56
Mg/(Mg+Fe)	58.0	63.9	39.2	48.1
	(structural formula based on 24 oxygen per formula unit)			
Si	5.9363	6.0217	6.0036	5.9363
Ti	0.8163	0.4764	0.5202	0.5834
Al	2.8699	3.0936	3.1551	3.1940
Fe	2.1897	1.9575	3.1679	2.6707
Mg	3.0289	3.4686	2.0409	2.4733
K	1.9421	1.8746	2.0215	1.9374
Na				0.1131
summe	16.7833	16.8923	16.9091	16.9083

Table II-8 MICROPROBE DATA FROM PLAGIOCLASE

sample No.	3217	4447	3205	4101	4107	4428
		(weight percentage %)				
SiO2	58.67	48.40	56.17	62.70	51.37	55.82
Al2O3	27.06	32.95	27.02	23.97	31.28	28.62
Cr2O3		0.13				
FeO					0.14	
MgO		0.21	0.16		0.16	0.17
CaO	8.46	15.87	9.25	5.44	13.72	10.26
K2O	0.08		0.08	0.32	0.11	0.14
Na2O	6.29	2.44	5.80	7.58	3.21	4.99
summe	100.49	100.00	98.48	100.00	100.00	100.00
	(structural formula based on 32 oxygen per formula unit)					
Si	10.4141	8.8559	10.2160	11.0759	9.3241	10.0127
Al	5.6476	7.1048	5.7919	4.9898	6.6929	6.0494
Cr		0.0191				
Fe					0.0216	
Mg		0.0581	0.0445		0.0437	0.0446
Ca	1.6083	3.1119	1.8029	1.0297	2.6692	1.9714
K	0.0183		0.0186	0.0726	0.0258	0.0324
Na	2.1654	0.8640	2.0464	2.5947	1.1297	1.7360
summe	19.8537	20.0138	19.9203	19.7627	19.9069	19.8465
Ca:Na:K	42:57:1	78:22:00	46:53:1	28:70:2	70:29:1	53:46:1

Table II-8 (continued) MICROPROBE DATA FROM PLAGIOCLASE

sample No.	3055	3055	3785	3641	3792	3735
			(weight percentage %)			
SiO2	62.90	68.52	55.78	45.48	57.04	60.19
Al2O3	24.16	19.85	29.02	35.49	27.90	25.81
CaO	5.14	0.28	10.94	19.06	9.98	7.48
K2O	0.14				0.14	0.07
Na2O	8.63	11.10	5.22	0.41	5.56	6.57
summe	100.97	99.74	100.97	100.44	100.68	100.10
	(structural formula based on 32 oxygen per formula unit)					
Si	11.0309	11.969	9.9357	8.3397	10.1626	10.6755
Al	4.9929	4.0862	6.0926	7.6687	5.8575	5.3946
Ca	0.9656	0.0515	2.0879	3.7447	1.9059	1.4206
K	0.0307				0.0434	0.0151
Na	2.9354	3.7601	1.8030	0.1449	1.9215	2.2578
summe	19.9555	19.8673	19.9193	19.8980	19.8909	19.7635
Ca:Na:K	24:75:1	1:99:00	54:46:0	96:4:0	49:50:1	38:61:1

Table II-9 MICROPROBE DATA FROM K-FELDSPAR

sample No.	4101	3055
	(weight percentage %)	
SiO2	65.16	65.13
TiO2	0.47	0.24
Al2O3	18.84	18.57
K2O	15.05	14.42
Na2O	0.48	1.29
summe	100.00	99.65
	(structural formula based on 32 oxygen per formula unit)	
Si	11.9561	11.9855
Ti	0.0649	0.0330
Al	4.0739	4.0272
K	3.5226	3.3839
Na	0.1716	0.4605
summe	19.7891	19.8901
Ca:Na:K	0:05:95	0:12:88

Appendix VI

Discussion on the paper by W.J.Collins and C.Teyssier.entitled: Crustal Scale Ductile Fault Systems in the Arunta Inlier, Central Australia,

P. Ding & P.R. James, Department of Geology and Geophysics, University of Adelaide, S.A. 5000, Australia.

Discussion

"Forcing, adjusting, abbreviating, omitting, padding, inventing, falsifying, and whatever else, is the essence of interpreting, -: Nietzsche, On the Genealogy of Morals"

In their paper, Collins and Teyssier argue that many of the shear zones in the Arunta Inlier can be interpreted as part of a single Palaeozoic thrust system which caused "most" of the uplift of the lower crustal high-grade metamorphics, and thus emphasise that there is no need to invoke extensive Proterozoic uplift on pre-Palaeozoic shear zones. Their work follows the earlier study of Teyssier (1985) and consists of "detailed mapping on three traverses," across the southeastern part of the Arunta Inlier. We do not find favour with any of their four conclusions, however we particularly disaggree with the presentation and interpretation of their first traverse (the Ruby Gap-Huckitta Traverse - see Figs. 3 & 4) as it crosses an area that we have been mapping in "detail" for more than five years (Ding, in prep; Ding and James, 1985; James et al, 1985, Lawrence et al, in press), and from which we have recently presented an interpretation in direct conflict with that outlined in their paper (James and Ding; in submission).

Following the preliminary presentation of James et al, (1985), James and Ding (in submission) present a compilation map and set of cross sections and block diagrams which includes all of the area north of the Illogwa Shear zone of Collins and Teyssier, (Fig. 3). In our interpretation, the zone between the Entia Gneiss and the Irindina Gneiss, and containing the intrusive Bruna Gneiss, is described as the Harts Range Detachment Zone, a zone of intense and long-lived, but mostly Proterozoic shearing. This conflicts directly with its interpretation by Collins and Teyssier, as a Palaeozoic shear zone of the Alice Springs Orogeny and linked to the Ruby Gap thrust structures. In our geological subdivision of the detachment zone we recognise an early major zone of reclined non-coaxial mylonitic shearing (the Florence/Leaky Shear zone) which took place under granulite facies metamorphic conditions at deep crustal levels. Recent work (Lui, pers comm) has shown much of this shearing to have occured with a sense of displacement of the upper (northern) block moving in a northerly direction relative to the southern block (ie in an extensional sense), and opposite to that described by Collins and Teyssier, as their "consistent southward shearing". Of most importance is the fact that the shear zone mylonites with their north trending lineations are intruded by the granitic precursor to the Early-Mid Proterozoic Bruna gneiss (1747 +5/-4 Ma. Mortimer et al., in press) which means that this major shearing at least, must be invoked as Proterozoic in age. The Bruna gneiss is variably sheared containing from gneissic to ultramylonitic LS

fabrics. In contradiction to Collins and Teyssier we have recognised weakly to undeformed N-S trending mafic dykes south of both Brumby Bore and Harding Springs Well (near the unidentified outlier in the Bruna Gneiss 10 km east of Mt Ruby in their Fig. 3) which transect and obviously postdate deformation within the Bruna Gneiss and closely resemble the 980 Ma Stuart Dykes exposed cutting across similar foliated augen gneisses of the Iwupataka Complex (Amri et al. 1987), 25 km west of Alice Springs. We have not recognised the possible mylonitised equivalents of the Stuart Dykes within Bruna Gneiss.

Collins and Teyssier further report the clustering of K-Ar and Rb-Sr mineral ages from shear zones around 300-550 Ma as supporting evidence for their activity during the Palaeozoic. Similar ages reported by Mortimer et al (1985 and in press) have been interpreted by them in terms of uplift and cooling not neccesarily related to shearing or mylonite development. Rather, from their U-Pb zircon and Rb-Sr data on the age of the Bruna Gneiss intrusion from near Mt Bruna, Mortimer et al show it to have been isotopically unaffected by Palaeozoic disturbances. Further support for significant pre-Palaeozoic shearing is also provided from the Entire Creek 520 Ma folded pegmatite, deformed by weak flattening or minor shearing, which cross-cuts early folds and LS fabrics with north trending lineations and which must thus post-date them.

In the Harts Range Area, most of which is shown in the figure 3 of Collins and Teyssier, we have recognised mylonites to have developed at many stages of a complex history of ductile folding and thrusting. The mylonites form in near layer-parallel zones within both the Entia Gneiss and Irindina Gneiss as well as in the Florence/Leaky Shear zone and at the margins of and within the Bruna Gneiss. Most of the zones are shallowly inclined and very few show the characteristic fine muscovite-chlorite-biotite retrograde schist assemblages which have been described from possible Palaeozoic shear zones elsewhere in the Arunta Inlier. In figure 4, Collins and Teyssier show a very schematic section across this area. They present no explanation as to why they insert a very large thickness of granulite beneath the Entia Gneisses. From our work we find that the Strangways Granulites have been sheared to form the Florence/Leaky shear zone which has then been thrust above the Entia and Bruna Gneisses, rather than below them. We further find it interesting that in the north of figure 4 the contact of the Entia Dome structures with the Maparta Fault Zone is masked by question marks though the most sensible interpretation would seem that the latter (Palaeozoic?) cross cuts the former (Proterozoic?) and, along with the Illogwa Shear Zone to the south, may form a set of conjugate steep thrusts, which caused minor uplift (pop-up) of the Harts Range area in Palaeozoic times.

At the southern margin of the Harts Range area our mapping shows the Illogwa Shear Zone to be represented by a few narrow retrograde shear zones. Some of the quartzites within this zone may represent Late Proterozoic Heavitree Quartzite, though they have not all been unequivocally demonstrated as such, and some are likely to belong to the basement. Finally, though the zones

may link-up to the south with the Ruby Gap thrusts, these thrusts certainly bear no resemblance to the mylonites of the Harts Range Area. We thus dispute the contention of Collins and Teyssier that the foliations and lineations can be "traced continuously across the area".

From the evidence just cited and from our preliminary work in the area of the Arunta Inlier south of the Harts Range area (Ding and James, in prep), we conclude that the majority of the shearing is most likely to be Early-Mid Proterozoic in age, with very little ductile deformation ascribable to Palaeozoic events. We further suggest that Collins and Teyssier, like other previous workers (Teyssier, 1985; Forman, 1971; Marjoribanks, 1976; Stewart, 1967) have significantly overestimated the effects of Palaeozoic deformation in central Australia. We consider that the Palaeozoic deformation is generally restricted to brittle faulting and brecciation of the basement and its overlying platform cover (Heavitree Quartzite), with minor prograde shearing of the latter, at the northern margin of the Amadeus Basin, and of minor retrograde shearing within the high-grade basement of the Arunta Inlier in narrow, mostly steeply inclined shear zones, with only limited uplift in Palaeozoic times. In their own map of figure 2 for example, Collins and Teyssier support this contention for the Redbank Shear Zone, which they describe as several kilometres thick, and as having suffered major Palaeozoic displacement, yet it, and its associated shear zones to the south, are shown as being unconformably overlain by the Heavitree quartzite , or truncating it without significant offset, between Alice Springs and the Arltunga Nappe Complex. We concur with this interpretation as we have also observed this relationship in the field at the northern corner of the Mordor Pound, and also north of Ross River where the basal Heavitree Quartzite conglomerate contains large clasts with randomly oriented intense muscovite fabrics . Thus most of the uplift on this (Redbank) zone must also have been pre-Palaeozoic. This relationship was recognised by Marjoribanks and Black (1974) for the Redbank Zone and by Allen and Black (1979) for the Harry Creek Zone, who also suggested that much of the later shearing may have occured by the reactivation of preexisting Proterozoic shear zones. An estimate of the amount of Proterozoic versus Palaeozoic uplift may be made from observations in the Arltunga area. Evidence of andalusite biotite schist layers which formed at 4-6 kb, or 15-22 km in basement rocks immediately beneath the Heavitree unconformity, indicate that this may reflect a likely amount of pre-Palaeozoic uplift. This early uplift would have brought granulites close to the surface at that time, though no such rocks have yet been found directly beneath the unconformity. Possible Palaeozoic uplift is difficult to estimate as most of the cover sequence in the northern block has been eroded. However it may have been a maximum of only 5-10 km, equivalent to the thickness of the Amadeus Basin cover sequence. In the Ruby Gap area (as also occurs in the Ormiston and Arltunga areas) limited Palaeozoic overthrusting has produced repeated imbricate slices, but we are unconvinced that duplex structures, "Tetes Plongeantes" or large scale overthrusting of basement gneisses has been clearly demonstrated. We thus consider that the term Orogeny should not be used in the context of the Alice Springs movements, which we consider are largely associated with intracontinental, epeirogenic (anorogenic) uplifts. Collins and Teyssier have

erected a geometric solution to describe the evolution of a Palaeozoic intracontinental orogeny in central Australia largely based on a popular thin-skinned tectonic model with most of their argument for its temporal unity based on indirect geochronological evidence and their "powerful" analysis technique of detailed structural traverses. We prefer the erection of interpretive models on the basis of rigourous geological and structural mapping and the presentation of those maps as supporting evidence.

REFERENCES (not duplicated in Collins and Teyssier)

Ding P. (in prep.) Geological evolution of the Harts Ranges in central Australia. Ph.D thesis, University of Adelaide.

Ding P. & James P.R. (in prep). The effects of Palaeozoic deformation at the southern margin of the Arunta inlier in central Australia: reinterpretation of the Alice Springs "Orogeny".

James P.R.,Ding P.,Rankin L. & Scales G. 1985. Displacement and strain within the nappe sequences of the Harts Range area, central Australia. Abstracts vol. of IGCP conference: Tectonics and geochemistry of Early to Middle Proterozoic Fold Belts, Darwin, August,1985.

James P.R. & Ding P. in submission. "Caterpillar Tectonics" in the Harts Range area: a kinship between two sequential Proterozoic orogenic belts within the eastern Arunta Inlier of central Australia.(Precambrian Res.)

Lawrence R.W.,James P.R. & Oliver R.L. (in press) Lithological and structural relationships within the Irindina supracrustal assemblage in the Harts Range ruby mine area of central Australia and their relevance to the occurence of ruby. Aust.J.Earth.Sci.

Mortimer G.E., Cooper J.A. & James P.R. (1985). U-Pb and Rb-Sr geochronology in the vicinity of the Harts Range ruby mine area, Arunta Inlier, central Australia.Abstracts vol. of IGCP conference: Tectonics and geochemistry of Early to Middle Proterozoic Fold Belts, Darwin, August,1985.

Mortimer G.E., Cooper J.A. & James P.R. (in press). U-Pb and Rb-Sr geochronology and geological evolution of the Harts Range ruby mine area of the Arunta Inlier, central Australia.

Stewart A.J. 1967. An interpretation of the Blatherskite nappe, Alice Springs, Northern Territory.J.geol.Soc.Aust.,14(2),175-184.

*
Chinese Affiliation - Institute of Geology, Chinese Academy of Geological Sciences, Baiwanzhuan Road, Beijing, China.

APPENDIX VII

EVIDENCE FOR AND LOCATIONS OF CRUCIAL RELATIONSHIPS FOR EACH PHASE OF THE FOLD SEQUENCE

Fold sequence	Evidence	Localities where crucial relationship occur
HRF_3 (CF_5)	Defined by a locallized refolding of the axial surfaces of the HRF_2 folds and the HRT_3 thrusts, which truncate the HRF_2 (CF_4) folds.	The best example can be seen at location No. 4258 (Map7).
HRF_2 (CF_4)	Defined by the large-scale and first folding of the axial surfaces of the HRF_1 (CF_3) folds and the HRT_2 thrust, which truncate the HRF_1 (CF_3) folds, without visible axial fabrics.	The best examples are the Oonagalabi Tongue and the Maud Window (Fig. 1-1) and also can be seen at location Nos. 3566, 3505 (Map7).
HRF_1 (CF_3)	Defined by the first folding of the HRT_1 and CT thrusts which truncate the BF_4 and CF_2 folds, and by the refolding of the axial surfaces of the CF_2 folds.	The best examples can be seen at location Nos. 3869, 4180 & 3566 (Map7) and the whole Florence Window (Fig. 1-1, Map 5 & 2), 8 km north of the Muller Flat Dam.
CF_2	Defined by the first folding of the CS_1 fabrics with a second and weak axial planar schistosity (BS_2).	The best examples can be seen at location Nos. 3588, 4194, 4206 (Map7).
CF_1	Regional metamorphic foliation and gneissic layering form intense axial planar schistosity (CS_1) of CF_1 folds which are defined by lithological boundaries (CS_0) within the HOB. The limbs of CF_1 folds have usually been transposed.	Best examples are at location Nos. 3520, 3553, 3588 & 3913 (Map7).
BF_4	Defined by the first folding of the axial surfaces of the BF_3 folds without visible axial planar fabrics.	The best examples are the folds exposed 7-8 km SE of Mt Mabel (see Geological Map of Oonagalabi Tongue, Map 3, and folds No.7 & 8 on Fig.3-2).
BF_3	Defined by the first folding of the axial surfaces of the BF_2 folds without visible axial planar fabrics.	The best examples are the Huckitta Fold (its northern closure is exposed about 7km NW of the Huckitta Bore) and the Inkamulla Fold (its SE closure is exposed 4 km SE of the Inkamulla Bore) on Map 4.
BF_2	Defined by the first folding of the BS_1 fabrics with a second and weak axial planar schistosity (BS_2).	The best examples can be seen within the steep zone in the central part of the Entia Dome (No. 3 on Map 4), 6 km east of the Inkamulla Bore.
BF_1	Regional metamorphic foliation and gneissic layering form intense axial planar schistosity (BS_1) of BF_1 folds which are defined by the boundaries between the amphibiloite and the granitic gneisses within the SOB.	The best large-scale example occurs at the NE end of the steep zone in the central part of the Entia Dome (Fold No. 1 on Map 4), 11 km NW of the Huckitta Bore.

Precambrian Research, 40/41 (1988) 199-216
Elsevier Science Publishers B.V., Amsterdam — Printed in The Netherlands

'CATERPILLAR TECTONICS' IN THE HARTS RANGE AREA: A KINSHIP BETWEEN TWO SEQUENTIAL PROTEROZOIC EXTENSION–COLLISION OROGENIC BELTS WITHIN THE EASTERN ARUNTA INLIER OF CENTRAL AUSTRALIA

P.R. JAMES and P. DING

Department of Geology and Geophysics, The University of Adelaide, Box 498, G.P.O., Adelaide, South Australia (Australia)

(Received November 11, 1986; revision accepted December 1, 1987)

Abstract

James, P.R. and Ding, P., 1988. 'Caterpillar tectonics' in the Harts Range area: a kinship between two sequential Proterozoic extension-collision orogenic belts within the eastern Arunta Inlier of central Australia. Precambrian Res., 40/41: 199-216.

We propose that in the Harts Range area of the Arunta Inlier of central Australia, a basement and cover relationship previously described by us, represents a thick complexly deformed contact zone between an Early-Middle Proterozoic fold belt, the Strangways Orogenic Belt (SOB) and a younger Middle Proterozoic orogenic belt, the Harts Range Orogenic Belt, both of which contain their own supracrustal sequences. Rocks of the SOB were deposited and possibly metamorphosed to a maximum grade of granulite facies at ~1800 Ma during an early phase of crustal extension. They were subsequently intruded by a significant proportion of acidic magmas at 1767 Ma and compressed to form a distinctively NNE-SSW trending orogenic belt. A WNW-ESE trending shallowly north-dipping zone of intense and repeated deformation, termed the Harts Range Detachment Zone (HRDZ), formed initially during a period of NNE-SSW crustal extension as a major low-angle normal shear/detachment zone within, and crosses at a high angle to the trend of, the basement rocks of the SOB. The HRDZ has been intermittently active as a zone of crustal weakness since its initiation. The first extensional movement on this zone began the formation of the Harts Range Mobile Belt (HRMB) which displays many of the characteristics of modern tectonic zones activated by plate movement. A supracrustal cover sequence, the Harts Range Cover (HRC), formed in the major geosynclinal basin which developed on the subsiding upper plate of the HRDZ. Continued crustal extension juxtaposed the cover sequence, which was then metamorphosed to a maximum grade of amphibolite facies, and granulite facies basement of the HRDZ, before a fundamental change in movement sense led to crustal contraction and a collision-related, thrusting phase. The HRMB which includes the HRDZ and the HRC, was then internally deformed over a relatively very short time span (15-20 Ma), before voluminous granitic magma intruded mainly along the HRDZ, during the Harts Range Orogeny (HRO). The intrusion of this major granitoid at 1747 Ma precisely fixes the time-scale of evolution for the earlier phases of the HRO. The HRO is documented in detail as a peculiar orogenic style of crustal contraction which was largely taken up by reverse-sense, discrete thrusting and shearing on faults and shear zones associated with the HRDZ. Displacement on the HRDZ was a stick-slip process with repeated punctuation of thrust-slip movement by pinning at points located progressively to the south. Each period of cessation of thrust-slip movement was followed by folding of discrete thrusts, of captured basement lobes within the HRDZ and of the overlying supracrustal sequence. The individual discrete movement phases and folding episodes are each named and described, as is a model of this unusual type of Proterozoic tectonic activity.

0301-9268/88/$03.50 © 1988 Elsevier Science Publishers B.V.

Introduction

There has been considerable recent interest in the proposal that large-scale subhorizontal extensional strains may be an important mechanism for intra-plate deformation and for regional metamorphism (McKenzie, 1978; Wernicke and Burchfiel, 1982; Wickham and Oxburgh, 1985; Sandiford and Powell, 1986). Following the recognition of extension values of 100–300% in the upper level crust of the Basin and Range Province (Davis and Coney, 1979; Angelier and Colletta, 1983), Wernicke (1981) developed a tectonic model of an extensional analogue to the popular thin-skinned compressional model, with extensional deformation concentrated in narrow shallow-dipping zones of continental decoupling. He later (Wernicke, 1985) enlarged the model of detachment tectonics proposing that large-scale, uniform-sense simple shear took place on low-angle detachment shear systems beneath normal fault systems with colinear ductile movement in subjacent highly deformed metamorphic core complexes. Wernicke (1985) further suggested that the upper crustal-shear systems may penetrate the entire lithosphere as single entities and that large extensions on such zones were the precursor to final plate separation and oceanic crust formation, as the lithosphere eventually broke under tension and the asthenosphere reached close to the Earth's surface.

Sandiford and Powell (1986) have recently widened the scope of this model, citing the increased heat flow and elevated geotherms associated with present-day extensional regimes, to suggest that it may be the cause of deep crustal metamorphism, which can be observed in modern and expected in ancient examples.They proposed that an increase in temperature from 450–500 °C at 30 km beneath stable cratons, to 700–900 °C beneath regions such as the extending Basin and Range Province is sufficient to generate granulite facies assemblages at that depth, resulting from dehydration reactions involving the breakdown of biotite and hornblende with probably the associated production of granitic melts. Sandiford and Powell (1986) concentrated on the mechanisms for heat transfer and upward perturbation of the geotherm in the mantle lithosphere and lower crust beneath extensional zones and reviewed the P–T–t paths expected in such zones. They further emphasized the asymmetry of such zones, whereby the region of most pronounced lithospheric thinning (and thus maximum heat flow) could be considerably displaced from the region of maximum crustal thinning. They did not, however, discuss the associated deposition of, and the prograde metamorphic paths imposed on, the supracrustal rocks, and therefore did not investigate the obviously important association of high-grade metasedimentary rocks with extension zones and the paradox of how surface-formed supracrustals reach the lower crust to be metamorphosed under such extreme conditions. Likewise, following the initial suggestion of McKenzie (1978) that rapid stretching of continental lithosphere could be the result of thinning and progressive upwelling of the asthenosphere associated with block faulting and subsidence and therefore lead to the progressive metamorphism of sedimentary piles in extensional basins, Wickham and Oxburgh (1985) investigated the transient thermal anomaly of the northeast Pyrenees as a possible rift/extensional orogen. However, they also studied the mechanisms for elevating the geothermal gradient in such regimes rather than studying the possible tectonic depression of the basin fill. They did, however, emphasize the significant contrasts between their Hercynian type tectonometamorphic regime where, owing to the active rifting and extension, the basin was still receiving sediment while metamorphism went on in the same sequence at depth, and the more normal (or more readily recognized) collisional orogenic setting of the Alpine/Himalayan chain.

Although crustal extension and subsidence of supracrustals fixed to the upper plate of a detachment model seems an ideal mechanism,

Wernicke (1985) did not extend the model to the development of metamorphic terranes. His extensional models (Wernicke, 1985; figs. 3 and 12) show supracrustals subsiding to at most 8–10 km and he favours the progressive flattening and flexing of detachment zones at depth, which would preclude further subsidence. Wynne-Edwards (1976), on the other hand, described platform sedimentary sequences near to basement–cover unconformities in the Grenville Province, reaching depths > 15 km during Proterozoic ensialic orogenesis.

Most modern authors (e.g., Bird, 1978; England, 1978; Shackleton, 1986) recognize the currently popular plate tectonic alternative mechanism of crustal convergence and sediment obduction as the mechanism of thickening continental crust and forcing sedimentary rocks to the depths where they can be metamorphosed to high grades with associated anatexis. Even in their recent proposition of melt-enhanced deformation with the association of deep crustal melts and high-deformation zones, Hollister and Crawford (1986) favoured subduction-related underthrusting of sediments, crustal thickening and slow heating to produce melts in lower crustal metasediments associated with detachment terranes.

In our recent review of the structure and tectonic history of the Harts Range area (Ding and James, 1985), we described a basement infrastructure and a cover sequence suprastructure, which underwent separate complex tectonothermal evolutions before being juxtaposed by major subhorizontal shearing and subsequently redeformed in a further complex orogenic episode. One of our main problems in interpreting the evolution of the area was in understanding the mechanism that could both metamorphose two supracrustal sequences to high grades at obviously deep crustal levels and subsequently overthrust the lower-grade over the higher-grade sequence in what was a classic thin-skinned thrusting regime. With the aid of more recent studies (see also associated papers, in this volume) we now enlarge on our discussion of the tectonothermal evolution of the Harts Range area and propose a new model for its evolution, which may have wider applications to Proterozoic tectonics.

Geological framework of the Harts Range area

The location of, and a simplified geological map of, the Harts Range area are shown in Fig. 1; and a refined tectonothermal history of the area is presented as a time–space diagram in Fig. 2, where the tectonic history of the area is divided into three stages; the Strangways Orogenic cycle, the Harts Range Orogenic cycle and post-orogenic events. This latter diagram is a more detailed version of table II from Ding and James (1985) with which it may be compared.

The area can be divided into an unreworked basement and a supracrustal cover, with a major detachment zone of reworked basement separating them. We correlate the basement areas with those affected by the Strangways Event of Shaw et al. (1984) in the Strangways Range, some 50 km to the west of the Harts Range area. In Fig. 2 we therefore assign these rocks to the Strangways Orogenic Belt (SOB), i.e., having been affected by the Early–Middle Proterozoic Strangways Orogeny. In our earlier review we proscribed the evolution of the basement domains to a Stage I, possibly Archaean history. This conclusion is not supported by recent isotope geochronology (Mortimer et al., 1986, 1987; Cooper et al., 1988).

The most significant of the unreworked basement areas are those situated to the south of, and thus as a lower/footwall plate to, the Muller Thrust (see Fig. 1). The Entia Dome represents a major tectonic window of unreworked SOB exposed due to much later crustal flexing of its bounding Entia Thrust, and the Atnarta window is a smaller example of the same type of feature.

We now define all of the area north of the Muller Thrust, as shown on Fig. 1, excepting those basement rocks exposed in the Entia

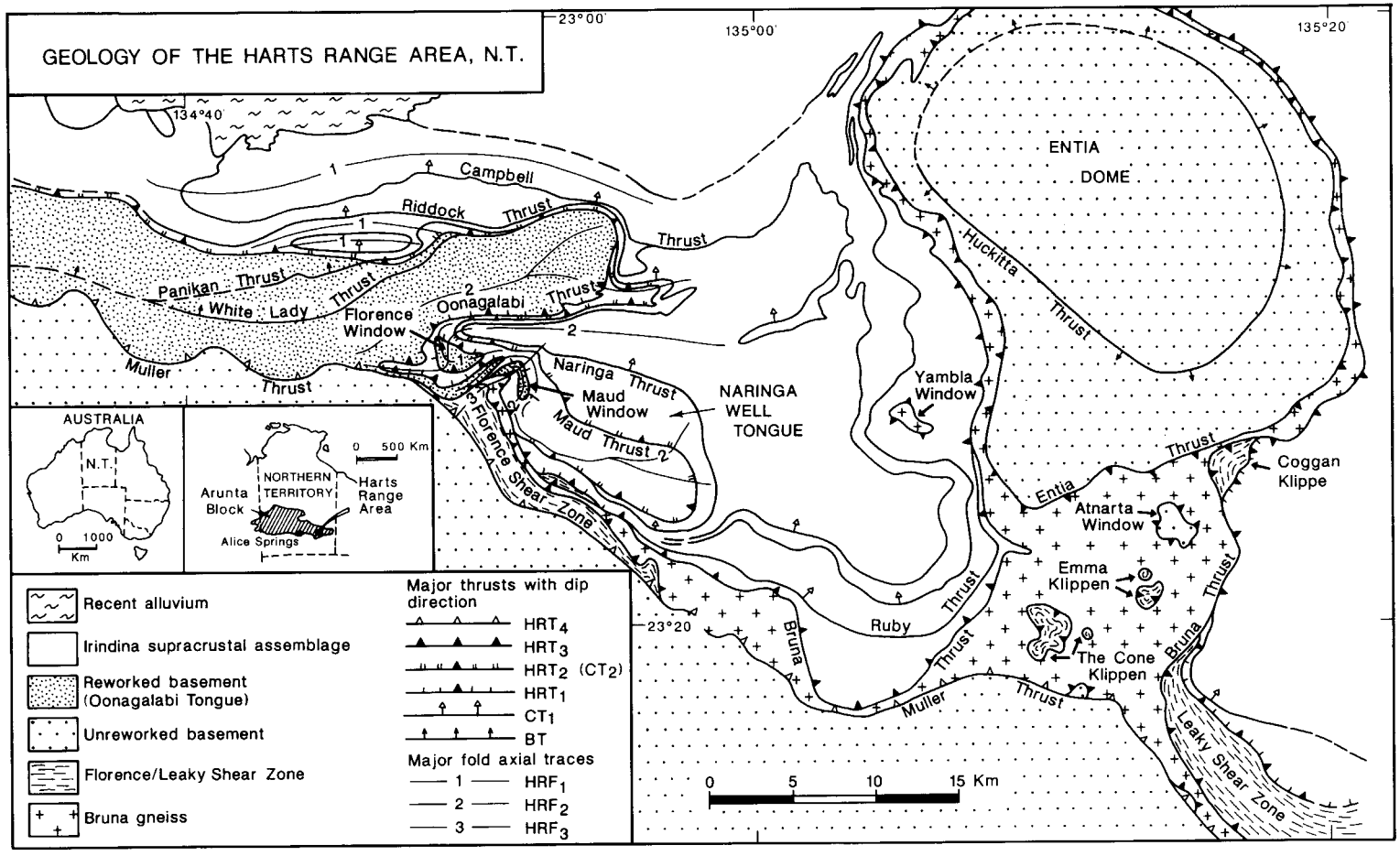


Fig. 1. Geological and tectonic map and location of the Harts Range area.

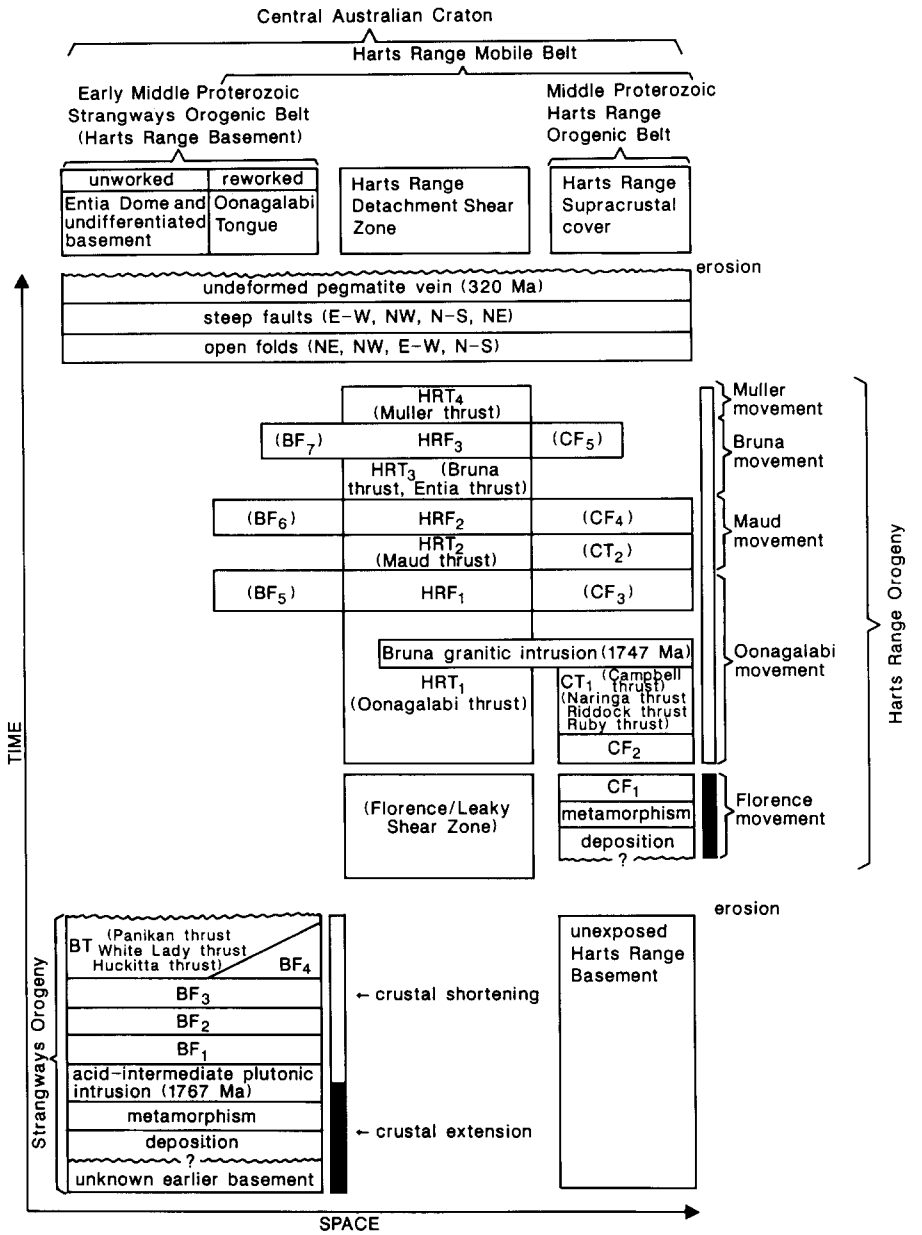


Fig. 2. Tectonothermal evolution of the Harts Range area.

Dome, as belonging to the Harts Range Mobile Belt (HRMB), and as having been affected in the Middle Proterozoic by a younger extension–collision orogeny, the Harts Range Orogeny (HRO) of Fig. 2. The areas of SOB basement unaffected by this orogeny (i.e., south of the Muller Thrust and in the Entia Dome) therefore represent a stabilized substrate and presumably a cratonic basement to this mobile belt.

The HRMB was initiated by the development of a low-angle extensional detachment zone, the Harts Range Detachment Zone, (HRDZ) within the pre-existing cratonic SOB basement (Fig. 2). This detachment zone was initiated as a thick complex zone with a major

displacement surface in the middle bounded on either side by wide mylonite zones. High-grade (granulite facies) mylonites and intense LS tectonites associated with an upper plate to the north (extensional) movement sense are found within this shear zone, which was reworked during the contraction phase of the HRO by folding and thrusting.

The Oonagalabi Tongue, bounded partly by the Oonagalabi Thrust, and partly by the Maud Thrust, represents the largest and most striking example of reworked basement within the HRDZ, while the Florence and Maud windows are smaller and more complex. The Florence Shear Zone and Leaky Shear Zone represent the other principal relicts of the earliest-formed parts of the HRDZ and occur in two significant exposures in the Harts Range area. Both occur in the southern part of the area close to the boundary between basement and cover, and both are intimately associated with outcrops of the Bruna granitic gneiss (Fig. 1). In the southwest, the Florence Shear Zone crops out spectacularly in the Florence Creek and forms a belt up to 2 km wide and 20 km long in the spinifex-covered low hills adjacent to it and its tributaries. In the far southeast of the area a range of hills exposes the Leaky Shear Zone (named after the adjacent Leaky Bore). These two shear zones, as described later, are identical, but have been named separately due to their 30 km separation and the complexity of the intervening geology.

Further minor exposures of the HRDZ (the Emma Klippen and The Cone and Coggan Klippen) crop out as tectonic/erosional klippen in the broad square outcrop of Bruna gneiss which occurs between the Entia, Muller and Bruna Thrusts in the southeast of the area (Fig. 1).

A thick plutonic acid sheet (the Bruna granitic gneiss) is associated with the HRDZ throughout most of the area. It forms a continuous ring around the Entia Dome between the Entia and Bruna Thrusts, and thins as a narrow WNW–ESE zone as it intrudes the Florence Shear Zone to the WNW and the Leaky Shear Zone to the ESE, where it is truncated to the south by the Muller Thrust.

A thick sequence of supracrustal sediments and mafic igneous rocks above the HRDZ is named the Harts Range Supracrustal Cover (HRC) which is now represented in the area by the Irindina supracrustal assemblage including the Harts Range meta-igneous complex (Sivell and Foden, 1985). This sequence forms the structurally overlying nappes of the HRMB and is from north to south progressively floored by the Maud, the Oonagalabi and then the Bruna Thrusts, and the thinness of the sequence in the east is shown by the window of Bruna gneiss (Yambla window) which occurs in the centre of the area (Fig. 1). Within the cover sequence the Ruby, Campbell, Riddoch, Naringa and Maud Thrusts separate major lithologic and structural domains which make up the cover nappes of the HRMB.

The HRC, some parts of the earlier-formed HRDZ (i.e., Florence and Leaky Shear Zones), intrusives into the HRDZ (i.e., Bruna gneiss) and part of the SOB basement (Oonagalabi Tongue) were finally deformed by the compressional phase of the HRO. As will be described later in detail, this deformation was concentrated in the HRDZ during crustal contraction by repeated thrusting and folding. Individual cycles of movement during this contraction (collision) phase, include the Oonagalabi, Maud, Bruna and Muller movement phases (Fig. 2).

Geological evolution of the Harts Range area

The Strangways orogenic cycle

Deposition

During the Early Proterozoic (Plumb and James, 1986) a sedimentary and possibly volcanic sequence was deposited in an extensional basin, forming sandstones, limestones, marls, siltstone, shale and possible basic and acid volcanic rocks, which together with mafic/ultra-

mafic intrusions, formed the earliest supracrustal deposits recognized in this area. In the Entia Dome such supracrustal rocks now form only a very minor component of the gneissic sequence owing to gross plutonic invasion (see later), whereas in the western part of the unreworked SOB, within 5–10 km south of the Oonagalabi Tongue, supracrustals with major continuous quartzo-feldspathic gneiss, pelitic gneiss and marble/calc-silicate horizons form a greater proportion (up to 50% of the sequence according to Goscombe (1984) and L. Rankin (personal communication, 1985)). No basement to these supracrustals has yet been discovered. However, the rocks are very similar to the bimodal sequence described from the Strangways Ranges (Warren, 1979, 1983; and Shaw and Langworthy, 1984), and the sequences from the two areas may have a common origin.

High-grade metamorphism

The supracrustals of the SOB in the Harts Range area were metamorphosed to upper amphibolite and granulite facies at ~ 1800 Ma (Fig. 2). Unlike Shaw et al. (1984) who describe a thermal culmination late in the tectonic evolution of their Strangways Event, we consider that maximum P–T conditions were reached during the formation of the first recognized metamorphic compositional layering and layer-parallel fabric in the metasediments and metaigneous layers (pre-BD_1). Goscombe (1984) describes this as being characterized by the presence of orthopyroxene plus plagioclase in mafic gneiss, and of microperthitic and disordered feldspars, indicating an early prograde metamorphism to transitional hornblende–granulite facies at 700–800°C and 7–8 kbar, from rocks just south of the western extent of our area. A few kilometres to the north, Sivell and Oliver (in preparation) describe a metamorphic peak in granulites of both the Cadney and Oonagalabi gneiss complexes of 870–960°C at nearly 9 kbar. In the Entia gneiss a slightly lower P/T regime of upper amphibolite facies (650–750°C at 7–9 kb) is described by Oliver et al. (1988). Thus the earliest high-grade metamorphism of the SOB appears to decrease in grade from WNW to ESE across the Harts Range area. This is supported by the work of Warren (1979, 1983) who recognized a granulite facies thermal peak in the Strangways Range to the northwest, with maximum conditions of 850–920°C at 8 kbar, decreasing in temperature locally from west to east, and which she also concluded must have occurred soon after original deposition of the SOB supracrustals. The presence of a basinal supracrustal sequence, and the early high-grade metamorphism within the SOB, both indicate that it may have formed in an early phase of extensional tectonism in the manner described by Sandiford and Powell (1986). This tentative interpretation is indicated on Fig. 2.

Voluminous early tectonic acid–intermediate plutonism

In the lower and middle levels of the SOB, acidic to intermediate plutonics were emplaced along the metamorphic layering and early foliation of the gneisses. In contrast to the metamorphic gradation of decreasing temperature from west to east, the most voluminous plutonism is to be found in the Entia Dome where it comprises often more than 80–85% of the total rocks (Foden et al., 1988), and forms the major plutonic Huckitta and Inkamulla bodies, which are multiple intrusions with individual granitic horizons up to 100 m in current thickness. Thus, in the Entia Dome, the metamorphosed supracrustals become discrete lenticular bodies and separated thin layers within a predominantly orthogneiss complex. In the northwest, high-grade orthogneisses make up 75–80% of the total rocks in the Oonagalabi Tongue. However, in the western part of the unreworked SOB, they are more subordinate to the SOB supracrustals, which retain their integrity as continuous horizons (Goscombe, 1984).

The granitoids of the Entia Suite intruded at or shortly before 1767 Ma (Mortimer et al.,

1986, 1987; Cooper et al., 1988 and thus provide an excellent time marker for the commencement of the early tectonothermal evolution of the SOB. The plutonism just post-dated the metamorphic maximum which appears to have occurred close to the commencement of SOB orogenic contraction.

Crustal shortening in the SOB

Basement comprising the Oonagalabi Tongue, the Entia Dome and the whole southern margin of the study area displays repeatedly superposed isoclinal folds developed under high amphibolite to granulite facies conditions, which fold both the metamorphosed supracrustals and their intrusive orthogneisses. The intense compositional layering and schistosity in the orthogneisses were developed as axial-planar fabrics associated with the earliest folding (BF_1). In the Oonagalabi Tongue, a change in metamorphic conditions is indicated by the intimate intercalation of amphibolite facies orthogneisses with partially retrogressed mafic granulites.

Such repeated refolding and repetition of lithologies about primarily recumbent axial surfaces, could only be produced by contraction and thickening of the crust (see Fig. 2, BF_1–BF_4). Three major fold generations have been recognized in the Entia Dome (Foden et al, 1988) and four generations in the other basement areas. Fold hinges of superposed phases are commonly coaxial, and intense LS to S > L fabrics with mineral/stretching lineations subparallel to the fold hinges attest to the overall intensity of the strain. The SOB deformation was caused by prolonged subhorizontal ductile strain with a predominant NNE–SSW principal elongation direction. Neither the sense of shear, nor the amount of strain can be estimated from the basement lithologies, although some individual mafic layers show ductile thinning from hundreds of metres down to less than one metre. The bulk strain, however, was much less than this, as while folding due to lateral (layer-parallel) compression thickened the sequence, flattening due to vertical (layer-normal) compression concomittantly attenuated the same sequence. The basement strain geometry thus appears to have been produced largely by subhorizontal flattening together with intense non-coaxial shear.

The folded SOB sequence was finally displaced internally by thrust-sense shear zones (BT of Fig. 2) which terminated the Strangways Orogeny. The Huckitta Thrust (Fig. 1) is a regionally layer-parallel discordance that formed following the BF_3 folding in the Entia Dome, while the Panikan and White Lady Thrusts transect the layering at a low angle following BF_4 in the Oonagalabi Tongue.

We find similar structural trends throughout the basement areas of the SOB in the Harts Ranges, which, together with the similar structural styles in the Strangways Ranges (B.D. Goscombe, personal communication, 1986) and the similarly NNE–SSW aligned metamorphic gradation and plutonic zonation, suggests that the SOB is a single orogenic belt.

The Harts Range Orogeny (HRO)

The Florence movement phase

Towards the end of the Strangways Orogeny the whole SOB must have been greatly thickened. The Florence movement (Fig. 2) was the beginning of a cycle of large-scale crustal extension, with at this time a NNE–SSW principal horizontal extension, initiating an ESE–WNW orogen which cut at a high angle across the trend of the SOB. This feature further confirms the fundamental relative temporal difference between the HRO and the Strangways Orogeny. It also emphasises the change in crustal stress conditions which must have occurred over a very short time period (a few million years, Cooper et al., 1988) just after 1767 Ma, from horizontal WNW–ESE compression to horizontal NNE–SSW extension.

Extensional movement concentrated along a discrete master detachment zone (the HRDZ) that became the locus for all further displace-

ments in the HRMB, and which we have been able to document in considerable detail. The form of the HRDZ is similar to the type of gently dipping low-angle normal shear or detachment zone, described as a model for explaining crustal extension within the Basin and Range Province (Davis and Coney, 1979; Wernicke, 1981, 1985), and also to explain deep crustal metamorphism (Sandiford and Powell, 1986).

During the initial development of the HRDZ, the zone consisted at deep crustal levels of a low-angle discrete detachment fault bounded on either side by high-grade, granulite facies shear zones. The preserved parts of this shear zone are now recognized as the separate relicts of the Florence and Leaky Shear Zones, each up to 2 km thick (Figs. 1 and 4(a)), together with the minor intervening tectonic klippen. These zones are identical, exhibiting intense, shallowly north-dipping, strongly layered protomylonites and mylonites, with intense layer-parallel foliation and consistently N–S to NE–SW trending lineations. Kinematic indicators including asymmetric augen and quartz and hornblende petrofabric diagrams show consistent extensional (i.e. hanging-wall north) movements (Liu, 1987; James et al., in press). The microstructure and mineralogy of these zones indicates deeply located shearing under high temperatures provisionally estimated as 800–850°C (i.e., similar to the SOB). The Oonagalabi gneisses which were later reactivated in the compressional phase of the HRO are also considered to have formed within the HRDZ, which therefore must have been at least 2–5 km thick.

The detachment zone may have traced updip to a Basin–Range type brittle extending orogen, which would have been located far to the south of the current HRMB position, and which would have been lost to erosion (Figs. 3 and 4). Continued extension may have resulted in the subsidence of the upper (northern) plate relative to the lower (southern) plate. New sediments of the HRC sequence were deposited into the subsiding basin under initially shallow-water conditions and formed the sandstones,

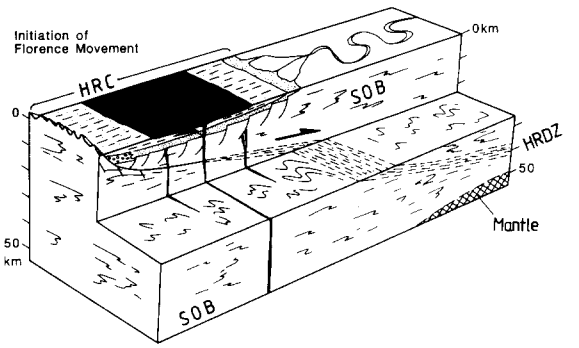


Fig. 3. Block diagram showing the early development of the Florence Movement phase, including the initiation of rifting, block subsidence and formation of the HRC.

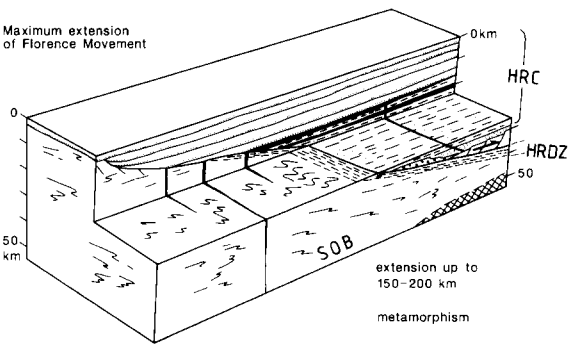


Fig. 4. Full extension and juxtaposition of the HRC over high-grade rocks of the HRDZ.

limestones, marls, siltstones and shales which now form the most southerly (and likely earliest) sequences of the Naringa Well area (Ding and James, 1985). Deeper water conditions producing arkoses and greywackes formed later in the deepening basin, and further to the north, where they now form semi-pelitic gneisses. Extension led to fracturing of the continental crust and the development of extensive basaltic lava flows (Fig. 3) accompanied by mafic and ultramafic intrusions of the Harts Range meta-igneous complex (Sivell and Foden, 1985). These igneous rocks are more closely associated with the northern exposures of the deeper water sediments as would be expected in an extending orogen over a thinning crust.

Continued extension drew the HRC supracrustals deeper within the crust until they eventually came into contact with the HRDZ

and lower plate granulites (Fig. 4). During this time they would have been affected by the increased confining pressure and elevated geotherm, and were metamorphosed to upper amphibolite facies with minor partial melting during the development of a metamorphic layering. The HRC underwent only moderate early deformation. The first-phase isoclinal folds (CF_1) are minor and uncommon with an axial planar fabric (CS_1) in pelitic gneiss and a weak N–S trending mineral lineation (CL_1).

The Oonagalabi movement phase

The end of the extensional Florence movement phase saw a major change in tectonic style. The HRO changed to a contractional orogen which developed an unusually complex style of thrusting and folding. This movement led to the southward shallow overthrusting and gradual relative uplift of the HRC on the upper plate of the HRDZ, with most intense deformation concentrated along the detachment zone and its bounding decollement surfaces. The earliest evidence of contraction during the HRO is provided by isoclinal folding on a major scale (CF_2) in the cover sequences in the northwest Harts Ranges north of the Naringa Well area. The folds trend mainly E–W, with shallow east and west plunges and a parallel weak axial mineral lineation and they thus lie at a high angle to the regional HRDZ shortening direction (Fig. 5). The bulk strain during CF_2 appears to be similar to that displayed in the basement, while strain shown by individual layers may be much less than that shown by such layers in the basement. This folding was followed by southwards thrusting along the top principal bounding fault of the HRDZ which reactivated the Oonagalabi Thrust (HRT_1), which was the first fault developed during the HRO, and which is preserved as the tectonic boundary between the SOB basement and HRC supracrustals, south of the Oonagalabi Tongue and in the Florence Creek areas (Figs. 1 and 6(a)). Displacement also took place along the bottom bounding fault of the HRDZ juxtaposing granulite facies within the HRDZ against the underlying amphibolite facies Entia gneiss complex, as can be seen in the Leaky Shear Zone and the Coggan Klippen. Concomitantly, southwards thrusting in the HRC occurred (CT_1) with successive formation and overriding of the major Campbell, Riddoch and Naringa Thrusts (Fig. 1).

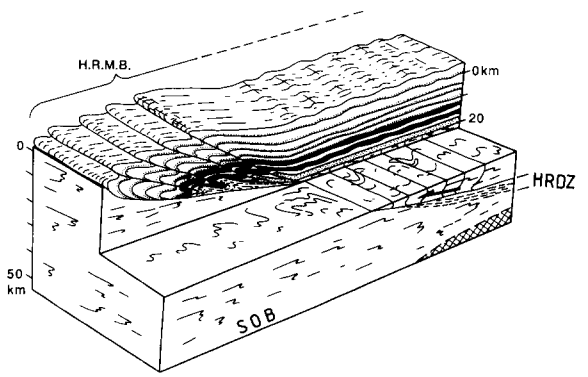


Fig. 5. Block diagram showing the HRF_1 folding developed during shortening of the Oonagalabi Movement phase.

Intrusion of the Bruna granite

The protolith to the Bruna gneiss, a coarsely porphyritic and potassic granite, preferentially intruded along the still active Florence/Leaky Shear Zone (Figs. 1 and 6(b)) at 1747 Ma (Cooper et al., 1988). This unit is thinnest in the west of the zone and thickens rapidly eastwards and southeastwards until it almost obscures the earlier high-grade mylonites of the zone. The body intrudes near the base of the HRDZ in the east and transgresses to intrude near the top in the west, where small stocks and sills cross-cut the HRC sequence (Fig. 1). Mylonites and other shear zone products remain as large xenolithic fragments within the Bruna gneiss. Further shearing occurred after solidification of the Bruna granite, which was thus deformed and mylonitized with the strain preferentially partitioned into shear zones at the margins and occasionally within the Bruna gneiss. Flattened and elongated feldspar megacrysts within the Bruna gneiss indicate both oblate and plane strains (James et al., 1985, in

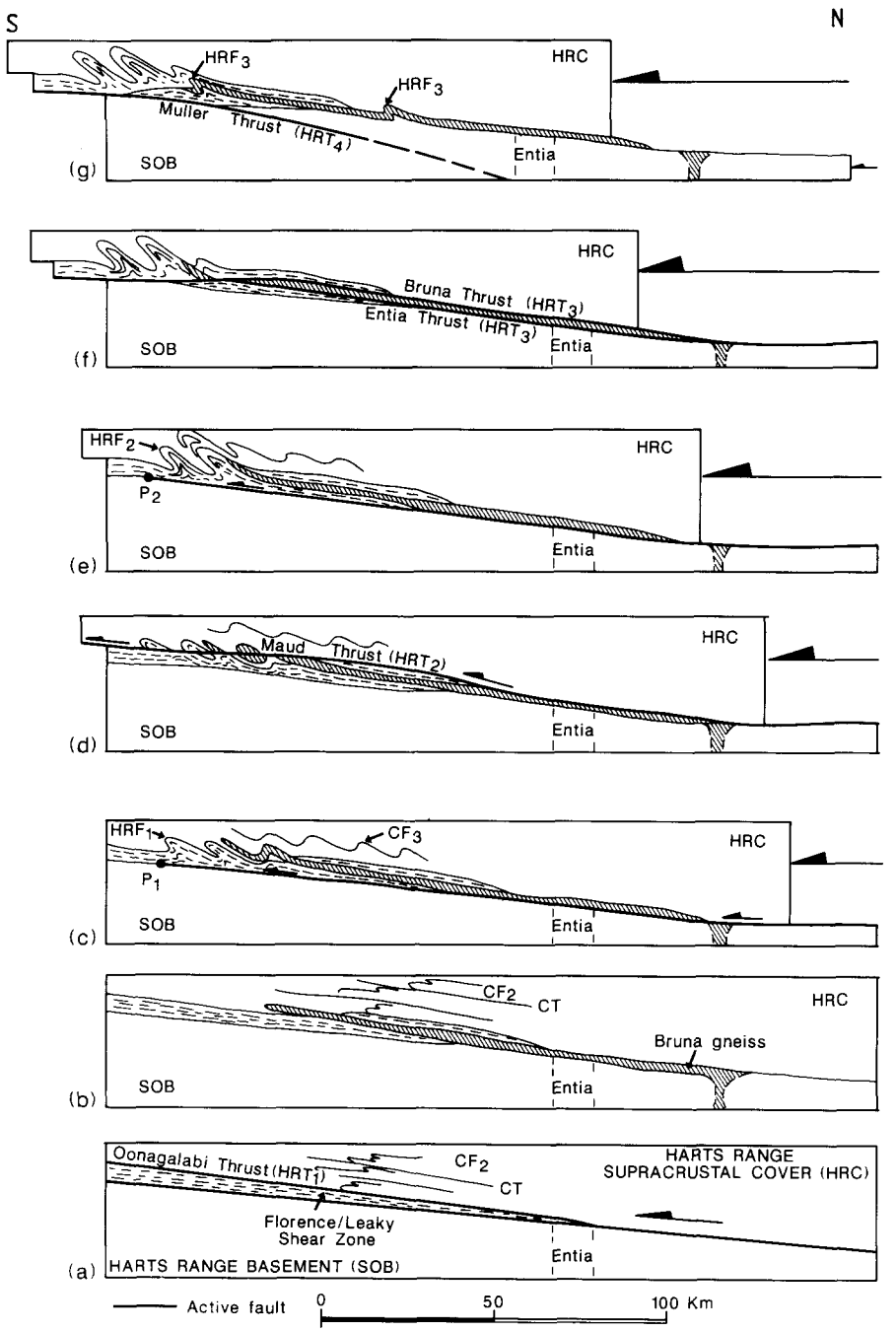


Fig. 6. Cartoon showing the evolution of the Harts Range orogeny. (a)-(c) Oonagalabi Movement phase, (d) and (e) Maud movement phase, (f) and (g) Bruna and Muller Movement phases.

press), whereas kinematic indicators suggest contractional movement senses of the upper plate primarily to the south (James et al., in press).

Oonagalabi movement phase (continued)

During continued activity of the Oonagalabi movement phase the displacement on the bottom bounding fault of the HRDZ was inter-

rupted by pinning of the active thrusting at point P_1 of Fig. 6(c). Continued movement of the upper plate sequence over the HRDZ then led to the development of buckles and subsequently major folds in that part of the basement previously incorporated within the major detachment/shear zone (e.g., see the Florence window of Fig. 1), and in the overlying already folded supracrustals, as well as in the intrusive Bruna gneiss. All major folds are very tight to isoclinal, but inclined and asymmetric with a consistent southerly vergence indicating continued overriding from the north caused by the consistent subhorizontal northerly compression. This is the first fold generation recognized to have affected the HRDZ thrust plane and is abbreviated as HRF_1 (Figs. 1 and 2), but it is the third fold generation recognized within the supracrustals (CF_3) and the fifth ductile fold generation affecting the rocks of the Oonagalabi Tongue (BF_5). The fold axes of HRF_1 or CF_3 folds trend E–W similar to those of CF_2 folds but the earlier folds (BF and CF) and thrusts (BT and CT_1) were all certainly involved in this fold generation as is shown by the detailed maps of Ding (1988).

The Maud movement phase

Folding of the detachment zone at the end of the Oonagalabi movement phase was succeeded by development of a new thrust plane, the Maud Thrust, which truncates the HRF_1 folds, and is abbreviated as HRT_2 (Figs. 1, 2 and 6(d)). The Maud Thrust has a complexly folded geometry, but on Fig. 1 can be seen to ramp up from its position as the basement–cover boundary at the northern edge of the Oonagalabi Tongue to a central, layer-parallel position within the Naringa Well Tongue, until it is finally truncated in the south by the Bruna Thrust (see later).

The Maud Thrust event was followed by a change to a major transpressional movement. The macroscopic geometry can be explained by thrust movement pinned at the base of the detachment zone, this time at point P_2 shown on Fig. 6(e), and a major slab of the reworked SOB basement, the Oonagalabi gneiss complex, which had earlier been intensely sheared in and incorporated into the HRDZ, and its overlying cover sequence together with all the pre-existing thrusts and folds of the detachment zone, were thrown into a regional reclined fold pair. In the north, the Oonagalabi Tongue has an amplitude and wavelength in the order of 5–10 km, and is wholly cored by SOB basement gneisses, which must have retained their ductility at least through this event. Smaller basement lobes and windows also core the similar magnitude fold of this generation in the Naringa Well Tongue, which is bounded by the folded CT_1 Naringa Thrust. This is the second fold generation that affected the detachment shear zone and is abbreviated as HRF_2 (Figs. 1 and 2), while it represents the fourth fold generation in the supracrustals (CF_4) and the sixth fold generation in the basement (BF_6). The HRF_2 folds are reclined or subneutral isoclinal folds, which have E–W trending fold axial planes and shallow to intermediate north-plunging fold axes.

The easterly vergence of these structures, plus their style, suggests E–W subhorizontal shearing of the hanging-wall upper plate as the most likely cause, with dextral transcurrent shear concentrated on the major northerly inclined HRDZ shear/detachment zone. The change from southerly overthrusting, to eastwards overfolding in a low-angle transpressional regime could well have been imposed on the zone as a local rotation or scissor movement of the moving upper plate, caused by the initial pinning of its thrust movement at a single point, rather than along a line, as appeared to occur during the earlier Oonagalabi phase.

The Bruna movement phase

Compression from the north continued with a return to intense thrusting and ductile shearing, which occurred within a major part of the

HRDZ. This movement, which transected the HRF_2 folding, was partitioned mainly along the top margin of the sill-like Bruna gneiss body, where it formed the Bruna Thrust (Figs. 1 and 6(f)). Movement also took place within the gneiss body forming stacked heterogeneous protomylonite, mylonite and ultramylonite zones, and also along its bottom margin forming the Entia Thrust of the Entia Dome. All stretching lineation trends indicate a N–S or NNE–SSW principal extension, while rotational criteria such as asymmetric augen (Simpson and Schmidt, 1983; Faure, 1985) and asymmetric shear bands (Lister and Snoke, 1984) indicate primarily overthrusting of the cover sequence towards the south (James et al., in press). Both the top and bottom thrusts are abbreviated as HRT_3 on Figs. 1 and 2, though their precise location is only regionally rather than locally known, as the shearing and thrusting tends to depart intermittantly from the boundaries of the Bruna gneiss by as much as several hundred metres. The mylonitic layering is commonly folded on a small scale within the Bruna gneiss, forming asymmetrical folds which indicate further local pinning and interruption of thrusting. After the HRT_3 thrusting event, mafic magma intruded into the Entia gneiss, the Bruna gneiss and the supracrustals, and formed dolerite–gabbro dykes and sills, which are undeformed or weakly deformed.

The HRT_3 thrusts and the detachment shear zone as well as the adjacent basement and supracrustals were then locally folded at a mappable scale (Fig. 1). This is the third fold generation to have affected the detachment shear zone and is abbreviated as HRF_3, and therefore represents BF_7 folding in the basement or CF_5 in the cover (Fig. 2). The HRF_3 folds are tight asymmetric to isoclinal, neutral folds with fold axes trending NNE–SSW, similar to the HRF_2 folds. Although they are local in effect, one HRF_3 fold is as large as a few kilometres in amplitude and this phase forms the last intense ductile deformation of the HRDZ (Fig. 6(g)).

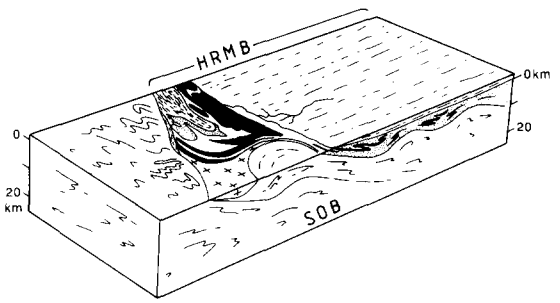


Fig. 7. Block diagram showing final relationships of the units as at the present erosion level.

The Muller movement phase

The Harts Range orogenic cycle was terminated by thrusting along the Muller Thrust (HRT_4), which cuts HRF_3 and the earlier thrusts and folds (Figs. 1 and 2) and bounds the southern margin of the Harts Range Mobile Belt. The thrust is marked by a narrow mylonite/schist zone which trends ENE–WSW across the whole area and varies from tens up to hundreds of metres across and dips from 45–55° N with a regular strong down-dip lineation. Muscovite and biotite developed in typical retrograde assemblages associated with epidotization. Relict high-grade mylonites suggest that this relatively narrow zone, which transects all earlier structures, became the locus of displacement for the whole area. It is gently warped by later flexures, but otherwise is undeformed and carried the Entia gneiss to its current position along with the remainder of the overlying HRMB (Fig. 7).

Discussion

The Harts Range Detachment Zone and the Harts Range Cover sequence are most significant in that they show a close spatial and temporal, and thus causal, relationship between a stratotectonic (geosynclinal) phase of basin development and an active basement detachment zone, for this Early–Middle Proterozoic region of central Australia. Although such relationships between kinematically active plate

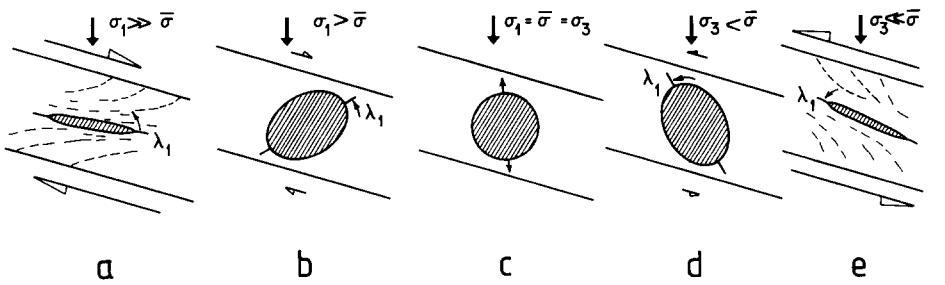


Fig. 8. Effect of reversal of sense of shear on a detachment zone dipping at 15°, with anticlockwise rotation of principal maximum deviatoric strain axis. Strain intensity during extension decreases from a to b, reverses at c and increases during crustal contraction from d to e.

and especially intra-plate boundaries should be expected due to the compatibility considerations involved in partitioning strains in a stressed crust, we consider that this is one of the first demonstrated examples of such a relationship so early in the geologic record. A similar model is proposed by Gordon and Hempton (1986) who provide convincing evidence of the temporal and spatial association of the Late Proterozoic Keewanawan Rift with the convergence and collision event which formed the Grenville Orogen. They also cite a number of recent actualistic models (Red Sea rift/Zagros–Bitlis system) and older rift/collision related tectonic comparisons to support their proposal, all of which demonstrates the inter-

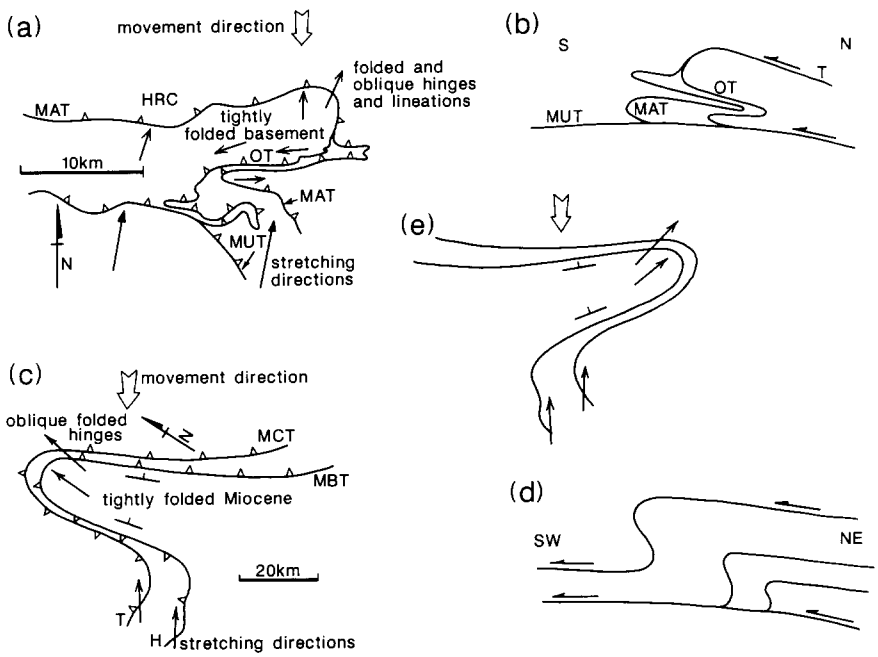


Fig. 9. (a) Sketch map of the Oonagalabi Tongue with (b) sketch section. MAT, Maud Thrust; MUT, Muller Thrust; OT, Oonagalabi Thrust. Sketch map (c) rotated to similar orientation as (a) for comparison, and section (d) of the Hazara syntaxis from Coward (1982). MCT, main central thrust, MBT, main boundary thrust; H, Hazara Thrust. The simplified sketch of the Hazara syntaxis (e) has been inverted (i.e., as if viewed upwards from beneath) to emphasize the great similarity with the Oonagalabi Tongue.

dependence and transfer of intra-plate strains.

Another significant feature of the two closely related orogenic episodes in the Harts Ranges is the development of the subconcordant plutonism which appears to be temporally related to the change from extension to contraction in both the SOB and the HRMB. This temporal association of the change in tectonic environment and the major plutonic event may indicate a possible genetic relationship. An extensional regime with a likely vertical maximum principal compressive stress would certainly not favour the bodily emplacement of thick volumes of granitic magma in a lit-par-lit fashion at varying scales in a gneissic pile. However, a change of stress regime from a horizontal principal tensile stress to a horizontal principal compressive stress (with a concomittant vertical principal tensile stress) would be more likely to affect the base of a thinned crust (before it became rapidly thickened by shortening and thrusting) and might favour the prising apart of layers, especially those with strong competence contrasts and an intense foliation, in the metamorphic pile (Fig. 8).

The common association of extensive concordant igneous bodies with ductile deformation zones has recently been discussed by Hollister and Crawford (1986). In their tectonic surge model, they suggest that melts derived by deep crustal anatexis or mantle addition weaken deep crust and accelerate movement to facilitate large-scale vertical displacement of metamorphic crust. They describe, from the cordilleran terranes of British Columbia, uplifts of the order of 12 km in 12 Ma (a rate of 1 mm a^{-1}), with sills of plutonic material hundreds of metres thick localized in zones of most penetrative deformation, and they further cite the coaxiality of igneous flow and metamorphic stretch lineations as evidence for the coincidence of melt transport and movement of the metamorphic country rock. The ubiquitous association of plutonic melts with intense deformation in the SOB (and with the Bruna gneiss) supports the interpretation that

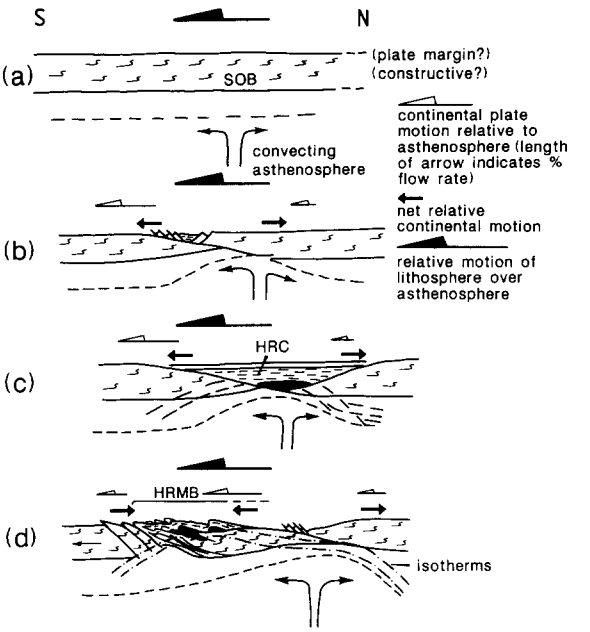


Fig. 10. Sketch sections showing a 'caterpillar tectonic' model (modified from the detachment model of Wernicke (1985) and the millipede model of Wynne-Edwards (1976) for the evolution of the HRMB. SOB, Strangways Orogenic Belt; HRC, Harts Range Supracrustal Cover; HRMB, Harts Range Mobile Belt.

this was a site of Proterozoic deep-crustal detachment.

The contractional phases of the HRO with the repeated development of discrete thrusts which formed a typical, but highly attenuated, ramp and flat morphology, together with the consistency of trends of principal stretch lineations, all provide supporting evidence that it formed as a typical thin-skinned response to crustal contraction. Thrusts developed in a piggy-back fashion (Butler, 1982) with the most northerly and uppermost thrusts (e.g., CT_1) formed first and succeeding and lower thrusts carrying the earlier ones.

Of special significance in this area is the Oonagalabi Tongue which provides the first and most striking evidence of alternating ductile and semi-ductile stick–slip deformation with the development of intensely folded major thrust boundaries. The geometry, scale, kinematic

pattern and tectonic position of the HRF_2 Oonagalabi Tongue all show a marked similarity to that described for the development of the Hazara and Nanga Parbat syntaxes of the western Himalayas in northern Pakistan (Coward, 1983). These isoclinally folded re-entrants of Eocene–Miocene molassic shales and sandstones developed in the upper plate of active detachments by sticking on lower thrusts. The Hazara syntaxis especially (Fig. 9) closely resembles the Oonagalabi Tongue and is described with a hingeline oblique to the main thrust movement likely to have been produced by, 'crumpling of higher thrusts into oblique folds', due to differential movement of the lower thrusts (Coward, 1983), i.e., a scissor action identical to that interpreted from the Oonagalabi Tongue.

Favoured models for the evolution of deformation belts in the Precambrian currently fall into two groups; those invoking strictly uniformitarian collisional orogeny following oceanic lithosphere subduction at destructive plate margins (B-subduction), and those involving mantle-plume-generated extension and limited lithospheric subduction following intra-lithosphere decoupling (A-subduction). These are extreme models of the many mechanisms invoked to cause collisional orogeny. Shackleton (1986) favours the former, largely due to the lack of evidence supportive of A-subduction models and thus the difficulty in demonstrating their existence, of which he is therefore "not convinced". We favour a new model which resembles the A-subduction model of Kroner (1983), because it provides a simple mechanism for repeated ensialic crustal reworking involving cyclical extension and compression and thus fits the pattern that we have interpreted from the Harts Range area. However, our preferred tectonic model for the production of Proterozoic ensialic mobile deformation belts more closely resembles a modified version of the 'millipede' model of Wynne-Edwards (1976). In his general review of Proterozoic tectonics Wynne-Edwards contrasted typical Phanerozoic plate margin orogenesis, involving eugeosynclinal volcaniclastic arcs, blue schists and ophiolites, with characteristic Proterozoic orogenesis which involved the ensialic reworking of granitic basement–gneiss complexes overlain by shallow miogeosynclinal platform sequences. He accounted for this latter tectonic style, as exemplified by the Grenville Province, by invoking a ductile spreading model involving hot sialic crust that underwent extensional and then compressional subhorizontal flow as it moved unidirectionally over a mantle plume.

In the Harts Range area we see all the characteristics of repeated ensialic orogenesis of granitic basement gneisses and cover sequences developed and tectonothermally worked and reworked, in firstly extending orogens similar to those recognized as metamorphic core complexes, and secondly in compressive subhorizontal flow regimes and fold thrust belts. In Fig. 10, we sketch a possible lithospheric model of evolution which most closely fits our spatial and temporal observations. Our model, though similar to the millipede model of Wynne-Edwards, does not rely on the variation of plutonic intrusive ages sequentially across a mobile belt. It is rather characterized by repeated extension and contraction. Thus we prefer the analogue of the active motion similar to that of a caterpillar moving unilaterally (but with the ability to change direction) over the ground to the movement of tectonic elements in our model and thus suggest the title of caterpillar tectonics to indicate this as a common style of Proterozoic orogenesis.

Acknowledgements

We thank our colleages John Cooper, John Foden, Robert Lawrence and Robin Oliver for reviewing early drafts of this paper, and Mike Sandiford, Mike Rickard and Mike Etheridge for helping to improve significantly the final version. Sherry Proferes and Rick Barrett for cartography and photography, respectively. The Adelaide University Geology Departments'

Harts Range Project is funded by the A.R.G.S. grant No. E8215617 for which we are grateful.

References

Angelier, J. and Colletta, B., 1983. Tension fractures and extensional tectonics. Nature, 301: 49-51.

Bird, P., 1978. Initiation of intracontinental subduction in the Himalayas. J. Geophys. Res., 83: 4957-87.

Butler, R.W.H., 1982. The terminology of structures in thrust belts. J. Struct. Geol., 4: 239-247.

Cooper, J.A., Mortimer, G.E. and James, P.R., 1988. Rate of Arunta Inlier evolution at the eastern margin of the Entia Dome, central Australia. Precambrian Res., 40/41: 217-231.

Coward, M.P., 1983. Thrust tectonics, thin-skinned or thick-skinned, and the continuation of thrusts to deep in the crust. J. Struct. Geol., 5: 113-123.

Davis, G.H. and Coney, P.J., 1979. Geologic development of Cordilleran metamorphic core complexes. Geology, 7: 120-124.

Ding, P., 1988. Geological evolution of the Harts Ranges in central Australia. Ph D. thesis, University of Adelaide (submitted).

Ding, P. and James, P.R., 1985. Structural evolution of the Harts Range area and its implication for the development of the Arunta Block, central Australia. Precambrian Res., 27: 251-276.

England, P.C., 1978. Some thermal considerations of the Alpine metamorphism, past, present, future. Tectonophysics, 46: 21-40.

Faure, M., 1985. Microtectonic evidence for eastward ductile shear in the Jurassic orogen of SW Japan. J. Struct. Geol., 7: 175-186.

Foden, J.D., Buick, I.S. and Mortimer, G.E., 1988. The petrology and geochemistry of granitic gneisses from the east Arunta Inlier, central Australia: implications for Proterozoic crustal development. Precambrian Res., 40/41: 233-259.

Gordon, M.B. and Hempton, M.R., 1986. Collision-induced rifting: the Grenville Orogeny and the Keweenawan rift of North America. Tectonophysics, 127: 1-25.

Goscombe, B.D., 1984. The structure, metamorphism, petrology and geochemsitry of the Paradise Well area in the Harts Ranges, Eastern Arunta Block. Honours thesis, University of Adelaide, 171 pp. (unpublished).

Hollister, L.S. and Crawford, M.L., 1986. Melt-enhanced deformation: a major tectonic process. Geology, 14: 558-561.

James, P.R., Ding, P., Rankin, L. and Scales, G., 1985. Displacement and strain within the nappe sequences of the Harts Range area, central Australia. Abstracts Volume of IGCP Conference: Tectonics and Geochemistry of Early to Middle Proterozoic Fold Belts, Darwin, August, 1985.

James, P.R., Macdonald, P. and Parker, M.D. (in press). Strain and displacement in the Harts Range Detachment Zone from the western margin of the Entia Dome, central Australia. Precambrian Res.

Kroner, A., 1983. Proterozoic mobile belts compatible with the plate tectonic concept. Geol. Soc. Am. Mem., 161: 59-74.

Lister, G.S. and Snoke, A.W., 1984. S-C Mylonites. J. Struct. Geol., 6: 617-638.

Liu, Y., 1987. Microstructural studies on the Florence Shear Zone, eastern Arunta Inlier, central Australia. Unpublished Report, University of Adelaide, 149 pp.

McKenzie, D.P., 1978. Some remarks on the development of sedimentary basins. Earth Planet. Sci. Lett., 40: 25-32.

Mortimer, G.E., Cooper, J.A. and James, P.R., 1986. Geochronological studies in the eastern Entia Dome, Arunta Inlier. Geol. Soc. Aust. 8th Aust. Geol. Congr. Absts., 15: 48-49.

Mortimer, G.E., Cooper, J.A. and James, P.R., 1987. U-Pb and Rb-Sr geochronology and geological evolution of the Harts Range ruby mine area of the Arunta Inlier, central Australia. Lithos, 20: 445-467.

Oliver, R.L., Lawrence, R.W., Goscombe, B.D., Ding, P., Sivell, W.J. and Bowyer, D.G., 1988. Metamorphism and crustal considerations in the Harts Range and neighbouring regions, Arunta Inlier, central Australia. Precambrian Res., 40/41: 277-296.

Plumb, K.A. and James, H.L., 1986. Subdivision of Precambrian time: recommendations and suggestions by the subcommission on Precambrian stratigraphy. Precambrian Res., 32: 65-92.

Sandiford, M. and Powell, R., 1986. Deep crustal metamorphism during continental extension: modern and ancient examples. Earth Planet. Sci. Lett., 79: 151-158.

Shackleton, R.M., 1986. Precambrian collision tectonics in Africa. In: M.P. Coward and A.C. Ries (Editors), Collision Tectonics. Geol. Soc. Spec. Pub., 19: 329-349.

Shaw, R.D. and Langworthy, A.P., 1984. Strangways Range region, Northern Territory. Aust., Bur. Miner. Resour., Geol. Geophys., 1: 100 000 Map Commentary.

Shaw, R.D., Stewart, A.J. and Black, L.P., 1984. The Arunta Inlier: a complex ensialic mobile belt in central Australia. Part 2: tectonic history. Aust. J. Earth Sci., 31: 457-484.

Simpson, C. and Schmidt, S.M., 1983. An evaluation of criteria to deduce the sense of movement in sheared rocks. Bull. Geol. Soc. Am., 94: 1281-1288.

Sivell, W.J. and Foden, J.D., 1985. Banded amphibolites of the Harts Range meta-igneous complex, central Australia: a bimodal basalt tonalite suite. Precambrian Res., 28: 223-252.

Warren, R.G., 1979. Volcanogenic and sedimentary origins to sapphirine-bearing rocks in the Arunta Block, central Australia. Nature, 278: 159-161.

Warren, R.G., 1983. Metamorphic and tectonic evolution of granulites, Arunta Block, central Australia. Nature, 305: 300–302.

Wernicke, B., 1981. Low-angle normal faults in the Basin and Range Province—nappe tectonics in an extending orogen. Nature, 291: 645–648.

Wernicke, B., 1985. Uniform-sense normal simple shear of the continental lithosphere. Can. J. Earth Sci., 22, 108–125.

Wernicke, B. and Burchfiel, B.C., 1982. Modes of extensional tectonics. J. Struct. Geol., 4: 105–115.

Wickham, S.M. and Oxburgh, E.R., 1985. Continental rifts as a setting for regional metamorphism. Nature, 318: 330–333.

Wynne-Edwards, H.R., 1976. Proterozoic ensialic orogenesis: the millipede model of ductile plate tectonics. Am. J. Sci., 276: 927–953.

Precambrian Research, 40/41 (1988) 277–295
Elsevier Science Publishers B.V., Amsterdam — Printed in The Netherlands

METAMORPHISM AND CRUSTAL CONSIDERATIONS IN THE HARTS RANGE AND NEIGHBOURING REGIONS, ARUNTA INLIER, CENTRAL AUSTRALIA

R.L. OLIVER[1], R.W. LAWRENCE[1], B.D. GOSCOMBE[2], P. DING[1], W.J. SIVELL[3] and D.G. BOWYER[4]

[1]*Department of Geology and Geophysics, University of Adelaide, Adelaide (Australia)*

[2]*Department of Geology, University of Melbourne, Melbourne (Australia)*

[3]*Nepean College of Advanced Education, Sydney, N.S.W. (Australia)*

[4]*Exploration Division, SANTOS Ltd, Adelaide, S.A., (Australia)*

(Received April 24, 1987; revision accepted December 22, 1987)

Abstract

Oliver, R.L., Lawrence, R.W., Goscombe, B.D., Ding, P., Sivell, W.J. and Bowyer, D.G., 1988. Metamorphism and crustal considerations in the Harts Range and neighbouring regions, Arunta Inlier, central Australia. Precambrian Res., 40/41: 277–295.

The Harts Range region consists of several segments, or terrains, which have behaved essentially independently, though some overlap of history, permitting correlation, is apparent. Some analogy with the 'terrane' concept is envisaged. The Harts Range terrains are: (1) the Strangways Orogenic Belt (SOB), south of the Muller Thrust, (2) the SOB of the Oonagalabi Tongue, (3) the SOB of the Entia Dome, together comprising a 'Basement', and (4) the Harts Range 'Cover' (HRC), all separated from each other by thrusts or faults.

The terrains consist of supracrustal sequences comprising metasediments and some metabasites, thought to have been deposited in extensional rift depressions, plus varying amounts of intrusive granitoids. Both granulite facies and amphibolite facies mineralogies characterise the basement terrain of the Oonagalabi Tongue and that south of the Muller Thrust. The Entia Dome and cover terrains have only amphibolite facies mineralogy.

A combination of thermobarometry and petrogenetic data suggests equilibration of the SOB south of the Muller Thrust at 700–800°C and 5–7 kbar and of the HRC in the Ruby Mine area at 680–780°C and 6–8 kbar. Some thickening of the supracrustal accumulations owing to compression is considered necessary for the development of these pressures.

Comparison of the Harts Range terrains with the Strangways terrain shows some similarities and some differences.

Introduction

A feature of the Arunta Inlier, according to Shaw et al. (1984), is that cycles of extension and convergence appear to have occurred five times, between 1800 and 4–300 Ma. In the Harts Range, a model proposed by James and Ding (1988) may be regarded as a modification of Shaw et al.'s earliest cycle in which accumulation of two supracrustal sequences (Division 1 and Division 2) is terminated by the Strangways event. In James and Ding's model the equivalents of these two subdivisions in the Harts Range, juxtaposed on a set of gently in-

0301-9268/88/$03.50 © 1988 Elsevier Science Publishers B.V.

clined thrust surfaces, have been termed the Harts Range Cover complex (HRC) and a lower Basement complex, the latter, only, constituting part of the Strangways Orogenic Belt (SOB), as defined by Ding and James (1985) and James and Ding (1988).

Compositionally, the two divisions have some similarity, but Division 1 is characterised by having a greater quartzofeldspathic content. A manifestation of the thrust surfaces, separating the two terrains, is depicted by the Florence Shear Zone, which is interpreted by James and Ding (1988) as part of a detachment zone relating the two complexes. The Bruna Gneiss is considered by these authors to have been emplaced into the detachment zone during detachment.

In general, rocks of the SOB are of a higher metamorphic grade (amphibolite–granulite facies) and display more migmatitic and granitoid development than the amphibolite facies HRC. The deformational histories of the two complexes seem to be distinct in that the SOB fold structures trend fairly consistently NNE–SSW, whereas those of the HRC are more variable. Within the SOB, also, the Oonagalabi Tongue, the area south of the Muller Thrust, and the Entia Dome can be distinguished as three separate terrains with recognisable metamorphic and tectonic differences, at least in part.

This paper, is a preliminary study in which the metamorphic conditions responsible for the mineralogy of the Basement and Cover rocks are described and an attempt made to reconcile these conditions with tectonic models.

Geology

Basement rocks

South of the Muller Thrust

In this area (see Fig. 1), deformation, during the Strangways Orogeny, has resulted in the development of four generations of predominantly NE trending, near-recumbent and upright ductile folds, which have not been affected significantly during subsequent deformation of the HRC.

Roughly west of Paradise Well (= Cadney metamorphics and part of the Bungatina metamorphics; Shaw et al., 1984), lithologies are, predominantly, mafic granulite, and high-grade metasediments, including pelites and abundant calc-silicates. East of Paradise Well, there are more granitic and tonalitic gneisses, associated with amphibolite facies mafics and metasediments.

In *metapelites* of the Paradise Well locality a common mineral assemblage is biotite–sillimanite – garnet – quartz–K-feldspar – plagioclase – cordierite – magnetite. Texturally, in one thin section there is some indication that garnet is being replaced by cordierite (Fig. 2a). In other cases, sillimanite fringes, and presumably post-dates, cordierite and K-feldspar (Fig. 2b). Elsewhere, garnet includes, and is supposedly later than, biotite and sillimanite (Fig. 2c). The composition of the cordierite, garnet and biotite are shown in Table I.

In the Paradise Well area *mafic gneisses* occur as 1–20 m thick discontinuous layers, intercalated with quartzofeldspathic and other lithologies, the layering being parallel to S_1. Constituent minerals, defining S_1, are orthopyroxene, clinopyroxene, hornblende, plagioclase and quartz.

The hornblende referred to is primary hornblende, crystallised together with pyroxenes and plagioclase (and quartz?). It is brownish green in colour and has relatively abundant TiO_2 (up to 2%: see Table II). Also occurring, to a variable extent, are fine-grained aggregates of secondary blue-green hornblende.

Compositional differences between primary and secondary hornblendes are evident in Table II and are displayed in Fig. 3a, 3b. The hornblende chemistry may be considered in the light of the compositional dependence of hornblende on P_{fluid}, T and f_{O_2} as experimentally determined by Spear (1981). This qualitative dependence, shown in Fig. 4a–c, indicates, in

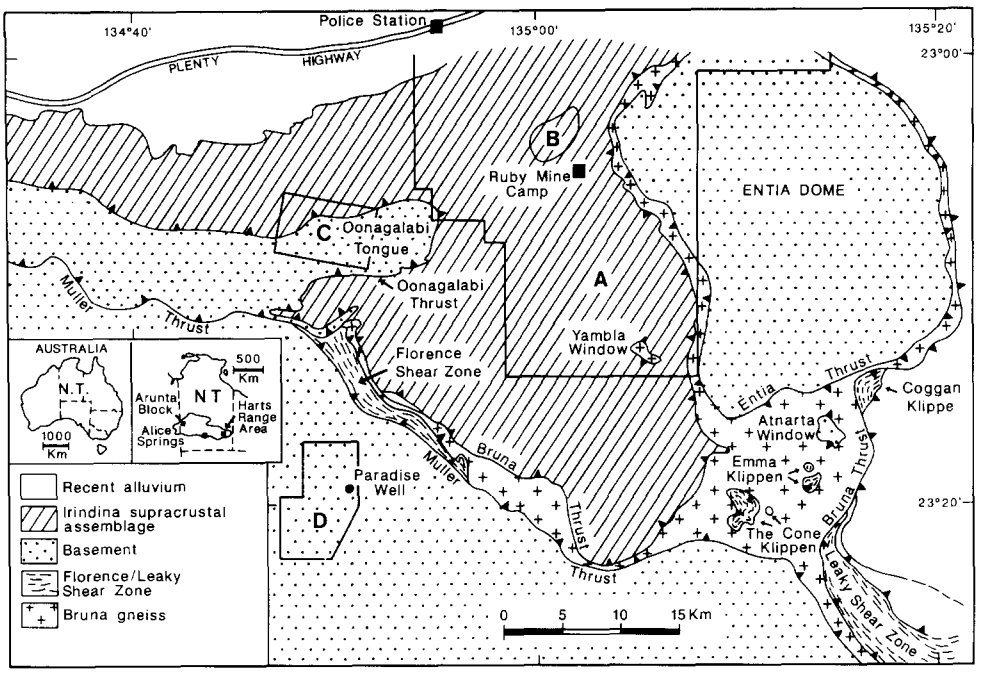


Fig. 1. Map of Harts Range showing the main lithological subdivisions. A = Ph. D. thesis area of R.W. Lawrence, B = Honours thesis area of D.G. Bowyer, C = Honours thesis area of L. Rankin, D = Honours thesis area of B.D. Goscombe. Note: Ph. D. thesis of P. Ding covers the whole area.

combination with Fig. 3a,b that:

(1) secondary hornblende crystallised at a lower temperature than primary hornblende;

(2) there is an increase of Al^{vi} with P_{fluid} increase, paralleling, seemingly, a decrease in metamorphic grade; increase of Al^{vi} however, is likely to be a consequence of Al^{iv} decrease, thus reflecting the decrease in temperature with retrogression, rather than P_{fluid} increase;

(3) retrograde metamorphism occurred with an increase in oxidation state, possibly as a result of influx of water into the terrain.

Quartzofeldspathic lithologies, in the Paradise Well area, consist of:

(1) layered medium- to coarse-grained gneiss, consisting of quartz + plagioclase + K-feldspar + biotite + garnet, of likely sedimentary origin according to the positive discriminant function values of Shaw (1972);

(2) coarse-grained quartz–plagioclase–K-feldspar–biotite-poor homogeneous metagranites in which garnet occurs only rarely; there are two varieties, (a) $Na_2O > K_2O$ granitic gneisses with weak foliation and (b) $K_2O > Na_2O$ granitoids with no foliation. Variety (a) is thought to have been emplaced slightly earlier than variety (b). In all the above quartzofeldspathic varieties, K-feldspar is perthitic or microperthitic.

Charnockitic gneisses, west of Paradise Well, contain quartz, perthite and antiperthite, 2–5% orthopyroxene, and variable clinopyroxene, hornblende, biotite, garnet and opaques. In typical Basement granitic gneisses, east of Paradise Well, the K-feldspar is predominantly microcline.

Calc-silicate lithologies are abundant in the Paradise Well area and further west. Layers vary in thickness from a few centimetres to 20 m. Layers consist of varying abundances of quartz, calcite, epidote, tremolite, green fassaiitic clinopyroxene, grossular plagioclase and scapolite. Reaction between garnet and plagioclase to produce epidote (Fig. 2d), and between

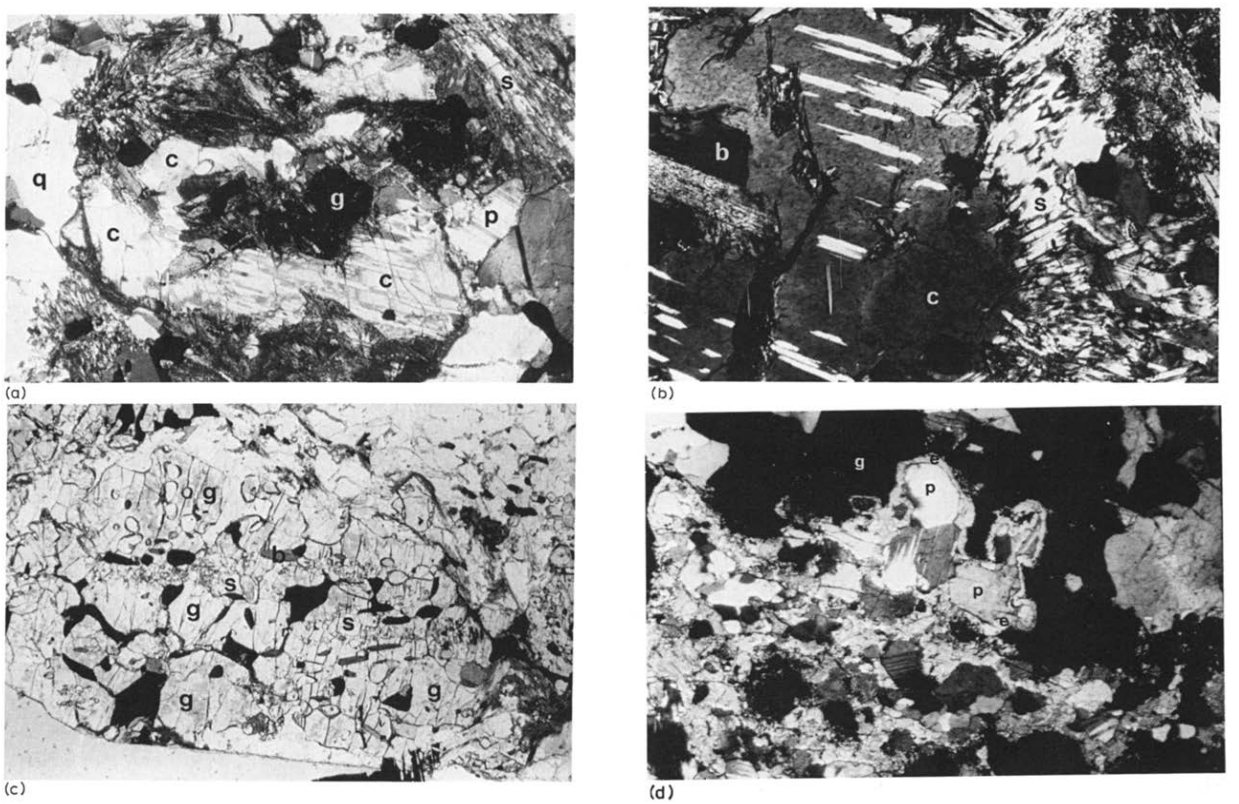


Fig. 2. Photomicrographs of metapelites from the Paradise Well locality. (a) Specimen 834/303, showing cordierite mantling garnet. Field of view 3.0 mm. (b) Specimen 834/238, showing sillimanite rimming cordierite. Field of view 0.9 mm. (c) Specimen 834/204, showing sillimanite and biotite inclusions in garnet. Field of view 3.0 mm. (d) Epidote sandwiched between (and formed by reaction of) garnet and plagioclase. Field of view 3.0 mm. c = cordierite, g = garnet, b = biotite, q = quartz, s = sillimanite, p = plagioclase, K = K-feldspar, e = epidote.

diopside and plagioclase to produce garnet, is evident.

Oonagalabi Tongue

In this area, refolding, or reworking, of Basement structures during several generations of deformation of the HCR is recognised. The rocks, referred to as the Oonagalabi gneiss by Ding and James (1985) and Sivell (1986) (see also Rankin (1983)) comprise intimately interlayered mafic and granitic gneisses. The granitic gneisses in places are garnetiferous. Migmatitic development is widespread.

Some of the mafic material shows granulite facies mineralogy. Assemblages typically comprise orthopyroxene, clinopyroxene, plagioclase and hornblende. Garnet may be present in addition (Fig. 5a). Mineral compositions are shown in Table III. Other mafic lithologies display amphibolite facies mineralogy, e.g., hornblende–plagioclase–scapolite–opaque, and hornblende–clinopyroxene–plagioclase. Near the sheared margin of the Oonagalabi Tongue, textures are more strongly foliated and biotite is commonly developed. The mineralogy of pelites and rare calc-silicates is similar to that in the basement rocks south of the Muller Thrust.

Entia Dome

The Entia gneiss complex (Ding and James, 1985) of the Entia Dome consists mainly (80–85%) of acidic to intermediate orthogneisses and migmatitic gneisses with subsidiary amphibolite facies mafic and ultramafic gneisses and metasediments. Granitic gneiss consists of K-feldspar (microcline), plagioclase, and quartz, with lesser amounts of biotite, musco-

TABLE I

Microprobe analyses of minerals from metapelites Paradise Well region

	Biotite		Garnet		Cordierite	
	1	2	3	4	5	6
SiO_2	36.83	37.29	38.52	39.16	48.22	49.55
TiO_2	4.09	2.31	-	-	32.62	33.51
Al_2O_3	16.88	16.87	22.07	22.09	-	-
Fe_2O_3	-	-	0.0	0.64	-	-
FeO_T	11.10	9.61	-	-	3.53	2.90
FeO	-	-	24.98	17.61	-	-
MnO	-	-	5.08	11.80	0.38	0.27
MgO	15.57	17.64	8.36	8.45	10.70	11.55
CaO	-	-	0.75	1.72	-	-
K_2O	9.71	9.91	-	-	-	0.07
Total	94.17	93.63	99.76	101.48	98.98	100.75
Cations	*22 oxygens*		*12 oxygens*		*18 oxygens*	
Si	5.4622	5.5235	2.9915	2.9883	5.0078	5.0031
Ti	0.4557	0.2577	-	-	-	-
Al	2.9506	2.9451	2.0200	1.9865	3.9925	3.9885
Fe^{3+}	-	-	0.0	0.0368	-	-
Fe_T^{2+}	1.3768	1.1897	-	-	0.3064	0.2452
Fe^{2+}	-	-	1.6222	1.1239	-	-
Mn	-	-	0.3345	0.7626	0.0333	0.0229
Mg	3.4426	3.8939	0.9677	0.9611	1.6557	1.7381
Ca	-	-	0.0626	0.1409	-	-
K	1.8375	1.8725	-	-	-	0.0094
$Mg/Mg + Fe^{2+}$	-	-	0.374	0.461	0.844	0.876

Specimen 834/238 = analyses 1, 3 and 5.
Specimen 834/303 = analyses 2, 4 and 6.

vite, hornblende, epidote and accessory minerals.

The mineralogy of metapelites in the Entia gneiss complex includes cordierite, phlogopite, kyanite and, in places, gedrite. There are numerous examples of kyanite being replaced by cordierite (Fig. 5b), and kyanite by sillimanite.

Amphibolite occurs as distinctive dark layers or lenticular bodies within the light-coloured granitic gneiss of the Entia Dome. Their modal composition is hornblende and andesine with subsidiary diopside, garnet, epidote, scapolite, biotite and quartz.

Florence Shear Zone and Bruna gneiss

This zone comprises a number of basement lithologies, deformed to various degrees. Some rocks, with protomylonitic texture, consist of lenticular aggregates of fine-grained orthopyroxene, clinopyroxene, plagioclase and hornblende replacing coarser-textured grains of the same phases, and suggest recrystallisation under granulite facies conditions (Fig. 5c) of probable SOB lithologies.

Typical Bruna gneiss mineral assemblages are muscovite–biotite–microcline–quartz, epidote – muscovite – microcline – plagioclase – quartz, biotite–hornblende–quartz–garnet–plagioclase–K-feldspar. Textures commonly indicate considerable strain-induced recrystallisation.

Cover rocks (HRC)

These rocks, which are part of the Harts Range Group of, e.g., Shaw et al. (1984), and

TABLE II

Microprobe analyses of minerals from mafic gneisses, Paradise Well region

	Orthopyroxene		Clinopyroxene		Primary hornblende		Secondary hornblende		Plagioclase	
	1	2	3	4	5	6	7	8	9	10
SiO_2	50.91	52.27	51.68	53.38	41.04	43.33	40.65	48.13	54.94	50.36
TiO_2	-	-	0.17	-	1.98	1.33	-	-	-	-
Al_2O_3	1.07	1.25	1.95	0.97	11.74	11.55	13.28	8.37	27.50	30.61
FeO_T	28.96	22.70	10.87	6.44	17.99	12.37	18.08	10.87	0.48	0.53
MnO	1.03	0.71	0.27	-	0.16	-	-	-	-	-
MgO	16.85	21.80	12.24	14.41	8.77	12.19	9.21	15.19	0.55	0.89
CaO	0.44	0.37	22.05	23.17	11.31	11.44	11.34	11.79	10.34	14.13
K_2O	-	-	-	-	1.60	1.33	1.60	0.45	0.21	0.17
Na_2O	-	-	-	-	1.52	1.30	1.52	0.66	5.72	3.74
Cl	-	-	-	-	0.45	0.46	0.50	0.14	-	-
P_2O_5	-	-	-	-	-	-	-	-	-	0.13
SO_3	-	-	-	-	-	-	-	-	-	0.16
Cr_2O_3	-	-	-	0.17	-	0.45	-	-	-	-
Total	99.26	99.10	99.22	98.54	96.57	95.72	96.18	95.60	99.75	100.71
Cations	*6 oxygens*		*6 oxygens*		*23 oxygens*		*23 oxygens*		*32 oxygens*	
Si	1.9784	1.9696	1.9596	1.9970	6.3489	6.5363	6.3056	7.0806	9.9622	9.1496
Ti	-	-	0.0048	-	0.2301	0.1506	-	-	-	-
Al	0.0489	0.0557	0.0870	0.0428	2.1408	2.0527	2.4278	1.4518	5.8774	6.5550
Fe_T^{2+}	0.9412	0.7154	0.3445	0.2016	2.3276	1.5606	2.3455	1.3369	0.0733	0.0802
Mn	0.0340	0.0226	0.0086	-	0.0204	-	-	-	-	-
Mg	0.9763	1.2245	0.6918	0.8036	2.0220	2.7401	2.1305	3.3295	0.1488	0.2400
Ca	0.0184	0.0148	0.8957	0.9288	1.8749	1.8487	1.8846	1.8587	2.0077	2.7501
Cr	-	-	-	0.0051	-	0.0534	-	-	-	
K	-	-	-	-	0.3155	0.2551	0.3167	0.0836	0.0475	0.0397
Na	-	-	-	-	0.4561	0.3795	0.4559	0.1880	2.0115	1.3190
Cl	-	-	-	-	0.1184	0.1171	0.1317	0.0351		
P	-	-	-	-	-	-	-	-	-	0.0201
S	-	-	-	-	-	-	-	-	-	0.0204
Mg/Mg + Fe	0.509	0.631	-	-	-	-	-	-	-	-
Ca:Na:K	-	-	-	-	-	-	-	-	49:50:1	67:32:1

Specimen 834/314 = analyses 1, 3, 5, 7 and 9.
Specimen 834/387 = analyses 2, 4, 6, 8 and 10.

which are referred to as the Harts Range supracrustal cover (HRC) by James and Ding (1988), are represented by the Irindina supracrustal assemblage which comprises both Irindina metasediments and meta-igneous rocks of the Harts Range Meta-igneous Complex (Ding and James, 1985).

Metasediments of the Irindina supracrustal assemblage are pelitic and semipelitic gneiss, with minor marble and quartzite. The Harts Range meta-igneous complex is predominantly amphibolite but also included are rare pods of ultramafic and a significant horizon of Entire Anorthosite (Lawrence, 1987; Lawrence et al., 1987).

Metapelites are schistose and consist typically of quartz, biotite, garnet, plagioclase, muscovite and sillimanite. K-feldspar occurs extremely rarely. The composition of some of these minerals is given in Table IV. An intense layer-parallel S_1 foliation, manifested by the preferred orientation of biotite, generally characterises these metapelitic gneisses. Parallel sillimanite defines an L_1 mineral-elongation lineation.

Mafic rocks comprise banded metabasaltic amphibolite and subsidiary tonalite, interlayered on a fine scale (see also Sivell and Foden, 1985). The amphibolites consist predominantly of calcic amphibole (edenite) and pla-

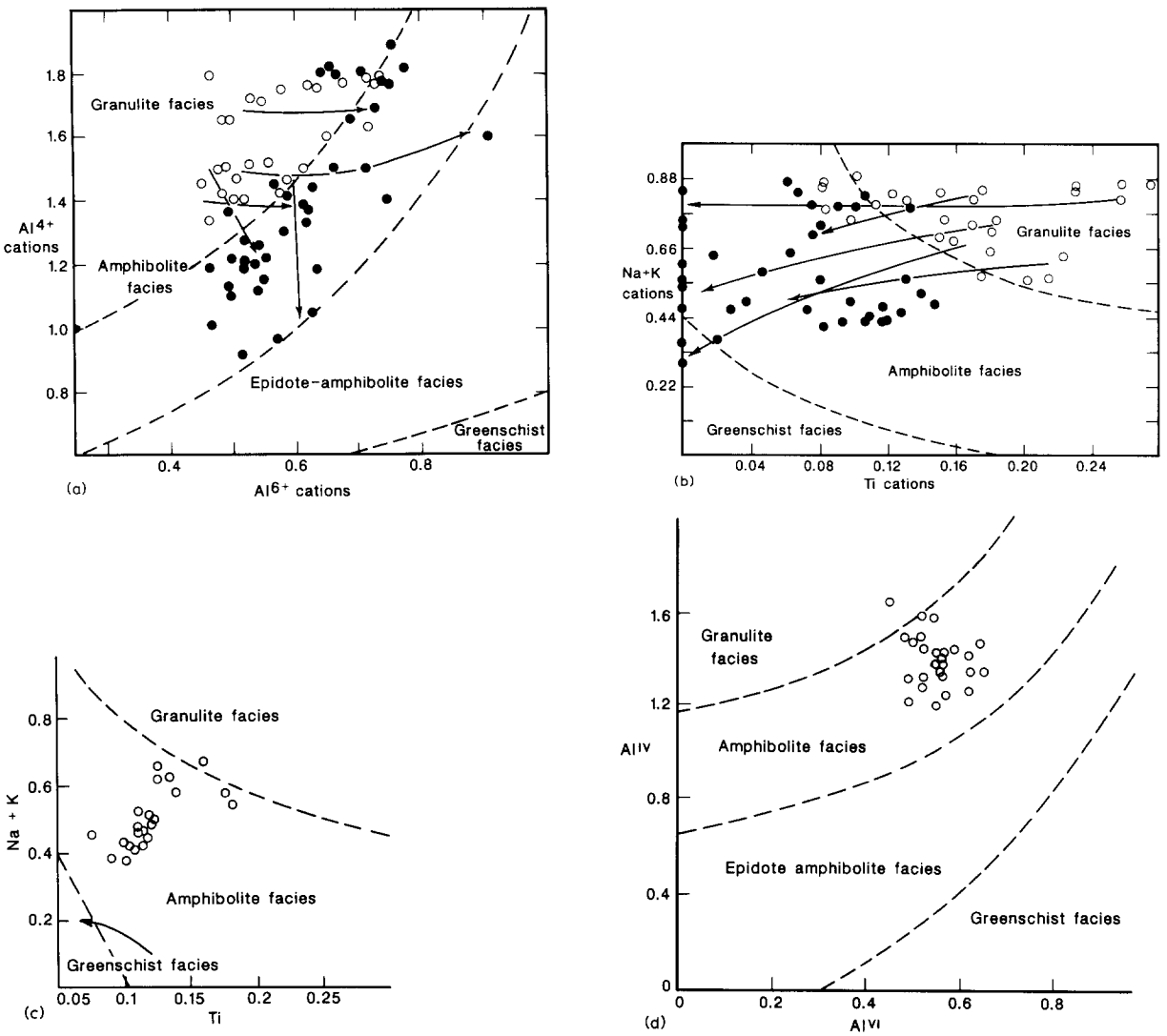


Fig. 3. Diagrams showing metamorphic grade of hornblendes. (a) and (b) from basement metabasites of the Paradise Well locality (c) and (d) from cover amphibolites of the Ruby Mine area. ○ = primary hornblendes, ● = secondary hornblendes, ← = direction of retrogression for a sample. Metamorphic facies boundaries modified from Zakrutkin (1968).

gioclase (labradorite) in approximately equal proportions. Subsidiary mineral phases include clinopyroxene, garnet, sphene and ilmenite (Fig. 5d). The major element compositions of hornblende, garnet and clinopyroxene are given in Table V. An indication of metamorphic grade (amphibolite facies), based on the hornblende analyses is given in Fig. 3c,d.

Within the *Entire Anorthosite*, pink corundum occurs where anorthositic and ultramafic lithologies (consisting predominantly of Mg-hornblende and chlorite, plus rare anthophyllite and enstatite) are closely intermixed as the result of tight folding and metamorphic differentiation of the Cover during D_1. Subsequent retrogression resulted in the Mg-hornblende being rimmed by tremolite, in association with Mg-rich chlorite. An ultramafic pod in area B,

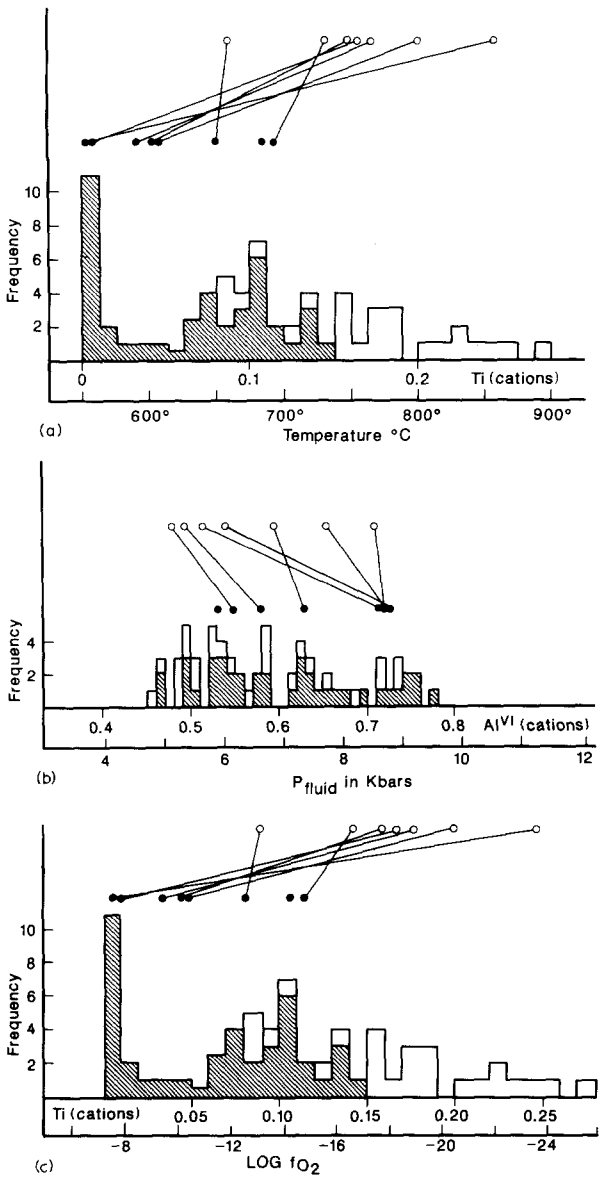


Fig. 4. Primary and secondary hornblendes from basement metabasites of Paradise Well region, showing (a) correlation of Ti with T, (b) correlation of Al^{vi} with P_f, (c) correlation of Ti with f_{O_2}, according to Spear (1981). □ primary hornblende; ▨ secondary hornblende; ●—○ tie line joins composition of average primary hornblende composition (○) to average secondary hornblende composition (●) within a single sample.

Fig. 1, consisting predominantly of Mg-hornblende, contains subsidiary sapphirine enclosing spinel.

Pressure–temperature–time considerations

SOB Lithologies

South of the Muller Thrust

Equilibrium temperatures given by nine basic, non-garnetiferous granulites from the Paradise Well area and basement localities east and west of Paradise Well, have been determined using the two-pyroxene geothermometers of Wood and Banno (1973) and Wells (1977). These temperatures range from 769 to 835 °C and 786 to 876 °C, respectively, an overall average being 821 °C. Application of Lindsley's (1983) two-pyroxene geothermometer to six of these samples from the Paradise Well area produces an average temperature of 730 ± 70 °C.

Textural indications of equilibrium of hornblende with orthopyroxene and clinopyroxene in many of the mafic gneisses means that a very approximate temperature can be derived from the position of the amphibole–pyroxene equilibrium curve if a_{H_2O} is known (hornblende composition not taken into account). On this basis, Fig. 6 shows a maximum possible temperature of ~ 850 °C at ~ 8 kbar for the non-garnetiferous basic granulites referred to earlier, assuming a negligible H_2O fluid phase. In places, intercalated with the pyroxene-plus hornblende-rich layers, there are thin, quartzofeldspathic S_1 layers, which may represent incipient synmetamorphic partial melting.

Only slightly more precise indications of P–T are provided by pelitic lithologies. Based on the assumed equilibrium of coexisting garnet, anhydrous cordierite, sillimanite, plagioclase, biotite and quartz in three metapelites from the Paradise Well locality, a temperature of 700–810 °C and pressure of 5–7 kbar are suggested, as indicated in Fig. 7. These estimates must be considered tentative, not only because of the thermodynamic uncertainties inherent in the thermobarometry depicted in Fig. 7 but also because the extent of equilibrium between these phases is uncertain, as indicated by their tex-

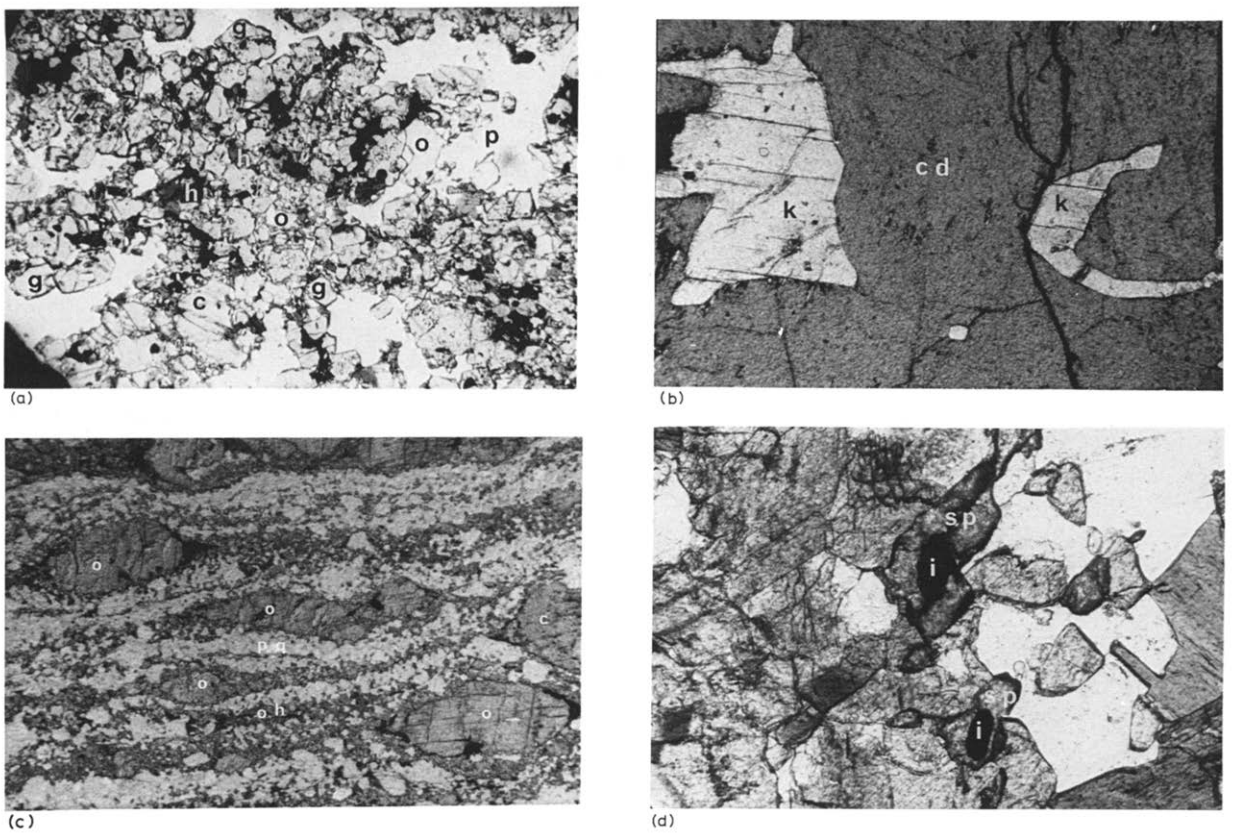


Fig. 5. Photomicrographs of (a) garnet-clinopyroxene-orthopyroxene-hornblende-plagioclase metabasite from the Oonagalabi Tongue (Specimen 823/25A), showing secondary garnet; (b) kyanite remnants in cordierite, metapelite, Entia Dome (Specimen 823/101R); (c) mylonitised metabasite (Specimen 796/4008) from Florence Shear Zone showing recrystallised orthopyroxene and hornblende; (d) Cover amphibolite, Ruby Mine locality (Specimen 790/R6), showing ilmenite mantled by sphene. Field of view for all photographs is 3.0 mm. g = Garnet, c = clinopyroxene, o = orthopyroxene, h = hornblende, p = plagioclase, pq = plagioclase + quartz, oh = secondary hornblende + orthopyroxene, b = biotite, s = sillimanite, q = quartz, i = ilmenite, sp = sphene, a = apatite, k = kyanite, cd = cordierite.

tural relationships described earlier.

The indicated 750 °C and 6.3 kbar under conditions of $P_{H_2O} = 0.4\ P_{tot}$ derived from Holdaway and Lee (1977) (see Fig. 7) is considered to be possible confirmation of the P–T suggested above because a value of $P_{H_2O} = 0.4\ P_{tot}$ falls within the range of a_{H_2O} estimates of 0.04385–0.71087 and 0.02522–0.40886 which have been calculated for two of the samples used in Fig. 7, Goscombe (1984). These a_{H_2O} estimates are derived from the composition of constituent cordierite, garnet and biotite (Table I) and estimates of pressure and temperature, according to the method described by Phillips (1980).

As mentioned above, orthopyroxene, clinopyroxene and primary hornblende in the mafic rocks manifest S_1 and this assemblage is considered to represent peak metamorphism. Whether garnet, cordierite, sillimanite, plagioclase and biotite in the metapelites are similarly part of S_1 and are associated with maximum P–T is not conclusive because of possible disequilibrium, suggested earlier (and see Fig. 2a–c). The suggested equilibration temperatures and pressures indicated by the two lithologies at least broadly overlap.

As described above, textural evidence for retrogression is provided by secondary hornblende in the metabasites, and garnet, and epidote, in the calc-silicates, but there is no definite evidence available to indicate the evolutionary stage when these formed. They possibly developed concomitantly with the replacement of cordierite by sillimanite (Fig. 2b), but some, at least, may have been later (see below).

TABLE III

Microprobe analyses of minerals from Oonagalabi basic granulites

	Orthopyroxene		Clinopyroxene			Garnet		Hornblende		Plagioclase	
	1	2	3	4	5	6	7	8	9	10	11
SiO_2	50.51	52.78	51.43	51.56	53.18	38.22	37.66	41.42	44.87	61.77	58.67
TiO_2	-	-	-	-	-	-	-	2.01	0.84	-	-
Al_2O_3	0.85	0.95	2.33	1.96	1.80	21.07	20.90	11.96	11.22	25.95	26.37
Cr_2O_3	0.20	-	0.15	-	0.19	-	-	-	0.51	-	-
FeO_T	33.46	23.62	13.49	11.34	7.19	29.67	29.08	20.23	11.22	-	-
MnO	0.51	0.75	0.13	0.13	0.26	1.24	0.85	-	-	-	-
MgO	14.18	21.89	10.31	11.43	14.10	3.64	3.99	8.11	13.13	-	-
CaO	0.42	0.28	21.56	21.70	22.53	6.71	6.87	11.10	10.86	6.88	8.05
K_2O	-	-	-	-	-	-	-	0.74	0.76	0.19	0.15
Na_2O	0.28	-	0.55	0.38	0.26	-	-	2.29	1.57	6.89	6.35
Cl	-	-	-	-	-	-	-	0.20	0.13	-	-
V_2O_3	-	-	-	-	-	-	-	0.24	-	-	-
Total	100.41	100.26	99.94	98.50	99.50	100.55	99.35	98.28	95.10	101.67	99.61
Mg/Mg + Fe	43.0	62.3	57.7	64.2	77.8	18.0	19.7	41.7	67.6	-	-
Ca:Na:K	-	-	-	-	-	-	-	-	-	35:64:1	41:58:1

Specimen 823/25A = analyses 1, 3, 6, 8 and 10.
Specimen 823/25B = analyses 2, 4, 5, 7 and 9.
Analysis 4 = clinopyroxene in association with garnet
Analysis 5 = clinopyroxene in association with orthopyroxene } different layers.

Oonagalabi Tongue

From geothermometry, using the two-pyroxene method of Wood and Banno (1973) and of Wells (1977), applied to three non-garnetiferous, orthopyroxene-, clinopyroxene- and hornblende-bearing mafic granulites, tentative temperatures of 781–818 °C and 803–863 °C are obtained.

Possible confirmation of such temperatures is the range of 813–873 °C at 7–8.5 kbar derived from the application of Ferry and Spear's (1978) garnet–biotite geothermometer to biotite and garnet cores from metapelites associated with the above granulites. Biotite plus garnet rims from two of the same metapelites, produce a slightly lower range of 729–850 °C at 7–8.5 kbar. These P–T conditions representing granulite facies metamorphism in the Oonagalabi Tongue are not significantly different from those in the basement terrain south of the Muller Thrust, represented by the Paradise Well locality.

Evidence of lower-grade metamorphism is also prevalent in the Oonagalabi Tongue in the form of mafic amphibolites, as mentioned above. The protolith of associated granitic gneisses is considered to be a likely accompaniment of amphibolite facies metamorphism, subsequent to earlier granulite facies. Ferry and Spear's (1978) geothermometry yields a tentative equilibration temperature range of 553–790 °C at 7–8.5 kbar, using biotite and garnet cores from five granite samples, and a similar range using garnet rims. A temperature of 655–658 °C at 6–7 kbar is derived from the application of Graham and Powell's garnet–hornblende geothermometer to an associated garnetiferous amphibolite.

A suggested transitional granulite–amphibolite facies mineral assemblage, of orthopyroxene – clinopyroxene – hornblende – garnet – plagioclase, is seen in two samples (e.g., Fig.

TABLE IV
9
Microprobe analyses of minerals from Cover pelites

	Garnet		Plagioclase		Biotite	
	1	2	3	4	5	6
SiO_2	37.91	37.94	58.70	59.00	37.00	37.25
TiO_2	-	-	-	-	2.93	2.37
Al_2O_3	21.05	21.00	26.47	26.37	18.53	18.27
FeO_T	31.84	33.12	-	-	19.81	19.18
MnO	2.62	2.47	-	-	0.05	0.50
MgO	3.70	3.97	-	-	9.26	10.19
CaO	2.80	2.18	8.71	8.37	-	-
K_2O	-	0.01	0.22	0.23	9.37	9.11
Na_2O	-	-	6.30	5.88	0.16	0.20
P_2O_5	-	0.07	-	-	-	-
Cr_2O_3	-	-	-	-	0.01	0.04
NiO	-	-	-	-	0.06	-
F	-	-	-	-	0.22	0.34
Cl	0.03	-	-	-	0.09	0.41
Total	99.93	100.76	100.42	99.85	97.49	97.43
Cations	*12 oxygens*		*32 oxygens*		*22 oxygens*	
Si	3.0250	3.0109	10.4486	10.5212	5.5083	5.5485
Ti	-	-	-	-	0.3280	0.2660
Al	1.9794	1.9644	5.5517	5.5432	3.2510	3.2077
Fe	2.1250	2.1981	-	-	2.4665	2.3887
Mn	0.1769	0.1660	-	-	0.0066	0.0065
Mg	0.4396	0.4698	-	-	2.0560	2.2622
Ca	0.2392	0.1854	1.6618	1.5992	-	-
K	-	0.0006	0.0511	0.0533	1.7792	1.7302
Na	-	0.0005	2.1757	2.0334	0.0472	0.0591

Analyses 1, 3 and 5 = Specimen 797/12-1.
Analyses 2, 4 and 6 = Specimen 797/34-1.

TABLE V

Microprobe analyses of minerals from Cover amphibolites

	Hornblende		Clinopyroxene		Plagioclase		Garnet	
	1	2	3	4	5	6	7	8
SiO_2	44.67	43.23	52.94	51.02	54.87	60.28	38.50	37.91
TiO_2	1.64	1.47	0.16	-	-	-	0.05	-
Al_2O_3	11.49	11.47	1.63	1.61	28.79	25.43	21.40	21.10
Fe_2O_3	-	-	-	-	-	-	-	0.53
FeO_T	14.66	17.13	8.95	11.67	0.02	0.00	23.61	-
FeO	-	-	-	-	-	-	-	25.06
MnO	0.09	0.22	0.12	0.34	0.05	-	1.76	1.73
MgO	11.28	9.27	12.66	10.45	-	0.15	3.70	3.81
CaO	11.63	11.49	23.30	21.93	11.44	7.16	10.72	9.16
K_2O	0.11	0.46	0.02	-	0.03	0.14	0.01	-
Na_2O	1.78	1.72	0.41	0.40	4.94	7.22	0.01	-
P_2O_5	0.28	-	-	-	0.03	-	0.11	-
Cr_2O_3	0.03	-	-	-	0.03	-	0.06	-
NiO	-	-	0.05	-	-	-	-	-
F	-	-	-	-	0.05	-	0.07	-
Total	97.67	96.47	100.25	97.42	100.25	100.40	99.98	99.29
Cations	*23 oxygens*		*6 oxygens*		*32 oxygens*		*12 oxygens*	
Si	6.5788	6.561	1.9743	1.983	9.8716	10.695	3.0107	3.000
Ti	0.1820	0.168	0.0045	-	0.0004	-	0.0027	-
Al	1.9946	2.051	0.0717	0.074	6.1044	5.314	1.9721	1.968
Fe^{3+}	-	-	-	-	-	-	-	0.032
Fe^T	1.8059	2.174	0.2792	0.379	0.0032	-	1.5441	-
Fe^{2+}	-	-	-	-	-	-	-	1.664
Mn	0.0110	0.028	0.0037	0.011	0.0072	-	0.1167	0.116
Mg	2.4769	2.098	0.7038	0.605	-	0.041	0.4319	0.449
Ca	1.8356	1.868	0.9312	0.913	2.060	1.360	0.8982	0.777
Na	0.5073	0.507	0.0296	0.030	1.7232	2.483	0.0013	-
K	0.0208	0.090	0.0012	-	0.0068	0.032	0.0009	-
Al^{iv}	1.7072	-	-	-	-	-	-	-
Al^{vi}	0.2007	-	-	-	-	-	-	-
Mg/Mg+Fe	57.8	-	71.6	-	-	-	-	-

Analyses 1, 3, 5 and 7 = Sample 797/30-1.
Analyses 2, 4, 6 and 8 = Sample 790/R6.

5a). The garnet (plus clinopyroxene) are considered to represent the low-temperature side of line No. 5, in Fig. 6. The relatively fine grain size of the garnet indicates its crystallisation as a secondary phase.

Retrogression from granulite to amphibolite facies in the Oonagalabi Tongue and in the basement south of the Muller Thrust is thought to have been approximately synchronous and, as mentioned, accompanied by the emplacement of granitic magmas (see below).

Cover rocks (HRC)

The presence of garnet only in the Cover metapelites, compared with the garnet plus cordierite in the basement metapelites, can be ascribed to one or more of a number of causes, viz., (1) different bulk compositions; (2) crystallisation of the Cover rocks at higher pressures than basement rock pressures; (3) higher temperatures in the Basement. It is possible that all these factors contribute.

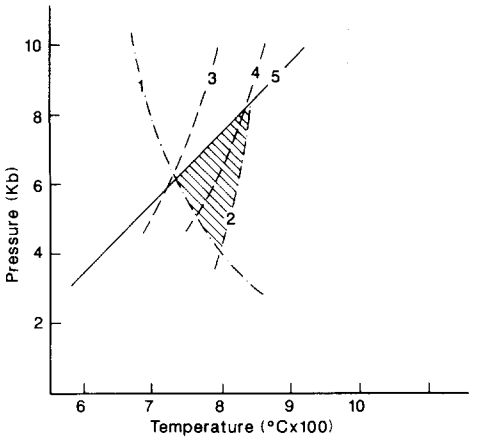


Fig. 6. Shaded area shows range of P-T equilibrium for Oonagalabi non-garnetiferous, two-pyroxene metabasite. (No. 1) saturated basalt solidus, (No. 2) beginning of amphibole vapour absent melting (Thompson and England, 1984), (No. 3) hornblende breakdown curve for P_{H_2O} = 0.2, (No. 4) hornblende breakdown curve for P_{H_2O} = 0.3 (Wells, 1979), (No. 5) equilibrium curve for reaction garnet + clinopyroxene = orthopyroxene + plagioclase (Green and Ringwood, 1967).

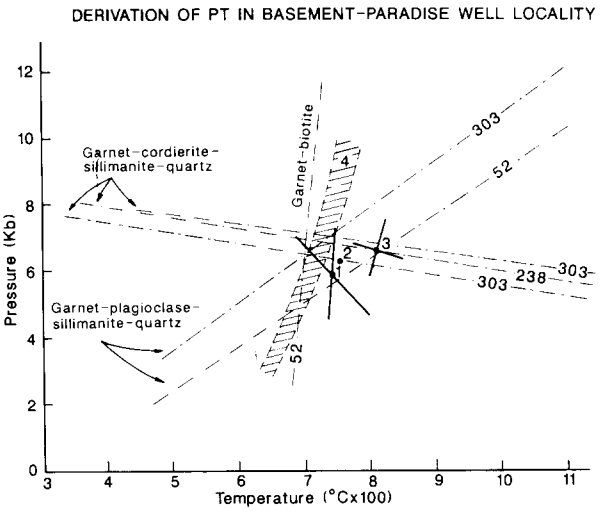


Fig. 7. Estimated equilibrium P-T of Paradise Well locality metapelites (Specimens 834/52, /238 and /303) from the intersection of the P-T lines derived from the garnet-cordierite-sillimanite-quartz geobarometer (Wood and Fraser, 1976) and the garnet-plagioclase-sillimanite-quartz geobarometer (Harris and Jayaram, 1982), unmodified by corrections for non-ideal Fe–Mg mixing according to the model of Ganguly and Saxena (1984). Also plotted is the line of P-Ts derived from the biotite-garnet geothermometer of Indares and Martignole (1985), involving a correction for non-ideality of Fe and Mg mixing according to Ganguly and Saxena (1984). Also indicated are: (No. 1) intersection of quartz + biotite + garnet + vapour = cordierite + orthopyroxene + liquid and cordierite + garnet = quartz + Al_2SiO_5 + orthopyroxene + vapour (Grant, 1985); (No. 2) intersection of the reactions biotite + sillimanite + quartz = cordierite + garnet + K-feldspar + vapour and cordierite = garnet + sillimanite + quartz for cordierite mg value of ~85 (see Holdaway and Lee, 1987, fig. 7b); (No. 3) intersection of same reactions as for No. 2 according to Thompson (1982, fig. 7); (No. 4) beginning of partial dry melting of pelites (Thompson, 1982).

The apparently stable association of biotite, garnet and sillimanite, without cordierite and significant K-feldspar, restricts the P-T range of these metapelites to the biotite–garnet–sillimanite field of the KFMASH petrogenetic grid depicted by Thompson (1976, part 2, Fig. 7). The boundaries of this field are represented by reactions (3) and (4) in Fig. 8. The virtual absence of K-feldspar in these rocks further restricts the temperature range to below the equilibrium temperature for the reaction muscovite + quartz = K-feldspar + Al_2SiO_5 + vapour (see Fig. 8). The position of the shaded area (6), in Fig. 8, corresponding to the initiation of vapour absent melting in pelites, according to Thompson (1982, Fig. 8), conforms with the small amount of melting, evidenced by limited migmatitic development in the Irindina pelitic metasediments.

Geothermometry applied to garnet–biotite pairs from a metapelite not represented in Fig. 8, and in which core and rim are discriminated, indicates a temperature of 698–705 °C, derived from biotite plus garnet cores and 645–652 °C from biotite plus garnet rims, at pressures of 7–8.5 kbar. An even lower temperature, viz., 564–571 °C, is obtained from garnet plus biotite inclusions, which may indicate more complete equilibrium on cooling.

P-T estimates derived from the assemblage hornblende + plagioclase + garnet + clinopyroxene in a Cover amphibolite, and garnet + plagioclase + sillimanite in a metapelite, are also depicted in Fig. 8. Textures indicate that phases within each of the two rocks are in equilibrium and field observations support the belief that the mineral assemblages of the two

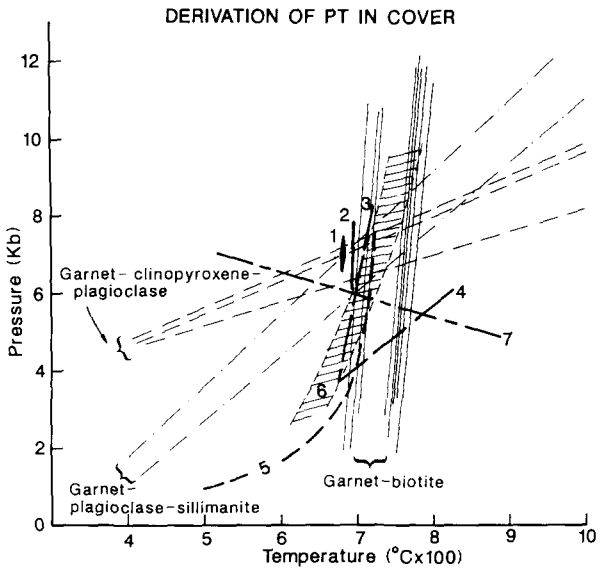


Fig. 8. Estimated equilibrium P-T of metapelites and amphibolites from the cover (Specimens 797/12,/34 and /30, 790/R6) based on the intersection of P-T lines derived from the garnet-plagioclase-clinopyroxene geobarometer of Newton and Perkins (1982) and Perkins and Chipera (1985), from the garnet-plagioclase-sillimanite thermobarometer of Newton and Haselton (1981) and from the garnet-biotite geothermometer of Ferry and Spear (1978). Also shown are: (No. 1) garnet-clinopyroxene geothermometer of Ellis and Green (1979); (No. 2) garnet-hornblende geothermometer of Graham and Powell (1984); (No. 3) univariant curve for the reaction staurolite = biotite + garnet + sillimanite (Thompson, 1976); (No. 4) univariant curve for the reaction sillimanite + biotite = garnet + cordierite + K-feldspar (Thompson, 1976); (No. 5) univariant curve for the reaction quartz + muscovite = K-feldspar + Al_2SiO_5 + vapour; (No. 7) approximate minimum pressure of Cover garnetiferous pelitic rocks (without cordierite), based on combination of garnet and whole-rock compositions, and derived from Thompson (1976, figs. 2A and 2B).

lithologies are also in equilibrium with each other.

Compatible with the 680–780 °C temperature range indicated in Fig. 8 is the coexistence of anthophyllite and enstatite in the ruby-bearing anorthosite–ultramafic lithology described earlier. The equilibrium of these two phases indicates a temperature in excess of 700 °C, with $P_{H_2O} = P_{tot}$ (Evans and Trommsdorff, 1970). The presence of secondary carbonate, however, in some of the ultramafic rocks suggests the presence of CO_2 in the fluid and the lessening of H_2O partial pressure and consequently a lowering of the temperature of the dehydration equilibrium.

Indications of retrogression in the ultramafics have been mentioned earlier. Also, in a number of the HRC amphibolites, retrogression is indicated by the occurrence of sphene, with an upper temperature stability limit (given by Liou et al., 1974) of ~ 550 °C, rimming (and presumably replacing) ilmenite (Fig. 5d).

Discussion

A combination of experimental and thermodynamically derived equilibria (Fig. 7) suggest that peak temperatures in basement south of the Muller Thrust approximated 700–800 °C at pressures of 5–7 kbar and that, in the Cover, temperatures of 680–780 °C were attained over a pressure range of 6–8 kbar. Given the presumed greater reliability of experimentally derived deductions, compared with those based on thermodynamics, the temperature range exhibited by the Cover could perhaps be lowered to 680–720 °C. It is thus apparent that the basement equilibrium temperatures referred to were slightly higher than those of the cover but that Basement pressures were, if anything, slightly lower than those of the cover. Basement pressures correspond to a crustal depth of ~ 17.5–24.5 km and Cover pressures to ~ 21–28 km.

The pressures and temperatures outlined above are broadly similar to those postulated for amphibolite–granulite facies terrains in other parts of the world and a further similarity is that granulites of such paired metamorphic terrains commonly represent a higher temperature than the amphibolite facies rocks but not a higher pressure (Bohlen, 1987).

There is general consensus that the Arunta protoliths of Division 1 equivalent and Division 2 equivalent supracrustals were deposited on the floor of an ensialic or continental rift depres-

sion or depressions which resulted from lithospheric extension (Warren, 1983; Shaw et al., 1984; Stewart et al., 1984; Windrum and McCulloch, 1986; James and Ding, 1988) and this is considered by the present authors to be a likely interpretation.

Subsequent metamorphism (and tectonics?) appear to have affected the two terrains similarly, but to different degrees, resulting in the distinction between Stewart et al.'s and Shaw et al.'s Divisions 1 and 2, and as implied above.

James and Ding (1988) suggest that metamorphism of the Basement may have occurred during "an earlier phase of extensional tectonism in the manner described by Sandiford and Powell (1986)". The implication of James and Ding's suggestion is that metamorphism is simply a consequence of gravity loading and heat accumulation in a sequence of virtually untectonised supracrustals. The development of pressures corresponding to >20 km depth in this way is not easy to verify. Recorded apparently untectonised supracrustal thicknesses are limited to 15 km (Wynne-Edwards, 1976; McKenzie, 1978; Wernicke, 1985), and there are uncertainties in the supply of heat. In Sandiford and Powell's (1986) model, perturbation of geotherms owing to lithospheric extension may result in the development of granulite facies temperatures at the bottom of the crust, but accumulation of substantial thicknesses of supracrustals are expected to occur later, during thermal subsidence.

That granulite terrains and the lower crustal environment can sometimes be independent is also emphasised by Windrum and McCulloch (1986), who state, as a result of their discussion of metamorphism in the Strangways Range (just west of the Harts Range), that "granulite terrains, in general, cannot be equated with lower continental crust but instead represent assemblages of (mainly) supracrustal rocks which in some instances have been involved in collision events". In the Strangways Range, granulite facies metamorphism at 1780 $\pm$ 40 Ma considered by Windrum and McCulloch to be due to large-scale underthrusting of terrain corresponding to the Basement rocks of the present paper was characterised by $T = 840\,^{\circ}C$ and $P = 8$ kbar, thus representing comparable, though somewhat higher, temperature and pressure conditions than are exemplified by the Harts Range Basement.

Retrograde metamorphism in the basement has been described, in the form of secondary amphibole, garnet zoning in metapelites, garnet and epidote in calc-silicates and, possibly, sillimanite after cordierite. The timing of these developments is uncertain but some, at least, may be associated with the early emplacement of the protoliths of granite gneisses in the Paradise Well area, referred to above. If so, it is tempting to correlate this retrogradation with the growth of retrograde biotite at 750 °C and 8 kbar, and associated anatexis of felsic rocks, in the Strangways Range (Windrum and McCulloch, 1986). Windrum and McCulloch quote a Rb–Sr date of 1690 $\pm$ 25 Ma for this Strangways Range event.

In the Entia Dome, somewhat older zircon dates of 1767 $\pm$ 2 Ma and 1766 $\pm^{6}_{7}$ Ma for granitic gneiss and leucogranite respectively (Cooper et al., 1988) are not dissimilar to the 1780 $\pm$ 40 Ma in the Strangways Range. It is suggested, therefore, that granulite facies metamorphism due to underthrusting of crustal blocks in the Strangways Range region may have been synchronous with supracrustal accumulation and presumed subsequent compression and the development of a metamorphic fabric, followed by the emplacement of voluminous granitoids, in the Entia Dome 'basin'. Supracrustal remnants within the predominantly granitoid terrain include metapelites containing gedrite + kyanite + quartz, the stability of which requires a pressure of 8–9.5 kbar (Green and Vernon, 1974). It is possible that these pressures are a consequence of underthrusting of the Entia Dome terrain beneath the HRC at 1745 $\pm^{9}_{7}$ Ma in accordance with the postulates of James and Ding, and Cooper et al. (1988, and see below). This would be in conflict

with Windrum and McCulloch (1986), who consider gedrite + kyanite + quartz to have been in equilibrium in cordierite-rich rocks in the Strangways Range at 1450 Ma. In the Entia Dome there is no indication, in the form of relict higher temperature phases, such as orthopyroxene, that the kyanite + gedrite represents a replacement assemblage, formed as the result of isobaric cooling, as apparently was the case in the Strangways Range (Warren, 1983). Therefore the kyanite + gedrite + quartz assemblage, if initially in equilibrium in the Entia Dome terrain at ~ 1745 Ma, may have remained in the Entia Dome terrain at 7–8 kbar and 700°C for ~ 300 Ma.

Insofar as metamorphism of the Cover and Basement represent the same order of pressure and temperature, the difficulties in accounting for the requisite heat and pressure for the Basement metamorphism, according to the James and Ding model (1988), apply also to metamorphism of the Cover. Metamorphism in both terrains would seem to have required pressures, at least, consequent on tectonic thickening or underthrusting, which means that the apparent S_1 in both cover and basement has developed during compression (cf., James and Ding, 1988).

Apart from indicating pressures and temperatures of presumed peak metamorphism, the mineralogy and textures of the Cover rocks provide few constraints on the history of the terrain. Ignorance of the age of the HRC means that support for HRC accumulation being subsequent to that of the SOB supracrustals is restricted to structural evidence (Ding and James, 1985; Ding, in preparation). The somewhat greater felsic content of the SOB supracrustals compared with the HRC suggests that the two supracrustal sequences accumulated in separate depressions. This is supported by the somewhat higher metamorphic temperatures but lower pressures of the SOB supracrustals compared with the lower temperatures and higher pressures of the HRC, suggesting lateral differences in the nature and quantity of heat supply. The possibility, however, that the SOB supracrustals represent the more proximal facies of one depositional basin cannot be ignored.

Evidence that the granitic protolith of the Bruna gneiss was intruded into the active Florence/Leaky shear zone is provided by James and Ding (1988), and the 1745 $\pm^{9}_{7}$ Ma zircon age of the Bruna gneiss (Cooper et al., 1988) is thus used as a fix on the dating of Florence/Leaky shear zone activity. Some of the retrograde metamorphism described above, such as the development of garnet in granulites in the Oonagalabi Tongue, may be associated with this activity. That some retrogradation is due to isobaric cooling is suggested by the equilibrium temperatures at 7–8 kbar of garnet cores and rims in both HRC and Oonagalabi SOB metapelites, and by the reaction of clinopyroxene and plagioclase to form garnet in calc-silicates, possibly corresponding to that which is thought to have taken place at 1690 ± 25 Ma in the Strangways Range.

In the Entia Dome, decompression is evidenced by the replacement of kyanite by cordierite (Fig. 5) and by sillimanite. Equilibria of identical phases in the Strangways Range are considered to represent ~650–680°C and 7–8 kbar, at 1095 Ma (Warren, 1983; Windrum and McCulloch, 1986). Synchronous decompression in these two regions must be considered a possibility. The consequent expectation of evidence for such uplift in the intervening terrain also, e.g., in the Paradise Well or Ruby Mine areas (Fig. 1) is not substantiated, however, except, perhaps, by the apparent replacement of spinel by sapphirine in HRC ultramafic in area B (Fig. 1).

Micas from undeformed pegmatites cutting the HRC in the Ruby Mine area, dated by Mortimer et al. (1987) at 322–332 ± 3 Ma, are likely manifestations of the Alice Springs Orogeny, an event which had widespread repercussions in the Arunta Block. There is no other incontrovertible evidence of the Alice Springs Orogeny in the Harts Ranges, though Dr W. Collins (personal communication, 1987) claims that

mica from a metapelite in the Entia Dome has an age compatible with the commonly accepted age of ~350 Ma (Mathur and Shaw, 1982) for the Alice Springs Orogeny.

Conclusion

Present indications are that the SOB south of the Muller Thrust, the Oonagalabi Tongue, the Entia Dome and the HRC, plus the Strangways Range, are separate terrains that have behaved independently though their P-T-t paths overlap to some extent and some correlation is possible. To the extent that they are independent, they may be considered to resemble "terranes" in the sense of Howell (1985). However, many more metamorphic, structural and geochronological data must be acquired before a satisfactory elucidation of the crustal history of the overall Harts Range is possible.

Acknowledgements

This paper comprises the work by a number of people within the Department of Geology and Geophysics, University of Adelaide, as participants of a joint project in the Harts Ranges, financed by the Australian Research Grants Scheme (ARGS). Included in the paper are data from the Ph.D. theses of R. Lawrence and P. Ding and the Honours theses of B. Goscombe and D. Bowyer. The authors acknowledge the background support of Drs P.R. James, J.A. Cooper and J.D. Foden, co-chief investigators of the project, and helpful comments by Dr M. Sandiford. Thanks are expressed to Mr G. Trevelyan and Mr W. Mussared for the preparation of thin sections, to Mr. J. Stanley and Mr P. McDuie for XRF and wet chemical analyses, to Dr B.J. Griffin for assistance with the electron microprobe, to Ms S. Proferes and Mrs Fleur de Laine for drafting of diagrams, to Mr R. Barrett for photography, to Mr J. Willoughby for computer assistance, to Ms Sofia Tsemitsidis and other members of the secretarial staff for typing. Reading of, and comments on, an early draft of the manuscript by Drs James and Foden, and of a subsequent draft by editorial referees, are appreciated. Some points in the discussion may not represent the views of all authors.

References

Bohlen, S.R., 1987. Pressure-temperature-time paths and a tectonic model for the evolution of granulites. J. Geol., 95: 617-632.

Bowyer, D.G., 1982. The geology of parts of the Harts Range, Northern Territory, Australia - petrology, geochemistry and structure. Honours Thesis, Univ. of Adelaide (unpublished).

Cooper, J.A., Mortimer, G.E. and James, P.R., 1988. Rate of Arunta Inlier evolution at the eastern margin of the Entia Dome, central Australia. Precambrian Res., 40/41: 217-231.

Ding, P. and James, P.R., 1985. Structural evolution of the Harts Range area and its implication for the development of the Arunta Block, central Australia. Precambrian Res., 27: 251-276.

Ellis, D.J. and Green, D.H., 1979. An experimental study of the effect of Ca upon garnet-clinopyroxene Fe-Mg exchange equilibria. Contrib. Mineral. Petrol., 71: 13-22.

Evans, B.W. and Trommsdorff, V., 1970. Regional metamorphism of ultramafic rocks in the central Alps: parageneses in the system CaO-MgO-SiO_2-H_2O. Schweiz. Mineral. Petrogr. Mitt., 50: 481-492.

Ferry, J.M. and Spear, F.S., 1978. Experimental calibration of the partitioning of Fe and Mg between biotite and magnetite. Contrib. Mineral. Petrol., 66: 113-117.

Ganguly, J. and Saxena, S.K., 1984. Mixing properties of aluminosilicate garnets: constraints from natural and experimental data, and applications to geothermo-barometry. Am. Mineral., 69: 88-97.

Goscombe, B.D., 1984. The structure, metamorphism, petrology and geochemistry of the Paradise Well area in the Harts Range, eastern Arunta Block. Honours Thesis, Univ. of Adelaide (unpublished).

Graham, C.M. and Powell, R., 1984. A garnet-hornblende geothermometer: calibration, testing and application to the Pelona Schist, southern California. J. Metamorphic Geol., 2: 13-31.

Grant, J.A., 1985. Phase equilibria in partial melting in pelitic rocks. In: J.R. Ashworth (Editor), Migmatites. Blackie, Glasgow, pp. 86-144.

Green, D.H. and Ringwood, A.E., 1967. An experimental investigation of the gabbro to eclogite transformation and its petrological applications. Geochim. Cosmochim. Acta, 31: 767-833.

Green, T.H. and Vernon, R.H., 1974. Cordierite breakdown

under high pressure hydrous conditions. Contrib. Mineral. Petrol., 46: 215-226.

Harris, N.B.W. and Jayaram, S., 1982. Metamorphism of cordierite gneisses from the Bangalore region of the Indian Archaean. Lithos, 15: 89-98.

Holdaway, M.J. and Lee, S.M., 1977. Fe-Mg cordierite stability in high-grade pelitic rocks based on experimental theoretical and natural observations. Contrib. Mineral. Petrol., 63: 175-198.

Howell, D.G. (Editor), 1985. Tectonostratigraphic terranes of the circum-Pacific region. Circum-Pacific Council for Energy and Mineral Resources, Earth Science Series No. 1. Houston, TX, pp. 581.

Indares, A. and Martignole, J., 1985. Biotite-garnet geothermometry in granulite-facies rocks: evaluation of equilibrium criteria. Can. Mineral., 23: 187-193.

James, P.R. and Ding, P., 1988. 'Caterpillar tectonics' in the Harts Range area: a kinship between two sequential Proterozoic extension-collision orogenic belts within the eastern Arunta inlier of central Australia. Precambrian Res., 40/41: 199-216.

Lawrence, R., 1987. The structure and metamorphism of the Irindina supracrustal assemblage on the western side of the Entia Dome, Harts Range, central Australia. Ph.D. Thesis, Univ. of Adelaide (unpublished).

Lawrence, R.W., James, P.R. and Oliver, R.L., 1987. Lithological and structural relationships within the Irindina supracrustal assemblage in the Harts Range Ruby Mine of central Australia and their relevance to the occurrence of ruby. Aust. J. Earth Sci., 34: 293-309.

Lindsley, D.H., 1983. Pyroxene thermometry. Am. Mineral., 68: 477-493.

Liou, J.G., Kuniyoshi, S. and Ito, K., 1974. Experimental studies of the phase relations between greenschist and amphibolite in a basaltic system. Am. J. Sci., 274: 613-632.

Mathur, S.P. and Shaw, R.D., 1982. Australian orogenic belts: evidence for evolving plate tectonics? Earth Evol. Sci., 4: 281-308.

McKenzie, D., 1978. Some remarks on the development of sedimentary basins. Earth Planet. Sci. Lett., 40: 25-32.

Mortimer, G.E., Cooper, J.A. and James, P.R., 1987. U-Pb and Rb-Sr geochronology and geological evolution of the Harts Range ruby mine area of the Arunta Inlier, central Australia. Lithos, 20: 445-467.

Newton, R.C. and Haselton, H.T., 1981. Thermodynamics of the garnet-plagioclase-Al_2SiO_5-quartz geobarometer. In: R.C. Newton, A. Navrotsky and B.J. Wood (Editors), Thermodynamics of Minerals and Melts. Springer-Verlag, New York, pp. 131-147.

Newton, R.C. and Perkins, D. III, 1982. Thermodynamic calibration of geobarometers based on the assemblages garnet-plagioclase-orthopyroxene (clinopyroxene)-quartz. Am. Mineral., 67: 203-222.

Perkins, D. III, and Chipera, S.J., 1985. Garnet-orthopyroxene-plagioclase-quartz barometry: refinement and application to the English River subprovince and the Minnesota River Valley. Contrib. Mineral. Petrol., 89: 69-80.

Phillips, G.N., 1980. Water activity changes across an amphibolite-granulite facies transition, Broken Hill, Australia. Contrib. Mineral. Petrol., 75: 377-386.

Rankin, L., 1983. The structural geology and fabric development in the Mt Mabel area of the Harts Range, eastern Arunta Block. Hons. Thesis, Univ. of Adelaide (unpublished).

Sandiford, M. and Powell, R., 1986. Deep crustal metamorphism during continental extension: modern and ancient examples. Earth Planet. Sci. Lett., 79: 151-158.

Shaw, D.M., 1972. The origin of the Apsley Gneiss, Ontario. Can. J. Earth Sci., 9: 18-35.

Shaw, R.D., Stewart, A.J. and Black, L.P., 1984. The Arunta Inlier: a complex ensialic mobile belt in central Australia, Part 2: tectonic history. Aust. J. Earth Sci., 31: 457-484.

Sivell, W.J., 1986. A basaltic-ferrobasaltic granulite association, Oonagalabi gneiss complex, Central Australia: magmatic variation in an early Proterozoic rift. Contrib. Mineral. Petrol., 93: 381-394.

Sivell, W.J. and Foden, J.D., 1985. Banded amphibolites of the Harts Range meta-igneous complex, central Australia: an early Proterozoic basalt-tonalite suite. Precambrian Res., 28: 223-252.

Spear, F.S., 1981. An experimental study of hornblende stability and compositional variability in amphibolite. Am. J. Sci., 281: 687-734.

Stewart, A.J., Shaw, R.D. and Black, L.P., 1984. The Arunta Inlier: a complex ensialic mobile belt in central Australia, Part I: stratigraphy, correlations and origin. Aust. J. Earth Sci., 31: 445-455.

Thompson, A.B., 1976. Mineral reactions in pelitic rocks: II. Calculations of some P-T-(Fe-Mg) phase relations. Am. J. Sci., 276: 425-454.

Thompson, A.B., 1982. Dehydration melting of pelitic rocks and the generation of H_2O-undersaturated granitic liquids. Am. J. Sci., 282: 1567-1595.

Thompson, A.B. and England, P.C., 1984. Pressure-temperature-time paths of regional metamorphism II. Their inference and interpretation using mineral assemblages in metamorphic rocks. J. Petrol., 25: 929-955.

Warren, R.G., 1983. Metamorphic and tectonic evolution of granulites. Nature, 305: 300-303.

Wells, P.R.A., 1977. Pyroxene thermometry in simple-complex systems. Contrib. Mineral. Petrol., 62: 129-139.

Wernicke, B., 1985. Uniform sense normal simple shear of the continental lithosphere. Can. J. Earth Sci., 22: 108-125.

Windrum, D.P. and McCulloch, M.T., 1986. Nd and Sr isotopic systematics of central Australian granulites: chronology of crustal development and constraints on the evolution of lower continental crust. Contrib. Mineral. Petrol., 94: 289-303.

Wood, B.J. and Banno, S., 1973. Garnet–orthopyroxene and orthopyroxene–clinopyroxene relationships in simple and complex systems. Contrib. Mineral. Petrol., 42: 109–124.

Wood, B.J. and Fraser, D.G., 1976. Elementary Thermodynamics for Geologists. Oxford University Press, Oxford, 303 pp.

Wynne-Edwards, H.R., 1976. Proterozoic ensialic orogenesis: the millipede model of ductile plate tectonics. Am. J. Sci., 276: 927–953.

Zakrutkin, V.V., 1968. The evolution of amphibolites during metamorphism. Vsesoyuznoe, Mineralogicheskoe, Obschchestvo, Zapiski (Verhandlungen), 97: 13–23.

Precambrian Research, 27 (1985) 251—276
Elsevier Science Publishers B.V., Amsterdam — Printed in The Netherlands

STRUCTURAL EVOLUTION OF THE HARTS RANGE AREA AND ITS IMPLICATION FOR THE DEVELOPMENT OF THE ARUNTA BLOCK, CENTRAL AUSTRALIA

P. DING and P.R. JAMES

Department of Geology and Mineralogy, University of Adelaide, S.A. 5000 (Australia)

ABSTRACT

Ding, P. and James, P.R., 1985. Structural evolution of the Harts Range Area and its implication for the development of the Arunta Block, central Australia. Precambrian Res., 27: 251—276.

A division of the high grade metamorphics of the Arunta Block in the Harts Range Area into two main groups on the basis of lithology, structure, metamorphism and igneous activity is suggested as a result of detailed mapping. The lower group is regarded as a basement terrain and comprises major layered felsic or granitic gneiss, minor amphibolite and mafic granulite, while the structurally overlying group is regarded as a cover sequence (Irindina supracrustal assemblage) and comprises predominantly metasediments (pelitic and semi-pelitic gneiss, calc-silicate and quartzite) and amphibolite, anorthosite and ultramafic rock of the Harts Range meta-igneous complex. The cover sequence might have been deposited in an aulacogen or adjacent to a continental margin which developed by rifting of a pre-existing basement.

The two groups both show early major ductile tectonothermal stages with four major fold generations and a later discrete shear event in the basement and two major fold generations and a later series of stacked nappes developing in the cover. The basement's early orogenic evolution with associated granulite facies metamorphism is typical of intensely reworked early Precambrian terrains and developed spatially and or temporally separated from the cover. Cover deformation closely resembles continental margin Cordillera type overthrusting and thus thin-skinned tectonics associated with large scale crustal shortening.

During the later Harts Range remobilization, the basement and cover were juxtaposed by displacement on a fundamental crustal dislocation (recumbent contraction fault). Mylonites repeatedly developed along the dislocation which was also isoclinally folded, intruded by a major megacrystic granitoid (Bruna gneiss) sheet and repeatedly rejuvenated. The history of development of the dislocation is documented and described as a process of underthrusting of basement beneath cover which led to the final termination of the orogenic activity.

INTRODUCTION

This paper presents a preliminary structural and tectonic synthesis after the detailed geological mapping of an area of ~2500 km^2 of, and to the south of, the Harts Range (subsequently referred to as the Harts Range

0301-9268/85/$03.30 © 1985 Elsevier Science Publishers B.V.

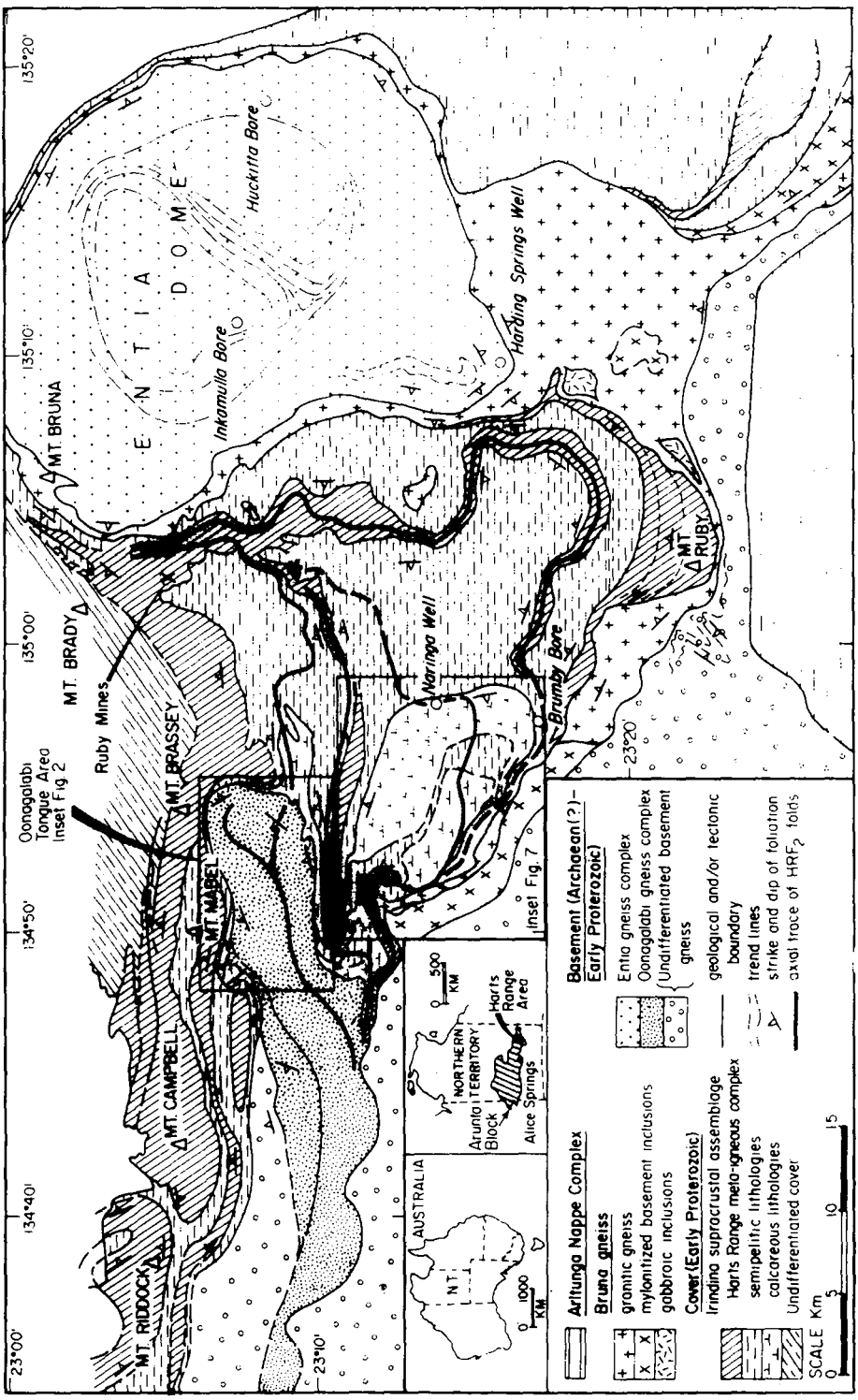


Fig. 1. Simplified geological map of the Harts Range Area.

Area of Fig. 1), which is situated some 100—150 km northeast of Alice Springs in central Australia. In the Harts Range Area we recognize a crystalline basement comprising intimately interlayered major felsic or granitic gneiss and minor mafic gneiss and a mixed metasedimentary and mafic meta-igneous supracrustal cover sequence both of which display distinctly different, intense and complex, high grade tectonothermal histories, including thrust development. After these stages of individual tectonic evolution, the basement and cover appear to have been juxtaposed by large scale thrusting.

The Harts Range Area lies within the eastern Arunta Block, a lower Proterozoic inlier surrounded by late Precambrian and younger platform sequences. According to Plumb et al. (1981) the Harts Range Area is situated wholly within the Central Tectonic Zone of the Arunta Block which consists of predominantly granulite and amphibolite facies rocks affected by the main development of the oldest (~1800 Ma according to Black et al., 1983), readily recognized metamorphism (Strangways Event).

Both Rutland (1981) and Plumb (1979) suggested that the Arunta Block lies astride a fundamental, deep, crust—mantle, east—west trending megastructure. The Harts Range Area lies at the northern margin of this megastructure which has recently been termed the Redbank granulite belt of the middle Proterozoic reworked Musgrave—Fraser Province (Rutland, 1981 and fig. 1.6). Rutland recognized the antiquity of this belt and suggested that it initially separated the essentially platformal early Proterozoic sequences of the Gawler Province, which clearly involved reworking of Archaean cratonic material (see for example Cooper et al., 1976 and Parker and Lemon, 1982), from the "geosynclinal" sequences of the North Australian Province. During its subsequent evolution in mid-late Proterozoic times tectonic activity was concentrated on thrusting associated with the easterly trending Redbank mylonite zone according to Marjoribanks (1976) and Marjoribanks and Black (1974). The area suffered its last major tectonic movements with again primarily north—south overthrust activity and nappe development during the Devono—Carboniferous Alice Springs orogeny.

Few well documented examples of major repeated overthrusting involving both reworked older basement and overlying younger cover sequences have been detailed from the high-grade mid-Proterozoic mobile belts which developed extensively between 1800 and 1000 Ma ago across Laurasia and Gondwanaland. Mobile belts such as the Eastern Ghats of India, the Ubendian and Kavirondian—Nyanzian of Africa and the major extensive mid-Proterozoic North Atlantic belt (Windley, 1977) are characterized by high (often granulite) grade polymetamorphism and discrete complex tectonothermal events superimposed on both frequently recognized Archaean basements and their unconformably overlying early Proterozoic supracrustal cover sequences. Characteristic features such as amphibolite dyke swarms, major intrusive anorthosite suites and granite—

migmatite complexes typify the mid-Proterozoic syn to post orogenic igneous activity whilst synmetamorphic deformation is recognized as producing complexly overprinted and ductilely deformed structural geometries, typically in major upright linear shear (mobile) belts.

In the Harts Range Area of the Arunta Block of central Australia we recognized a new and striking pattern of early Proterozoic tectonic development. Although no examples of radiometrically dated Archaean crust have as yet been described from the Arunta Block, Rutland (1981) regarded all of the Australian Proterozoic Provinces as being ensialic and most likely a product of vertical accretion on, and within, a pre-existing Archaean proto-continental crust. We consider the Harts Range Area to display contiguous reworked Archaean(?) crystalline basement and Proterozoic supracrustal cover. The area represents the former east—west trending extensional passive margin of a north—south rifting Archaean(?) proto-continent. The subsequent orogenic activity formed the remarkable feature of repeated semi-ductile to brittle (thrusting) and ductile (isoclinal folding) deformations which appear to have resulted from the progressive northwards underthrusting of the basement associated with (plate tectonic activated ?) crustal shortening.

LITHOLOGICAL SUBDIVISION OF THE HARTS RANGE AREA

Joklik (1955) was the first to carry out a systematic geological study of the area, and he established a preliminary stratigraphic sequence which he termed the Harts Range Group. The subdivision of the Harts Range Area was modified after systematic reconnaissance mapping of the Arunta Block by B.M.R. workers during 1970—1974 (for details see Shaw et al. 1979, 1982 and in prep.). This work, which was for the production of 1:100 000 and 1:250 000 sheet areas, was based on photointerpretation of 1:25 000 colour air photographs associated with field traverses and checking of lithologies and geological relationships and was not accompanied by detailed mapping or structural studies. Preliminary results first published by Shaw and Stewart (1975a and b) subdivided the rocks of the Harts Range Area into the two lower of their three loosely chronological divisions of the Arunta Block, which were based on metamorphic character and associations (Table I). They described rocks of the lowest unit (Division One) as consisting of granulites of pelitic, felsic and mafic compositions (with subordinate amphibolite facies calc-silicates and gneisses). Stewart and Warren (1977) considered the mafic and felsic granulites to represent the chemical equivalents of basic and acid volcanics. This unit was considered to be everywhere in discordant contact (fault or possible unconformity) with the second unit (Division Two) which consisted of amphibolite grade felsic, pelitic and calcareous gneisses with associated mafic flows or sills. This second unit was considered to be characterized by a much higher proportion of mature original sediments than the first unit and concom-

itantly a lower proportion of meta-igneous rock.

From detailed mapping and structural interpretation of this study we considerably revise the pre-existing lithological subdivision and nomenclature. We subdivide the Harts Range Area into two distinct primary groupings (see legend to Fig. 1) on the basis of lithology, metamorphism, igneous activity and structure. Gneisses found in three subareas, the Oonagalabi Tongue, the Entia Dome and those to the south and west of Mt. Ruby, are considered to represent crystalline basement, whilst the second grouping comprises the cover sequence of the Irindina supracrustal assemblage and includes the Harts Range meta-igneous complex. A third minor grouping comprises predominantly the Bruna granitic gneiss which occupies a restricted location along part of the basement—cover boundary and though clearly of plutonic origin, with minor xenoliths, lenses and interlayers of mainly basement, its position or age of intrusion in regard to either basement or cover is equivocal.

TABLE I

Lithological subdivision of the Harts Range according to Shaw et al. (1982 and 1983)

Division Two — Harts Range Group
Brady Gneiss
Irindina Gneiss
-Riddock Amphibolite Member
—Naringa Calcareous Member
Bruna Gneiss
Entia Gneiss
Division One — Strangways Metamorphic Complex
Cadney metamorphics
Bungitina metamorphics

Basement

Shaw et al. (1979 and in prep.) subdivided the Strangways Metamorphic Complex of their Division 1 into a number of spatially separate metamorphic units defined within fault bounded blocks. They make only tentative lithological correlations between blocks and thus between the metamorphic units. Within the Oonagalabi Tongue (renamed as it does not represent a domal structure (see later) as is implied in the term Oonagalabi Dome of Shaw and Wells, 1983) lay basement gneisses of the Bungitina metamorphics of Shaw et al. (1979 and in prep.). We prefer not to use this term, as Bungitina metamorphics are also described from south of our major thrust boundaries (see later), but rather refer to these gneisses as

the Oonagalabi gneiss complex of the crystalline basement (Fig. 1). This gneiss complex comprises biotite gneiss, biotite hornblende gneiss, feldspathic gneiss, amphibolite, mafic granulite and granitic gneiss. It is characterized by a variably developed compositional layering defined by continuous and discontinuous lithological units. Fine scaled interlayering frequently precludes mapping of individual horizons, but occasional groupings of dominant sequences of mafic lithologies or granitic gneiss are discrete enough to provide marker horizons which have been mapped to outline the complex fold geometry as is shown later in Fig. 2. As the layering is mainly the product of the complex tectonothermal history which developed this geometry, it is also more fully discussed later.

Samples displaying granulite facies assemblages are widely distributed within the Oonagalabi Tongue and along with their similar lithologies and overall gneissic morphology suggest equivalence of this basement with the Strangways Metamorphic Complex which makes up the predominantly charnockitic granulites of the Strangways Range to the west (D.F. Windrum, personal communication, 1983). Typical metamorphic assemblages within the Oonagalabi gneisses, however, display amphibolite facies mineralogies.

Shaw et al. (1982) included the Entia Gneiss of their Entia Domal Structure as part of the Division 2 Harts Range Group (Table I) which overlies the Strangways Metamorphic Complex. In contrast, we see no clear distinction between the Entia gneiss complex (we prefer to retain the name but as an informal and non capitalized term) and the Oonagalabi gneiss complex. Both gneiss complexes comprise predominantly felsic with minor mafic, layered gneisses, and both display similar structural styles (though due to their different subsequent evolution they have different precise structural geometries) and similar tectonothermal histories, and both clearly underly the supracrustal cover sequence along disjunctive contacts.

We define the Entia gneiss complex as basement which is restricted to the Entia Dome (Fig. 1) and is separated from the main outcrops of crystalline basement by the continuous outcrop of a thin superficial layer of Bruna gneiss. The Entia gneiss complex comprises mainly feldspathic gneiss, amphibolite and a few layers of phlogopite—kyanite schist mostly showing evidence of amphibolite facies assemblages. The metamorphic history of this gneiss complex was the subject of a detailed study by Dobos (1978).

The general character of the Entia gneiss complex is similar to the Oonagalabi gneiss complex except for a distinctly lower proportion of mafic layers. Within the Entia gneisses Joklik (1955) recognized two granitic bodies, the Huckitta and Inkamulla Granodiorites, as intruding the cores of the Huckitta and Inkamulla "domes" (see also Shaw et al., 1982). Our work and that of Buick (1983) has shown that the intrusive granites are, in fact, sheet like bodies of granitic gneiss (of a complex granitoid suite), refolded into uniformly plunging isoclinal folds (not open domes) and are deformed by all deformation phases along with their host gneisses.

The undifferentiated gneisses shown in Fig. 1 in the south of the Harts Range Area are similar in lithology and metamorphism to the other basement gneisses. Immediately SW of Mt. Ruby they display a structural geometry and history identical to, and contiguous with, that found within the upper part of the Entia gneiss complex.

Cover

We no longer use the term Harts Range Group of Shaw et al. (1982) to describe supracrustal rocks of the Harts Range Area, because they included the Entia gneiss (of our crystalline basement) and the Bruna gneiss within that group (compare Fig. 1 legend with Table I). Within their Harts Range Group (Table I), Shaw et al. (1982) subdivided the sequence into a number of conformable Gneiss units, implying the establishment of a stratigraphy for the cover. Throughout our field investigations no primary sedimentary depositional or igneous (intrusive or extrusive) features have been identified within any units of the cover sequence (or of the crystalline basement). Small scale layering is grossly transposed and refolded by isoclinal recumbent folds (see later) and nowhere can be shown to conclusively represent original sedimentary or igneous layering. No stratigraphic younging or way-up criteria have been recognized to enable identification of the obviously commonly repeated and inverted lithological units. On a large scale major lithological contacts have generally been recognized as of primarily tectonic origin (thrusts, slides or décollements), and thus mappable lithological units can nowhere be interpreted as sedimentary formations. Thus owing to the complexity of the imposed tectonothermal activity, the recognition of a formal stratigraphy in the cover sequence is precluded, and we therefore prefer not to use the nomenclature of Shaw et al. (1982) but present a simplified lithological subdivision of the cover sequence of the Harts Range Area as shown in Fig. 1.

The Irindina supracrustal assemblage comprises both sediment (pelitic and semipelitic gneiss, calcareous rock and quartzite) and the Harts Range meta-igneous complex. The biotite schists and biotite gneisses are poorly layered and strongly foliated and contain infrequent minor layers and lenses of calcareous and quartzose metasediments and conformable amphibolite as competent units. Structurally near to the base of the Irindina supracrustals lies a major unit consisting of layers of biotite gneiss, pure and impure quartzite and marble, calc-silicate rock and calcareous quartzite, as a contiguous sequence mappable around many folds in the Naringa Well area (see later Fig. 7). This gradual change in lithotype from more quartz rich to calcareous lithologies across relatively continuous compositional layering may represent an original bedded sequence of mature (platformal/shallow shelf) sediments. However, the lack of way-up criteria does not allow the bottom or top of the sequence to be recognized. In conformity with our revision of the lithological subdivision of the cover

sequence we do not retain the name Naringa Calcareous Member of Shaw et al., 1982 (see Table I) for this unit.

The major layered amphibolites of the Harts Range Area were included as the Riddock Amphibolite Member of the Irindina Gneiss of the Harts Range Group by Shaw et al. (1982) (Table I). The Riddock Amphibolite Member is here renamed as part of the Harts Range meta-igneous complex within the Irindina supracrustal cover sequence. This complex may comprise major mafic metavolcanic components or it may represent the deformed equivalent of a major intrusive layered mafic suite or possibly a combination of both. Detailed petrographic and geochemical studies are in progress (W. Sivell, personal communication, 1984). The complex is now dominated by layered mafic amphibolites with minor leucocratic amphibolites, rare pods of ultramafic and a significant horizon of anorthosite (Katz, 1981), the Entire anorthosite of Ding et al. (1983), near its base. Minor interlayers of pelitic biotite gneiss are also structurally intercalated within the amphibolites.

Bruna gneiss

The Bruna gneiss which was previously placed within the Harts Range Group of Shaw et al. (1982) (see Table I) is typically a homogeneous, mylonitized, potash feldspar megacrystic, granitic gneiss which forms a major sheet separating basement and cover over most of the eastern Harts Range Area (Fig. 1). It is clearly of igneous origin, containing numerous xenoliths of amphibolite, gabbro, mafic granulite and pyroxene gneiss and has been recognized intruding both basement and cover.

STRUCTURAL EVOLUTION OF THE HARTS RANGE AREA

Plumb et al. (1981) considered that both Division 1 and Division 2 rocks of Shaw and Stewart (1975a) were deposited in the Arunta Block area during the early Proterozoic and were then together subjected to multiple metamorphism and deformation during the Strangways Event (1800–1850 Ma ago). They did not recognize any difference in structural evolution between the two Divisions, whilst allowing the possibility of an unconformity between them. Plumb et al. (1981) further offered a simple structural interpretation, pointing out that three distinct phases of folding were evident in the Central Tectonic Zone of the Arunta Block. They did not, however, elaborate on their individual styles or superposition relationships.

From the current detailed field mapping study we have recognized a complex sequence of deformation events which individually affected the crystalline basement and supracrustal cover sequence and subsequently juxtaposed and remobilized them as a single mobile zone. Table II outlines the sequence of orogenic stages and associated structures.

At least three directions of late open folding can be seen in both the basement and the cover as a later phase of the stage three remobilization. These folds produce the major fold interference patterns and complex outcrop traces of the Harts Range Area but are of relatively minor geometrical significance and are therefore not discussed further in this paper.

TABLE II

Orogenic stages and associated structures developed in the Harts Range Area

	Deformation(D)	Fold(F)	Fabric(S/L)	Thrust(T)
Stage 4 — Alice Springs orogeny				
Stage 3 — Remobilization — Harts Range Event(HR)				
	HRD_{4-6}	HRF_{4-6}		
		----------		HRT_3
	HRD_3	HRF_3		
		----------		HRT_2
	HRD_2	HRF_2		
	HRD_1	HRF_1		
		----------		HRT_1
Stage 2 — Cover (C)				
				CT
	CD_2	CF_2	CL_2	
	CD_1	CF_1	CS_1/CL_1	
Stage 1 — Basement (B)				
				BT
	BD_4	BF_4		
	BD_3	BF_3		
	BD_2	BF_2		
	BD_1	BF_1	BS_1/BL_1	
	pre BD_1 (?)			

The following abbreviations are used throughout the text — Basement structures of Stage 1 (B), cover structures of Stage 2 (C), remobilization structures of Stage 3 (HR), ductile deformation phase (D), fold generation (F), foliation (S), lineation (L), major thrust event (T). Use of subscripts for particular generation of structures follows standard structural geology usage i.e., BF_1 indicates the first fold generation developed within the basement etc.

Stage 1 — basement structures

Three discrete subareas of outcropping basement have been investigated in the Harts Range Area, being the Entia gneiss complex of the Entia Dome, the Oonagalabi gneiss complex of the Oonagalabi Tongue and the undifferentiated layered basement gneisses immediately south and west of Mt. Ruby (Fig. 1). Though precise geometries of the three basement areas differ because of their different subsequent tectonic development during

the remobilization stage (Stage 3) of orogenic evolution, they all display similar sequences and styles of early structures.

The Oonagalabi Tongue

The Oonagalabi area has been studied in most detail (a full account of the geology of the Oonagalabi Tongue is in preparation). Detailed structural mapping of this area (Fig. 2) reveals that the structural history began with the formation of an intense layer-parallel metamorphic foliation (BS_1) and mineral lineation (BL_1), which developed along with intensely transposed continuous and lenticular, fine to coarse (10^{-2}—10^2 m) compositional layering (see Figs. 2 and 3). This fabric which developed during the first recognizable deformation of the basement, BD_1, is defined by preferred orientation of largely amphibolite facies minerals. The amphibolite facies mineralogy is superposed on an earlier granulite facies assemblage which may define an earlier (pre BD_1?) fabric (see Table II).

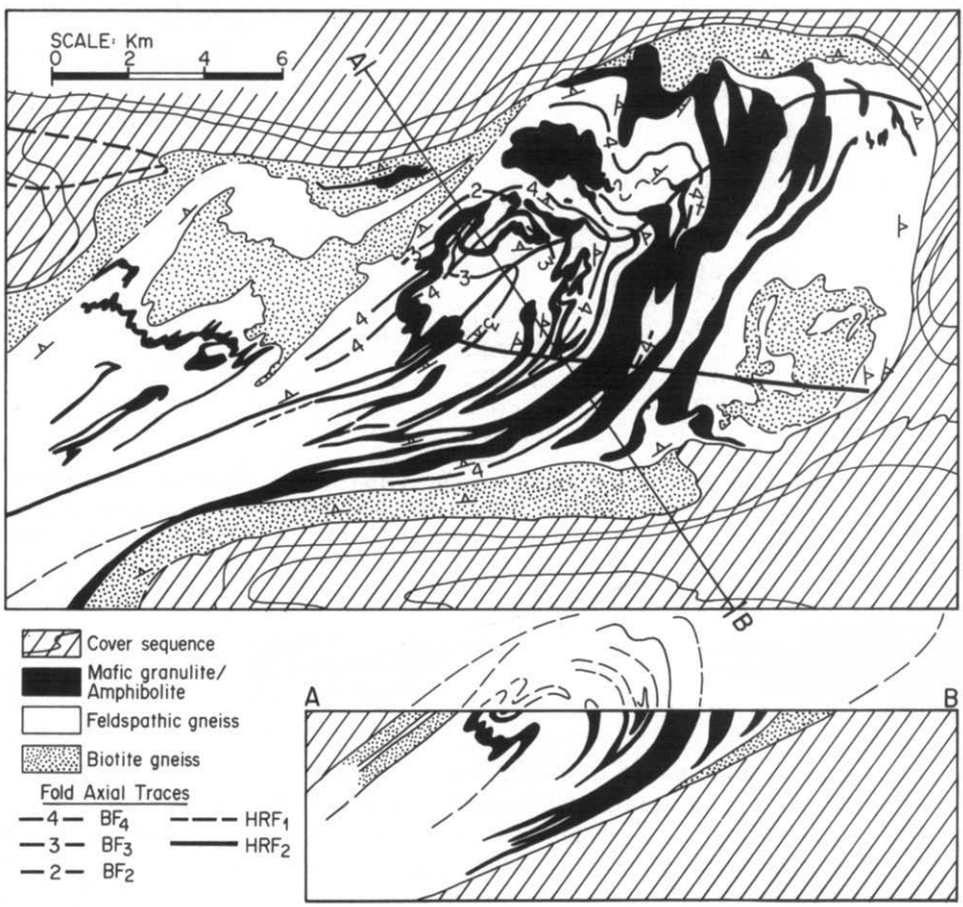


Fig. 2. Geological map of the Oonagalabi Tongue.

The relationship between the two mineral fabrics is currently being studied, but the extent and intensity of later deformations is likely to preclude the recognition of significant pre-D_1 geometry or structures. Even within the BD_1 event no major BF_1 folds have been recognized, and the orientation of the BS_1 and BL_1 structural elements is quite variable due to refolding and overprinting by later events.



Fig. 3. Finely interlayered amphibolite, feldspathic gneiss and biotite—amphibole—plagioclase gneiss within the Oonagalabi gneiss complex.

The layering and early fabric were folded around major recumbent isoclinal folds (BF_2), the hinges of which are characteristically small with rounded parallel closures (i.e., retaining layer thickness) in profile and long continuous parallel limbs (see, for example, the upper centre area of Fig. 2). On a small scale the relationship is recognized in mafic layers where the BF_2 fold closures clearly fold BS_1 without the formation of a new axial plane foliation or axial lineation. BL_1 lineations can often be observed folding around BF_2 folds with a variable intersection angle of up to 45° (Figs. 4 and 5). Occasionally a new axial foliation (BS_2) defined by biotite and a new mineral lineation appears in the hinges of B_2 folds.

BF_3 folds refold the parallel limbs of the BF_2 folds (map and section of Fig. 2), forming a series of major isoclinal folds of typically hundreds



Fig. 4. BL_1 lineation with different orientations (shown parallel to the knife and pencil) within either limb of an isoclinal BF_2 fold from the Oonagalabi gneiss complex.



5 (a)

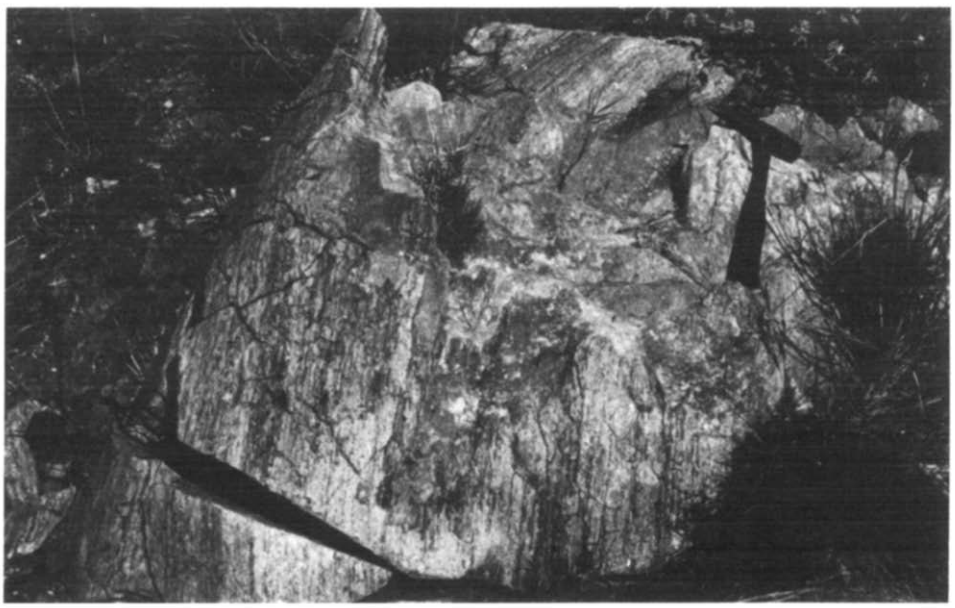


Fig. 5. BL_1 lineation occurs at 30° to the hinge of BF_2 isoclinal fold (a) which clearly folds it (b). The BF_2 fold plunges 55/20°. The BL_1 lineation plunges (022°/41°) on the northwest limb and 075/0° on the southeast one. The fold occurs within feldspathic gneisses from undifferentiated basement west of the Oonagalabi Tongue.



Fig. 6. The BS_1 fabric within layered amphibolite is folded about an isoclinal BF_2 fold which is itself folded by a very tight, possibly BF_4 fold. This example is located north of Harding Springs' Well (Fig. 1) within the Entia gneiss complex.

of metres to kilometres in amplitude, though few minor BF_3 folds can be found. The closures of BF_3 folds are similar to the generally smaller BF_2 closures, with again subparallel limbs. The axial planes and hinges of BF_3 and BF_2 folds are generally parallel, with trends varying slightly around NE—SW with shallow NE plunges (Fig. 2). Superposition of these two structures develop type III interference patterns of Ramsay (1967) as can be clearly seen on both the map (Fig. 2) and outcrop (Fig. 6) scale.

The largely parallel sequence defined by the dominant limb regions of BF_2 and BF_3 folds was refolded during BD_4 to form the most commonly observed folds in the area. Major BF_4 folds are tight with shorter limbs and parallel hinges again coaxial with BF_2 and BF_3.

After this series of ductile structural events, major schists and mylonite zones, trending ENE and dipping moderately NNW, transect the basement lithologies and earlier structures. They are interpreted as semi-ductile overthrusts (BT of Table II). Figure 1 shows two examples of map scale thrusts.

The Entia Dome and extension of the basement SW of Mt. Ruby

The structural history of the Entia gneiss complex, which developed during the basement orogenic stage (Stage 1), appears to be identical to that described from the Oonagalabi Tongue. Two isoclinal (BF_2 and BF_3) and one tight (BF_4) ductile fold generations coaxially refold an intense early (BD_1) layer parallel tectonothermal fabric as is shown in Fig. 6 (this work and Buick, 1983). The major ductile geometries (see Fig. 1) resemble large northeasterly plunging sheath folds and their precise morphology is still under study.

The strong NE–SW tectonic grain defined by BD_4 structural trends in the Entia Dome reappears to the southwest of Mt. Ruby from beneath the thin cover of Bruna gneiss. These two areas share an identical structural history and geometry, and they appear to have acted together as stable crust during the subsequent remobilization period of Stage 3.

Stage 2 — cover structures

The sedimentary sequence of the Irindina supracrustals, including the largely basic rocks of the Harts Range meta-igneous complex, were metamorphosed to amphibolite facies syntectonically with CD_1 (Table II). Minor folds at the boundaries of ultramafic boudins exposed in workings at the Harts Range Ruby mine site (Fig. 1) are described as possible CF_1 by Lawrence, James and Oliver (unpublished). Throughout the cover rocks an intense CS_1 foliation is manifested as a mica schistosity in biotite schist or biotite rich gneiss and as a transposed tectonic layering and layer-parallel foliation in amphibolite, quartzite and calc-silicate. A weak CL_1 mineral lineation strikes predominantly from NE—SW in the south, through north—south to more northwesterly in the north.

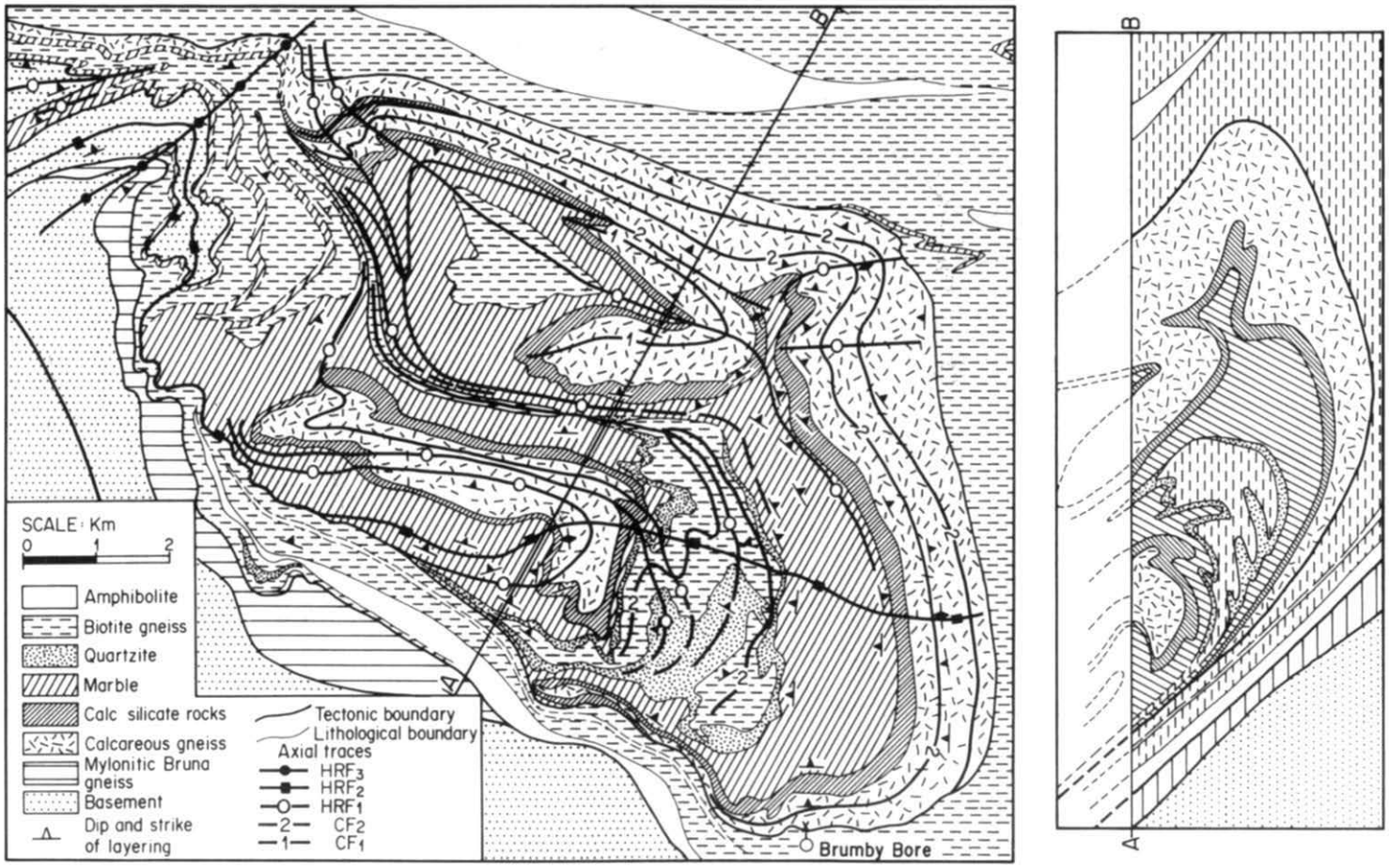


Fig. 7. Geological map of the Naringa Well area.

The best area to unravel the complex history and geometry of superposed structures is within the cover sequence from the Naringa Well area where they are illustrated by many distinct and continuous lithological layers whose boundaries may represent transposed sedimentary bedding (Fig. 7). A few CF_1 isoclinal folds have been mapped within the calc-silicate units of this area. It is difficult to map out CF_1 folds in pelitic gneiss units. Many isoclinal folds within individual lithologic units may represent possible minor CF_1 folds (Fig. 8). CF_1 folds display tight closures with fold axes and CL_1 lineations plunging NE, while the fold axial surfaces trend E—W.

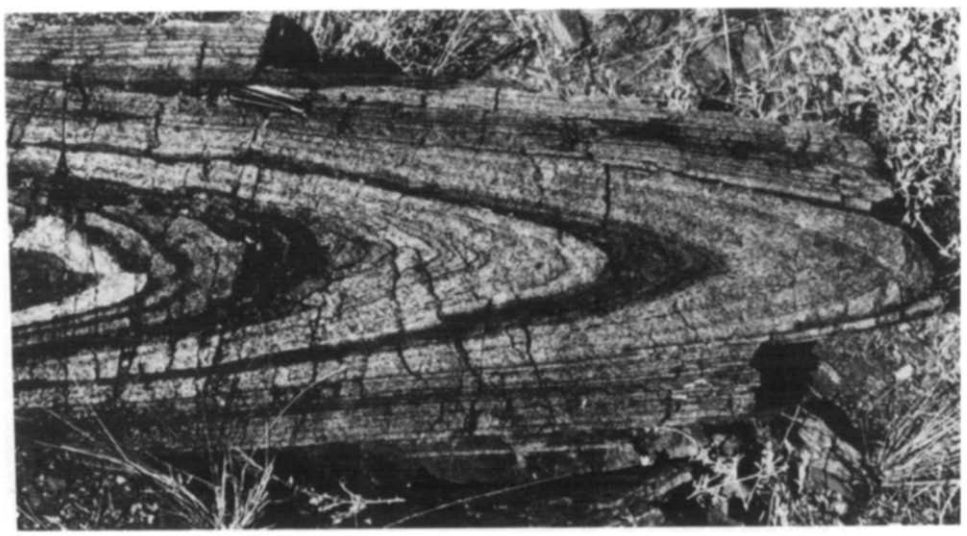


Fig. 8. CF_1 fold flattened by ductile shearing related to HRT_2 within the Naringa Well area.

CF_2 major isoclinal folds (Fig. 7) occur with fold axes and a CL_2 lineation plunging shallowly E—W and paralleling fold axial surface trends. Both CF_1 and CF_2 folds developed under high grade (amphibolite facies) metamorphic conditions.

Major CF_2 folds are transected by major thrust boundaries (CT) throughout the cover sequence (Table II and Fig. 9). The thrusts broadly follow the boundaries of major lithological units on a large (map) scale and therefore resemble décollement surfaces. However, the presence of mylonites along the thrusts and the frequent low angle discordances at the thrusts show the cover sequences to have the form of a duplex of thrust sheets or nappes, each containing a complexly folded package of supracrustals.

Four major nappes are recognized in the cover sequence, though subsequent ductile folding has largely modified their original morphologies.

The lowest nappe (I of Fig. 9) comprises the calcareous and quartzose assemblages of the Naringa Well area (Fig. 7) but also contains minor pelitic

gneiss. A thick calcareous gneiss is largely conformable with the bounding thrust, but small scale layering in the adjacent nappe is clearly discordant with the thrust boundary. This boundary is also marked by very fine grained-mylonitic calcareous and quartzose gneisses. The second nappe (II) comprises primarily pelitic gneisses in the central portion of the cover sequence of the Harts Range Area. It contains minor interlayered amphibolite and calcareous gneiss and is structurally overlain by the third thrust sheet (III) which comprises predominantly the Harts Range meta-igneous complex and its tectonically interleaved units of pelitic gneiss. The structurally highest thrust sheet (IV) of the Harts Range Area comprises intimately interleaved and isoclinally folded pelitic gneiss and amphibolites. The precise definition of the major amphibolite unit, which forms Mt. Ruby and can be traced as a continuous unit for 40 km to the north and 20 km to the west (Fig. 1), and of its structurally overlying pelitic gneiss as either a repetition of the two former nappe units (II and III) by subsequent isoclinal folding or as two different thrust sheets (see Fig. 9) is not possible. This is due to the complexity of subsequent ductile deformation.

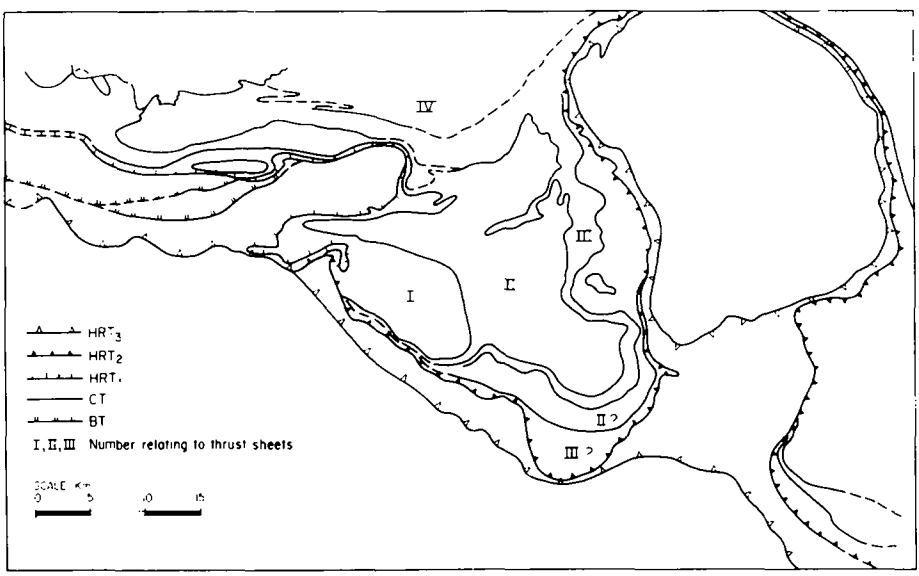


Fig. 9. Simplified map showing major thrusts within the Harts Range Area.

Stage 3 Harts Range Event — remobilized basement and cover structures

After the development of BF_4 folds in the crystalline basement and CF_2 folds in the supracrustal cover sequence a major discordant thrust boundary developed juxtaposing the basement and cover. This thrust (HRT_1) is now only recognized in the Oonagalabi area (Figs. 1 and 2), where it

forms the boundary of the Oonagalabi Tongue and in the Naringa Well area (Fig. 7). The HRT_1 thrust is locally parallel to adjacent layering in both basement and cover. However, basement fold axial surface traces and the BT thrust zones are clearly sheared into parallelism width HRT_1, close to the thrust which is defined by a belt of mylonites up to 20 m wide. On a regional scale the major lithological boundaries of the Irindina supracrustals, the CT décollements, CF_2 fold axial traces and all earlier folds are all also sheared into parallelism and ultimately transected by the HRT_1 thrust.

The HRT_1 thrust boundary, and both the basement below and cover above, were refolded about originally open to tight asymmetric upright HRF_1 folds which are best developed in the cover sequence around Mt. Riddock and Mt. Campbell and in the Naringa Well area (Figs. 1 and 7). HRF_1 folds are now largely tight to isoclinal and recumbent and trend predominantly E–W, coaxially with the CF_2 folds. Amphibolite and quartzite horizons display smoothly rounded parallel style HRF_1 closures while those in the pelitic gneisses elsewhere are tight and disharmonic. HRS_1 axial plane foliations occur sporadically, being most easily recognized as they transect earlier foliations in the HRF_1 closures, while a new HRL_1 lineation is often difficult to distinguish from the coaxial CL_2 (Fig. 10).



Fig. 10. HRF_1 folds with an incipient axial fabric within the Naringa Well area.

The HRF_1 folds and all earlier structures were refolded by HRF_2 during a largely transcurrent ductile movement. HRF_2 folds are neutral, recumbent, isoclinal folds with shallow northerly plunges. Two major fold

pairs of this generation are shown in Figure 1, where they are most evidently folding the HRT_1 boundary, the CT décollements between nappes I and II, and II and III and the HRF_1 folds. On a smaller scale the style of HRF_2 folds is more difficult to describe. Different lithologies show vastly different fold geometries, and because of their differing mechanical properties HRF_2 show the styles of disharmonic folds as reviewed by Ramsay (1983).

Within the Oonagalabi basement HRF_2 folds (which are therefore the sixth generation folds of the local sequence) display rounded closures but are isoclinal with parallel limbs as is the folded shape of the HRT_1 boundary. The influence of HRF_2 on the Irindina supracrustals and layered mafics, where major and minor HRF_2 folds are common (e.g., Fig. 11), is complex due to interference with earlier fold closures of competent horizons which are found in HRF_2 hinge areas and to localized parasitic folds with mylonitized limbs.



Fig. 11. Low elevation oblique aerial photograph of HRF_1 fold refolded by HRF_2, attenuated close to HRT_2, Naringa Well area (see also Fig. 7).

The next major thrust HRT_2 forms the base of the cover sequence in the south and east of the Harts Range Area and extends into the basement to the west. The thrust mostly separates Irindina supracrustals from the laterally continuous underlying Bruna gneiss and other basement gneisses and is not deformed by HRF_2 major folds. In the area immediately west of the Naringa Well area HRT_2 transect a small portion of Oonagalabi gneiss complex which had previously been folded by HRF_2 folds and its bounding HRT_1 thrust. Intense shearing and drag occurred along the HRT_2 thrust with a strong flattening and rotation of HRF_1 folds near both the northeast (near the Ruby Mine area) and southwest (west of the Naringa area) edges of the overriding nappe. This thick (up to 1 km) development of mylonites occurred under granulite facies conditions in a major recumbent ductile shear zone. It appears that the Bruna gneiss intruded into this shear zone, near its top in the west and near its base in the east, and was subsequently itself deformed by the same continuous event. The Bruna gneiss and its related mafic granulite xenoliths and country rock were strongly mylonitized during this period of thrusting (Fig. 12).

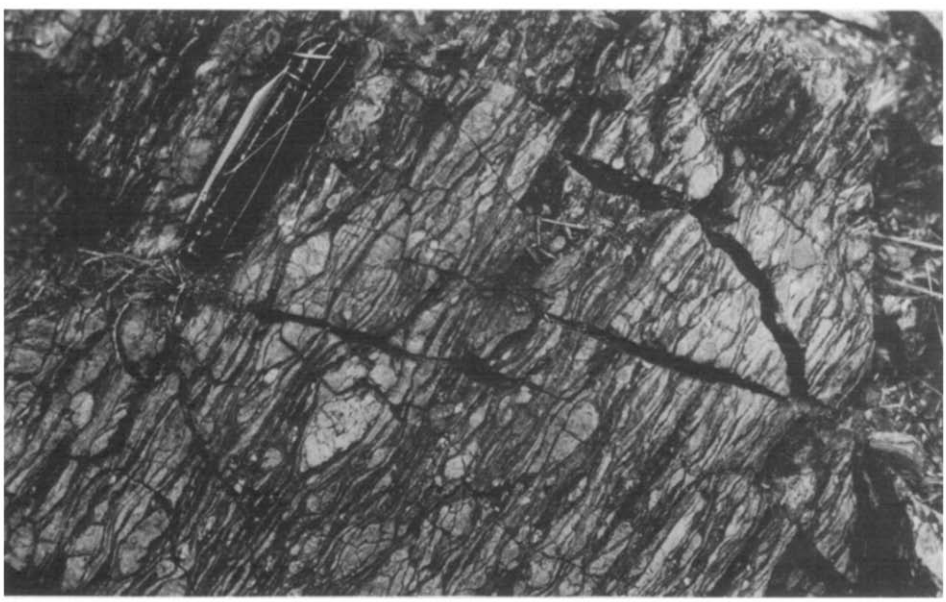


Fig. 12. Typical mylonitic fabric (XZ section) within Bruna granitic gneiss west of Brumby Bore.

The HRT_2 thrust plane and its overlying sequence are sporadically folded by asymmetric minor folds trending ENE and with axial planes inclined moderately to the NNW. These HRF_3 folds are tight and also fold the mylonitic foliation of the Bruna gneiss. In one sample a mylonitic (biotite) fabric is recognized developing parallel to the axial plane of HRF_3 folds.

The final major thrust (HRT_3) of the Harts Range Event forms the lower boundary between the Bruna gneiss and basement in the eastern part of the Harts Range Area, while in the west it truncates earlier major folds and thrusts (Fig. 1) and, as a mylonite or schist zone up to 100 m wide, separates overlying Oonagalabi gneiss basement from basement to the south. The Bruna gneiss suffered further mylonite development during this period of thrusting.

SUMMARY OF COMPARISONS AND CONTRASTS BETWEEN BASEMENT AND COVER

The similarity between basement terrains of three areas (the Oonagalabi Tongue, the Entia Dome and the area south of Mt. Ruby) and the differences between basement and the Irindina supracrustal assemblage are listed below:

(1) Felsic and granitic gneisses are the predominant lithologies within the basement while pelitic or semi-pelitic gneiss or schist, calcareous rocks and quartzite are the predominant lithology within the Irindina supracrustal assemblage.

(2) Mafic rocks within the supracrustals are all of amphibolite facies while those within the basement are of granulite facies (though some contain lower grade assemblages).

(3) Mafic rocks within the supracrustals are mainly layered, continuous, thick units which may represent metabasaltic flows (W. Sivell, unpublished) intercalated with thin layers of metasediments, while within the basement mafic rocks are distinctly different, appearing mainly as thin layers or lenses (some of which are of clearly intrusive origin) intercalated with predominant feldspathic gneiss and granitic gneiss.

(4) The volume of mafic rock within the supracrustals is about equal to the metasediments, while mafic rocks within the basement represent only about one tenth of the sequence.

(5) Significant features of anatexis, including migmatitization and granitic magma intrusions, can be seen everywhere within the basement, while in the supracrustals only weak migmatitization and small granite sills have been found.

(6) Before HRF_1 the main trend of folds in the basement was NE, while that of folds in the supracrustals was E—W.

(7) More uniform and intense fabrics (foliations and lineations) are found within the basement. Only weak mineral lineations with more varied trends occur within the supracrustals.

A MODEL FOR THE TECTONIC EVOLUTION OF THE HARTS RANGE AREA

Figure 13 shows a series of simplified cartoon models describing the tectonic development of the Harts Range Area. The period of formation

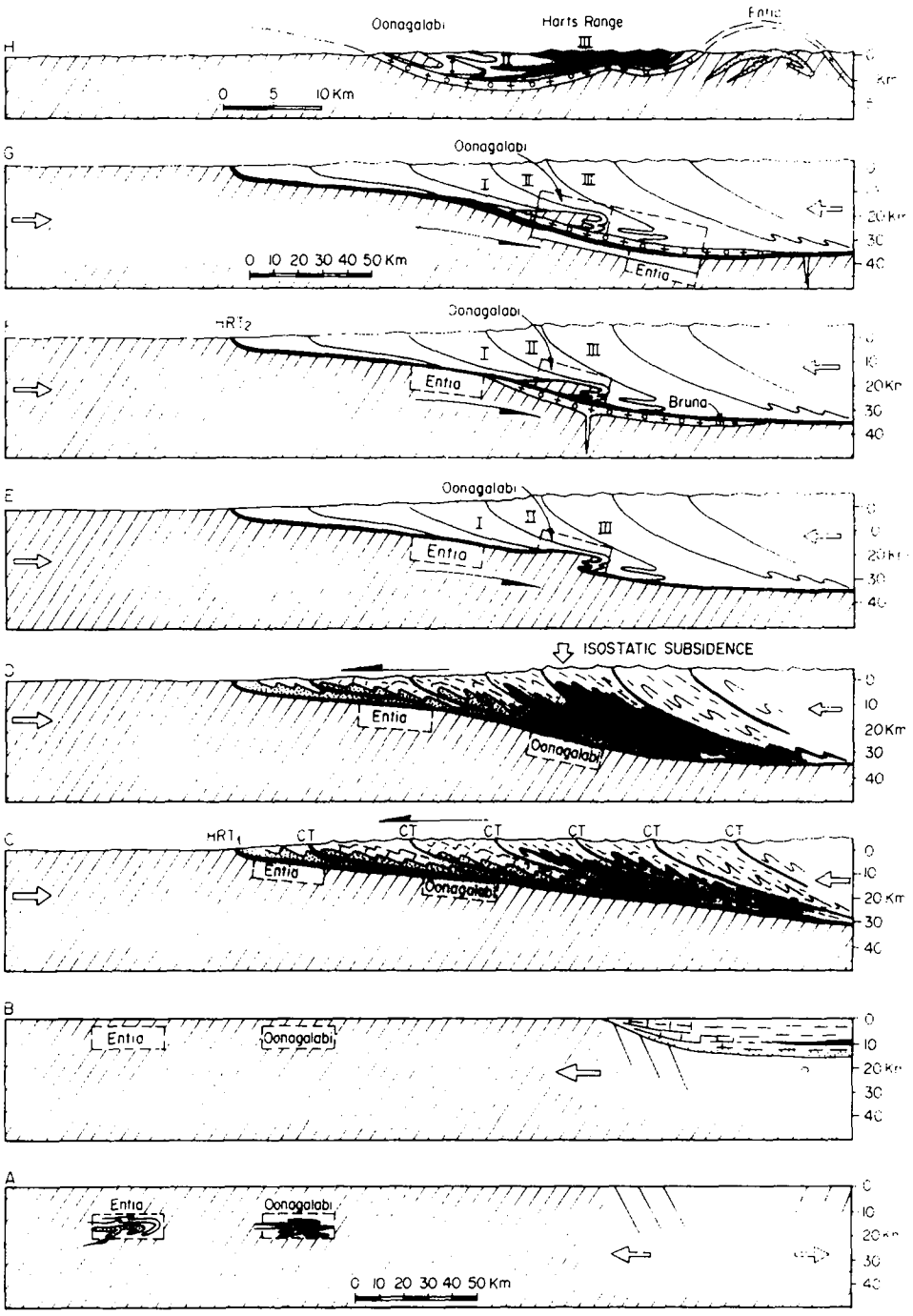


Fig. 13. Schematic section representation of a model for the tectonic evolution of the Harts Range Area. A = Stage I evolution, B—D = Stage II evolution, E—H = Stage III evolution, Harts Range Event. A—G sections are S—N, H section is W—E.

of the layered crystalline basement areas was one of interleaving of acid and mafic horizons and intrusion of homogenous potassic granitic and granodioritic bodies, followed by intense ductile deformation with repeated isoclinal fold development at uniformly elevated temperatures and pressures under largely granulite facies conditions. The continental crust developed by this process closely resembles areas of layered high grade crystalline gneisses which have been described from Archaean terrains of Australia and elsewhere. Morphologically similar terrains include the Archaean gneisses of the Fiskanaesset region of West Greenland (Myers, 1981), the Ancient Gneiss Complex of Swaziland (Hunter, 1970 and Barton, 1981) and the Shaw batholith of Western Australia where the tectonic interleaving of high grade gneisses, syntectonic granites and greenstone belt intercalations was recognized by Bettenay et al. (1981). A reconnaissance Rb—Sr geochronological study of the basement (Division 1) areas of the southern Arunta Block adjacent to the Harts Range Area by Black et al. (1983) revealed only lower Proterozoic maximum ages. However, subsequent tectonothermal activity in the rocks highlighted in our work may have assisted in later isotopic reequilibration of a pre-Proterozoic craton.

Ductile thrusting (BT) within the basement in the Oonagalabi Tongue before its juxtaposition with the cover formed high grade mylonitic schist zones and attests to early shear zone development.

The Irindina supracrustals appear similar to a geosynclinal basin sequence, varying from platform-shelf facies (orthoquartzite—carbonate) to (deeper water?) monotonous pelites and semi-pelites. The sequence may represent a simple aulacogen developed on the underlying rifted crystalline basement gneisses. The present regional distribution of the cover sequence further suggests that this may have been the site of an E—W through which separated the North Australian craton from the Gawler craton, tough whether continental crust separated sufficiently to develop a proto-ocean is not certain. The Harts Range layered meta-igneous complex might have intruded into the cover sequence as a typical mafic lopolithic sheet with minor extrusive layers. Alternatively, the Irindina supracrustals and Harts Range layered meta-igneous complex may represent the now severely interleaved and distorted remnants of an oceanic mafic crust/sediment (i.e., ophiolite) sequence.

The cover sequence was subjected to an orogenic evolution typical of compressional/collision tectonics of a continental margin. This might have been initiated as a Cordilleran orogeny with the early metamorphism of the sequence to amphibolite facies and subsequent (post CD_2) deformation predominated by shallow contraction faults (CT) developing on lithological (décollement) horizons to form a stacked overthrust pile of thin nappes. The inferred southerly motion of this continental shortening is evidenced by the pervasive and uniform N—S trend of the CL_1 lineation and E—W trend and southerly overturned asymmetric vergence of CF_2 and HRF_1 folds. This typical thin-skinned tectonic pattern did not involve the basement to the sequence initially (Coward, 1983) and probably de-

veloped on the continental foreland to the main Cordilleran fold belt (Price, 1981) on a major basement/cover (HRT_1) basal décollement. The semi-brittle nature of this movement is evidenced by its formation as a discrete structure with only thin ductile mylonites on the boundary and limited shear of adjacent structures.

The development of resistance to continued overriding of the nappes leading to crustal thickening and associated isostatic subsidence of the basement (Price, 1973) might have then caused the drastic change in orogenic evolution which marked the initiation of Stage 3, the Harts Range Event. At the beginning of this stage the basement and cover, which previously were being continuously juxtaposed by the major thrust (HRT_1), were welded together. The subsequent evolution of HRT_1 clearly involves its ductile folding by an E—W horizontal transcurrent stress which formed the isoclinal, neutral, shallowly north-plunging HRF_2 folds. This ductile deformation suggests that HRT_1 was further depressed within the crust either by continued isostatic subsidence or by the process we favour which is that of the initiation of underthrusting of the basement below the now static nappes of the cover sequences.

The process of underthrusting of basement below the overlying sequence appears to have continued, with subsequent development of the HRT_2 thrust as a major shear zone located largely at the mechanical discontinuity of the cover—basement contact, but which also transected the basement alone along part of its length. The Bruna granitic gneiss appears to have intruded during this event and controlled its subsequent development. A constant intense lineation trending at 020—040° indicates the NNE-NE direction of the underthrusting. This thrust again ceased to be an active displacement horizon and was then folded before similarly oriented underthrusting continued along the HRT_3 thrust plane at the base of the Bruna gneiss.

The model for the development of the Harts Range orogenic stage, therefore, involves the progressive southwards migration of shallowly northerly inclined thrusts which underrode an already developed orogenic supracrustal sequence. Late stage continued underthrusting was most likely halted by the isostatic resistance of low specific gravity continental crust/basement to further subsidence, and open upright buckling of the Harts Range Area to develop its complex outcrop patterns attests to the cessation of orogenic activity.

CONCLUSIONS

(1) As is summarized earlier, two distinct lithological groupings have been recognized in the Harts Range Area. One is a crystalline basement of layered felsic and mafic gneisses which may represent the high grade and highly deformed equivalent of a granite—greenstone (thus originally Archaean?) terrain. The second group comprises a suite of metasedimentary supracrustals and interlayered amphibolites which represent the fill

an E—W basin which formed either as a aulacogen or proto-ocean produced by the extension and rifting of the pre-existing crystalline basement.

(2) Basement lithologies show the development of a high amphibolite and granulite facies assemblage, isoclinal folds and tectonothermal fabric, all subsequently deformed by three isoclinal fold phases and a later semi-ductile thrust.

(3) The cover sequence displays an amphibolite facies fabric refolded by isoclinal folds and then complexly thrust to form a series of stacked nappes. The nappes and their bounding thrusts are themselves tightly folded. Both fold and thrust geometries indicate thrusting of cover over basement in a southerly direction.

(4) Basement and cover were juxtaposed by progressive underthrusting of basement beneath the cover sequence. A series of three thrusts were sequentially developed and then incorporated in subsequent ductile folds.

(5) Examples of complexly infolded and interthrust cover and basement in orogenic zones are rare except in well documented Phanerozoic examples. The Harts Range Area provides a classic example of such a tectonic pattern within the Arunta Block of central Australia. It has thus a significant potential for future intensive integrated study of its structural, petrologic, geochemical and isotopic evolution. This study is currently in progress.

ACKNOWLEDGEMENTS

The logistic support for this paper and for the Adelaide University Harts Range Project is provided by A.R.G.S. grant number E8215617 I.

Bronwyn Hosking and Lorna Lucas, Rick Barrett and Sharon Proferes are, respectively, thanked for word processing, photography and cartography. The paper was improved by discussions with R. Lawrence whose mapping around the Harts Range Ruby Mine is included in Fig. 1. R.W.R. Rutland and M.A. Etheridge are thanked for their critical reviews of the first draft.

REFERENCES

Barton, J.M., Jr., 1981. The pattern of Archaean crustal evolution in southern Africa as deduced from the evolution of the Limpopo Mobile Belt and the Barberton Granite—Greenstone Terrain. In: J.E. Glover and D.J. Groves (Editors), Archaean Geology. Geol. Soc. Aust., Spec. Publ., 7: 21—31.

Bettenay, L.F., Bickle, M.J., Boulter, C.A., Groves, D.I., Morant, P., Blake, T.S. and James, B.A., 1981. Evolution of the Shaw Batholith — an Archaean Granitoid—Gneiss Dome in the Eastern Pilbara, Western Australia. In: J.E. Glover and D.J. Groves (Editors), Archaean Geology. Geol. Soc. Aust., Spec. Publ., 7: 361—372.

Black, L.P., Shaw, R.D. and Stewart, A.J., 1983. Rb—Sr geochronology of Proterozoic events in the Arunta Inlier, Central Australia. Bur. Min. Res. J. Aust. Geol. Geophys., 8: 129–137.

Buick, I., 1983. The geology, petrology and geochemistry of the Huckitta granodioritic gneisses and associated granitoids. Honours thesis, University of Adelaide (unpublished) 28 pp.

Cooper, J.A., Fanning, C.M., Flook, M.M. and Oliver, R.L., 1976. Archaean and Proterozoic metamorphic rocks on southern Eyre Peninsula, South Australia. Geol. Soc. Aust. J., 23: 287–292.

Coward, M.P., 1983. Thrust tectonics, thin skinned or thick skinned, and the continuation of thrusts to deep in the crust. J. Struct. Geol., 5, 2: 113–124.

Ding, P., James, P.R. and Lawrence, R.W., 1983. Structural evolution of the Harts Range Group, central Australia. Geol. Soc. Aust., Abstract Series 9: 67, 68.

Dobos, S.K., 1978. Phase relations, element distributions, and geochemistry of metamorphic rocks from the eastern Arunta Block, Northern Territory. Ph.D. thesis, Macquarie University (unpublished) 313 pp.

Hunter, D.R., 1970. The ancient Gneiss Complex in Swaziland. Trans. Geol. Soc. S. Afr., 83: 107–150.

Joklik, G.F., 1955. The geology and mica-fields of the Harts Range, central Australia. Bur. Min. Res., Australia, Bulletin 26.

Marjoribanks, R.W., 1976. The relation between microfabric and strain in a progressively deformed quartzite sequence from central Australia. Tectonophysics, 32 209–293.

Parker, A.M. and Lemon, N.M., 1982. Reconstruction of the Early Proterozoic stratigraphy of the Gawler Craton, South Australia. Geol. Soc. Aust. J., 29: 221–238.

Plumb, K.A., 1979. The tectonic evolution of Australia. Earth-Sci. Rev., 14: 205–249.

Plumb, K.A., Derrick, G.M., Needham, R.S. and Shaw, R.D., 1981. The Proterozoic of northern Australia. In: D.R. Hunter (Editor), Precambrian of the Southern Hemisphere, pp. 205–307, Development in Precambrian Geology, 2. Elsevier, Amsterdam.

Price, R.A., 1973. Large-scale gravity flow of supracrustal rocks, southern Canadian Rockies. In: K.A. de Jong and R. Scholten (Editors), Gravity and Tectonics. Wiley New York, pp. 491–502.

Ramsay, J.G., 1967. Folding and Fracturing of Rocks. McGraw-Hill, New York, 568 pp.

Ramsay, J.G., 1983. Rock ductility and its influence on the development of tectonic structures in mountain belts. In: K.J. Hsü (Editor), Mountain Building Processes. Academic Press Inc., New York, 263 pp.

Rutland, R.W.R., 1981. Structural framework of the Australian Precambrian. In: D.R. Hunter (Editor), Precambrian of the Southern Hemisphere.

Shaw, R.D. and Stewart, A.J., 1975a. Arunta Block-regional geology. In: C.L. Knight (Editor), Econ. Geol. Aust. Papua New Guinea, Monogr. Ser. 5.

Shaw, R.D. and Stewart, A.J., 1975b. Towards a stratigraphy of the Arunta Block. In: Proterozoic Geology. Geol. Soc. Aust., Abstracts of the First Australian Geological Convention, p. 35.

Shaw, R.D. and Wells, A., 1983. Alice Springs, Northern Territory (Second Edition). 1:250 000 Geological Series – Explanatory Notes. Bur. Min. Res., Geol. Geophys.

Shaw, R.D., Langworthy, A.P., Offe, L.A., Stewart, A.J., Allan, A.R., Senior, B.R. and Clarke, D., 1979. Geological report on 1:100 000 scale mapping of the southeastern Arunta Block, Alice Springs 1:250 000 Sheet area, Northern Territory. Bur. Min. Res., Record 1979/47 (unpublished).

Shaw, R.D., Freeman, M.J., Offe, L.A. and Senior, B.R., 1982. Geology of the Illogwa creek 1:250 000 Sheet Area, central Australia – Preliminary Data, 1979–80 surveys. Bur. Min. Res. Geol. Geophys., Record 1982/23 (unpublished).

Shaw, R.D., Stewart, A.J. and Rickard, M.J., in prep. Geology of the Arltunga–Harts Range region, Northern Territory. Bur. Min. Res., Australia, 1:100 000 Map Commentary.

Stewart, A.J. and Warren, R.G., 1977. The mineral potential of the Arunta Block. Bur. Min. Res. J. Aust. Geol. Geophys., 2: 21–34.

Windley, B.F., 1977. The Evolving Continents. Wiley, London, 385 pp.